

การสำรวจแผ่นดินไหวบรรพกาลตามเขตรอยเลื่อนระนอง ภาคใต้ของประเทศไทย



นางสาว สุมาลี ทิพยไภาส

ศูนย์วิทยทรัพยากร
จุฬาลงกรณ์มหาวิทยาลัย

วิทยานิพนธ์นี้เป็นส่วนหนึ่งของการศึกษาตามหลักสูตรปริญญาวิทยาศาสตรมหาบัณฑิต

สาขาวิชาธรณีวิทยา ภาควิชาธรณีวิทยา

คณะวิทยาศาสตร์ จุฬาลงกรณ์มหาวิทยาลัย

ปีการศึกษา 2553

ลิขสิทธิ์ของจุฬาลงกรณ์มหาวิทยาลัย

PALEOEARTHQUAKE INVESTIGATION ALONG THE RANONG FAULT ZONE,
SOUTHERN THAILAND



Miss Sumalee Thipyopass

ศูนย์วิทยทรัพยากร
จุฬาลงกรณ์มหาวิทยาลัย
A Thesis Submitted in Partial Fulfillment of the Requirements
for the Degree of Master of Science Program in Geology

Department of Geology

Faculty of Science

Chulalongkorn University

Academic Year 2010

Copyright of Chulalongkorn University

Thesis Title PALEOEARTHQUAKE INVESTIGATION ALONG THE RANONG
FAULT ZONE, SOUTHERN THAILAND
By Miss Sumalee Thipyopass
Field of Study Geology
Thesis Advisor Associate Professor Punya Charusiri, Ph.D.
Thesis Co-advisor Thanu Harnpattanapanich, Ph.D.

Accepted by the Faculty of Science, Chulalongkorn University in Partial
Fulfillment of the Requirements for the Master's Degree



..... Dean of the Faculty of Science
(Professor Supot Hannongbua, Dr.rer.nat.)

THESIS COMMITTEE



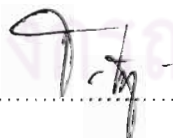
..... Chairman
(Associate Professor Montri Choowong, Ph.D.)



..... Thesis Advisor
(Associate Professor Punya Charusiri, Ph.D.)



..... Thesis Co-advisor
(Thanu Harnpattanapanich, Ph.D.)



..... Examiner
(Thanop Thitimakorn, Ph.D.)



..... External Examiner
(Suwith Kosuwan, M.Sc)

สุมาลี ทิพย์โยภาส : การสำรวจแผ่นดินไหวบรรพกาลตามเขตรอยเลื่อนระนอง ภาคใต้ของประเทศไทย. (PALEOEARTHQUAKE INVESTIGATION ALONG THE RANONG FAULT ZONE, SOUTHERN THAILAND) อ. ที่ปริกษาวิทยานิพนธ์หลัก : รองศาสตราจารย์ ดร.ปัญญา จารุศิริ, อ.ที่ปริกษาวิทยานิพนธ์ร่วม: ดร.ธนู หาญพัฒน์พานิช, 316 หน้า.

การศึกษาเขตรอยเลื่อนระนองภาคใต้ของประเทศไทยมีวัตถุประสงค์เพื่อให้ทราบลักษณะเฉพาะและตำแหน่งของรอยเลื่อนมีพลัง จำนวนเหตุการณ์แผ่นดินไหว ขนาดความรุนแรงในอดีต และอัตราการเคลื่อนตัวของรอยเลื่อน โดยอาศัยข้อมูลโทรสัมผัส การสำรวจคลื่นไหวสะเทือน กลไกการเคลื่อนตัวของเหตุการณ์แผ่นดินไหว และข้อมูลภาคสนามเป็นหลัก

ผลจากการศึกษาพบว่ารอยเลื่อนระนองเป็นรอยเลื่อนที่วางตัวในแนวตะวันออกเฉียงเหนือ-ตะวันตกเฉียงใต้ และมีการเอียงเทด้วยมุมชันไปในทางทิศตะวันออกเฉียงจากนั้นยังพบว่ารอยเลื่อนระนองต่อเลยออกไปในทะเลทั้งอ่าวไทยและทะเลอันดามันด้วย สำหรับบนแผ่นดินพบว่ารอยเลื่อนยาว 300 กิโลเมตรจากจังหวัดประจวบคีรีขันธ์ไปยังจังหวัดระนองและประกอบด้วยรอยเลื่อนย่อย 19 รอยเลื่อน ส่วนรอยเลื่อนที่ต่อออกไปในทะเลมีความยาวประมาณ 45-100 กิโลเมตร โดยข้อมูลจากการสำรวจคลื่นแผ่นดินไหวพบว่า รอยเลื่อนดังกล่าวตัดเข้าไปถึงพื้นผิวทะเล รอยเลื่อนระนองที่อยู่บนพื้นแผ่นดินมีการเคลื่อนตัวในแนวระนาบแบบซ้ายเข้า ส่วนรอยเลื่อนที่เคลื่อนตัวไปในทะเลเป็นรอยเลื่อนตามแนวเฉียงที่มีการเคลื่อนตัวแบบปกติเป็นหลักและมีการเคลื่อนตัวในแนวระนาบแบบซ้ายเข้าร่วมด้วย ซึ่งสอดคล้องกับข้อมูลกลไกการเกิดแผ่นดินไหวที่เกิดในอ่าวไทยและข้อมูลจากสนามที่แสดงให้เห็นถึงลักษณะภูมิลักษณะการแปรสัณฐานหลายรูปแบบเช่นทางน้ำหักงอ ภูเขารูปสามเหลี่ยม ภูเขา รอยเลื่อน สันเขาขนาน ผารอยเลื่อน เป็นต้น

ผลการศึกษการลำดับชั้นตะกอนจากร่องสำรวจแผ่นดินไหวโบราณ 2 ร่องจากรอยเลื่อนและข้อมูลการหาอายุในอดีตและปัจจุบัน ประกอบกับข้อมูลการวิเคราะห์โครงสร้างภาคตัดขวางจากคลื่นไหวสะเทือนในทะเลอันดามันและอ่าวไทย สรุปได้ว่าเคยเกิดแผ่นดินไหวทั้งหมด 6 ครั้ง และที่เกิดอายุน้อยที่สุดเมื่อประมาณ 2,000 ปีมาแล้ว และรอยเลื่อนระนองทำให้เกิดแผ่นดินไหวใหญ่ที่สุด 7.4 Mw โดยอาศัยหลักฐานจากรอยเลื่อนย่อยระนอง และรอยเลื่อนนี้มีอัตราการเคลื่อนตัวมากที่สุดคือ 0.7 มม/ปี โดยใช้ข้อมูลรอยเลื่อนย่อยหนองกี่ ดังนั้นจึงสรุปได้ว่ารอยเลื่อนระนองเป็นรอยเลื่อนมีพลังโดยนัยการเคลื่อนตัวเป็นแบบซ้ายเข้าในปัจจุบันและมีความอุบัติซ้ำประมาณ 2,000 ปี

ภาควิชา.....ธรณีวิทยา.....ลายมือชื่อ นิสิต.....*สุมาลี ทิพย์โยภาส*.....
 สาขาวิชา.....ธรณีวิทยา.....ลายมือชื่อ อ.ที่ปริกษาวิทยานิพนธ์หลัก.....*Th. Y. Jai*.....
 ปีการศึกษา.....2553.....ลายมือชื่อ อ.ที่ปริกษาวิทยานิพนธ์ร่วม.....*Th. Y. Jai*.....

5072532823 : MAJOR GEOLOGY

KEYWORDS : RANONG FAULT / MACROSEISMIC / PRACHUP KHIRI KHAN /
ACTIVE FAULT / THERMOLUMINESCENCE DATING

SUMALEE THIYOPASS : PALEOEARTHQUAKE INVESTIGATION ALONG
THE RANONG FAULT ZONE, SOUTHERN THAILAND. ADVISOR :
ASSOCIATE PROFESSOR PUNYA CHARUSIRI, Ph.D., CO-ADVISOR : THANU
HARNPATTANAPANICH, Ph.D., 316 pp.

Investigation along the Ranong Fault Zone (RNF) in southern Thailand is aimed at identifying its characteristics, locating active faults, identifying numbers of earthquake faulting, and determining paleoearthquake magnitudes and slip rates using remote sensing and field survey, enhanced seismic data, dating data, and focal mechanism. The result shows that the RNF strikes in the northeast- southwest direction and dips eastward at steep angles. It is also discovered that the RNF extends into the sea to the Gulf of Thailand and the Andaman sea. The RNF on land is estimated to have the length of 300 km from Prachuab Khirikhan to Ranong province. The RNF consists of 19 fault segments and its extended segments to the sea have the length between 45 and 100 km. Seismic reflection data reveal that the RNF cuts through the seafloor. On land the RNF is the strike-slip fault with the left lateral sense of movement, whereas in the sea the RNF is the oblique-slip fault with the major normal sense of movement. The result confirms very well with the focal mechanism data and field relation regarding several morphotectonic features including trigular facet, offset stream linear valley, pressure ridge and fault scarp.

The stratigraphic – log results from two paleoseismic trenches across the RNF along with the previous and recent geochronological data and structural section from seismic interpretation lead to the conclusion that there are at least 6 earthquake events and the latest movement occurred at about 2,000 yrs. The RNF used to trigger the largest earthquake with the magnitude of 7.4 Mw as evidenced by the Ranong segment and the fault has the maximum slip rate 0.7 mm/yr from the Nong Ki segment. It is therefore concluded that the RNF is active fault with the sinistral sense of movement and the recurrences interval of 2,000 yr.

Department : Geology

Field of Study : Geology

Academic Year : 2010

Student's Signature Sumalee Thiyopass

Advisor's Signature Punya Charusiri

Co-advisor's Signature Thanu Harnpattanapanich

ACKNOWLEDGMENTS

The author wishes to express my profound and sincere appreciation to my advisor, Associate Professor Punya Charusiri, and the thesis co-advisor, Dr.Thanu Hampattanapanich, for their enthusiastic support, continuous guidance and invaluable advice throughout the period of this study.

Sincere thanks and appreciation are extended to the Royal Irrigation Department for the grants and accessibility usefully data of detail 2 meters contour map in southern Thailand, color orthophotograph and the satellites images from Landsat 5 TM and The CGIAR Consortium for spatial Information (CGIAR-CSI) for SRTM DEM data.

A special thank to the Secretary and staff of Office of Atoms for Peace (OAEP), especially Mr.Pisarn Tungpitayakul for his help in sample analysis with NAA method. I also would like to express my sincerely gratitude to Mr.Arag Vitittheeranon for his help in working in gamma ray issues.

Thanks are also extended to Mr.Pathinya Pornsopin, the senior official of Thai Meteorological Department, Mr.Tananchai Mahattanachai, the senior geologist of The Department of Mineral Fuels, and Dr. Pasakorn Pananoon, Department of Earth Science, Faculty of Science, Kasetsart University, for providing permission suggestions in my graduate study.

Special thanks extend to Mr.Sarun Keawmaungmoon, Mr.Weerachat Wiwegwin, and Mr. Aukkaravit Maneerut for their helping at the fieldwork and manage collectiong all samples, Mr.Wasin Wachiradilok for complie data into English version. I would like to thank to Associate Professor Montri Chuwong, Dr. Pitsanupong Kanjanapayont, Dr. Santi Pailoplee and staffs of the Department of geology, Chulalongkorn University for all their help and support.

This research was supported by several agency including the 90th Chulalongkorn University Fund from Graduate School Chulalongkorn University.

Finally, a very special thank to my family, my parents for continuous financial and emotional supports throughout the program. No amount of his gratitude of them would be sufficient. Last, but not least, my colleague, Mr. Krerksak Leenanon , thank you for your help and being a budget supporter. Your responses make her work a better one.

CONTENTS

	PAGE
ABSTRACT IN THAI.....	iv
ABSTRACT IN ENGLISH.....	v
ACKNOWLEDGEMENTS.....	vi
CONTENTS.....	vii
LIST OF TABLES.....	xi
LIST OF FIGURES.....	xiii
CHAPTER I INTRODUCTION.....	1
1.1 Background.....	1
1.2 Objectives.....	3
1.3 Study Area.....	6
1.4 Methodology.....	6
1.5 Research Output.....	8
1.6 A Brief Guide to the Thesis.....	9
CHAPTER II GEOLOGICAL TECTONIC SETTINGS.....	10
2.1 Regional Setting.....	10
2.1.1 Structural and geology setting of mainland	10
2.1.2 Structural and geology setting of Andaman sea	18
2.1.3 Structural and geology setting of Gulf of Thailand	26
2.2 Neotectonic Evolution.....	30
2.3 Active Faults in Thailand.....	34
2.3.1 Previous earthquake studies in Thailand.....	34
2.3.2 Definition of active faults.....	41
2.3.3 Some thoughts on Active Faults in Thailand.....	46
2.4 Ranong Fault.....	47
CHAPTER III REMOTE-SENSING INVESTIGATIONS.....	51
3.1 Materials.....	51
3.1.1 Landsat 5 TM+.....	51

	PAGE
3.1.2 Digital Elevation Model.....	52
3.1.3 Arial Orthographic image.....	56
3.1.4 Airbone geophysic data.....	56
3.2 Interpretation and Result	58
3.2.1 lineaments.....	58
3.2.2 Sediment basins and boundary.....	67
3.3 Fault segmentation.....	67
3.3.1 Concept of fault segmentation.....	67
3.3.2 Result of fault segment.....	73
CHAPTER IV MACROSEISMIC INVESTIGATION AND FOCAL MECHANISM.....	125
4.1 Macroseismic intensity map (on the 2006 earthquake event in Prachuab Khiri Khan).....	125
4.1.1 Method of work.....	128
4.1.2 Result of the study.....	132
4.1.3 Discussion and Conclusion.....	132
4.2 Focal Mechanism (on 8 th October 2006 earthquake event in Prachuab Khiri Khan).....	146
4.2.1 Basic concept of Focal mechanism.....	146
4.2.2 Methodology.....	146
4.2.3 Preliminary Result.....	151
4.2.4 Discuss and Conclusion.....	153
CHAPTER V SEISMIC INTERPRETATION.....	160
5.1 Seismic interpretation in Andaman Sea	160
5.1.1 Preliminary Result	164
5.1.1.1 Seismic line survey AN1	164
5.1.1.2 Seismic line survey AN2	169
5.1.1.3 Seismic line survey AN3.....	175
5.1.1.4 Seismic line survey AN4	181
5.1.2 Summary of seismic interpretation in Andaman sea	188

	PAGE
5.2 Seismic interpretation in Gulf of Thailand	190
5.2.1 Preliminary Result	198
5.2.1.1 Seismic survey line G1	198
5.2.1.2 Seismic survey line G2	207
5.2.1.3 Seismic survey line G3	214
5.2.2 Summary of seismic interpretation in Gulf of Thailand	219
CHAPTER VI FIELD INVESTIGATIONS	224
6.1 Previous Investigations	224
6.1.1 Natural Hot Spring	224
6.1.2 Radon gas survey	226
6.2 Tectonic Geomorphology	228
6.2.1 General Geology	228
6.2.2 Field investigations	230
6.3 Paleoseismic Trench	230
6.3.1 Trench 1: Si Yeak Ban Krut.....	238
6.3.2 Trench 2: Ban Neon Kraut.....	243
CHAPTER VII THERMOLUMINESCENCE DATING	248
7.1 Basic Concept	248
7.2 Laboratory Processes	251
7.2.1 Crushing and Sieving	251
7.2.2 Annual Dose Evaluation	253
7.2.3 Paleodose or Equivalent Dose Evaluation	254
7.2.4 Error Determination	261
7.3 Dating result from this study	261
CHAPTER VIII DISCUSSIONS	268
8.1 Characteristics of the RF	268
8.2 Geomophic Features and Paleoearthquake Magnitudes	274
8.3 Age, Slip Rates and Recurrence Interval	282
8.4 Neotectonic Evolution of The RF	286

	PAGE
CHAPTER IX CONCLUSIONS	291
References.....	294
Appendix.....	303
Biography	316



ศูนย์วิทยทรัพยากร
จุฬาลงกรณ์มหาวิทยาลัย

LIST OF TABLES

	PAGE
Table 2.1 Active fault rank, criteria, and examples in Thailand (modified after Charusiri et al., 2001).....	43
Table 2.2 Activity of faults in Thailand based upon age-dating data (modified after Charusiri et al., 2001).....	44
Table 3.1 Band spectrum and wavelength interval of Landsat Thematic Mapper (Landsat 5), (USGS, 2009).	52
Table 3.2 Image information from satellite, Landsat 5 TM applied in this research.....	52
Table 3.3 Image information from STRM DEM used in this research.....	53
Table 3.4 Types of fault segments and criteria used for active fault segmentation in this study (McCalpin,1996).	71
Table 3.5 Fault segment lengths proposed for active fault by various authors (modified after (McCalpin,1996).	72
Table 4.1 Coordinates of the epicenter and the magnitude of the earthquake base on different seismic center (TMD, 2006).....	126
Table 4.2 Number of data and time of investigation of the earthquake in this study.....	128
Table 4.3 Modified Mercalli Scale (Bolt, 2006)	130
Table 4.4 The relocated coordinates of the epicenter and the magnitude of the earthquake from TMD (2007) and different seismic center.....	135
Table 4.5 Seismic station , location and first time of P-wave arrival in this study.	151
Table 4.6 Parameters used for calculation of focal mechanism.....	151
Table 5.1 Displacement of faults in seismic line survey AN1.....	169
Table 5.2 Displacement of faults in seismic line survey AN2.....	175
Table 5.3 Displacement of faults in seismic line survey AN3.....	181
Table 5.4 Displacement of faults in seismic line survey AN4.....	188
Table 5.5 Displacement of Ranong fault which cutting to the seafloor	189

	PAGE
Table 5.6 Displacement of Ranong fault cutting the top of basement	189
Table 5.7 Displacement of faults in seismic line survey G1	207
Table 5.8 Displacement of faults in seismic line survey G2	214
Table 7.1 TL dating results of quartz concentrates sediments for sample collected from the study area, Prachuab Khiri Khan and Ranong, Southern Thailand.	265
Table 8.1 Paleoearthquake magnitudes of the KMF in southern Thailand, estimation from Well & Coppersmith (1994).....	279
Table 8.2 Numbers of Earthquake faultings and recurrence interval of the fault segments belonging to RNF.	285
Table 8.3 Slip rate and regional slip rate in long term of active fault.	286



ศูนย์วิทยทรัพยากร
จุฬาลงกรณ์มหาวิทยาลัย

LIST OF FIGURES

	PAGE	
Figure 1.1	Map of Pacific ocean region showing subduction zones on the ring of Fire (Modified after http://standeyo.com/Reports/041222.EQ.warning/050827.Deyo.EQs.html).....	2
Figure 1.2	Map of regional South East Aisa showing earthquakes of different depths 0-800 km (http://umfacts.um.edu.my/gallery/index.php?menu=research_hp?menu=search_details&cid=110)	2
Figure 1.3	Map of mainland Southeast Asia showing epicentral distribution from 1912-2009 (Data from Nutalaya et al., 1985; Thai Meteorological Department, 2009 and http://neic.usgs.gov/neis/epic/epic_global.html .)	4
Figure 1.4	Map of Part of southern Thailand showing the location of study area (A) Study area in main land (red square),(B) Study area in Andaman Sea (purple area),and (C) Study area in Gulf of Thailand (orange square).....	5
Figure 1.5	Flow chart showing the methodology used in this study	7
Figure 2.1	Tectonic map of central- east Asia illustrating 'extrusion' model and its relationship with Cenozoic structures in the region. Numbers in white arrows indicate the relative order in which certain continental blocks were extruded toward the southeast (after Tapponnier et al., 1982).	11
Figure 2.2	Regional setting of South and East Asia showing major tectonic sedimentary basins and main structural features (Morey,2002).....	12
Figure 2.3	Structure map showing distribution and orientation of major Cenozoic basin in the Gulf of Thailand. Inserted map shows dextral transtensional shear movement (Polachan and Sattayarak,1989).	13

Figure 2.4	Detail of the Thai Peninsula showing the Ranong (RF) and Khlong Marui fault zones. (a) Fault map, dark grey, metamorphic cores and granite outlines stippled-west of the RF-belonging to the Western Province and dotted-east of the RF-belonging to the Eastern Province (modified from Department of Mineral Resources, 1982) and basin outlines from Intawong (2006). (b) SRTM (Shuttle Radar Topography Mission) digital elevation model of the same area (Watkinson et al., 2008). Also shown in (b) is the location of the study area (in box).	14
Figure 2.5	Geological map showing orientations and distribution of the Ranong Fault. (RF) Note that northern part of RN passes through Bangsaphan and Thup Sakae districts of Prachuab Khiri Khan province whereas the southern part passes through Ranong and Kraburi cities of Ranong province (Modified from Department of Mineral Resources, 2007).	16
Figure 2.6	Explanation of geological map along the RF (Modified from Department of Mineral Resources, 2007) showing in Figure 2.5. ...	17
Figure 2.7	Structural geology map of Andaman Sea (Modified from DMR., STS. And BEICIP-FRANLAB, 1996).....	23
Figure 2.8	Physiographic map of the Mergui Basin, Andaman Sea (Mahatanachai, 1996).....	24
Figure 2.9	Stratigraphic Correlation of Mergui and N-sumatra Basin (Mahatanachai, 1996).....	25
Figure 2.10	Structure map of Gulf of Thailand showing relationship between conjugate strike-slip faults and the development of N-S trending pull-apart basins. (1) Sakhon, (2) Paknam, (3) Hua Hin, (4) North western, (5) Prachuab, (6) Western, (7) Kra, (8) Pattani, (9) Chumporn, (10) Nakhon, (11) Songkhla, (12) Malay (Polachan and Sattayarak, 1989).....	27

	PAGE
Figure 2.11 Generalised chronostratigraphic summary of basins in the northern part of the Gulf of Thailand (Pradidtan and Dook, 1992).....	28
Figure 2.12 Stratigraphy of Cenozoic basins in the Gulf of Thailand (Polachan et al.,1991).	31
Figure 2.13 Three successive stages (I to III) and extrusion-tectonic model (IV to VI) with plasticine experiment (plain view). In unilaterally confined experiment, two major faults (F1 and F2) guide successive extrusion of two blocks. In stage VI, blocks 1 and 2 can be compared to Indochina and southern China, and open gap 1, 1+2, 2 to South China Sea, Andaman Sea, and northeastern China, respectively (after Tapponnier et al., 1982).	33
Figure 2.14 Tectonic evolution during Tertiary Period : 44 Ma (A), 32 Ma (B), 23 Ma (C), 15 Ma (D), and 4 Ma (E), showing the change in the sense of movement of the Ranong and Khlong Marui Faults (RF & KMF), respectively, between 32 and 23 Ma of the Andaman Sea (Curry, 2005).	37
Figure 2.15 Tectonic map of SE Asia showing major fault systems and the relative movement of the SE Asian crustal blocks in response to India-Asia collision (modified from Poolachan, 1989, Charusiri et al., 2002) (Notes: SMF = Sumatra Fault; SGF = Sagaing Fault; RNF = Ranong Fault; KMF = Khlong Marui Fault; TPF = Three Pagoda Fault; MPF = Mae Ping Fault; SCB = South China Block; STB = Shan Thai Block; LCB = Lamgpang Chaingrai Block; NTB = Nakhon Thai Block; WBB = West Burma Block and ICB = Indo Chian Block (Charusiri et al., 2007).	38

Figure 2.16	Map of Peninsular Thailand and nearby regions showing major active faults : Ranong Fault (RF) and Khlong Marui Fault(KMF) and epicenter distribution (A). (modified after Department of Mineral Resources, 2007). Noted that the study area is located as blue box in (B). The study area with epicentral distribution and RF is shown in (C).	39
Figure 2.17	Map of Thailand showing major active faults and quaternary age dating results along the major active faults (Charusiri et al., 1998). The study area covers along the fault line No.11.	40
Figure 2.18	Index map of Thailand showing major active faults (Department of Mineral Resources, 2006). Noted that the study area is show as red box.	45
Figure 2.19	Major active RNF and its segments in the northern part: Prachuab Khiri Khan (A) and the southern part: Ranong province (B), as identified by Department of Mineral Resources (2007).	49
Figure 2.20	Major active faults and their segments in Prachuab Khiri Khan province, as Identified by Pananon et al. (2009).	50
Figure 3.1	SRTM DEM index map of the world (A) showing location and the data Sheet 56-10 that cover the study area (http://strm.csi.cgiar.org).	54
Figure 3.2	Arial photograph type-orthograph which was used in this research, (http://www4.oginfo.com).	54
Figure 3.3	Map of the study area showing contrasting output constructed using (a) Contour line (b) DEM from contour line resolution 2 m. (c) SRTM DEM.	55

Figure 3.4	Airborne geophysics map of Prachuab Khiri Khan province. (a) Total magnetic field map. (b) Total count of radioactive intensity map (c) Ternary colour map (d) lineament map interpreted using airborne geophysics (modified from DMR, 1989). Note that the NNW-SSE lineaments show in (d) is almost in the same trend as those found in figure.3.5.....	57
Figure 3.5	Enhanced Landsat 5 TM map with the false colour composite data of bands 4:5:7 (red: green: blue) showing the physiographic features of Prachuab – Khiri Khan area, south central Thailand.	60
Figure 3.6	Enhanced Landsat 5 TM map with the false colour composite data of band 4:5:7 (red: green: blue) showing the physiographic feature of Chumphon and Ranong areas, southern Thailand. Good example is a sharp lineament which is Sawi segment.....	61
Figure 3.7	Enhanced Landsat 5 TM map with the false colour composite data of band 6/3:2:4/5 (red: green: blue) showing the physiographic features of Prachuab Khiri Khan area. Note that identification of Cenozoic basins (show herein as yellow-colour) can be seen easily after the enhancement process.	62
Figure 3.8	Shaded relief image from DEM data showing prominent structures and fracture in study area.	63
Figure 3.9	Map of the study and regional areas showing orientations and distribution of lineaments. Noted that the NW-SE trending lineament near Prachuab Khirikhan is quite prominent.....	64
Figure 3.10	Lineament maps after enhancement in the DEM format showing (a) the north-south trend with 158 lineaments, (b) the east-west trend with 60 lineaments, (c) the northeast-southwest trend with 294 lineaments and (d) the northwest-southeast trend with 158 lineaments.	65

	PAGE	
Figure 3.11	Map showing Cenozoic deposits (yellow) after combined data of enhanced Landsat5TM and DEM data. Noted that the Cenozoic basins in the Ranong Province are mainly from DMR (2007).....	66
Figure 3.12	Assemblage of landforms associated with active tectonic strike – slip faulting (modified after Keller and Pinter, 1996).	70
Figure 3.13	Active fault segments of the northern part of the Ranong fault in Prachuab- Khiri Khan area based on result of remote sensing interpretation and geomorphology. (Yellow color = Cenozoic deposit and grey colour = hard rocks).	78
Figure 3.14	Active fault segments of the southern part of the Ranong fault in Chumphon and Ranong area base on result of remote sensing interpretation and geomorphology. (Yellow color = Cenozoic deposit and grey colour = hard rocks). Noted that the Cenozoic basins in the Ranong Province area mainly from DMR (2007).....	79
Figure 3.15	(a) 2m contour interval DEM image and (b) topographic map showing orientation and evidence of Thap Sakae segment.....	80
Figure 3.15 (Cont.)	Enlarged image data (Fig. 3.16a) of Thap Sakae fault segment shown as color orthographic image (c) and sketch image (d) showing fault orientation and two series of trigular facets.	81
Figure 3.16	(a) 2m contour interval DEM image and (b) topographic map showing the orientation and evidence of Khao Mun segment of the northern part of RNF. Note that a series of offset streams, trigular facets and linear valley.....	82
Figure 3.16 (Cont.)	Enlarged image data (Fig.3.16a) of Khoa Mun segment showing (c) colour-ortho photographic image and (d) topographic map with showing offset streams (OS) with the left lateral displacement.	83
Figure 3.17	Landsat and (a) 2m contour interval DEM image (b) showing the orientation of the Bangsaphan segment in the northern part of RNF.	84

Figure 3.17	Enlarged of Bangsaphan segment (Fig.3.18b) appear as aerial	
(Cont.)	photographic image (c) and DEM data (d) showing offset stream, a	
	series of trigular facets ,linear valley and linear ridge.....	85
Figure 3.17	Aerial photographic image (e) and topographic map (f) with	
(Cont.)	interpreted series of triangular facet at Khao Samianma.	86
Figure 3.18	Landsat image (a) and 2m contour interval DEM image (b)	
	showing orientation of the Nong Ya Plong segment in the northern	
	part of RNF.	87
Figure 3.18	Active fault evidence of Nong Ya Plong fault segment (enlarged	
(Cont.)	from figure 3.18 b) (c) DEM data and (d) topographic map showing	
	a series of offset stream, parallel ridge, pressure ridge and linear	
	ridge, suggesting the sinistral sense of movement.....	88
Figure 3.18	(e) DEM 2m interval and (f) topographic map with interpreted	
(Cont.)	beheaded stream (BH) and offset streams as well as a series of	
	triangular facets (h). Noted that the electric power line was	
	constructed following the Nong Ya Plong segment.	89
Figure 3.18	The 3D image data of the Nong Ya Plong segment (g) with this	
(Cont.)	study interpretation (h) showing a series of trigular facets in Khoa	
	Nakkarat area.	90
Figure 3.19	Landsat image (a) and 2m contour interval DEM image (b)showing	
	Khao Khirilom segment in the central of RNF.....	91
Figure 3.19	Enlarged DEM image (c) from northern part of the Khao khirilom	
(Cont.)	segment (figure 3.19 b) showing offset streams (OS) with the left	
	lateral displacement, linear valley in 3D colour-orthographic image	
	(d).....	92
Figure 3.19	Active fault evidence enlarged of Khao Khirilom fault segment	
(Cont.)	(figure 3.19c) from colour-ortho photographic image (e) showing	
	offset streams (OS) with the left lateral displacement interpreted in	
	this study (f).....	93

Figure 3.20	Landsat map (a) and 2m contour interval DEM (b) showing the orientation and active fault evidence of Khao Deang Noi fault segment from such as a series of trigular facets and linear valley...	94
Figure 3.21	Enhanced Landsat map (a) showing Bangsaphan Noi fault segment and 2m contour interval DEM image (b) showing offset streams (OS) with the left lateral displacement.....	95
Figure 3.22	Landsat map (a) and 2m contour interval DEM image (b) showing Khao Kwang segment of RNF.	96
Figure 3.22 (Cont.)	Active fault evidence along Khao Kwang segment enlarged from figure 3.23b shown as DEM image (c) and topographic map (d) showing a series of offset stream, linear valley ,pressure ridge and trigular facets.	97
Figure 3.23	Topographic map (a) and 2m contour interval DEM image (b) showing the orientation of the Tha Sae segment.....	98
Figure 3.23 (Cont.)	Active fault evidence along the Tha Sae segment enlarged from figure 3.23b) from DEM image with 2m contour interval (c) and topographic map with the interpreted result (d)showing parallel ridge, linear valley and trigular facets, at Ban Hin Khe in Khlong Lakhla river valley.....	99
Figure 3.24	Enhanced Landsat TM5 image (a) and 2m contour interval DEM image (b) showing the orientation of Khlong Nam Khoa segment of RNF.	100
Figure 3.24 (Cont.)	Active fault evidence along the Khlong Nam Khoa segment (enlarged figure 3.24b) from Dem image data with 2m interval contour (c) and topographic map (d) showing offset streams, parallel ridges, linear valley and a series of trigular facets (d). Note that there is a prominent linear valley in the north of the segment that runs in the NW-SE direction.....	101

	PAGE
Figure 3.24 Active fault evidence of Khlong Nam Khoa segment (enhanced (Cont.) from figure 3.24d) showing a series of trigular facets in Khoa Plai Khlong Hin Phao.	102
Figure 3.25 Active fault evidence of Pak Jun fault segment from 2m interval contour DEM image (a) and topographic map (b) showing offset streams, linear valley, linear ridge and series of trigular facet.....	103
Figure 3.25 Active fault evidence of Pak Jun segment enlarged from figure (Cont.) 3.25b shown as DEM image (c) showing offset streams (OS) with the left lateral displacement and (d) showing a series of trigular facets in Khao Hin Song.	104
Figure 3.26 Active fault evidence of Tha Mai Lai segment (a) DEM interval contour 2m and (b) topographic map (b) showing, linear valley and trigular facet.....	105
Figure 3.26 Active fault evidence of Tha Mai Lai segment enlarged from figure (Cont.) 3.26d shown as 3D colour-orthographic map (g) showing a series of trigular facets in Khoa Phae Ma.....	106
Figure 3.27 Topographic map (a) and 2m contour interval DEM image (b) showing the oreintation of Sawi segment at the middle part of RNF.	107
Figure 3.27 Active fault evidence of Sawi segment (enlarged from figure 3.27b) (Cont.) shown as DEM image(c) and topographic map (d) showing parallel ridges, linear valley, a series of trigular facets and offset streams...	108
Figure 3.27 3D colour-orthographic map of Sawi fault segment (enlarged figure (Cont.) 3.27b) showing a set of trigular facets and parallel ridges near Ban Nong Tum Soa.	109
Figure 3.28 Landsat image (a) and 2m contour interval DEM image (b) showing the NE-SW trending of Nong Ki segment which is almost parallel to the Sawi segment.	110

Figure 3.28	Active fault evidence of Nong Ki segment (enlarged figure 3.28b)	
(Cont.)	displayed as DEM image (c) and topographic map (d) showing parallel ridges, linear valley, a series of trigular facets and offset streams. These fault segment are considered to control the Cenozoic basin formation.	111
Figure 3.28	Active fault evidence of Nong Ki segment (enlarged figure 3.28c)	
(Cont.)	from ortho-color photographic image (e) and topographic map (f) showing a series of offset streams.....	112
Figure 3.28	Active fault evidence of Nong Ki segment (enlarged figure 3.29c)	
(Cont.)	appear in 3D colour-orthographic image (g) and interpreted in this study (h) showing a series of trigular facets in Khoa Choan Chan...	113
Figure 3.29	Active fault evidence of La-un segment from DEM image (a) and topographic map (b) showing linear valley, trigular facets and offset streams. Note there is a fault segment parallel to Khlong Rawi, which pass La-un district.....	114
Figure 3.29	Active fault evidence along La-un fault segment (enlarged figure 3.29b) showing 2 series of trigular facets facing at opposite Directions. These two segments which control the development of Khlong Rawi linear valley.....	115
Figure 3.30	Topographic maps (a) showing two subparallel subsegment of Ranong segment of the southern part of RNF and 2m contour interval DEM image (b).....	116
Figure 3.30	3D colour-orthographic interpretation image (c) along the Ranong segment (enlarged figure 3.31b) showing trigular facets at Khoa Phra Narai.	117
Figure 3.30	Active fault evidence of Ranong segment (enlarged figure 3.30b)	
(Cont.)	shown as DEM image (e) and interpreted in this study (f) showing parallel ridges, a set of trigular facets and offset streams.	118

Figure 3.31	Topographic maps (a) and 2m contour interval DEM image (b) showing the orientation of Kraburi segment of the southern part of RNF.	119
Figure 3.32	Topographic maps (a) and 2m contour interval DEM image (b) showing the orientation of Pato segment of the southern part of RNF.	120
Figure 3.32 (Cont.)	3D colour-orthographic interpretation image (c) along the Pato segment (enlarged figure 3.32b) showing trigular facets at Khoa Nom Soa area, in the Pathui Patho district.	121
Figure 3.33	Topographic maps (a) and 2m contour interval DEM image (b) showing the orientation of Pathui segment in the southern part of RNF and prominent linear valley (g).	122
Figure 3.33 (Cont.)	Active fault evidence of Pathui segment (enlarged figure 3.33b) from DEM with 2 m contour interval image (c) and enlarge colour-orthographic map from black box in figure 3.33c (d) showing offset streams with left lateral movement.	123
Figure 3.33 (Cont.)	Active fault evidence along the Pathui segment (enlarged figure 3.34b) shown as 3D colour-orthographic map (e) and interpreted in this study (f) showing a series of trigular facets in Khoa Hin Cheang area.....	124
Figure 4.1	Topographic map of Prachuap Khiri Khan area showing earthquake epicenters on 27 th -28 th September 2006 and 8 October 2006 measured by seismological network stations.....	127
Figure 4.2	Flow chart showing the methodology used in macroseismic investigation.	129
Figure 4.3	Map showing investigated points in Prachuab Khiri Khan province. (Data from Department of Mineral Resources, 2006).	131

Figure 4.4	Earthquake intensity map showing the result from macroseismic investigation (Thipyopass et al., 2009) for the earthquake taking places on 27 th September 2006 (base on the Modified Mercalli Intensity scale (MMI)). (a) From this study (b) Data modified from Department of mineral resource.....	136
Figure 4.5	Earthquake intensity map showing the result from macroseismic investigation (Thipyopass et al., 2009) for the earthquake taking places on 28 th September 2006 (base on the Modified Mercalli Intensity scale (MMI)). (a) From this study (b) Data modified from Department of mineral resource.	137
Figure 4.6	Earthquake intensity map showing the result from macroseismic investigation (Thipyopass et al., 2009) for the earthquake taking places on 8 th October 2006 (base on the Modified Mercalli Intensity scale (MMI)).	138
Figure 4.7	Distribution of Cenozoic deposits in Prachuab Khiri Khan area (DMR, 2005) after superimposing with intensity contour of earthquake event on 27 th October 2006 (based on the Modified Mercalli Intensity scale (MMI)).	139
Figure 4.8	Distribution of Cenozoic deposits in Prachuab Khiri Khan area (DMR, 2005) after superimposing with intensity contour of earthquake event on 28 th October 2006 (base on the Modified Mercalli Intensity scale (MMI)).	140
Figure 4.9	Distribution of Cenozoic deposits in Prachuab Khiri Khan area (DMR, 2005) after superimposing with intensity contour of earthquake event on 8 th October 2006 (base on the Modified Mercalli Intensity scale (MMI)).	141

Figure 4.10	Map of Pracuab Khiri khan and nearby regions showing the epicenter of earthquake event on 27 th -28 th September and 8 th October 2006 and fault segments of the RNF.....	142
Figure 4.11	Map of Pracuab Khiri khan and nearby region showing the epicenter of earthquake event on 27 th -28 th September and 8 th October 2006 and interpreted lineament from magnetic data (Kenting Earth Sciences International LTD,1989).....	143
Figure 4.12	Map of Pracuab Khiri khan and the nearby region indicating the epicenter of earthquake event on 27 th -28 th September and 8 th October 2006 comparing with basin geometry of Gulf of Thailand (DMR,2006).....	144
Figure 4.13	Map shows the epicenter of the earthquake, lineaments of active faults, and oil fields in the gulf of Thailand.(DMF, 2009)	145
Figure 4.14	Schematic diagram of a focal mechanism showing three types of faulting and their stereo-plot results.....	147
Figure 4.15	Direction of P-first motions (Vince Cronin, 2004).	148
Figure 4.16	The angle (from vertical) that the ray leaves the earthquake is the take-off angle (http://www.learninggeoscience.net/free/00071).....	148
Figure 4.17	The map of seismic station which recorded seismograph of the earthquake event on 8 th October 2006.....	150
Figure 4.18	Recorded seismic waveforms from seismic station which recorded the earthquake event on October 8, 2006.....	154
Figure 4.19	First motion of the enlarged P waves from seismic station which recorded the earthquake event on October 8, 2006.....	155
Figure 4.20	Plots of P-wave first motion data in the stereonet with data from this study.....	156
Figure 4.21	The preliminary results of probable focal mechanism identified from this study.....	157

Figure 4.22	Plots of P-wave first motion data in the stereonet with data from Pananon (2009).....	158
Figure 4.23	The results of probable focal mechanism identified from this study and data from Pananon, 2009.....	159
Figure 5.1	Map showing seismic survey lines used in study area (pink Block)..	162
Figure 5.2	Map showing seismic line survey in Andaman sea (black line). Note that several epicenters detected at both ends of the seismic lines AN1, AN2, AN3 and AN4.....	163
Figure 5.3	(a) seismic cross-section of seismic line survey AN1. (b) Map showing seismic line survey AN1 and distribution of epicentral in Andaman sea. (c) Map showing seismic line survey AN1 and structure map of Andaman sea. Note that there are 2 interesting faults F1(Ranong fault) and F2 (Eastern Andaman Fault) which produce intermediate EQ (3.4-4.0 ML).....	165
Figure 5.4	Model of sediment formation layers of seismic line survey AN1. (b) Map showing seismic line survey AN1 and distribution of epicentral (c) Map showing seismic line survey AN1 and structure map of Andaman sea. (d) Map showing seismic line survey AN1 and Physiographic map of the Mergui Basin, Andaman Sea.	166
Figure 5.5	Seismic cross section of seismic line survey AN1 at Ranong ridge showing normal movement at RNF into seafloor. Note that F1, F2 and F3 reach the seafloor.	167
Figure 5.6	Seismic cross section of the enlarged seismic line survey AN1 at Ronong ridge showing F1, F2 and F3 reach to the seafloor (point A, B, C and D).	168
Figure 5.7	Seismic cross section of the enlarged seismic line survey AN1 at Ronong ridge showing dip angle of F1, F2 and F3 at point A, B, C, D and E).	168

Figure 5.8	(a) seismic cross-section of seismic line survey AN2. (b) Map showing seismic line survey AN2 and distribution of epicentral in Andaman sea. (c) Map showing seismic line survey AN2 and structure map of Andaman sea.	170
Figure 5.9	(a) Model of sediment formation layers of seismic line survey AN2. (b) Map showing seismic line survey AN2 and distribution of epicentral c) Map showing seismic line survey AN2 and structure map of Andaman sea. (d) Map showing seismic line survey AN2 and Physiographic map of the Mergui Basin, Andaman Sea.	171
Figure 5.10	Seismic cross section of seismic line survey AN2 at Ranong ridge showing normal movement at RNF into seafloor. Note that F1 reach the seafloor.	172
Figure 5.11	Seismic cross section of the enlarged seismic line survey AN2 at Ronong ridge showing F1 reach to the seafloor (point A).	173
Figure 5.12	Seismic cross section of seismic line survey AN2 near Ranong ridge showing normal movement of F2 cut Thalang formation.	174
Figure 5.13	(a) seismic cross-section of seismic line survey AN3. (b) Map showing seismic line survey AN3 and distribution of epicentral in Andaman sea. (c) Map showing seismic line survey AN3 and structure map of Andaman sea.	176
Figure 5.14	(a) Model of sediment formation layers of seismic line survey AN3. (b) Map showing seismic line survey AN3 and distribution of epicentral c) Map showing seismic line survey AN3 and structure map of Andaman sea. (d) Map showing seismic line survey AN3 and Physiographic map of the Mergui Basin, Andaman Sea.	177
Figure 5.15	Seismic cross section of line survey AN3 at Ranong ridge showing normal movement at RNF into seafloor. Note that the F1 reaches the seafloor.	178
Figure 5.16	Seismic cross section of the enlarged seismic line survey AN3 at Ranong ridge showing the F1 reaches to the seafloor (point A).....	179

Figure 5.17	Seismic cross section of line survey AN3 near Ranong ridge showing normal movement F2 cut basement.	180
Figure 5.18	(a) seismic cross-section of seismic line survey AN3. (b) Map showing seismic line survey AN3 and distribution of epicentral in Andaman sea. (c) Map showing seismic line survey AN3 and structure map of Andaman sea	182
Figure 5.19	(a) Model of sediment formation layers of seismic line survey AN3. (b) Map showing seismic line survey AN3 and distribution of epicentral .(c) Map showing seismic line survey AN3 and structure map of Andaman sea.(d) Map showing seismic line survey AN3 and Physiographic map of the Mergui Basin, Andaman Sea.	183
Figure 5.20	Seismic cross section of line survey AN4 at Ranong ridge showing normal movement at F1 cut Thalang formation and almost reach to seafloor.	184
Figure 5.21	Seismic cross section of the enlarged line survey AN4 at Ranong ridge showing F1 almost reaching to the seafloor (point A).....	185
Figure 5.22	Seismic cross section of seismic line survey AN4 near Ranong ridge showing normal movement at F2 cutting to the seafloor.....	186
Figure 5.23	Seismic cross section of the enlarged line survey AN4 near Ranong ridge showing F2 reaching to the seafloor (point A).....	187
Figure 5.24	Map showing the direction of Ranong F1 and Ranong F2 from seismic interpretation in Andaman area. (The legend and explanation are as the same as these of Figure 5.14).....	191
Figure 5.25	Map showing Ranong F1 Ranong F2 and Ranong F3 which are related to epicenters of earthquake with magnitudes about <3-5 ML and correspond with the structure map of Andaman (DMR,1996).....	192
Figure 5.26	Structural model from strike slip fault (Cunningham and Mann, 2007).	193

Figure 5.27	Map showing direction of movement of the RNF in the Andaman Sea and the main physiographic features of the Mergui Basin, Andaman Sea (Mahatanachai, 1996). Note that the RNF fault from structure map of Andaman by DMR (1996).....	194
Figure 5.28	Map showing the computed average regional slip rates at the points which the Andaman seafloor was cut by Ranong F1 and Ranong F2. Note that the Ranong F1 from AN1 and AN2 is extrapolated based on the interpretation made by staff of DMF.....	195
Figure 5.29	Map showing the computed average regional slip rate at the points which top of basement was cut by Ranong F1 and Ranong F2.....	196
Figure 5.30	Map showing seismic line survey of this study (black line) and the extrapolated RNF in Gulf of Thailand.....	197
Figure 5.31	seismic cross-section of seismic line survey G1. (b) Map showing seismic line survey G1, distribution of epicentral in Gulf of Thailand, lineament of Ranong fault zone and basin in gulf of Thailand.	199
Figure 5.32	(a) Model of seismic line survey G1 showing direction of movement. (b) Map showing seismic line survey G1, distribution of epicentral in Gulf of Thailand, lineament of Ranong fault zone and basin in gulf of Thailand.	200
Figure 5.33	Seismic cross section of the enlarged seismic line G1 at Point A (Fig 5.31a) showing negative flower structure (F2, red line), suggesting the normal movement and F1 is the normal fault controlling the edge of Prachuab basin and cutting through into seafloor, layer.	201
Figure 5.34	Seismic cross section of the enlarged seismic line survey G1 at the edge of prachuab basin in the west side showing normal movement of F1 reach to the seafloor.	202

Figure 5.35	Seismic cross section of the enlarged seismic line survey G1 at Point A (Figure 5.31a) showing and reverse senses of normal movement in the flower structure reach to the seafloor.	203
Figure 5.36	Seismic cross section of the enlarged seismic line survey G1 at Point B (Figure 5.31a) showing the normal movement of F3 that reaches to the seafloor.	204
Figure 5.37	Seismic cross section of the enlarged seismic line survey G1 Point C (Figure 5.31a) showing the normal movement of F4 reach to the seafloor.....	205
Figure 5.38	Map showing faults in seismic survey G1 and extended of lineament of RNF. Point A founded negative flower structure and it is location of epicenter of earthquake on 27 September 2006.....	206
Figure 5.39	(a) seismic cross-section of seismic line survey G2. (b) Map showing seismic line survey G2, distribution of epicentral in Gulf of Thailand, lineament of Ranong fault zone and basin in gulf of Thailand.	208
Figure 5.40	(a) Model of seismic line survey G2 showing direction of movement. (b) Map showing seismic line survey G2, distribution of epicentral in Gulf of Thailand, lineament of Ranong fault zone and basin in gulf of Thailand. ...	209
Figure 5.41	Seismic section of the enlarged line G2 at Point C (Fig 5.39a) showing the negative flower structure (F2, red line), suggesting the normal fault cutting through sediments into seafloor.....	210
Figure 5.42	Seismic section of the enlarged line survey G2 at Point C (Figure 5.39a) showing normal movement in the negative flower structure with one fault reaching to the seafloor.	211
Figure 5.43	Seismic section of the enlarged line survey G2 at Point D and E (Figure 5.39a) showing normal movement of F3 and F4 (green line and pink line) reach to the seafloor.	212

Figure 5.44	Map showing faults in seismic survey G2 and extended of lineament of RNF. Point C founded negative flower structure and Point D is location of epicenter of earthquake on 27 September 2006.....	213
Figure 5.45	seismic cross-section of seismic line survey G3. (b) Map showing seismic line survey G3, distribution of epicentral in Gulf of Thailand, lineament of Ranong fault zone and basin in gulf of Thailand.	215
Figure 5.46	(a) Model of seismic line survey G3 showing direction of movement. (b) Map showing seismic line survey G3, distribution of epicentral in Gulf of Thailand, lineament of Ranong fault zone and basin in gulf of Thailand.	216
Figure 5.47	Seismic section of the enlarged line G3 at Point F (Figure 3.45a) showing normal movement along the F1 and F2 (blue line and green line) which cut through sediment into seafloor.....	217
Figure 5.48	Map showing structure model of seismic line G3, epicenters of earthquake and extending lineament of Ranong Fault zone.	218
Figure 5.49	Map showing the newly proposed edge of basin (blue line) based on seismic interpretation in this study.....	221
Figure 5.50	Map showing fault segments of the RNF (Nong Ya Plong segment, Bangsaphan segment and Bangsaphan Noi segment) that are extrapolated to the gulf of Thailand.....	222
Figure 5.51	Map showing regional (or long-term) slip rate of the extrapolate lines of the RNF in Gulf of Thailand in this study.....	223
Figure 6.1	Map showing relationship between hot spring locations in Ranong province and active fault traces (data from Department of Mineral Resources, 2004).....	225
Figure 6.2	Detailed topographic map of Ban Neon Kruat, Bangsaphan district of Prachuab Khirikhan area, showing movement along the RNF segment with its left lateral sense of movement.	227

Figure 6.3	Plots of gas radon concentrations and distance in radon survey lines at Ban Neon Kruat area (Artyotha, 2007), showing the peak of random content immediately at the fault line (in Fig. 6.2)...	227
Figure 6.4	Locations of paleoseismic trenches along the Nong Ya Plong and the Khao Khrilom segments of the RNF	229
Figure 6.5	Topographic map of Si Yeak Ban Krut area showing the location of Nong Ya Plong segment and morphotectonic features offset streams, series of trigular facets, linear ridge and linear valley. Note that the red box represent the areas of photographs taken from field investigation.....	231
Figure 6.6	(a) color ortho- image showing location of Siyeak Ban Krut trench. (b) The artificial pool (Si Yeak Ban Krut Trench) at Ban Si Yeak Ban Krut , Thap Sakae district, Prachuab Khirikhan province. Note that the offer stream in (a) shows the left lateral sense of movement along the Nong Ya Plong segment of the RNF.	232
Figure 6.7	The artificial pool near Nakkarat mountain which cross cut by Nong Ya Plong segment and showing subduced trigular facets..	233
Figure 6.8	Quarry of weathered granite at Ban Nong Chun, Thap Sakae district, Prachuab Khirikhan showing the orientation of quartz vein in $20^{\circ}/68^{\circ}$, almost following the regional trend of the fault.	233
Figure 6.9	A panoramic view showing a series of trigular farcets along the Nong Yaplong segment of the RNF Ban Hin Thung, Thap Sakae district, Prachuab Khirikhan province. (Looking west). Note that the electric power line is behind this mountain	234
Figure 6.10	Topographic map of Ban neon Kruat area showing the location of Khoa Khrilom segment, offset stream and trigular facet. Note that the red box represent the areas of photographs taken from field investigation.....	235

	PAGE
Figure 6.11 Color -Orthographic image showing offset stream and location of Neon Kruat trench	236
Figure 6.12 A close-up view (Fig. 6.12) part of Khlong Loi river show offset stream at Ban Neon Kruat area.(Looking west)	236
Figure 6.13 Color -Orthographic image showing offset stream evidence of Khoa Khirilom area and location of Neon Kruat trench (yellow colour).....	237
Figure 6.14 Topo graphy view of Neon kruat area around Neon Kruat trenching.Note that the electric power line are located following the Kho Khirilom Segment.	237
Figure 6.15 View of paleoseismic trench section on the north-east wall, Si Teak Ban Krut, Thap Sakae. Prachuab Khirikhan	240
Figure 6.16 Trench log section of the north-west wall, Si Yeak Ban Krut, Thap Sakae, Prachuab Khirikhan showing 5 major straigraphic units, major faults orientation and sample location for dating.	241
Figure 6.17 Trench log section at the northeast wall of Si Yeak Ban Krut showing structure of normal fault and clearly offset of Unit B which displacement approximately 56 cm.	242
Figure 6.18 Trench log section at the northeast wall of Si Yeak Ban Krut showing The orientation of normal fault and clearly offset of quartz vein which was separated approximately 15-25 cm.	242
Figure 6.19 View of paleoseismic trench section (A-A'-A''-A''') on the north-east wall, Neon Kruat, Bangsaphan. Prachuab Khirikhan showing Cenozoic sediment	245
Figure 7.1 Applied thermoluminescence method for dating by showing relationship between amount electron in electron trap and time, (modified after Won-in, 2002).....	249

Figure 7.2	Simplified diagram of lattice structure and ionic crystal showing (a) ideal model of completely lattice (b) negative-ion vacancy occurred in ionic crystal cause negative-ion interstitial and substitution impurity center (c) electron capture by electron trap in negative ion vacancy and (d) electron escape from electron trap by heat or Light,(http://www.rses.anu.edu.au).	252
Figure 7.3	Simplified model showing energy states in Thermoluminescence processes,(Aitken, 1985).	252
Figure 7.4	Chart of calculate annual dose and equivalent dose for TL and OSL dating, (modified after Takashima and Honda, 1989).	255
Figure 7.5	Summary of neutron activation analysis (NAA) procedures with sample preparation and annual dose determination.	255
Figure 7.6	TL equipment component.(a) Thermoluminescence Detector (TLD) at geology department, faculty of science, chulalongkorn university (b) Main equipment that comprises the “reader”, which is necessary for measuring the paleodose, irradiating the sample, heating the sample, and deriving a “growth” curve,(Lian, 2007).....	258
Figure 7.7	Result of example diagram after run with Thermoluminescence Detector for calculated equivalent dose (a) growth curve (b) grow curve.....	259
Figure 7.8	(a)Schematic charts of regeneration technique (Takashima et. al., 1989). Note that several portions are used for measurement of the TL intensity; N is natural sample; I ₀ is residual intensity from sample; H is 350°C heated sample; and γ is known dosage that irradiated sample (b) Thermoluminescence remaining after bleaching by exposes to sunlight for various time, (Aitken, 1985)....	260
Figure 7.9	Trench log stratigraphy showing faults oriental and TL ages of sedimentary layers on northeast wall, SiYeak Ban Krut Trench.	266

Figure 7.10	Trench log stratigraphy showing faults oriental and TL ages of sedimentary layers on northeast wall, Ban Neon Kruat Trench.....	267
Figure 8.1	Regional distribution of tin -bearing granite belts in South-East asia (Garson et al., 1975)..	269
Figure 8.2	Map showing active fault segments of the RNF on main land and faults segments in the sea..	272
Figure 8.3	(a) Map showing the S46 ⁰ W- trending Bangsaphan Noi extending to site of epicentral event on 8 October. (b) Beach balls of the same earthquake event on 8 October 2006..	273
Figure 8.4	2m contour interval DEM showing (a) Bangsaphan segment from DMR (2007) and (b) Khoa Khirilom segment and Bangsaphan segment, Khoa Samianma, Bangsaphan district, Prachub Khilikhan province.	276
Figure 8.5	(a)2m contour interval DEM showing (b) Na Khoa segment from DMR (2007) and (b) Khlong Nam Khoa segment from this study, Ranong -Kraburi district, Ranong province.	277
Figure 8.6	(a)2m contour interval DEM showing (b) Ranong segment from DMR (2007) and (b) Ranong segment from this study, Ranong province	278
Figure 8.7	Map showing active fault segments, their length and estimated maximum credible earthquakes of paleomagnitudes of The Ranong Fault Zone in Prachuab Khirikhan province.	280
Figure 8.8	Map showing active fault segments, their length and estimated maximum credible earthquakes of paleomagnitudes of Ranong Fault Zone in Chumphon and Ranong province. (Cenozoic deposits data from DMR,	281

	PAGE
Figure 8.9 Trench log section at the northeast wall of Ban Neon Kruat, Prachuab Khirikhan showing principle stratigraphy and TL of this study, TL ages of Department of Mineral Resource (2007) and Carbon-14 dating of Department of Mineral Resource (2007).	283
Figure 8.10 (a) Map showing slip rate on main land. (b) map showing regional slip rate -long term in Andaman Area. (c) Map showing regional slip rate - long term in gulf of Thailand.	288
Figure 8.11 Simplified model of the RNF based on this study.	289
Figure 8.12 Geometry and anatomy of strike-slip fault showing releasing bend and restraining bend, which help in explaining evolution of Sinistral movement of the Ranong Fault Zone (Crowell, 1974). ...	290

CHAPTER I

INTRODUCTION

1.1 Background

Earthquake is a natural phenomenon which is unable to control and unpredictable when it will be occurring. As known, earthquakes can cause large damages in many parts of the world including Thailand such as the earthquake that happen on 12 May 2008 ,7.9 Mw at western China in Sichuan Province killed more than 8000 people.

There are two main theories on earthquakes, viz. the elastic rebound model and the dilation source theory. The elastic rebound model states that at a geological fault between two moving plates, stress occurs and deforms the rocks. This theory supports the idea that earthquake mechanisms are directly related to tectonic especially, active tectonic. Large faults within the Earth's crust result from the action of tectonic forces. Energy release associated with rapid movement on active faults is the cause of most earthquakes.

The earthquake is the result of a sudden release of energy in the Earth's crust that creates seismic waves. The seismicity or seismic activity of an area refers to the frequency, types and sizes of earthquakes experienced over a period of times. As commonly known, the earthquakes can occur along subduction zones on the ring of fire (Figure 1.1).The occurrence of earthquakes in Southeast Asia coincides with tectonic boundaries. Subduction zones are clearly marked by earthquakes of different depths (Figure 1.2)

Although Thailand has not been considered to be a seismically active country due to the disappearance of the large earthquakes in the past. Thailand was not absolutely to be save from earthquakes because annals and stone inscriptions indicated that large earthquakes have been recorded many times in several parts of Thailand, magnitude earthquakes. Thailand Meteorology Department shows that the distribution of most epicenters place in boundary of Thai-Burma, Thai-Loas, Burma-China and

Andaman sea, those reveal that earthquake concern with major faults in this region

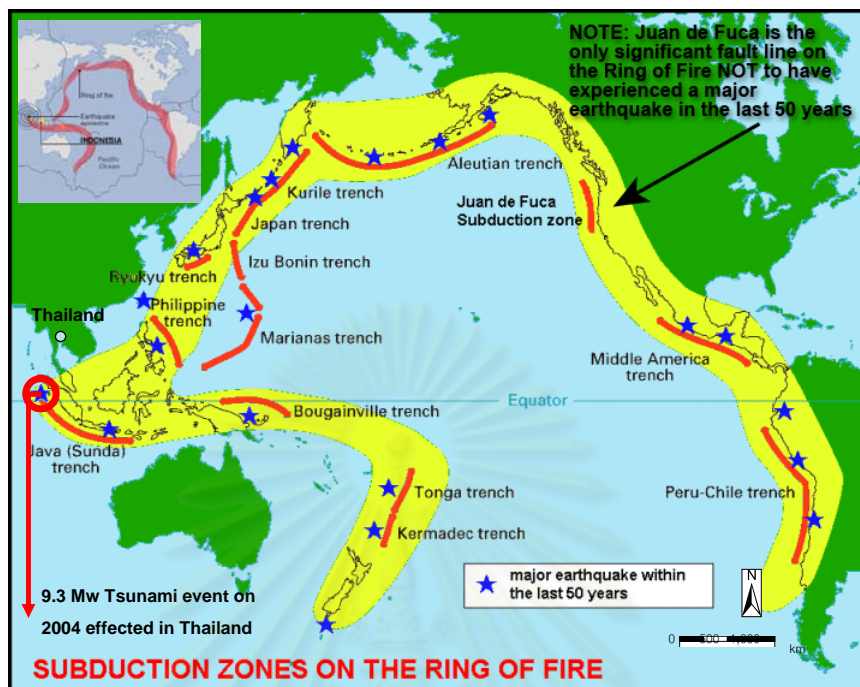


Figure 1.1 Map of Pacific ocean region showing subduction zones on the ring of fire. (Modified after <http://standeyo.com/Reports/041222.EQ.warning/050827.Deyo.EQs.html>).

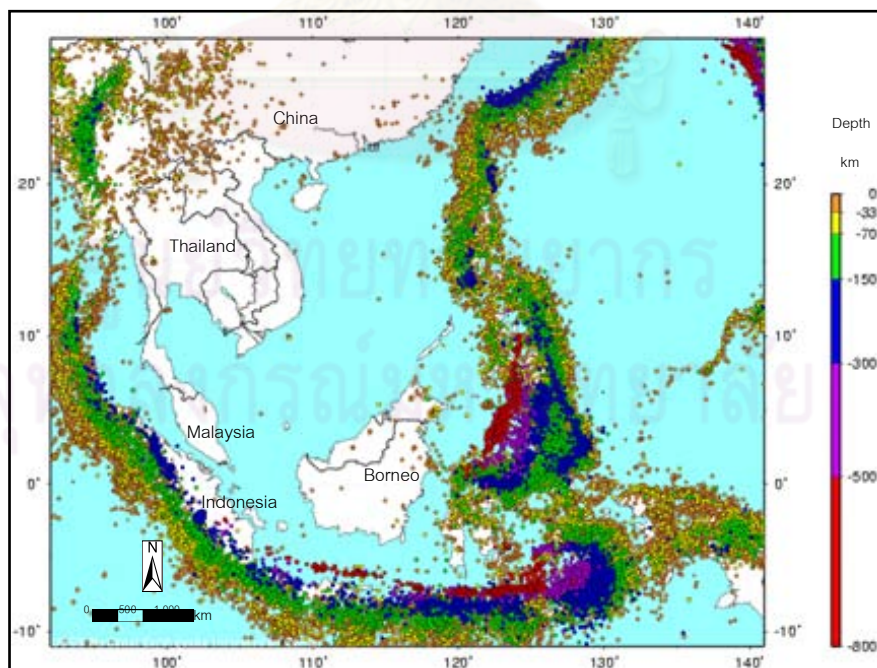


Figure 1.2 Map of regional South East Asia showing earthquakes of different depths

(0-800 km (http://umfacts.um.edu.my/gallery/index.php?menu=research_details&cid=110).

(Figure 1.3).

There are two major faults in the Southern Thailand, including the Ranong (RF in this study) and the Khlong Marui fault. RF was first classified as the potentially active fault by Hinthong (1997) based on preliminary TL dating results. Earlier than that, Chauviroj(1991) only mentioned that the Ranong Fault and KMF were the major northeast-southwest trending faults but he did not defined clearly if or not they are active. Recently, the Sumatra earthquake on 26 December 2004 with magnitude 9.3 Mw effected around the Andaman Sea and nearby regions. Then, In gulf of Thailand on 27-28 September, 8 October 2006 earthquake 4.8-5.0 Mb power quakes make people alarmingly and home are damaged. This result lead to investigate the Ranong Fault Zone. In this study, special emphasis is placed on the application of remote-sensing, seismic data, TL - datings to delineate the fault and to classify fault segments.

1.2 Objective

The main purposes of this research are to characterize of the Ranong Fault (RF) Zone, in detail and to clarify the paleoearthquakes along the studied fault zone. The main knowledge and techniques used for paleoearthquake investigation in this study include remote-sensing interpretation in addition to investigations on morphotectonic analyses, seismic anaysis, and luminescence-dating results. The prime goal of the output is to help design of building or large construction and planning in order of preventing damages from earthquakes in the future. Consequently, the results of this research are fulfils the following four fold:

1. Identifying characteristics of the Ranong Fault Zone
2. Delineating active fault traces of the Ranong Fault Zones
3. Determining the ages of the Ranong Fault Zone movement; and
4. Estimating the paleoearthquake magnitudes and slip-rates of these fault movement.

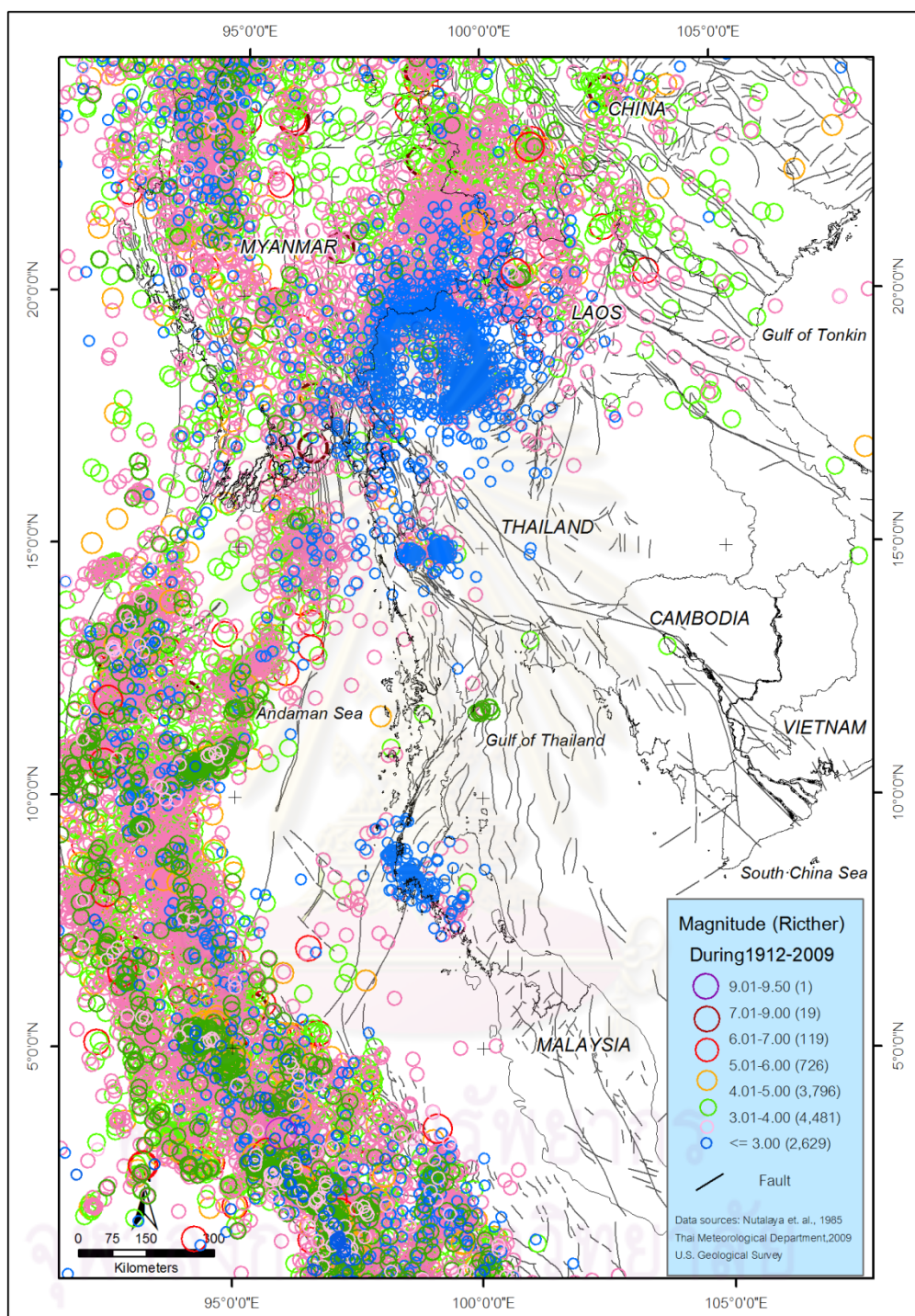


Figure 1.3 Map of mainland Southeast Asia showing epicentral distribution from 1912-2009. (Data from Nutalaya et al., 1985; Thai Meteorological Department, 2009 and http://neic.usgs.gov/neis/epic/epic_global.html).

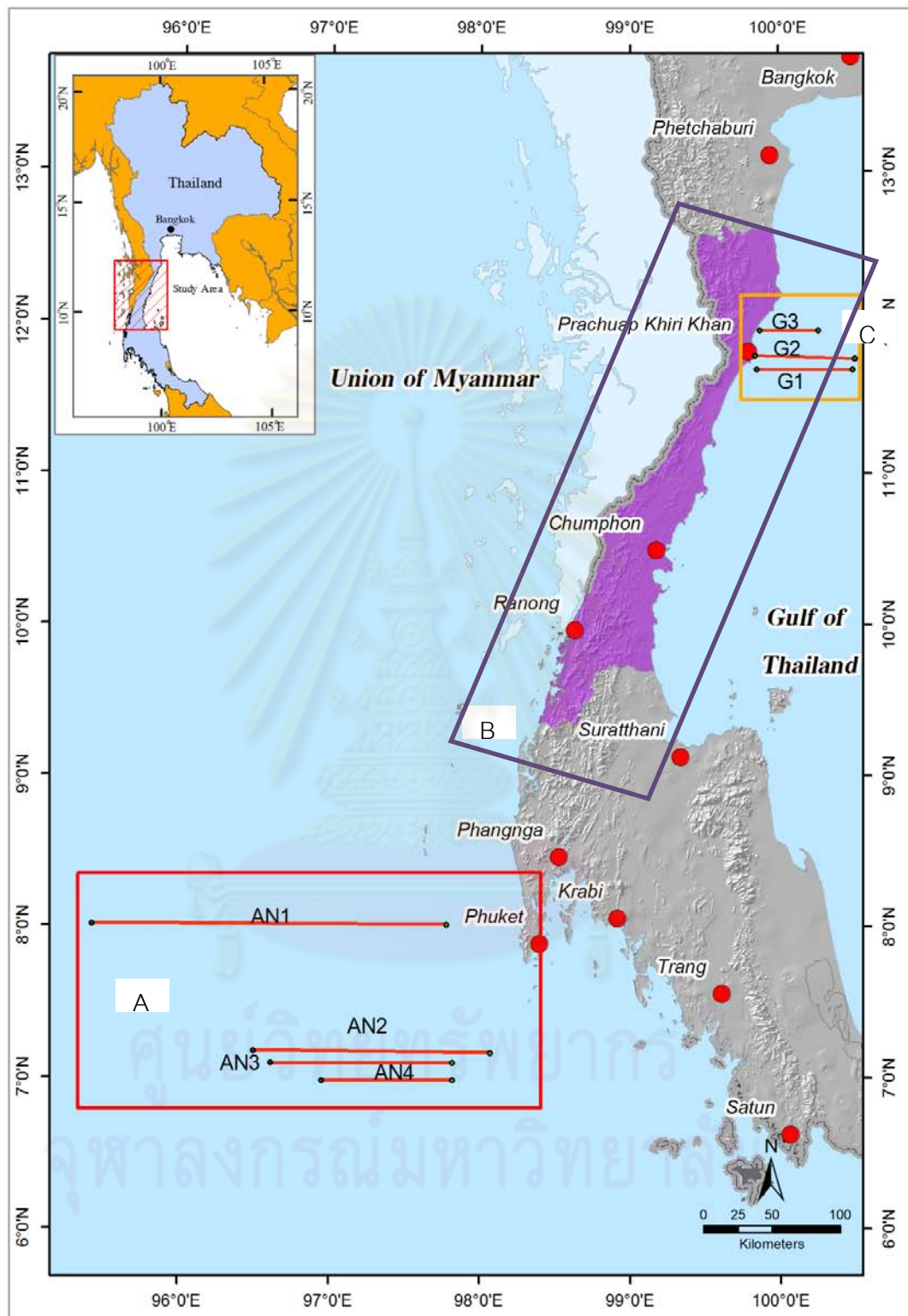


Figure 1.4 Map of Part of southern Thailand showing the location of study area (A) Study area in Andaman Sea (red square), (B) Study area in main land (purple area), and (C) Study area in Gulf of Thailand (orange square).

1.3 Study area

The study area selected for the present research is located within the RF zone. Study areas consist 3 parts (Figure 1.4)

1. Mainland area bounded by latitudes $9^{\circ}0'0''\text{N}$ to $13^{\circ}0'0''\text{N}$ and longitudes $98^{\circ}0'0''\text{E}$ to $10^{\circ}0'0''\text{E}$ to cover most Prachuab Khirikhan, Chumphon and Ranong.

2. Gulf of Thailand area bounded by latitudes $11^{\circ}0'0''\text{N}$ to $12^{\circ}45'0''\text{N}$ and longitudes $99^{\circ}30'0''\text{E}$ to $100^{\circ}0'0''\text{E}$

3. Andaman area bounded by latitudes $7^{\circ}0'0''\text{N}$ to $8^{\circ}0'0''\text{N}$ and longitudes $95^{\circ}30'0''\text{E}$ to $98^{\circ}15'0''\text{E}$

The total study area is about $90,000\text{ km}^2$ and the study area is approximately 250-900 km far from Bangkok, the capital city of Thailand.

1.4 Methodology

The study methodology is divided into 7 steps (Figure 1.5) including:

1.4.1 To collect the report data

The first step involves collecting data for supporting further steps of study. This data is composed of reviewing literatures for pervious work, selecting topographic maps, analyzing geological maps, screening earthquake epicenters, acquiring remotesensing images and aerial photograph, and other related technical and nontechnical documents.

1.4.2 To interpret remote-sensing images

The second step involves remote-sensing interpretation. Commencement of the stage is to study the small scale using digitally enhanced satellite imageries and interpretation on a large scale with aerial photographs. Basic data for the interpretation is enhanced Landsat 5, SRTM DEM, DEM from detail survey resolution 2 m. and Airborne geophisic data for determining lineaments, their attitudes and orientations as well as delineating Cenozoic basins. Interpretation was also performed along with the aerial photographs (1:50,000) and color-orthographs (1:4,000) for geomorphology evidence of active tectonic landforms.

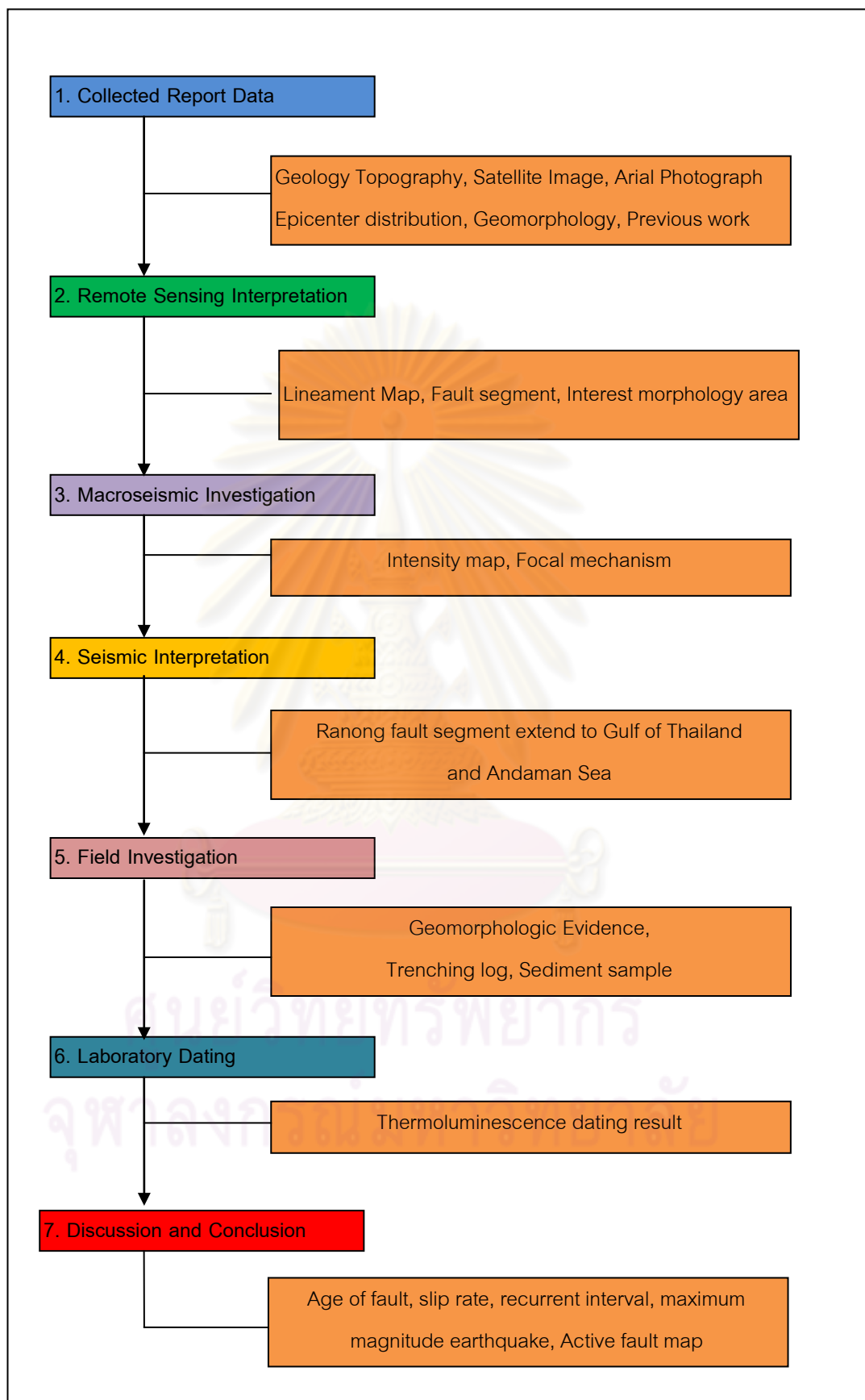


Figure 1.5 Flow chart showing the methodology used in this study.

1.4.3 To investigate Macroseismic

In this step, used three earthquake events that took place in Prachaub Khiri Khan area of south Central Thailand on September 27 and 28 and October 8, 2006. These earthquake events were redetermined and investigated for the construction of the iso-seismal maps. The purpose of this study is to evaluate the probable source of the epicenters which happened in that area and evaluate the most probable location of the epicenters. Including, study about focal mechanical earthquake of these earthquake events.

1.4.4 To interpret seismic

Interpreted seismic data from 7 surveys are located within the RF zone were provided by Department of Mineral Fuel (DMF). Data separated in 2 parts, 4 surveys in Andaman sea area and 3 surveys in gulf of Thailand area for determining lineaments, their attitudes and orientations.

1.4.5 To do field investigation

This step starts with compilation of previous field data related to fault evidence. Sub sequentially identifying sequences of faulting in the selected area with exploratory trenching. Then geological data and sample collection.

1.4.6 To do age-dating

Dating is the fifth step with the main purpose of collecting samples for dating by Thermoluminescence (TL) method. The dating method follows that of Takashima and Watanabe (1994), commencing at collecting suitable geological samples related to active faults, treatment of quartz-enriched samples for dating, and analyzing both of equivalent and annual doses of quartz concentrates.

1.4.7 To discuss the result and make a conclusions

The last step includes integration of all the available investigated and surveyed results for discussion on fault characteristic, geomorphic features and paleoearthquake magnitudes, recurrence intervals, slip rates, and neotectonic evolution of the RF.

1.5 Research output

The clearly-defined segments of RF and the active fault map at a scale 1:50,000 form the main output of this study.

1.6 A Brief Guide to the Thesis

This thesis provides an emphasis on tectonic geomorphology and geochronology of the Ranong Fault Zone in succession of Chapters as following :

Chapter I mentions about an introduction, objective, study area, methodology and research output to the study project research.

Chapter II notifies the regional setting, neotectonic evolution of tectonic plate in southern Thailand. Active faults studies in Thailand and some investigations on The RF zone area are included.

Chapter III is the part of detailed remote-sensing investigation including the process of enhancement and interpretation of Landsat 5 images, DEM data and aerial photographs to determine the tectonic landform evidence.

Chapter IV is the part of detailed macroseismic investigation including the process of Interview results were converted to intensity scale to make intensity maps and seismic data from earthquake events in Prachaub Khiri Khan area of south Central Thailand on October 8, 2006 can be evaluated to focal mechanical of these event.

Chapter V interpreted seismic survey in Andaman area and Gulf of Thailand area to determine characteristic of RF in these area.

Chapter VI provides the previous investigation related to active fault evidence. Tectonic geomorphology was applied to indicate the active-fault evidences and show the sedimentary layers in trenches with collecting sample location.

Chapter VII mentions the uses of the dated sedimentary ages to approximate the fault ages.

Chapter VIII compares the dating and the summary of earlier investigations to discuss on characteristics of the RF and neotectonic evolution.

Chapter IX is the conclusion deduced from the result of study project research.

CHAPTER II

GEOLOGICAL TECTONIC SETTINGS

2.1 Regional Setting

Regional setting of the South East Asia has been accepted as the result of the collision of the Indian against Eurasian plates and the UrAsian plate seems to stop its movement, while the Indian plate was still moved northwards. This gave rise to the Southeast Asian region moved with clockwise rotation. (Figure 2.1) These mentioned by many researchers (Tapponier et al., 1982,1986; Daly et al., 1991; Dewey et al., 1989; Rangin et al., 1990; Lee and Lawver, 1995; Hall, 1996; Packham, 1996; and Mathews et. al., 1997) Cenozoic basins were formed in response to this tectonic process (Figure 2.2). South-East Asia consists of the continent assembles, which called "Sundaland Block" and link up with the China Block in the north and with the subduction zone of Indian plate in the west and connected with the Chinese Sea in the east.

2.1.1 Structural and geology setting of mainland

The Southern Thailand or the Thai Peninsula has the large-scale fold structures with the major fold axis in the north-south trend and some areas have been related to the magmatism and metamorphism. This scenario may have created the mountainous area, which extends from Phetchaburi in the north to Satun in the south. In the Western Thailand and the upper Southern Thailand, there exist several important fault traces collectively called " Three Pagoda Fault " (Figure 2.3) lying in the northwest - southeast trend. In the middle of southern Thailand, the structural geology is dominated by the Ranong fault (RF) and the lower almost parallel fault, the Khlong Marui fault (KMF), both of them lying in the NNE-SSW trend. Their fault types are the strike-slip fault zones with ductile deformation in Tertiary (Figure 2.4). According to Watkinson et al. (2008), These faults are bounded and overprinted by brittle strands, which are part of a population of parallel and branching sinistral faults, and they are localised into the two similar, but discrete fault zones.

Geology of the region is depicted as a geologic map with scale 1:1,000,000 and modified geologic map scale 1:50,000 of Prachuab Khiri Khan, Chumphon, Ranong and

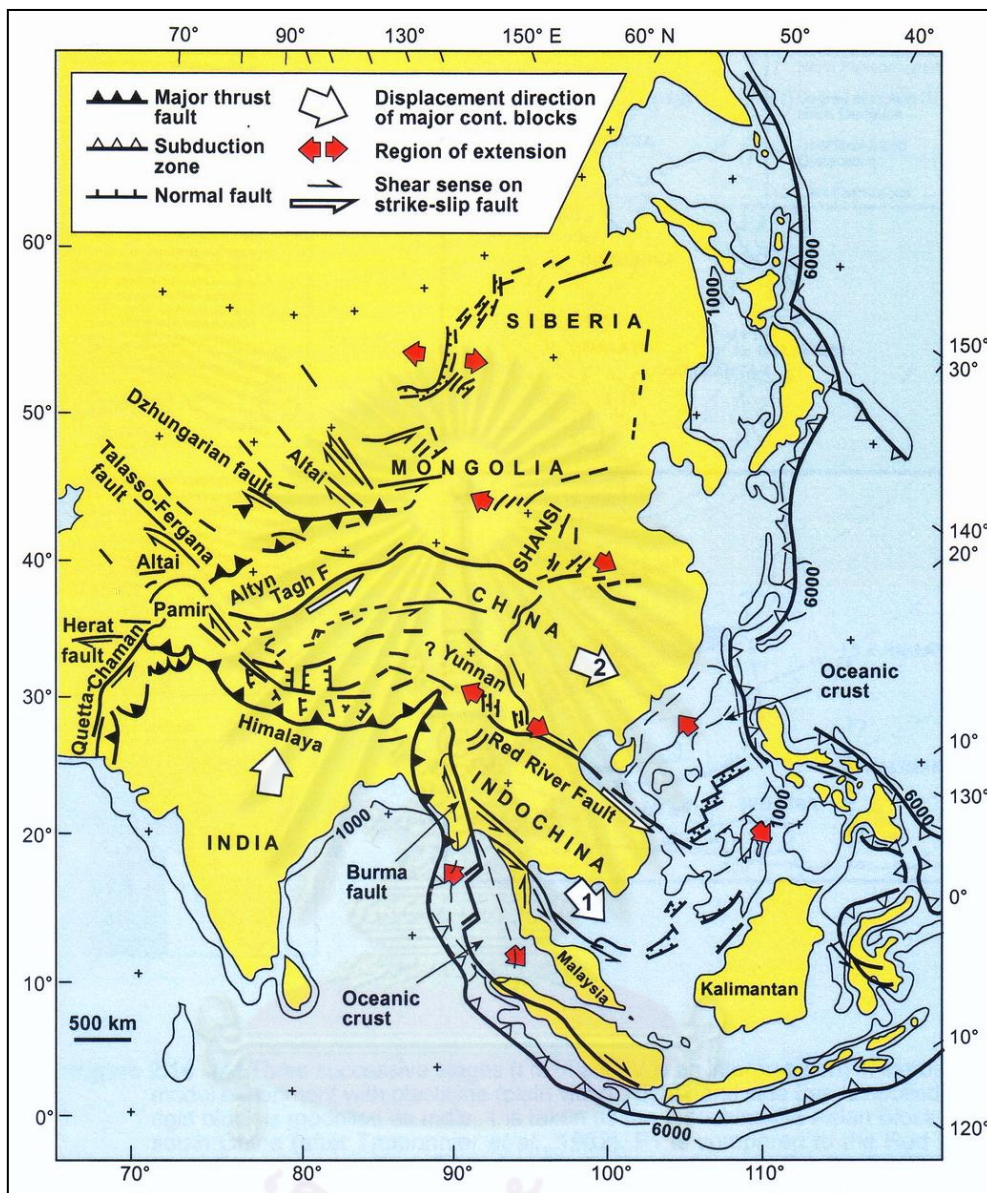


Figure 2.1 Tectonic map of central- east Asia illustrating 'extrusion' model and its relationship with Cenozoic structures in the region. Numbers in white arrows indicate the relative order in which certain continental blocks were extruded toward the southeast (after Tapponnier et al., 1982).

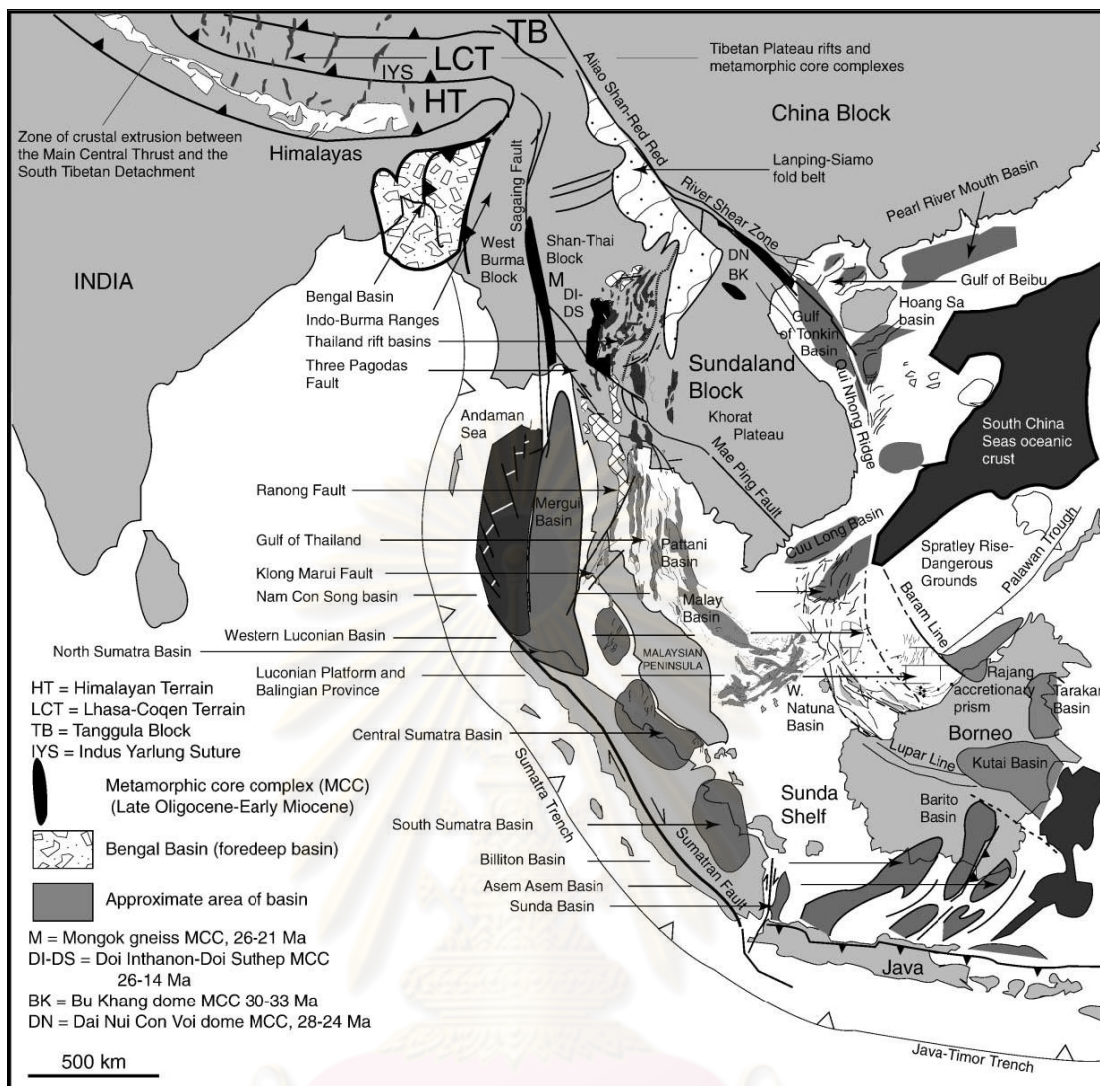


Figure 2.2 Regional setting of South and East Asia showing major tectonic sedimentary basins and main structural features (Morey,2002).

ศูนย์วิทยทรัพยากร
 จุฬาลงกรณ์มหาวิทยาลัย

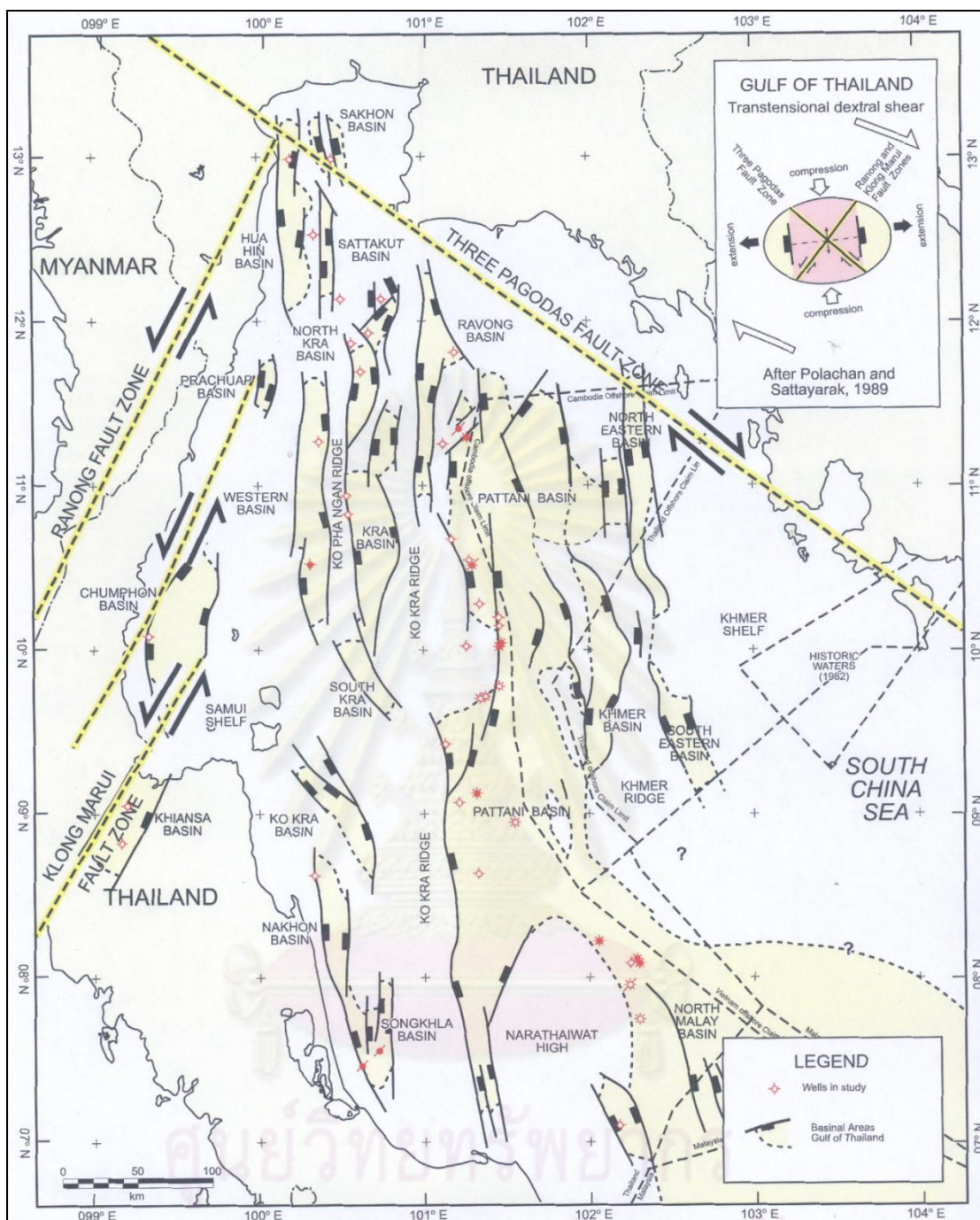


Figure 2.3 Structure map showing distribution and orientation of major Cenozoic basins in the Gulf of Thailand. Inserted map shows dextral transtensional shear movement (Polachan and Sattayarak, 1989).

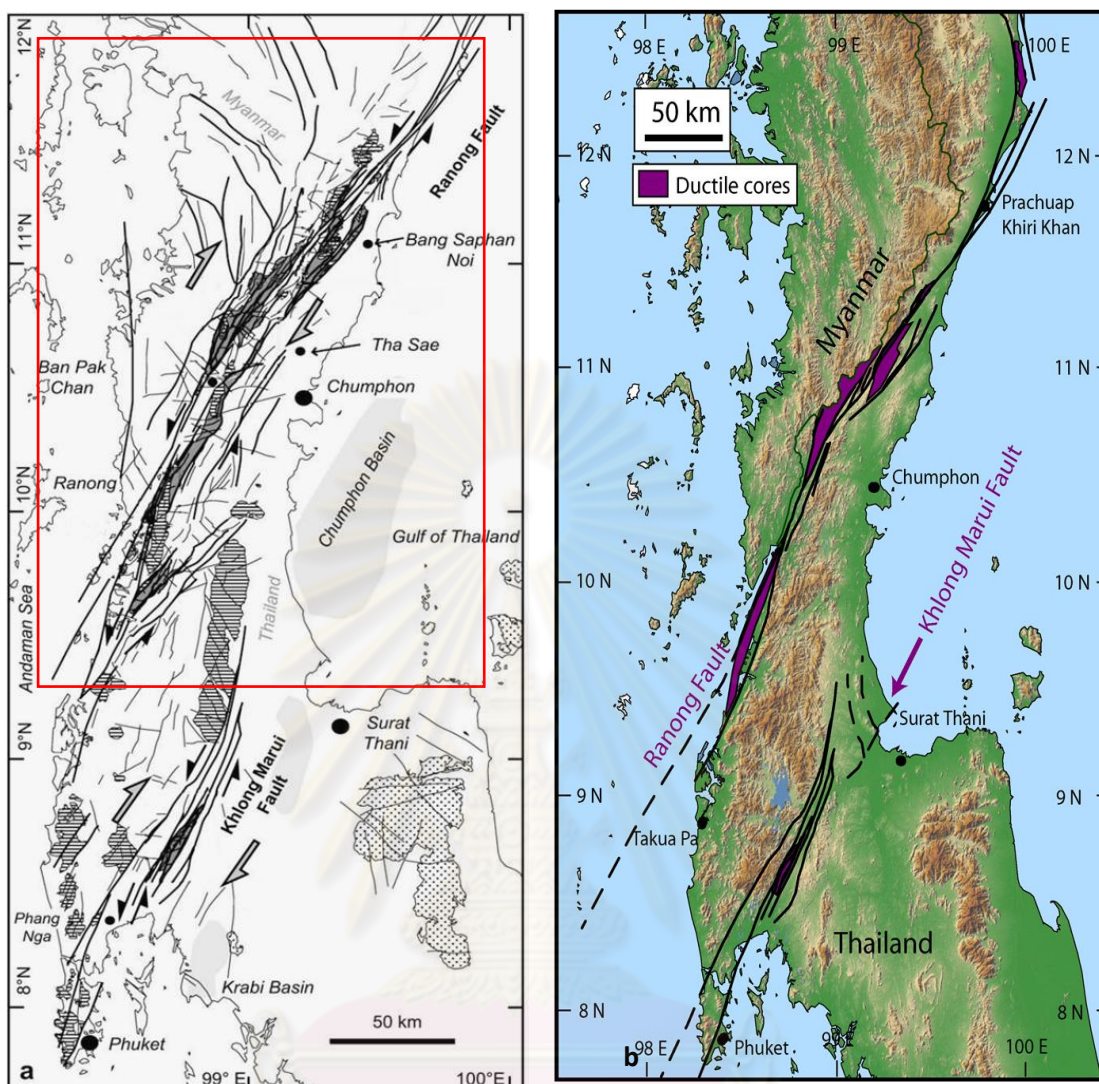


Figure 2.4 Detail of the Thai Peninsula showing the Ranong (RF) and Khlong Marui fault zones. (a) Fault map, dark grey, metamorphic cores and granite outlines stippled-west of the RF-belonging to the Western Province and dotted-east of the RF-belonging to the Eastern Province (modified from Department of Mineral Resources, 1982) and basin outlines from Intawong (2006). (b) SRTM (Shuttle Radar Topography Mission) digital elevation model of the same area (Watkinson et al., 2008). Also shown in (b) is the location of the study area (in box).

it consists of several units of metasediments and sedimentary rocks and few granite intrusive rocks. Ages of the rocks vary from Carboniferous to Quaternary. Almost all rock units were cut by the RF. In this thesis, the geology is explained only along and within the RF (Figure 2.5 and Figure 2.6), based on the work of DMR (2005).

2.1.1.1 Kaeng Krachan Group (CP) covers most of the study area and composed of gray pebble mudstone, shale, siltstone and sandstone of Carboniferous – Permian period behaves continuously sequence and overlain by the limestone of Ratchaburi group, which in Permian period. This group is subdivided based on textures, structures, and occurrences, into five formations from bottom upward, namely Laem Mai Pai, Ko He, Khao Phra and Khao Chao formation, respectively.

I Laem Mai Pai Formation(CP_{lp}) composed mudstone, grey, well laminated, interlaminated with sandstone, dull white, fine grained, subrounded, low sphericity; intercalated with felspathic sandstone, white, medium grained, subrounded, low sphericity at the middle part.

II Ko He Formation(CP_{kh}) composed pebbly sandstone and pebbly mudstone, greenish grey, grey, fine to medium grained, dense and clasts are scattering, 2x3 mm. in average size of quartz, mudstone, sandstone, limestone and granite, subangular- to subrounded, low to moderately sphericity, poor sorted, exfoliation and gravel oriented near fault zone; quartzite, hornfels and meta-sandstone at granite contact.

III Khao Phra Formation(CP_{kp}) comprises mudstone, greenish grey, grey, well laminated; lenticular fine grained sandstone, intercalated with quartzitic sandstone, fine to medium grained, subrounded, moderately sphericity; and conglomerate lens near the upper part, thin to thick bedded, mudstone showing cleavage near fault zone.

IV Khao Chao Formation(CP_{kc}) comprises arkosic sandstone, white to light grey, good sorted, medium grained, thin bedded with *Posidonomiya* sp.

2.1.1.2 Ratchaburi Group (P) is sedimentary sequence which is dominated by thick-bedded to massive the Permian limestone, dolomitic limestone, dolomite, grey to dark grey, massive, locally chert nodules, interbedded with sandstone and shale with fusulinid.

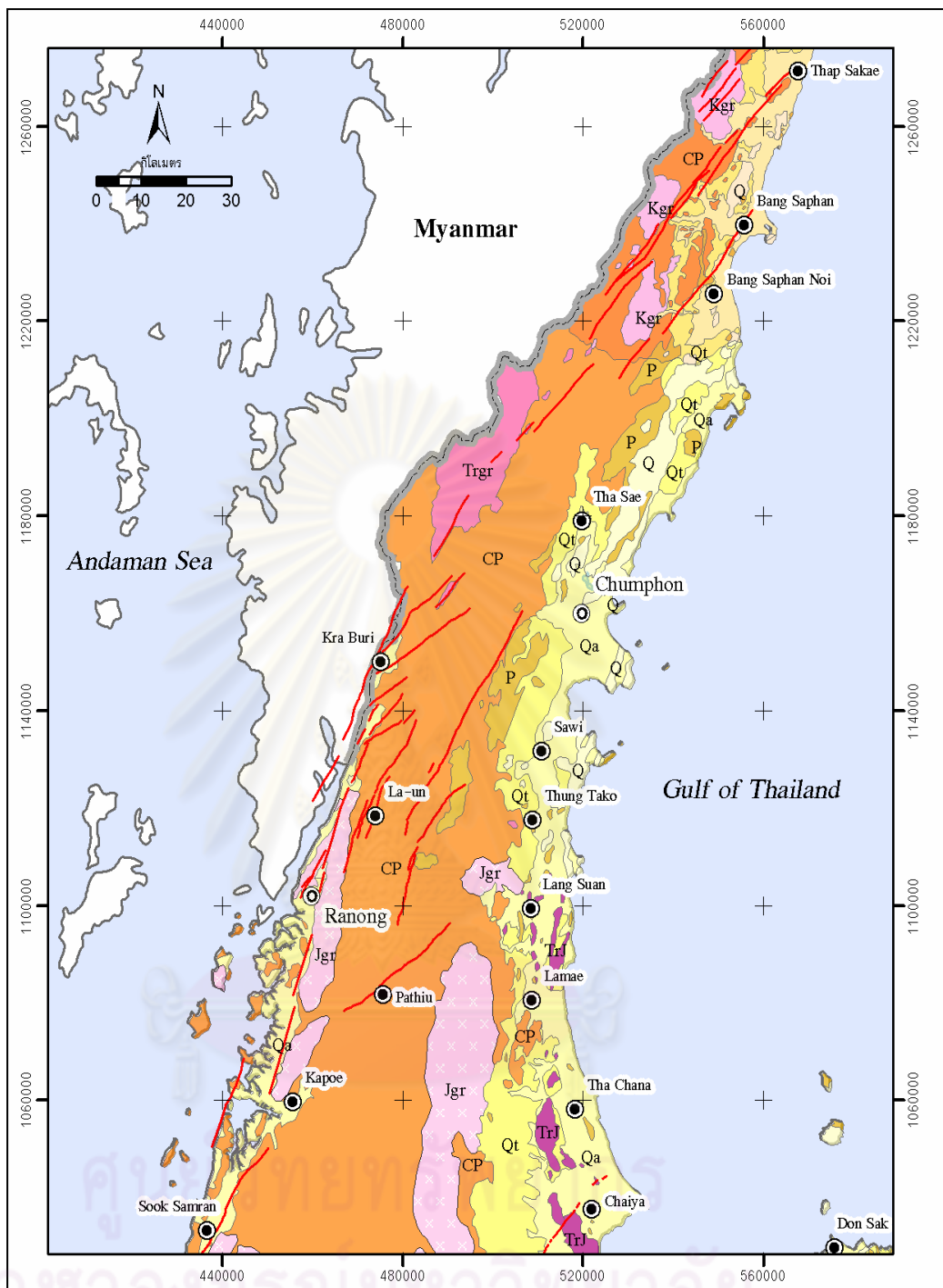


Figure 2.5 Geological map showing orientations and distribution of the Ranong Fault. (RF) Note that northern part of RN passes through Bangsaphan and Thup Sakae districts of Prachuab Khiri Khan province whereas the southern part passes through Ranong and Kraburi cities of Ranong province (Modified from Department of Mineral Resources, 2007).

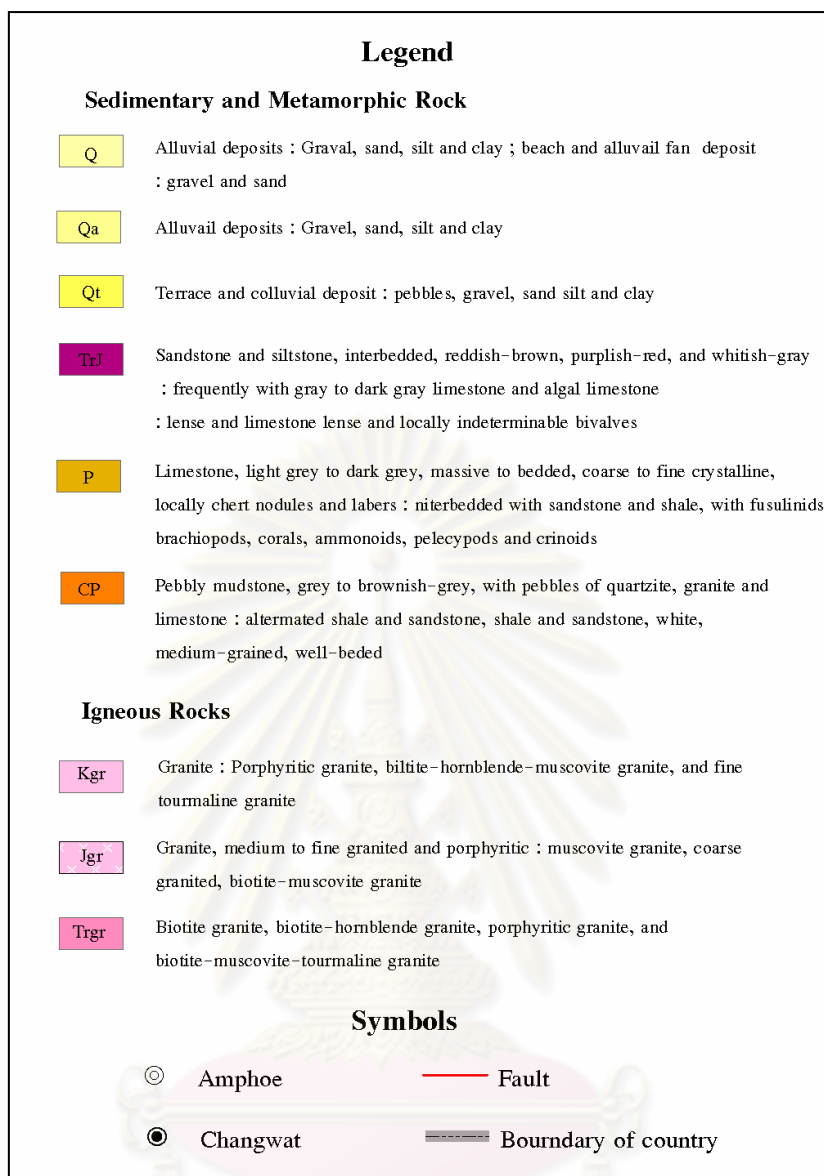


Figure 2.6 Explanation of geological map along the RF (Modified from Department of Mineral Resources, 2007) showing in Figure 2.5.

2.1.1.3 Triassic-Jurassic Sedimentary Rocks is distributed along the shore line in the eastern side of the KMF. Rocks are marine siltstone interbedded sandstone and with limestone lenses in some area.

2.1.1.4 Triassic-Cretaceous Sedimentary Rocks expose around the eastern side of the KMF. The rocks are non-marine shale, siltstone, and sandstone from reddish-brown to red colors. In some area, cross beddings and ripple marks are discovered.

2.1.1.5 Cenozoic sediments are young and semi-consolidated deposits. It also includes the shoreline deposits. Shoreline sediment (Q) is composed of unconsolidated near-shore sediment, such as sand and fine sand with shell leavings and corals.

I Alluvial sediment (Qa) is deposited from active rivers covering some coast and tidal flat plain. Terrace deposits consist of pebble, sand, clay, and mud.

II Colluvial sediment (Qt) is terrace deposits includes of gravel, sand, laterite and alluvial terrace this sediment often appear to follow the foothills and short hill.

2.1.1.6 Igneous Rocks are mainly granites of Triassic & Jurassic ages (Trgr & Jgr), distributed within the narrow area on the western part of the RF with the large sized massive (batholiths and plutons) intrusives. (Department of Mineral Resources, 2005). Granite is mainly characterized by large-sized sediment xenoliths and composed largely of feldspar, quartz, biotite and muscovite. In some small stocks, granites contain hornblende and magnetite. Most granites, particularly in the study area, are of Cretaceous age (Kgr).

2.1.2 Structural and geology setting of Andaman Sea

2.1.2.1 Structure

Within the study area, the physiography consists of ten major structural domains: East Andaman Fault Zone, Mergui Ridge, Western Mergui Basin, Eastern Mergui Basin, Central High, Ranong Ridge, Ranong Trough, Mergui Fault Zone, and Ranong- Klong Marui Fault Zone, Mergui-Malacca Shelf (Sunda Shelf) and Similan Basin (Figure 2.7, Figure 2.8). All basin suppose happen since early tertiary, especially sediment which deposited in Mergui basin beyond territorial Thai waters has the thickness more than 8,000 meter. Basement of the Mergui basin is granite, volcanic, and low grade metamorphic rock from late cretaceous to late Eocene period.

2.1.2.1.1 Mergui Ridge

Mergui Ridge is a longitudinal NE-SW trending, paleo-high structure, which separated the Andaman spreading center (Andaman Basin) in the west from the Mergui Basin in the east. The Ridge is approximately 70 km wide. The ridge is bounded to the west by NE-SW trending steeply westward dipping faults (East Andaman Fault Zone), and cut in the north by NW-SE Strike-slip faults (Mergui Fault Zone).

2.1.2.1.2 Mergui Shelf

Mergui Shelf consists of folded Paleozoic and Mesozoic rocks, overlying Precambrian granitoids and high-grade metamorphic rocks (Nakapadungrat and Putthapiban, 1992).

2.1.2.1.3 Mergui Basin

The Mergui Basin. (Polachan et. al., 1991) is a transtensional backarc basin that extends southward to the North Sumatra Basin. The Mergui Basin can be separated into three main sub-basin: the Western Mergui Sub-Basin, Eastern Mergui Sub-Basin and Ranong Trough (Polachan and Racey, 1994). The Central High separates the Western Mergui and Eastern Mergui sub-basins, and the Ranong Ridge separates the Eastern Mergui sub-basins and the Ranong Trough. Sedimentary thickness is estimated to be up to 10 km in the depocenter of the Western Mergui sub-basin (Polachan, 1988). Faults in Mergui basin can be divide into 2 type as follow;

(1) Strike-slip fault consists of 2 sub directions, one is NNW-SSE and another one is NNE-SSW.

(2) Normal fault consists of 2 main faults the major fault, N-S trending which controls opening of the Cenozoic basin and affect N-S trending half-graben basin pattern. The NNE-SSW fault is the conjugated fault of the N-S Mergui fault but almost quietly subsided along the fault plain. Other structures in Mergui basin are folds and can separate into 2 folds namely NW-SE and N-S trending with en-echelon characterize for former and rollovers characterize for later.

2.1.2.1.4 The Western Mergui Sub-Basin

The Western Mergui Sub-Basin is the N-S trending half-graben, which lies between the Mergui Ridge and Central High. The basin is bounded to the east by the steep westward dipping Mergui Fault Zone. Over 3,000 meters of sediment were drilled by the Trang and Mergui wells. Sediments in this sub-basin thicken eastwards.

2.1.2.1.5 The Eastern Mergui Basin

The Eastern Mergui Sub-Basin lies between the Central High to the west and the Mergui Shelf to the northeast or the Ranong Fault Zone to the southeast. The geological structures within this sub-basin comprise a series of westward tilting N-S trending half-grabens separated by a series of east-dipping N-S trending normal faults. Sediments in this basin thicken westwards and southwards.

2.1.2.1.6 The Central High

The Central High is a complex horst block extending along the Mergui Fault Zone, which is N-S trending in northern part of the Central area and bends into a SW trend in the Southern Area. This ridge is bounded to the east and west by easterly and westerly dipping normal faults, respectively. The Central High appeared to rise in Late Oligocene (Polachan et. al., 1991, and Beicip-franlap, 1996) and stop during Early Miocene time, which allowed mainly Early Miocene reefal and carbonate rocks in the Mergui Basin to be deposited on this ridge.

2.1.2.1.7 The Ranong Ridge

The Ranong Ridge is a westward tilting N -S trending basement high, bounded to the east by a steeply eastward-dipping N-S trending normal fault. This ridge has been offset left-laterally by the NE-SW trending Ranong Fault Zone. Sediments deposited on this ridge are generally thin and mainly of Plio-Pleistocene age.

2.1.2.1.8 The Ranong Trough

The Ranong Trough can be described as a deep, narrow half-graben NE-SW trending along the Ranong Fault Zone. The Ranong Trough lies between the Ranong Ridge and the Mergui-Malacca Shelf. Sediments thicken southward and westward toward the Ranong Fault Zone.

2.1.2.1.9 The Similan Basin

Similan Basin, half- graben which lied in north – south trending and link up to Ranong Basin at the north direction. The total length of the basin is estimate at about 50 km and average width of about 30 km with deeply west about 2 km.

2.1.2.1.10 The Andaman Basin

The Andaman basin was located between Nicobar Islands and Mergui Ridge, north-south trending that start from northern Sumatra Island in the south and terminate at Moetama bay in the north.

2.1.2.2 Stratigraphy of Mergui basin

From accumulate sedimentary environment can arrange the sediment from oldest to youngest into 9 formations(Pollachan,1989) (Figure 2.9) as follow;

2.1.2.2.1 Ranong Formation

The Ranong Formation is dominated by shallow marine sandstones which grade vertically and laterally fine upward into the Yala Formation. Data from fauna and flora studies suggest that the Ranong and Yala. Formations include Late Oligocene to Early Miocene sediment.

2.1.2.2.2 Yala Formation

The Yala Formation consists of outer shelf to bathyal shales and submarine fan sediments. The Yala Formation is a marine shale facies (benthic foraminifera and glauconitic shale), which is laterally related to the top of the Ranong Formation. Yala Formation that is Late Oligocene to Early Miocene.

2.1.2.2.3 Payang Formation

The Payang Formation contains mainly sandstone interbedded with shales.. The Payang Formation is Early Miocene age and overlain unconformably by the Surin Formation. Based on fossils found in the formation, this formation is suggested to be a shallow marine environment, which progressively deepens towards the top.

2.1.2.2.4 Tai Formation

The Tai Formation is a Lower Miocene carbonate rock lying on basement highs in the Central and upper Southern Area of the Mergui Basin. This formation is a reefal Limestone. Phangha. This formation corresponds to theregional unconformity at the top of Lowermost Miocene in the Mergui Basin. Paleontology suggests that the Tai Formation is an Early Miocene carbonate build up, which was deposited in a shallow marine environment.

2.1.2.2.5 Kantang Formation

The Kantang Formation is Lower Miocene age (based on Paleontology), consisting mainly of shales with minor sandstones. The Kantang Formation can be correlated to the Payang and Tai Formations, which are similar in age but different lithologies.

2.1.2.2.6 Surin Formation

The Surin Formation is equivalent to the Trang formation, which was deposited more regional than the Surin formation. The Surin Formation consists mainly of sandstones interbedded with shales and limestones of Middle Miocene age overlying the Payang Formation. Fossils of foraminifera, gastropod and shellfragments, contained within the Surin Formation suggests that the Surin Formation was deposited in a shallow marine environment during the Middle Miocene.

2.1.2.2.7 Trang Formation

The Trang Formation consists of shales overlying the Kantang Formation. The Trang Formation is present in most wells in the Mergui Basin. Abundant foraminifera contained in the Trang Formation suggest Middle Miocene age sediments deposited in lower bathyal, in the lower unit, and progressively shallowing to middle/upper bathyal in the upper unit.

2.1.2.2.8. Thalang Formation

The Thalang Formation is the Upper Miocene sediment and contains indicator foraminifera for Late Miocene age, which consists mainly of silty shales . Based on foraminifera, environment of deposition of the Thalang Formation is interpreted to be deep lower bathyal at the base and gradually changes into shallower in the upper part. In specific areas, depositional environment of this formation is recognized as basin floor deep water environment. Upward-coarsening sequences in the lower part and upward-fining in the upper part, initiated partly in the Mergui Basin indicates a progradational fan lobe with distal channel fill in a lower fan environment.

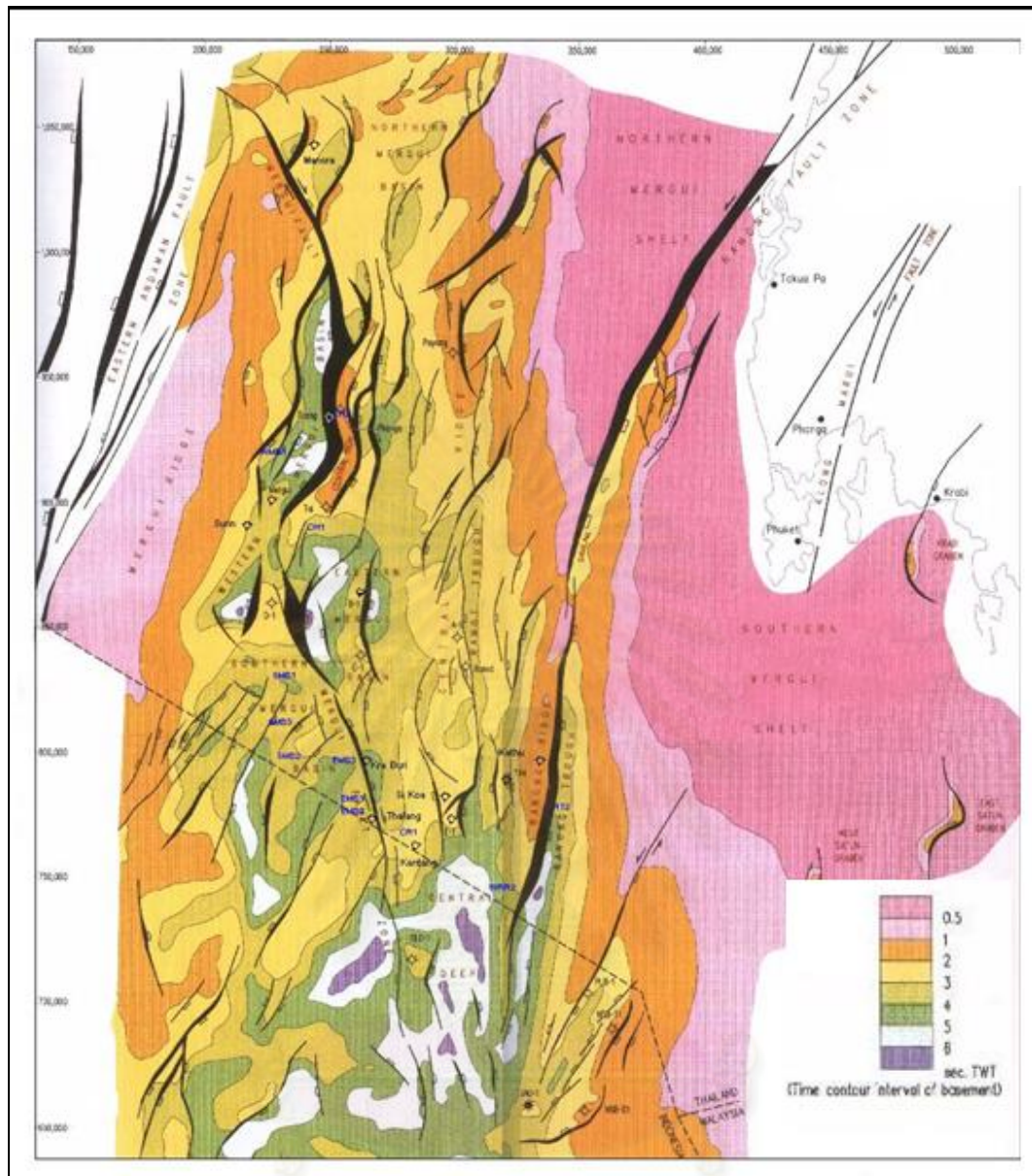


Figure 2.7 Structural geology map of Andaman Sea (after DMR., STS.
And BEICIP-FRANLAB, 1996)

คู่มือวิทยานิพนธ์
จุฬาลงกรณ์มหาวิทยาลัย

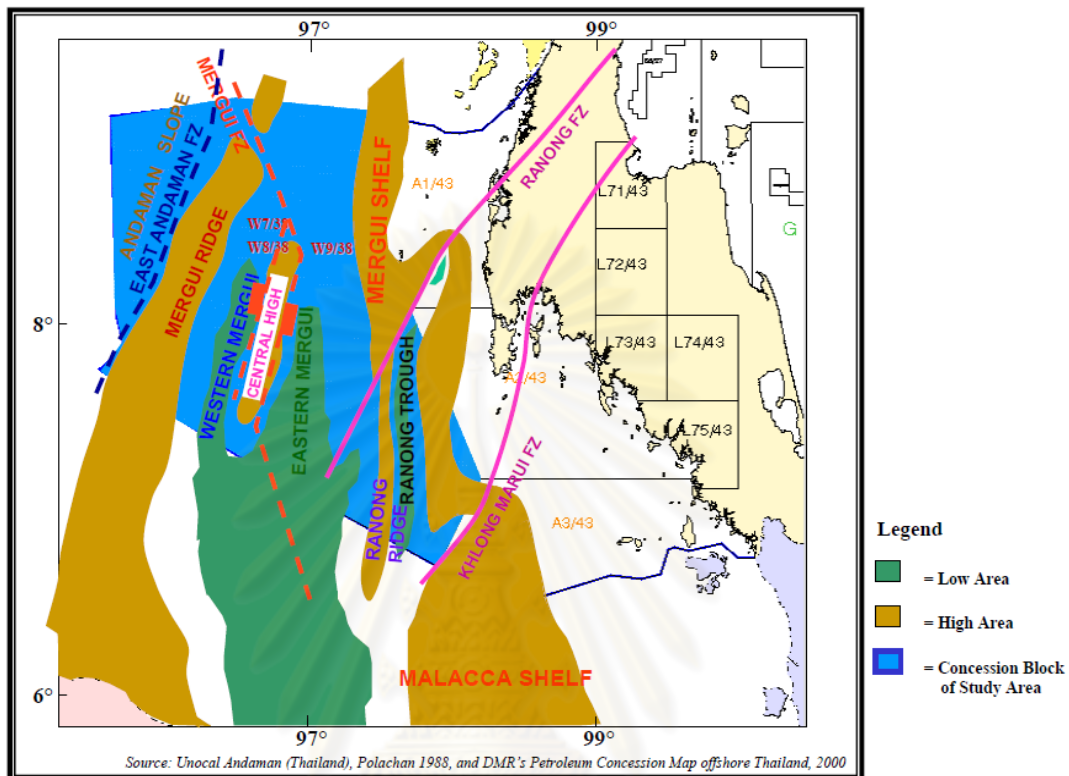


Figure 2.8 Physiographic map of the Mergui Basin, Andaman Sea (Mahatanachai, 1996).

ศูนย์วิทยทรัพยากร
จุฬาลงกรณ์มหาวิทยาลัย

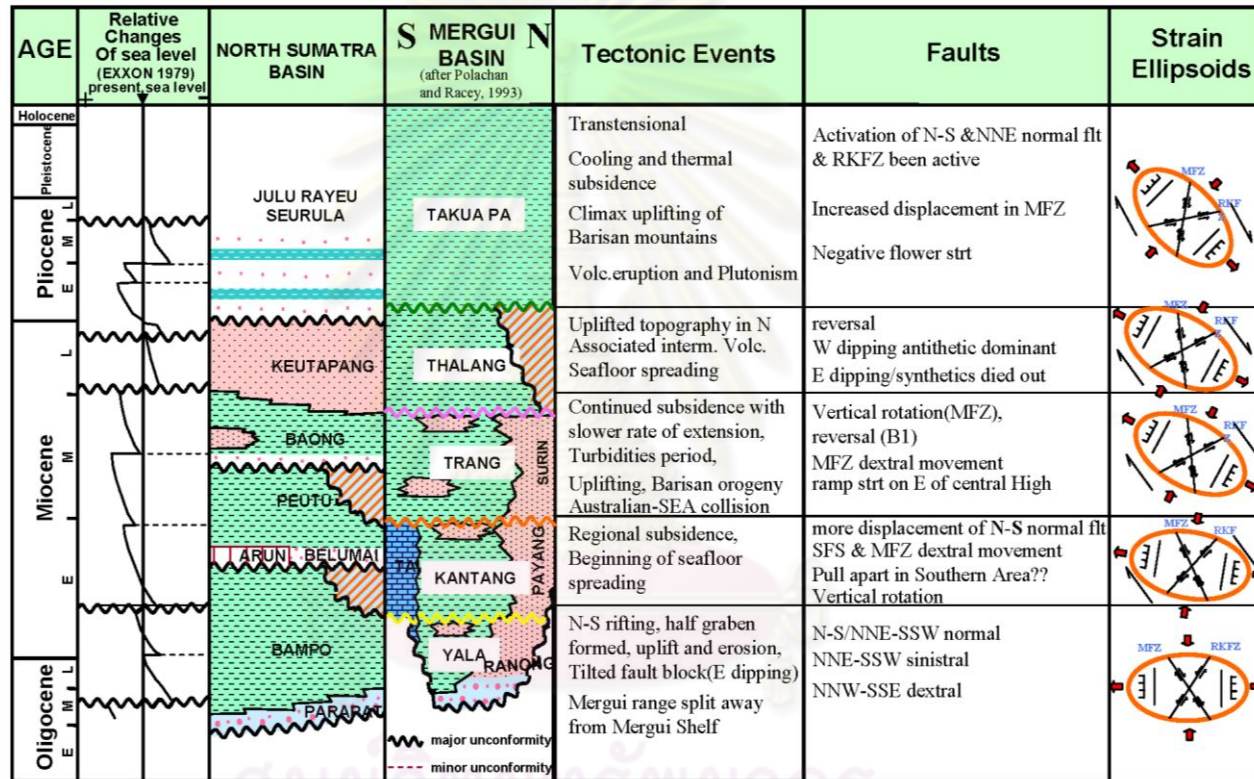


Figure 2.9 Stratigraphic Correlation of Mergui and N-sumatra Basin (Mahatanachai,1996)

2.1.2.2.9 Takua Pa Formation

The Takua Pa Formation primarily contains calcareous, glauconitic shales with abundant planktonic foraminifera, and occasional siltstones. The Takua Pa Formation overlies the Trang Formation with an unconformable contact between the formations. Palaeontology of the Takua Pa Formation suggest that deposition in various environments from lower bathyal in the lower part of the unit to shallower in the upper part. The age of Takua Pa Formation is Pliocene / Pleistocene to recent.

2.1.3 Structural and geology setting of Gulf of Thailand

2.1.3.1 Tectonic Setting

Tertiary basins in Thailand are classified as intracratonic rift basin (Woollands and Haw, 1976 and Chinbunchorn et al., 1989) and as transtensional pull-apart basins (Ponlathan and Sattayarak, 1989). Generally, these basins resulted from the Eocene to Oligocene collision of the Indian plate with Southern Asia and the subsequent extrusion and rotation of Indochina. During the initial contact of India with Southern Asia, Southeast Asia lay to the east of India and was probably oriented in the NW-SE direction. It was progressively rotated clockwise into a northerly orientation by the northward progress of India into Southern Asia. The progressive rotation of Southeast Asia had changed the angle of subduction of the Indian Ocean Plate beneath the southwestern margin of Southeast Asia from perpendicular to oblique. Increasing oblique subduction led to a cessation of the subduction related magmatic arc (Lower Cretaceous-Late Eocene) in Western Thailand and an accelerated strike-slip motion associated with the development of transtensional Cenozoic basins in this region. The onset of the beginning of the main phase of the strike-slip regime is at about 38 Ma (Polachan et al., 1991).

Cenozoic basins in the Gulf of Thailand are related to the dextral movement of NW-SE trending principal strike-slip faults, Three Pagoda, and the conjugate NE-SW trending transcurrent faults, Ranong and Khlong Marui, exhibiting sinistral motion (Figure 2.10). These basins are formed more or less parallel in the N-S direction as grabens or half grabens. In addition, structural grain of the Pre-Tertiary rocks in this region lies in N-S direction and influenced the basin trends (Pradidtan and Dook, 1992

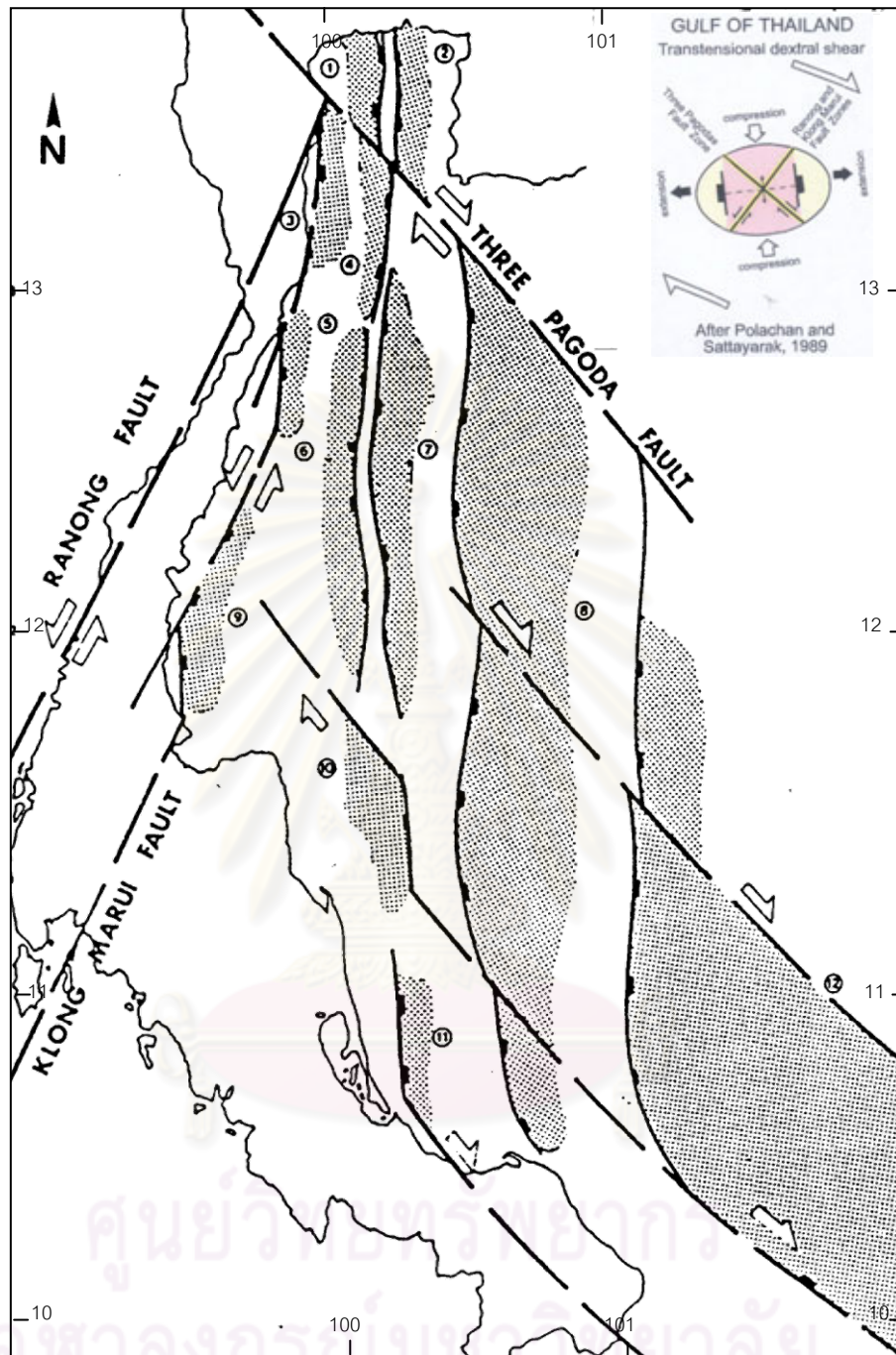


Figure 2.10 Structure map of Gulf of Thailand showing relationship between conjugate strike-slip faults and the development of N-S trending pull-apart basins. (1) Sakhon, (2) Paknam, (3) Hua Hin, (4) North western, (5) Prachuab, (6) Western, (7) Kra, (8) Pattani, (9) Chumporn, (10) Nakhon, (11) Songkhla, (12) Malay (Polachan and Sattayarak, 1989).

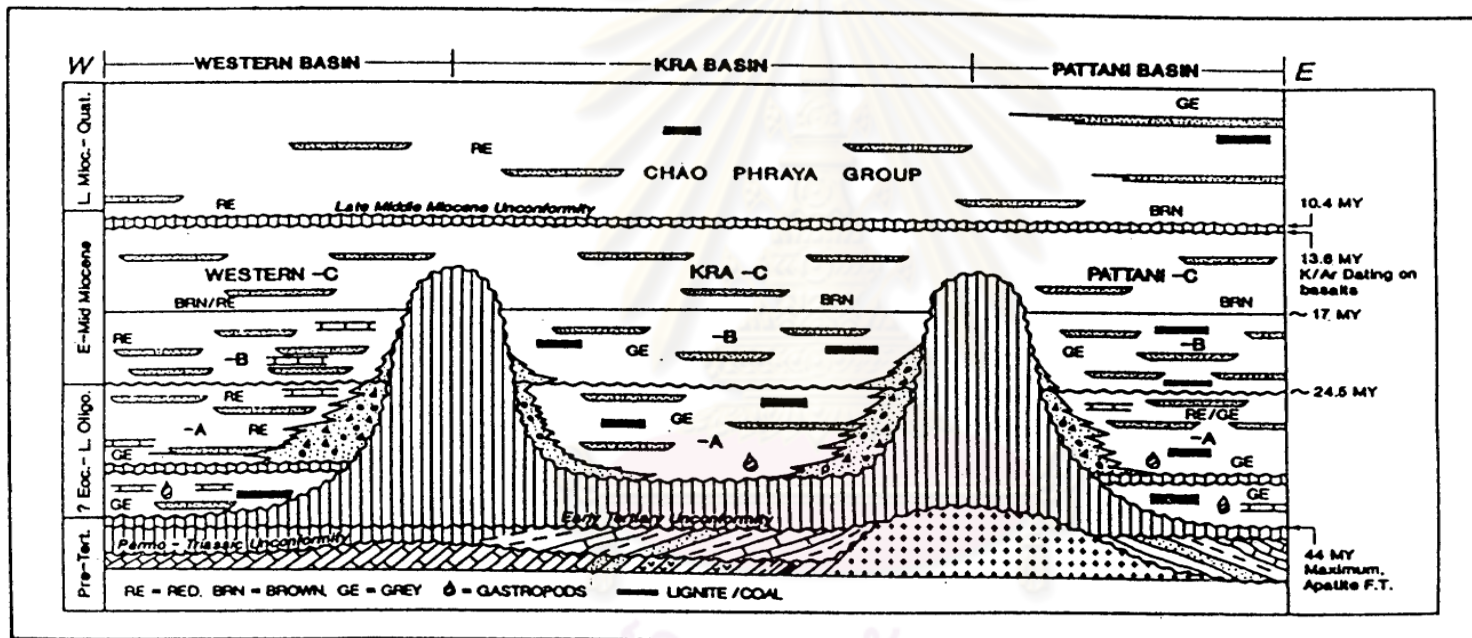


Figure 2.11 Generalised chronostratigraphic summary of basins in the northern part of the Gulf of Thailand

Praditdan and Dook, 1992)

and Packham, 1993). Hua Hin and North Western basins are bounded to the north by the Three Pagoda fault and to the west by the Ranong and Khlong Marui faults. They are formed as pull-apart basins by fault stepping of the Three Pagoda, Ranong and Khlong Marui.

2.1.3.2 Basin Formation

There is difficulty in dating the sequences of Cenozoic basin formation in Thailand because it has been noted that the biostratigraphic controls throughout the Tertiary are very limited due to the generally non-marine nature of deposition which has led to conflicting age designation (Polachan et al., 1991). Packham (1993) summarised the sequence of events associated with the development of Cenozoic basins in Thailand as follows. Early Oligocene (or possibly older). Commencement of rifting and basin formation induced by dextral shear. Early Oligocene to Middle Miocene. Relative tectonic quiescence but with continued extension, progressive expansion of deposition outwards from the initial rifting sites. Late Middle Miocene. Possible increase in dextral shear with local basin inversion and erosion, concurrent with sea level fall. Late Middle Miocene. Inception of Burma Plate and switching off regional lithospheric strain except near active strike-slip faults. Late Miocene to Quaternary. Decrease in tectonism, lithospheric cooling, and marine transgression in the Gulf of Thailand.

2.1.3.2.1 General Stratigraphy of the Northern Part of the Gulf of Thailand

General stratigraphy of Cenozoic basins in the Gulf of Thailand has been established by many authors. Woollands and Haw (1976) separated the Tertiary sediments in the Gulf of Thailand into three cycles of sedimentation which are particularly focused on the Eastern Basinal Area, Pattani and Malay basins). Chinbunchorn et al.(1989) divided the stratigraphy of Cenozoic basins in Thailand into two major sequences, Syn-rift and Post-rift sequences. Lian and Bradley(1986) and Polachan et al.(1991) divided the stratigraphy of Cenozoic basins in the Gulf of Thailand into four units(Figure 2.11). Pre-Tertiary basement in the northern part of the Gulf of Thailand, penetrated by several wells, compose of Permian carbonates, Mesozoic carbonates, Paleozoic metaclastics and Cretaceous granite. Tertiary sequences, unconformably overlying the Pre-Tertiary, are almost entirely non-marine

sediments and the biostratigraphic controls throughout the Tertiary are limited. Pradidtan and Dook (1992) reviewed the stratigraphy of the northern part of the Gulf using Late Miocene unconformity to divide the Tertiary succession into two sequences, Post-rift and Syn-rift sequences (Figure 2.12).

2.1.3.2.2 The Post-rift sequence

Since the formation of the unconformity, generally quiescent thermal subsidence has been taking place. The lithology of the Chao Phraya group is rather homogeneous. Flood plain and fluvial sediments are predominant, with more littoral and paludal sediments occurring in the upper part of the group.

2.1.3.2.3 The Syn-rift sequence

The stratigraphic groups below the unconformity are syn-rift related and were deposited in separate basin. In general, three distinct units, Upper, Middle and Lower, can be recognised from the Syn-rift sequence. Generally, the Syn-rift sequence comprises alluvial and lacustrine sediments. In the Kra and Chumphon basins, lacustrine sediments predominate in the Middle and Lower Units. The upper unit appears to be dominated by alluvial sediments, with associated braided and meandering stream deposits.

2.2 Neotectonic Evolution

Deformation of Thailand throughout Cenozoic Period is a result of the collision between the Shan Thai block and Indochina block in the first collision (Paleotectonic) and between Indian plate and Eurasian plate in the second collision (neotectonic). The interaction of Shan Thai and Indochina blocks at late Paleozoic age is the reason of main conjugate fractures system in northeast line and the northwest line in Thailand (Bunopas and Vella, 1983, Charisiri, 1989). The major northeast fractures and faults are Nam Pat, and Thoen-Long-Phrae Faults in northern Thailand and Ranong and Khlong Marui Faults in southern Thailand.

The experiments with plasticine of Tapponnier et al. (1982) are shown in Figure 2.13 They indicated many similarities between the results of their experiments and those of the geology of the Southeast Asia. For instance, they proposed that the F2 fault in the experiment corresponds to the Altyn Tagh Fault, and the F1 corresponds to the Red

AGE	UNIT	THICKNESS (UP TO)	LITHOLOGY		ENVIRONMENT	FOSSILS
LATE MIOCENE - RECENT	IV	1,700 m.	WESTERN GRABEN AREA CLAYS/SHALES/SANDSTONES Clays/Shales, brown - grey, varicoloured, silty Sandstones, fine - very coarse grained, occasionally gravel.	PATTANI & MALAY BASINS CLAYS/SHALES/SANDSTONES) Clays/Shales, grey, silty Sand(stones), grey fine - very coarse grained, channel characteristics.	Flood Plain with more Mangrove Swamp and Marine in upper part	Dacrydium Podocarpus Florschuetzia meridionalis Stenochlaena laurifolia
MIDDLE MIOCENE - LATE MID-MIOCENE	III	1,200 m.	SHALES /CLAYSTONE /SANDSTONES Shales /Claystones, varicoloured, redbrown, silty, sandy. Sandstones, brown, varicoloured, fine - coarse grained, average thickness 5m. restricted lateral extent. Limestone streaks & lignite are occasionally present.		Flood Plain with Local Delta Plain	Florschuetzia meridionalis Spinizonocapites echinatus
EARLY MIOCENE - MIDDLE MID-MIOCENE	II	800 m.	SHALES / SANDSTONES Shales / grey, organic rich Sandstones, brown - grey, very fine - medium grained, average thickness 4.5 m., significant lateral extent.		Lacustrine and Restricted Marine	Florschuetzia levipoli Echiperiporites estelae Pediastrum
↑ LATE OLIGOCENE - EARLY MIOCENE	I	5,000 m.	SHALES / SANDSTONES Shales, brown - grey, varicoloured. Sandstones, brown - grey, fine - coarse grained, fining upwards, channel characteristics.		Alluvial & Flood Plains with Ephemeral Lacustrine	Monoporites annulatus Magnastriatites howardi Picea, Pinus, Pediastrum
PRE-TERTIARY BASEMENT			MESOZOIC CLASTICS AND GRANITES, PALEOZOIC CLASTICS AND CARBONATES			

Figure 2.12 Stratigraphy of Cenozoic basins in the Gulf of Thailand (Polachan et al., 1991).

River Fault. The tectonics of eastern of eastern Asia would thus reflect the succession in time of two major phases of the continental extrusion. The gap between block 2 and block 1, which are compared to the southern China and the Indonesia, respectively (Figure 2.12); would be analogous to the South China Sea, whereas the gap A, between the rigid block and block 1, corresponds to the Andaman Sea.

Focus on the neotectonic crash, the soft collision (early collision) between Indian and Eurasian plates commenced during Late Paleocene to Middle Eocene (58-44 Ma), whilst the hard collision began in the Middle Eocene (44 Ma) (Curry, 2005). The Cenozoic tectonic evolution of this region can be separated into four stages, related to the northward movement of the Indo-Australian plate relative to the Eurasian plate. It is postulated by Srisuwan (2002) that the Cenozoic tectonic evolution of this region can be discussed in four stages as follows.

Stage I: Early Eocene to Early Oligocene (50 to 32 Ma): the South China Sea margin extension commenced earlier than the collision of Indo-Australian with Eurasian and the supposed time of initiation of the Red River Fault. The more extensive rifting in the South China Sea is noted and the first time rifting in the West Natuna Basin area is also mentioned to commence at this stage. The Malay, Mekong Delta and parts of Gulf of Thailand had been opening at 40-35 Ma.

Stage II: Early Oligocene to Early Miocene (32 to 23 Ma): end of the lateral Mea Ping Fault was approximately 30 Ma. Simultaneously, the onset of widespread extension in the Gulf of Thailand, Malay and West Natuna Sea Basins began during Late Oligocene, and continued to Early Miocene. The northern Thailand basins probably developed at this stage. The Mea Ping and Three Pagodas Faults changed to dextral sense of movement whereas the Mea Chan, Uttaradit, and Phrae-Thoen Faults became sinistral.

Stage III: Early to Middle Miocene (23 to 15 Ma): clockwise rotation of the entire Greater Sunda Block and increasing in the convergence rate along the Sunda Arc. North Sumatra Basin and Central Thailand Basins were still undergoing extension. During 20-15 Ma, clockwise rotation of Southern Thailand and counter-clockwise rotation of Malay Peninsular and Sumatra were reported. Inversion in the Malay and West Natuna

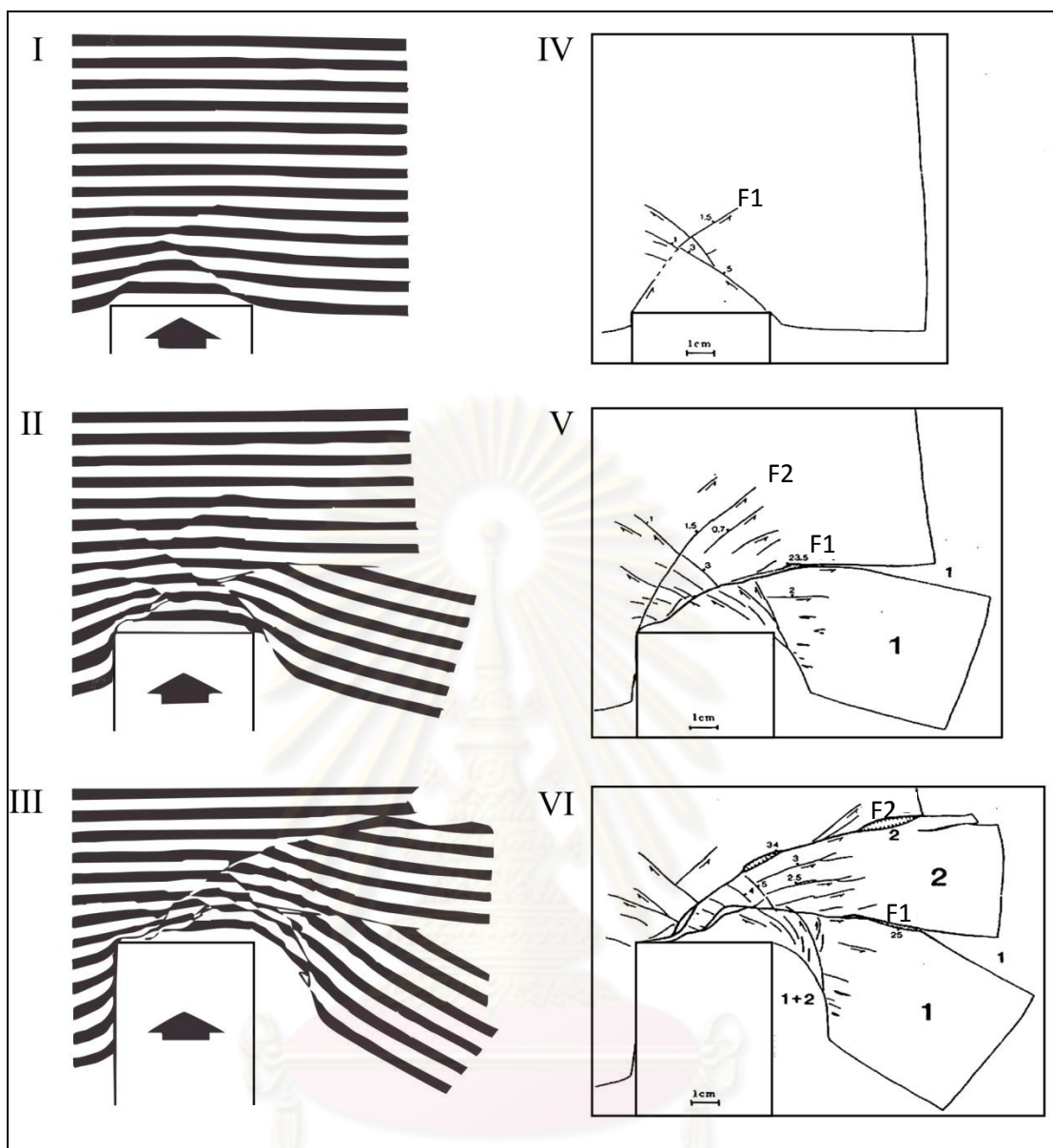


Figure 2.13 Three successive stages (I to III) and extrusion-tectonic model (IV to VI) with plasticine experiment (plain view). In unilaterally confined experiment, two major faults (F1 and F2) guide successive extrusion of two blocks. In stage VI, blocks 1 and 2 can be compared to Indochina and southern China, and open gap 1, 1+2, 2 to South China Sea, Andaman Sea, and northeastern China, respectively (after Tapponnier et al., 1982).

Basin, most Cenozoic basins in the Gulf of Thailand and onshore Thailand experienced uplift and erosion that corresponded to a pervasive Middle-Miocene unconformity.

Stage IV: Middle Miocene to Recent (<15 Ma): the counter-clockwise rotation of Borneo still continued while rotation of the Thai-Malay Peninsular and Sumatra ceased, and continued northward moving of Australia. North Sumatra had rotated counterclockwise with south Malaya and the rotation proceeded the orientation of the Sumatran margin became less oblique to the Indian plate motion vector. This caused the dextral Sumatran strike-slip system, and extension in the Andaman Sea region.

Extension occurred in the Gulf of Thailand and inversion in the Malay and West Natuna Basins, whereas the Andaman Sea continued opening toward its present extent. All NW trending strike-slip fault zones in the Sunda region were dextral. The inversion and uplift episode, the structural activity in the Cenozoic basins of the Sunda region slowed down toward quiescence around 10 Ma to 5 Ma, during which period regional subsidence occurred and was probably induced by post-rift thermal re-equilibrium. This late-stage subsidence has continued to the recent time (Figure 2.14).

According to the convergent of Indian plate and Eurasian plate in late Cenozoic, there were development of the South China Sea, and Cenozoic basins of offshore Vietnam, Cambodia and in Northern Thailand, have also been attributed to movement on the NW-trending strike-slip faults (Tapponnier et al., 1986), and offshore extensions of the KMF and RF have been linked to extension in the Andaman Sea and the Gulf of Thailand. However, Pacific plate still move to go to the northwest but Eurasian plate almost still motionless while Indian and Indonesia-Australian plate moves to upward in the north in the character clockwise, all about these were cause of continuously evolution of structure in the South-east Asia (Watkinson et al., 2008) (Figure 2.15).

2.3 Active Faults in Thailand

2.3.1 Previous earthquake studies in Thailand

In Thailand, the first explanation on the earthquakes has been recorded directly from annals or stone inscription and astronomy. At present, there are many earthquake have been reported in Thailand, especially western and northern part of Thailand.

However, a few researches have been reported, they have been more or less concerned with structural geology and tectonic geomorphology of southern Thailand.

Nutalaya et al. (1985) first studied characteristic earthquakes and described seismic source zones in the Myanmar, Thailand and Indochina areas. Twelve seismotectonic zones were identified. They located Thailand within zone F and zone G on the west and the north, respectively. However, from their report, southern Thailand and parts of northeastern Thailand were identified in the area without seismic source zones.

Siribhakdi (1986) studied seismogenic areas in Thailand and periphery and reported that earthquakes in Thailand throughout past 1,500 years history. The foci and epicenters of the seismicity have been located both in Thailand and neighboring countries. Many of the earthquakes in Thailand have close relation with four major faults including the Three pagoda, the Si Sawat, the Moei-Uthai-Thani and the Mea Hong Son-Mea Sariang Faults. He also mentioned that earthquakes in Thailand are associated with Tectonism, which is believed to be related to the subduction zone and spreading ridge in Andaman Sea (Figure 2.16).

Chuavirote (1991) studied major faults in Thailand and identified 13 faults including Ranong and Khlong Marui faults. He said that Ranong and Khlong Marui Faults were strike-slip faults and mainly trend in the northeast-southwest direction.

Tapponnier et al (1986) investigated the mechanics of the collision between India and Asia, and suggested that the Ranong Fault was sinistral movement, and at the same time the KMF was dextral. However, in the middle Cretaceous, they commended that the KMF was sinistral as the Ranong Fault.

Charusiri et al (1996) applied several remote sensing techniques to study geological structures related to earthquakes in Thailand and neighboring countries. The results are useful in determining the seismic source zones to indicate the earthquake prone areas. A new seismotectonic (or seismic-source) map is also proposed. According to this study, the Ranong and the KMF were located in zone G of their seismic-source map.

Hinthong (1997) reported "Study of Active Faults in Thailand" and first produced the active fault map of Thailand. Based upon geologic and geochronological available

data, and with exclusion of the tentatively inactive and inactive classification, fault activity can be classified as three classes namely, active, potentially active and tentatively active. Basically, there are three major criteria for recognition of active faults, namely, geologic, historic and seismologic criteria. Four classes have been proposed of active faults in Thailand including, potentially active, historically and seismologically active, neotectonically active, and tentatively active, respectively.

Charusiri et al. (1998) reclassified the active faults in Thailand into three classes, namely active, potentially active, and tentatively active based on results of morphotectonic and TL dating results. The RF have been classed as tentatively active fault, except at Kraburi area is active fault class. (Figure 2.17).

Royal Irrigation Department (2006) studied seismotectonic investigation in the project "Tha-Sae Dam" in Chumphon province for consideration of suitability and environment effect of Thasae Reservoir. The results revealed that the Ranong fault show no movement during Holocene and these faults are not active, but classified them to tentatively active fault.

After an accident earthquake event on 27-28 September 2006 and 8 October 2006, Department of Mineral Resources (2006) and Royal Irrigation Department (2006) reported the macroseismic investigation and produce intensity maps from earthquake. The maps indicated that the most probable location of those epicenters are in the Gulf of Thailand rather than the Kungyangale Fault in southern Myanmar.

Department of Mineral Resources (2007) investigated the Ranong and Khlong Marui Faults with integration of data from remote-sensing, field work, and TL dating data. The result shows that both faults were sinistral strike-slip faults and have the latest movement at about 40,000 and 1,200 years ago, respectively.

Watkinson et al. (2008) studied the kinematic history of the Khlong Marui and Ranong Faults, southern Thailand. They suggested that the Ranong Fault was the zone of strike-slip faulting with 4 stress phases. They are, D1: low grade ductile dextral strike slip shear complete before 87 Ma ; D2: medium to high grade ductile dextral strike-slip shear after 72 Ma and before 56 Ma; D3: brittle sinistral and sinistral reverse oblique strike-slip shear after 52 Ma; and D4: brittle dextral strike-slip shear at about 23 Ma.

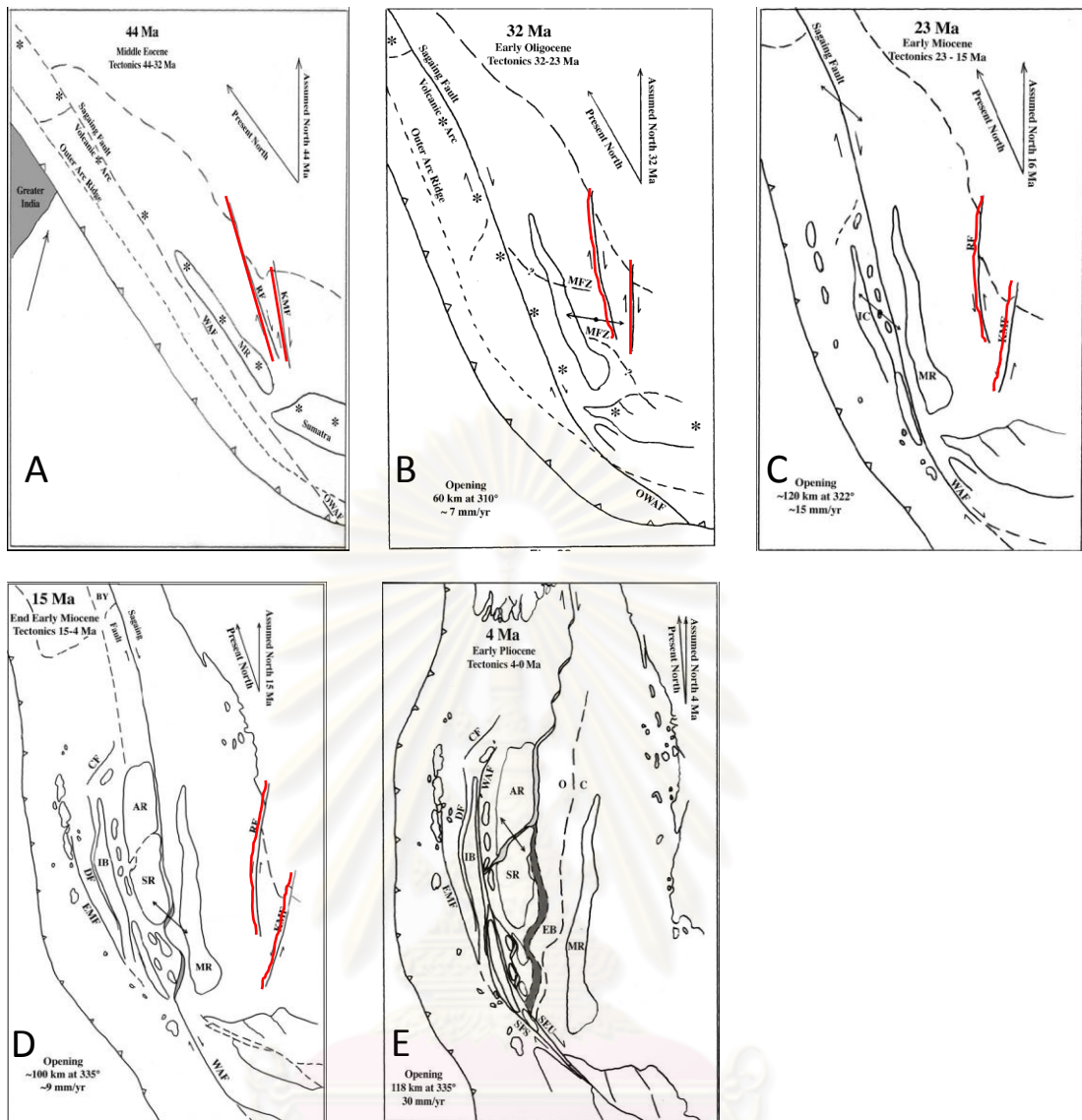


Figure 2.14 Tectonic evolution during Tertiary Period : 44 Ma (A), 32 Ma (B), 23 Ma (C), 15 Ma (D), and 4 Ma (E), showing the change in the sense of movement of the Ranong and Khlong Marui Faults (RF & KMF), respectively, between 32 and 23 Ma of the Andaman Sea (Curry, 2005).

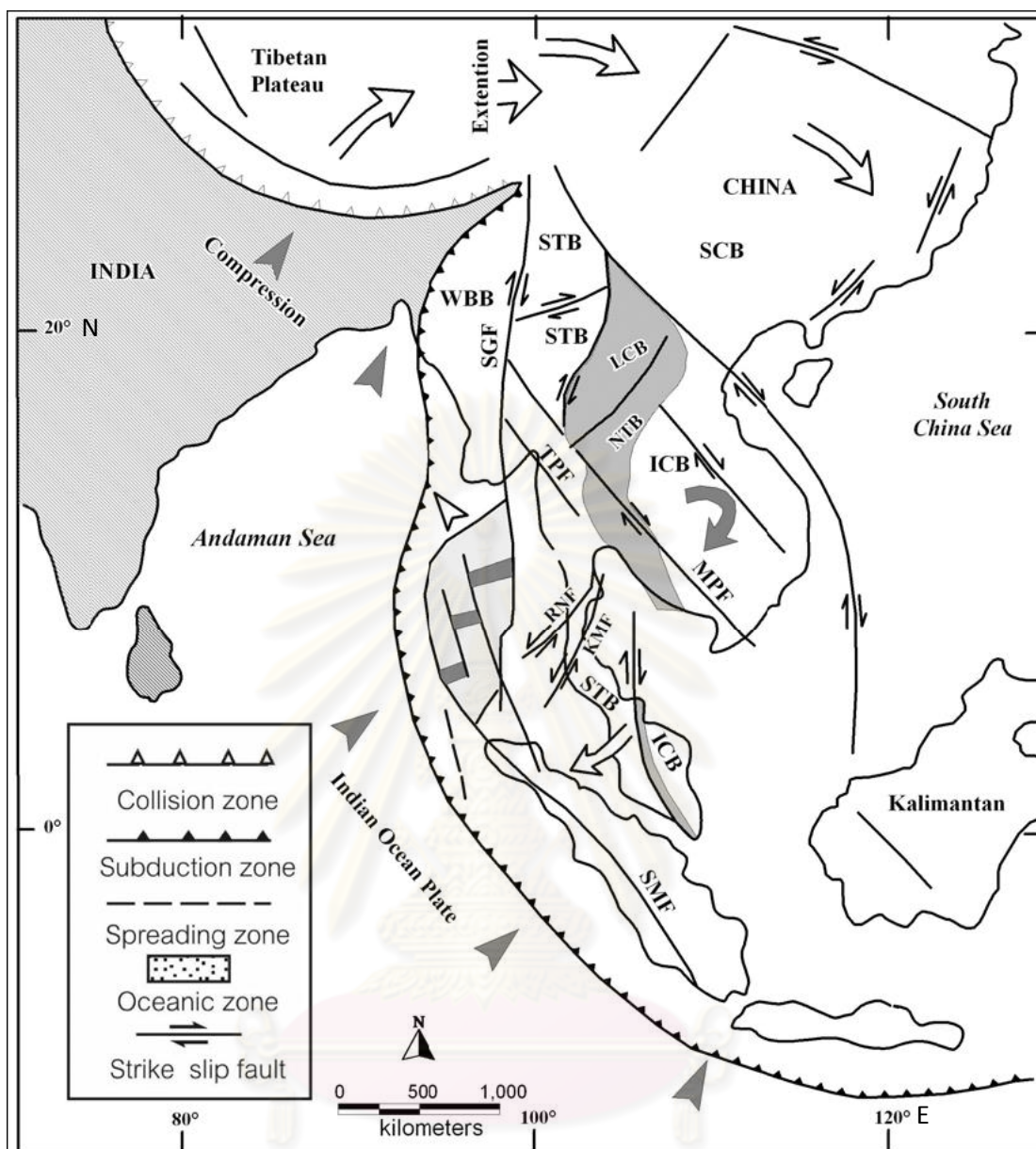


Figure 2.15 Tectonic map of SE Asia showing major fault systems and the relative movement of the SE Asian crustal blocks in response to India-Asia collision (modified from Poolachan, 1989, Charusiri et al., 2002) (Notes: SMF = Sumatra Fault; SGF = Sagaing Fault; RNF = Ranong Fault; KMF = Khleng Marui Fault; TPF = Three Pagoda Fault; MPF = Mae Ping Fault; SCB = South China Block; STB = Shan Thai Block; LCB = Lamgang Chaingrai Block; NTB = Nakhon Thai Block; WBB = West Burma Block and ICB = Indo Chian Block (Charusiri et al., 2007).

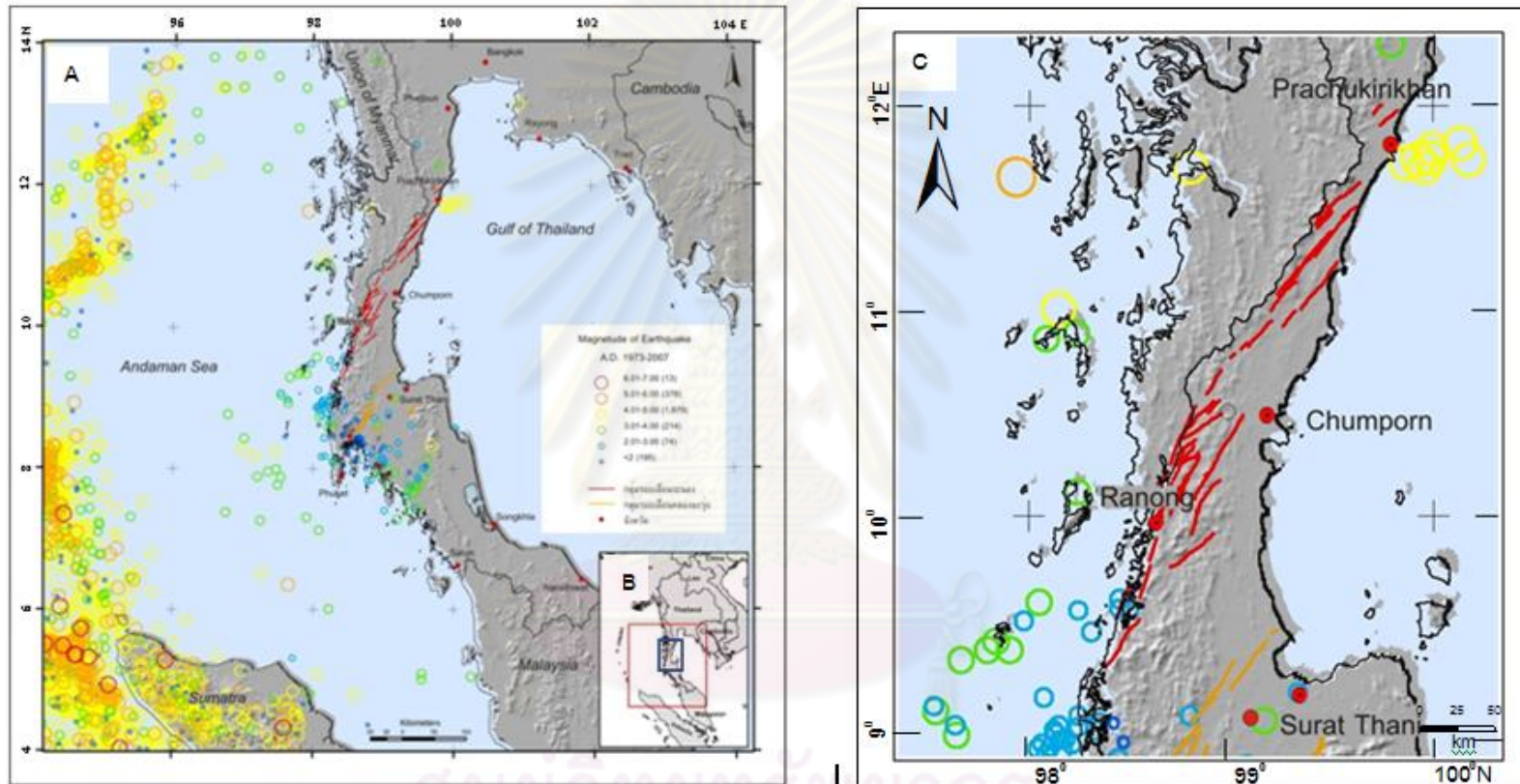


Figure 2.16 Map of Peninsular Thailand and nearby regions showing major active faults : Ranong Fault(RNF) and Khlong Marui Fault (KMF) and epicenter distribution (A). (modified after Department of Mineral Resources, 2007). Noted that the study area is located as blue box in (B). The study area with epicentral distribution and RNF is shown in (C).

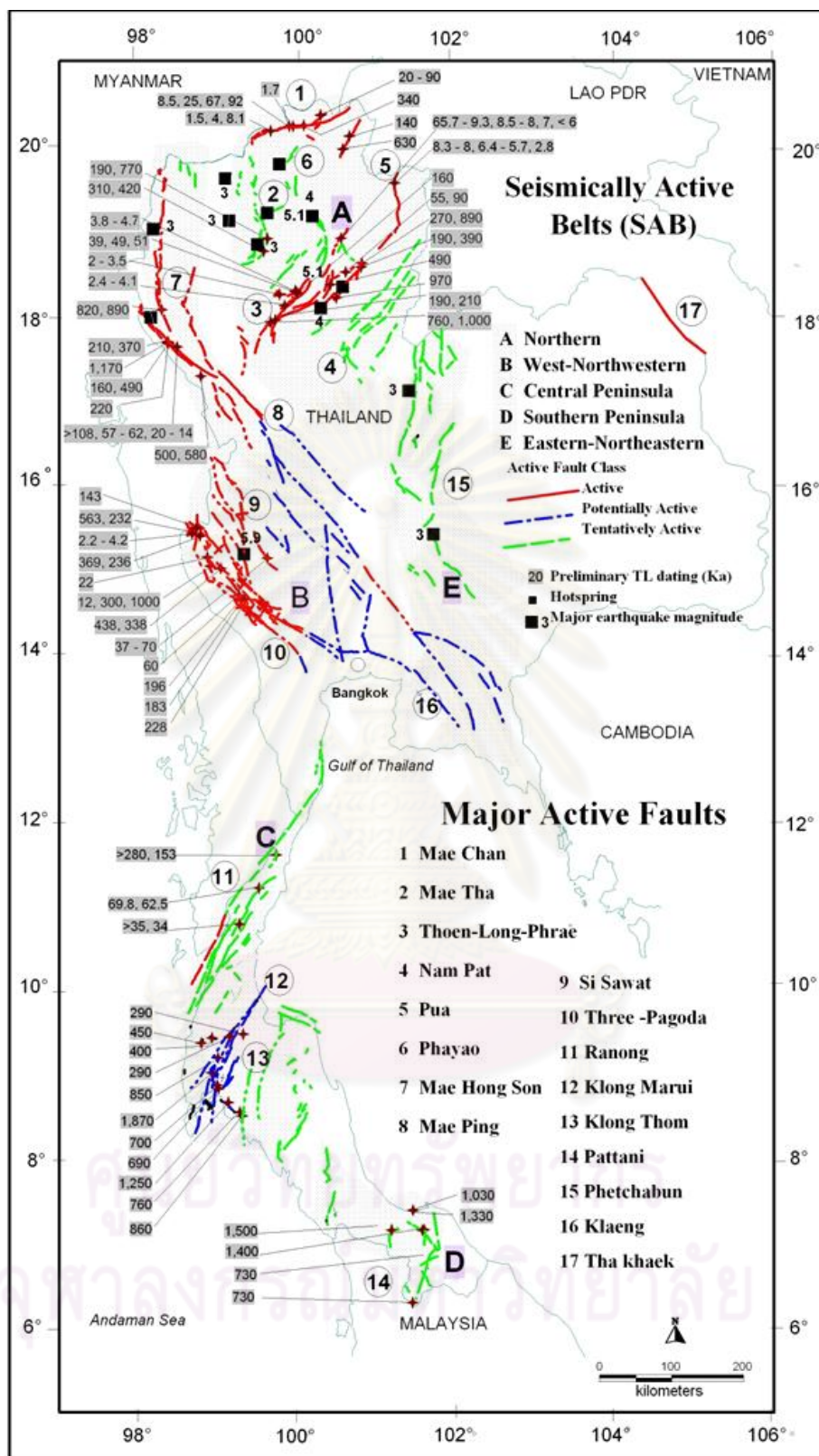


Figure 2.17 Map of Thailand showing major active faults and quaternary age dating results along the major active faults (Charusiri et al., 1998). The study area covers within the fault line No.11.

Pananon et.al. (2009) studied the project of earthquake hazard risk in Prachuab Khiri Khan province and adjacent area. They can divided fault segment of Ranong fault zone in Prachuab Khiri Khan area into 11 fault segments and have range of movement about 4,500-16,000 years ago.

Kaewmuangmoon (2010) studied about paleoearthquake investigation along Khlong Marui Fault Zone. He divided KMF into 16 fault segments based on geomorphic index and remote-sensing data and conclude that KMF is active sinistral fault .

2.3.2 Definition of active faults

The definition of active faults varies widely, depending on proposal. Willis (1923) defined an active fault as the fault on which a slip is likely to occur in the future, and a dead fault as the one on which no movement may be expected.

Albee and Smith (1996) proposed a definition of an active fault in a geologic sense as a fault which has moved in the past and will eventually break again in the future. The activeness of a fault is not just a single state that depends on the degree of activity.

An active fault in the definition of Wood (1915) refers to the historic movement that shows evidence of recent surface movement known as the trace phenomena.

Cluff and Bolt (1969) said that a fault should be considered active if it has displaced recent alluvium or other recently formed deposits, whose surface effects have not been modified to an appreciable extent by erosion.

Allen et al. (1965) stated that faults, which have had sufficiently recent movement to displace the ground surface are usually considered active by geologists simply because the ground surface is a very young and ephemeral feature. If stream offsets and scarps in alluvium are to be the criteria for activity of faults, then the term "active" must be applied to events dating back into the Pleistocene Epoch, perhaps as much as 100,000 years.

In engineering design, fault activity is restricted to fault movement during the last 10,000 years, to the Holocene Epoch. This study adopted the definition proposed by the United States Bureau of Reclamation that an active fault is the fault that has a relative displacement within the past 100,000 years.

At present, methods for estimating future hazards of faults are deficient. The

designation of a fault merely as active provides an inadequate indication of the attendant hazard. Restricting of the definition of active faults to those having had displacement within a defined past period of time, such as 10,000 or 100,000 years, provides little assessment of the hazard. In addition, the adoption of different restricted definitions by different agencies has caused confusion. An accurate expression of the probability of occurrence of future displacement, of earthquakes generated, and of the size of such events is needed in evaluating the hazards of active faults (Wallace, 1980).

The active fault, as used by United State Geological Survey (USGS), is a fault that is likely to have another earthquake some times in the future. Faults are commonly considered to be active if they have moved one or more times in the last 10,000 years.

The active fault based on International Committee on Large Dam (ICOLD, 1989), is a fault reasonably identified and located, known to have produced historical fault movements or showing geologic evidence of Holocene, around 11,000 years, displacements and which, because of its present tectonic setting, can undergo movement during the anticipated life of man-made structures.

The Western States Seismic Policy Council (WSSPC, 1997) recommends that the following guidelines be used in defining active faults in the Basin and Range physiographic province. Active faults can be categorized into three types, recognizing that all degrees of fault activity exist and that it is the prerogative of the user to decide the degree of anticipated risk and what degree of fault activity is considered "dangerous". They are: "Holocene Active Fault" – a fault that has moved within the last 10,000 years; "Late Quaternary Active Fault" – a fault that has moved within the last 130,000 years; and "Quaternary Active Fault" - a fault that has moved within the last 1,600,000 years. It should be emphasized in this thesis that half of the historic magnitude 6.5 or greater earthquakes in the Basin and Range province have occurred on faults that did not have Holocene activity, furthermore, earthquakes in the province will occur on faults in all three categories.

Site investigations for foundations of nuclear power plants and research reactors (IAEA, 1988 and 1992; U.S. Nuclear Regulatory Commission, 1982.) states that a "capable fault" is a fault which has exhibited one or more of the following characteristics:

Movement at or near the ground surface at least once within the past 35,000 years or

Table 2.1 Active fault rank, criteria, and examples in Thailand (modified after Charusiri et al., 2001).

<i>Rank</i>	<i>Historic</i>	<i>Geologic</i>	<i>Seismologic</i>	<i>Examples</i>
Active (AF):				
<i>Tectonic fault which displays a history of strong earthquake or surface faulting in the past 35,000 yrs, or a series of quakes during 100,000 yrs, and is expected to occur within a future time span of concern to human society.</i>				
Surface faulting and assoc. strong quakes, also with geodetic evidence.				
<i>Young Quaternary deposits cut by fault, distinct youthful geomorphic features.</i>				
Epicenters along that fault.				
<i>Mae Chan, Phrae, Thoen, Pua.</i>				
Potentially Active (PAF):				
<i>A tectonic fault without historic surface offset, but with a recurrence interval sufficient to human concern, and with an earthquake within 100,000 yrs.</i>				
Surface faulting unclear.				
<i>Subdued & eroded geomorphic features, faults not known to cut young alluviums, but offset older Quaternary deposits.</i>				
Alignment of epicenters but with low confidence of assigned locations.				
<i>Mae Tha, Mae Hong Son, Srisawat, Three - Pagoda.</i>				
Tentatively Active (TAF):				
<i>A fault with insufficient data to define past activity and its recurrence interval is relatively very long or poorly defined, or displaying an earthquake within 500,000 yrs.</i>				
Data indicate fault evidences, but evidences may not be definitive.				
<i>Traced clearly by remote-sensing data with some hot springs.</i>				
Scarce and low seismicity.				
<i>Payao, Nam Pat, Ranong, Klong Marui, Klong Thom, Southern Peninsula.</i>				

Table 2.2 Activity of faults in Thailand based upon age-dating data (modified after Charusiri et al., 2001).

Era	Period	Epoch	Yrs before	Fault activity
C E N O Z O I C	Quaternary		0	Active fault is categorized within one of these events: 1) Active - if one quake within 35,000 yrs, or several within 100,000 yrs. 2) Potentially active - if one quake within 100,000 yrs 3) Tentatively active - if one quake within 500,000 yrs Neotectonic fault (difficult to determine-active or inactive)
		Holocene	11,000	
		Pleistocene		
	Tertiary	Pliocene	160,000	
		Pre-Pleiocene	350,000	(Paleo-)Tectonic fault (or inactive)
			650,000,00	
Pre-Cenozoic				

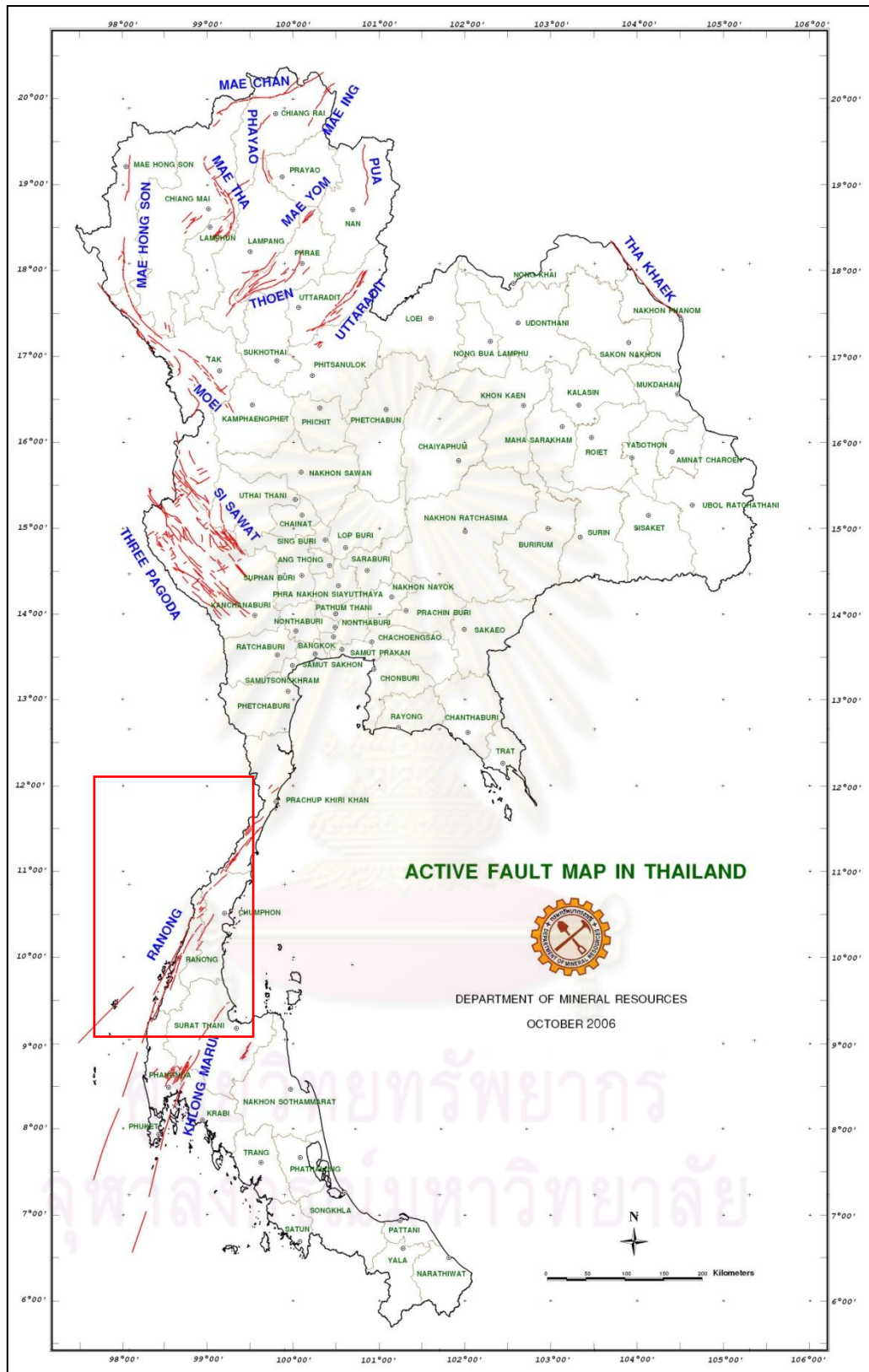


Figure 2.18 Index map of Thailand showing major active faults (Department of Mineral Resources, 2006). Noted that the study area is shown as red box.

movement of a recurring nature within the past 500,000 years; Macroseismicity instrumentally was determined with records of sufficient precision to demonstrate a direct relationship with the fault; and a structural relationship to a capable fault according to characteristic 1) or 2) such that movement on one could be reasonably expected to be accompanied by movement on the other.

In this study the writer applied the definition of active fault following that of Charusiri et al. (2001).

2.3.3 Some thought on Active Faults in Thailand

Hinthong (1995, 1997) reviewed the present status of the study of active faults program in Thailand. Apart from the knowledge of the importance of understanding of active faults, the various basic concepts, principles or even the implications have been laid out for refining. Approaches towards refining their definitions and classifications, as well as their criteria for recognition of active faults have been compiled from various sources. The importance of active fault evaluation to society is that it provides the basis for design, siting, zoning, communication, and response to earthquake hazards. It is necessary for all types of major engineering structures in order to reduce potential loss of life, injury or damage.

According to various authors and researchers, three approaches to define active faults can be distinguished and applied. These three definitions are characterized as general technical definition, engineering definition, and regulatory definition. Those three applications of definitions were discussed, based primarily on its original definition which was proposed in the context of a two-fold classification of dead and alive or active faults, and with respect to their potential for future renewal or recurrence of displacement or offset.

In consideration that based upon available data, and with the exclusion of the tentatively inactive and inactive classifications, fault activity can be classified as three classes, namely active, potentially, and tentatively, active. Basically, there are three major criteria for recognition of active faults: geologic, historic, and seismologic criteria. In order to scope with the problems of the study of active faults in Thailand, the adoption of active fault classifications, specifically for the benefit of the utilization only in

Thailand, four classes have been proposed, namely, potentially active, historically and seismologically active, neotectonically active, and tentatively active faults.

Consequently, with the restriction, deficiency of necessary data, and the lack of various seismologic, geodetic, geophysical, and other subsurface methods of analysis, not only supported by some thermoluminescence dating, the inventory of twenty-two preliminary active faults in Thailand have been outlined. The related purpose was to lay out major faults and fault zones for the preparation of preliminary active faults map of Thailand, scale 1:1,000,000.

Consequently, Charusiri et al, (2001), ranked the active faults, based upon historic, geologic, and seismologic data (Table 2.1). Since Thailand is not the main site for present-day large earthquakes as compared with those of the nearby countries, the best definition used herein is from the combination and modification of those above mentioned definitions. Additionally, the age of the fault is also essential in their justification, it is proposed that the fault becomes “active” if it displays a slip movement in the ground at least once in the past 35,000 years ago or a series of quakes within 100,000 years. If the fault shows only one movement within 100,000 years, it would be defined as “potentially active”. Furthermore, if only once in the past 500,000 years, it would be become “tentatively active”. All of these faults are expected to occur within a future time span of concern to society. The fault becomes “neotectonic” if it occurred in Pliocene or Late Tertiary, and it is regarded as “paleotectonic” or “inactive” if it occurred before Pliocene (Table 2.2).

2.4 Ranong Fault

Based on the work of Polachan and Sattayarak (1989), it is likely that there are two sets of the Ranong faults (RNF) on land (see R_1 & R_2 in fig. 2.10). However the locations of these two faults are very rough.

Chuavirote (1991) studied major faults in Thailand and identified 13 faults including Ranong faults. He said that Ranong fault was strike-slip faults and mainly trend in the northeast-southwest direction .

The Ranong Fault (RF) has been suggested as one of thirteen active faults in Thailand (Figure 2.18) base on the report by Department of Mineral Resources (2006).

The Ranong Fault (RF) and Khlong Marui Fault (KMF) are the major NNE trending strike-slip faults which dissect peninsular Thailand. They have been assumed to be conjugate to the NW-trending Three Pagodas Fault (TPF) and Mae Ping Fault (MPF) in Northern Thailand, which experienced a diachronous reversal in shear sense during India-Eurasia collision (Watkinson et al., 2008)

Department of Mineral Resources (2007) investigated the paleosiesmicities in southern Thailand using the remote-sensing interpretation and dating in some selected areas. Base on their study in Prachuab Khiri Khan and Ranong provinces Ranong Fault is defined as the lateral faults. The RF has the length of about 300 km and consist of 16 segments (Figure 2.19). The maximum paleoearthquake magnitude can be estimated from the length of fault segment (Well and Coppersmith, 1994) deduced from remote-sensing interpretation. The result revealed that the Ranong fault also generated several paleoearthquakes with magnitudes of about 6.2 -7.1. and the latest movement at about 40,000 and 1,200 years ago.

Pananon et al. (2009) studied the project of earthquake hazard risk in Prachuab Khirikhan province and adjacent area. They divided fault segments of Ranong fault zone in Prachuab Khiri Khan area into 11 fault segments with the earthquake range of movement occurring between 4,500 and 16,000 years ago. (Figure 2.20).

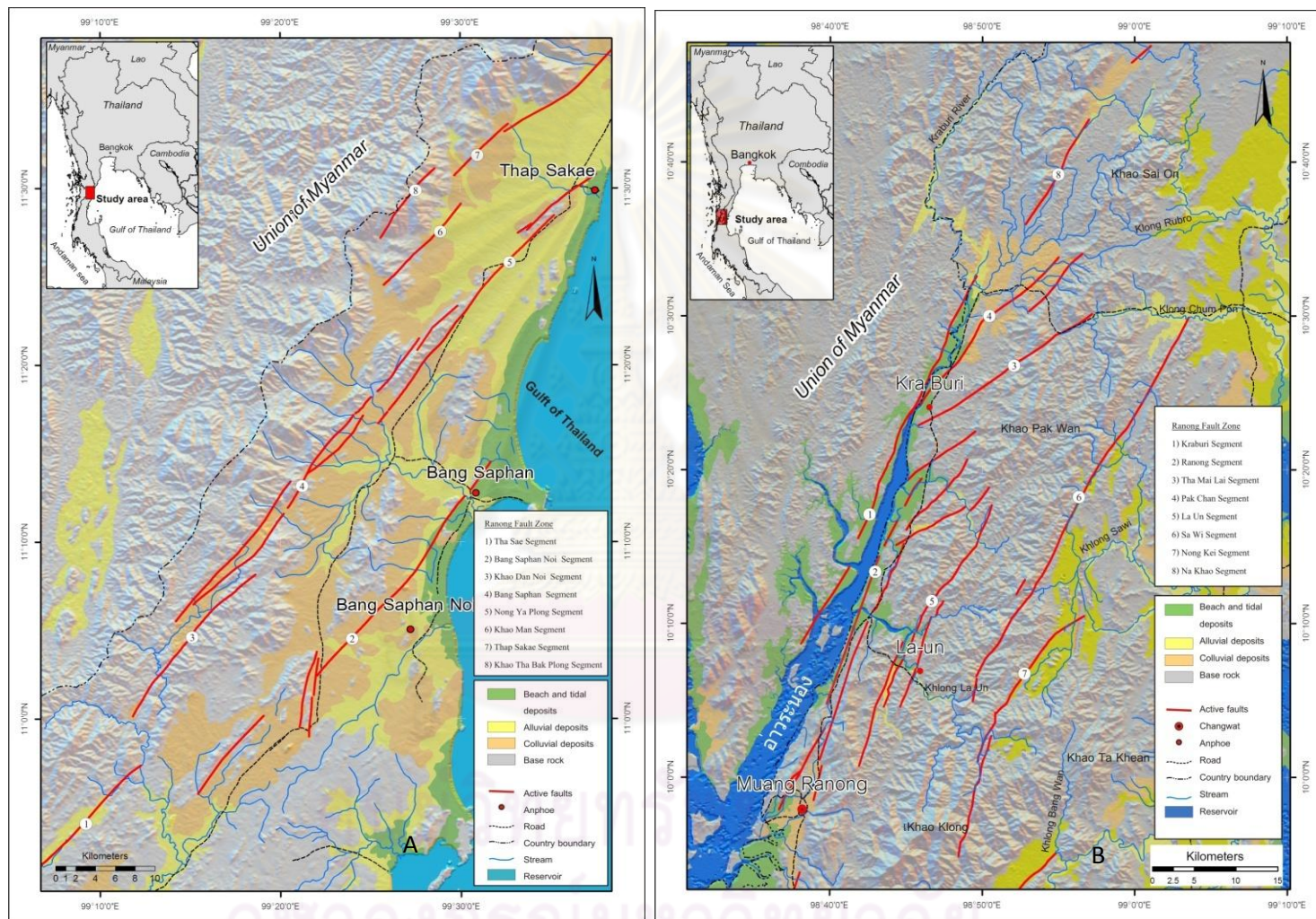


Figure 2.19 Major active RNF and its segments in the northern part: Prachuab Khiri Khan (A) and the southern part:

Ranong province(B), as identified by Department of Mineral Resources (2007).

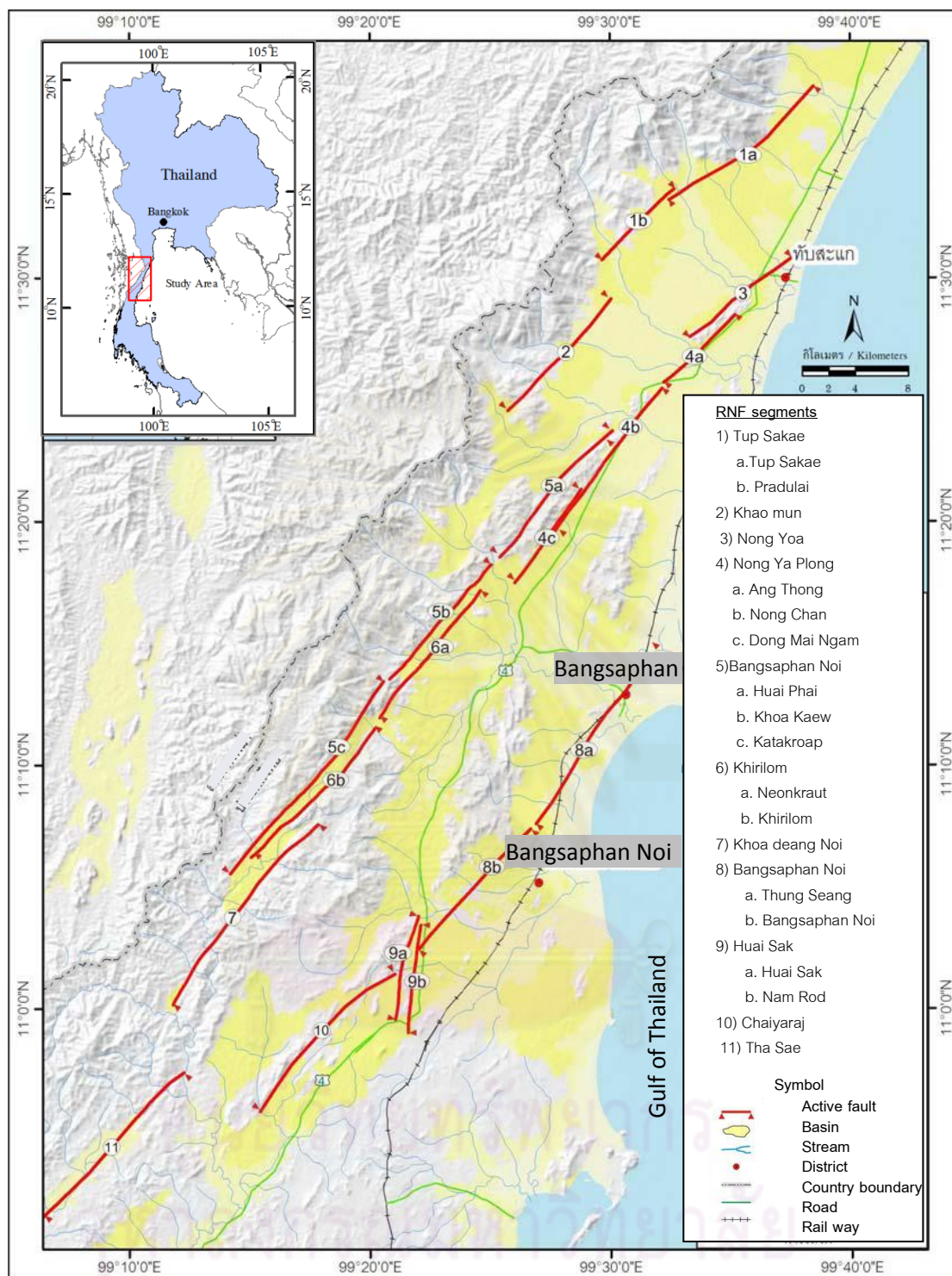


Figure 2.20 Major active faults segment and their subsegments in Prachuab Khiri Khan province, as Identified by Pananon (2009).

CHAPTER III

REMOTE-SENSING INVESTIGATIONS

In this paleoearthquake research the remote-sensing data have been used to interpret geology and structure geology. Remote-sensing data for this study comprises of satellite images, digital elevation model (DEM) data and aerial photographs satellite image were applied to cover the overall study area between $9^{\circ}0'0''\text{N}$ to $13^{\circ}0'0''\text{N}$ and longitudes $98^{\circ}0'0''\text{E}$ to $10^{\circ}0'0''\text{E}$ The result from the remote sensing interpretation can be helpful in the study of geomorphic indices investigation and field investigation.

3.1 Materials

The image data from Landsat 5 TM+ (enhanced thematic mapping), shuttle radar topography mission digital elevation model (SRTM DEM), digital elevation from detail survey resolution 2 m. and aerial photographs were applied in this investigation.

3.1.1 Landsat 5 TM+

The pictorial information was obtained from the satellite Landsat 5 TM+, which liberated to the space since April year 1982. This satellite takes electromagnetic wave signal that release out from earth surface The Earth's surface has the ability in reflecting definite frequency waves spectrum (Figure 3.1). Because the pictures have the difference of contrast following signal electromagnetic wave. Satellite Landsat 5 TM+ receive 7 wave bands, of which bands 1-3 are visible wavelength, bands 4, 5 and 7 are infrared wavelength, and wave band 6 is thermal infrared.

While the satellite orbited around the world, it toke a photograph, which covers 185×185 square kilometer areas. to keep running rounded orbit line, such as path 129/row 53 of Landsat 5TM+ image in this study, which were received from The Global Land Cover Facility.

Table 3.1 Band spectrum and wavelength interval of Landsat Thematic Mapper

(Landsat 5)(USGS, 2009).

Sensor TMMission 4-5	Spectral Sensitivity (μm)	Nominal Spectral Location	Ground Resolution (m)
Band 1	0.45-0.52	Blue	30 x 30
Band 2	0.52-0.60	Green	30 x 30
Band 3	0.63-0.69	Red	30 x 30
Band 4	0.76-0.90	Near-IR	30 x 30
Band 5	1.55-1.75	Mid-IR	30 x 30
Band 6	10.4-12.5	Thermal-IR	120 x 120
Band 7	2.08-2.35	Mid-IR	30 x 30

In this research 3 images data from the satellite Landsat 5 TM were used for interpreting structural geomorphology in the study area. The informative image detail is shown in tables 3.2.

Table 3.2 Image information from satellite, Landsat 5 TM applied in this research

No.	Path/Row	Data of Acquisition	Spectral Bands (no.)	Spatial Resolution (m)
1	129/51	05-03-2008	7	30 m (MX), 30 m (TI)
2	129/53	24-03-2009	7	30 m (MX), 30 m (TI)
3	130/53	11-02-2009	7	30 m (MX), 30 m (TI)

3.1.2 Digital Elevation Model

Digital Elevation Model are gray scale images wherein the pixel values are actually elevation numbers. The pixels are also coordinated to world space (longitude

and latitude), and each pixel represents some variable amount of that space (foot, meter, mile, etc.) depending on the purpose of the model and land area involved. They produced using elevation data derived from existing contour maps, digitized elevations and photogrammetric stereo-models based on aerial photographs and satellite remote-sensing images. In this study use DEM created from SRTM and contour line.

3.1.2.1 SRTM DEM data

Shuttle Radar Topography Mission Digital Elevation Model or SRTM DEM, which is a kind of data from the satellite was used in this research. It was digital format that altitudes of world surface. The image data is the mathematic model for delineating real topography and can be expressed in truthfully topographic map (or 3 dimension model). DEM pictures had applied the advantage for many research that related to topography work. DEM data was very useful to use in geology, especially study geomorphology for separate stone types and geological structure. SRTM DEM in this research received data assistance from CGIAR-CSI by the area researches cover lower southern Thailand (Figure3.1).

Table 3.3 Image information from STRM DEM used in this research

No.	Path/Row	Data of Acquisition	Spatial Resolution (m)
1.	STRM 56-10	29-06-2006	90x90

3.1.2.2 DEM produce by contour line

In this study use contour line from detail survey resolution 2 m.(Royal Irrigation Department, 2006) which cover study area to construct model and registered wgs-1984 zone 47N coordinates. Elevation data were investigate on 2006 supported by Royal Irrigation department. These are cover Prachuab Khirikhan, Chumphon and Ranong

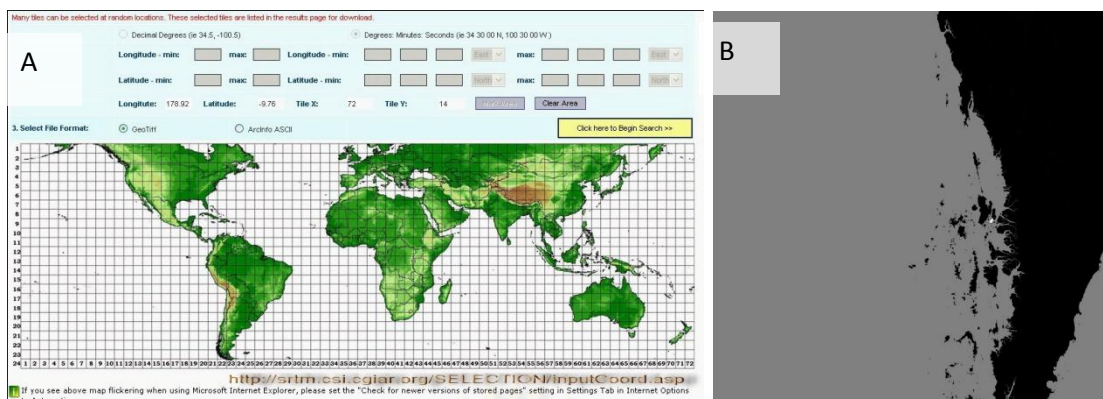


Figure 3.1 SRTM DEM index map of the world (A) showing location and the data sheet 56-10 that cover the study area (<http://srtm.csi.cgiar.org>).



Figure 3.2 Aerial photograph type-orthograph which was used in this research, (<http://www4.oginfo.com>).

ศูนย์วิทยทรัพยากร
จุฬาลงกรณ์มหาวิทยาลัย

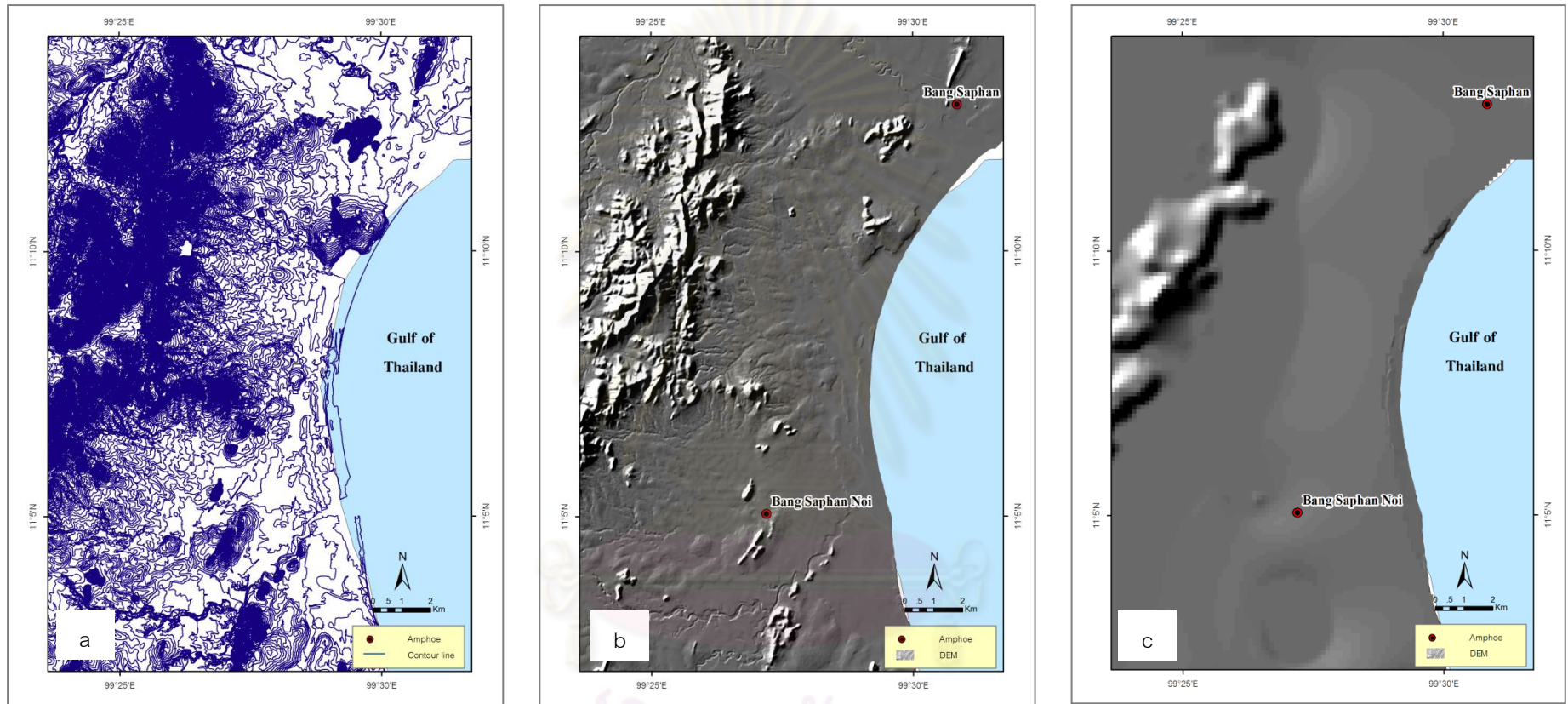


Figure 3.3 Map of the study area showing contrasting output constructed using (a) Contour line (b) DEM from contour line resolution 2 m. (c)

SRTM DEM.

คู่มือวิทยุพัชรากร
จุฬาลงกรณ์มหาวิทยาลัย

province There are more detail than SRTM DEM and helpful to provide lineament.(Figure 3.3)

3.1.3 Aerial Orthographic image

Aerial photography is the taking of photographs of the ground from an elevated position. The term usually refers to images in which the camera is not supported by a ground-based structure. Cameras may be hand held or mounted, and photographs may be taken by a photographer, triggered remotely or triggered automatically. Platforms for aerial photography include fixed-wing aircraft, helicopters, balloons, blimps and dirigibles, rockets, kites, poles and parachutes (Figure 3.2). Aerial photography should not be confused with Air-to-Air Photography, when aircraft serve both as a photo platform and subject (http://en.wikipedia.org/wiki/Aerial_photography).

As opposed to a bird's-eye view, photographs can be directed vertically. These are often used to create orthophoto – photographs which have been "corrected" so as to be usable as a map. In other words, an orthophoto is a simulation of a photograph taken from an infinite distance, looking straight down from nadir. Perspective must obviously be removed, but variations in terrain should also be corrected. Orthophotos are commonly used in geographic information systems, such as are used to create maps. Once the images have been aligned, or 'registered', with known real-world coordinates, they can be widely deployed. Orthophotos at a scale of 1:50,000 in this research were obtained from Department of Public Works and Town & Country Planning, and color-orthophoto at a scale of 1:4,000 were obtained from Royal Irrigation Department, covering Prachuab Khiri Khan, Chumphon and Ranong province. All of them were registered wgs-1984 zone 47N coordinates.

3.1.4 Airbone geophysic data

The three main airborne geophysics procedures are magnetic, electromagnetic, and radioactive. Airborne magnetometry (aeromag) is quite common and aeromag maps

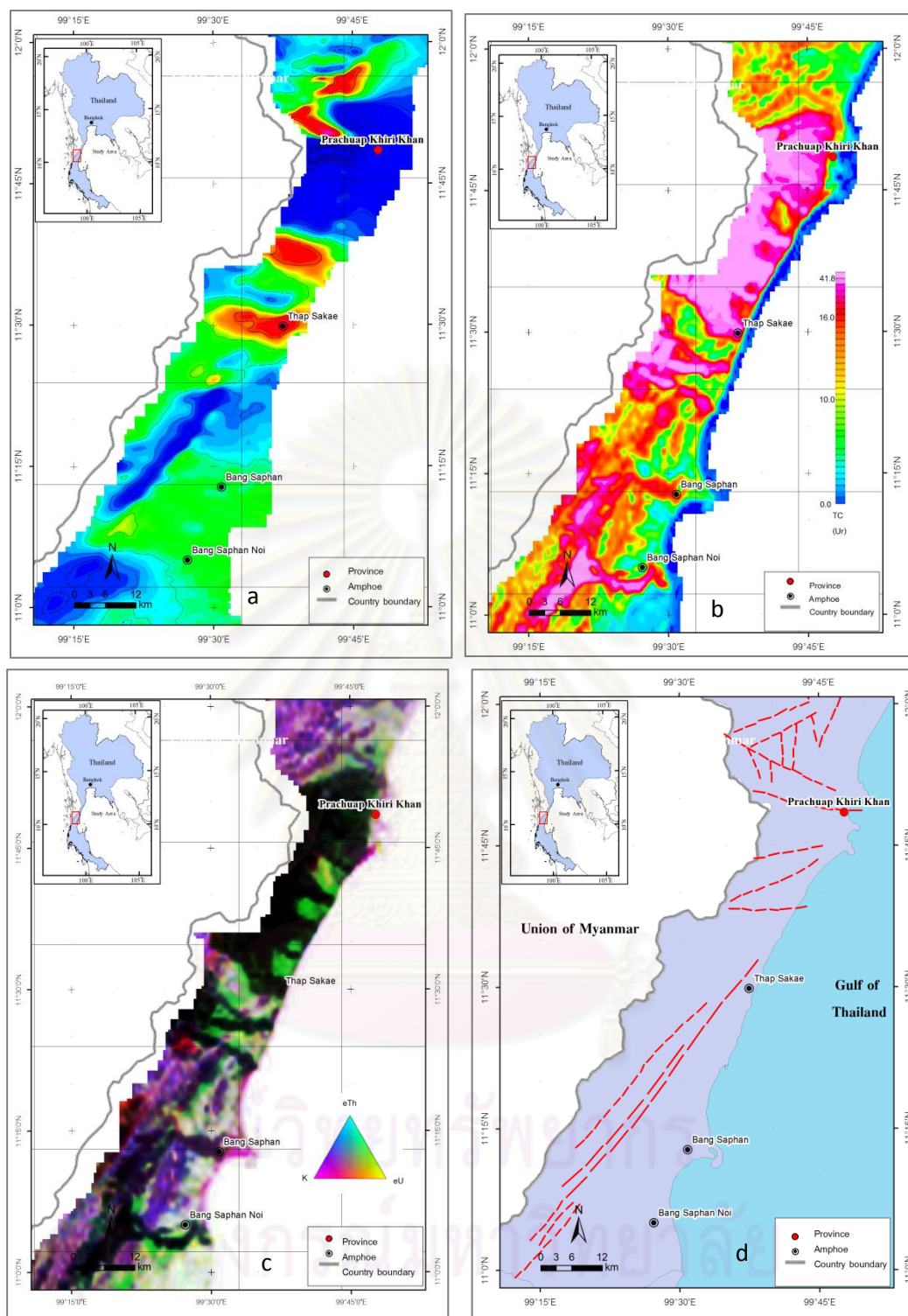


Figure 3.4 Airborne geophysics map of Prachuab Khiri Khan province. (a) Total magnetic field map. (b) Total count of radioactive intensity map (c) Ternary colour map (d) lineament map interpreted using airborne geophysics (modified from DMR,1989). Note that the NNW-SSE lineaments show in (d) is almost in the same trend as those found in figure.3.5

are available for most of the United States. Aeromagnetic mapping is very useful for mineral exploration and geological studies of magnetic rocks. Airborne electromagnetic methods are used in both the frequency and time domains. Ore body exploration is the chief use of airborne EM methods. Airborne radioactive measurements of gamma rays may be used for uranium and thorium exploration. In this study use the result of The mineral resources development project of Department of mineral resources, Thailand which cover only Prachuab Khiri Khan province. The fracture data from aeromagnetic survey and radiometric survey. (Figure 3.4)

3.2 Result/Interpretation

Satellite and space-borne images for geomorphotectonic investigation in this research are integrated data from LANDSAT 5 TM+ and DEM data acquired during 2006-2009. All of satellite data are collected in digital platform and using ENVI software for image enhancement and identification. In this study, lineaments and Cenozoic basins were performed by visual justification with the assistance of ArcGIS software. For the image processing and enhancement, the author used methods, such as false-coloured composite, principle component, band ratio, contrast stretching, and topographic modeling. These methods are helpful with the best image appearance and useful for delineation of major structures and Cenozoic basins.

3.2.1 lineaments

In an attempt to understand regional characteristics and patterns of geological lineaments in the study area and nearby, Landsat 5 TM+ imageries and DEM data were conducted for lineament interpretation approach. The Landsat 5 TM+ image with scale 1:250,000 is a false-coloured composite, bands 4, 5, and 7 represented in red, green, and blue (Figure 3.5, 3.6), respectively. The other is false coloured composite of spectral band 7/3 (red), band ratio 2 (green), and band ratio 4/5 (blue) to separate basin (Figure 3.7). In addition, DEM data were used for creating a hill shade image or virtual terrain model as shown in Figure 3.8. Those images as mentioned above covers study area and nearby areas. Figure 3.5 shows prominent the NE-SW trending lineament of Bangsaphan and Khoa Kwang segments from the enhanced image. It is clear that

Bangsaphan segment extends northeastward to the Gulf of Thailand. Figure 3.6 display the obvious lineament also in the NE-SW trend which is here in called Sawi segment. It is also noticed that the sharp lineaments at Ranong city seems to control the kraburi estuary. Additionally, as shown in figure 3.7 the NNW-SSE- trending lineament in southern Myanmar near Prachuab Khirikhan city is sharp as shown as the colour band/ ratio 6/3 :2:4/5 (red: green: blue).

The interpretation result from both enhanced Landsat 5TM+ images and DEM for neotectonic evidence is displayed in Figure 3.9. Hill shade image interpretation is used to assist in delineating large scale neotectonic features and to define orientations and directions of the investigated fault segments (McCalpin, 1996). The result shows the appearance of several neotectonic features including fault scarps, triangular facets, offset streams, and shutter ridges. Based upon Landsat and DEM interpretation, there exists a series of faults trending in the northeast-southwest, northwest- southeast, north-south, and east- west directions .

The major lineaments of faults lines, which are in the northeast-southwest direction, play a major role in shaping up the coast lines of Thailand Peninsular. Earlier works (such as Polachan, 1988, Charusiri et al., 2009) considered these fault zones were developed in Cenozoic time relative to the opening of basins in the Gulf of Thailand. The minor lineaments, which lie in the northwest-southeast and east-west directions, forming the conjugate sets of the major northeast – southwest – trending lineaments. As shown in Figure 3.9, most of lineaments which oriented in the northwest-southeast direction situate in the area dominated by basement rocks, whereas the lineament in the northeast-southwest direction situate in the area occupied by both basement rocks and sedimentary basin. Additionally, those structural lineaments in the northeast – southwest accompanies mountain range lines.,

There are about 158 lineaments in the north–south direction (Figure 3.10a), 60 lineaments in the east-west direction (Figure 3.10b), 294 lineaments which align in the northeast – southwest direction and 90 lineaments in the northwest – southeast direction

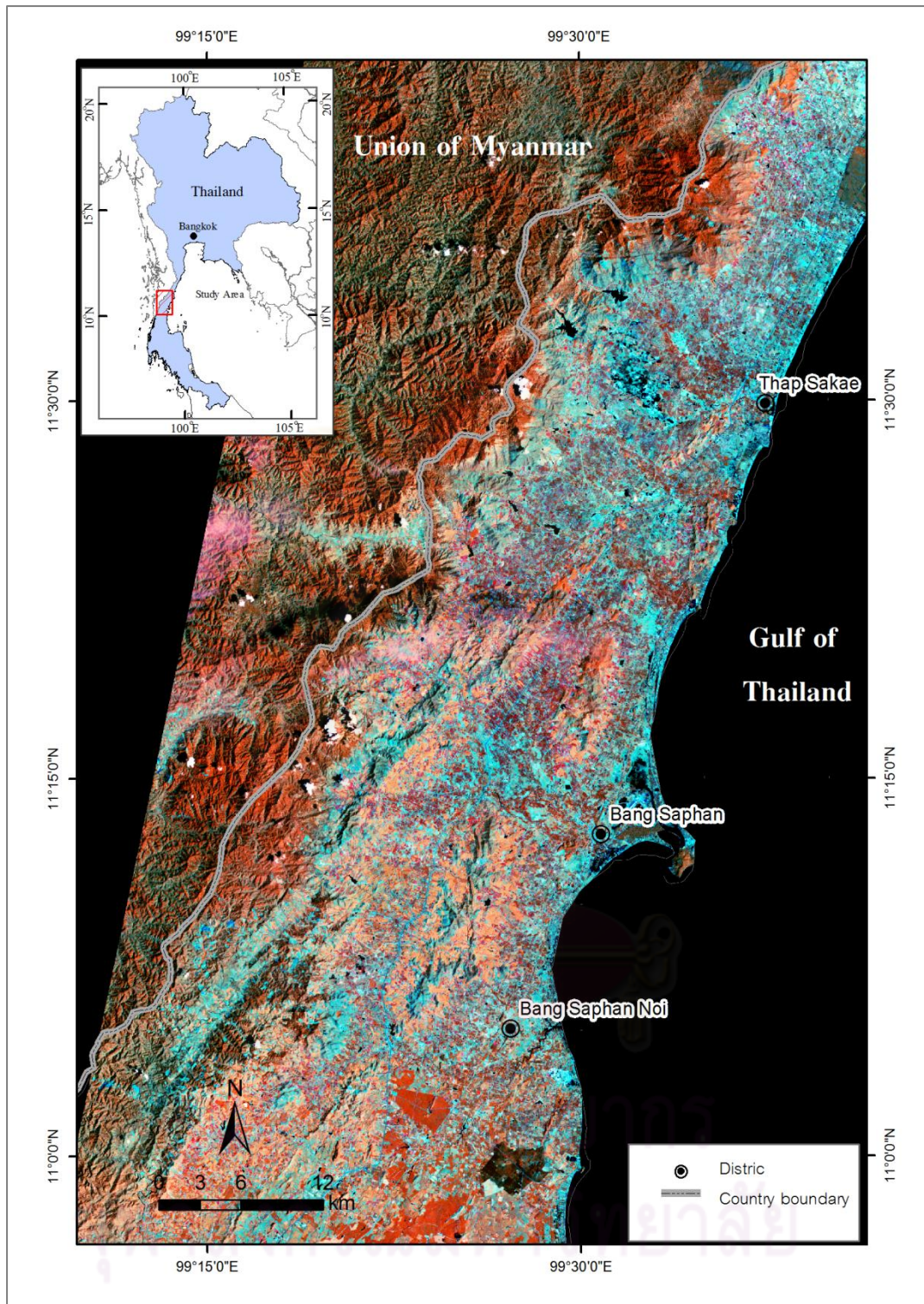


Figure 3.5 Enhanced Landsat 5TM map with the false colour composite data of bands 4:5:7 (red: green: blue) showing the physiographic features of Prachuab – Khiri Khan area, south central Thailand.

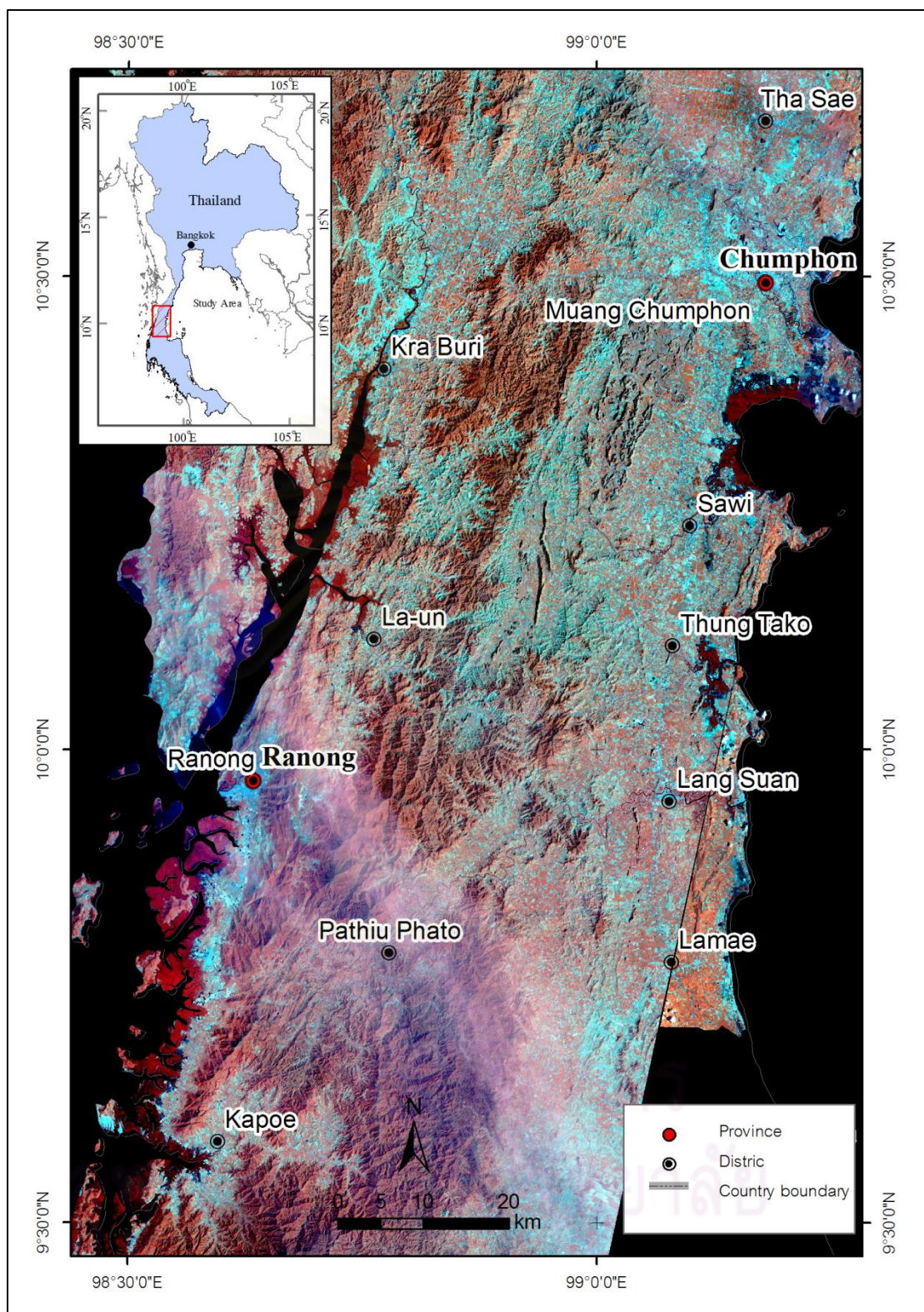


Figure 3.6 Enhanced Landsat 5TM map with the false colour composite data of band 4:5:7 (red: green: blue) showing the physiographic feature of Chumphon and Ranong areas, southern Thailand. Good example is a sharp lineament which is Sawi segment.

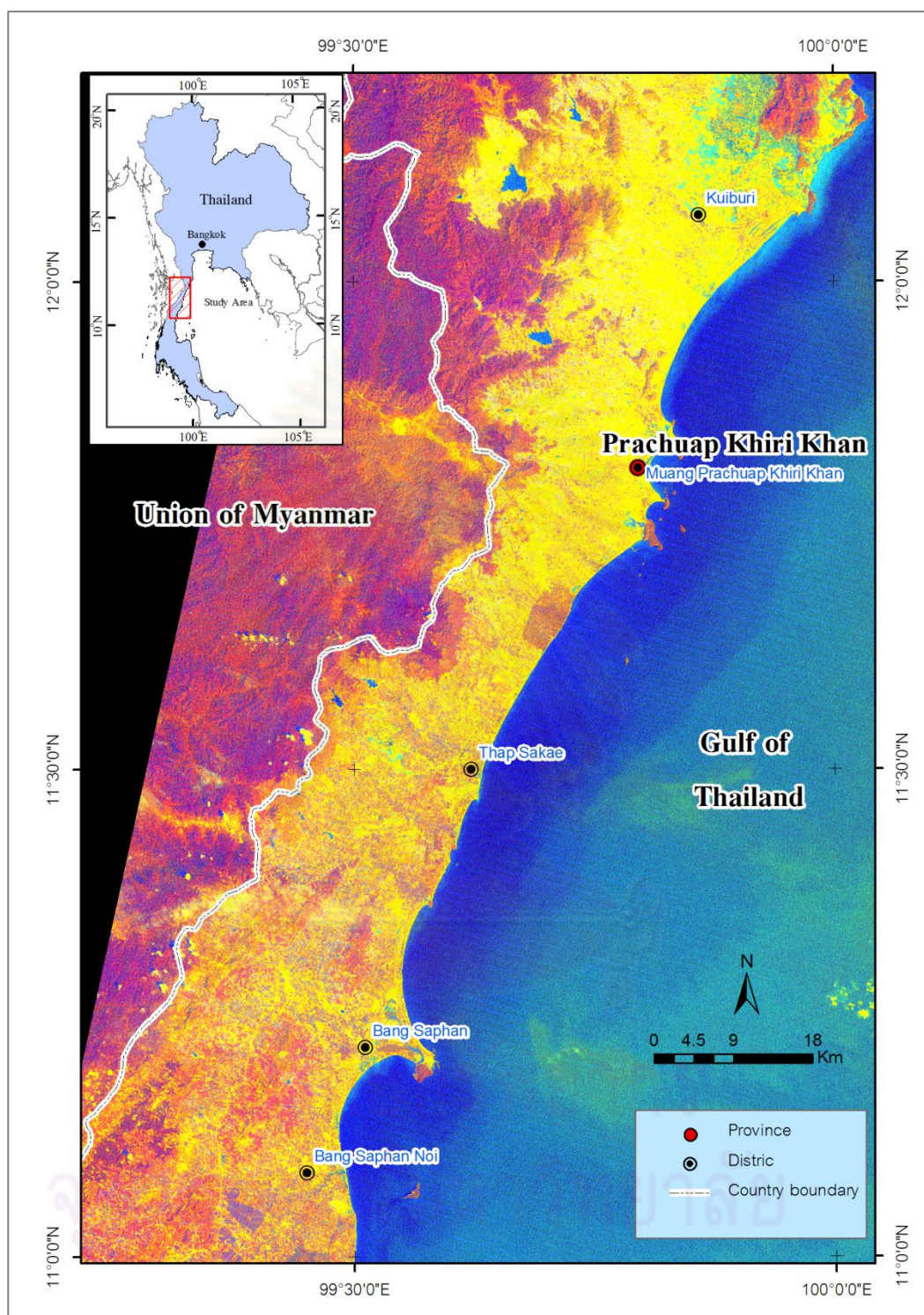


Figure 3.7 Enhanced Landsat 5TM map with the false colour composite data of band 6/3:2:4/5 (red: green: blue) showing the physiographic features of Prachuab Khiri Khan area. Note that identification of Cenozoic basins (shown herein as yellow-colour) can be seen easily after the enhancement process.

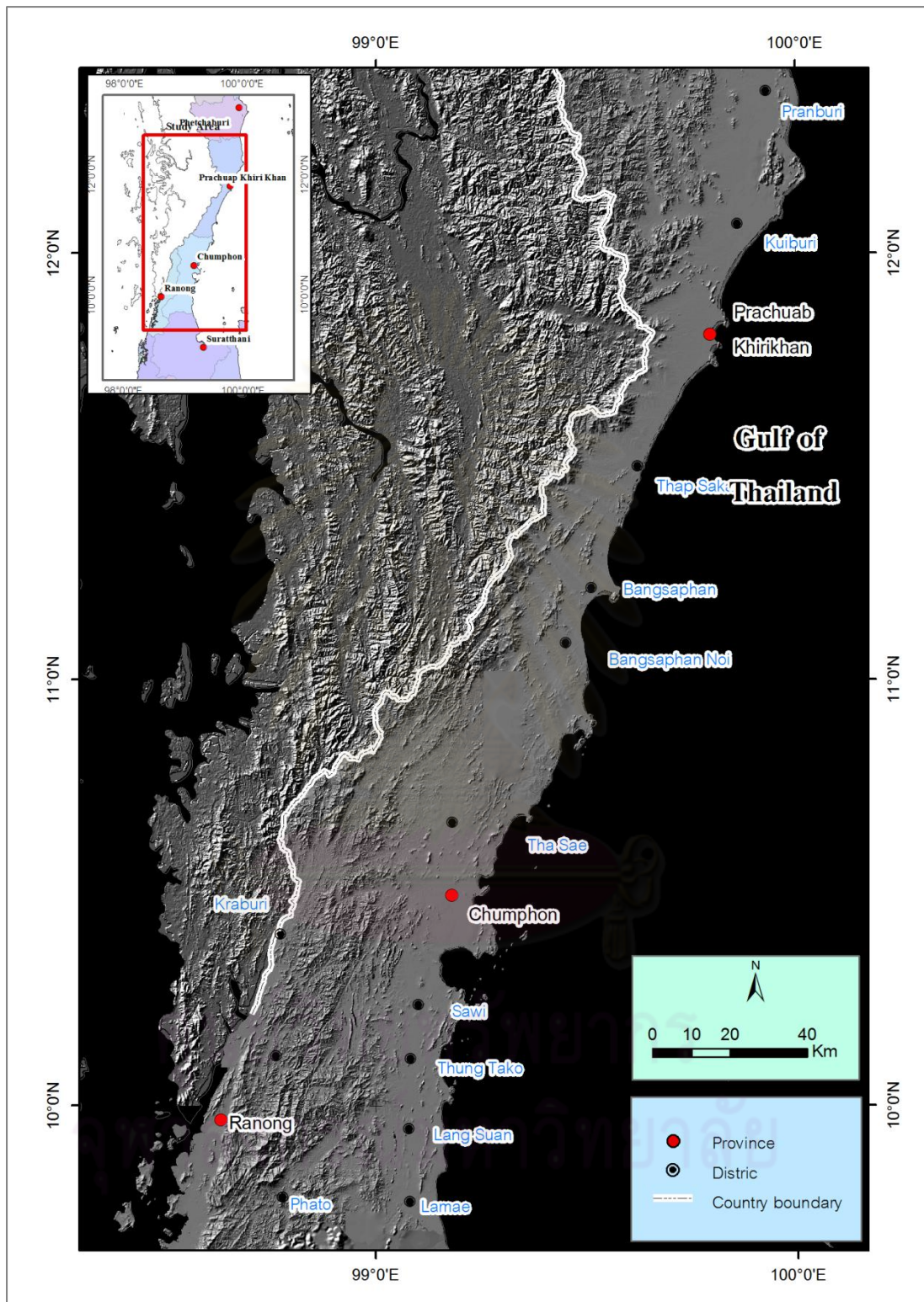


Figure 3.8 Shaded relief image from DEM data showing prominent structures and fracture in study area.

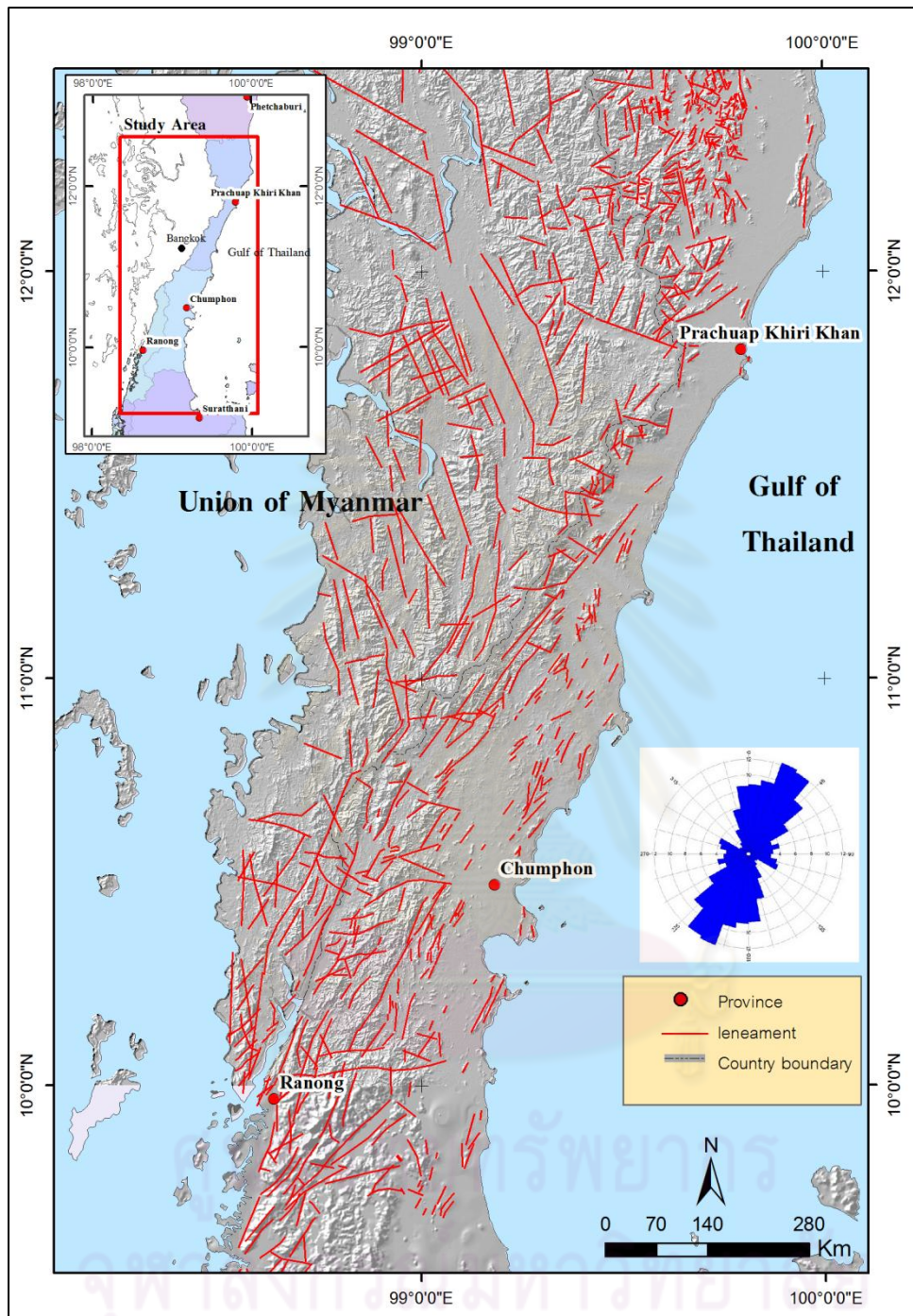


Figure 3.9 Map of the study and regional areas showing orientations and distribution of lineaments. Noted that the NW-SE trending lineament near Prachuab Khirikhan is quite prominent.

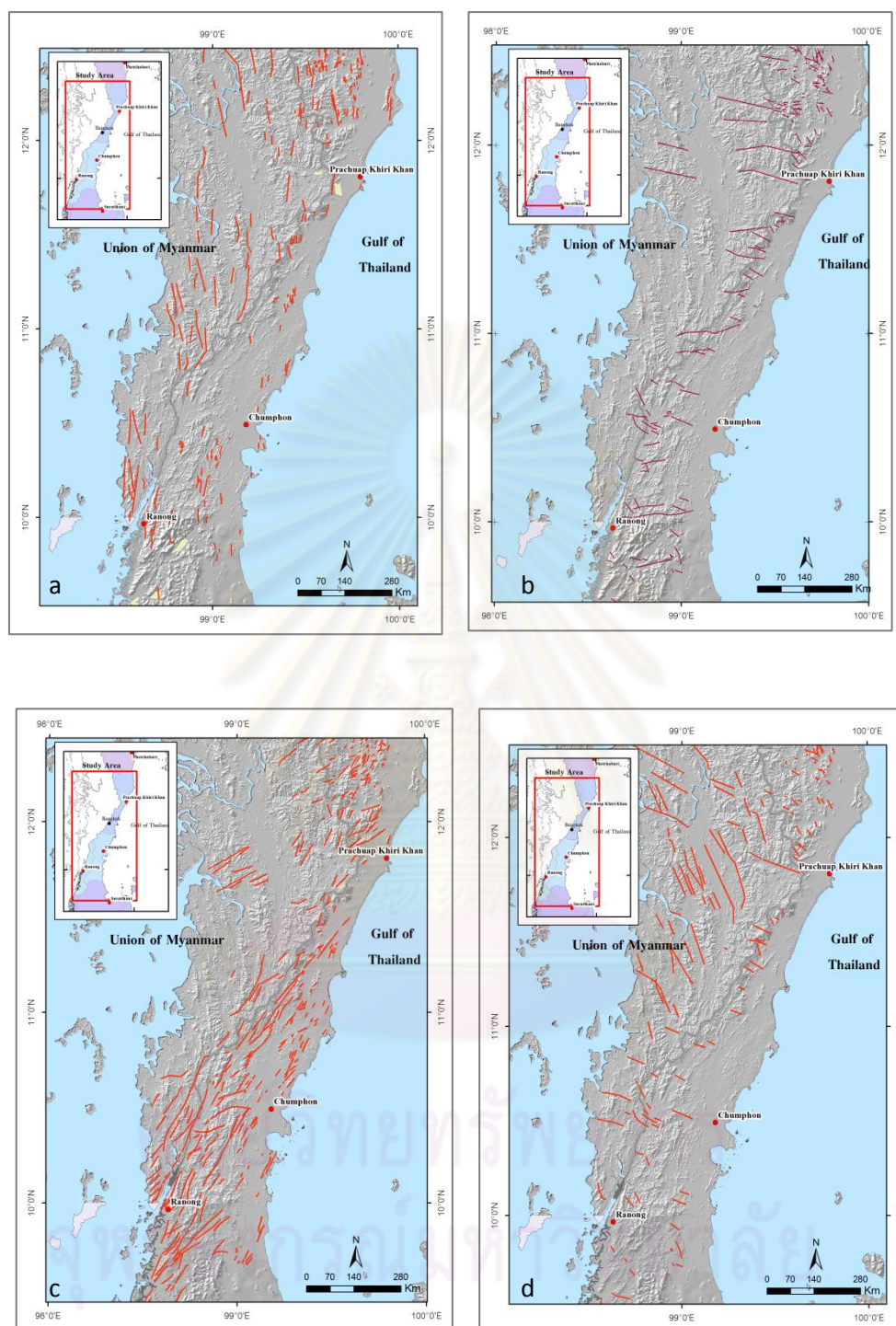


Figure 3.10 Lineament maps after enhancement in the DEM format showing (a) the north-south trend with 158 lineaments, (b) the east-west trend with 60 lineaments, (c) the northeast-southwest trend with 294 lineaments and (d) the northwest-southeast trend with 158 lineaments.

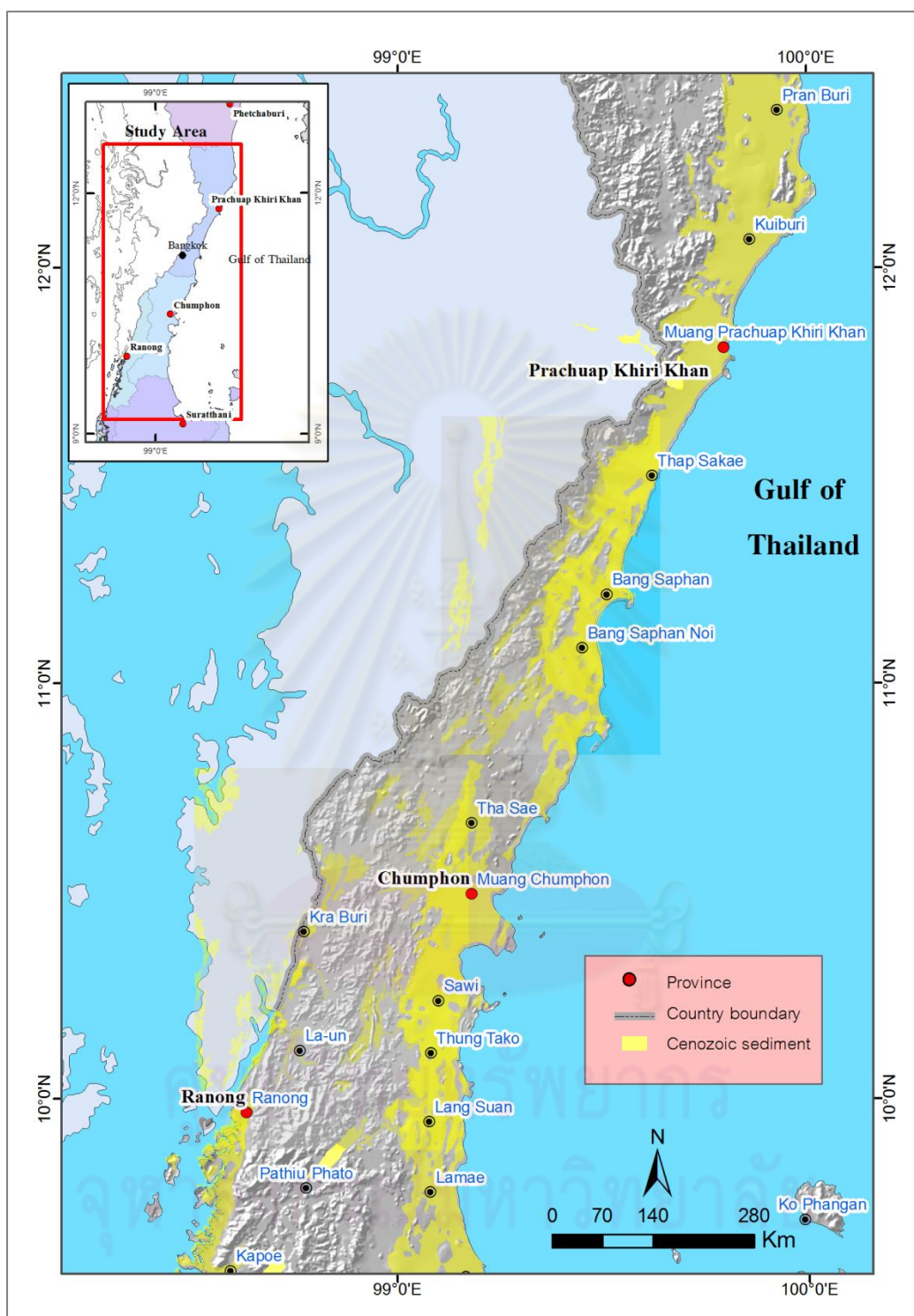


Figure 3.11 Map showing Cenozoic deposits (yellow) after combined data of enhanced Landsat5TM and DEM data. Noted that the Cenozoic basins in the Ranong Province are mainly from DMR (2007).

(Figure 3.10c) and (Figure 3.10d). The total of 602 lineaments were used to construct the rose diagram as shown in Figure 3.9. The result indicates that the northeast – southwest – trending lineaments are much more distinctive.

3.2.2 Sediment basins and boundary

From the interpretation it is suggested that the characteristic of topography in the study area is the prominent mountain range in the west. The mountains lie in the northeast-southwest trend. In the east part of the study area are almost alluvial plain and coastal plain. Sediment layers deposited in basins are alluvium and colluviums, these are quite contrast to the highland or mountains in the west.(Figure 3.11)

3.3 Fault segmentation

3.3.1 Concept of fault segmentation

Concept of fault segmentation is elucidated by the fact that historical surface ruptures triggered by earthquakes along the long faults seldom occurred throughout the entire length, and just only one or two segments became ruptures during large earthquake (McCalpin, 1996). For instance, the San Andreas Fault zone of California was divided into four segments based on difference of historical surface rupture (Allen, 1968). The long fault trace is composed of numerous discrete segments (Segall and Pollard, 1980). The segmentation of fault systems is related to the identification of individual fault segments, based on continuity, character and orientation. It is recommended that a segment can rupture as a unit (Slemmons, 1982). Aki (1984) suggested that the delineation of segments is related to the identification of discontinuities in the fault system. Discontinuity can be divided into two main 75 groups: geometric and inhomogeneous group. Note that this statement has borrowed from seismologists who have used these terms for asperities and barrier. In addition, it is believed that fault may be segmented at a variety of scale that is from a few meters to several tens of kilometers in length (Schwatz, 1989).

All fault segments have their own boundaries. In this study, the segment boundary is a portion of a fault where at least two preferable successive rupture zones have ends (Wheeler, 1989). There are several geomorphic features related to fault boundary or termination. For example, releasing bends and steps, restraining bends, branch and cross-cutting structures, and change in sense of slips are commonly observed at segment termination of strike-slip fault (Knuepfer, 1989). For normal and reverse faults, geomorphic features for definition segment endpoints are not clear (McCalpin, 1996).

Since late 1970s, many workers have found that not all faults have historical rupture records along their fault zone. Thus numbers of criteria have been conducted in order to work on fault segmentation approach, such as geometric, structural, geophysical, and geological criteria. McCalpin (1996) had summarized criteria for fault segmentation into five types (see Table 3.2). According to new criteria of fault segmentation have arisen, one fault has been segmented by various authors depending upon different criteria. For example, the San Andreas Fault was divided into segments by at least four authors (Table 3.3).

In the part of interpretation, detailed geomorphology was used to indicate features associated with active tectonic landforms for strike-slip faulting (Keller and Pinter, 1996). There were several explanation of each tectonic landform associated with active fault as explained below (Figure 3.12)

1) Linear valleys was generated from a transform faulting (strike-slip fault), which controls straight of the stream channels.

(2) Shutter ridge is a long and narrow mound that obstructs stream flow. The shutter ridge effected fault cutting through the hill ridge and appeared the ridge moved out from the originally mountain line, It is common evident of strike-slip fault.

(3) Offset stream which was a result of strike-slip fault by cutting through the stream, effect stream, which originally flow straight line was moved out and distance of movement from the originally stream line can be refered to displacement of fault movement.

(4) Beheaded stream, one of the cause of strike-slip fault, was formed by stream, which appears as a straight line and was cut from originally line. A new stream shows no connection with the main stream.

(5) Fault scarp, the characterized slanting cliff, was caused of fault cut through that area, which can be controlled by both of normal fault and strike-slip fault. Common appear in the topography that showed steep cliff next to the basin and saw in rows a trace moves distinctly.

(6) Sag pond, which was effected from strike-slip fault and caused of subsidence of the land in the area, where fault cut through and filled by parallel fault water pond, normal fault and strike-slip fault can be caused of them.

(7) Spring and hot spring, which generated open gap of fracture subsurface consequence the underground water in that area flows out from subsurface. Somewhere was related to hydrothermal in hot spring form.

(8) Triangular facet, the result of vertical movement of normal fault, was effected by surface erosion until have the look like triangle cliff character.

(9) Bench, the topography landform, that was developed from later triangular facet landform, where happen from normal fault until cause resemble like steps.

(10) Wine glass canyon; effected from normal fault, which cut through a stream channel and continue developed in erosional surface from horizontal erosion changed to vertical erosion. The result of valley that had resemble in wine glass, that is to say, the top of valley rather wide and below part will narrow and deep.

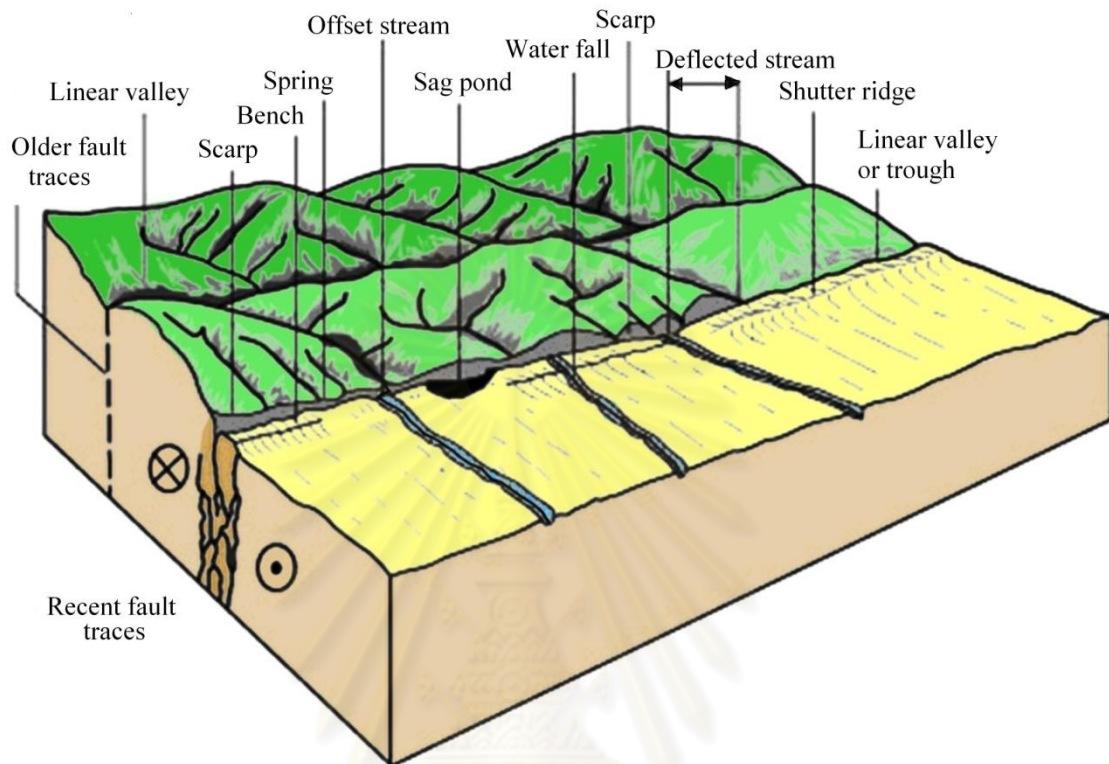


Figure 3.12 Assemblage of landforms associated with active tectonic strike – slip faulting (modified after Keller and Pinter, 1996).

ศูนย์วิทยทรัพยากร
จุฬาลงกรณ์มหาวิทยาลัย

Table 3.2 Types of fault segments and criteria used for active fault segmentation in this study (McCalpin,1996).

Type of Segment ^a	characteristics used to define the segment ^a	Likelihood of being An earthquake segment ^b
1.Earthquake	Historic rupture limits.	By definition, 100% ^c
2.Behavioral	1) Prehistoric rupture limits defined by multiple, well-dated paleoearthquakes. 2) Segment bonded by changes in slip rates, recurrence intervals, elapsed times, sense of displacement, creeping versus locked behavior, fault complexity.	High Mod. (26%)
3.Structural	Segment bounded by fault branches, or intersections with other faults, folds, or cross-structures.	Mod.-High (31%)
4.Geologic	1) Bounded by Quaternary basins or volcanic fields. 2) Restricted to a single basement or geologic terrain. 3) Bounded by geophysical anomalies. 4) Geomorphic indicators such as range-front morphology, crest elevation.	Variable ^d (39%)
5.Geometric	Segments defined by changes in fault orientation, stepovers, separations, or gaps in faulting.	Low-Mod. (18%)

^a Classification following the segment boundary types of dePolo et al. (1989, 1991) and Knuepfer (1989).

^b Percentages = percent of cases where historic ruptures have ended at this type of boundary, as opposed to rupturing through it (Knuepfer, 1989, Table 3).

^c However, restriction of a single historic rupture to the segment does not mean that all future ruptures will be similarly restricted.

^d Small number of observations, accuracy questionable (Knuepfer, 1989, Table 3).

Table 3.3 Fault segment lengths proposed for active fault by various authors (modified after (McCalpin,1996).

Fault name	Type ^a	Number of segments	Total fault length (km)	Mean segment length (km)	Modal segment length (km)	Criteria used for recognition ^b
1. Wasatch fault zone ^c	N	10	343	33	35	B,P,S,G,M
2. NE Basin and Range, >100 km ^c	N	10	-	25	20-35	B,P,S,G,M
3. NE Basin and Range, <100 km ^c	N	20	-	20	10-20	B,P,S,G,M
4. Idaho ^d	N	20	280	22	20-25	B,P,S,G,M
5. North-central Nevada ^e	N	70	-	10	10	M
6. San Andreas ^f	S	4	980	245	15-175?	B,P,S,G,M
6. San Andreas ^g	S	7	980	140	300?	B,P,S,G,M
6. San Andreas ^h	S	784	980	1.2	1	M
6. San Andreas ⁱ	S	68	980	14	12	M
7. San Jacinto ^j	S	20	250	12	10-15	M
8. Elsinore ^k	S	7	337	48	-	M,P
9. Xianshuihe ^l	S	1	220	220	-	M
10. Transverse Ranges ^m	R	-	-	20-30	-	M
11. Oued Fodda, Algeria ⁿ	R	3	32	11	11-12	B,P,S,M

^aN,normal; S,strike-slip; R,reverse.

^bB,behavioral; P,paleiseismic; S,structure; G,geological; M,geometric.

^cMachette et al. (1992a).

^dCrone and Haller (1991).

^eWallace (1989).

^fAllen (1968).

^gWallace (1970).

^hWallace (1973).

ⁱBilham and King (1989).

^jSanders (1989).

^kRockwell (1989).

^lAllen et al. (1989).

^mZiony and Yerkes (1985).

ⁿKing and Yielding (1983).

(11) Parallel ridge, the landform characterized not height hill and there was the wideness more than the length very much. It would be often appearance within 2 parallel fault segments, relative with horizontal fault movement rather than vertical fault movement.

3.3.2 Result of fault segments

In this study we use three criteria for fault segmentation which are structural, geological and geometric applied following those purposed by McCalpin (1996). Previous sections play an important role not only for locating and delineating the fault but also for segmenting fault. Based on the results of fault segmentation integrated with the previous study (Department of Mineral Resource, 2007), the RF can be divided into 19 fault segments see Figures 3.13 and Figure 3.14 shows the overall fault segments. Individual segments are Thap Sakae (11 km), Khao Mun (7 km), Bangsaphan (45 km), Nong Ya plong (44 km), Khoa Khiri Lom (22 km), Khao Deang Noi (22 km), Bangsaphan Noi (28 km), Khao Kwang (28 km), Tha Sae (34 km), Khlong Nam Khoa (50km), Pakjun 20(km), Tha Mai Lai (20 km), Sawi (65 km), Nong Ki (28 km), Laun (54km), Ranong (98 km), Kra buri (65 km), Pato (70 km) and Pathui (32 km). In this study Ranong segment is the longest segment.

(1)Thap Sakae segment commences from Ban Hup Phak and terminates at Ban Rai Noen of Tup Sakae district (Figure3.15). Important morphotectonic features are linear ridge and trigular facets (Figures 3.15a-3.15d). Offset streams show the left lateral movement The trend of the Thap Sakae segment is in the northeast-southwest direction ($N50^{\circ}E$, $S50^{\circ}W$). The total length of this segment is 11 km.

(2) Khao Mun segment segment commences from Ban Khoa Mun in the north of Bangsaphan distric to Khao Taback Prong in the west to of Tup Sakae district (Figure 3.16). The total length of segment is 7 km. Important morphotectonic features are a linear valley and offset stream suggestion shows the left lateral movement (Figures

3.16c-3.16d). The trend of the Khao Mun segment is in the northeast-southwest direction ($N42^{\circ}E$, $S42^{\circ}W$).

(3) Bangsaphan segment starts from Ban Khlong Kum of Bangsaphan district to Ban Morasuop of Tup Sakae district. (Figure 3.17) The total length of segment is 45 km. Important morphotectonic features are offset streams show left lateral movement, linear ridges and trigular facets (Figures 3.17c-3.17f). The trend of the Bangsaphan segment is in the northeast-southwest direction ($N40^{\circ}E$, $S40^{\circ}W$).

(4) Nong Ya Plong segment commences from Thap Sakae district near the town to Ban Neon Kruat of Bangsaphan district (Figure 3.18). The total length of segment is 44 km. Important morphotectonic features are offset streams show left lateral movement, parallel ridge, pressure ridge, linear ridge and trigular facets (Figure 3.18c-3.18h). The trend of the Nong Ya Plong segment is in the northeast-southwest direction ($N40^{\circ}E$, $S40^{\circ}W$).

(5) Khao Khirilom segment commences from Ban Khirilom to Ban Neon Kruat of Bangsaphan district (Figure 3.19). The total length of segment is 22 km. It consists of 2 subsegments including Khao Khirilom -1 in the east (12 km long) and Khao Khirilom in the west (10 km long) Important morphotectonic features are offset streams which show left lateral movement and trigular facets (Figures 3.19c-3.19f). The trend of Khoa Khirilom segment is in the northeast-southwest direction ($N40^{\circ}E$, $S40^{\circ}W$).

(6) Khoa Daeng Noi segment start from the southern of Ban Khirilom to Ban Duang Di of Bangsaphan district (Figure 3.20). The total length of segment is 22 km. Important morphotectonic features are linear valley and trigular facets (Figure 3.20a-3.20b). The trend of the Khoa Dang Noi segment is in the northeast-southwest direction ($N38^{\circ}E$, $S38^{\circ}W$).

(7) Bangsaphan Noi segment start from Amphoe Bangsaphan to Ban Bo Kop of Bangsaphan Noi district. The total length of segment is 28 km. Important morphotectonic feature is offset streams show left lateral movement (Figure 3.21). The trend of the Bangsaphan Noi segment is in the northeast-southwest direction ($N37^{\circ}E$, $S37^{\circ}W$). This segment runs mainly into the unconsolidated deposit.

(8) Khao Kwang segment commences from Ban Yang King Khong southern of Bangsaphan to Ban Thong In of Bangsaphan Noi district (Figure 3.22). The total length of segment is 28 km. Important morphotectonic features are offset streams show left lateral movement, linear ridge, pressure ridge and trigular facets (Figure 3.22c-3.22d). The trend of the Khao Kwang segment is in the northeast-southwest direction ($N37^{\circ}E$, $S37^{\circ}W$).

(9) Tha Sae segment commences from Ban Nong Hoi Khom to Ban Pak Phru of Tha Sae district (Figure 3.23). The total length of segment is 34 km. It consists of 3 subsegments including Tha Sae -1 which is the upper lineament (18 km long), Tha Sae -2 is the middle line (14 km long) and Tha Sae -3 is the lower line (11 km long) Important morphotectonic features are offset streams show left lateral movement, trigular facets, parallel ridge and linear valley (Figures 3.23c-3.23d). The trend of Tha Sae segment is in the northeast-southwest direction ($N42^{\circ}E$, $S42^{\circ}W$).

(10) Khlong Nam Khoa segment start from Ban Kuan Din Deang of Tha Sae to Ban Tup Lee of Kraburi district (Figure 3.24). The total length of segment is 50 km. Important morphotectonic features are offset streams show left lateral movement and trigular facets (Figures 3.24c-3.24e). The trend of the Khlong Nam Khoa segment is in the northeast-southwest direction ($N26^{\circ}E$, $S26^{\circ}W$).

(11) Pak Jun segment commences from Ban Chan Thueng of Tha Sae district to Ban Plai Khlong Wan of Kraburi district (Figure 3.25). The total length of segment is 20

km. It consists of 3 subsegments including Pak Jun -1 which is the east line (12 km long), Pak Jun-2 is the west line(4.5 km long) and Pak Jun -3 is the lower line (6.5 km long) Important morphotectonic features are offset streams show left lateral movement, linear valley, pressure ridge and trigular facets (Figure 3.25c-3.25d). The trend of Pak Jun segment is in the northeast-southwest direction ($N68^{\circ}E$, $S68^{\circ}W$).

(12) Tha Mai Lai segment start from Ban Na Sae of Tha Sae to Ban Tup Lee of Kraburi district (Figure 3.26). The total length of segment is 20 km. Important morphotectonic features are linear valley and trigular facets (Figures 3.26a-3.26c). The trend of the Tha Mai Lai segment is in the northeast-southwest direction ($N67^{\circ}E$, $S67^{\circ}W$).

(13) Sawi segment start from Ban Tha Mapring of Chumphon district to Ban Khun Luang Ya of Laun district (Figure 3.27). The total length of segment is 65 km. Important morphotectonic features are offset streams, linear valley, parallel ridge and trigular facets (Figures 3.27c-3.27e). The trend of the Sawi segment is in the northeast-southwest direction ($N30^{\circ}E$, $S30^{\circ}W$).

(14) Nong Ki segment commences from Ban Pho Thong of Sawi district to Khlong Nek of Laun district (Figure 3.28). The total length of segment is 28 km. Important morphotectonic features are offset streams show left lateral movement, linear valley, parallel ridge and trigular facets(Figures 3.28c-3.28h). The trend of the Nong Ki segment is in the northeast-southwest direction ($N25^{\circ}E$, $S25^{\circ}W$).

(15) Laun segment commences from Ban Phrack Sai of Kraburi district to Khlong Mai Pai of Muang Ranong (Figure 3.29). The total length of segment is 54km. It consists of 4 subsegments including Laun -1 which in the northern part of segment (35.5 km long), Laun -2 is the middle line(8 km long), Laun -3 is the middle line(7 km long and Laun -4 is the lower line (24 km long) Important morphotectonic features are linear valley and trigular facets (Figures 3.29a-3.29c). The trend of Laun segment is in the

northeast-southwest direction ($N24^{\circ}E$, $S24^{\circ}W$). This segment lies almost at boundary between granite rock and unconsolidated deposit.

(16) Ranong segment commences from Ban Thap Chak of Laun district to Sook Sumran district (Figure 3.30). The total length of segment is 98km. It consists of 9 subsegments. The shortest subsegment is about 3 km at Ban Sai Dang of Laun district and the longest subsegment is about 38 km from Ban Hin Chang to Ban Hat Sai Dum of Ranong district. Important morphotectonic features are parallel ridge, offset streams and trigular facets (Figures 3.30c-3.30e). The trend of Ranong segment is in the northeast-southwest direction ($N18^{\circ}E$, $S18^{\circ}W$).

(17) Kraburi segment commences from Ban Rang Taen of Kraburi district to Ban Salam in Myanmar (Figure 3.31). The total length of segment is 65km. Important morphotectonic features are offset streams and trigular facets. The trend of Kraburi segment is in the northeast-southwest direction ($N24^{\circ}E$, $S24^{\circ}W$).

(18) Pato segment commences from Ban Pak Nam Tako of Tung Tako district to Ban Chi Mi of Kapoe district (Figure 3.32). The total length of segment is 70km. Important morphotectonic features are offset streams and trigular facets. The trend of Pato segment is in the northeast-southwest direction ($N47^{\circ}E$, $S47^{\circ}W$).

(19) Pathui segment commences from Ban Thon Phong of Tung Tako district to Ban Hang Kae of Kapoe district (Figure 3.33). The total length of segment is 32km. Important morphotectonic features are offset streams (Figures 3.33c-3.33f) and trigular facets. The trend of Pato segment is in the northeast-southwest direction ($N48^{\circ}E$, $S48^{\circ}W$).

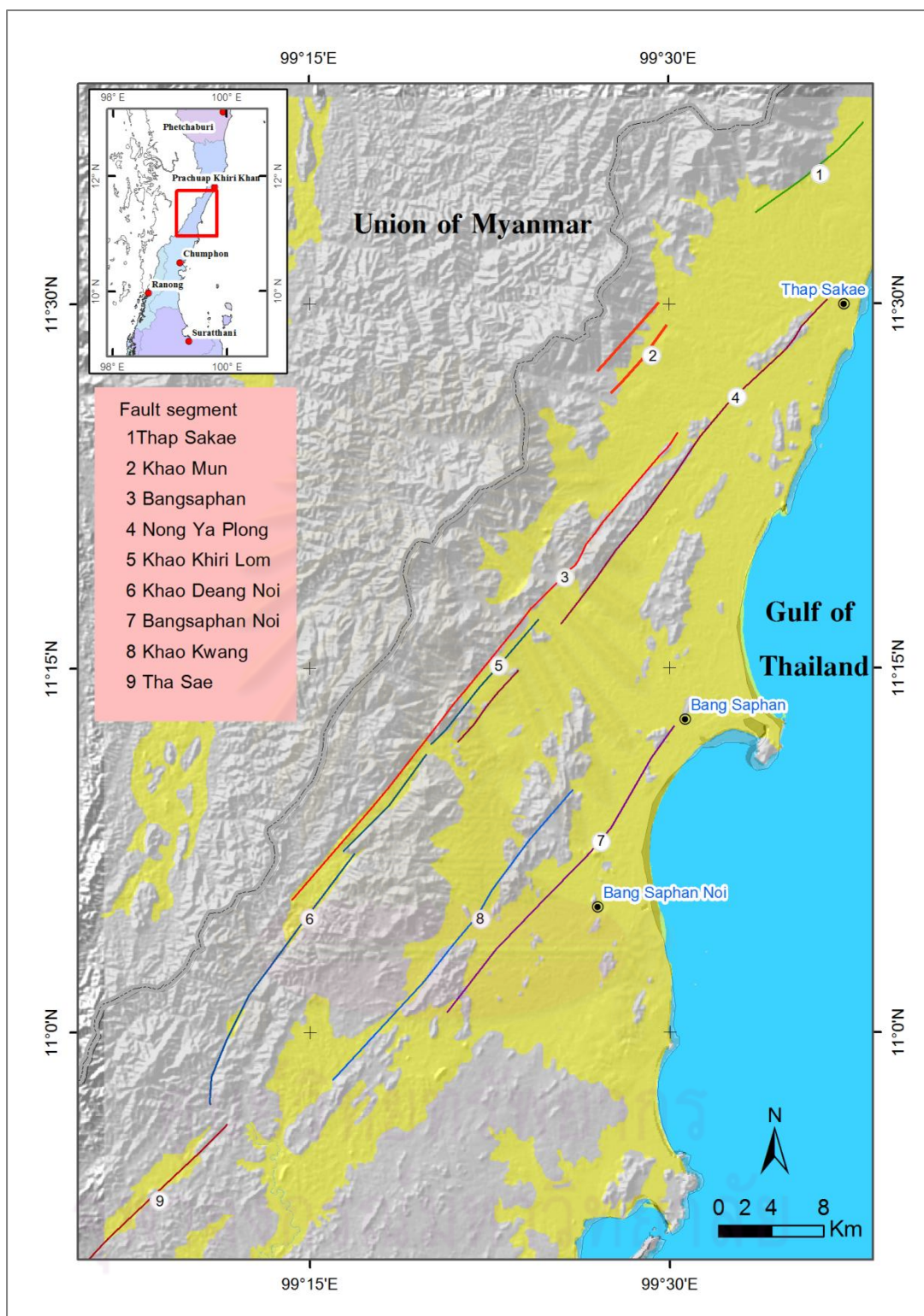


Figure 3.13 Active fault segments of the northern part of RNF in Prachuab-Khiri Khan area based on result of remote sensing interpretation and geomorphology. (Yellow color = Cenozoic deposits and grey colour = hard rocks).

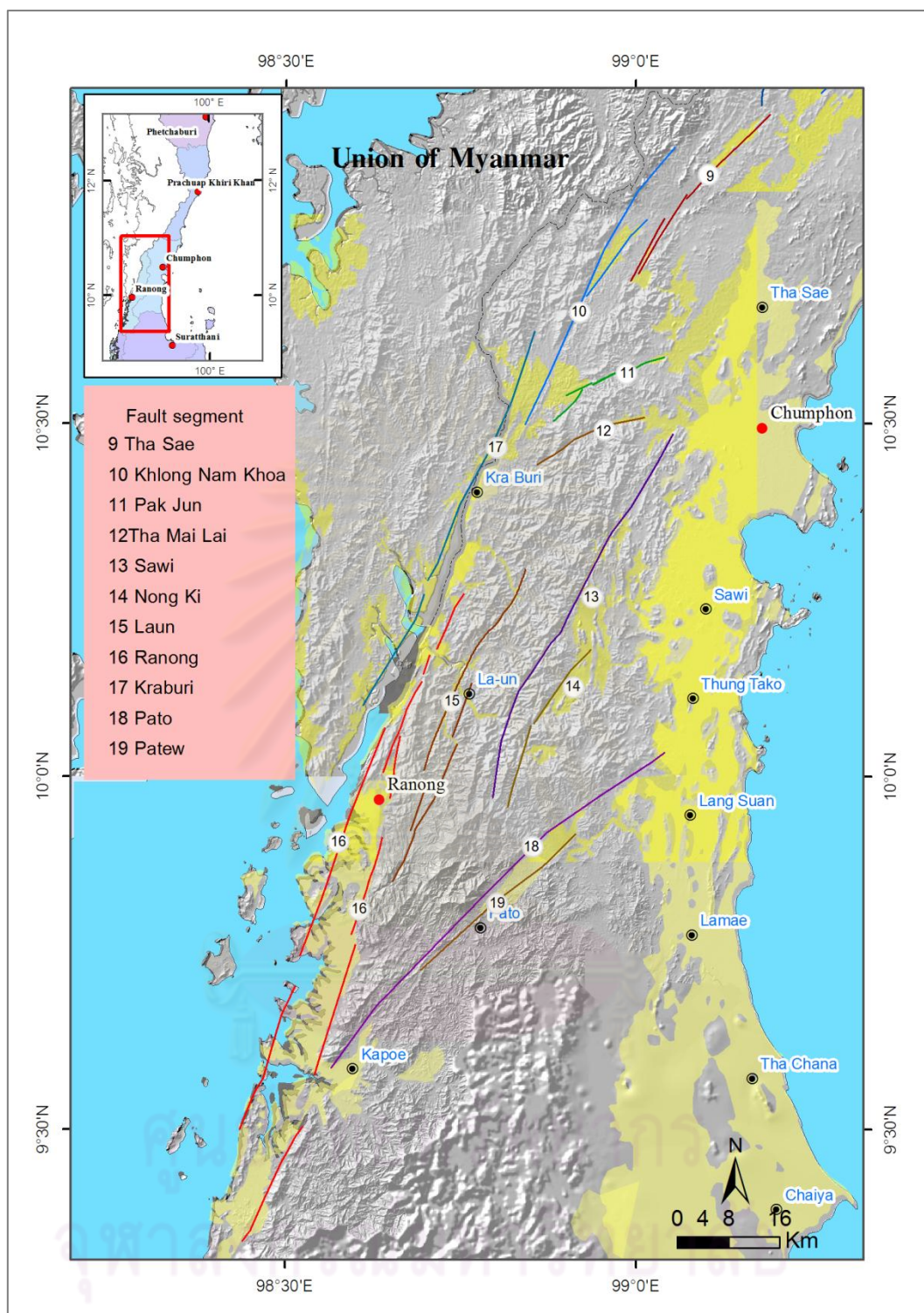


Figure 3.14 Active fault segments of the southern part of RNF in Chumphon and Ranong area base on result of remote sensing interpretation and geomorphology. (Yellow color = Cenozoic deposits and grey colour = hard rocks). Noted that the Cenozoic basins in the Ranong Province area mainly from DMR (2007).

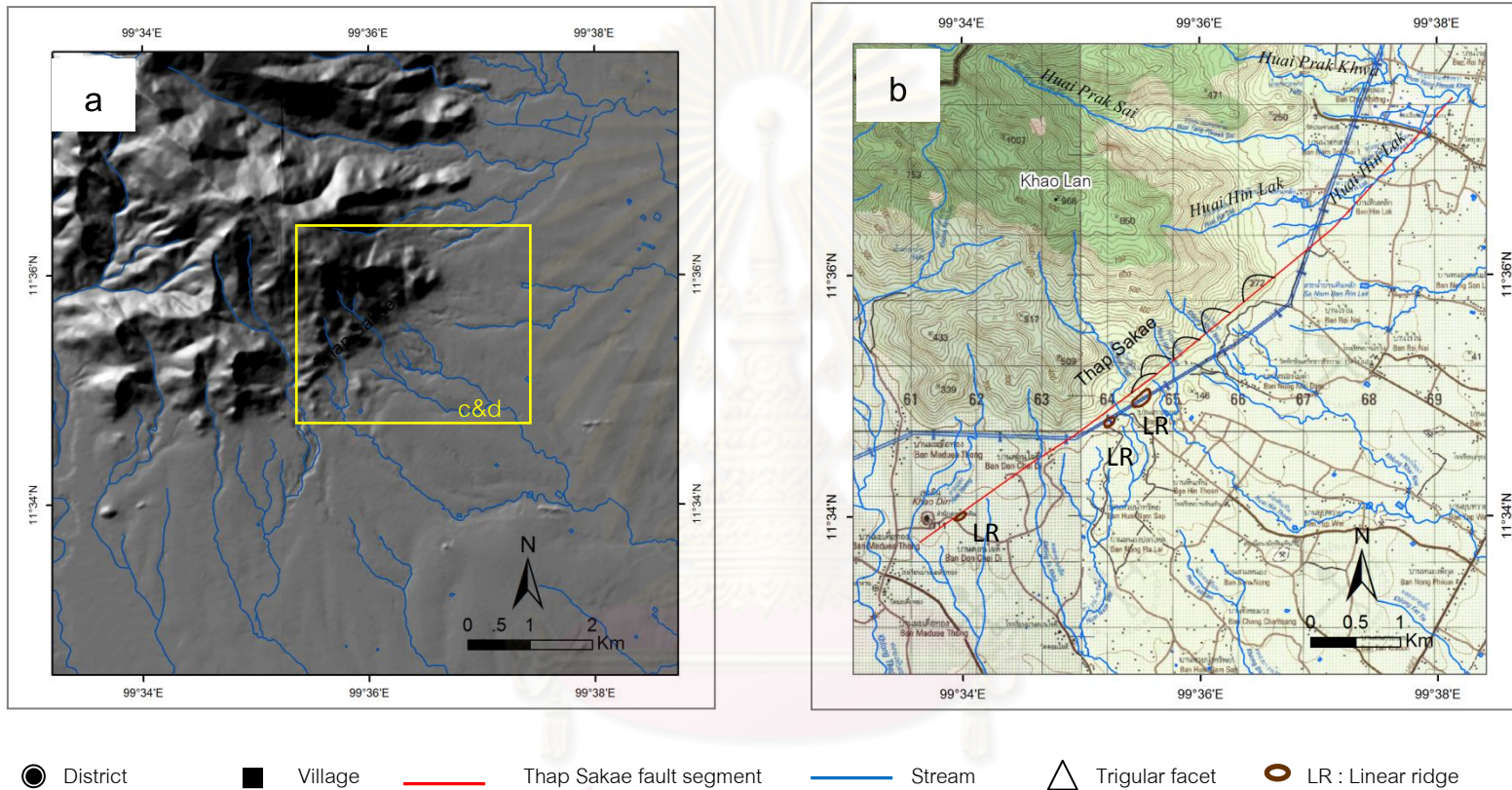


Figure 3.15 (a) 2m contour interval DEM image and (b) topographic map showing orientation and evidence of Thap Sakae segment.

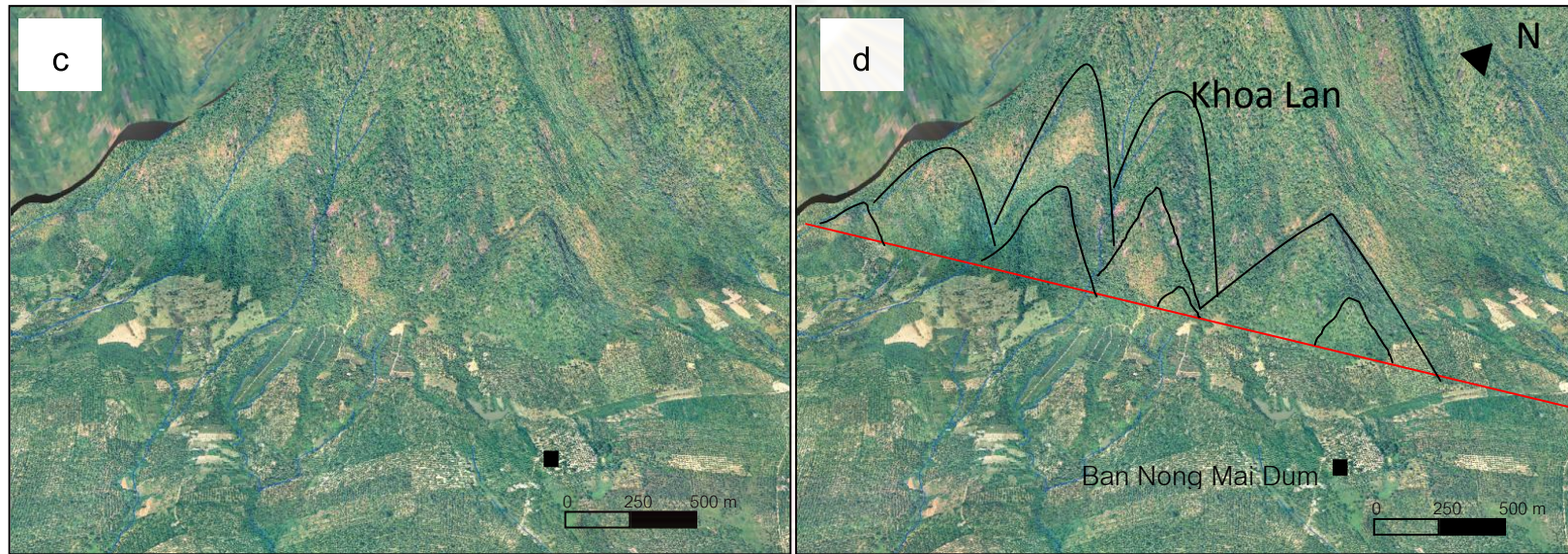
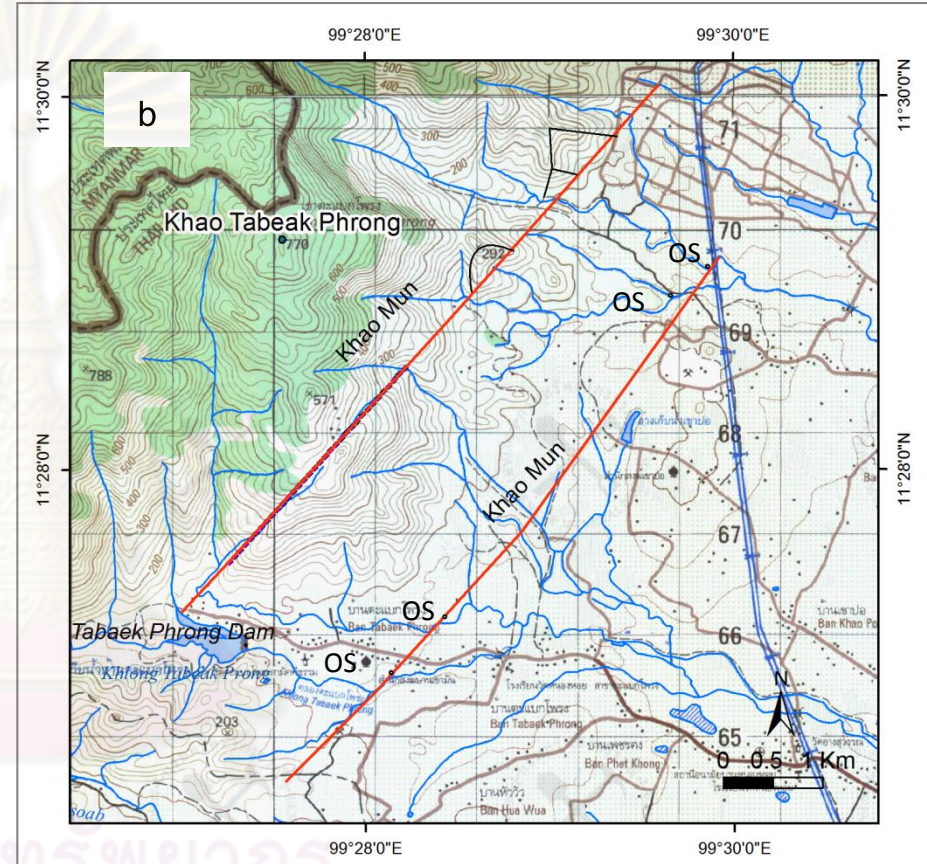
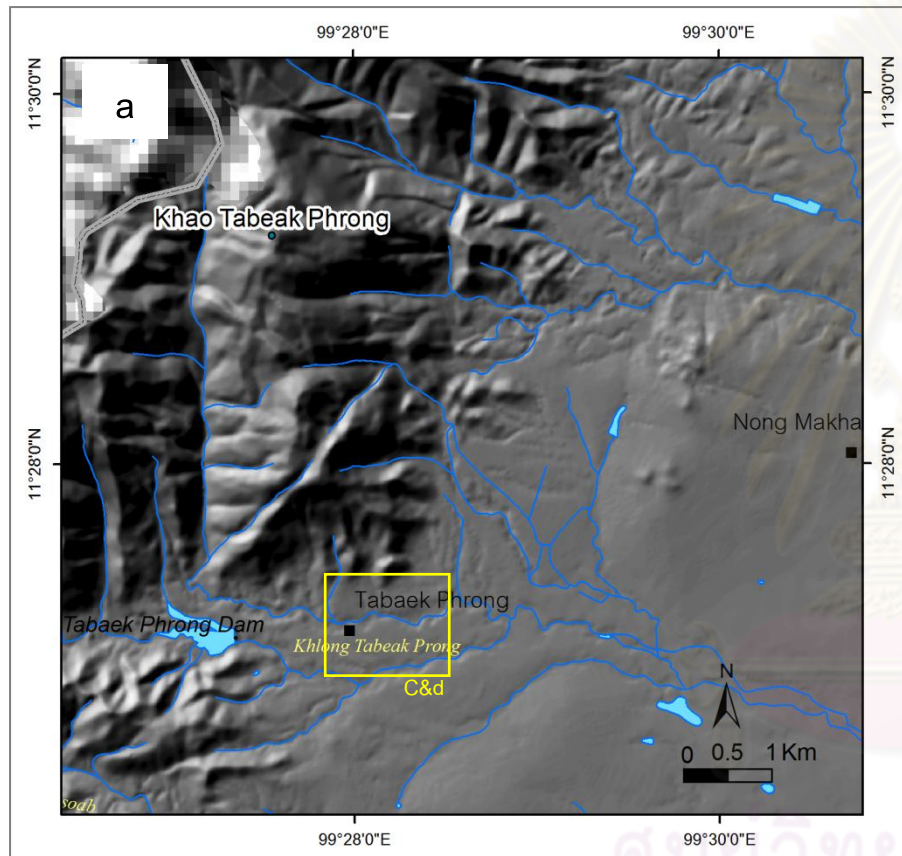


Figure 3.15 (Cont.) Enlarged image data (Fig. 3.16a) of Thap Sakae fault segment shown as color orthographic image (c) and sketch image (d) showing fault orientation and two series of trigular facets.



Village
 Khao Mun fault segment
 Stream
 OS Offset stream
 Trigular facet
 LV Linear valley

Figure 3.16 (a) 2m contour interval DEM image and (b) topographic map showing the orientation and evidence of Khao Mun segment of the northern part of RNF. Note that a series of offset streams, trigular facets and linear valley.

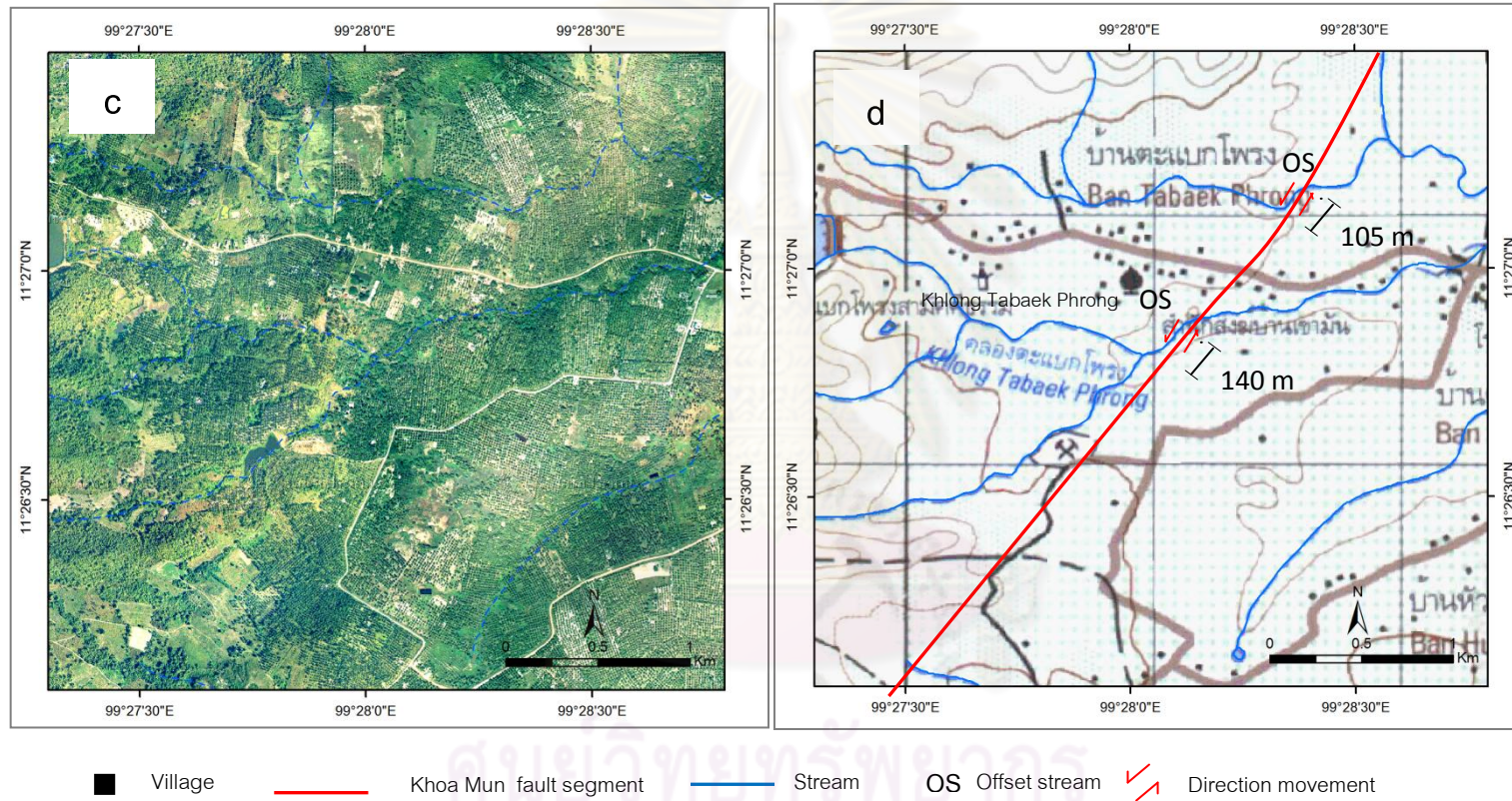


Figure 3.16 (Cont.) Enlarged image data (Fig.3.16a) of Khoa Mun segment showing (c) colour-ortho photographic image and (d) topographic map with showing offset streams (OS) with the left lateral displacement .

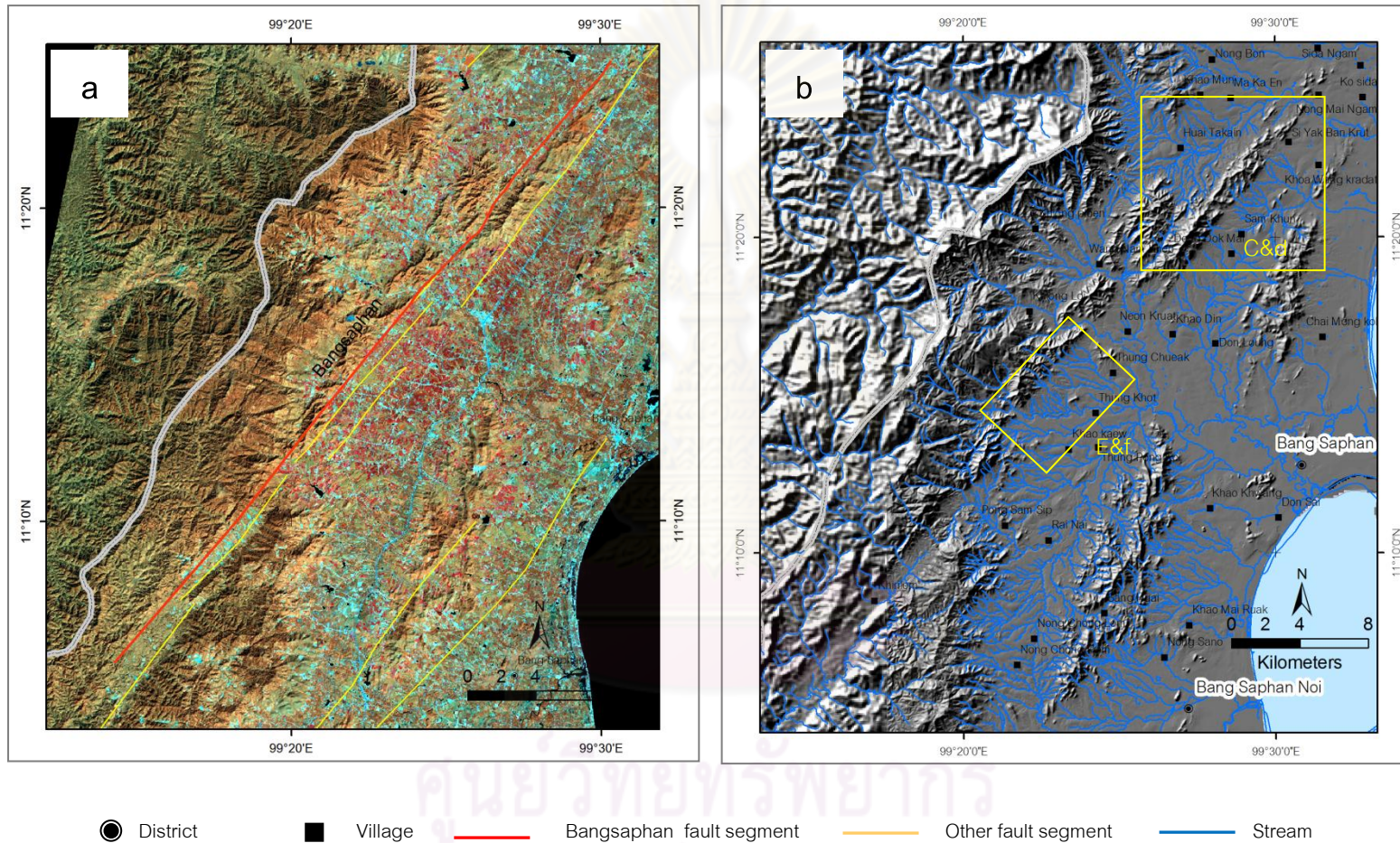
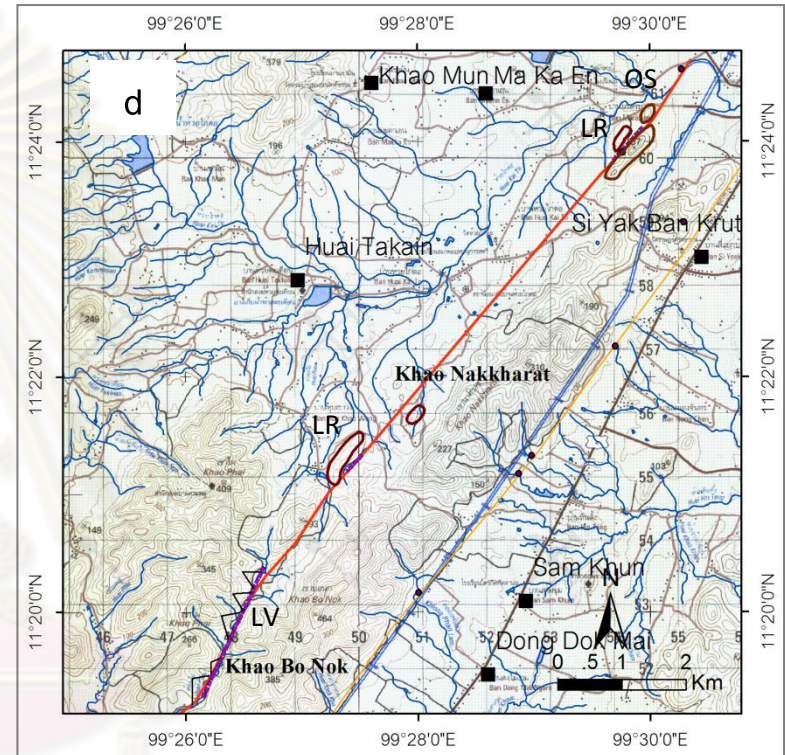
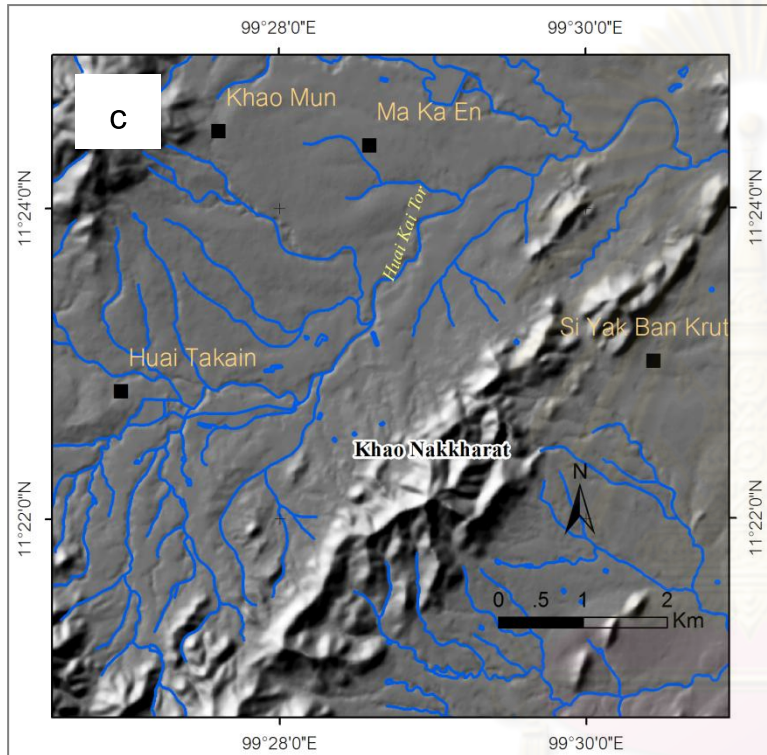
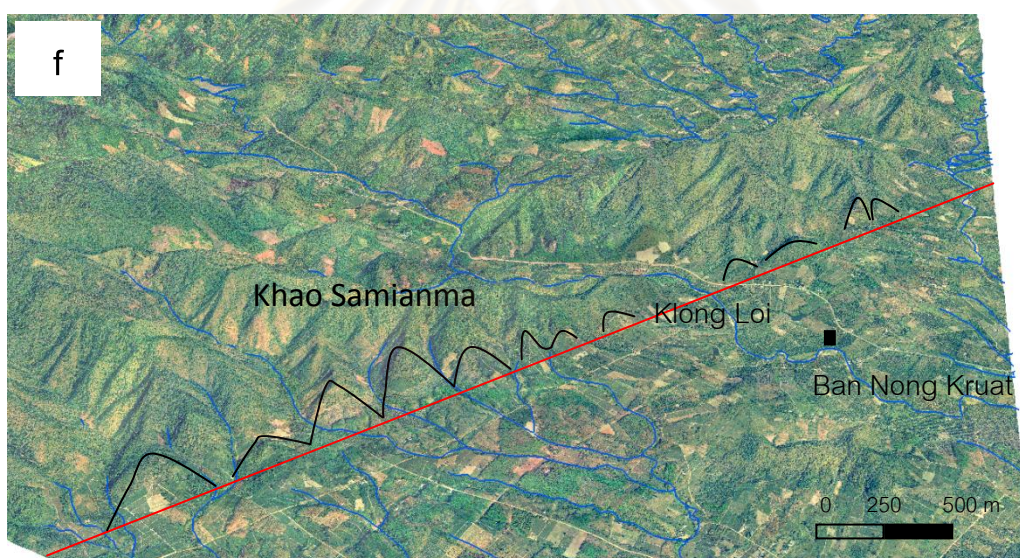
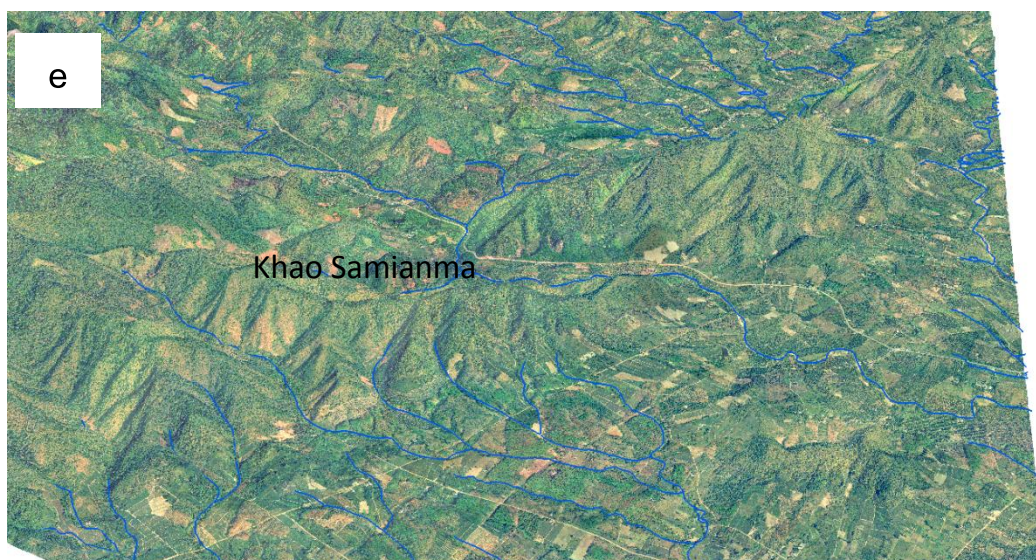


Figure 3.17 Landsat and (a) 2m contour interval DEM image (b) showing the orientation of the Bangsaphan segment in the northern part of RNF.



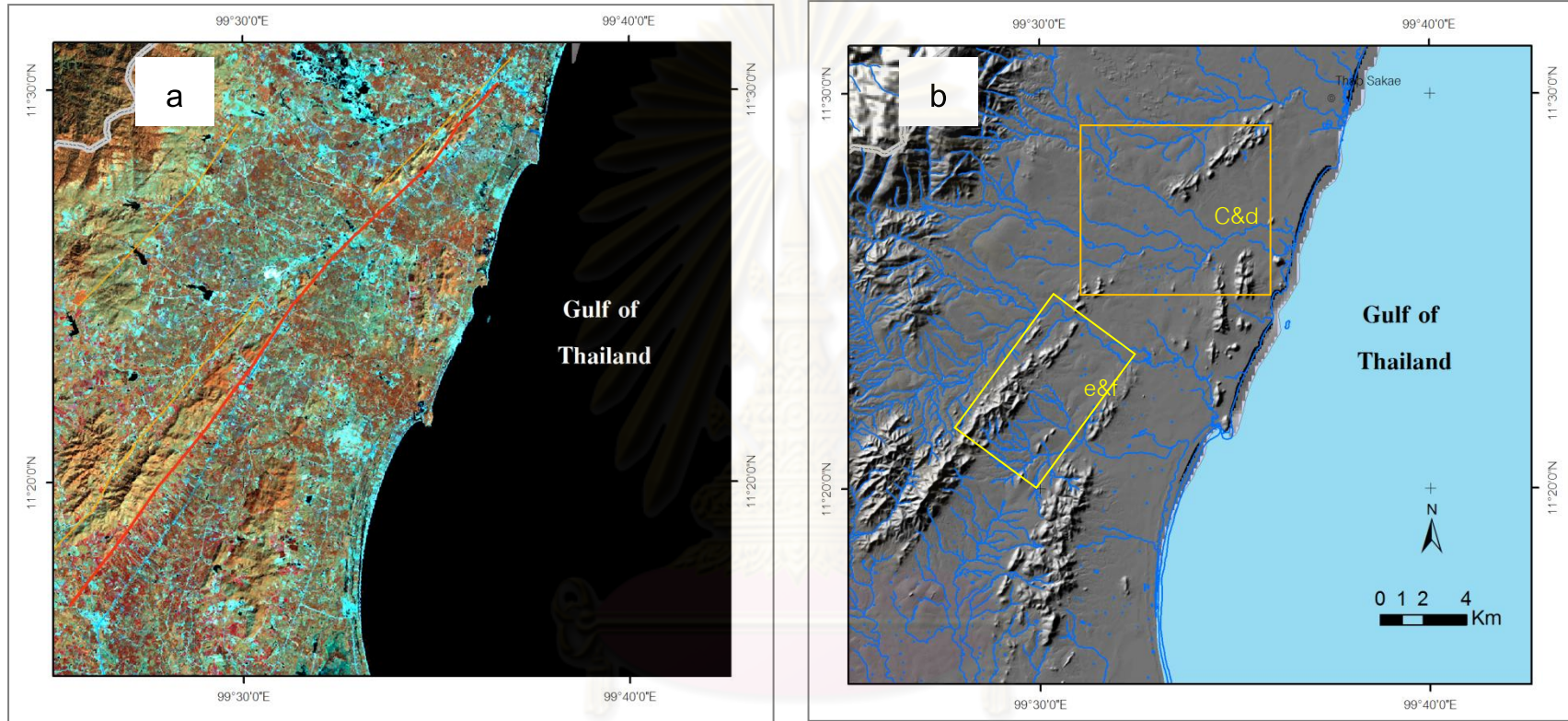
- Village
- (red line) — Bansaphan fault segment
- (blue line) — Stream
- OS Offset stream
- △ Trigular facet
- (dotted purple line) — LV Linear valley
- (brown oval) — Linear ridge

Figure 3.17 (Cont.) Enlarged of Bansaphan segment (Fig.3.18b) appear as aerial photographic image (c) and DEM data (d) showing offset stream, a series of trigular facets ,linear valley and linear ridge.



Village
 Bangsaphan fault segment
 Stream
 Trigular facet

Figure 3.17 (Cont.) Aerial photographic image (e) and topographic map (f) with interpreted series of triangular facet at Khao Samianma.



District
 Village
 Nong Ya Plong fault segment
 Other fault segment
 Stream

Figure 3.18 Landsat image (a) and 2m contour interval DEM image (b) showing orientation of the Nong Ya Plong segment in the northern part of RNF.

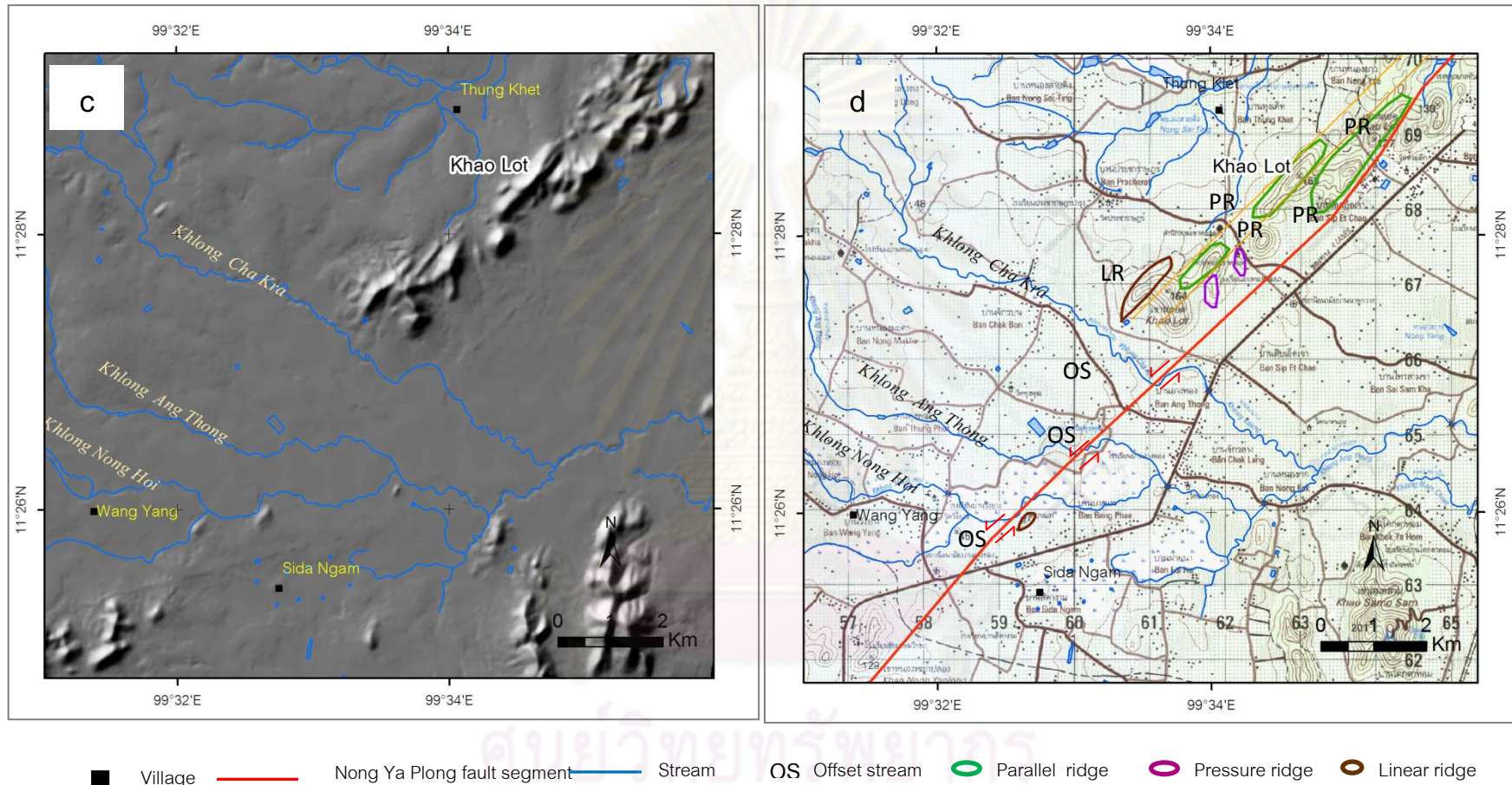
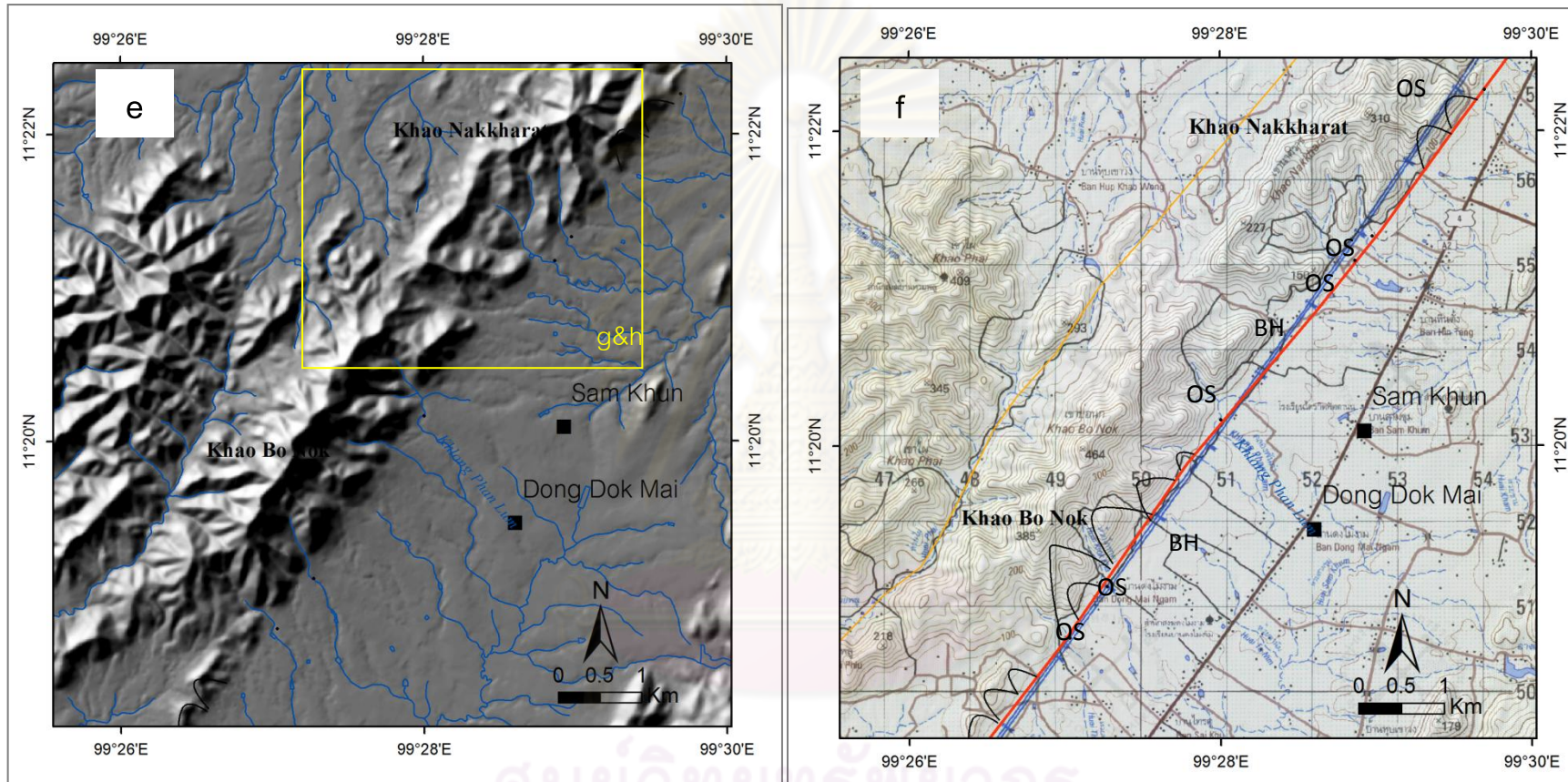
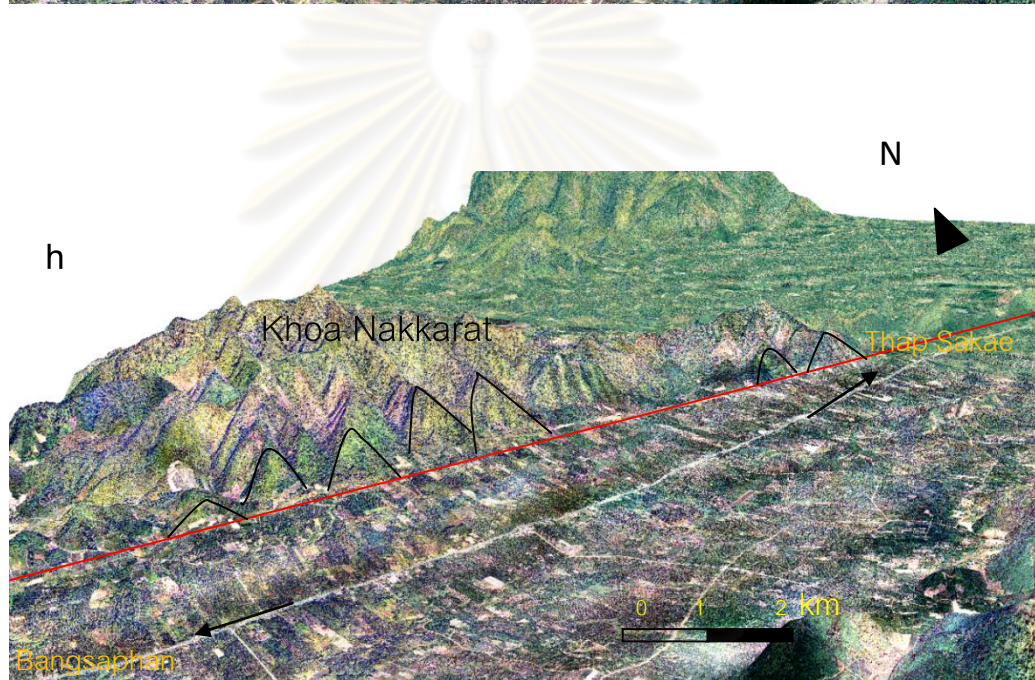
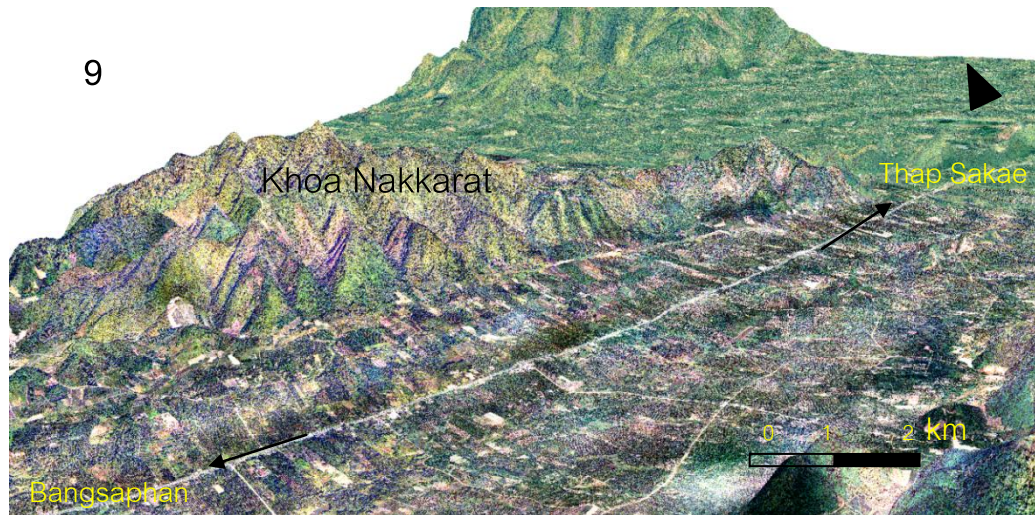


Figure 3.18 (Cont.) Active fault evidence of Nong Ya Plong fault segment (enlarged from figure 3.18 b) (c) DEM data and (d) topographic map showing a series of offset stream, parallel ridge, pressure ridge and linear ridge, suggesting the sinistral sense of movement.



Village
 Nong Ya Plong fault segment
 Other fault segment
 Stream
 OS Offset stream
 Trigular facet
 BH Beheaded stream

Figure 3.18 (Cont.) (e) DEM 2m interval and (f) topographic map with interpreted beheaded stream (BH) and offset streams as well as a series of triangular facets (h). Noted that the electric power line was constructed following the Nong Ya Plong segment.



Village
 Nong Ya Plong
 Stream
 Offset stream
 Trigular facet

Figure 3.18 (Cont) The 3D image data of the Nong Ya Plong segment (g) with this study interpretation (h) showing a series of trigular facets in Khoa Nakkarat area.

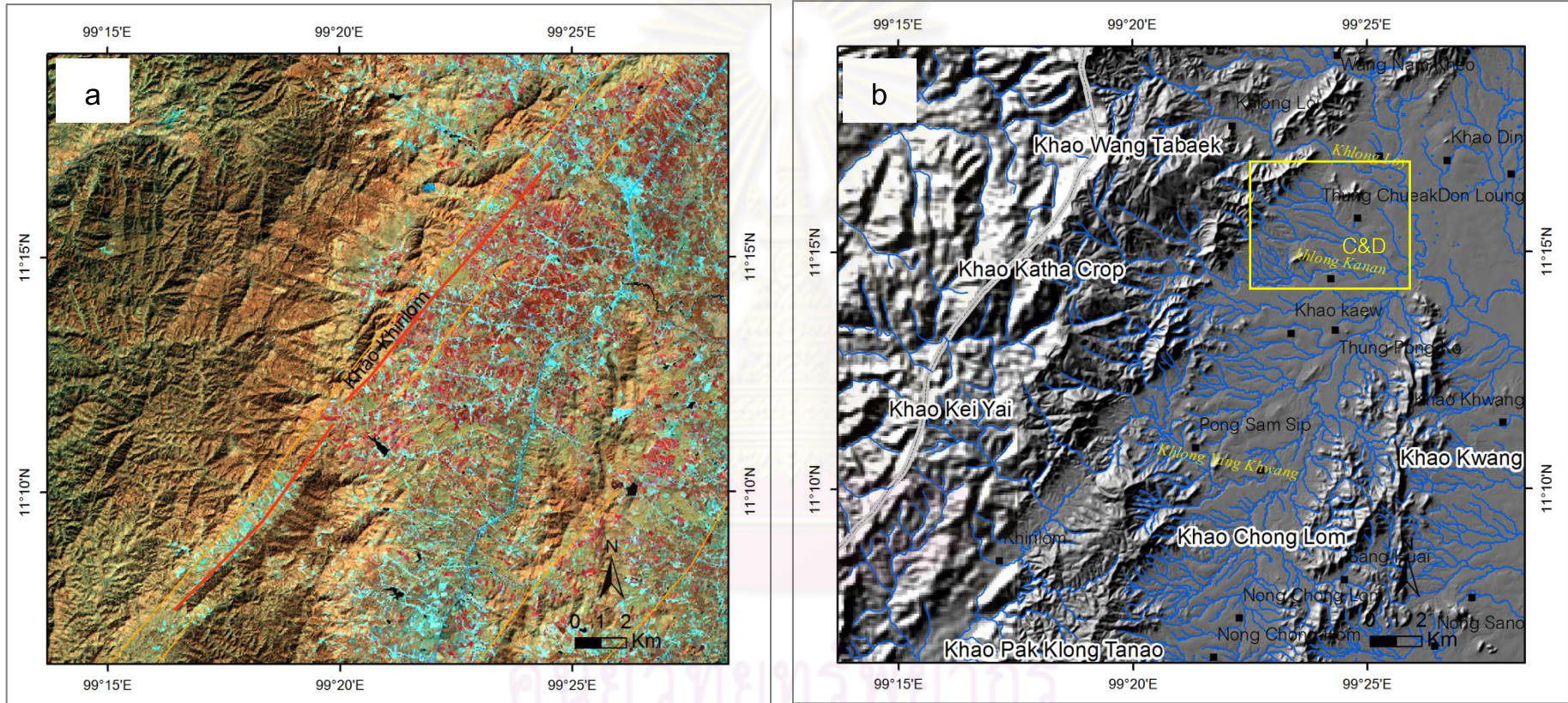
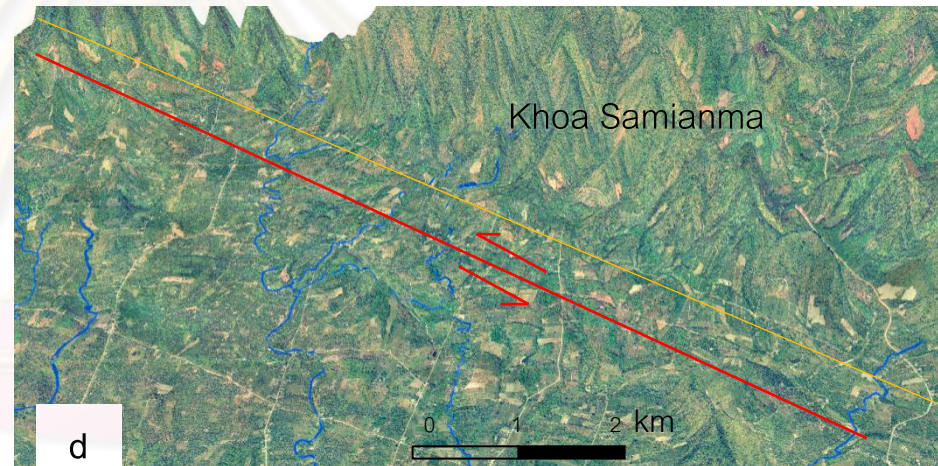
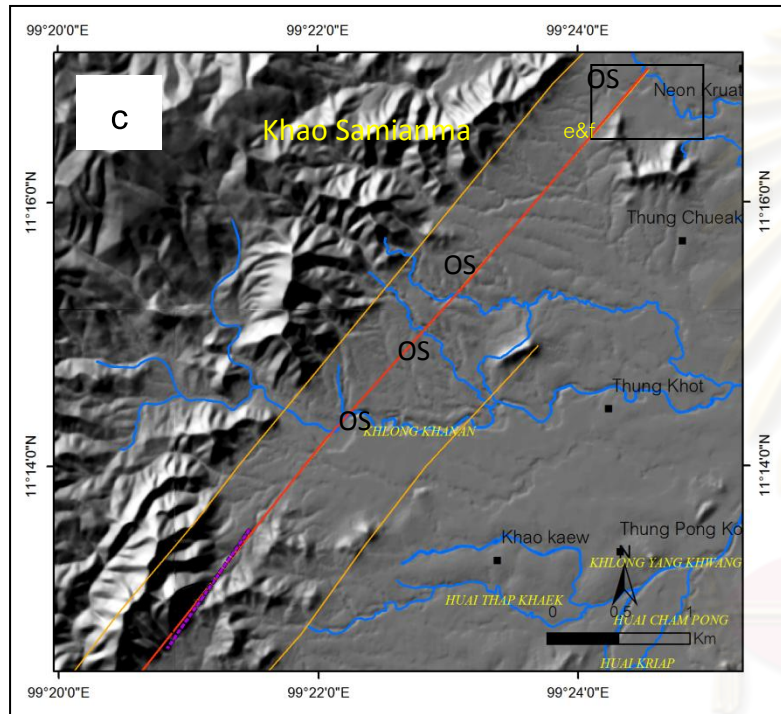
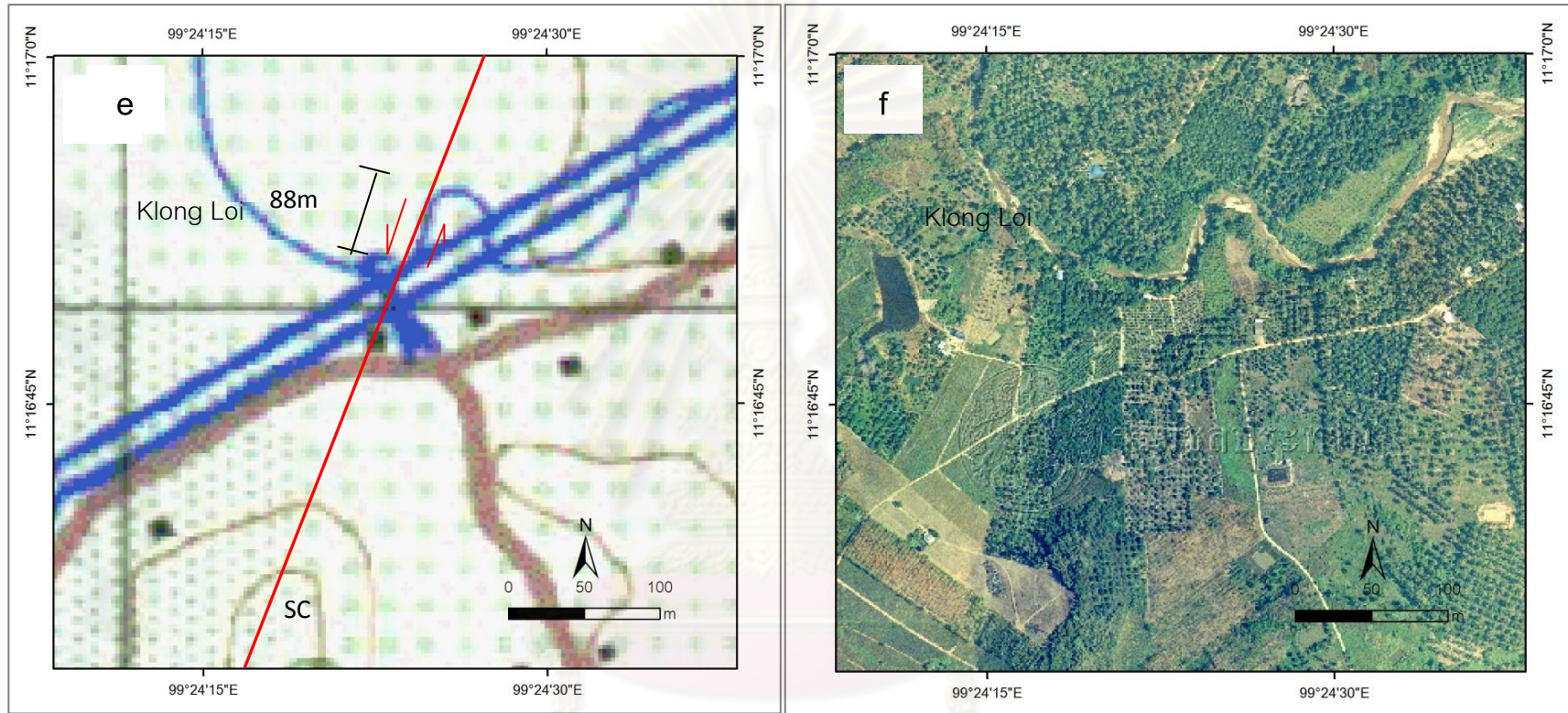


Figure 3.19 Landsat image (a) and 2m contour interval DEM image (b) showing Khao Khirilom segment in the central of RNF.



- Village
- Khao Khirilom fault segment
- Bangsaphan fault segment
- Stream
- OS Offset stream
- △ Trigular facet
- LV Linear valley

Figure 3.19 (Cont.) Enlarged DEM image (c) from northern part of the Khao khirilom segment (figure 3.19 b) showing offset streams (OS) with the left lateral displacement, linear valley in 3D colour-orthographic image (d).



Village
 Khao Khirilom fault segment
 Stream
 OS Offset stream
 Direction movement
 Parallel ridge
 SC Scarplet

Figure 3.19 (Cont.) Active fault evidence enlarged of Khao Khirilom fault segment (figure 3.19c) from colour-ortho photographic image (e) showing offset streams (OS) with the left lateral displacement interpreted in this study (f).

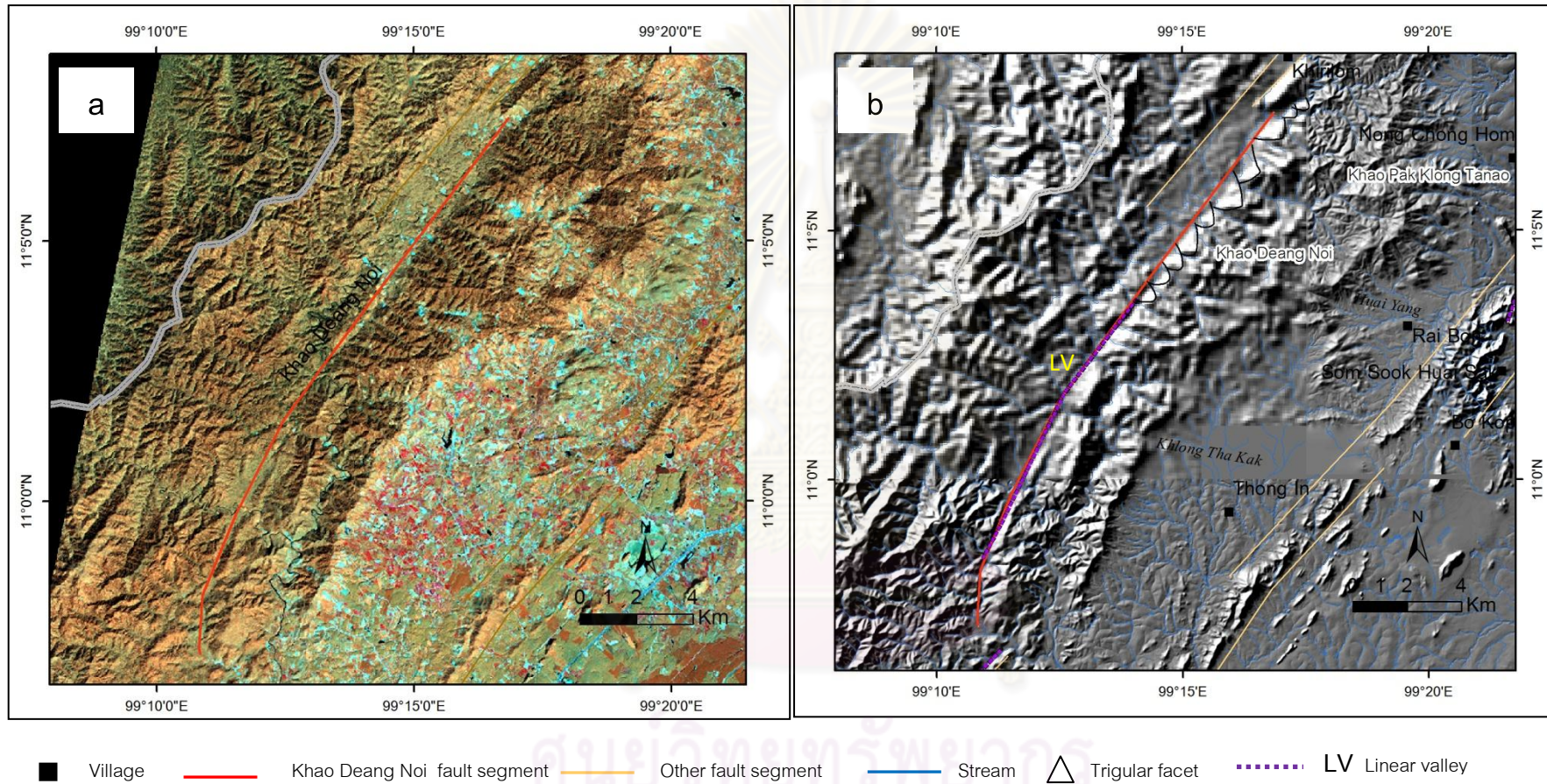


Figure 3.20 Landsat map (a) and 2m contour interval DEM (b) showing the orientation and active fault evidence of Khao Deang Noi fault segment from such as a series of trigular facets and linear valley.

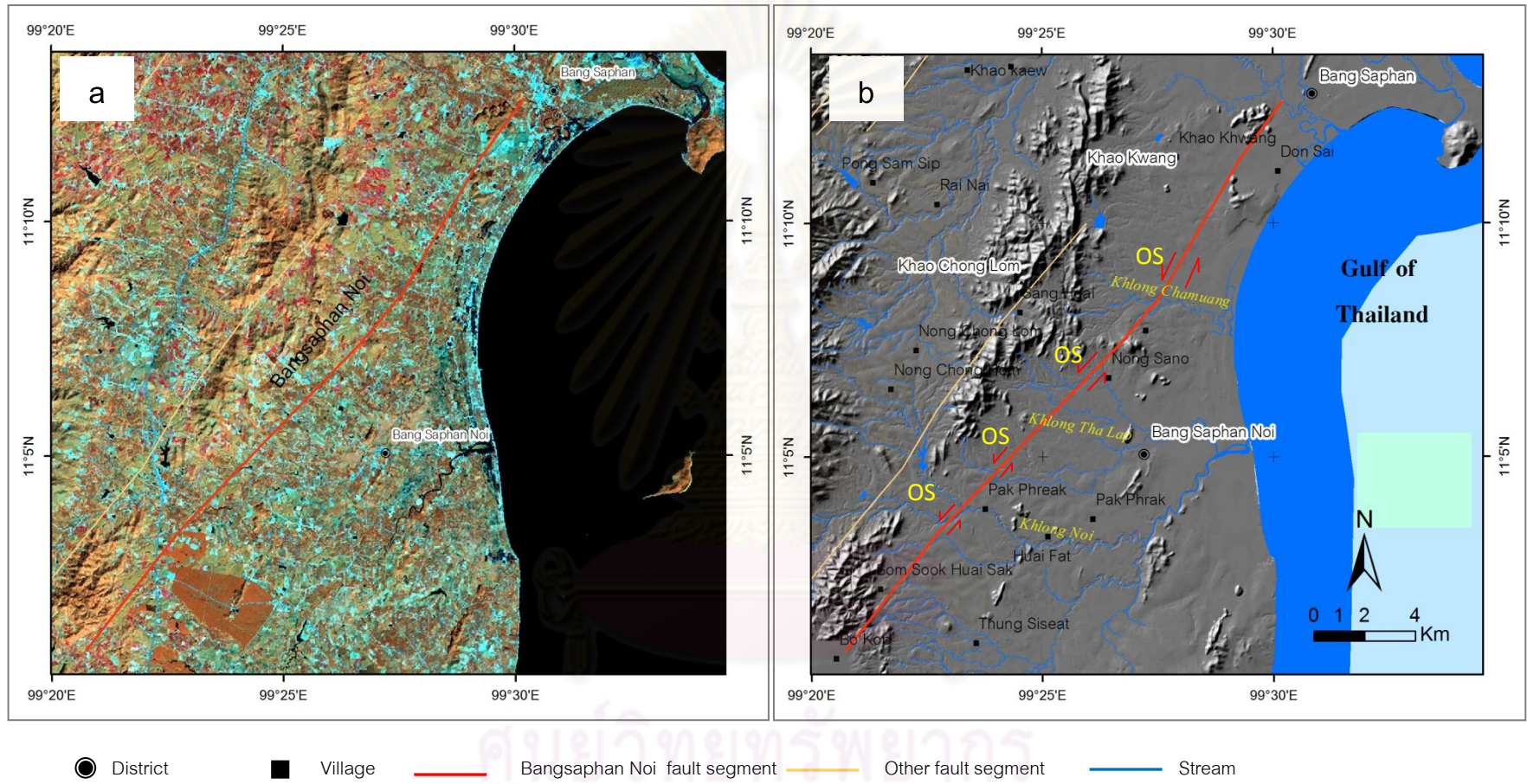
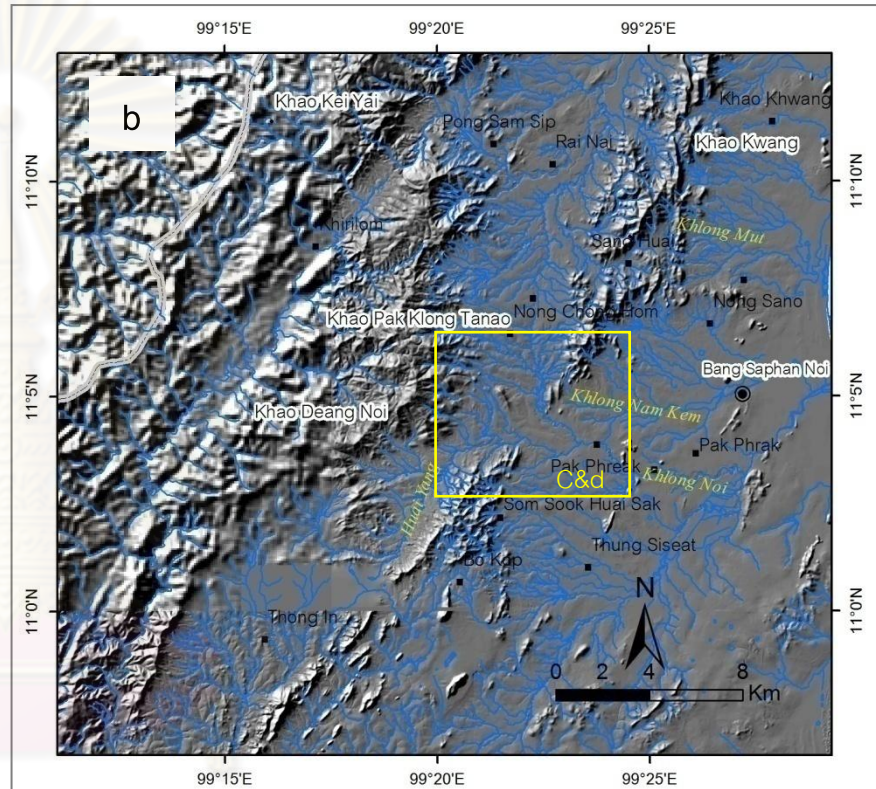
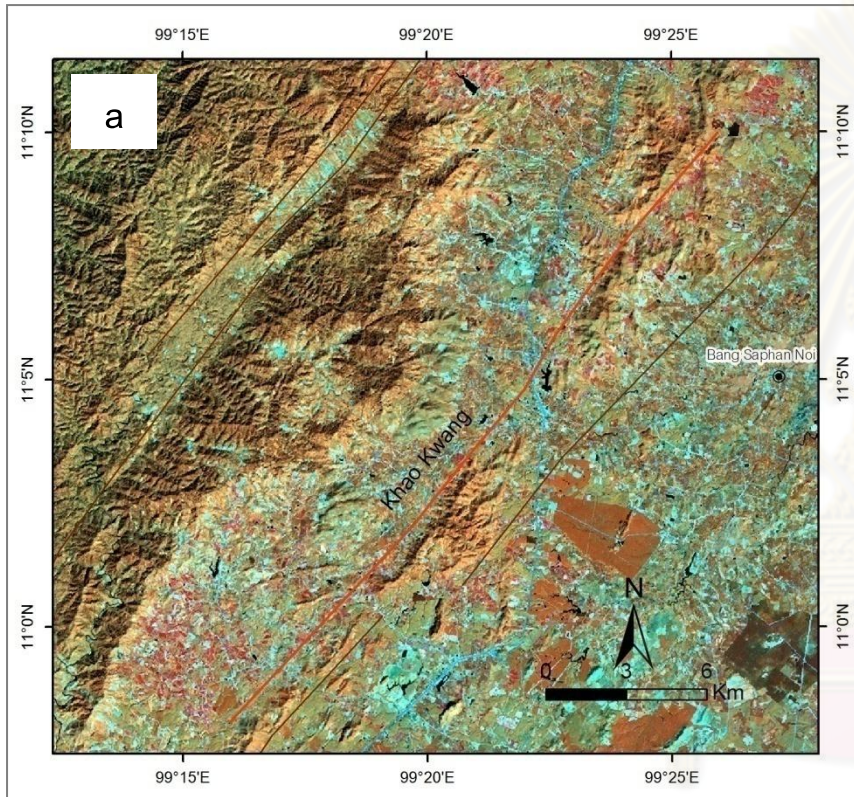
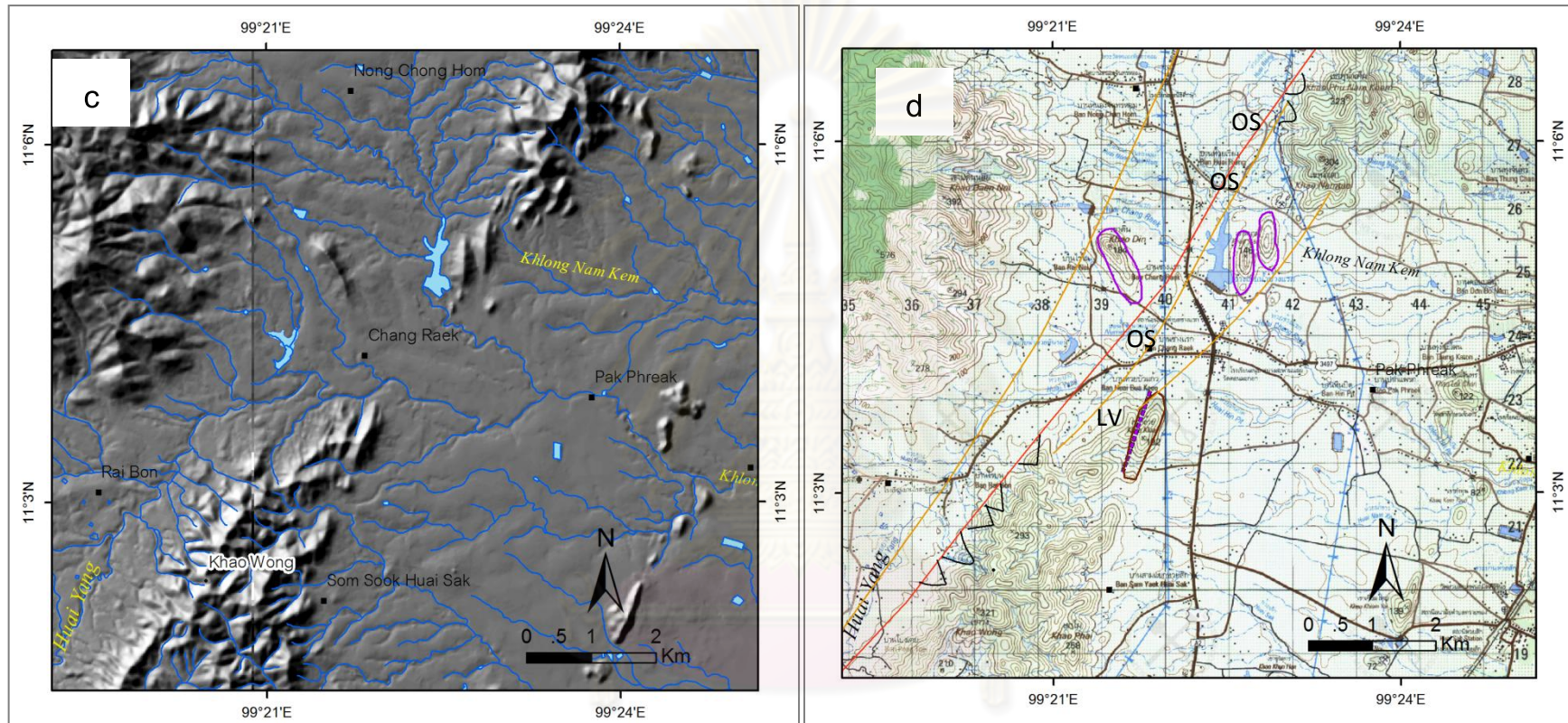


Figure 3.21 Enhanced Landsat map (a) showing Bangsaphan Noi fault segment and 2m contour interval DEM image (b) showing offset streams (OS) with the left lateral displacement.



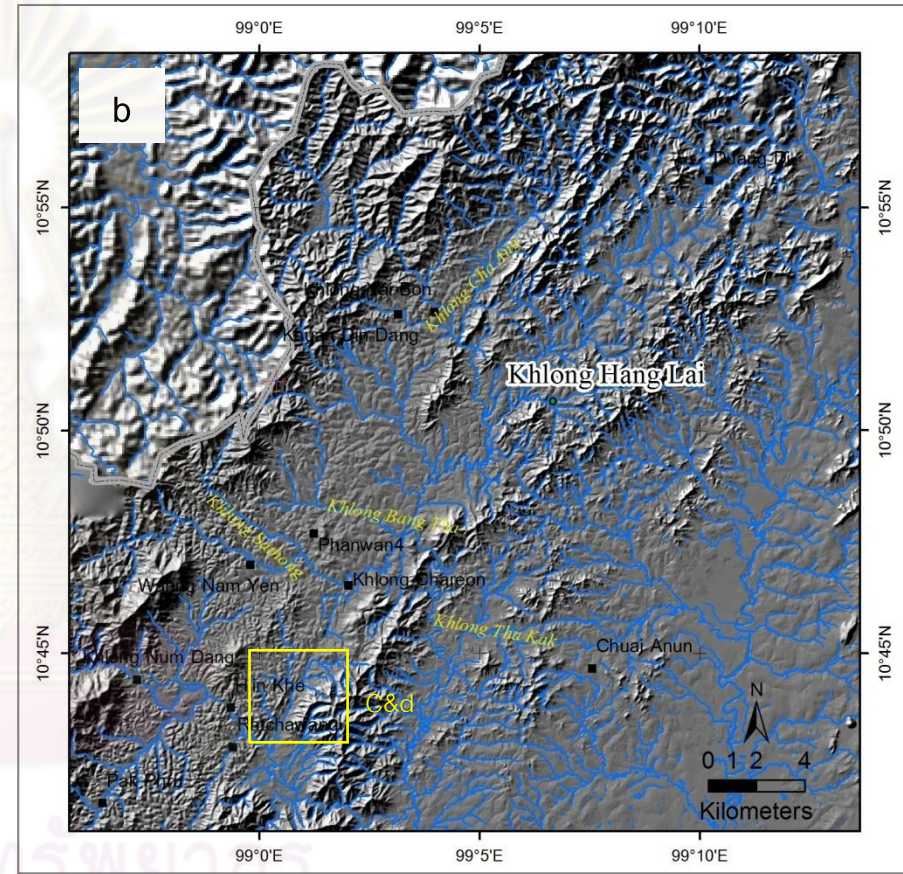
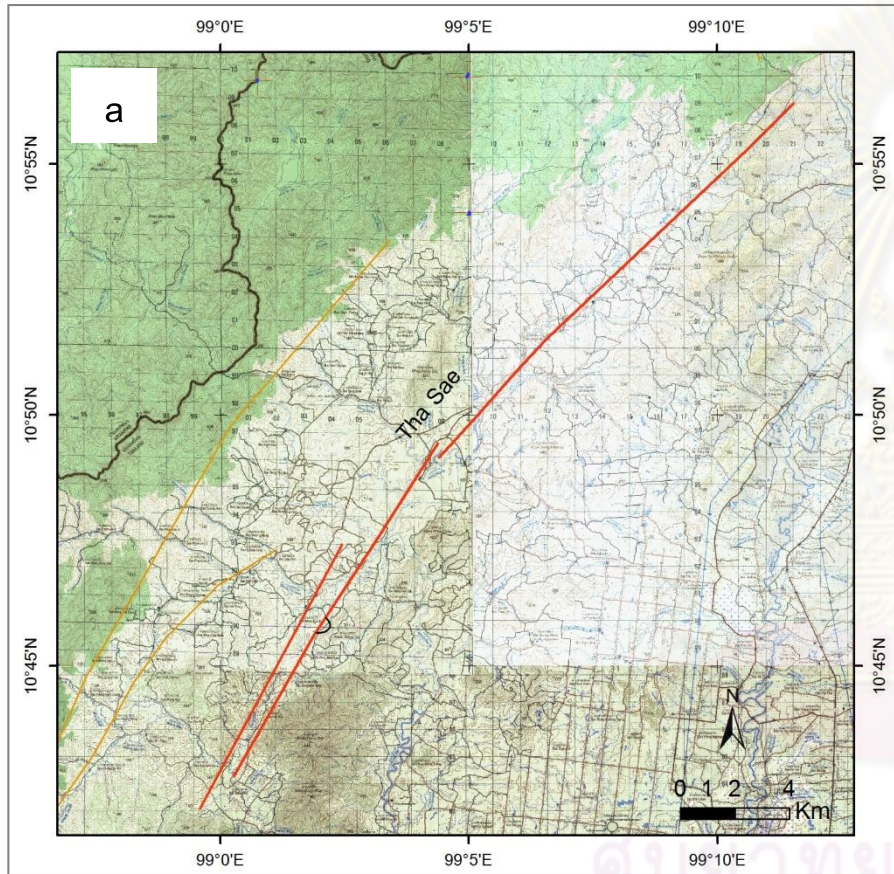
District
 Village
 Khao Kwang fault segment
 Other fault segment
 Stream

Figure 3.22 Landsat map (a) and 2m contour interval DEM image (b) showing Khao Kwang segment of RNF.



- Village
- Khao Kwang segment
- Stream
- OS Offset stream
- △ Trigular facet
- LV Linea valley
- Pressure ridge
- Linear ridge

Figure 3.22 (Cont.) Active fault evidence along Khao Kwang segment enlarged from figure 3.23b shown as DEM image (c) and topographic map (d) showing a series of offset stream, linear valley ,pressure ridge and trigular facets.



Village
 Tha Sae fault segment
 Other fault segment
 Stream

Figure 3.23 Topographic map (a) and 2m contour interval DEM image (b) showing the orientation of the Tha Sae segment .

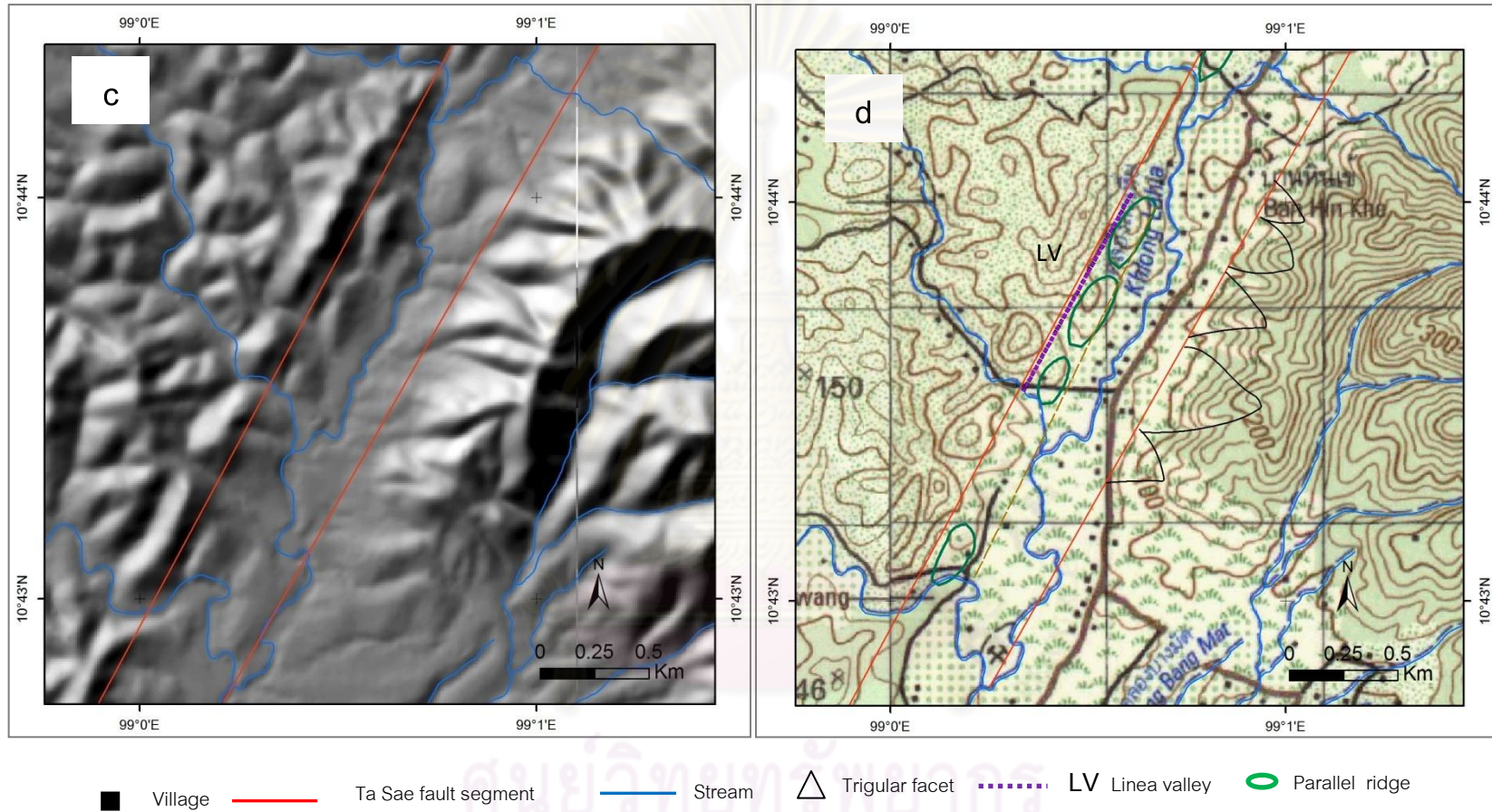


Figure 3.23 (Cont.) Active fault evidence along the Tha Sae segment enlarged from figure 3.23b) from DEM image with 2m contour interval (c) and topographic map with the interpreted result (d) showing parallel ridge, linear valley and trigular facets, at Ban Hin Khe in Khlong Lakhla river valley.

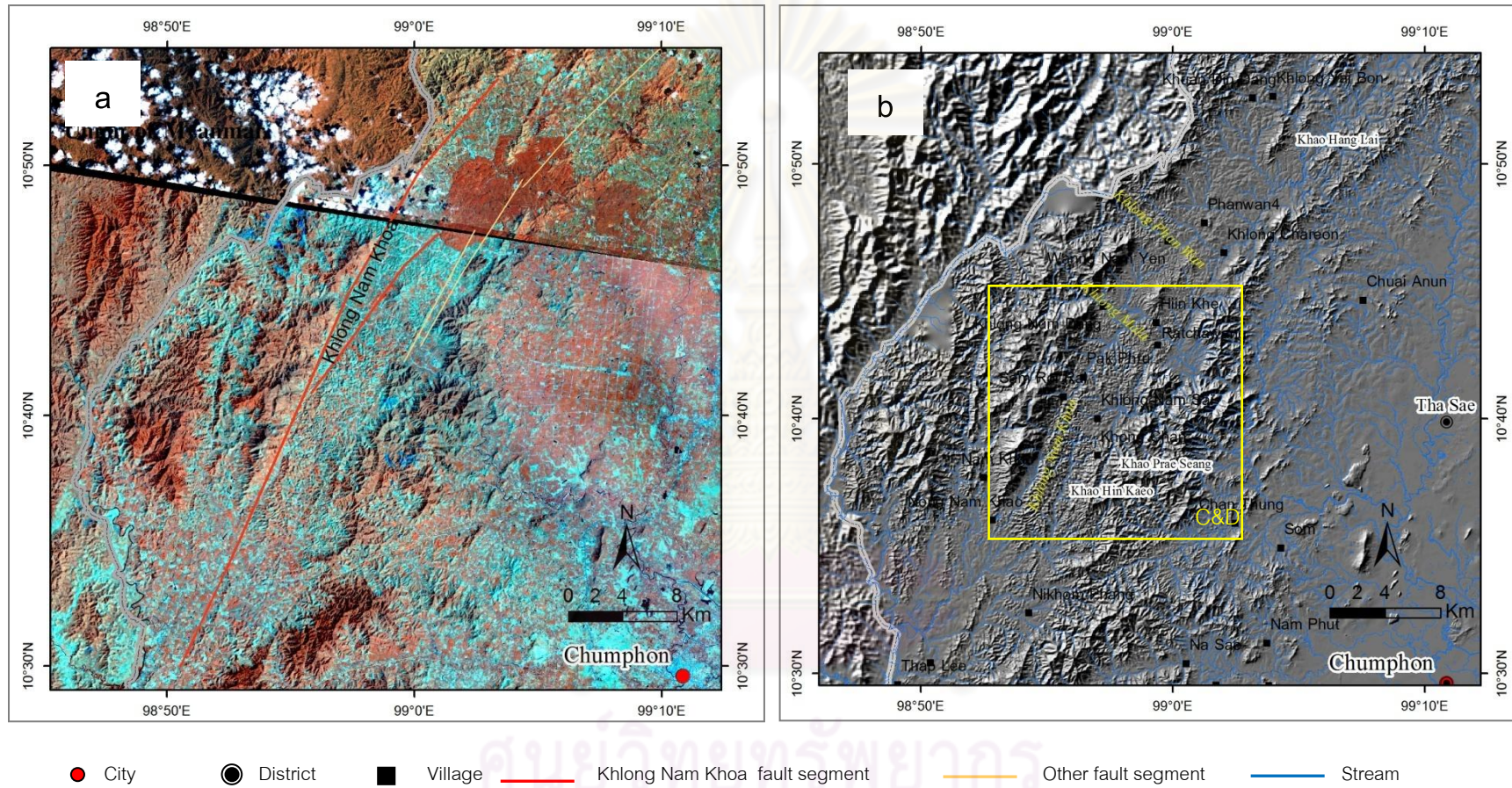
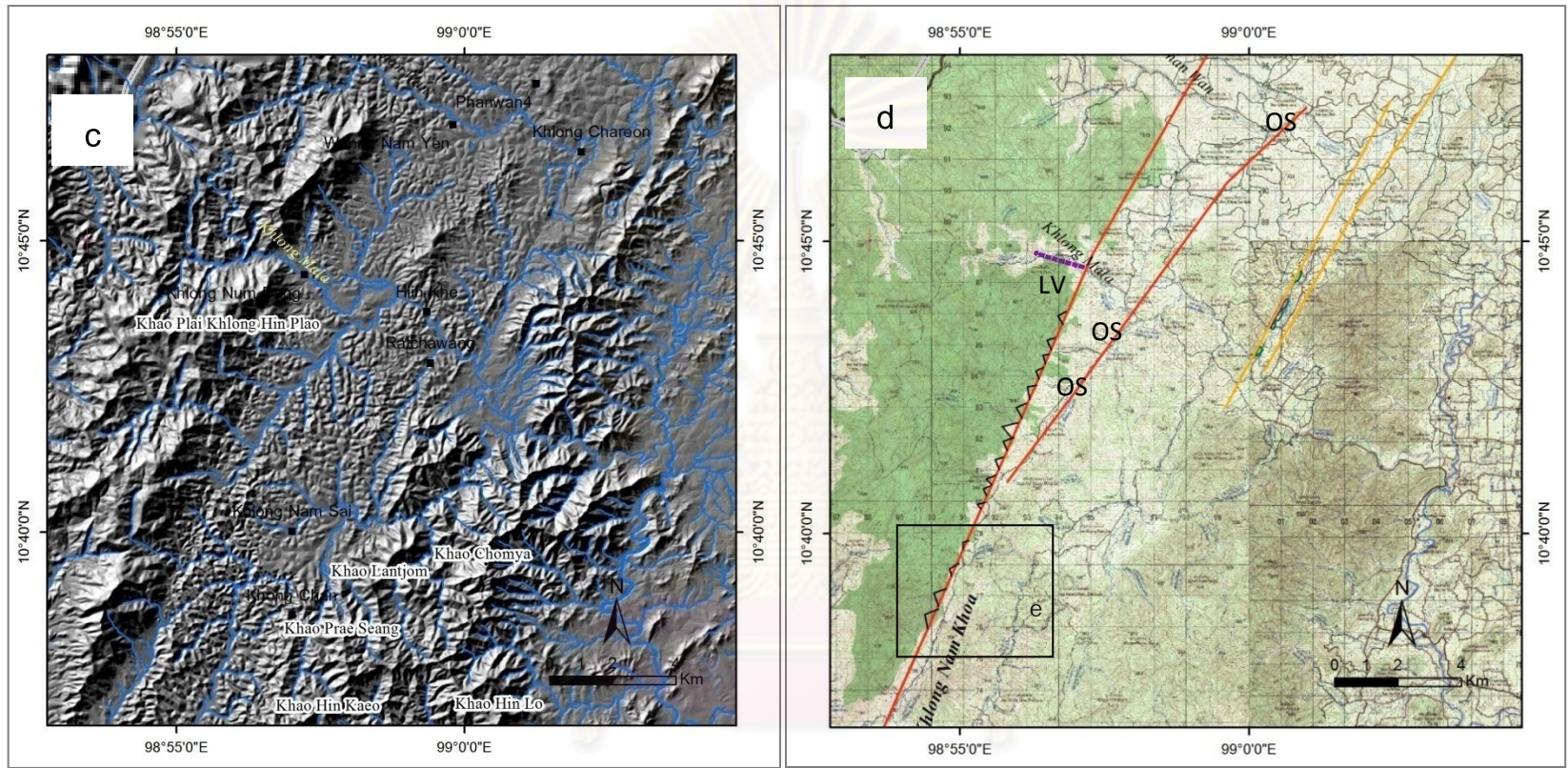
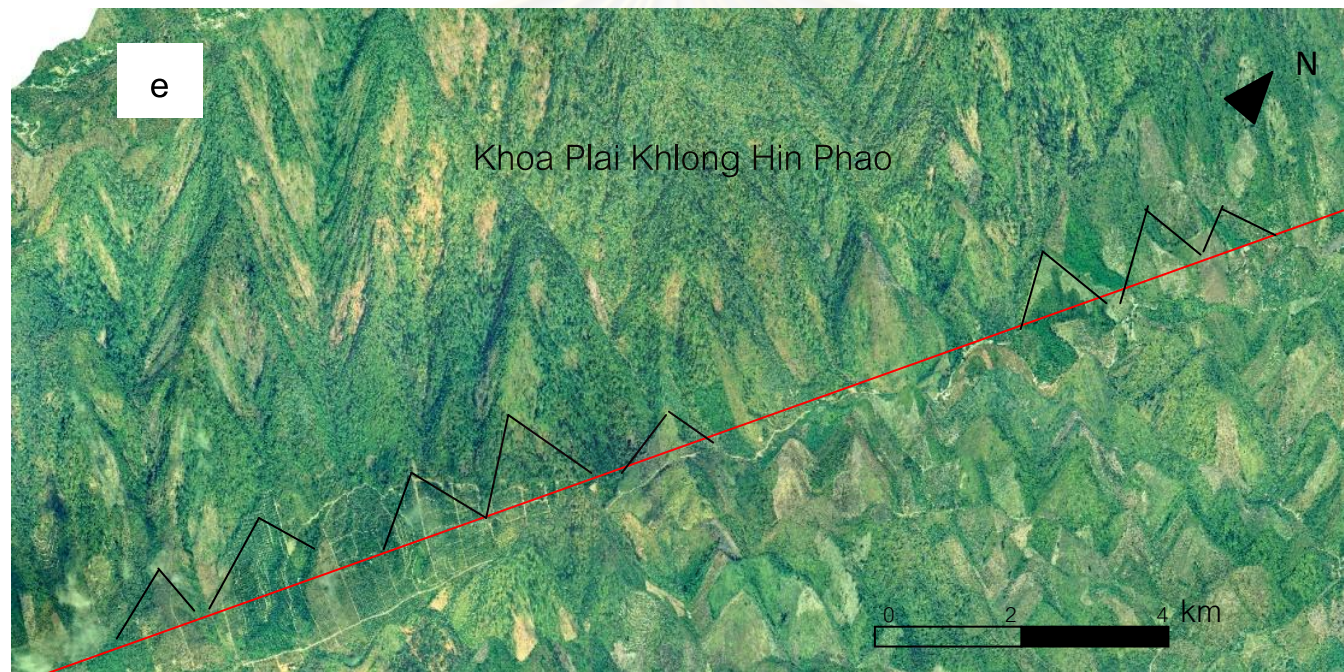


Figure 3.24 Enhanced Landsat TM5 image (a) and 2m contour interval DEM image (b) showing the orientation of Khlong Nam Khoa segment of RNF.



Village
 Khlong Nam Khoa segment
 Stream
 Trigular facet
 LV Linear valley
 Parallel ridge
 OS Offset stream

Figure 3.24 (Cont.) Active fault evidence along the Khlong Nam Khoa segment (enlarged figure 3.24b) from Dem image data with 2m interval contour (c) and topographic map (d) showing offset streams, parallel ridges, linear valley and a series of trigular facets (d). Note that there is a prominent linear valley in the north of the segment that runs in the NW-SE direction.



— Khlong Nam Khoa fault segment — Stream △ Trigular facet

Figure 3.24 Active fault evidence of Khlong Nam Khoa segment (enhanced from figure 3.24d) showing a series of trigular facets in Khoa Plai Khlong Hin Phao.

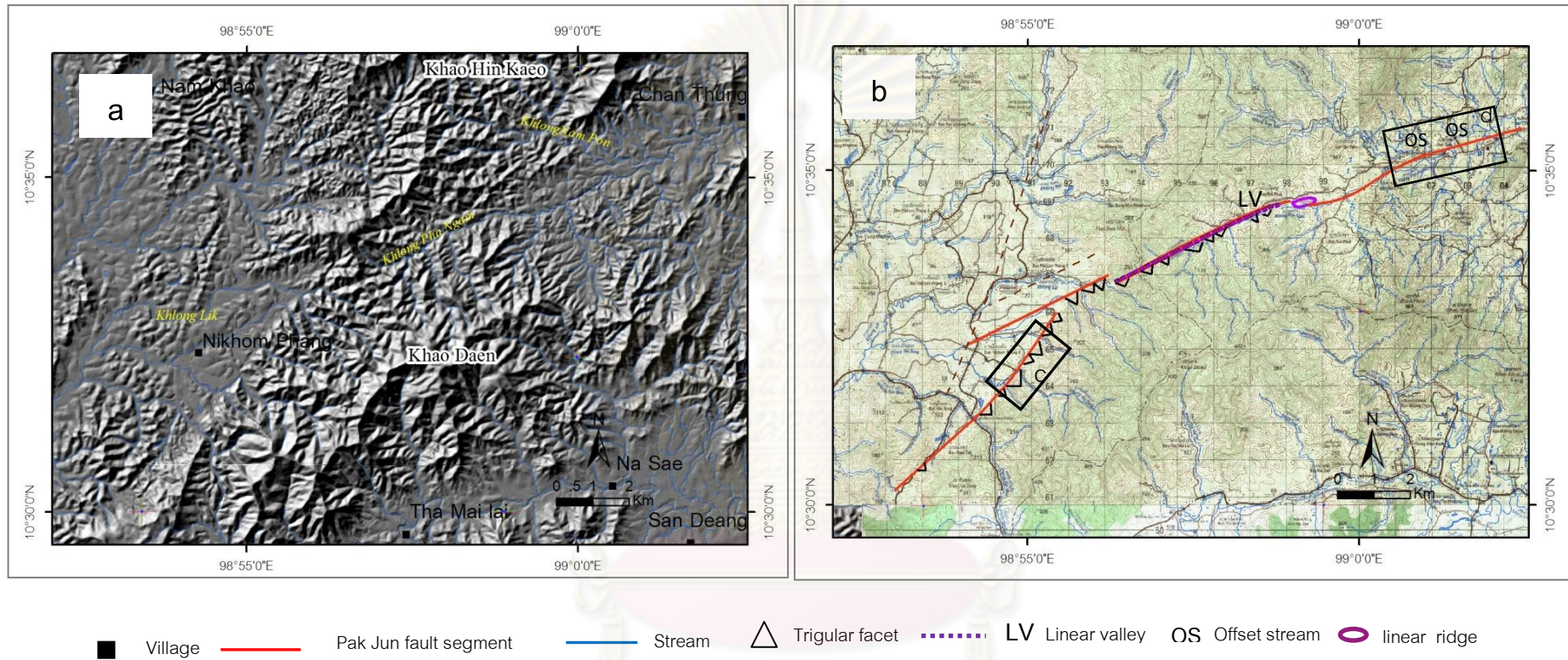


Figure 3.25 Active fault evidence of Pak Jun fault segment from 2m interval contour DEM image (a) and topographic map (b) showing offset streams, linear valley, linear ridge and series of trigular facet.

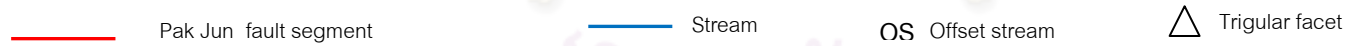
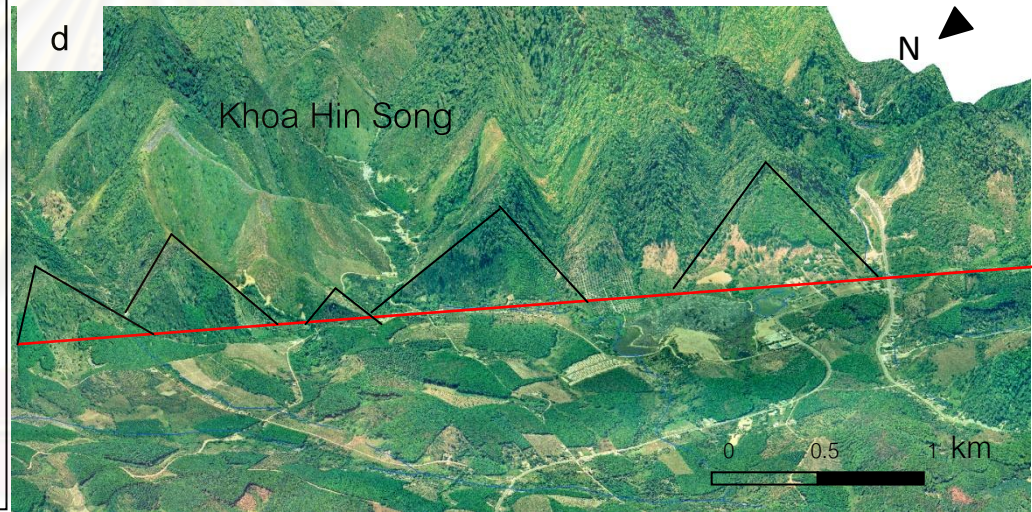
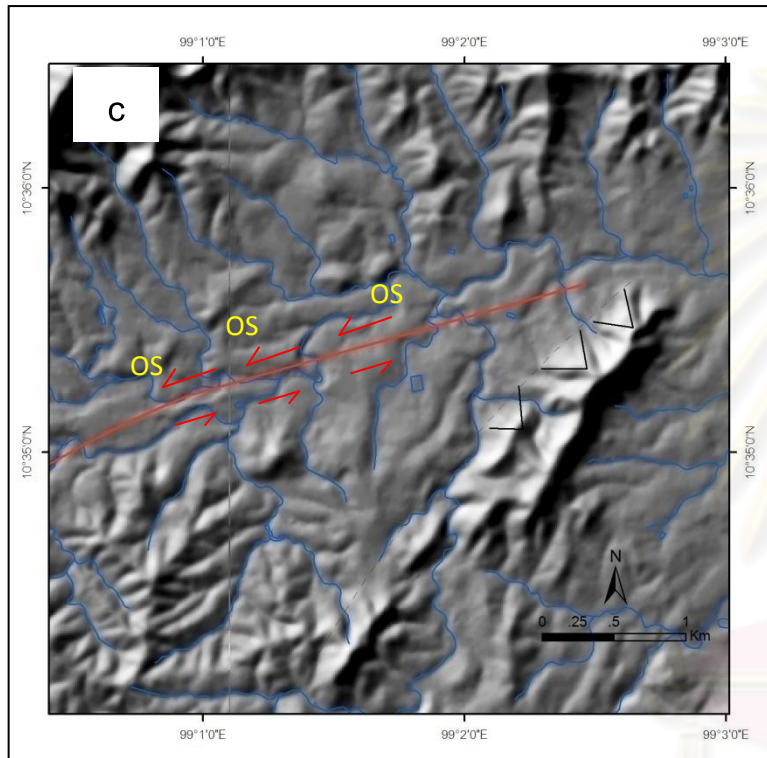
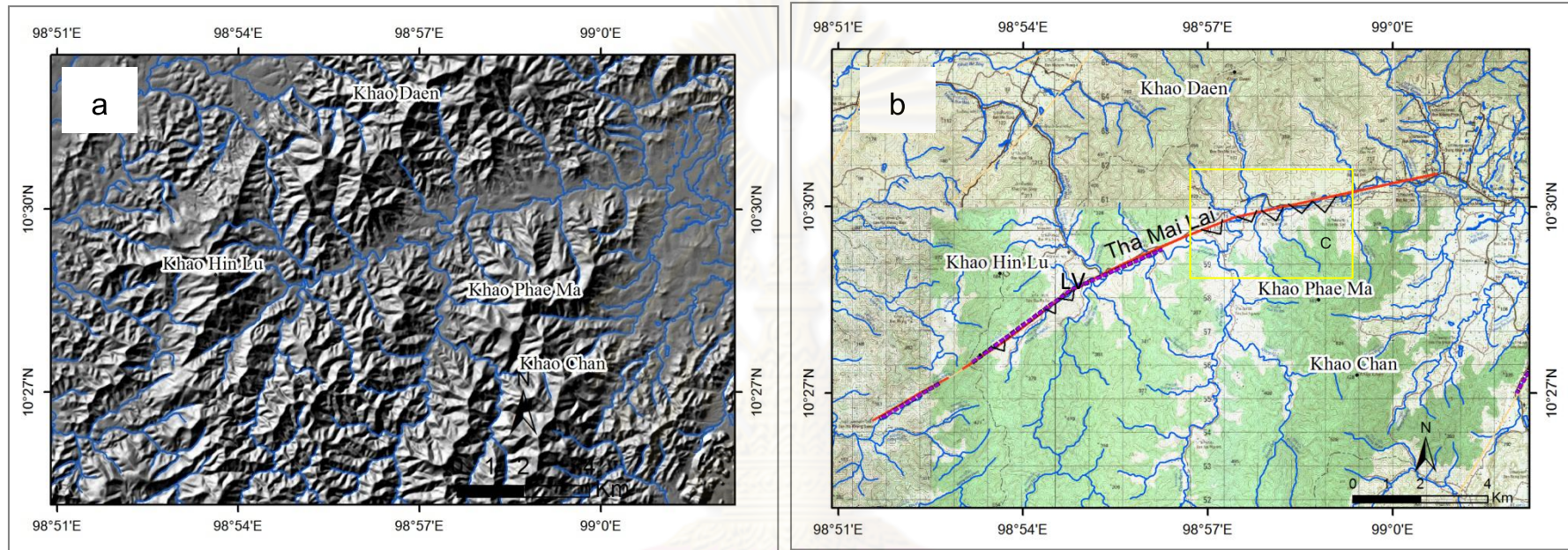


Figure 3.25 (Cont.) Active fault evidence of Pak Jun segment enlarged from figure 3.25b shown as DEM image (c) showing offset streams (OS) with the left lateral displacement and (d) showing a series of trigular facets in Khao Hin Song.



Village
 Tha Mai Lai fault segment
 Pak Jun fault segment
 Stream
 Trigular facet
 LV Linear valley

Figure 3.26 Active fault evidence of Tha Mai Lai segment (a) DEM interval contour 2m and (b) topographic map (b) showing, linear valley and trigular facet .

ศูนย์วิทยทรัพยากร
 จุฬาลงกรณ์มหาวิทยาลัย



Figure 3.26 (Cont.) Active fault evidence of Tha Mai Lai segment enlarged from figure 3.26d shown as 3D colour-orthographic map (g) showing a series of trigular facets in Khoa Phae Ma.

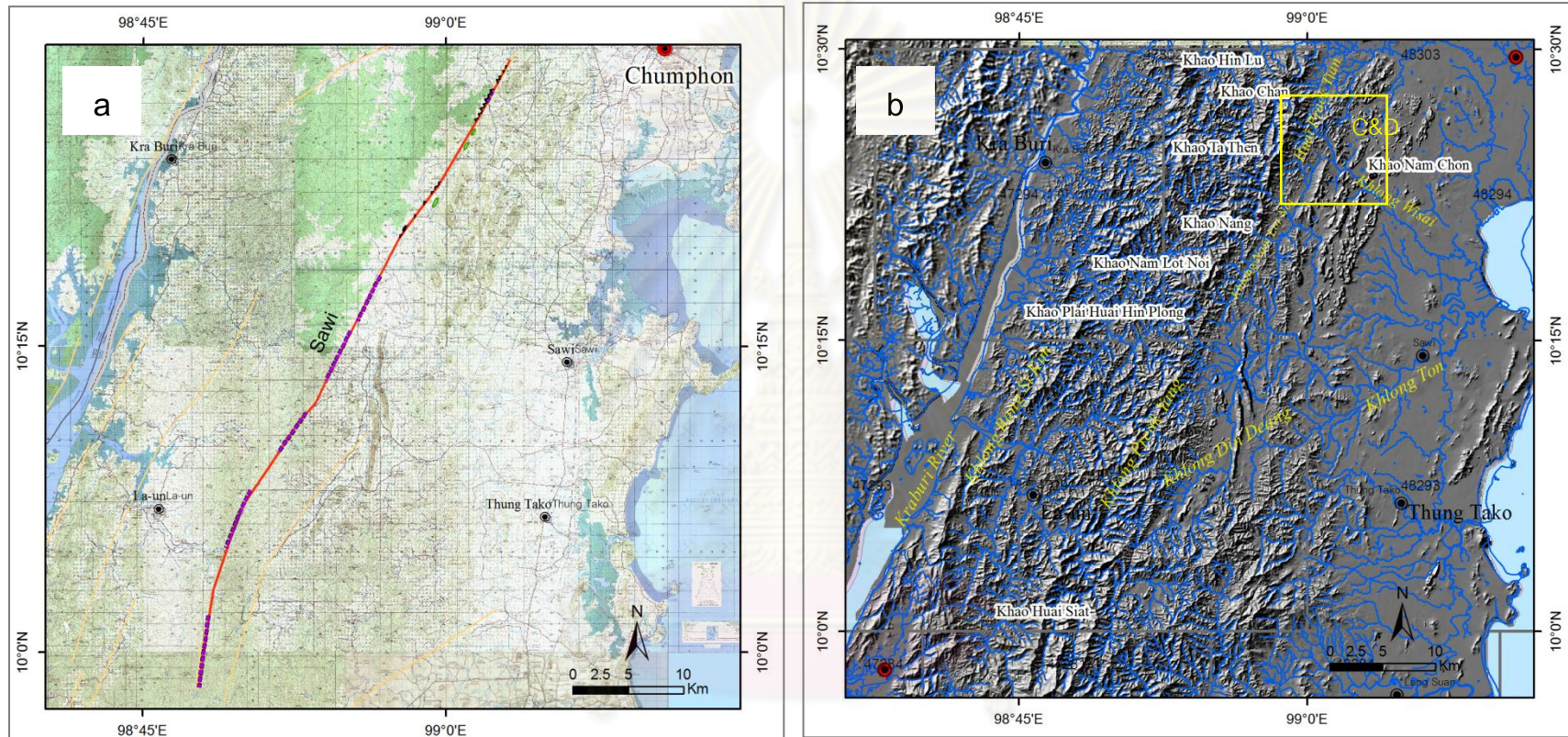
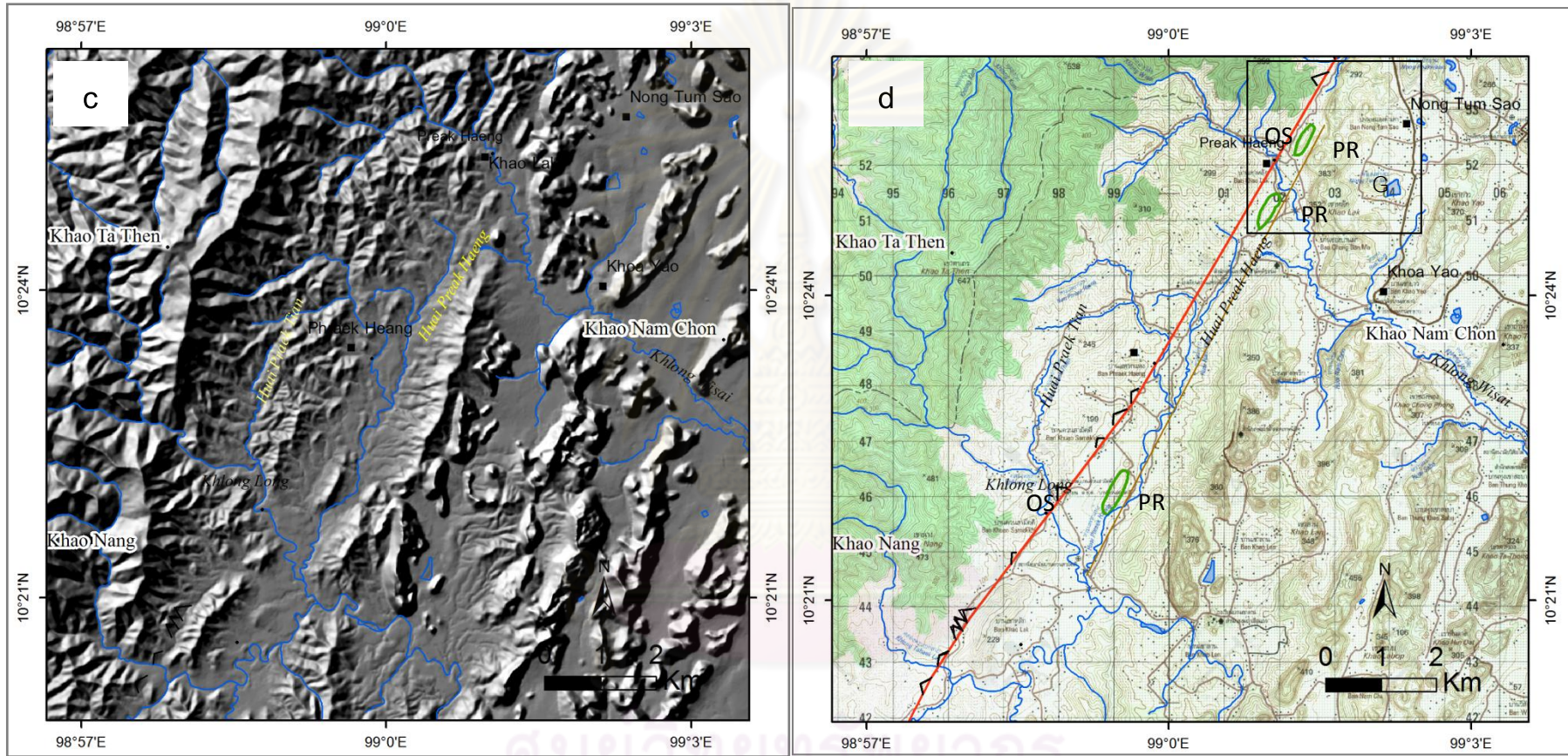


Figure 3.27 Topographic map (a) and 2m contour interval DEM image (b) showing the orientation of Sawi segment at the middle part of RNF.



Village
 Sawi fault segment
 Stream
 Tringular facet
 LV Linear valley
 OS Offset stream
 Parallel ridge

Figure 3.27 (Cont.) Active fault evidence of Sawi segment (enlarged from figure 3.27b) shown as DEM image (c) and topographic map (d) showing parallel ridges, linear valley, a series of trigular facets and offset streams.

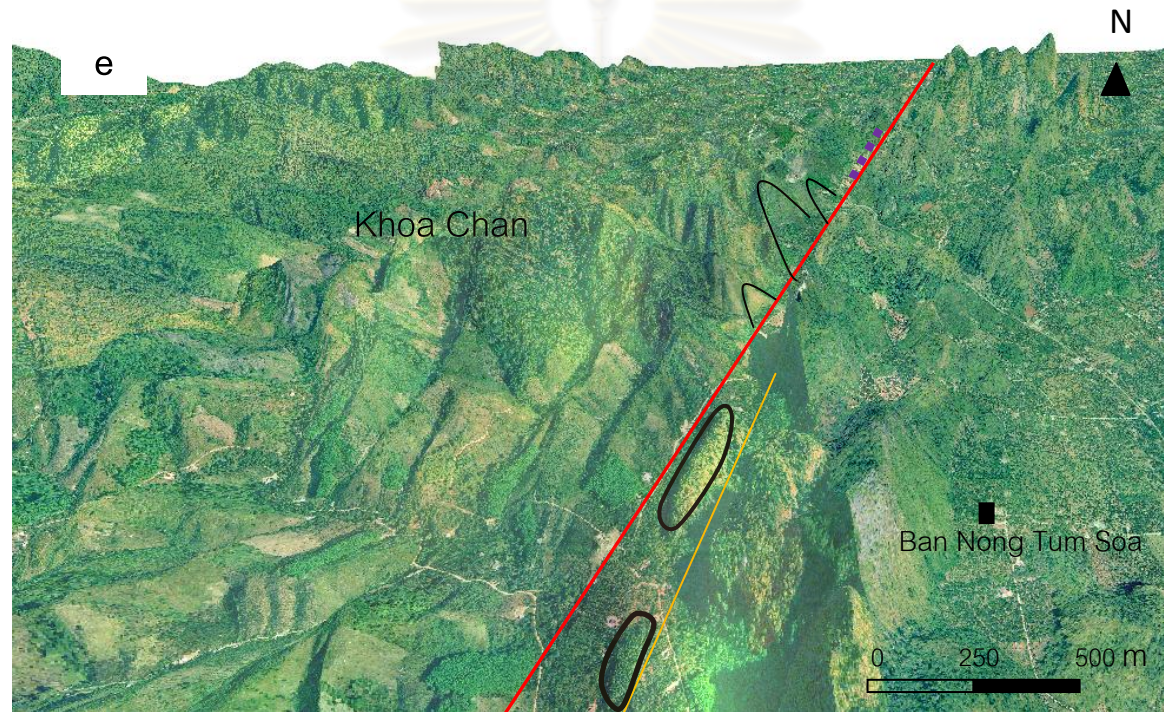
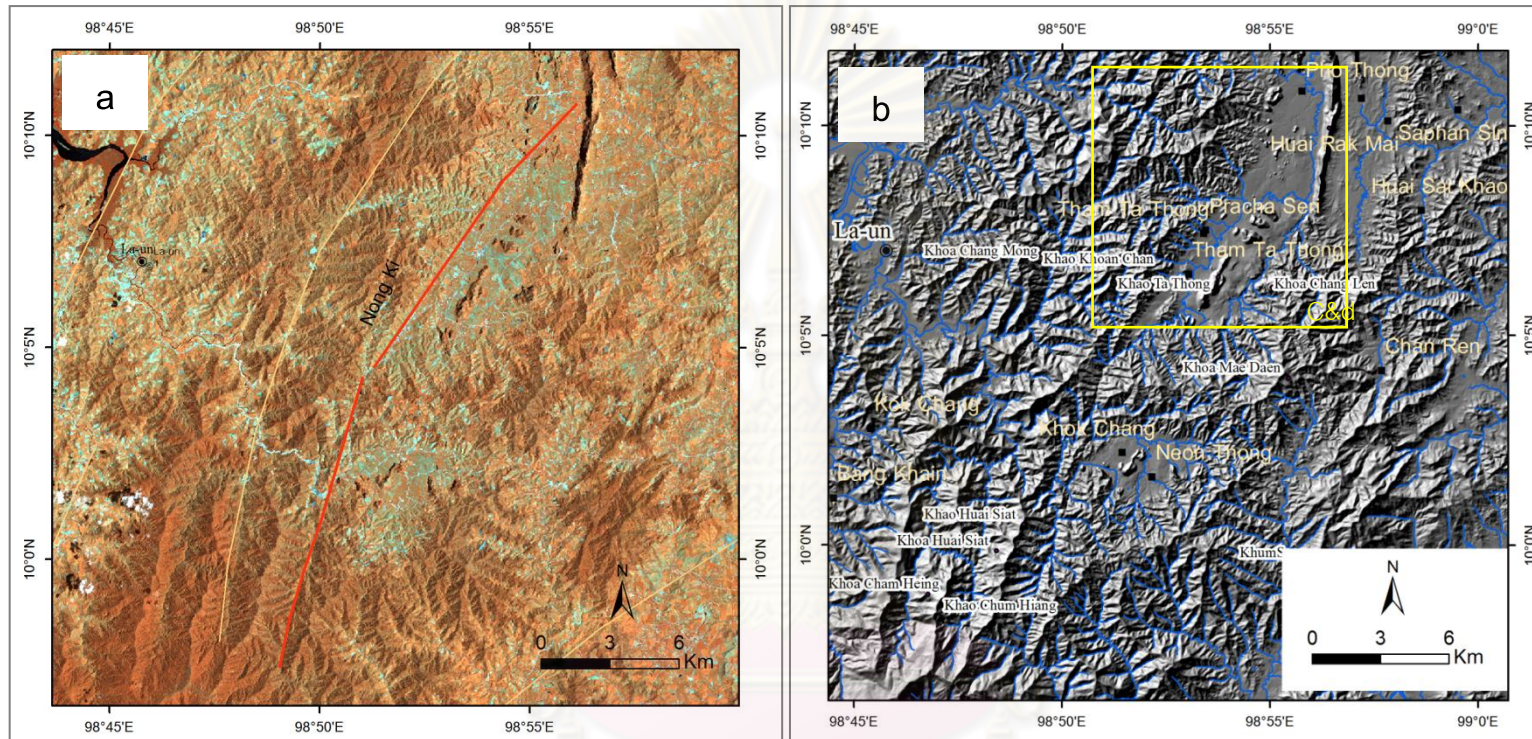


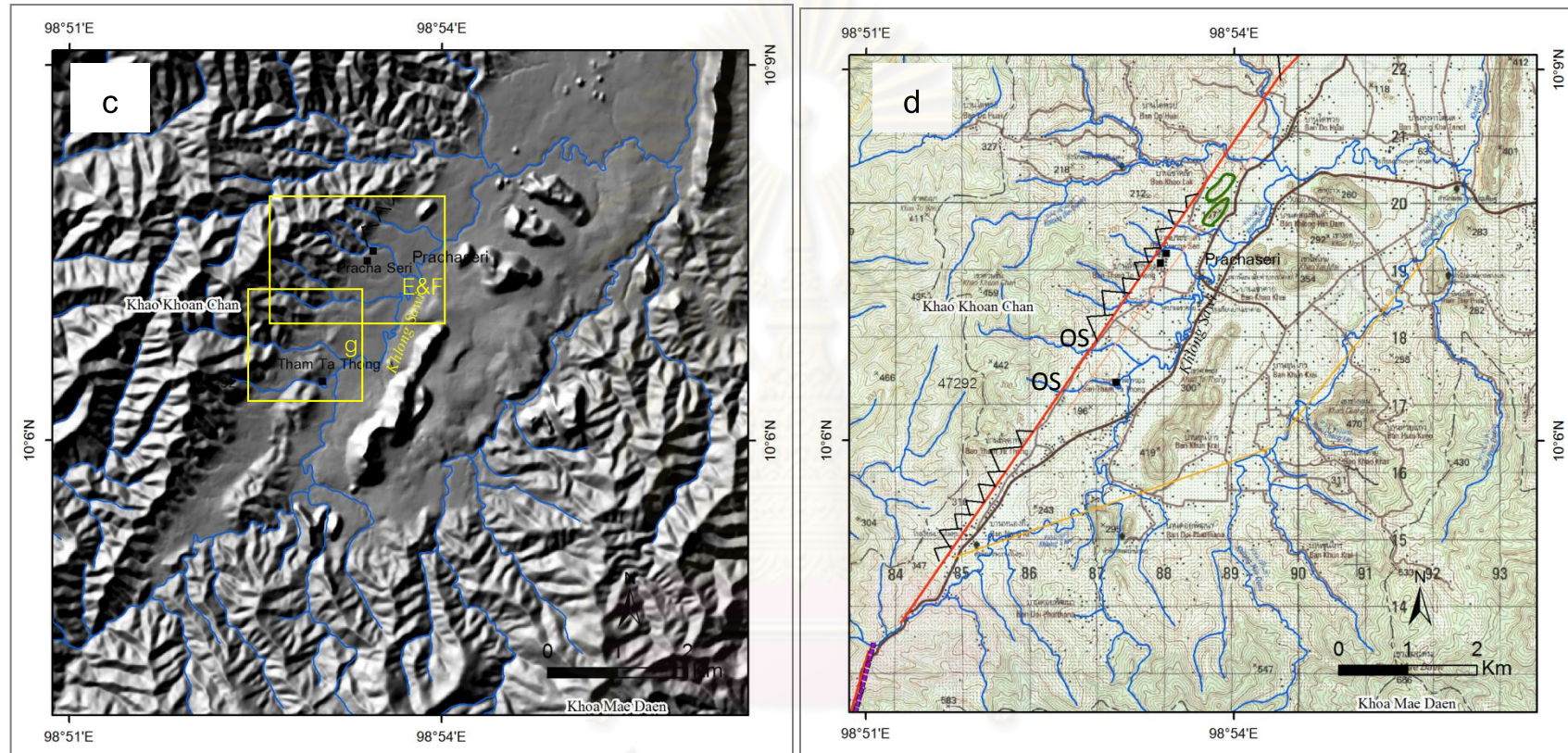
Figure 3.27 (Cont.) 3D colour-orthographic map of Sawi fault segment (enlarged figure 3.27b) showing a set of trigular facets and parallel ridges near Ban Nong Tum Soa.



Distric
 Village
 Nong Ki fault segment
 Other fault segment
 Stream

Figure 3.28 Landsat image (a) and 2m contour interval DEM image (b) showing the NE-SW trending of Nong Ki segment which is almost parallel to the Sawi segment.

ศูนย์วิจัยทรัพยากรธรณี
 จุฬาลงกรณ์มหาวิทยาลัย



- Village
- Nong Ki fault segment
- Stream
- △ Trigular facet
- LV Linear valley
- OS Offset stream
- Parallel ridge

Figure 3.28 (Cont.) Active fault evidence of Nong Ki segment (enlarged figure 3.28b) displayed as DEM image (c) and topographic map (d) showing parallel ridges, linear valley, a series of trigular facets and offset streams. These fault segment are considered to control the Cenozoic basin formation.

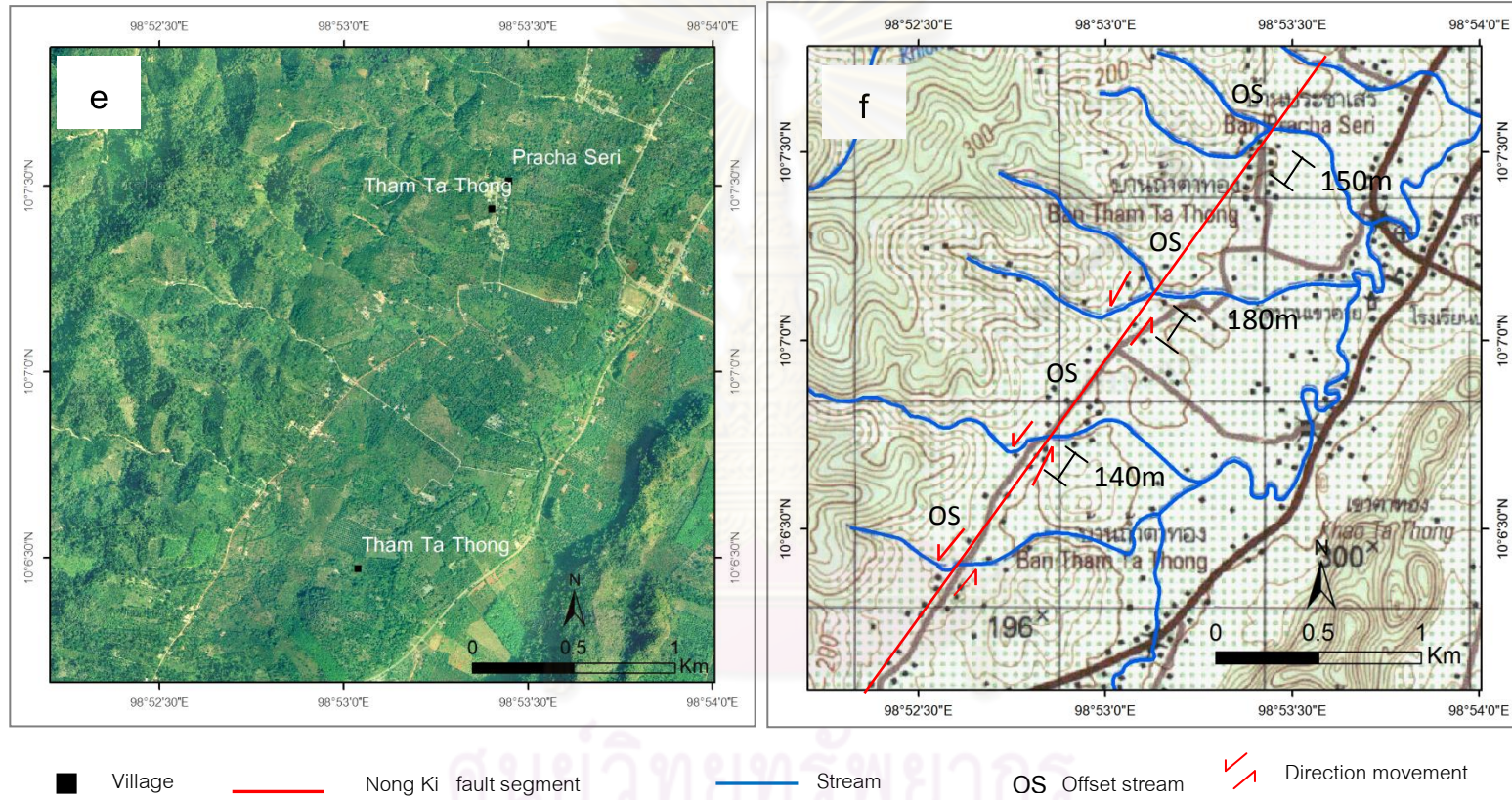
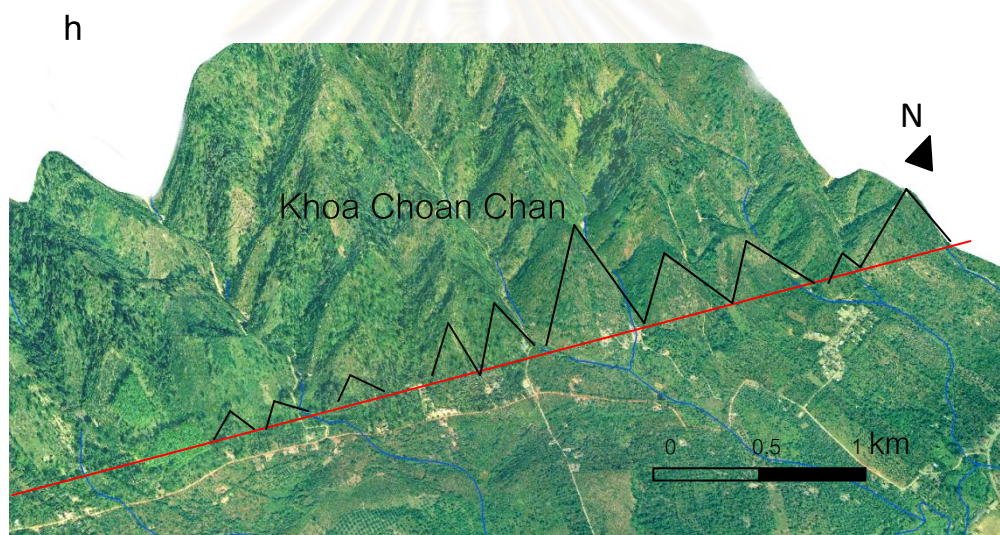
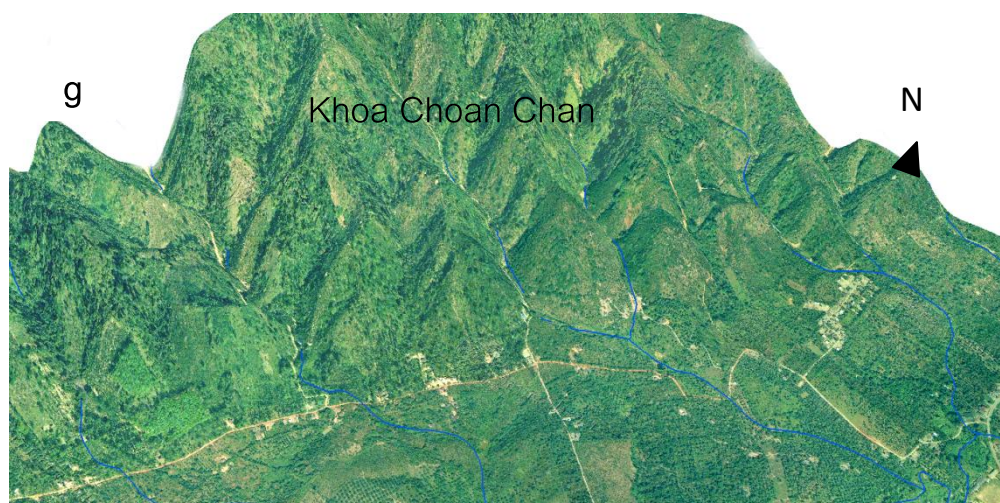


Figure 3.28 (Cont.) Active fault evidence of Nong Ki segment (enlarged figure 3.28c) from ortho-color photographic image (e) and topographic map (f) showing a series of offset streams.



■ Village — Nong Ki fault t — Other fault segment — Stream △ Trigular facet

Figure 3.28 (Cont.) Active fault evidence of Nong Ki segment (enlarged figure 3.29c)

appear in 3D colour-orthographic image (g) and interpreted in

this study (h) showing a series of trigular facets in Khoa Choan Chan.

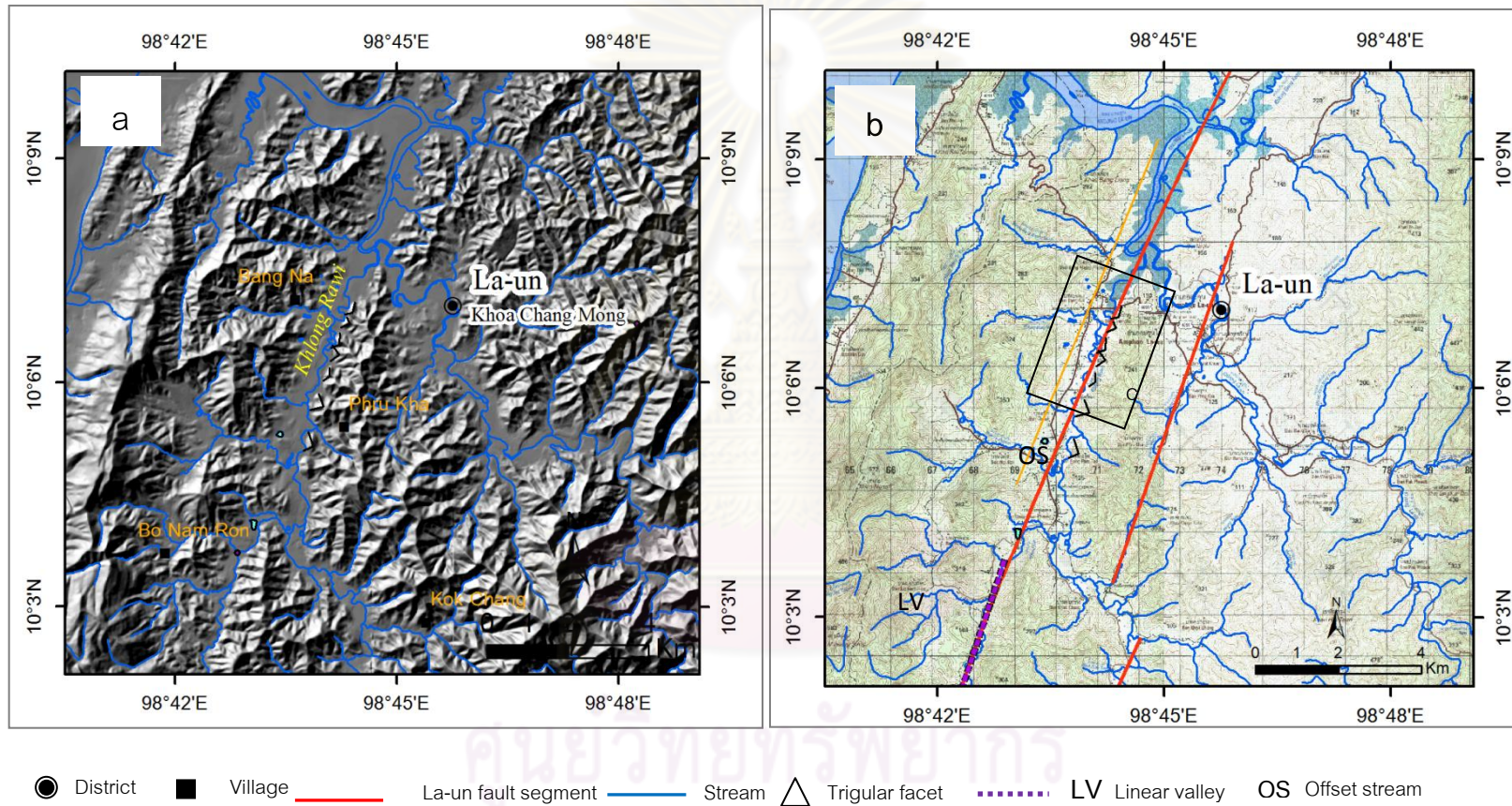
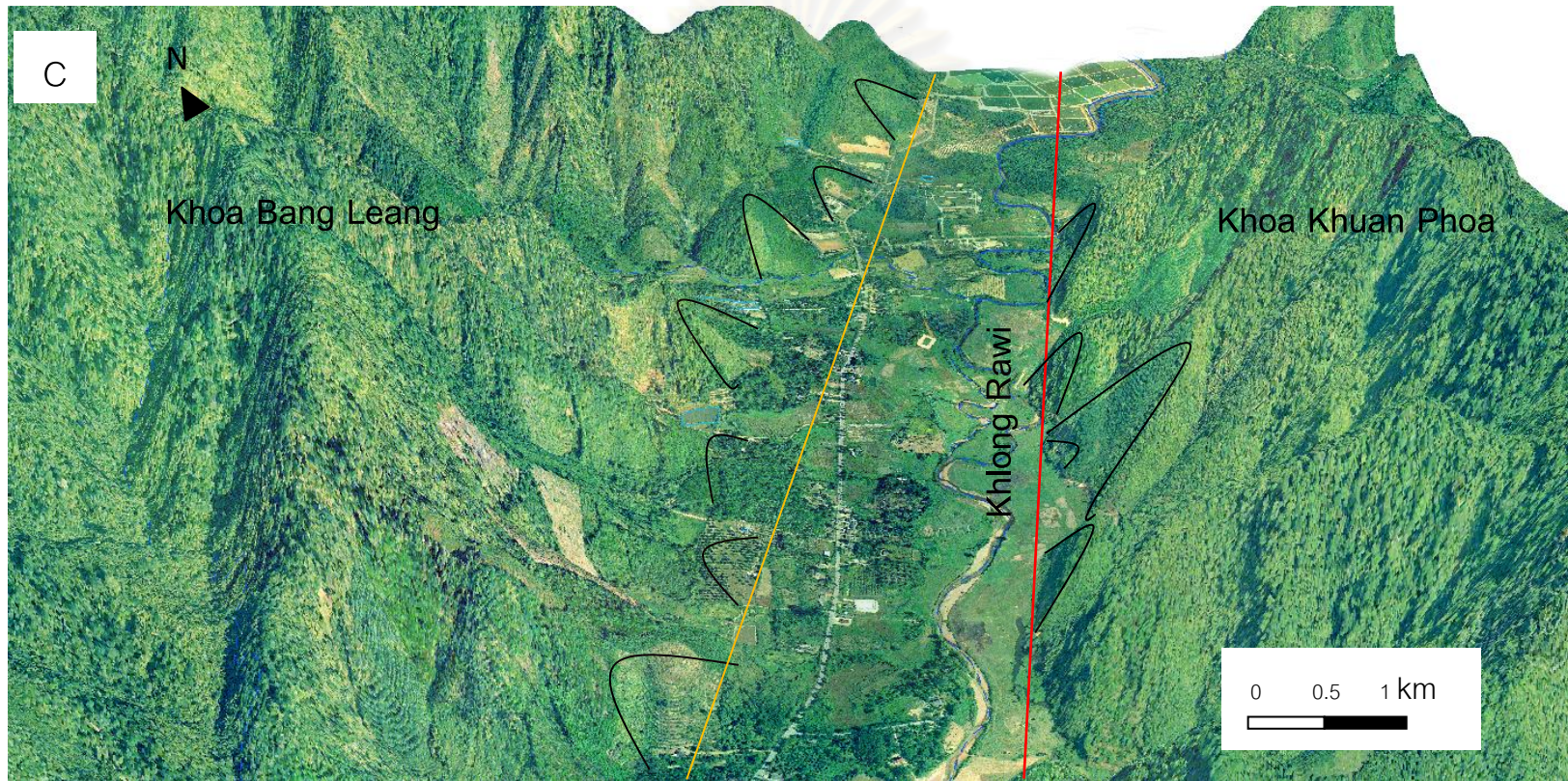
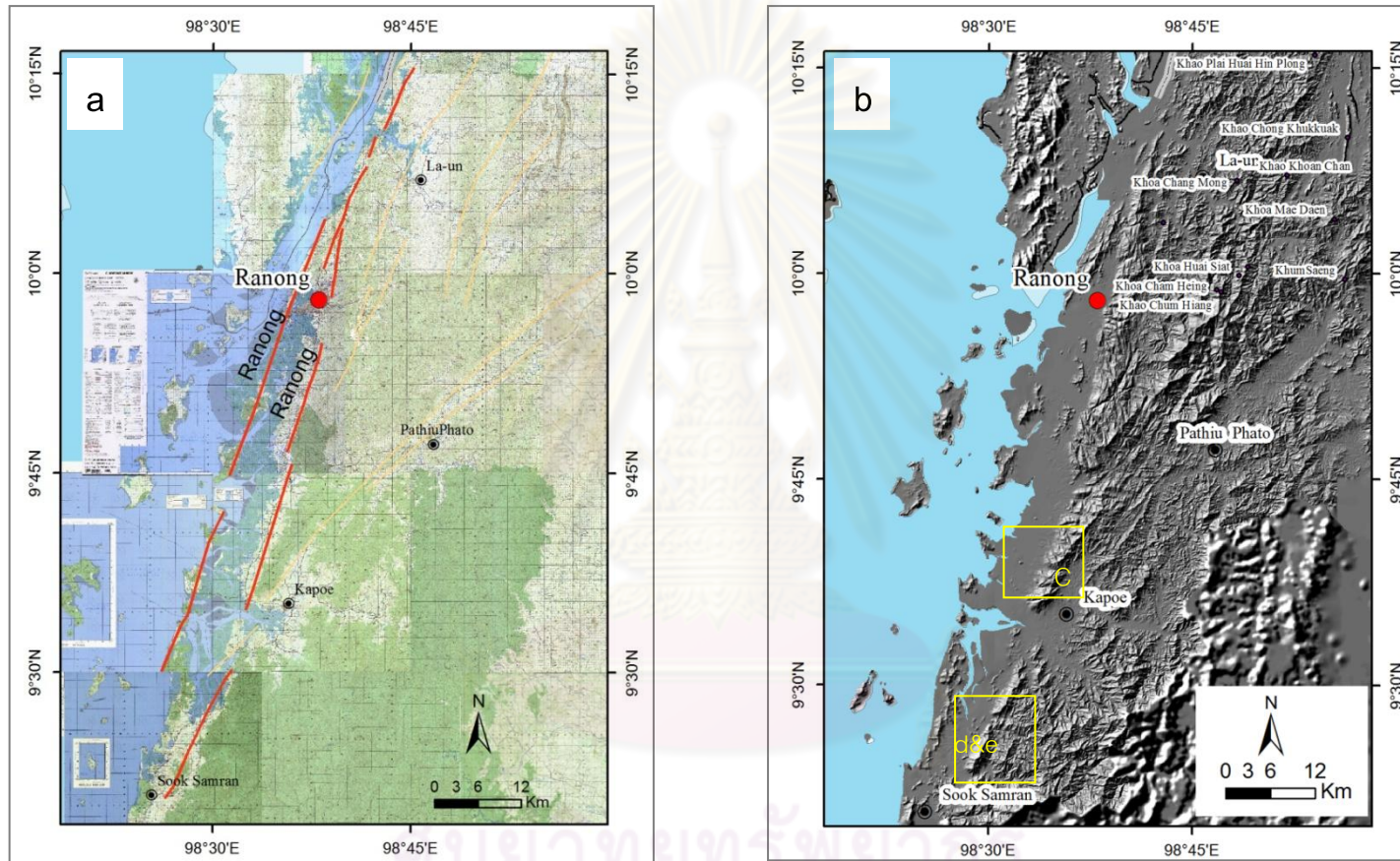


Figure 3.29 (Cont.) Active fault evidence of La-un segment from DEM image (a) and topographic map (b) showing linear valley, trigular facets and offset streams. Note there is a fault segment parallel to Khliong Rawi which pass La-un district.



— La-un fault segment
 — Stream
 △ Trigular facet

Figure 3.29 (Cont.) Active fault evidence along La-un fault segment (enlarged figure 3.29b) showing 2 series of trigular facets facing at opposite Directions. These two segments which control the development of Khlong Rawi linear valley.



● City
 ● District
 — Ranong fault segment
 — Other fault segment
 — Stream

Figure 3.30 Topographic maps (a) showing two subparallel subsegment of Ranong segment of the southern part of RNF and 2m contour interval DEM image (b).

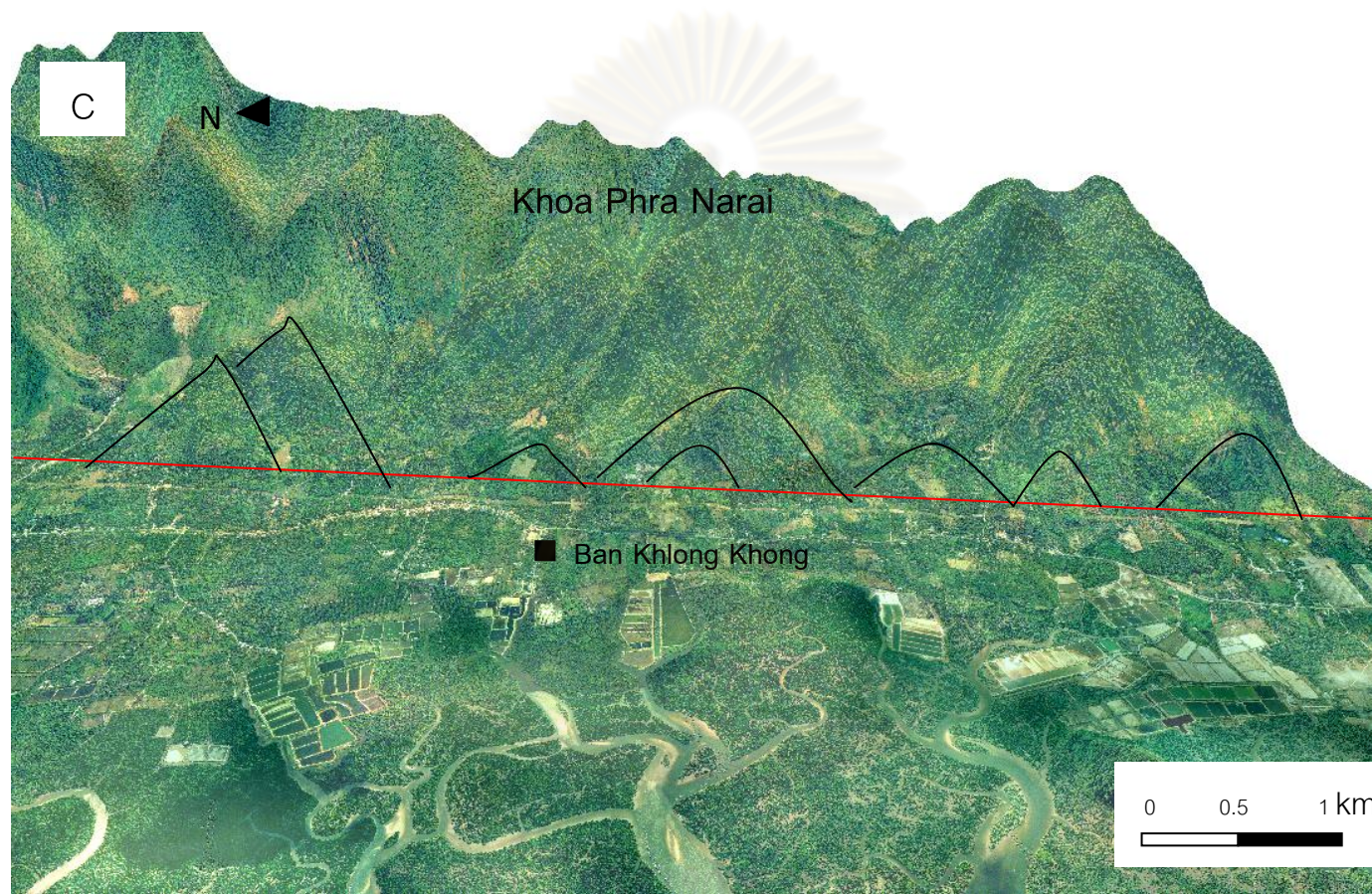


Figure 3.30 (Cont.) 3D colour-orthographic interpretation image (c) along the Ranong segment (enlarged figure 3.31b) showing trigular facets at Khoa Phra Narai.

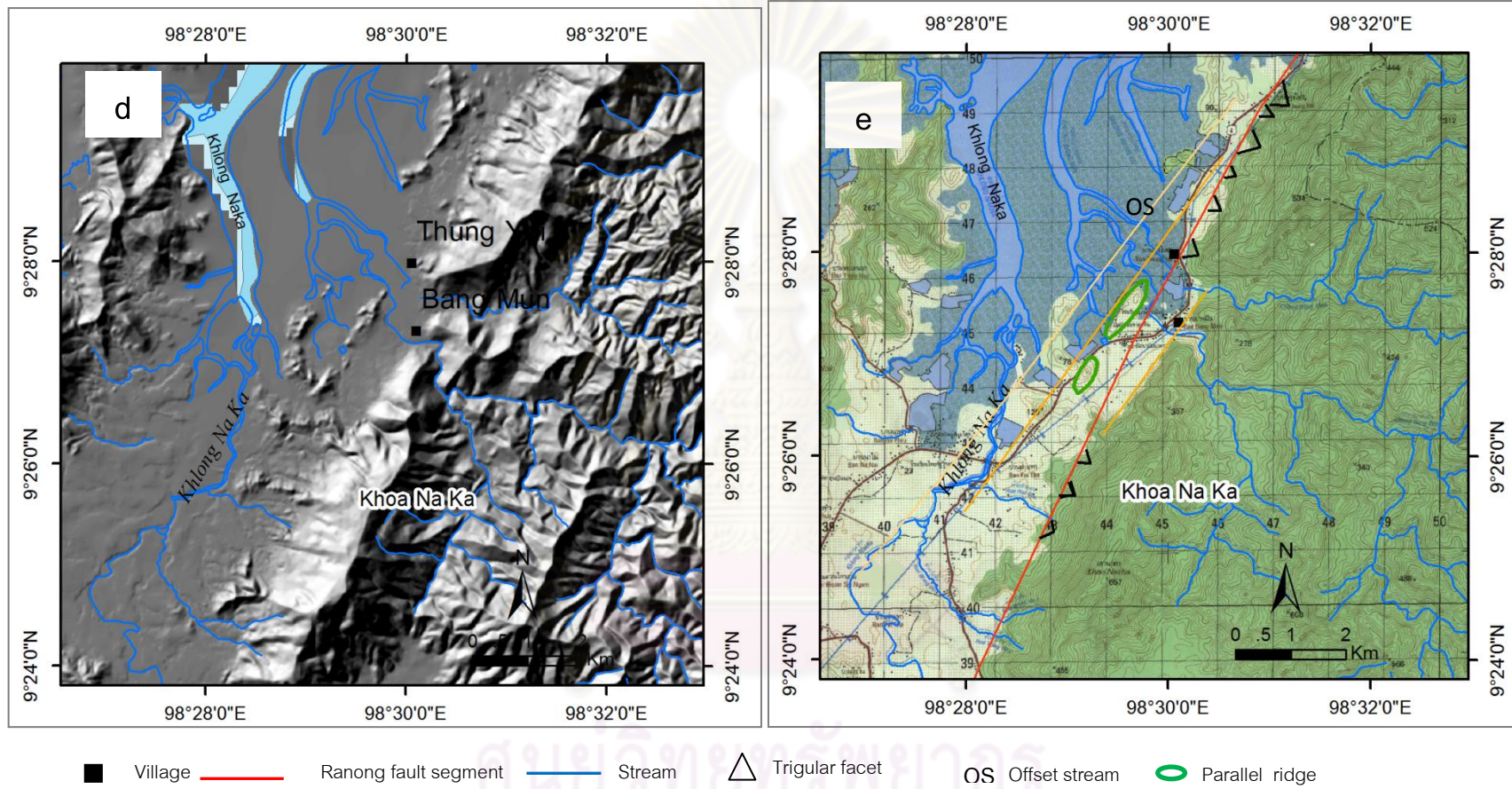


Figure 3.30 (Cont.) Active fault evidence of Ranong segment (enlarged figure 3.30b) shown as DEM image (e) and interpreted in this study (f) showing parallel ridges, a set of trigrular facets and offset streams.

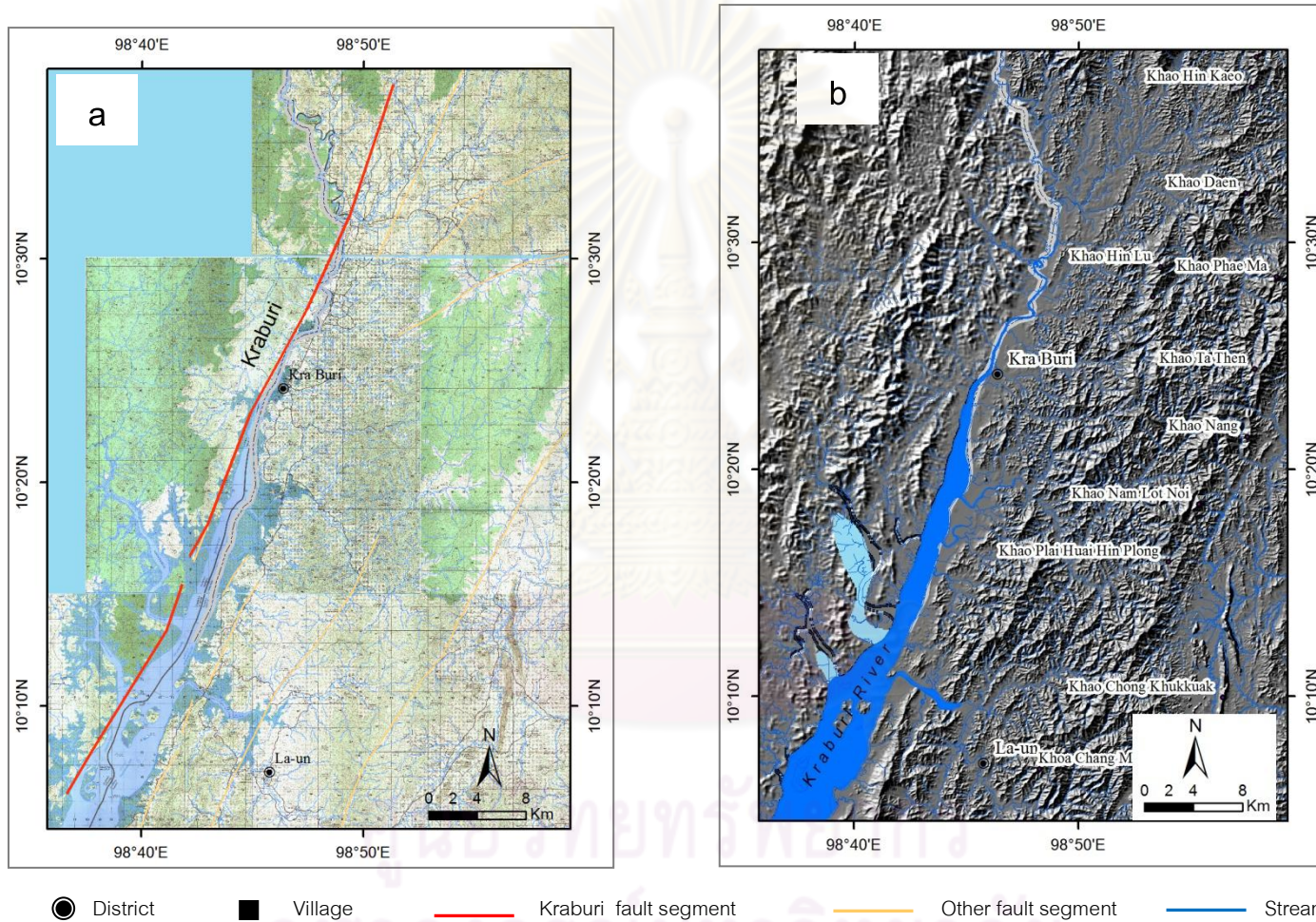


Figure 3.31 Topographic maps (a) and 2m contour interval DEM image (b) showing the orientation of Kraburi segment of the southern part of RNF.

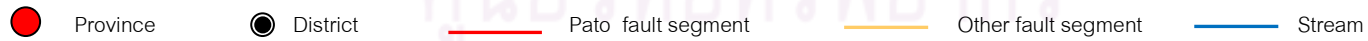
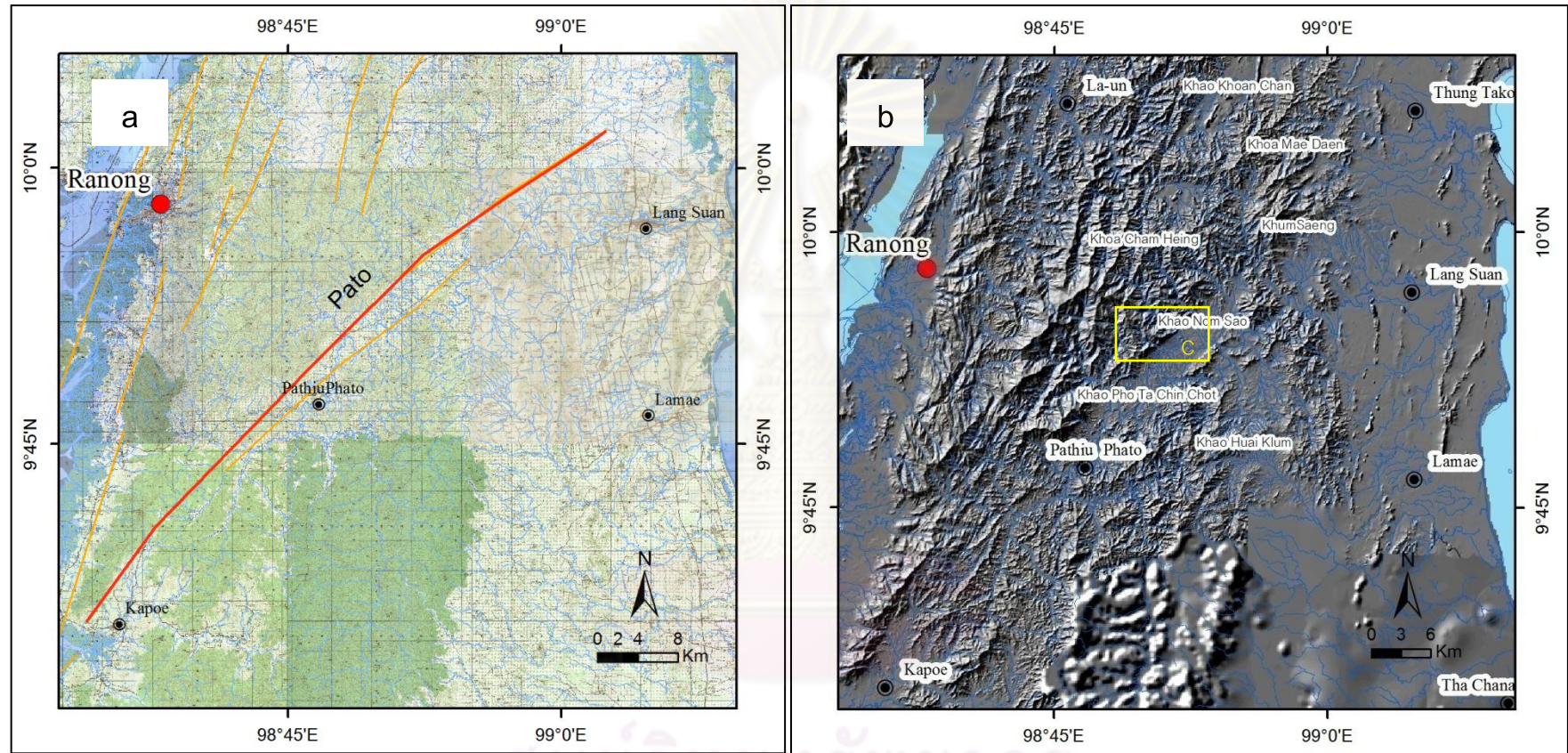


Figure 3.32 Topographic maps (a) and 2m contour interval DEM image (b) showing the orientation of Pato segment of the southern part of RNF.

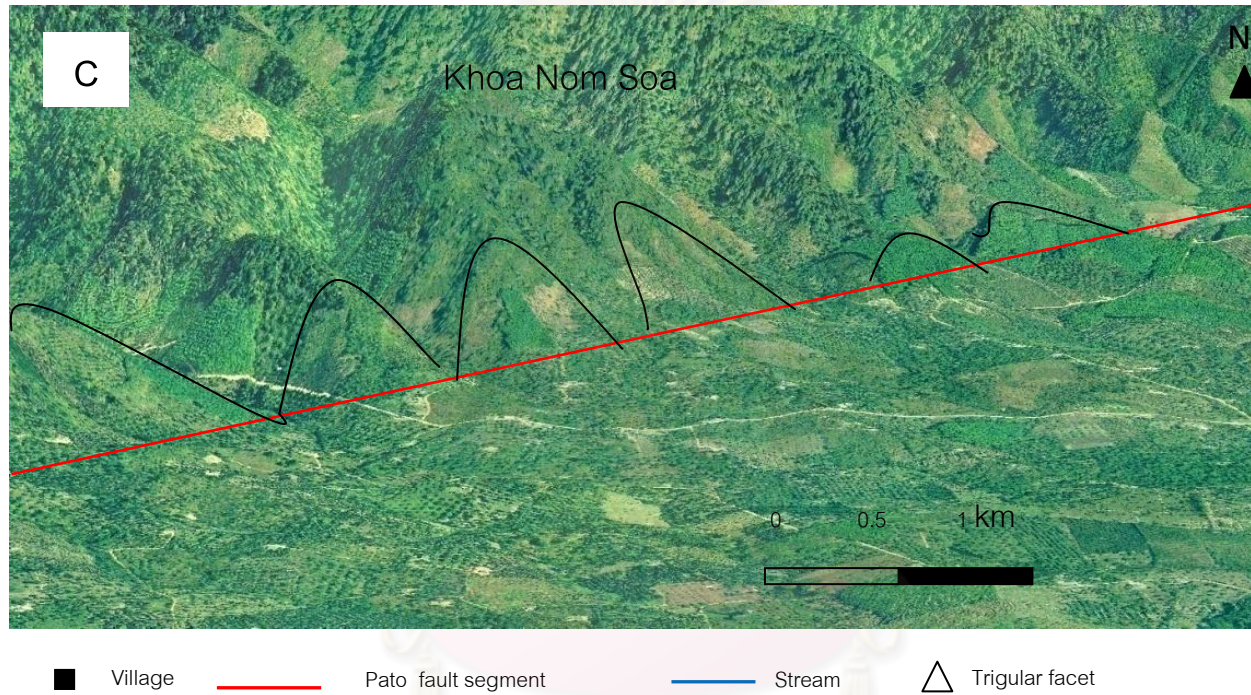
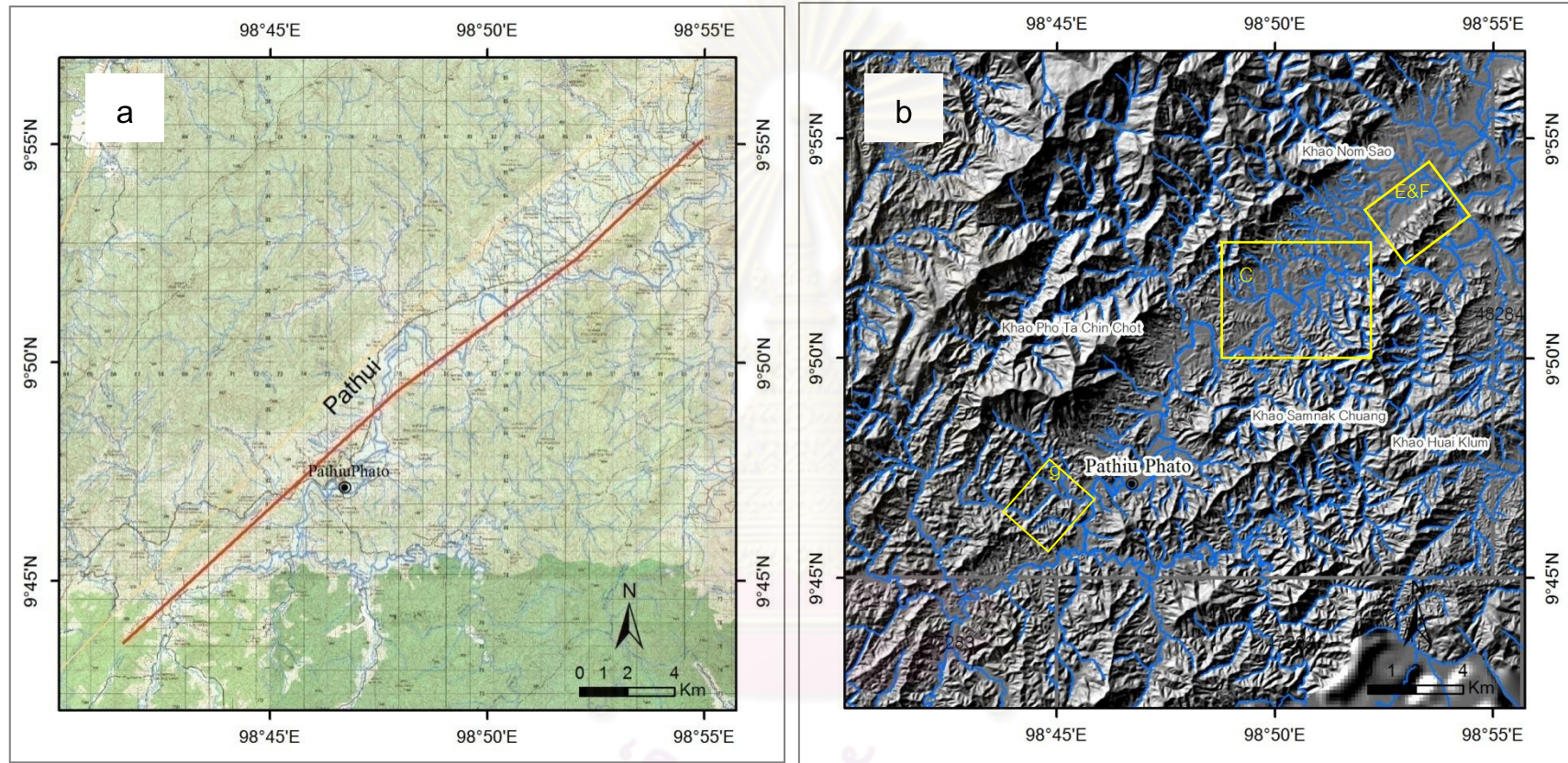


Figure 3.32 (Cont.) 3D colour-orthographic interpretation image (c) along the Pato segment (enlarged figure 3.32b) showing trigular facets at Khoa Nom Soa area, in the Pathui Patho district.



District
 Village
 Pathui fault segment
 Other fault segment
 Stream

Figure 3.33 Topographic maps (a) and 2m contour interval DEM image (b) showing the orientation of Pathui segment in the southern part of RNF and prominent linear valley (g).

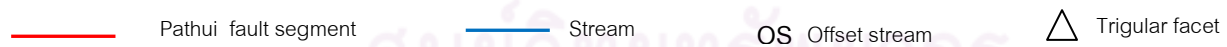
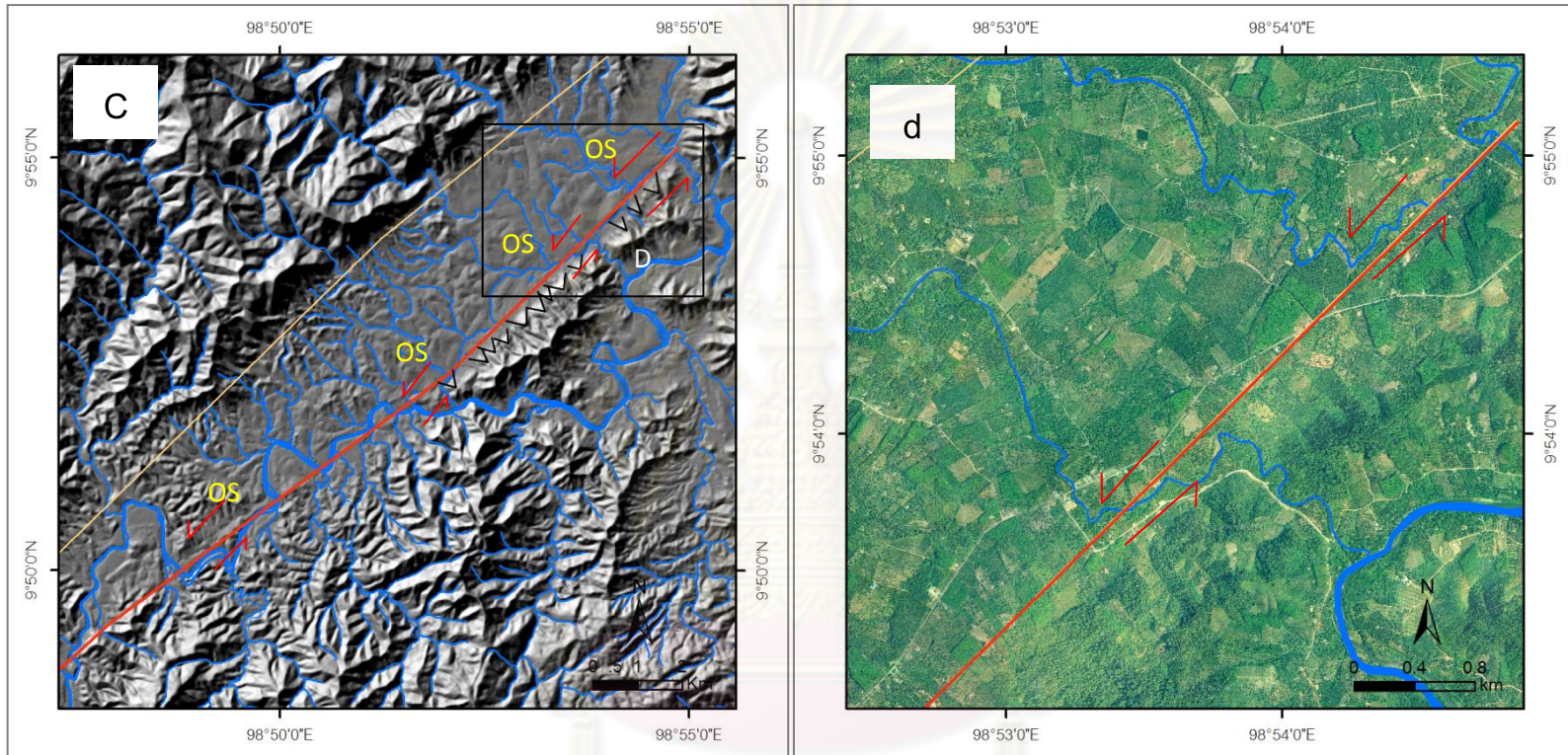
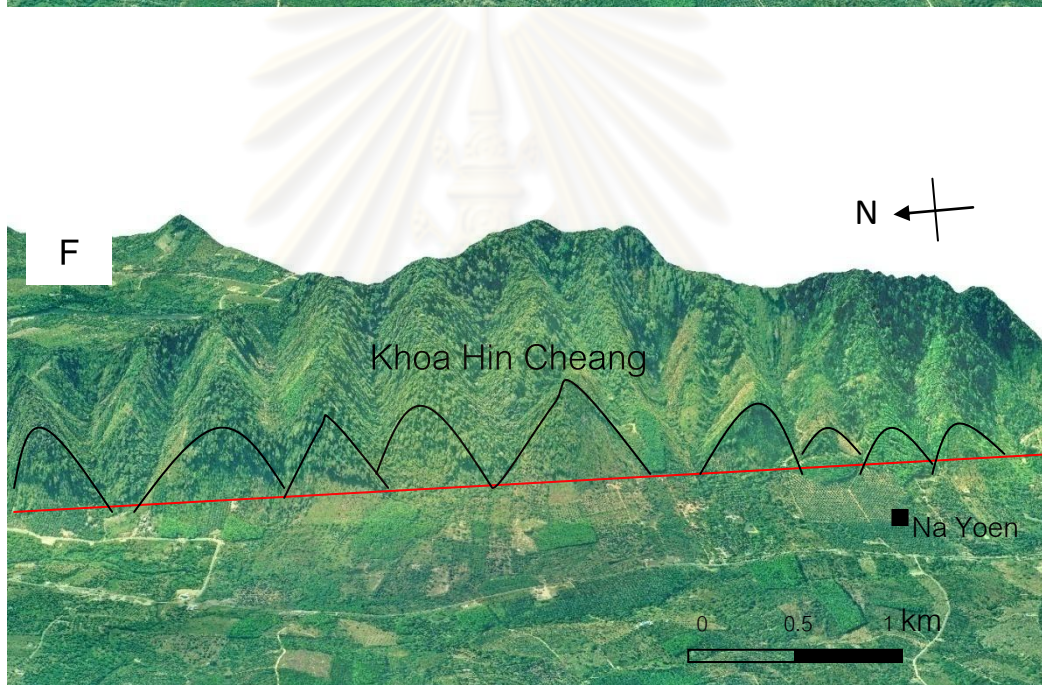


Figure 3.33 (Cont.) Active fault evidence of Pathui segment (enlarged figure 3.33b) from DEM with 2 m contour interval image (c) and enlarge colour-orthographic map from black box in figure 3.33c (d) showing offset streams with left lateral movement.



Village
 Pathui fault segment
 Stream
 OS Offset stream
 Trigular facet

Figure 3.33 (Cont.) Active fault evidence along the Pathui segment (enlarged figure 3.34b) shown as 3D colour-orthographic map (e) and interpreted in this study (f) showing a series of trigular facets in Khoa Hin Cheang area.

CHAPTER IV

MACROSEISMIC INVESTIGATION AND FOCAL MECHANISM

4.1 Macroseismic intensity map (on the 2006 earthquake event in Prachuab Khiri Khan)

Many articles have been published in the newspaper and other media (Thairath newspaper 2006 and Matichon Daily Newspaper 2006) about the earthquake event at Prachuab Khiri Khan on 27th-28th September 2006 and 8th October 2006. The people living in many areas of Prachuab Khiri Khan were able to experience the vibration clearly, attracting more attention from the Thai population as well as the neighborhood countries to the event.

According to the Thailand Meteorological Department (TMD), the center of the earthquake locates in the area of Burma at the latitude of 12.02 degree North longitude of 99.17 degree East with the distance about 70 Kilometers west from Prachuab Khiri Khan(TMD, 2006).

However, the network of seismic centers in other countries (Table no.1) argued that the center of the earthquake was located in Gulf of Thailand. The Earthquake has occurred at the depth between 10-29 kilometers on 27th-28th September and at the depth of 35 kilometers on 8th October.

Earthquake can occur both on land and in the sea because of the descent of the Earth crust, volcanic eruption or the movement of the Earth crust. Yet, the epicenter and the magnitude measured by different stations are not the same in this event (See Table 4.1 and Figure4.1). There is still no conclusion about where it occurs; Burma according Thailand Meteorological Department or it could be gulf of Thailand according to the USGS. Therefore, in order to understand the nature of this earthquake, there is a need to carry out this study which covers three objectives, including: 3 main tasks

1. to locate the correct location of the epicenter of the earthquake.
2. to find out the cause of the earthquake, and
3. to create the intensity map.

Table 4.1 Coordinates of the epicenter locations and the magnitude of the earthquake base on different seismic centers (TMD, 2006).

No.	Date and Time	TMD	USGS (Depth, Km)	GEOFON (Depth, Km)	EMSC (Depth, Km)	GSRC (Depth, Km)
1	27 Sep 2006 2027	N	11.70N,99.96E 4.1 Mb (29)	N	N	N
2	27 sep 2006 2257	N	11.72N,99.87E 4.5 Mb (10)	N	N	N
3	28 sep 2006 0038	12.02N,99.17E 4.2 ML	11.79N,100.0E 4.2 Mb (19)	N	N	N
4	28 Sep2006 0146	12.02N,99.17E 4.8 ML	11.82N,100.14E 4.3 Mb (10)	N	N	N
5	28 Sep 2006 1647	12.02N,99.17E 5.0ML	11.75N,99.99E 4.5 Mb (10)	N	N	N
6	8 Oct 2006 0412	12.02N,99.17E 5.6ML	11.74N,100.18E 5.0 Mb (35)	11.82N,99.85E 4.7 Mb (10)	11.76N,100.06E 4.9 Mb (34)	11.87N,100.15E 5.4 Mb (35)

Note * According to Thai local time USGS USGS= United State Geological Survey,USA

EMSC = European-Mediterranean Seismological Center, Italy

GEOFON = GEOFON Network central geo science research institution, Germany.

GSRC = Geophysical Survey Russian Academy of Sciences, Russia.

TMD = Thailand Meteorological Department (data reported in 2006)

N = No data recorded, Mb = Body-wave magnitude,

ML = Richter magnitude

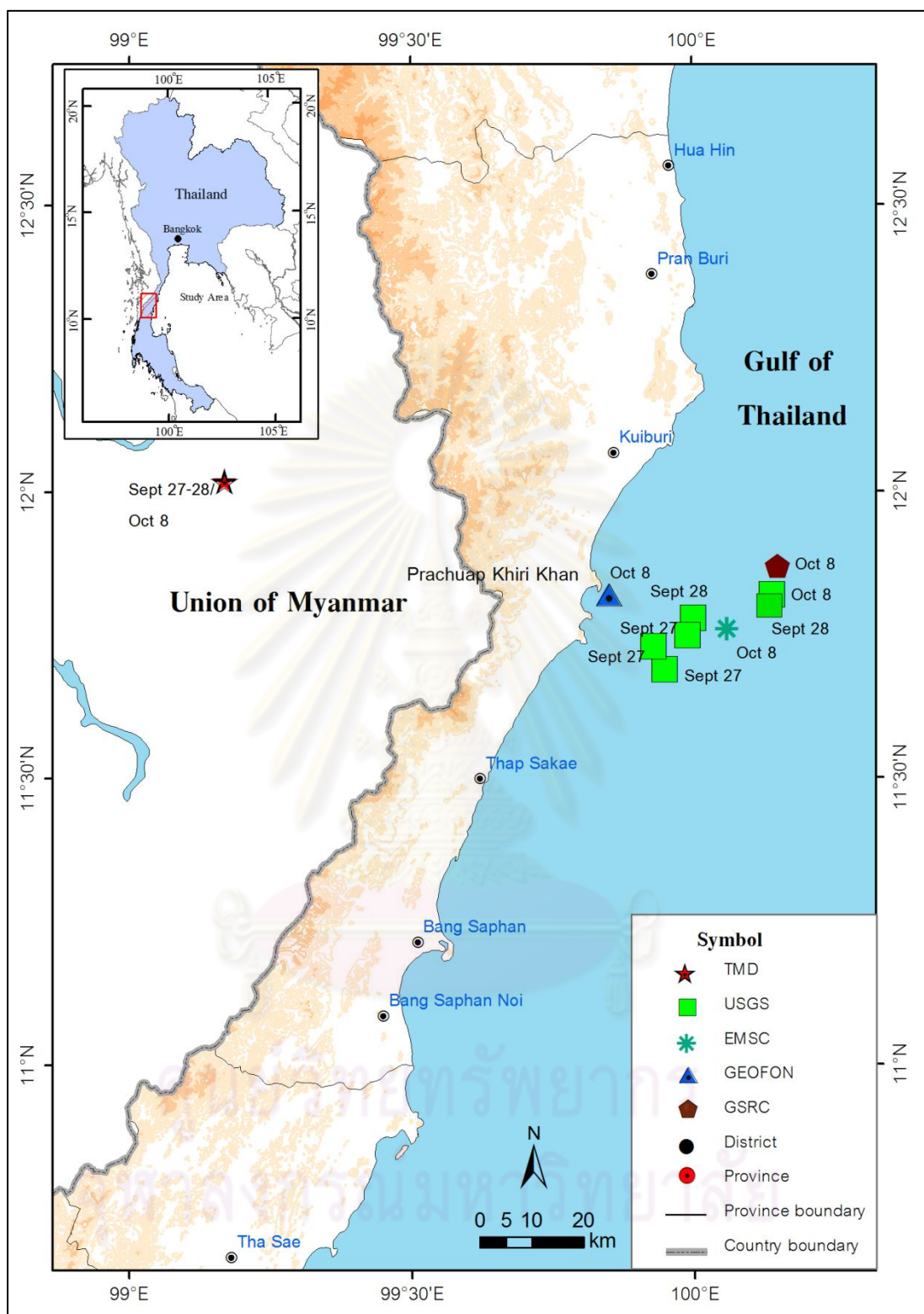


Figure 4.1 Topographic map of Prachuap Khiri Khan area showing earthquake epicenters on 27th-28th September 2006 and 8 October 2006 measured by seismological network stations.

4.1.1 Method of work

In this study, the procedure is divided into many steps as seen in the Figure 4.2. It will be the study of the vibration that can be sensed and seen in a wide area or it can be a field study without any assisted equipment .The study is called macroseismic investigation. There are three major steps:

- 1) Gathering data on the earthquake intensity and field investigate.
- 2) Setting up and comparing the intensity.
- 3) Creating the intensity map using Arc GIS program when all the data is collected. Analyze and codify at the end of the study before concluding.

4.1.1.1 Gathering the Earthquake intensity

There are 3 steps to collect the data:

1. Collect the general data such as topographical map, geological map and the data of the earthquake event occurred in the past.
2. Collect the information of the earthquake on the 27th -28th September 2006 and 8th October 2006 from the other seismic networks (See Table 4.1)
3. Carry out survey regarding the public's opinion of the earthquake intensity. The targeted group will be the people who have place to reside at the time the earthquake occurred with the total of 177 people.(Details are shown in Figure 4.3 and Table 4.2). Furthermore, the data will be collected from the Department of mineral resource which uses survey with the same format as our survey form with the Modified Mercalli Intensity Scale (Table 4.3). The scale was used to investigate the on the 29th September 2006 (Data of the earthquake on 27th-28th September 2006) and 9th October 2006. The numbers of data are 100,150 and 68 respectively following the order of the three events.

Table 4.2 Number of data and time of investigation of the earthquake in this study

Time	Earthquake incident	Number of survey
4 - 5 Oct 2006	27 Sep 2006	68
4 - 5 Oct 2006	28 Sep 2006	68
15 – 16 Oct 2006	8 Oct 2006	41

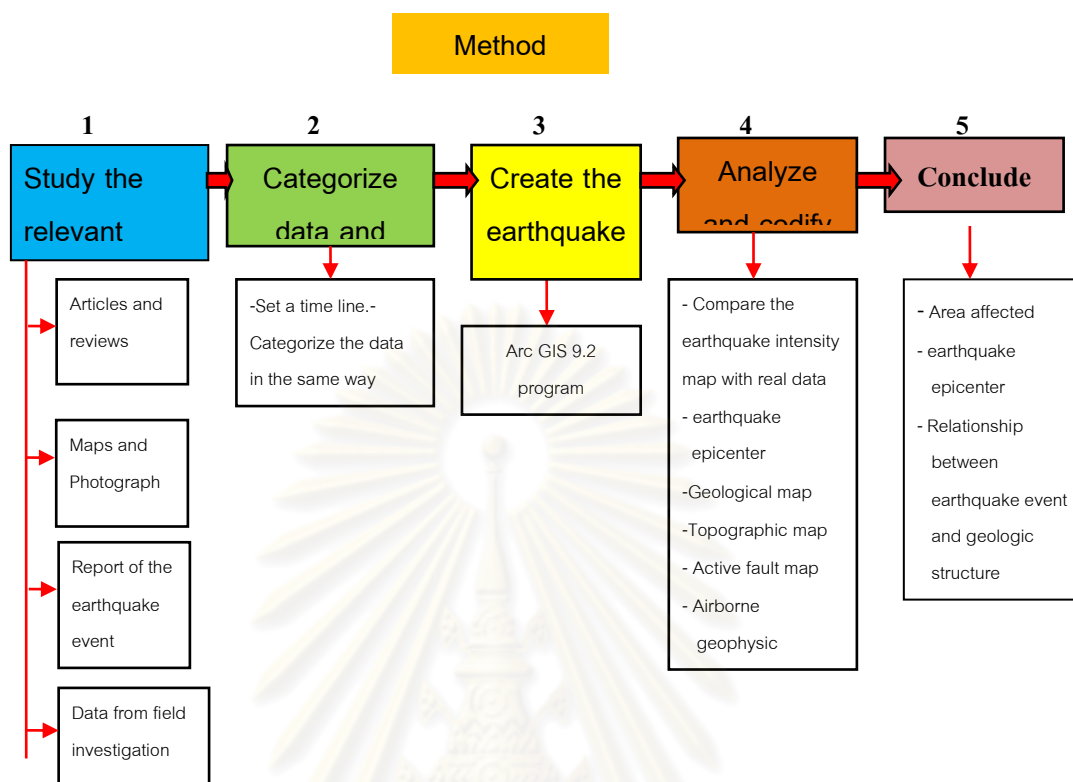


Figure 4.2 Flow chart showing the methodology used in macroseismic investigation.

ศูนย์วิทยทรัพยากร
จุฬาลงกรณ์มหาวิทยาลัย

4.1.1.2 Setting up and comparing the intensity

In this study, the earthquake intensity data collected from the people who felt the vibration. This can be done by considering the people reaction or the vibration of the different types of objects as well as everything that has been destroyed as a result of the earthquake as the criteria to compare with the Modified Mercalli Intensity Scale of Richter(1956). The scale has 12 levels (Table 4. 3) with the distinction in each level at different intensity.

4.1.1.3 Creating the earthquake intensity map

After comparing the earthquake intensity with the standard scale (Table 4.3), the seismic intensity map can be created with Arc.GIS 9.2(2006). Thus, the map can be displayed in the form of isoseismal map so that the data can be analyzed and codified. The overview of the whole procedure is shown in Figure 4.2

Table 4.3 Modified Mercalli Scale (Bolt, 2006)

Intensity	Modified Mercalli Scale
I	Felt by only a few people under very special circumstances
II	Felt by only a few people at rest, especially on the upper floors of buildings
III	Felt noticeably indoors especially on the upper floors of buildings
IV	Felt indoors by many people, outdoors by a few ; some awake
V	Felt by nearly everyone; many awake; dishes and windows break; plaster cracks
VI	Felt by everyone; many frightened and run outdoors; heavy furniture moves
VII	Everyone runs outdoors; slight to moderate damage in ordinary structures
VIII	Considerable damage in ordinary structures; Chimney and monuments fall
IX	Considerable damage in all structures; ground cracks; underground pipes break
X	Most structures destroyed; rails bend; landslides occur; water splashes over banks
XI	Few structures left standing; bridges destroyed; broad fissures in the ground; underground pipes break
XII	Damage total; waves seen on ground surfaces; objects thrown in air

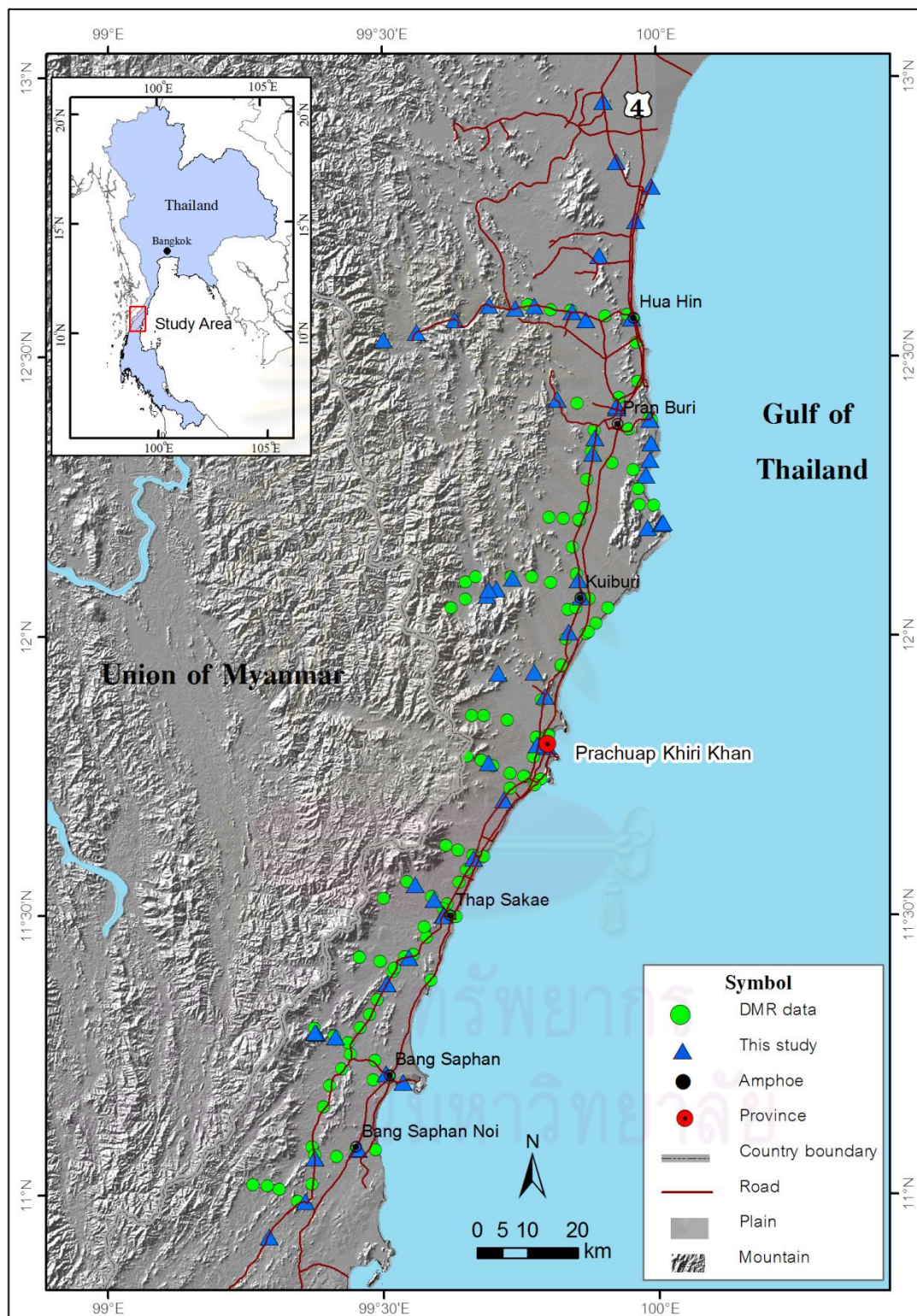


Figure 4.3 Map showing investigated points in Prachuab Khiri Khan province.

(Data from Department of Mineral Resources, 2006).

4.1.2 Result of the study

After analyzing 177 collected data, the intensity can be estimated and the intensity map in Prachuap Khiri Khan Region can be created with the details below.

1) After analyzing 168 data on the 27th September 2006, the magnitude of the earthquake is about 4.2 ML (4.3 Mb). This result in the intensity level from II to V (Figure 4.4). The intensity is high in the northern region and the intensity decreases when the point measured is far from the shore of Pranburi and Kuiburi district in the South and West direction. It can be concluded that the earthquake felt at the flat land at Tub Sakae and Bangsaphan district and have a lower intensity as compared to the intensity in the northern region which are Amphor Muang, Pranburi and Kuiburi district.

2) After analyzing 218 data on the 28th September 2006, the magnitude of the earthquake is about 5.0 ML (4.5 Mb). This results in the intensity level from III to V (Figure 4.5). Though the intensity is higher than that of 27th September 2006, the earthquake felt was divided equally in different regions. It can be felt in Amphor Muang, Pranburi and Kuiburi district and the intensity also subsided offshore.

3) After analyzing 109 data on the 8th October 2006, the magnitude of the earthquake is about 5.0 ML (5.6 Mb). This result in the intensity level from III to V (Figure 4.6). The vibration felt throughout reaches Hua Hin district (Figure 4.6). The vibration spread in the region around the shore of Pranburi and Kuiburi district as well as Amphor Muang

4.1.3 Discussion and Conclusion

4.1.3.1 The location of the earthquake epicenter

From the intensity maps which are shown in the Figure 4.4, 4.5 and 4.6, the idea of the location of earthquake neither conformed to the point estimated by the Thailand Meteorological Department nor the United State Geological Survey, USGS. The researchers try to superimpose the map of the spread of tertiary basin from Qa,

Quaternary alluvium and the map of Qt, Terrace sediment with the earthquake intensity map on the 27th-28th September 2006 and 8th October 2006 according to the GIS procedure (Figure 4.7, 4. 8 and 9). The result indicates that the earthquake occurred mostly on the flat land near the sea. Its intensity decreases in the region of hard rocks. Thus, we believe that the possible epicenter of the earthquake should locate in the offshore area in the Gulf of Thailand. The possibility is higher than the region of Burma (Figure 4.4, 4.5, 4.6, 4.7, 4.8 and 4.9) which I think it may have some relationship with the Kungyaungale Fault WCFS, 1998 which branched from Tennassarim Fault, Bender, 1983. This is because the decrease in intensity will go with the real data if the epicenters locate in the sea for all 3 events.

4.1.3.2 Cause of the Earthquake

According to the remote -sensing interpretation by the Lansat 5TM satellite, the epicenter of the earthquake reported by the Thailand Meteorological Department go with the powerful fault locating in the southern Burma (Figure 4.6), Kungyaungale Fault, WCFS, 1998, which locates in Northeast –Southwest direction and is a branch of Tennassarim Fault . However, when compare the point of the earthquake that occurred in the sea and the above mentioned fault as well as the study of topography, the epicenter of the earthquake should have a stronger relationship to the Ranong fault (Figure 4.10)and structure in gulf of Thailand (Figure 4.12) . Moreover, if we extend the Ranong fault line (Figure 4.10), the line will appear in the sea where the earthquake occurred.

Compared the structural lineament from airborne geophysical interpretation data (DMR, 1989) (Figure 4.11) with the epicenter of the earthquake from different organizations. That found the structural lineament in Prachuap Khiri Khan locates in a group in the East-West direction .This complex structural line may have some relationship with this event. Many people might suspect that if the epicenter of the earthquake occurred in 2006 in Prachuap Khiri Khun locates offshore from the Thai gulf, there may have something to do with the effect of the petroleum or the natural gas production through pumping. The vibration wave may have expanded and causes the earthquake. This case has happened before in the North Sea region between England

and Norway on 7th May 2005. The earthquake has the magnitude about 4.1-4.4 Mw near the petroleum source in EKOFISK. The vibration can be felt on the drilling machine and in the radius of 3-5 kilometers. The cause of the earthquake was that during the drilling process whereby the osmotic pressure in the upper structure increases drastically resulting in the collapsing (Ottemiller and the group, 2005). That case is very different from this event because epicenter of the earthquake has the depth of 10-35 kilometers which is deeper than the level of soft rock in the Thai gulf (Morley, 2001) and the epicenter of the earthquake is very far from the petroleum source (Figure 4.13). Thus, it can be concluded that the drilling/pumping process at the petroleum source is not the true cause of the events.

4.1.3.4 Conclusion

From the research study about the earthquake event at Prachuap Khiri Khan, the results are as followed.

- 1) The intensity of the earthquake (MMI) is at level II to V. The area affected mostly locates near the shore area from Tayang district of Petchburi province to Bangsapan district of, Prachuab Khiri Khan province.
- 2) The satellite photograph shows the active fault with one part in the northern most of the Ranong fault and another is the fault group in Burma.
- 3) From the epicenter of the earthquake appeared in the gulf of Thailand, there might be some relationship with the Ranong fault zone when Bangsaphan segment Bang sapan Noi fault segment , Nong Ya Plong fault segment and Tub Sakae fault segment which lie across the sea.
- 4) The airborne geophysical data demonstrate the structural lineament that lies in the east -west direction which might have some relationship with the epicenter of earthquake.
- 5) The epicenter of the earthquake might be relationship with the structural lineament in gulf of Thailand which lies in north –south direction and near the epicenters.

Note, that the epicentral location as reported by TMD were relocated in Prachuab Khirikhan Earthquakes and its aftershocks project, 2007. The new record shows the epicenter of earthquake event on 27th-28th September 2006 and 8th October 2006 occurred in offshore areas in the Gulf of Thailand (Table 4.4)

Table 4.4 The relocated coordinates of the epicenter and the magnitude of the earthquake from TMD (2007) and different seismic center.

No.	Date and Time	TMD	USGS (Depth, Km)	GEOFON (Depth, Km)	EMSC (Depth, Km)	GSRC (Depth, Km)
1	27 Sep 2006 2027	11.73N, 99.75E 4.4 ML	11.70N,99.96E 4.1 Mb (29)	N	N	N
2	27 sep 2006 2257	11.80N, 99.75E 4.6 ML	11.72N,99.87E 4.5 Mb (10)	N	N	N
3	28 sep 2006 0038	11.87N, 99.68 E 4.8 ML	11.79N,100.0E 4.2 Mb (19)	N	N	N
4	28 Sep2006 0146	11.73N, 99.74 E 4.8 ML	11.82N,100.14E 4.3 Mb (10)	N	N	N
5	28 Sep 2006 1647	11.80N, 99.89E 5.1 ML	11.75N,99.99E 4.5 Mb (10)	N	N	N
6	8 Oct 2006 0412	11.67N, 100.06E 5.23 ML	11.74N,100.18E 5.0 Mb (35)	11.82N,99.85E 4.7 Mb (10)	11.76N,100.06E 4.9 Mb (34)	11.87N,100.15E 5.4 Mb (35)

Note * According to Thai local time USGS USGS= United State Geological

Survey, USA

EMSC = European-Mediterranean Seismological Center, Italy

GEOFON = GEOFON Network central geo science research institution, Germany.

GSRC = Geophysical Survey Russian Academy of Sciences, Russia.

TMD = Thailand Meteorological Department (data reported on 2007)

N = No data recorded, Mb = Body-wave magnitude,

ML = Richter magnitude

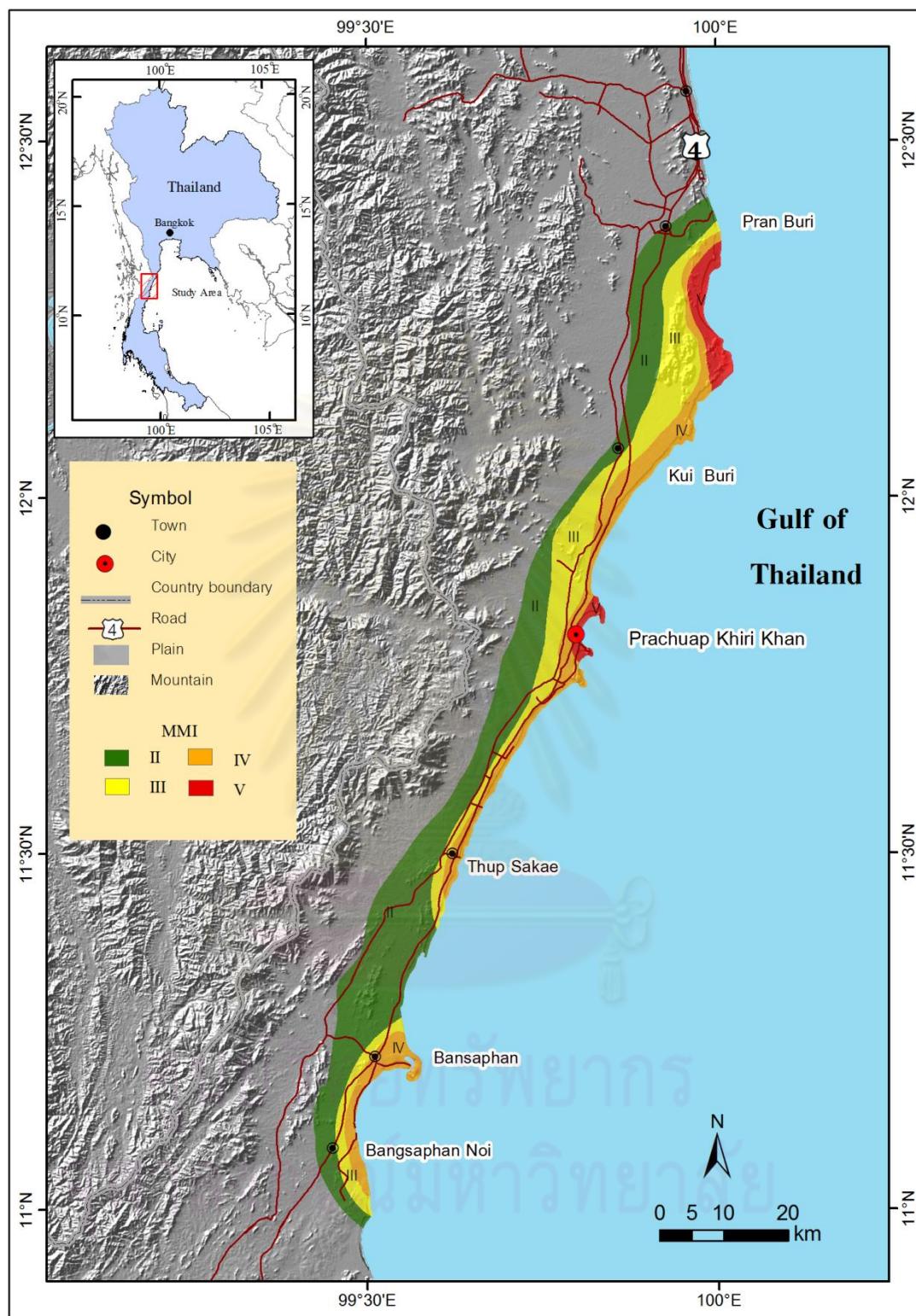


Figure 4.4 Earthquake intensity map showing the result from macroseismic investigation (Thipyopass et al., 2009) for the earthquake taking places on 27th September 2006 (based on the Modified Mercalli Intensity scale (MMI)).

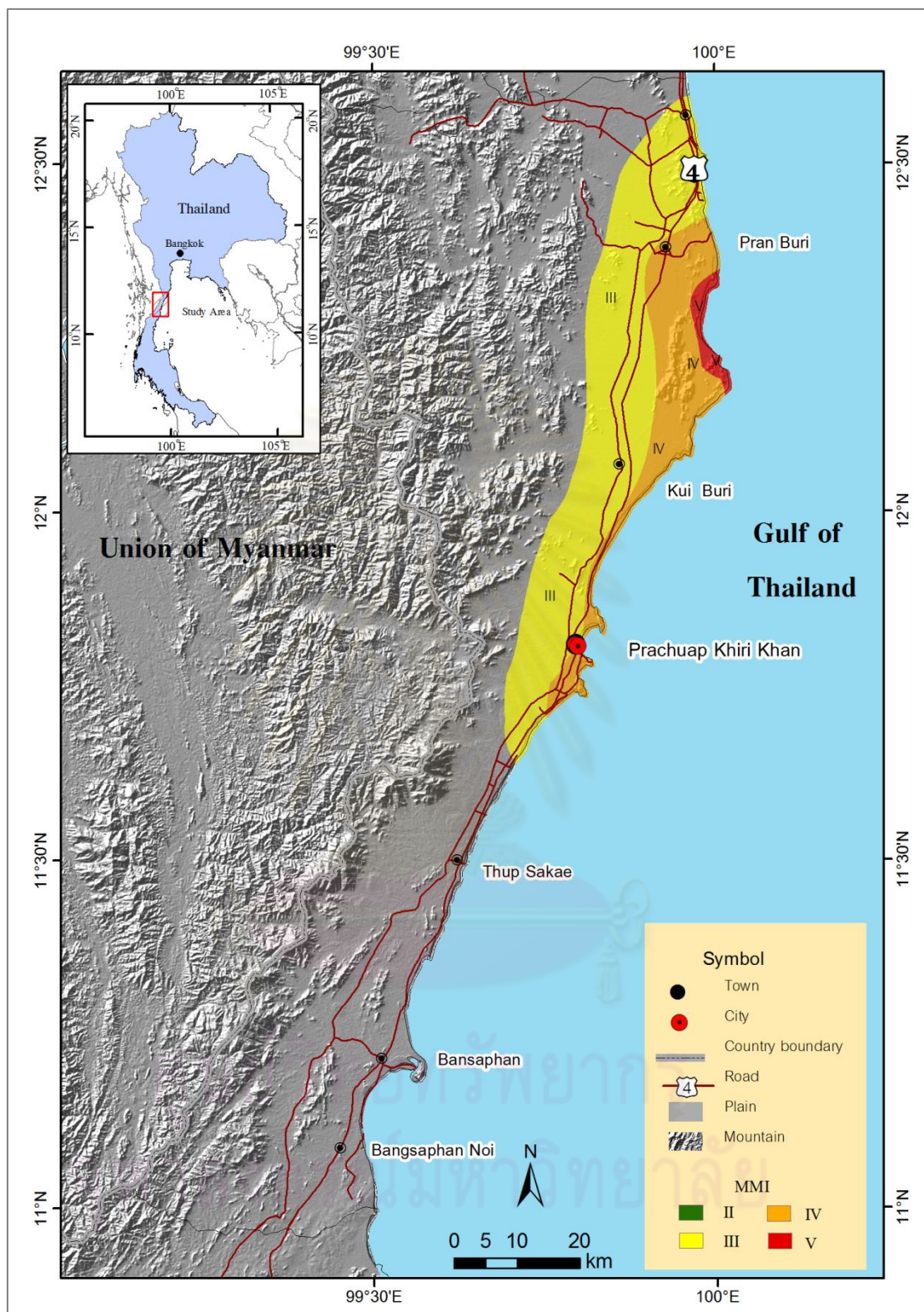


Figure 4.5 Earthquake intensity map showing the result from macroseismic investigation (Thipyopass et al., 2009) for the earthquake taking places on 28th September 2006 (based on the Modified Mercalli Intensity scale (MMI)).

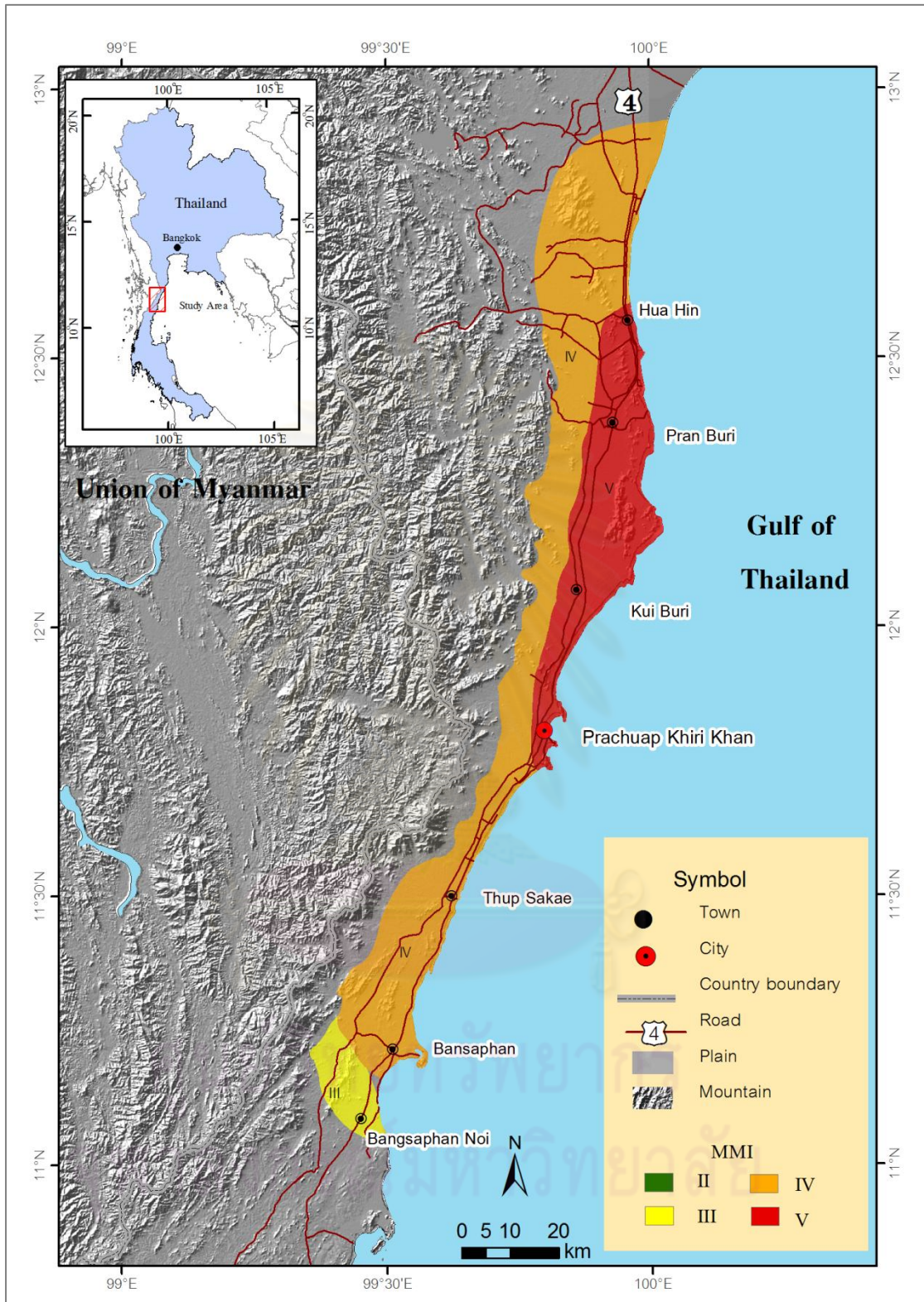


Figure 4.6 Earthquake intensity map showing the result from macroseismic investigation (Thipyopass et al., 2009) for the earthquake taking places on 8th October 2006 (base on the Modified Mercalli Intensity scale (MMI)).

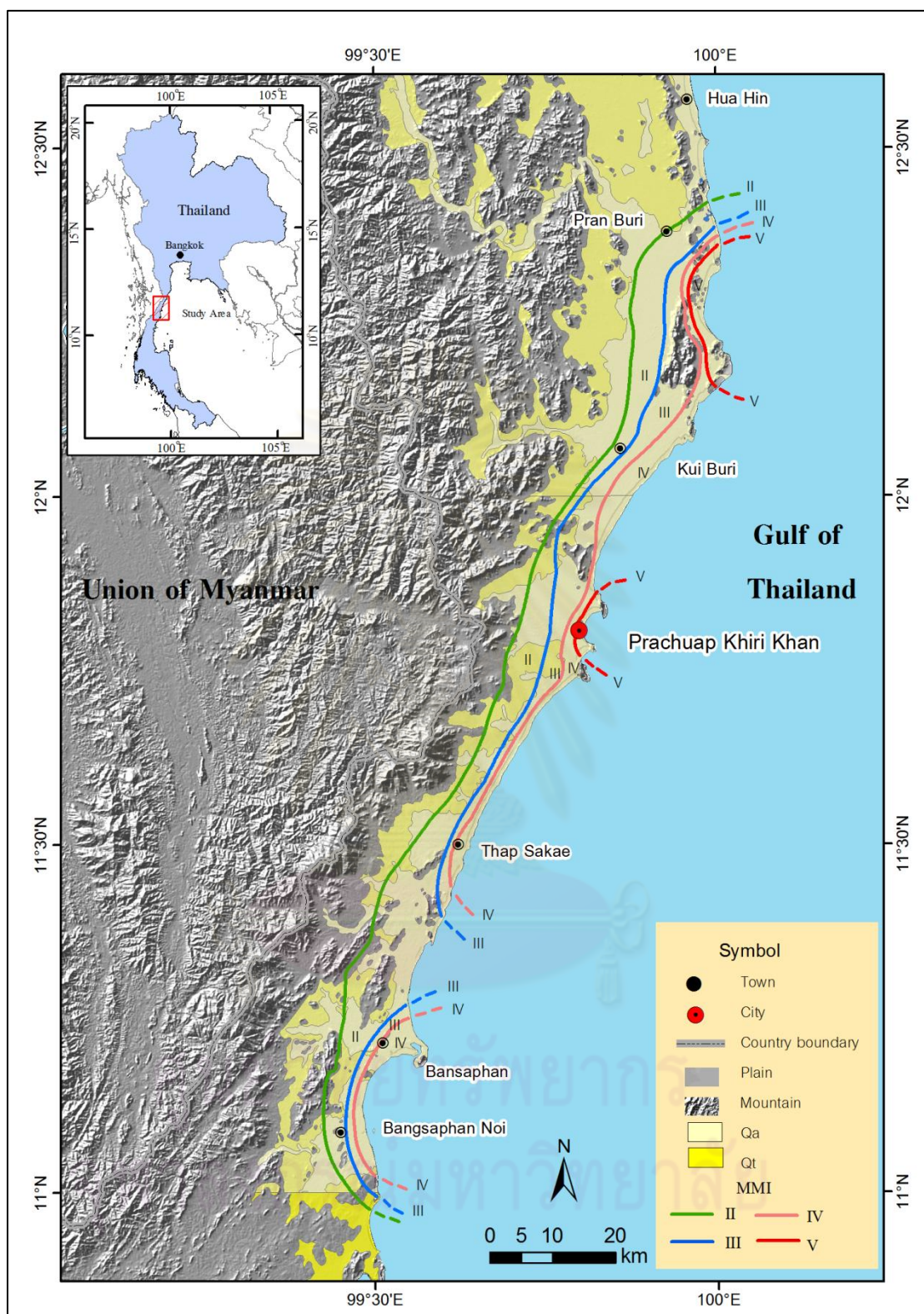


Figure 4.7 Distribution of Cenozoic deposits in Prachuab Khirikhan area (DMR, 2005) after superimposing with intensity contour of earthquake event on 27th October 2006 (based on the Modified Mercalli Intensity scale (MMI)).

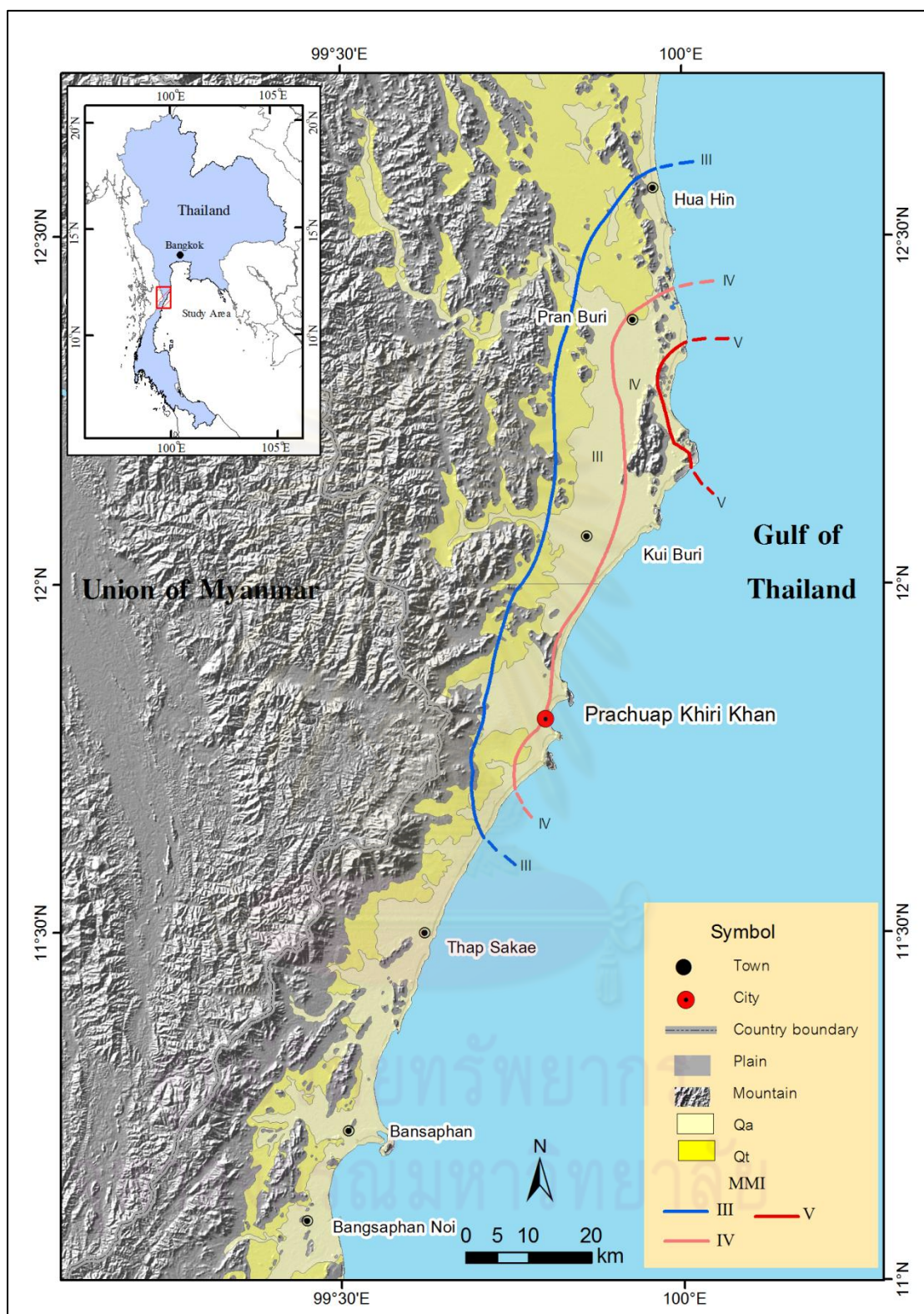


Figure 4.8 Distribution of Cenozoic deposits in Prachuab Khirikhan area (DMR, 2005) after superimposing with intensity contour of earthquake event on 28th October 2006 (based on the Modified Mercalli Intensity scale (MMI)).

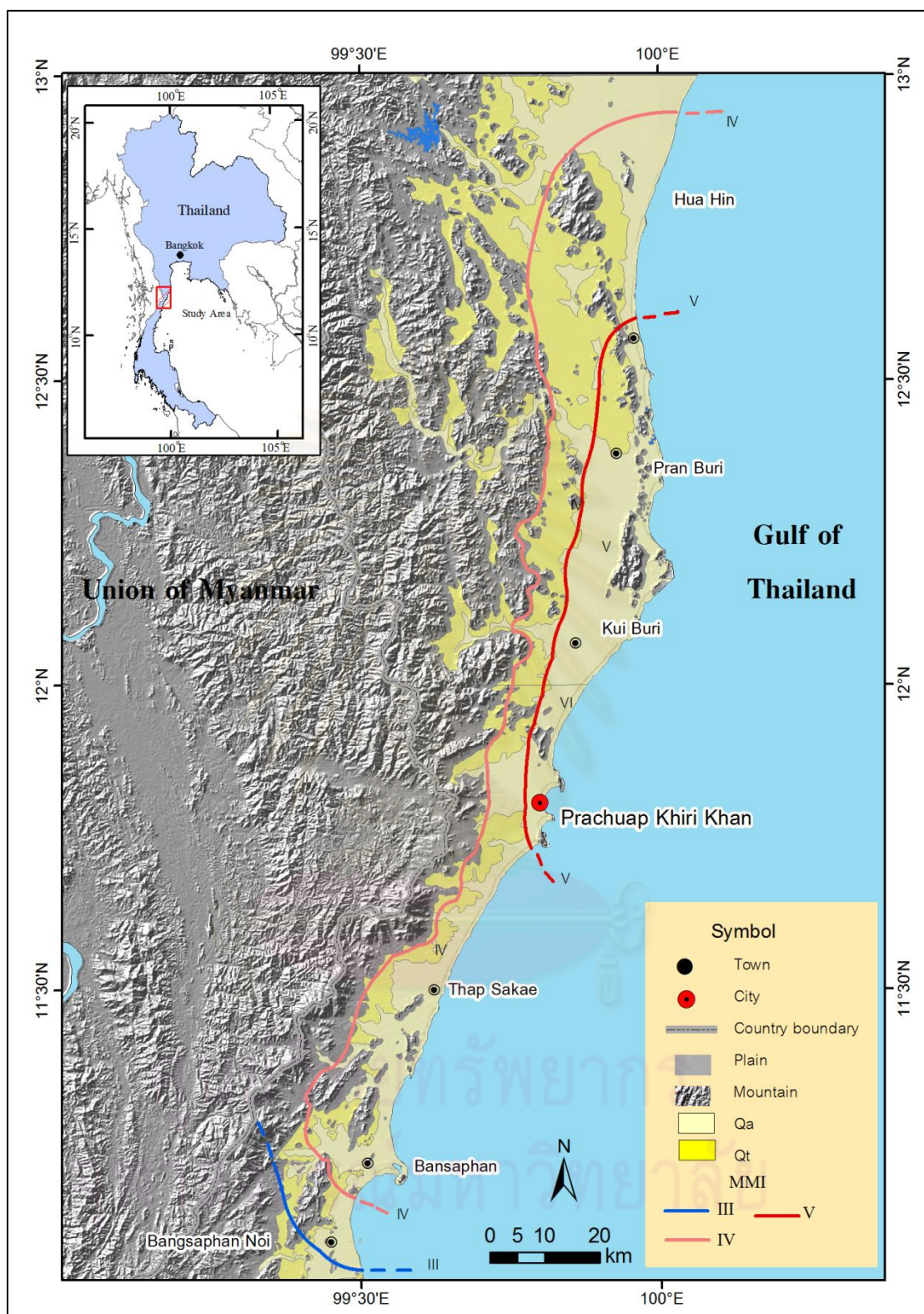


Figure 4.9 Distribution of Cenozoic deposits in Prachuab Khirikhan area (DMR, 2005) after superimposing with intensity contour of earthquake event on 8th October 2006 (based on the Modified Mercalli Intensity scale (MMI)).

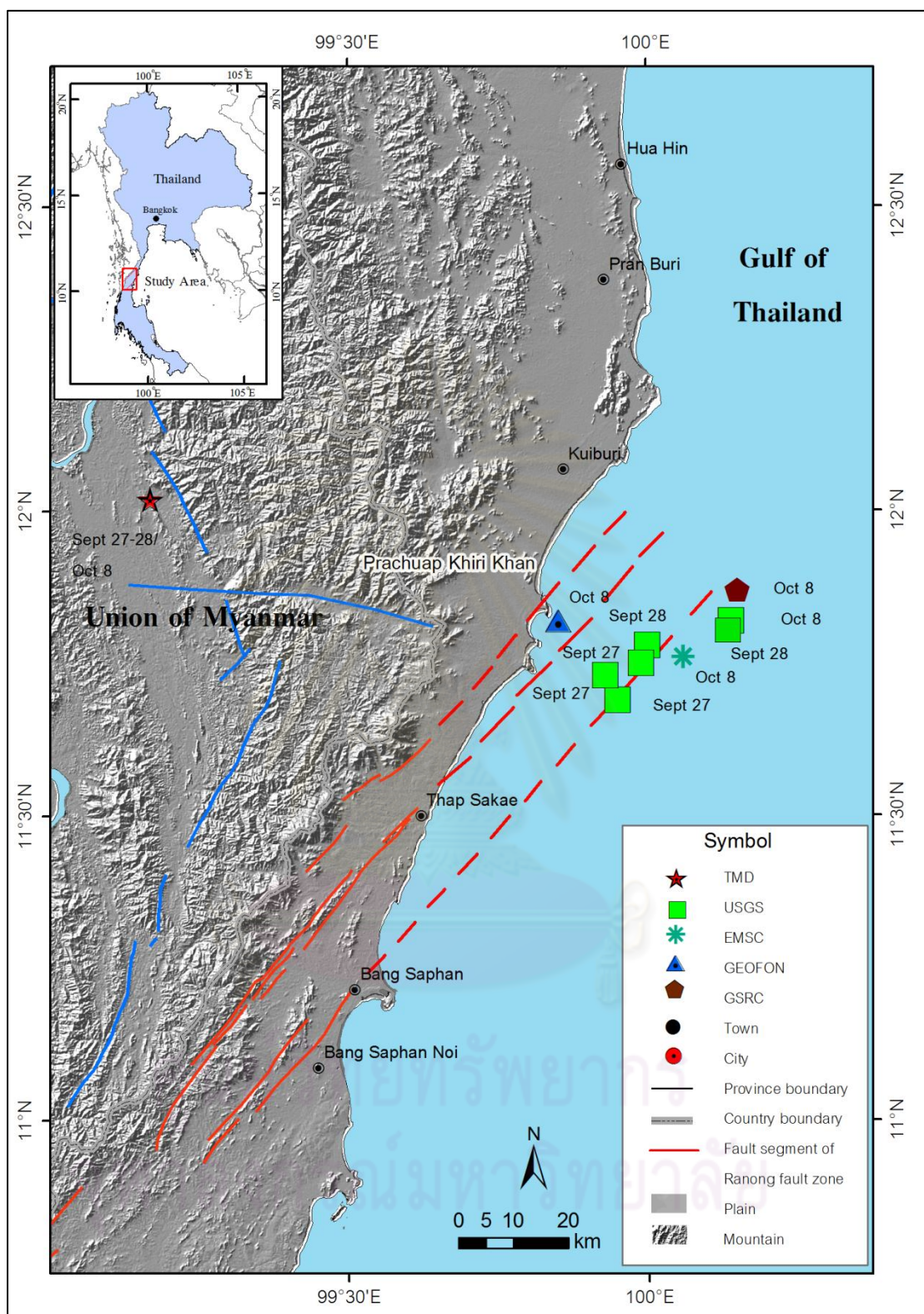


Figure 4.10 Map of Prachuab Khiri Khan and nearby regions showing the epicenter of earthquake event on 27th-28th September and 8th October 2006 and fault segments of the RNF.

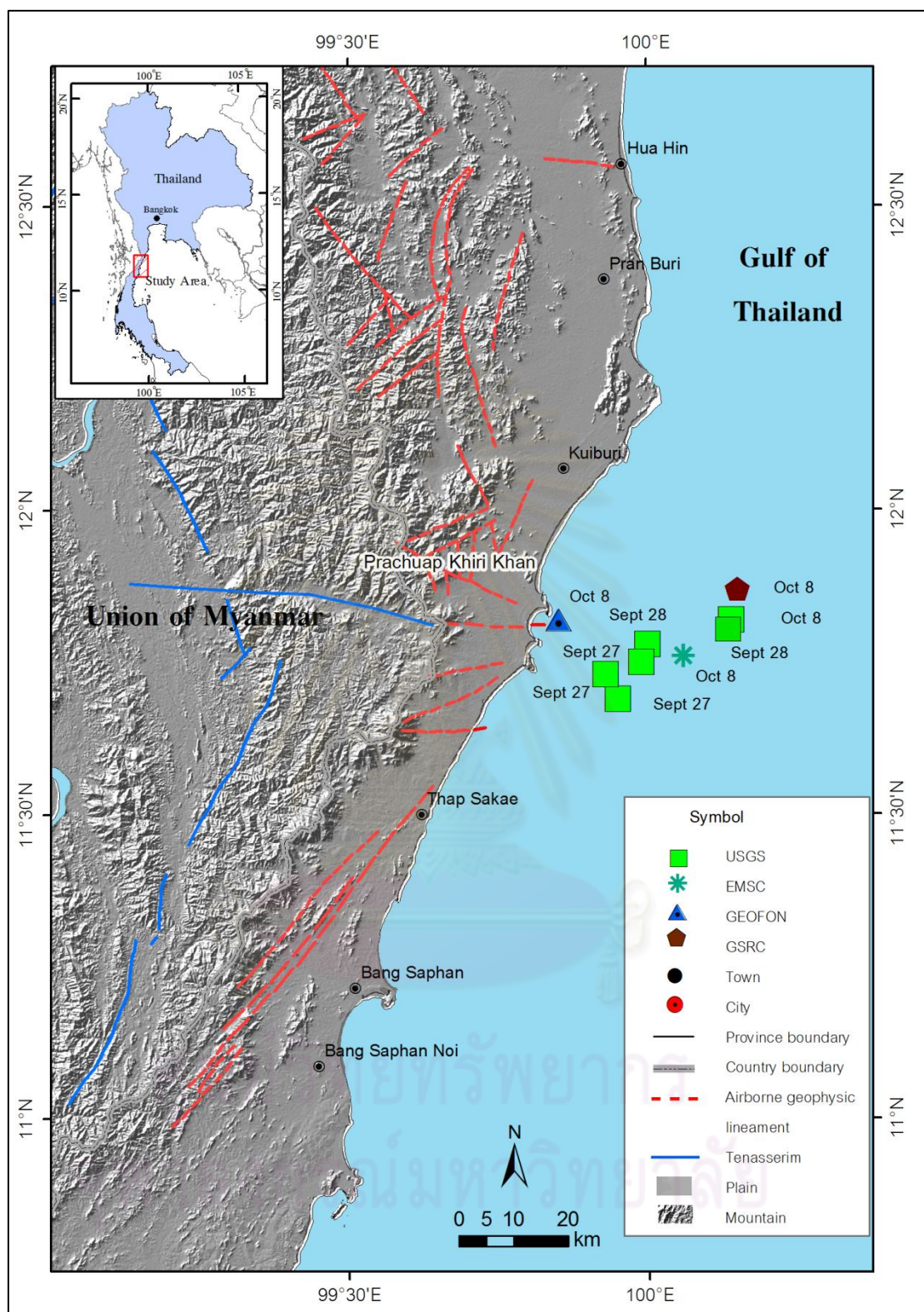


Figure 4.11 Map of Prachuab Khiri Khan and nearby region showing the epicenter of earthquake event on 27th-28th September and 8th October 2006 and interpreted lineament from magnetic data (Kenting Earth Sciences International LTD,1989).

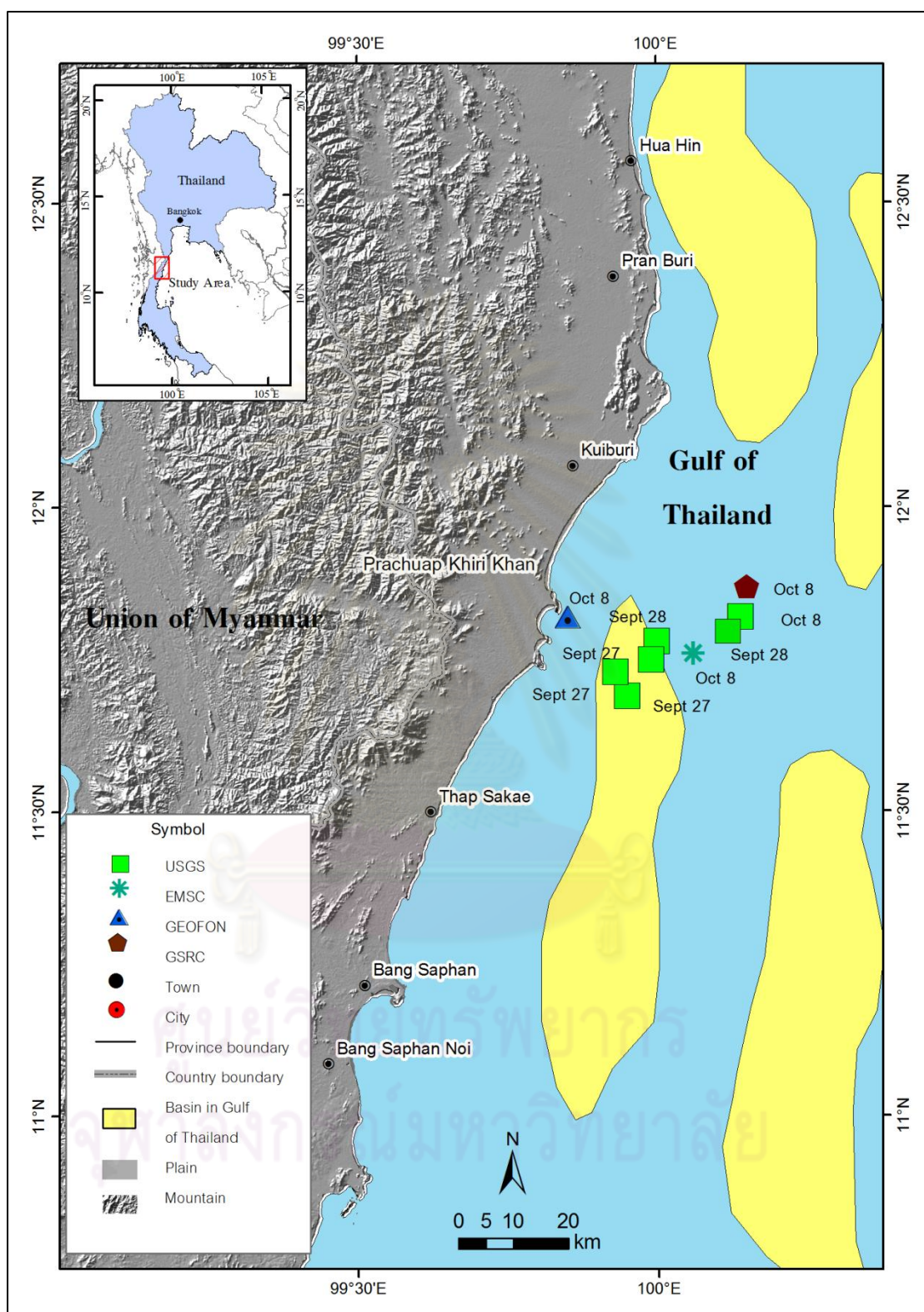


Figure 4.12 Map of Prachuab Khiri Khan and the nearby region indicating the epicenter of earthquake event on 27th-28th September and 8th October 2006 comparing with basin geometry of Gulf of Thailand (DMR,2006).

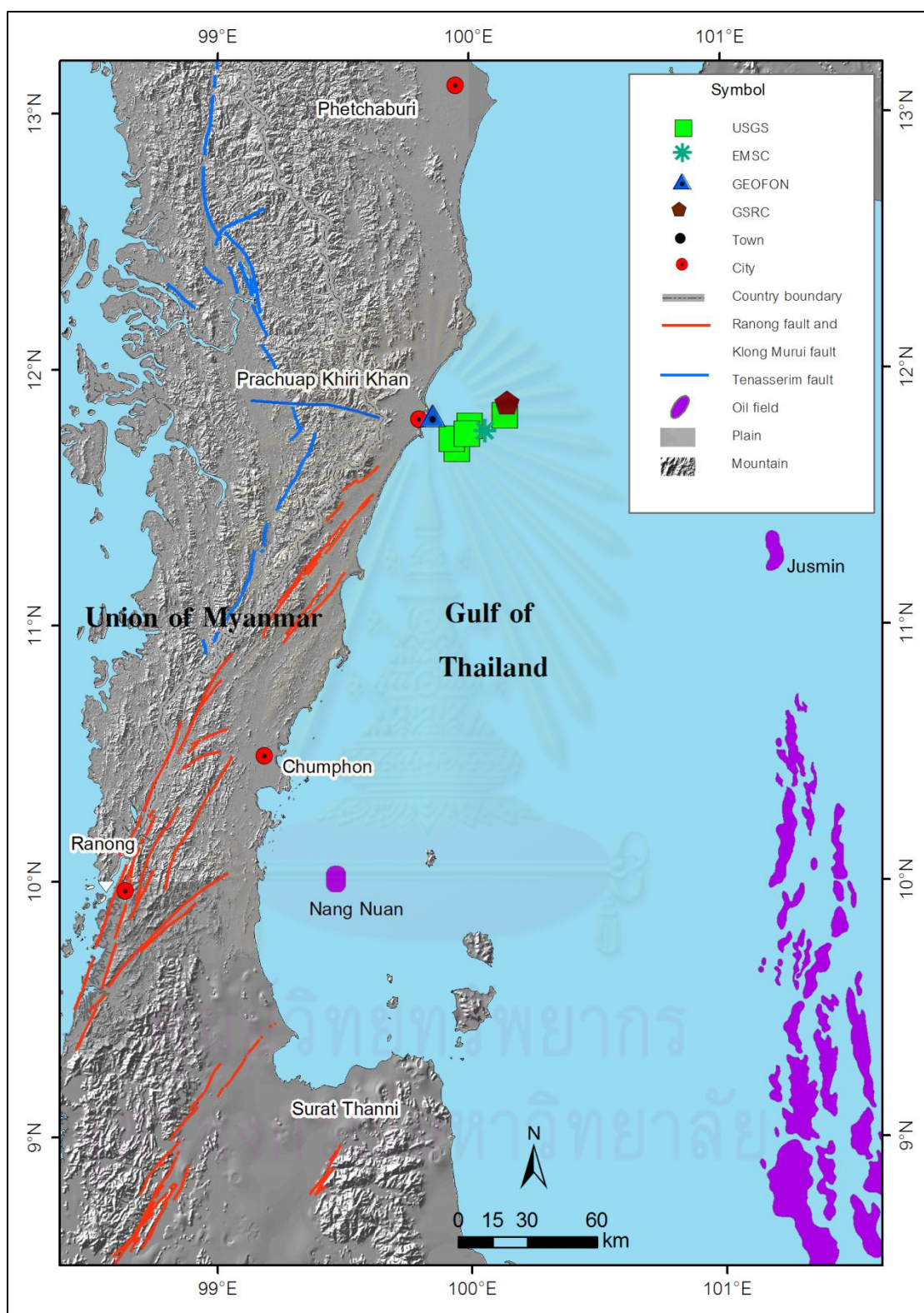


Figure 4.13 Map shows the epicenter of the earthquake, lineaments of active faults, and oil fields in the gulf of Thailand (DMF, 2009).

4.2 Focal Mechanism(on 8th October 2006 earthquake event in Prachuab Khiri Khan)

From macrosiesmic investigation of earthquake event on 8th October 2006 about 5.0 Mb found that epicenter of these event in Gulf of Thailand. It may be related with major structures of southern Thailand (Ranong fault zone) or major structure in Gulf of Thailand (North-South structure), Thus will be use seismic waveform to find focal mechanism of this event

4.2.1 Basic concept of Focal mechanism

The focal mechanism of an earthquake describes the inelastic deformation in the source region that generates the seismic waves. In the case of a fault-related event it refers to the orientation of the fault plane that slipped and the slip vector and is also known as a fault-plane solution. Focal mechanisms are derived from a solution of the moment tensor for the earthquake, which itself is estimated by an analysis of observed seismic waveforms. The focal mechanism can be derived from observing the pattern of "first motions", that is, whether the first arriving P waves break up or down. This method was used before waveforms were recorded and analysed digitally and this method is still used in this study for earthquakes too small for easy moment tensor solution.

Seismologists use information from seismograms to calculate the focal mechanism and typically display it on maps as a "beach ball" symbol. This symbol is the projection on a horizontal plane of the lower half of an imaginary, spherical shell (focal sphere) surrounding the earthquake source (Figure 4.15). A line is scribed where the fault plane intersects the shell. The stress-field orientation at the time of rupture governs the direction of slip on the fault plane, and the beach ball also depicts this stress orientation. In this schematic, the gray quadrants contain the tension axis (T), which reflects the minimum compressive stress direction, and the white quadrants contain the pressure axis (P), which reflects the maximum compressive stress direction. The computed focal mechanisms show only the P and T axes and do not use shading.

4.2.2 Methodology

1) From the preliminary determination of the epicenter, we know the location and origin time of the earthquake. Computed the distance between each station and the

Schematic diagram of a focal mechanism

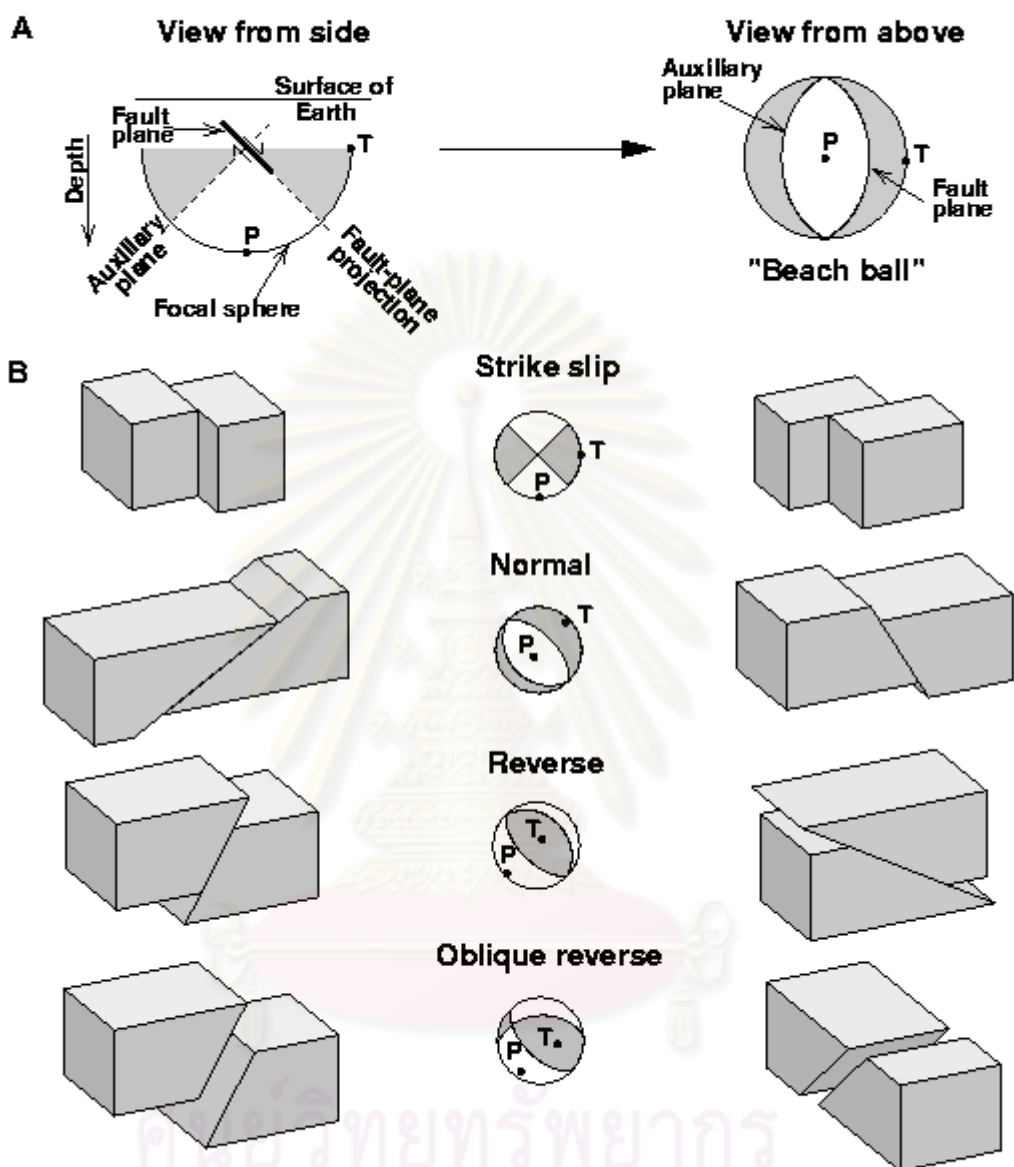


Figure 4.14 Schematic diagram of a focal mechanism showing three types of faulting and their stereo-plot results.

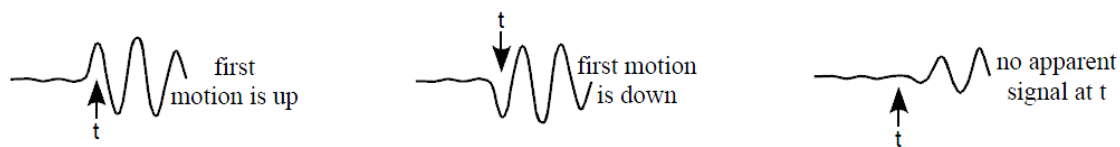


Figure 4.15 Direction of P-first motions (Vince Cronin, 2004)

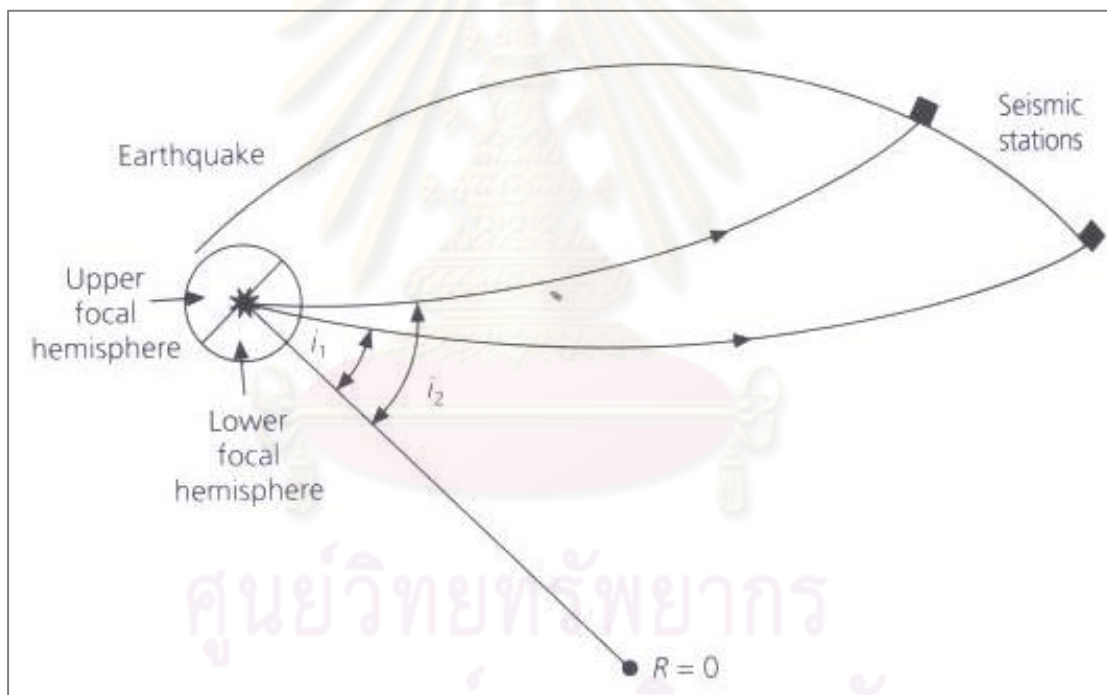


Figure 4.16 The angle (from vertical) that the ray leaves the earthquake is the take-off angle (<http://www.learninggeoscience.net/free/00071>)

epicenter. Then use a standard seismic-velocity model of Earth to define the exact time (t) that the P-wave of the earthquake should have arrived at each station. Consulting the seismogram recording the vertical component at each station, evaluate whether the first motion detected at that station was an “up” motion, a “down” motion, or no apparent signal at the expected time. (Figure 4.15)

2) The portion of the energy received by each seismograph, that left the earthquake focus in the form of a compressional P-wave, can be thought of as having traveled along a *ray path* from the focus to the seismograph. We have to know two things about that ray for each station: the *azimuth* along which it traveled from the earthquake focus to the station, and its take-off angle (also known as angle of emergence). The take-off angle is the angle between the ray as it just emerges from the focus and an imaginary vertical line extending through the focus. In routine work, the take-off angle is interpreted from a table that relates take-off angle to distance between the focus and the station. (Figure 4.16)

Next step, plot the data on a lower-hemisphere stereographic projection use an equal-area stereonet. For each station, the symbol is placed along a line extending from the center of the plot toward the azimuth of the station relative to the earthquake focus, and the take-off angle defines the angular distance from the center of the plot to the symbol.

In this study additionally data from 6 seismic stations of Thailand Meteorological Department were taken from 2 stations from the report of Earthquake hazard Risk study in Prachuab Khiri Khan Province and adjacent Area (Pananon, 2009) to analyze as shown in Table 4.5 (Figure 4.17)

From 8 seismograph stations, it is observed that the first motion of P wave that 6 station in this study were up (Figures 4.18-4.19) and 2 data from Pananon(2009) were down. The overall picture shows that the calculated distance and azimuth between hypocenter and each seismic stations (Table 4.5). Take -off angle can interpreted from table of take off angle (Japan Meteorological Department, 1990). Then plot data on a stereographic projection (Figure 4.20).

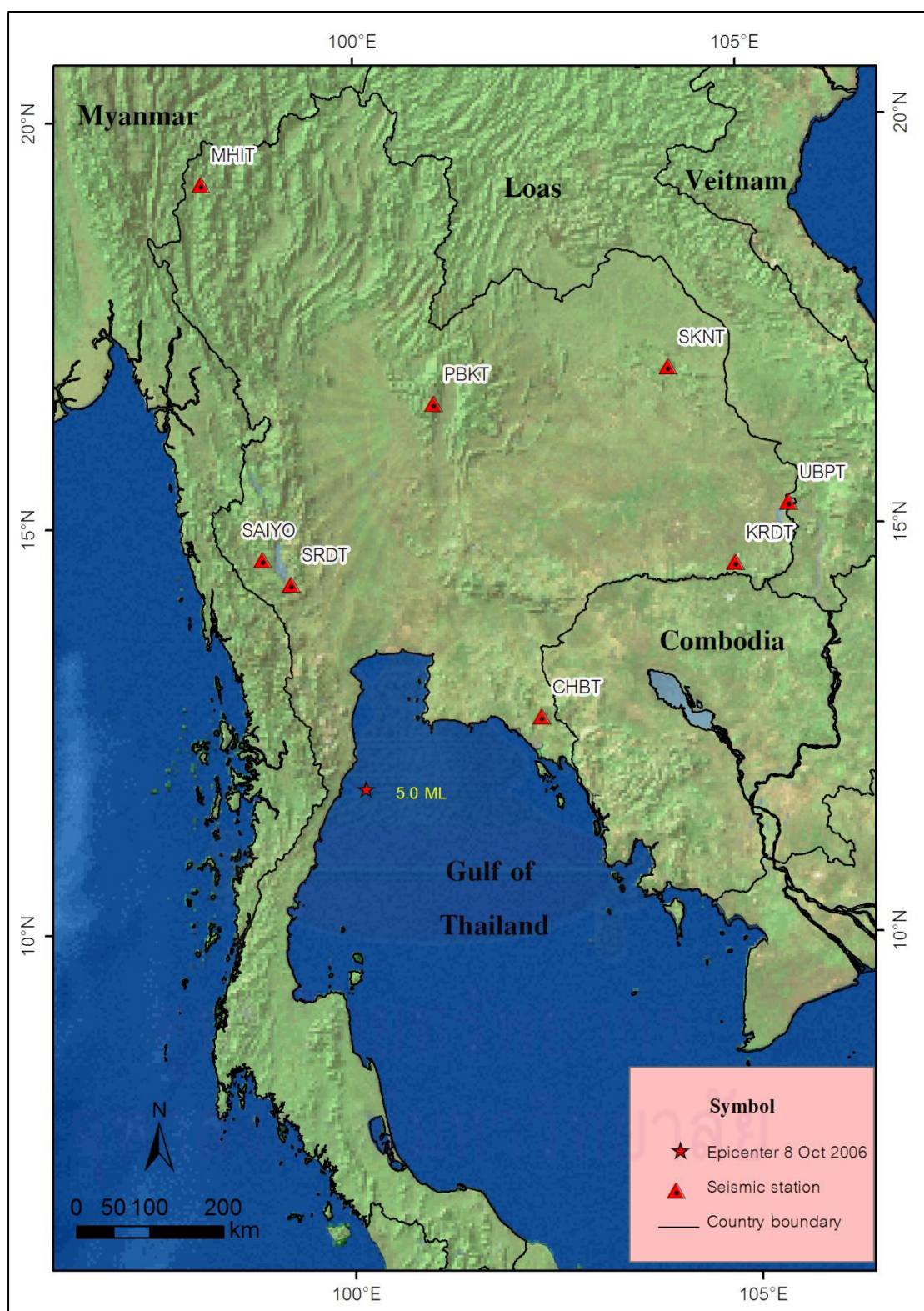


Figure 4.17 The map of seismic station which recorded seismograph of the earthquake event on 8th October 2006.

Table 4.5 Seismic station , location and first time of P-wave arrival in this study

Station code	Location	Longitude	Lattitude	Time (GMT)
CHBT	Chantaburi	102.329	12.7526	21:13:03.9187
MHIT	Mae Hong Son	97.9632	19.3148	21:14:19.3898
PBKT	Phetchaboon	100.9687	16.5733	21:14:33.7568
SRDT	Kanchanaburi	99.1212	14.3945	21.13.10.2578
UBPT	Ubonrachatani	105.4695	15.2773	21:15:08.3346
SAIYO	Kanchanaburi	99.6633	14.56722	21.13.08.9700
KRDT	Nakornratchasima	104.4482	14.5905	-
SKDT	Sakonnakorn	103.9150	16.9742	-

Note KRDT and SKDT from Pananon, (2009)

Table 4.6 Parameters used for calculation of focal mechanism

Station code	Distance (km)	Azimuth (degree)	Take- off angle (degree)
CHBT	270.56	68	21
MHIT	870.58	345	27
PBKT	545.06	10	25.5
SRDT	310.97	340	22.5
UBPT	704.09	55	26.3
SAIYO	319.58	350	26.6
KRDT	606.60	60	26
SKNT	718.10	36	26.5

4.2.3 Preliminary Result

The seismological data(6 stations) that have been used to create beach ball as shown in Fig. 4.21. It is found that the earthquake caused by movement of fault can happen in three variations which are normal fault, reverse fault and oblique fault.

If the angle of the fault is lower than 15 degree or between 75-85 degree, the movement of the fault can occur in all three ways. The Normal fault can be possibly

caused by the fault with fault plane lie in the direction of N70E-N30W(70-330 degree). The reverse fault can be possibly triggered by the fault with fault plane lie in the direction N65E-S25E(65-155 degree). The oblique fault can be possibly generated by the fault with fault plane lie in the direction N20W-N64W(296-340 degree) and S30E-S70E(110-150 degree).

If the angle of the fault is lower than 30-60 degree, the movement of the fault can occur in two ways- Normal fault and Oblique fault (normal fault and strike slip fault). In the case of normal fault, it can be possibly caused by the fault with fault plane lie in the direction N80E-N35W (80-325 degree). For the case of oblique fault, it is just the movement along the normal fault with strike slip fault. The range of value of the fault plane is steeper than that of the normal fault. If the angle of the fault dip is set at 30° or 60° , the fault planes lie in the directions of NS, N8 E, N28, N56E, S30W, S10E-S80E and S50W-N40W. If the angle of the fault dip is set at 40° or 50° , the fault planes lie in the directions of N 20E, N30W,S70E,S60W,S85E,N35W. If the angle of the fault dip is set at 45° , the fault planes lie in the direction of N80E, N30W, S60E, S35E, N70W and N85W.

We can see that the plotting of low number of data can result in many variations of the fault plane direction. Therefore, in this study, seismological data derived from the seismograph from the report of Earthquake. Pananon (2009) were added for analysis as shown in Table 4.5, and the new beach ball was presented as shown in Fig. 4.23. After putting the data from the 2 seismic stations from Pananon (2009) with the current research data, I found that the first motion of P wave from the two new stations was down. This enables me to narrow down the direction of the fault plane and allow me to construct beach ball as shown in figure 4.23. We have discovered that the movement of fault can happen in two ways either normal fault or oblique fault.

The possibility of being the normal case is very low because the earthquake is caused by the fault plane in the direction of N45E, S50W with the dip at 45° . Otherwise, in the case of oblique fault, the movement along the fault became normal with the strike slip component in the ranges of N36E-N60E (36-60 degree) and S40W-S70W (200-250 degree).

4.25 Discuss and Conclusion

From the result of this research study, the focal mechanism based on beach ball analysis is compared with the main structure which may be the cause of this earthquake (8 Oct 2006) such as the fault in the north- south direction which is the main structure creating the main basins in Gulf of Thailand. The studied faults may have moved in the normal fault type and the group of Ranong fault with movement in the left lateral direction largely strikes in the northeast-southwest. I have found that:

1. The earthquake has occurred along the normal fault plan which strikes in North-south direction following to the main structure in the Gulf of Thailand. If the beach ball has the relationship as stated, it will have the movement of the fault plane in the oblique sense type with the dip angles from 30-60 degree (Fig.4.23).

2. If the earthquake has the relationship with the group of Ranong fault that cut through the Gulf of Thailand, it will show the same beach ball with the focal mechanism of the oblique fault with the dip angle from 30-60 degree as well (Fig.4.23).

3. Therefore, we can conclude that the earthquake is related to the oblique fault rather than the normal fashion.

4. As the data from this research study has low quantity, this study of the fault plane and focal mechanism might not be accurate. This is because the low quantity of data prevents me from assessing the accuracy of the movement in each station which in turn use to translate the First Motion of P-wave. Since the data cannot be compared with other stations which locate around the same area, I cannot check whether it is the same which will allow us to remove the error from the station due to the different types of noise wave thus the result from this research is only preliminary result.

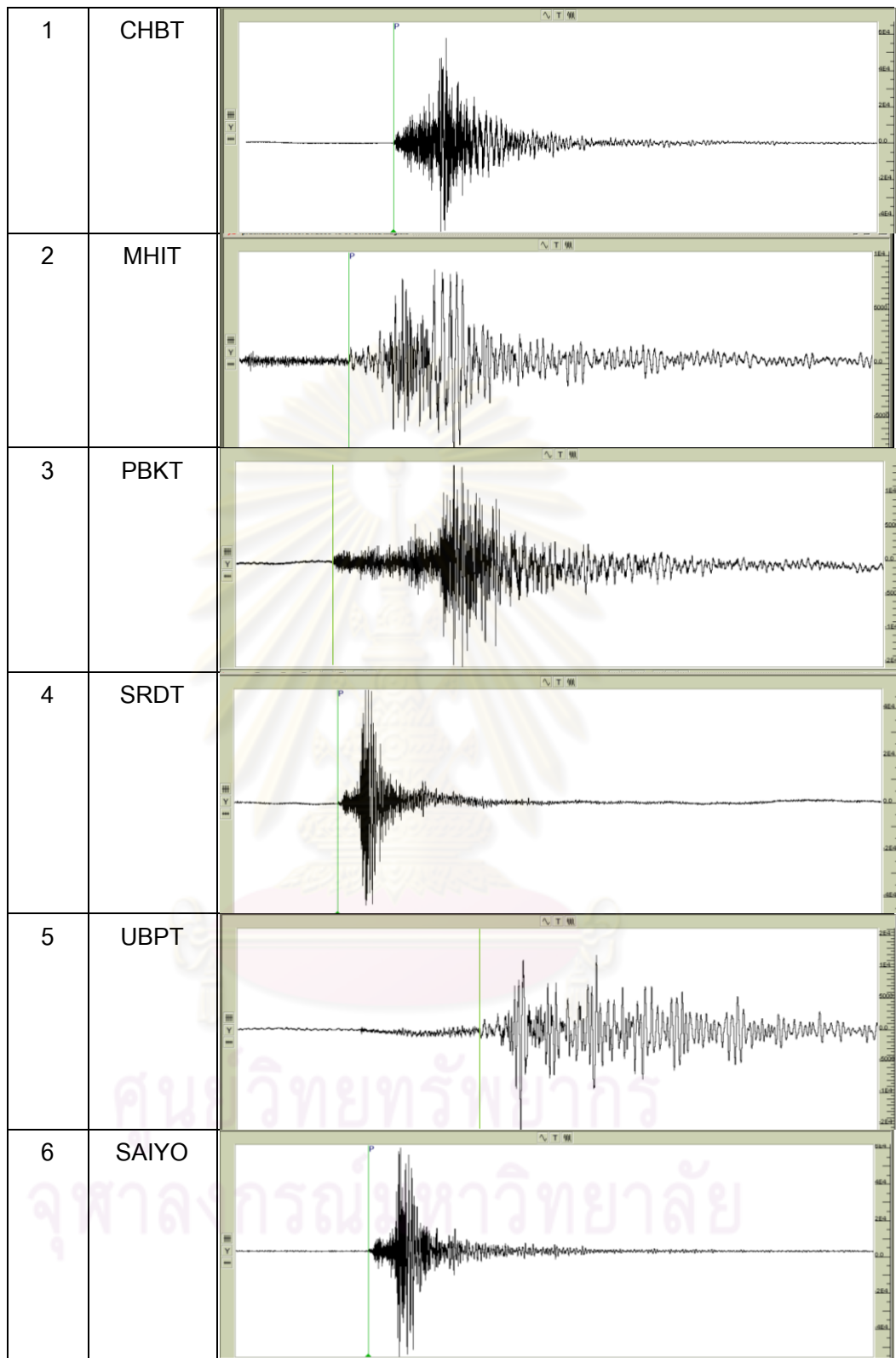


Figure 4.18 Recorded seismic waveforms from seismic station which recorded the earthquake event on October 8, 2006.

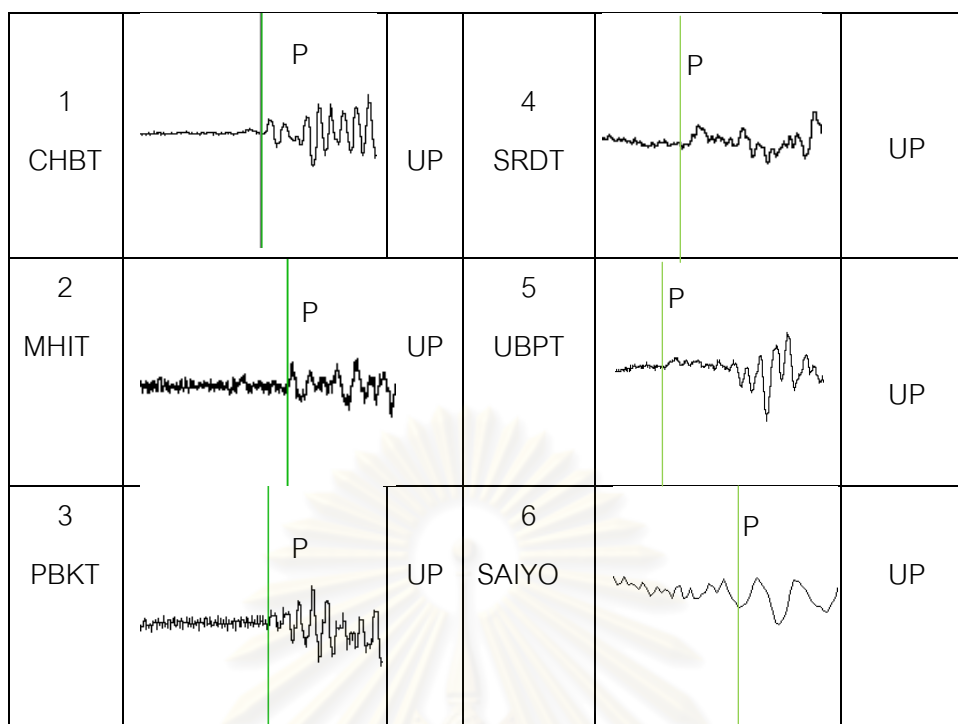


Figure 4.19 First motion of the enlarged P waves from seismic station which recorded the earthquake event on October 8, 2006.

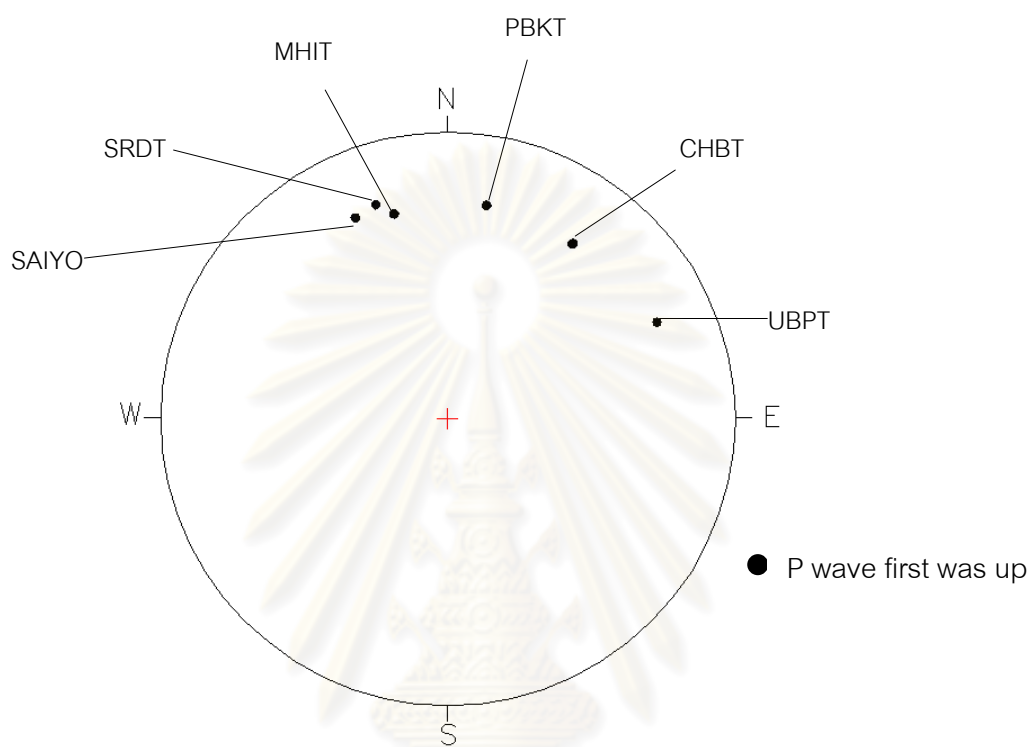


Figure 4.20 Plots of P-wave first motion data in the stereonet with data from this study.

ศูนย์วิทยทรัพยากร
จุฬาลงกรณ์มหาวิทยาลัย

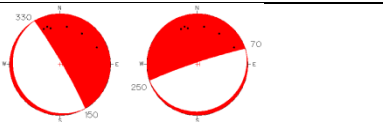
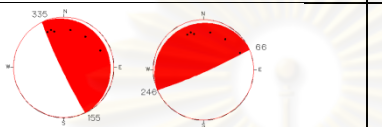
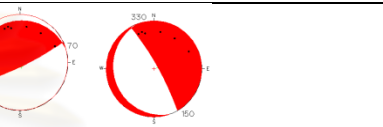
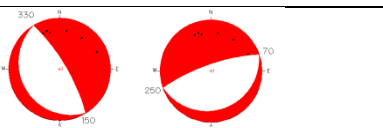
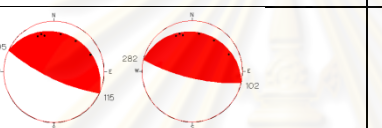
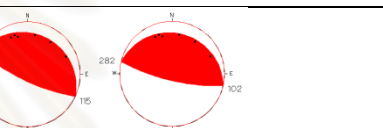
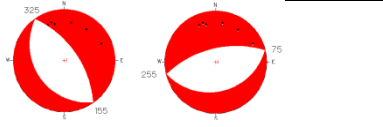
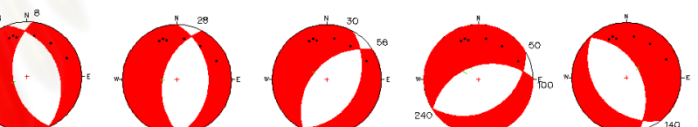
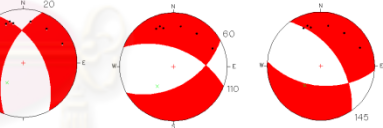
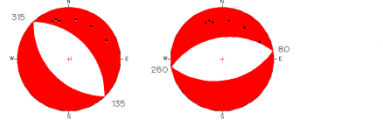
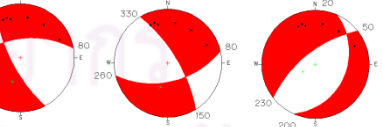
Dip Angle	Normal fault	Reverse fault	Oblique
Dip 5 ⁰ and Dip 85 ⁰	 N70E-N30W	 N65E-S25E, S65W-N25W	 N64E-S30E, S70W-N30W
Dip 15 ⁰ and Dip 75 ⁰	 N40E-N30W	 S65E-S78E, N65W-N78W	 N20W-N64W, S30E-S70E
Dip 30 ⁰ and Dip 60 ⁰ Dip 0 ⁰	 N75E-N35W	-	 N8E, N22W, NS, N28E, S30W, N56E, S10E-S80E, S50W-N40W
Dip 40 ⁰ and Dip 50 ⁰	-	-	 N20E, N30W, S70E, S60W, S85E, N35W
Dip 45 ⁰	 N80E-N45W	-	 N80E, N30W, S60E, N70W, S35E, N85W

Figure 4.21 The preliminary results of probable focal mechanism identified from this study.

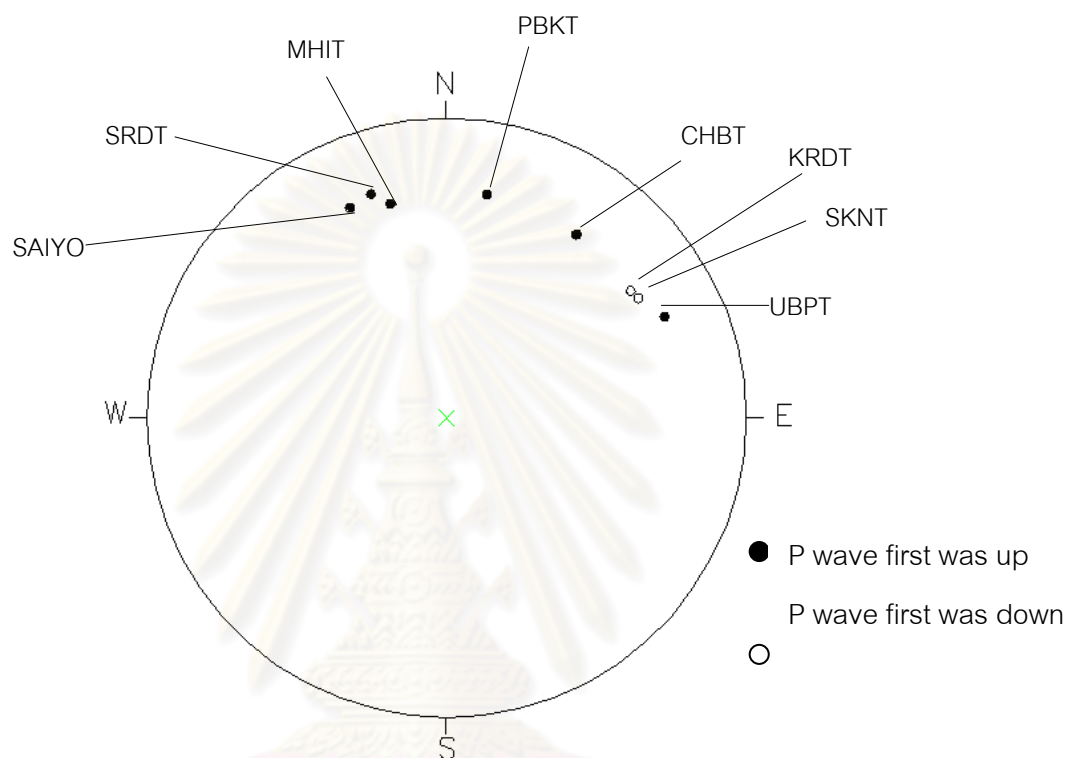


Figure 4.22 Plots of P-wave first motion data in the stereonet with data from Pananon (2009).

ศูนย์วิทยทรัพยากร
จุฬาลงกรณ์มหาวิทยาลัย

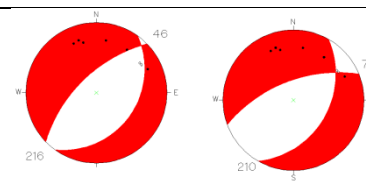
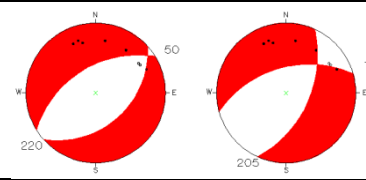
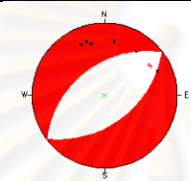
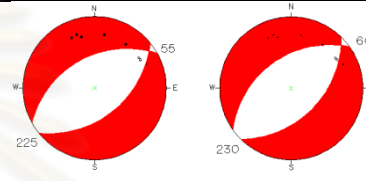
Dip Angle	Normal fault	Oblique fault
Dip 30° and Dip 60° Dip 0°	-	 N36E-N46E, S46W-S70W
Dip 40° and Dip 50°	-	 N20E-N45E, S50W- S75W
Dip 45°	 N50E, S50W	 N55E – N60E, S55W- S60W

Figure 4.23 The results of probable focal mechanism identified from this study and data from Pananon, 2009.

ศูนย์วิทยทรัพยากร
จุฬาลงกรณ์มหาวิทยาลัย

CHAPTER V

SEISMIC INTERPRETATION

From the remote sensing interpretation in chapter 3, the Ranong fault (RNF) zone trends in the northeast-southwest direction. From this direction, it is possible that the Ranong fault zone will extend into the Gulf of Thailand and Andaman Sea (Polachan and Sattayarak, (1989). Moreover, from the epicenter of the earthquake in the area of Andaman sea with the magnitudes of 3-5 Richter scale around the transition part in the continental plate and the sea surface, the earthquake that happened could be the result of the movement of the Ranong fault zone which is an active fault. Therefore, we have to interpret seismic data in the gulf of Thailand and Andaman (Figure. 5.1). The first report on the RNF cutting through the seafloor of Andaman is that of Chuntong (2010).

5.1 Seismic interpretation in Andaman Sea

The deep survey of seismic lines, which are assumed to be across the Ranong Fault, have been selected for this study as shown in (Figure 5.2). Taking Kingdom program 8.4 is applied and seismic line survey from Department of Mineral Fules, Ministry of energy which comprise of Line survey AN1, AN2, AN3 and AN4.

In this interpretation, borehole drilling log data and horizons distribution were used and can be distinguished into 6 line markers based on the work by Mahattanacha, (1996). They are :

1. light blue line marker representing sea floor
2. green line marker representing the Top of Thalang formation
3. dark blue line marker representing the Top of Trang formation
4. orange line marker representing the Top of Kantang formation
5. yellow line marker representing the Top of Ranong – Yala formation, and
6. pink/ dark red line marker representing the Top of besement

Based on stratigraphic correlation of the Mergui Basin and the geological time, we can approximate ages of these formations as follows:

1. The ages of Top of Thalang – Top of Trang are between 5.3 and 11.6 Ma ;
2. The ages of Top of Trang – Top of Kantang are between 11.6 and 16.0 Ma ;

3. The ages of Top of Kantang – Top of Ranong are between 16.0 and 20.0 Ma ;
4. The ages of Top of Ranong – Top of Basement are between 120.0 and 28.4 Ma ;
5. The ages of Top of Basement- lower Basement are between 28.4 Ma.

The depth in these seismic sections can be calculated by the following formula (eq. 5.1).

$$V_{int}^2 = [(V_{rms_2})^2 \times T_2 - (V_{rms_1})^2 \times T_1] \dots \dots \dots (5.1)$$

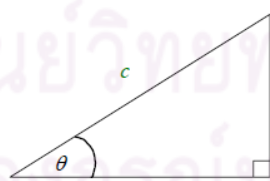
$$Z = [(T_2 - T_1) \times V_{int}] / 2$$

$$D = \sum Z$$

$$V_a = 2D / T$$

- Where
- V_{int} = Interval velocity (m/s),
 - V_{rms_1} = Upper root mean square velocity (m/s),
 - V_{rms_2} = Lower root mean square velocity (m/s),
 - V_a = Average velocity (m/s),
 - T = Two way time to a horizon (sec),
 - T_1 = Upper time (Two way-sec),
 - T_2 = Lower time (Two way-sec),
 - Z = Thickness (m), and
 - D = Depth (m).

In this study, V_{rms} from the table of V_{rms} of each seismic lines have been used to calculate depth. The dip angle in these seismic sections can be calculated by the formula (eq.5.2)



$$\tan \theta = a/b \dots \dots \dots (5.2)$$

- Where
- a = SP1 at T_1 - SP1 at T_2
 - b = SP2 at T_1 - SP2 at T_2
 - SP1 = short point No.1 , and
 - SP2 = short point No.2

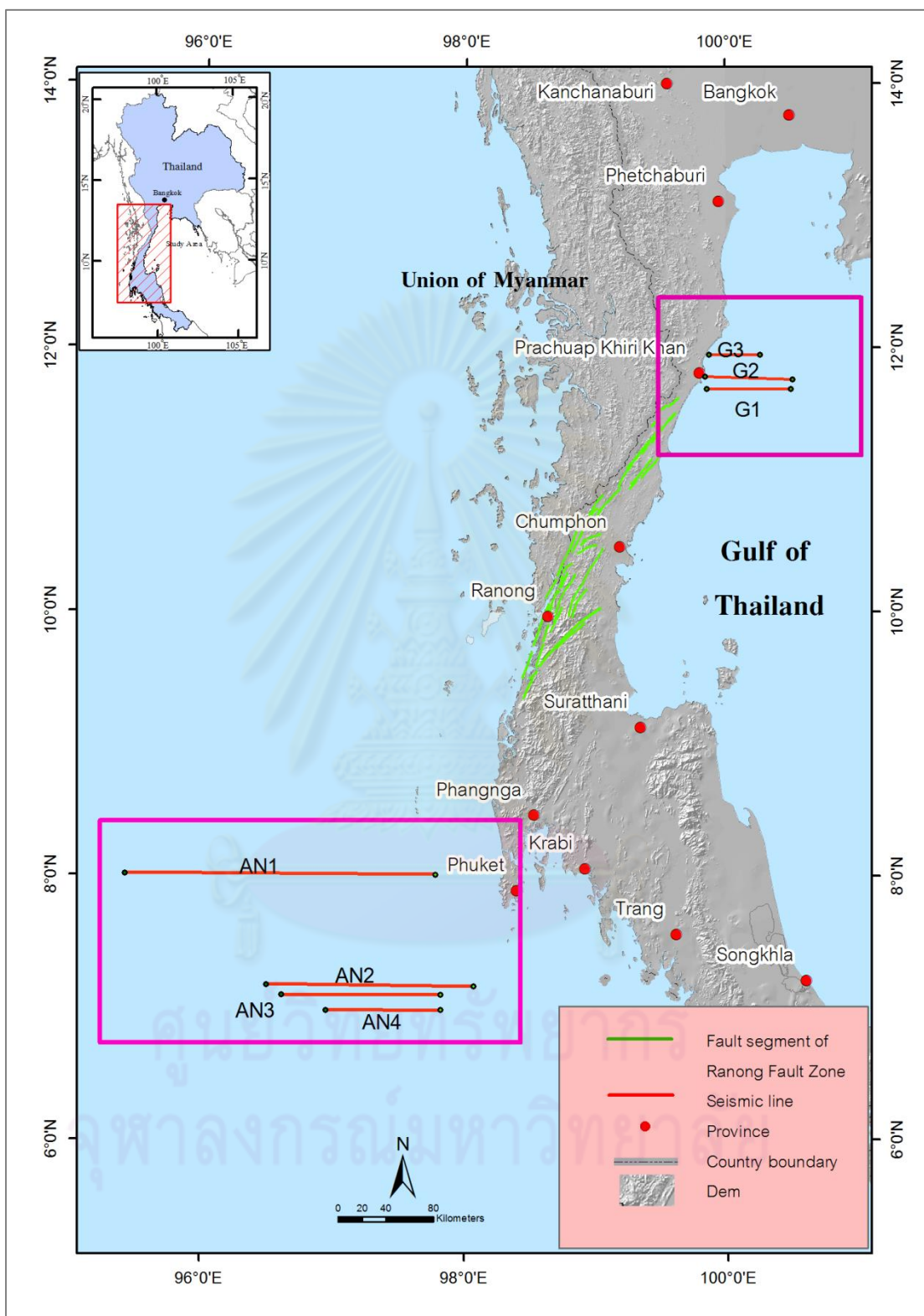


Figure 5.1 Map showing seismic survey lines used in the study Andaman sea and Gulf of Thailand areas (pink blocks).

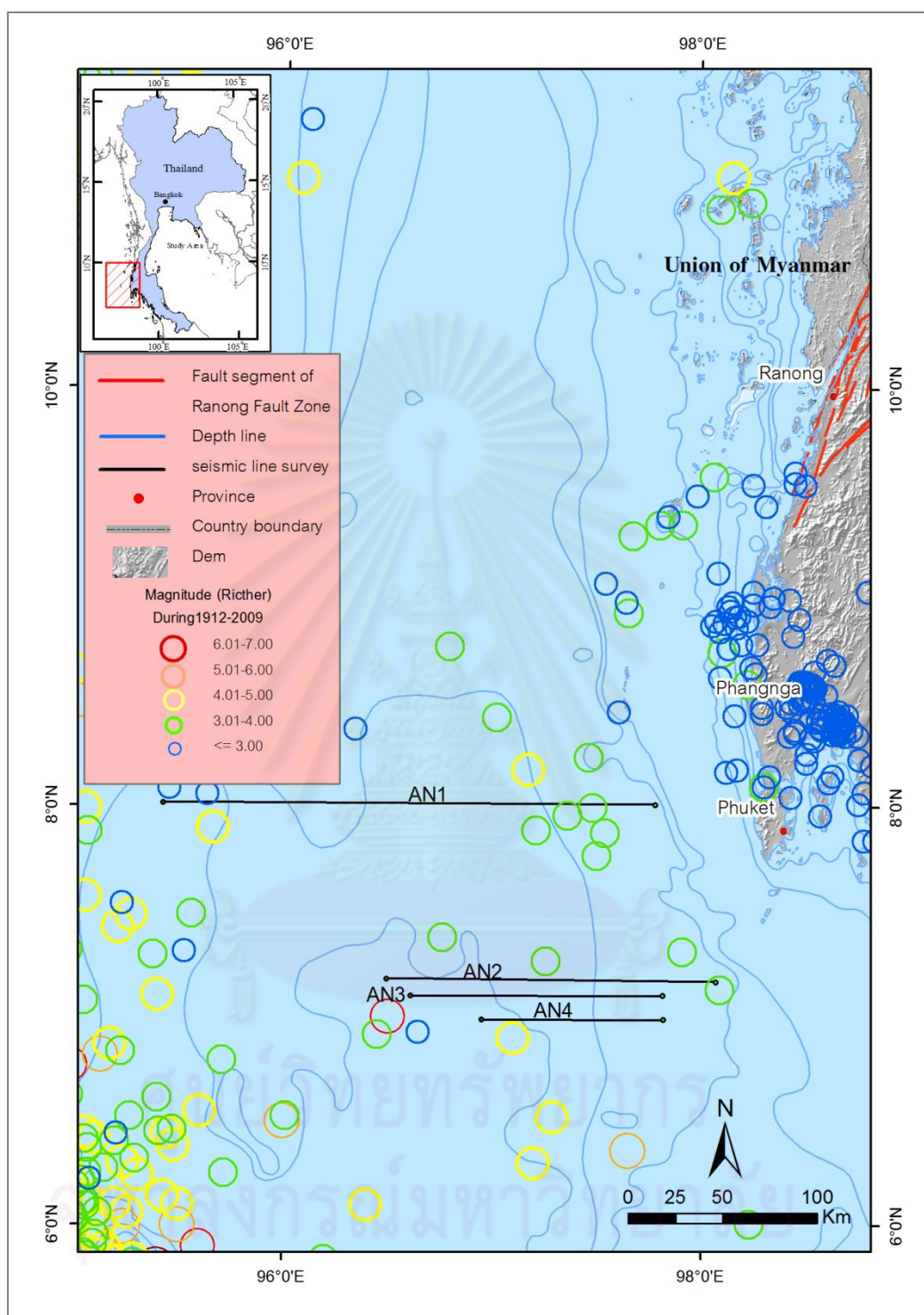


Figure 5.2 Map showing seismic line survey in Andaman sea (black line). Note that several epicenters detected at both ends of the seismic lines AN1, AN2, AN3 and AN4.

5.1.1 Preliminary Result

Although, the seismic data were enhanced properly, it is noted that the result of this research work is preliminary due to the scarcity of the seismic survey lines. The offsets taken from the estimation are frequently approximate due to the inaccuracy of the enhanced data.

5.1.1.1 Seismic line survey AN1

From the result movement along the RNF was found at the Ranong ridge and this RNF segment cuts sediment into seafloor. Table 5.1 shows the displacement along the RNF. Movement of the RNF caused the displacement or slip which its distance can be measured as shown table 5.1.

F1 cuts sediment layers up to the seafloor. The faults offsets the seafloor with the dip angle of 75 degree to the east. The fault has the vertical slip of 47m (0.039sec), and the slip rate of about 0.0029 mm/yr. It also offsets top of basement with the dip angle of 56 degree to east and the vertical slip of 3,640 m (1.617 sec) and slip rate of about 0.1282 mm/yr.

F2 cuts sediment layers up to the seafloor. The fault offsets the seafloor with the dip angle of 70 degree to the west. The fault has the vertical slip of 74m (0.058 sec), and the slip rate of about 0.0036 mm/yr. It also offsets top of Ranong with the dip angle of 65degree to west and the vertical slip of 76m (0.041 sec) and slip rate about 0.0038 mm/yr.

F3 cuts sediment layers up to the seafloor. The fault offsets the seafloor with the dip angle of 74 degree to the west. The fault has the vertical slip of 36m (0.029 sec), and the slip rate about 0.0031 mm/yr. (Figure 5.5-5.6).

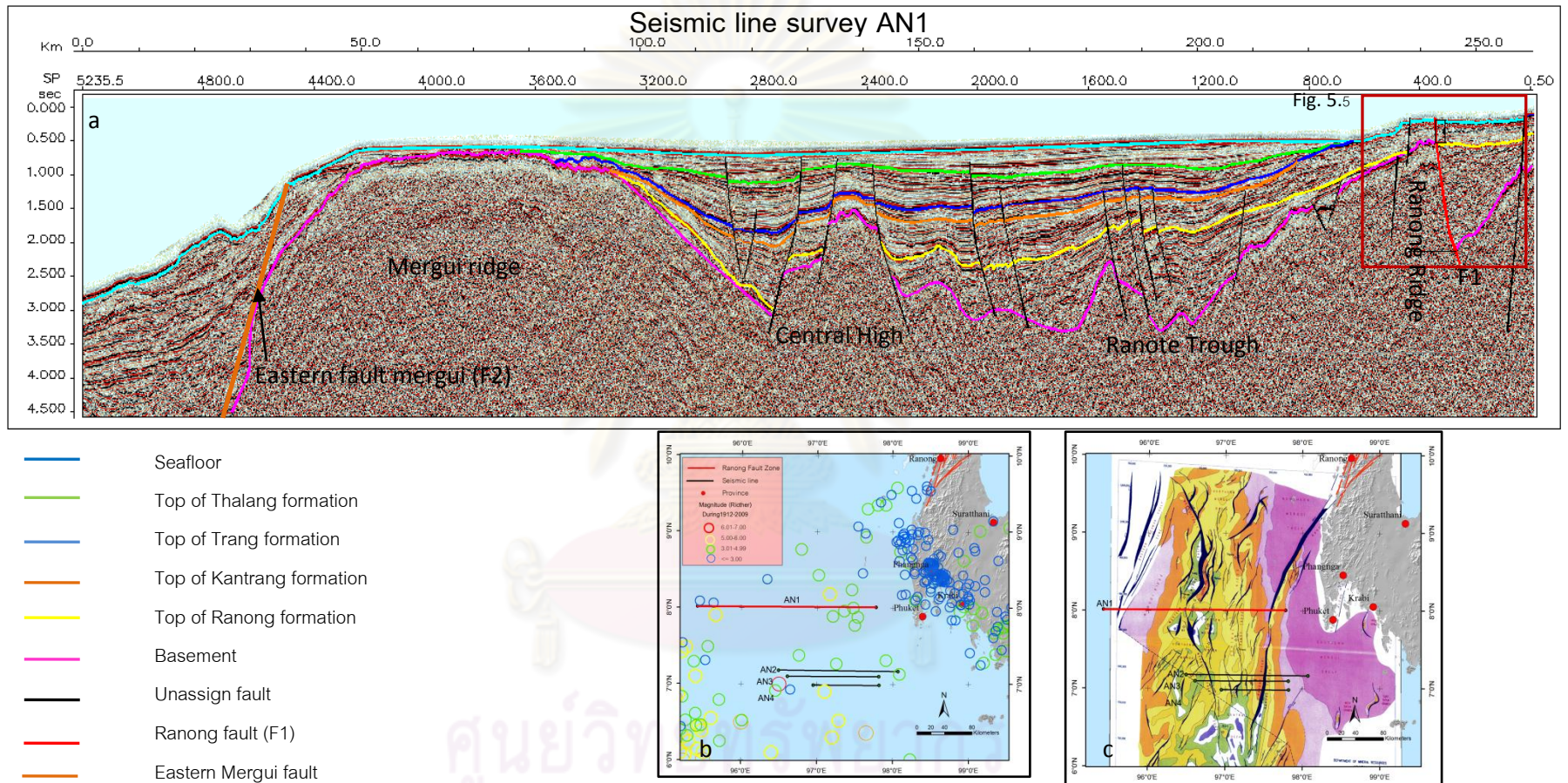
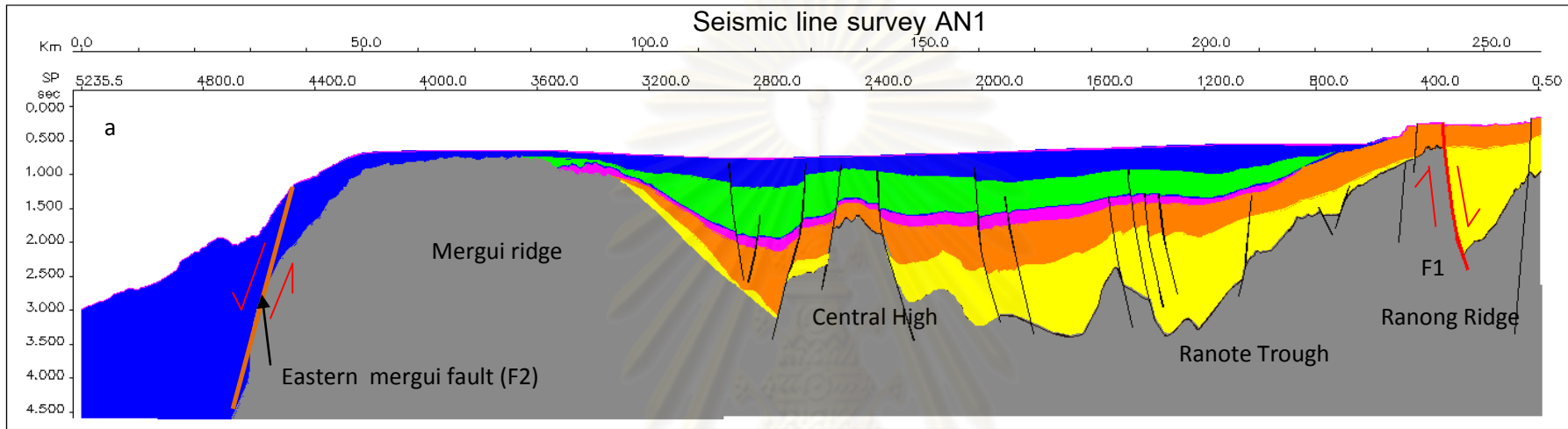
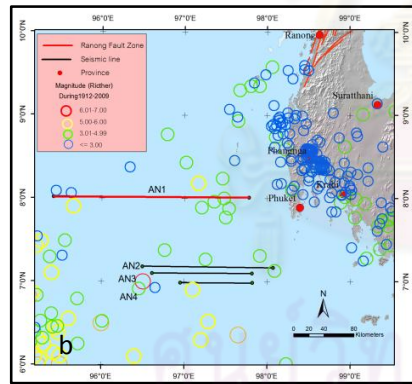


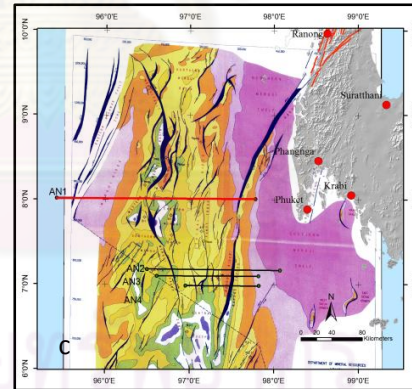
Figure 5.3(a) seismic cross-section of seismic line survey AN1. (b) Map showing seismic line survey AN1 and distribution of epicentral in Andaman sea. (c) Map showing seismic line survey AN1 and structure map of Andaman sea. Note that there are 2 interesting faults F1(Ranong fault) and F2 (Eastern Andaman Fault) which produce intermediate EQ(3.4-4.0 ML).



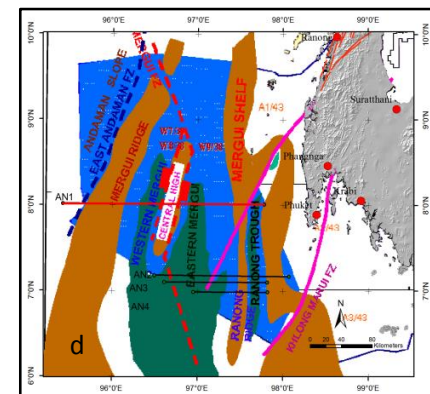
- Takuapa formation
- Thalang formation
- Trang formation
- Kantrang formation
- Ranong formation
- Basement
- Unassign fault
- Ranong fault
- Eastern Mergui fault
- Direction of movement



(DMF, TMD and USGS, 2009)

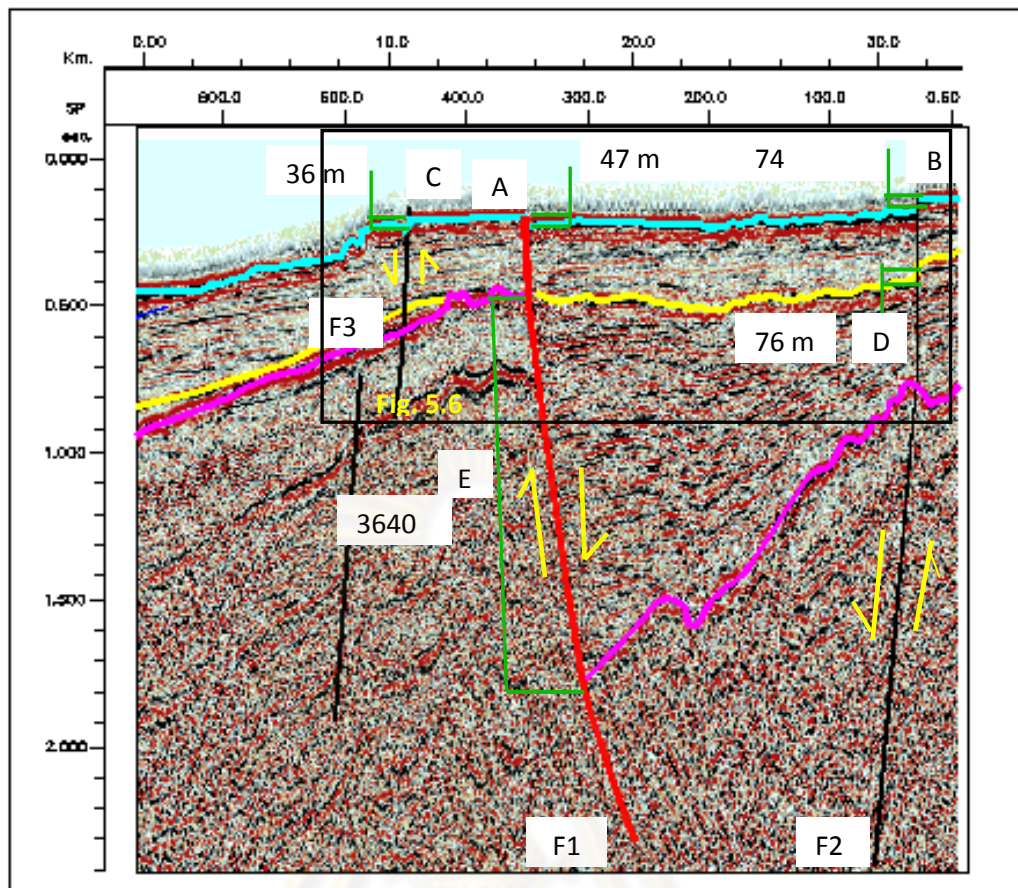


(DMR and Beicip Franlab, 1996)



(Mahatanachai, 1996)

Figure 5.4 Model of sediment formation layers of seismic line survey AN1. (b) Map showing seismic line survey AN1 and distribution of epicentral magnitude (Mmax) during 1972-2009. (c) Map showing seismic line survey AN1 and structure map of Andaman sea. (d) Map showing seismic line survey AN1 and Physiographic map of the Mergui Basin, Andaman Sea.



- | | | | |
|--|-------------------------|--|------------------------------------|
| | Seafloor | | Unassign fault |
| | Top of Ranong formation | | Fault segment of Ranong fault zone |
| | Basement | | Direction of movement |

Figure 5.5 Seismic cross section of seismic line survey AN1 at Ranong ridge showing normal movement at RNF into seafloor. Note that F1, F2 and F3 reach the seafloor.

ศูนย์วิทยทรัพยากร
จุฬาลงกรณ์มหาวิทยาลัย

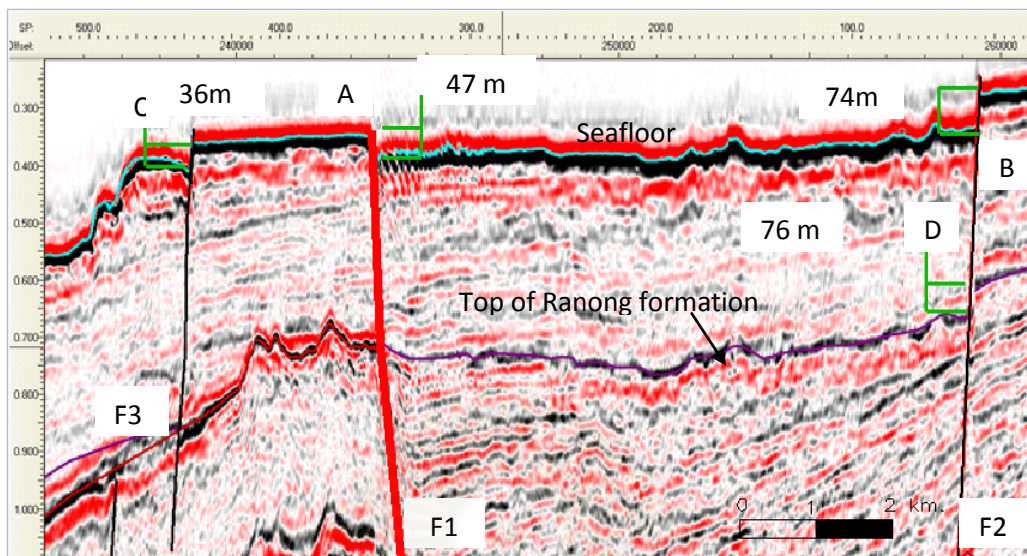


Figure 5.6 Seismic cross section of the enlarged seismic line survey AN1 at Ronong ridge showing F1, F2 and F3 reach to the seafloor (point A, B, C and D).

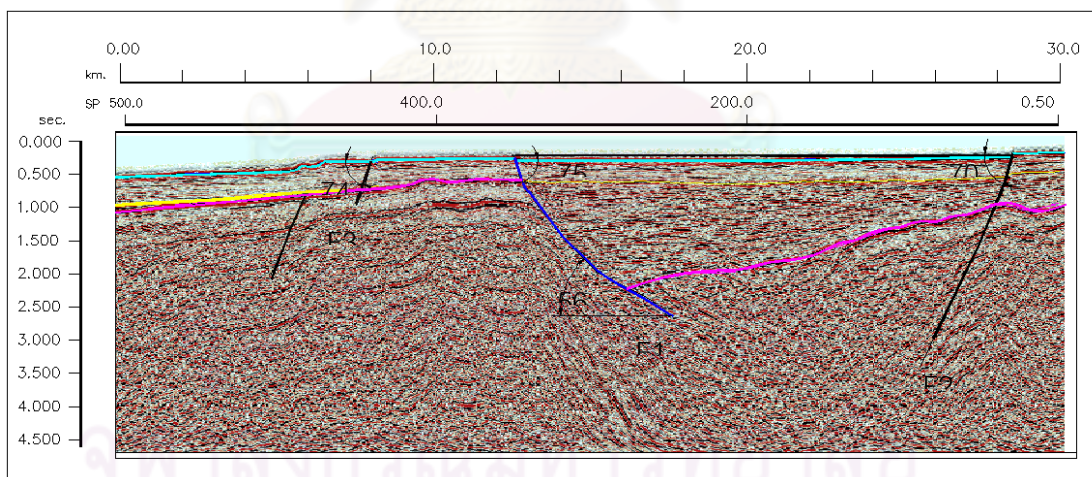


Figure 5.7 Seismic cross section of the enlarged seismic line survey AN1 at Ronong ridge showing dip angle of F1, F2 and F3 at point A, B, C, D and E).

Table 5.1 Displacement of faults in seismic line survey AN1.

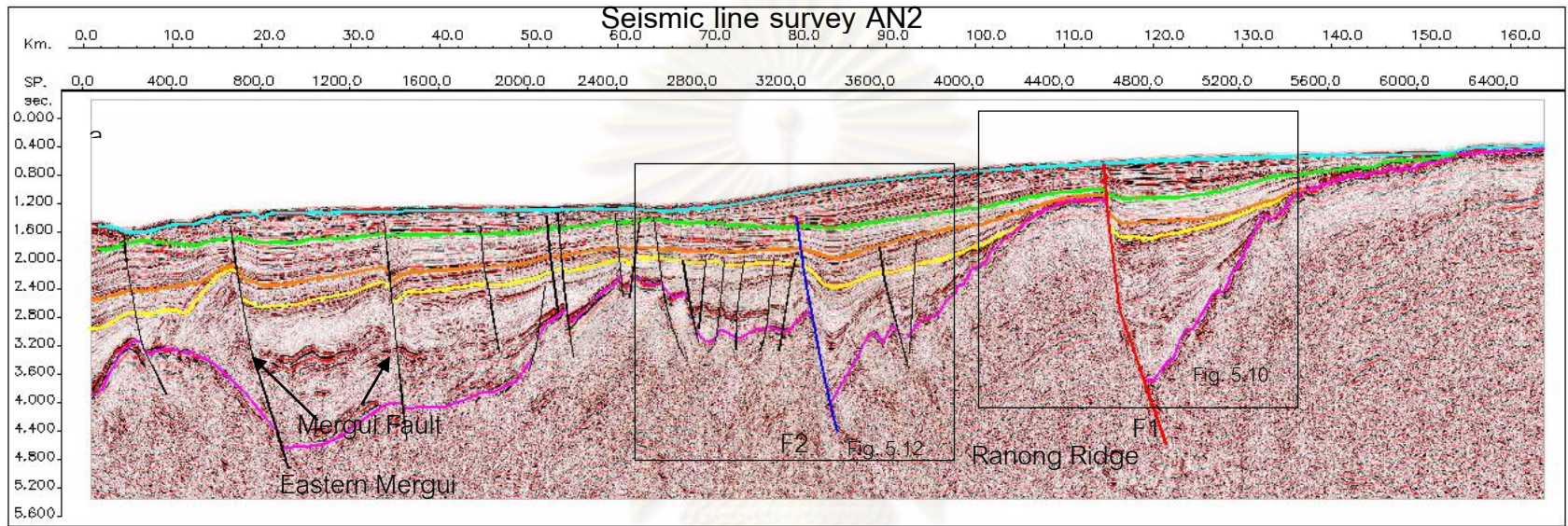
Point	Vertical displacement		Vertical slip rate mm./yr	Dip angle (degree)	Age of top layer Ma
	Sec	m			
A	0.039	47	0.0029	75	16
B	0.058	74	0.0036	70	16
C	0.029	36	0.0031	74	16
D	0.041	76	0.0038	65	20
E	1.617	3640	0.1282	56	28.4

5.1.1.2 Seismic line survey AN2

The result of movement along the RNF was found at the Ranong ridge and this RNF segment cut sediments into seafloor (F1). Far from Ranong ridge around 70 kilometers synthetic fault of Ranong fault (F2) cuts basement into Takuapa formation, developing the half graben (Figure 5.8 and 5.9). Table 5.2 shows the displacement along the RNF. Movement of along the RNF make sediment layer moved and the offset can be measured as shown table 5.2.

F1 cuts sediment layers up to the seafloor. The faults offsets the Thalang formation with the dip angle of 55 degree to the east. The fault has the vertical slip of 36m (0.040 sec), slip rate of about 0.0068 mm/yr. It also offsets top of Kantrang with the dip angle of 47 degree to east and the vertical slip of 230 m (0.202 sec) and slip rate of about 0.0144 mm/yr. the fault offsets top of basement with the dip angle of 47 degree to east and the vertical slip of 4,328 m (2.407 sec) and slip rate of about 0.1524 mm/yr. (Figure 5.10-5.11).

F2 cuts sediment layers into Takuapa formation. The fault offset top of Ranong with the dip angle of 46 degree to east . The fault has the vertical slip rate of 91m (0.050 sec) and slip rate of about 0.0046mm/yr. It also offsets top of basement with the dip angle of 48 degree to east with vertical slip rate of 2,736 m (1.617 sec), slip rate of about 0.0963 mm/yr. (Figure 5.12).



- Seafloor
- Top of Thalang formation
- Top of Kantrang formation
- Top of Ranong formation
- Basement
- Unassign fault
- Fault segment of Ranong fault zone (F2)
- Fault segment of Ranong fault zone (F1)

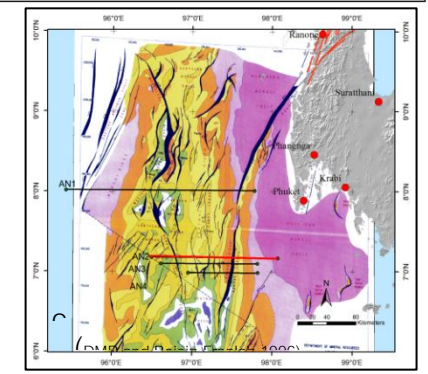
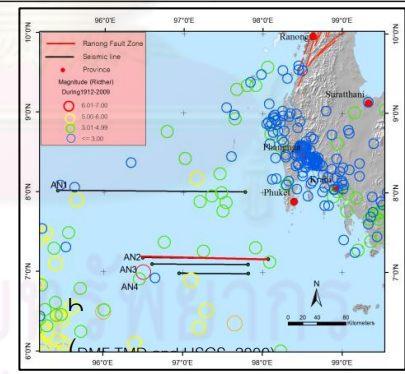
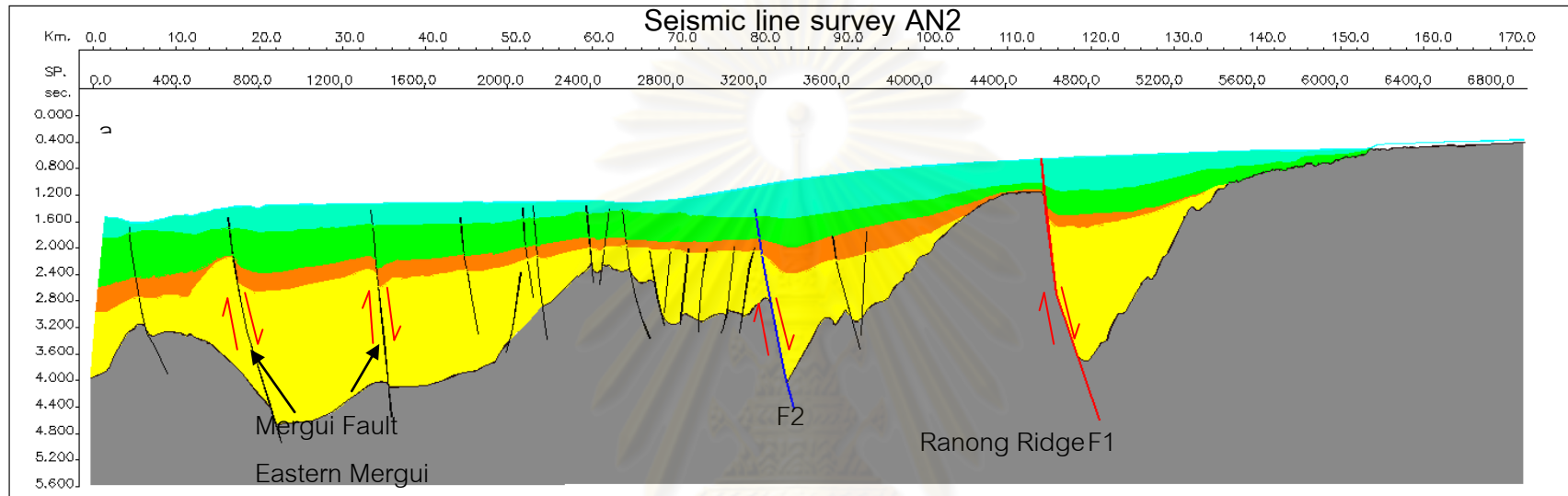


Figure 5.8 (a) seismic cross-section of seismic line survey AN2. (b) Map showing seismic line survey AN2 and distribution of epicentral in Andaman sea. (c) Map showing seismic line survey AN2 and structure map of Andaman sea.



- Takuapa formation
- Thalang –Trang formation
- Kantrang formation
- Ranong formation
- Basement
- Unassign fault
- Fault segment of Ranong fault zone (F2)
- Fault segment of Ranong fault zone (F1)
- Direction of movement

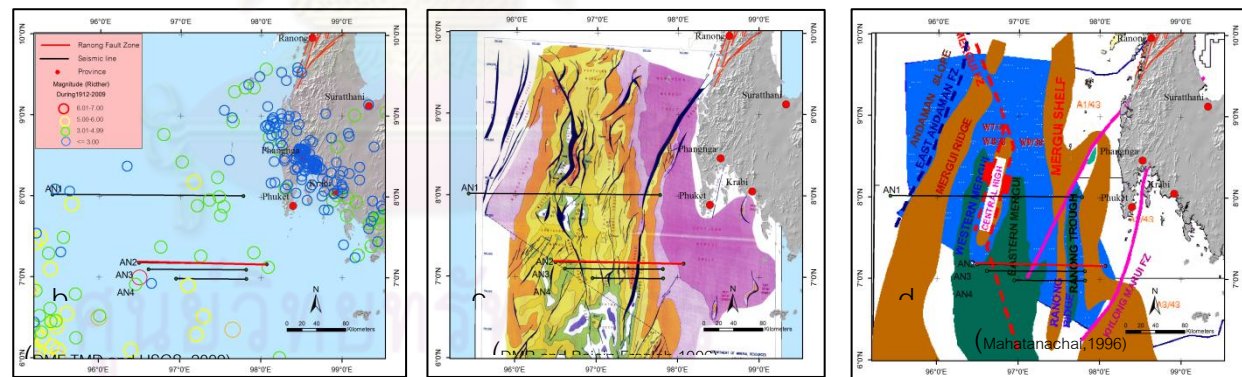
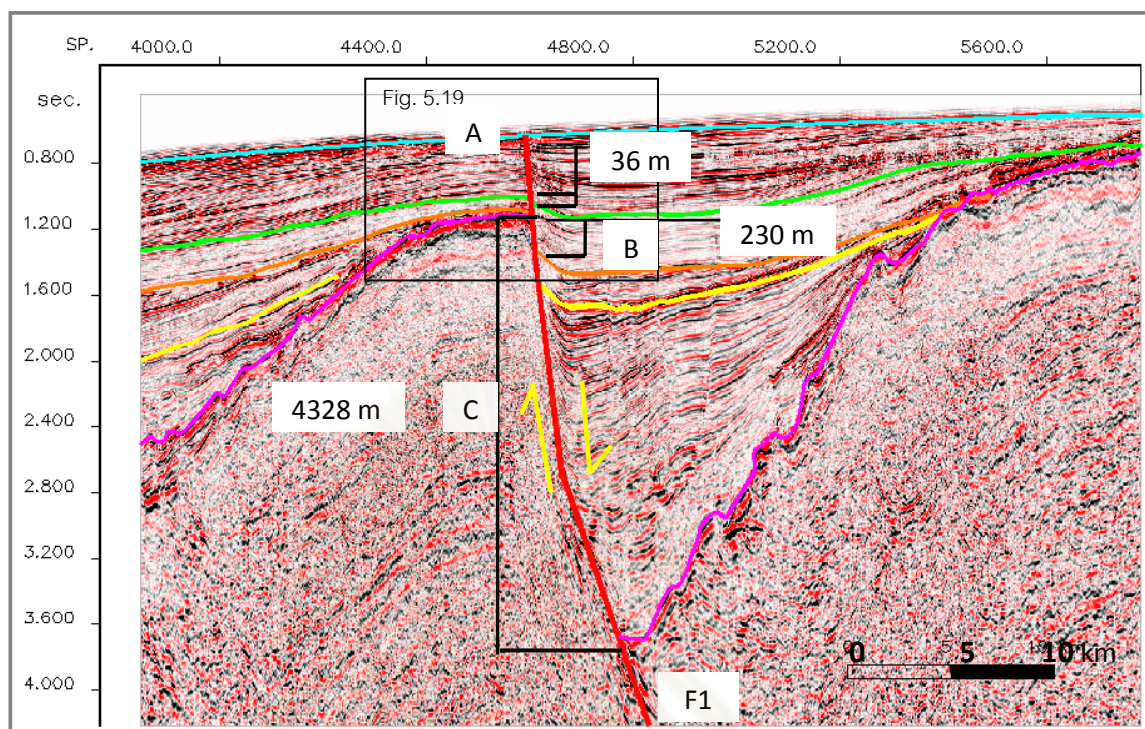


Figure 5.9 (a) Model of sediment formation layers of seismic line survey AN2. (b) Map showing seismic line survey AN2 and distribution of epicentral c) Map showing seismic line survey AN2 and structure map of Andaman sea. (d) Map showing seismic line survey AN2 and Physiographic map of the Mergui Basin, Andaman Sea.



- | | | | |
|--|---------------------------|--|---|
| | Seafloor | | Basement |
| | Top of Thalang formation | | Unassign fault |
| | Top of Kantrang formation | | Fault segment of Ranong fault zone (F1) |
| | Top of Ranong formation | | Direction of movement |

Figure 5.10 Seismic cross section of seismic line survey AN2 at Ranong ridge showing normal movement at RNF into seafloor. Note that F1 reach the seafloor.

ศูนย์วิทยทรัพยากร
จุฬาลงกรณ์มหาวิทยาลัย

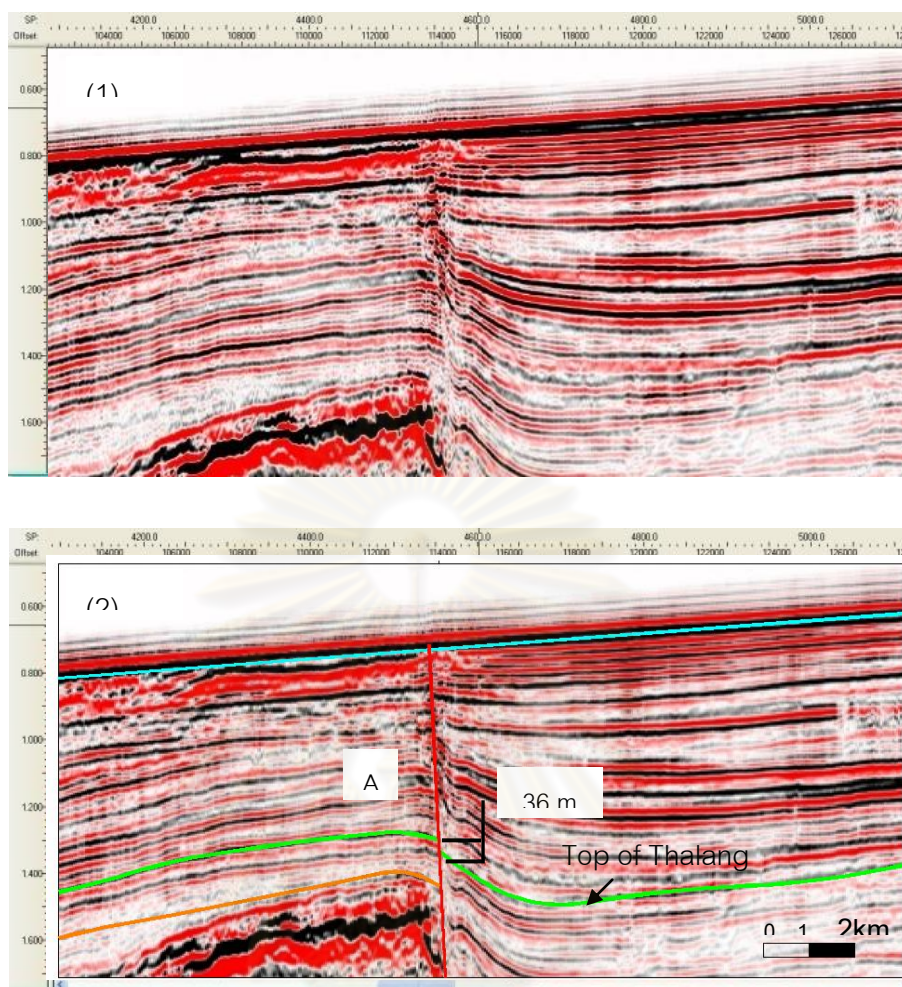


Figure 5.11 Seismic cross section of the enlarged seismic line survey AN2 at Ronong ridge showing F1 reach to the seafloor (point A).

ศูนย์วิทยทรัพยากร
จุฬาลงกรณ์มหาวิทยาลัย

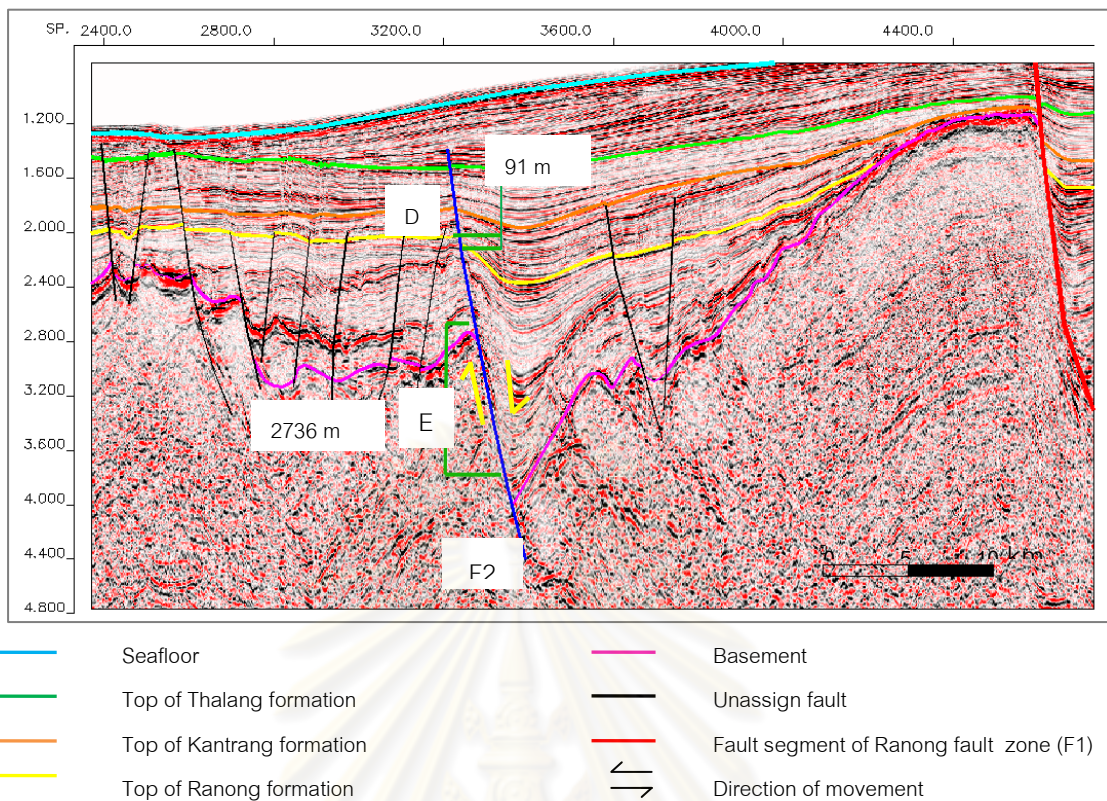


Figure 5.12 Seismic cross section of seismic line survey AN2 near Ranong ridge showing normal movement of F2 cut Thalang formation.

Table 5.2 Displacement of faults in seismic line survey AN2.

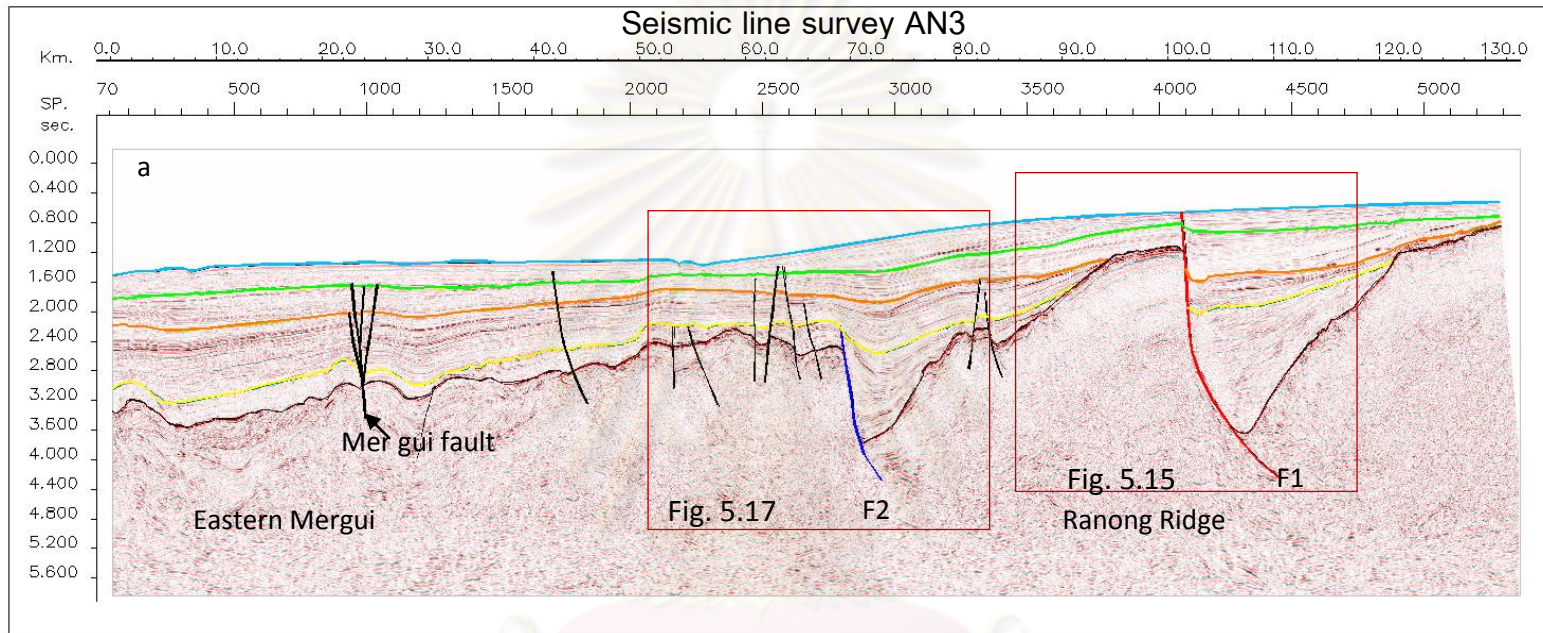
Point	Vertical displacement		Vertical slip rate mm./yr	Dip angle (degree)	Age of top layer Ma.
	Sec.	m.			
A	0.040	36	0.0068	55	5.3
B	0.202	230	0.0144	47	16
C	2.407	4328	0.1524	47	28.4
D	0.050	91	0.0046	46	20
E	1.169	2736	0.0963	48	28.4

5.1.1.3 Seismic line survey AN3

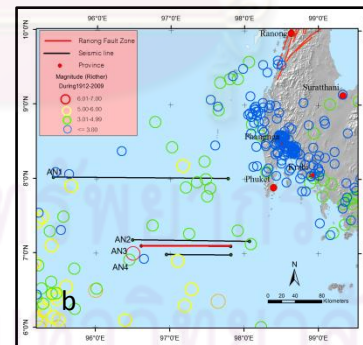
Interpretation of the result of this seismic line indicates that the RNF Ranong fault cuts through seafloor at Ranong ridge(F1) and far from Ranong ridge around 30 kilometers, synthetic faults of the RNF (F2) cut basement up to top of Ranong formation and from the half garben structure (Figures 5.13and 5.14). Movement along the Ranong Fault offset sediment layers with the distance ranging from 30 to more than 3,000 m (table 5.3).

F1 cuts sediment layers up to seafloor. The fault offsets top of Thalang formation with the dip angle of 55 degree to east with the thickness of 30 m (0.036 sec) and the slip rate of about 0.0056 mm/yr. The F1 offsets top of basement with the dip angle of 47 degree to east with the thickness of 4,419 m (2.487 sec) and the slip rate of about 0.1556 mm/yr.(Figure 5.15-5.16)

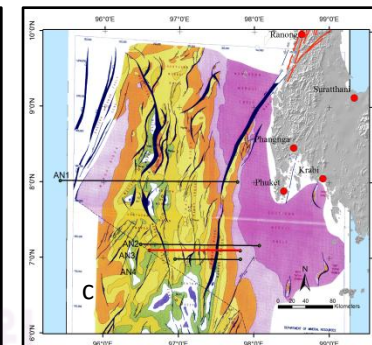
F2 cuts sediment layer into top of Ranong formation. The fault offsets top of basement with the dip angle of 47 degree to east with the thickness of 3,342 m (1.204 sec), slip rate of about 0.1177 mm/yr. (Figure 5.17).



- Seafloor
- Top of Thalang formation
- Top of Kantrang formation
- Top of Ranong formation
- Basement
- Unassign fault
- Fault segment of Ranong fault zone (F2)
- Fault segment of Ranong fault zone (F1)

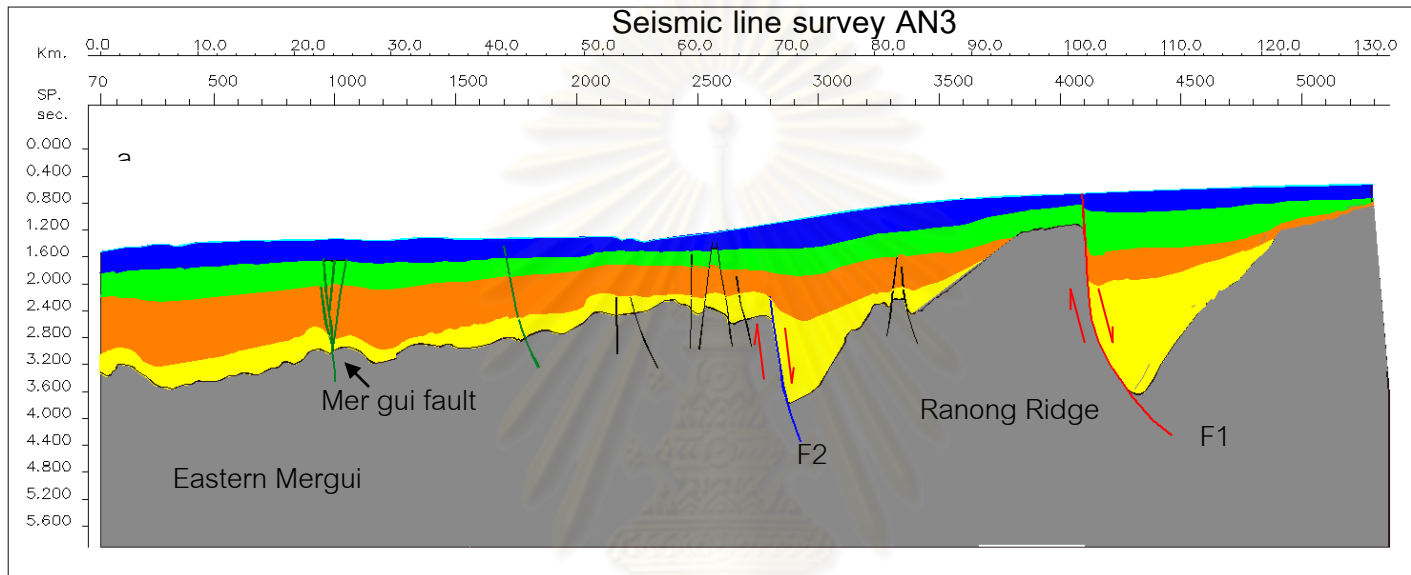










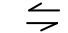
(DMF, TMD and USGS, 2009)

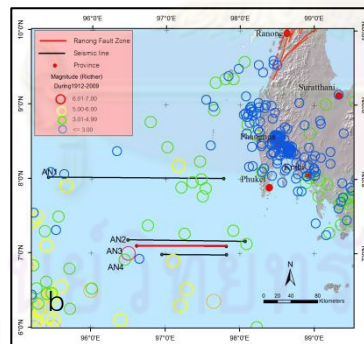


(DMR and Beicip Franlab, 1996)

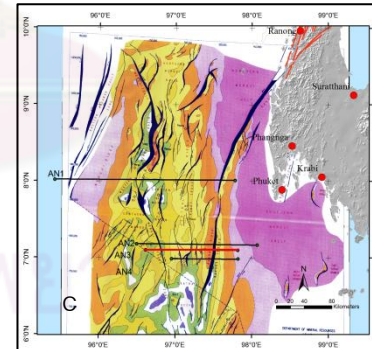
Figure 5.14 (a) Model of sediment formation layers of seismic line survey AN3. (b) Map showing seismic line survey AN3 and distribution of epicentral (c) Map showing seismic line survey AN3 and structure map of Andaman sea. (d) Map showing seismic line survey AN3 and physiographic map of the Mergui Basin, Andaman Sea.



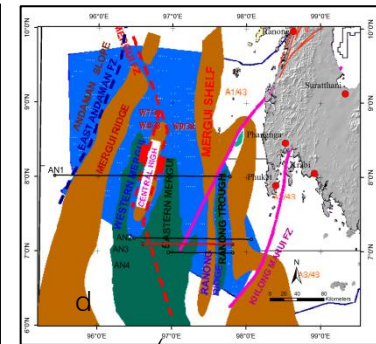
-  Seafloor
-  Top of Thalang formation
-  Top of Kantrang formation
-  Top of Ranong formation
-  Basement
-  Unassign fault
-  Fault segment of Ranong fault zone (F2)
-  Fault segment of Ranong fault zone (F1)
-  Direction of movement



(DMF, TMD and USGS, 2009)

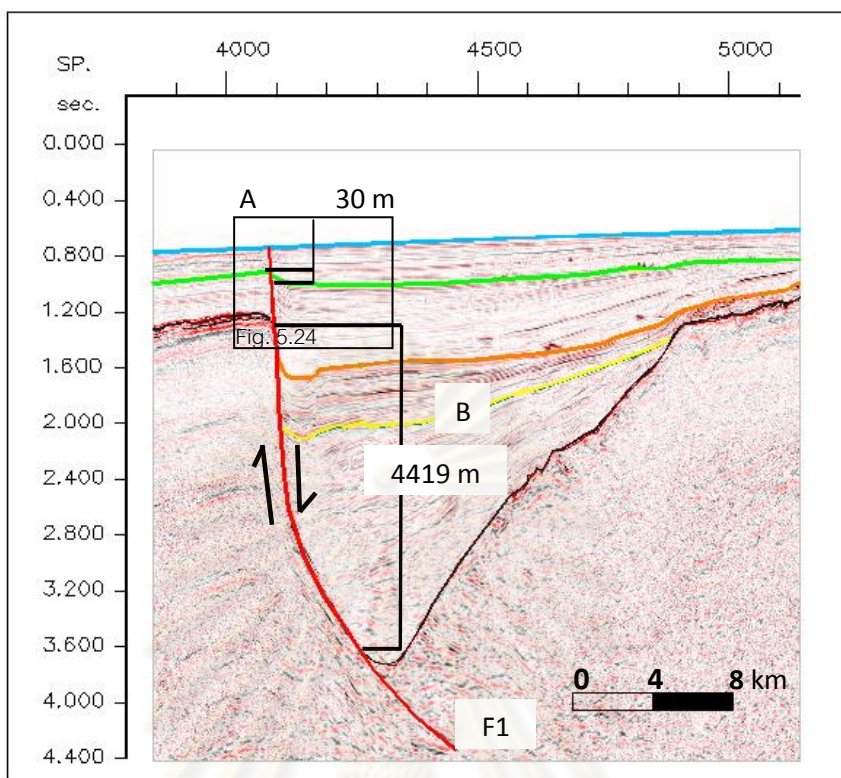


(DMR and Beicip Franlab, 1996)



(Mahatanachai, 1996)

Figure 5.14 (a) Model of sediment formation layers of seismic line survey AN3. (b) Map showing seismic line survey AN3 and distribution of epicentral (c) Map showing seismic line survey AN3 and structure map of Andaman sea. (d) Map showing seismic line survey AN3 and physiographic map of the Mergui Basin, Andaman Sea.



- | | | | |
|--|---------------------------|--|---|
| | Seafloor | | Basement |
| | Top of Thalang formation | | Unassign fault |
| | Top of Kantrang formation | | Fault segment of Ranong fault zone (F1) |
| | Top of Ranong formation | | Direction of movement |

Figure 5.15 Seismic cross section of line survey AN3 at Ranong ridge showing normal movement at RNF into seafloor. Note that the F1 reaches the seafloor.

ศูนย์วิทยทรัพยากร
จุฬาลงกรณ์มหาวิทยาลัย

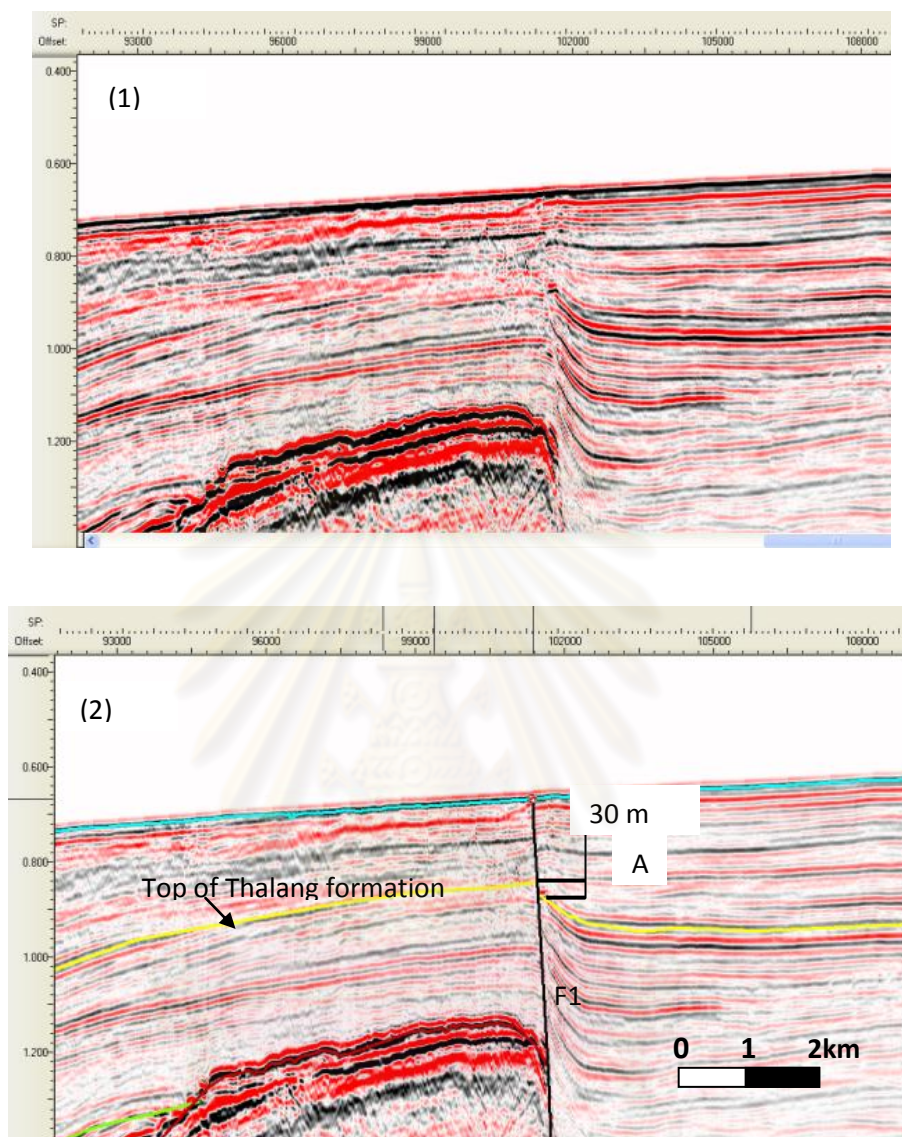
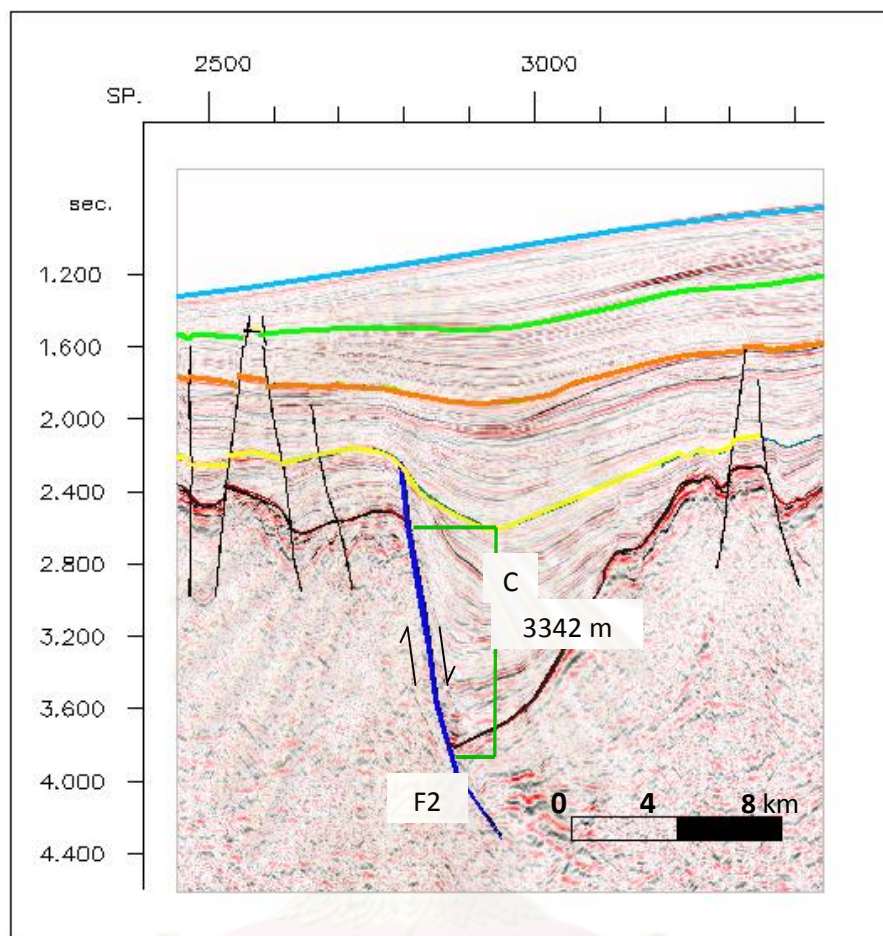


Figure 5.16 Seismic cross section of the enlarged seismic line survey AN3 at Ranong ridge showing the F1 reaches to the seafloor (point A).



- | | | | |
|---|---------------------------|---|---|
|  | Seafloor |  | Basement |
|  | Top of Thalang formation |  | Unassign fault |
|  | Top of Kantrang formation |  | Fault segment of Ranong fault zone (F1) |
|  | Top of Ranong formation |  | Direction of movement |

Figure 5.17 Seismic cross section of line survey AN3 near Ranong ridge showing normal movement F2 cut basement.

Table 5.3 Displacement of faults in seismic line survey AN3.

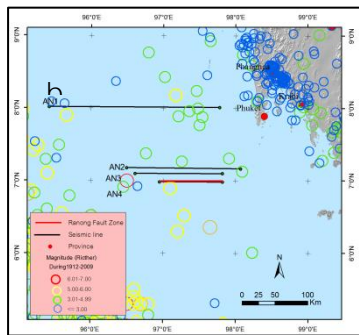
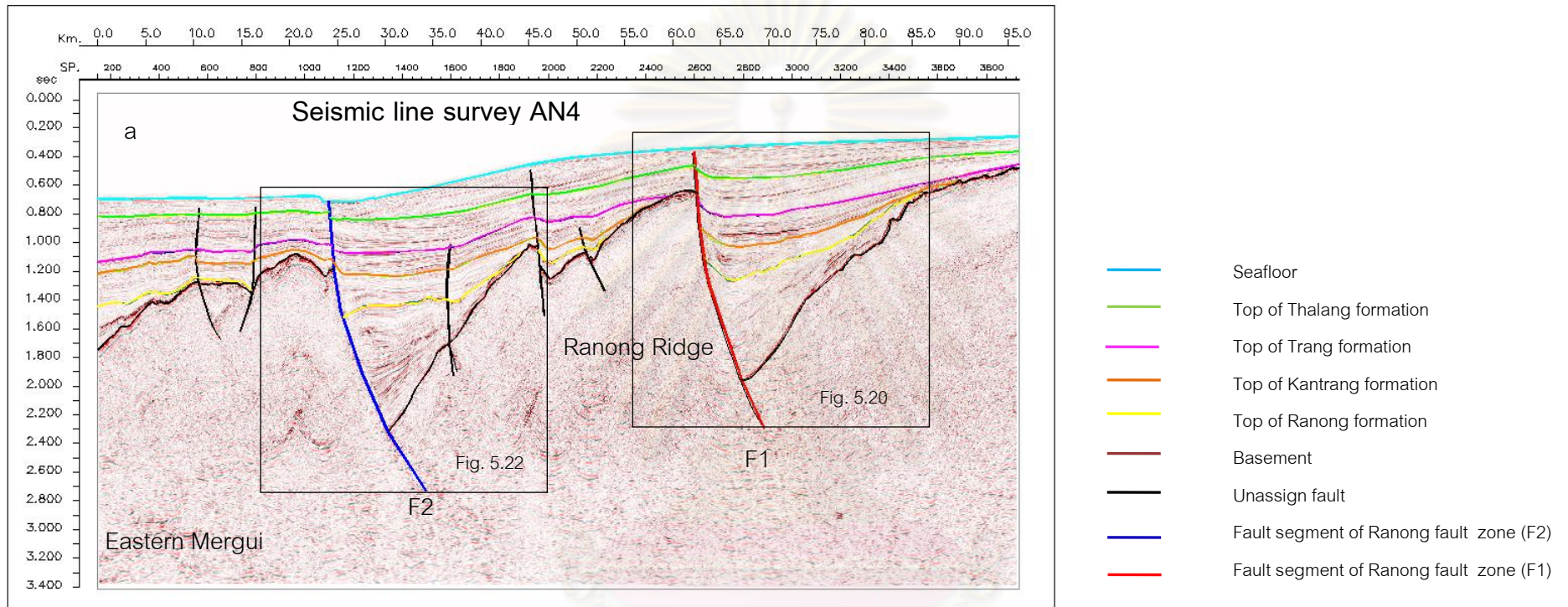
Point	Vertical displacement		Vertical slip rate mm./yr	Dip angle (degree)	Age of top layer Ma
	Sec	m			
A	0.036	30	0.0057	55	5.3
B	2.487	4419	0.1556	47	28.4
C	1.204	3342	0.1177	47	28.4

5.1.1.4 Seismic line survey AN4

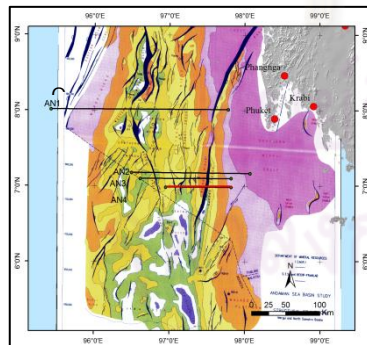
From the result of this seismic interpretation, it is found that the RNF moved almost to seafloor at Ranong ridge(F1) and far from Ranong ridge around 40 kilometers founded fault segment of Ranong fault(F2) cut into seafloor (Figures 5.18 and 5.19). Movement along the Ranong Fault offset sediment layers with the distance ranging from 40 to more than 8,000 m (Table 5.4).

F1 cuts top of Thalang formation to top of Takuapa formation. The end of fault is 61 m from seafloor (Figure 5.21). The faults offsets top of Thalang formation with the dip angle of 53 degree eastward and the vertical slip of 40 m (0.047 sec) The result indicates slip rate of about 0.0056 mm/yr. It also offsets top of basement with the dip angle of 47 degree eastward with the vertical slip of 7,039 m (2.615 sec). The result give the slip rate of about 0.2478 mm/yr.

F2 cuts sediment layers through the seafloor. The fault offsets top of Thalang with the dip angle of 60 degree to the eastward and the vertical slip of 81m (0.086 sec) and slip rate of about 0.0153 mm/yr. It offsets top of Trang formation with the dip angle of 60 degree to east with the vertical slip of 69 m (0.057 sec) and slip rate of about 0.0060 mm/yr. It also offsets top of basement with the dip angle of 56 degree to east and the vertical slip of 8,251 m (2.254 sec) and slip rate of about 0.2905 mm/yr.(Figure 5.22-5.23).

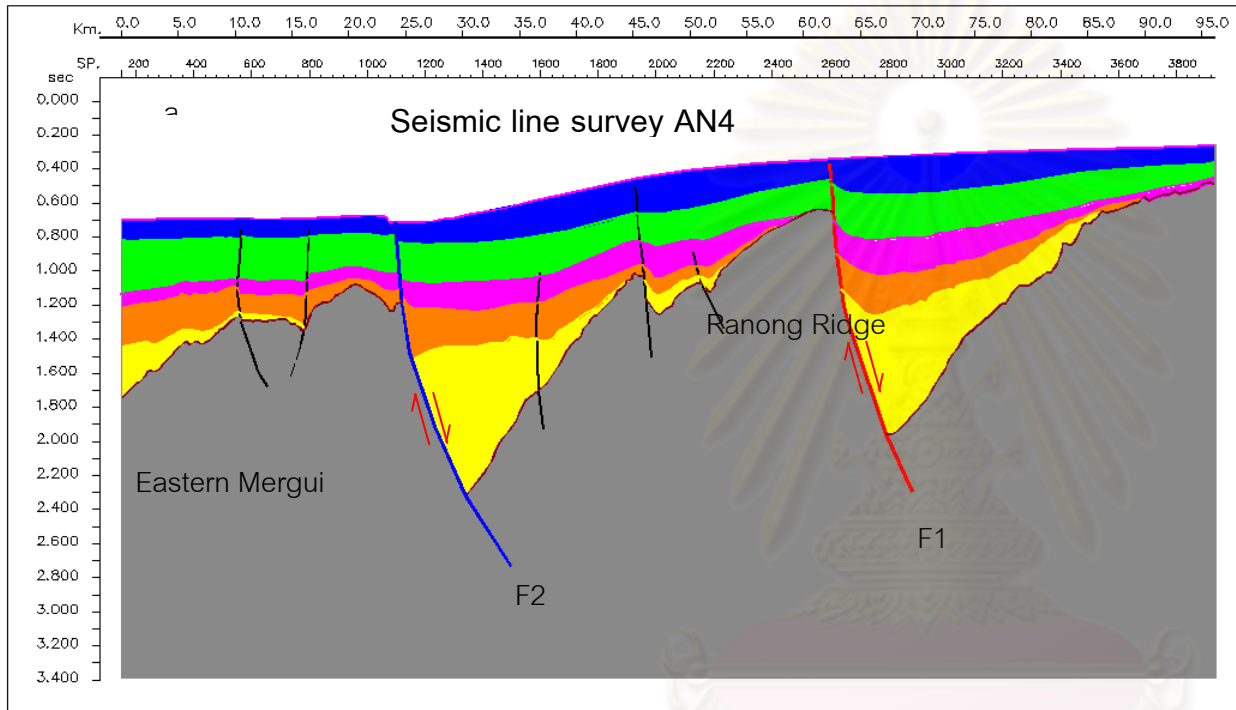


(DMF, TMD and USGS, 2009)



(DMR and Beicip Franlab, 1996)

Figure 5.18 (a) seismic cross-section of seismic line survey AN3. (b) Map showing seismic line survey AN3 and distribution of epicentral in Andaman sea. (c) Map showing seismic line survey AN3 and structure map of andaman sea.



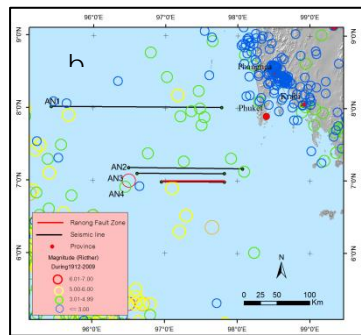
- Takuapa formation
- Trang formation
- Thalang formation
- Kantrang formation
- Ranong formation
- Basement
- Unassign fault
- Fault segment of Ranong fault zone (F2)
- Fault segment of Ranong fault zone (F1)
- Direction of movement

Figure 5.19 (a) Model of sediment formation layers of seismic line survey AN3.

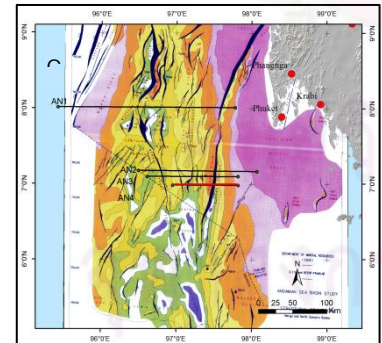
(b) Map showing seismic line survey AN3 and distribution of epicentral .

(c) Map showing seismic line survey AN3 and strcture map of Andaman sea.

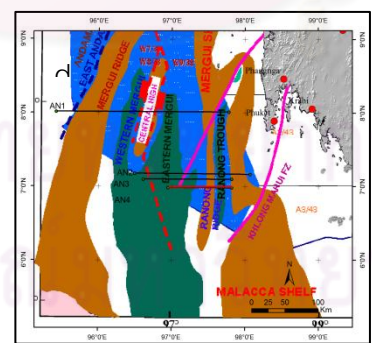
(d) Map sowing seismic line survey AN3 and Physiographic map of the Mergui Basin, andaman Sea.



(DMF,TMD and USGS, 2009)



(DMR and Beicp Franlab, 2009)



(Mahatanachai, 1996)

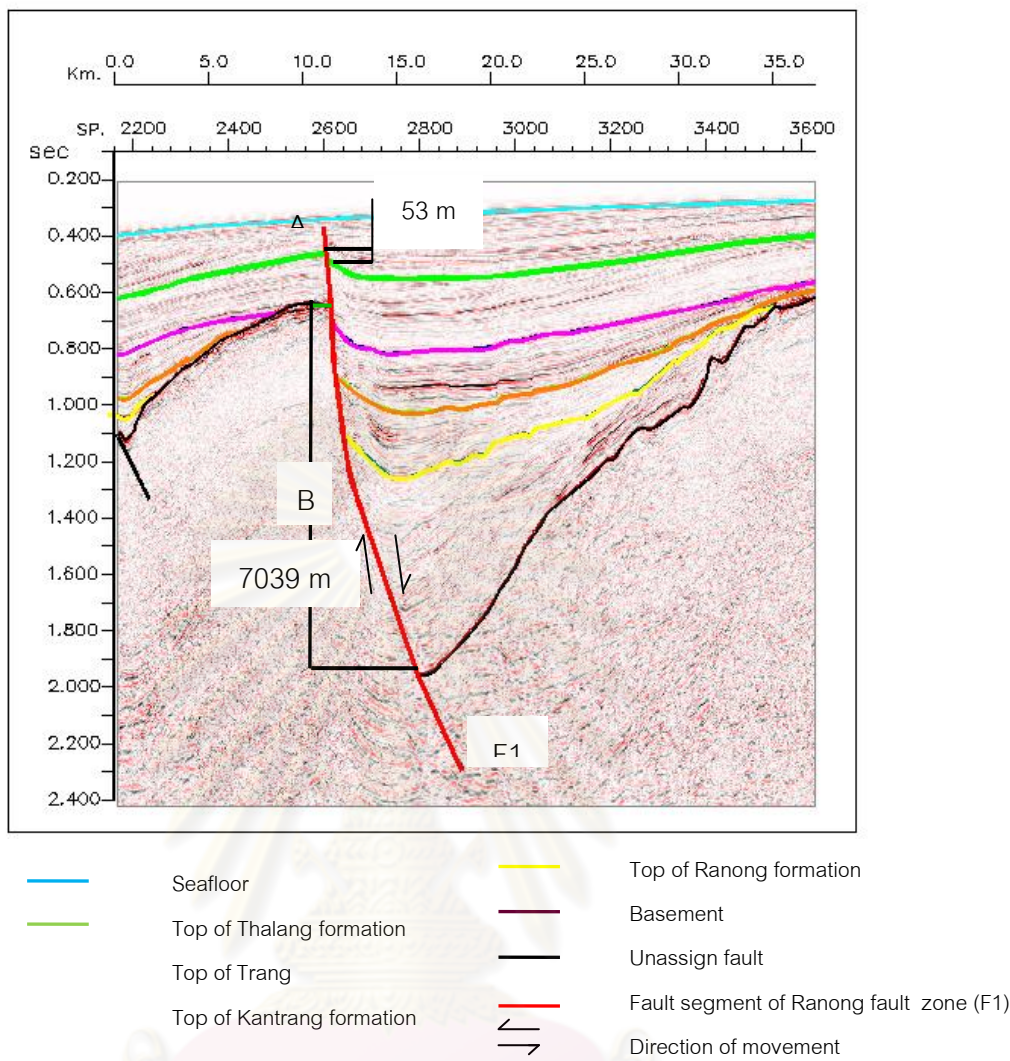


Figure 5.20 Seismic cross section of seismic line survey AN4 at Ranong ridge showing normal movement at F1 cut Thalang formation and almost reach to seafloor.

ศูนย์วิทยทรัพยากร
จุฬาลงกรณ์มหาวิทยาลัย

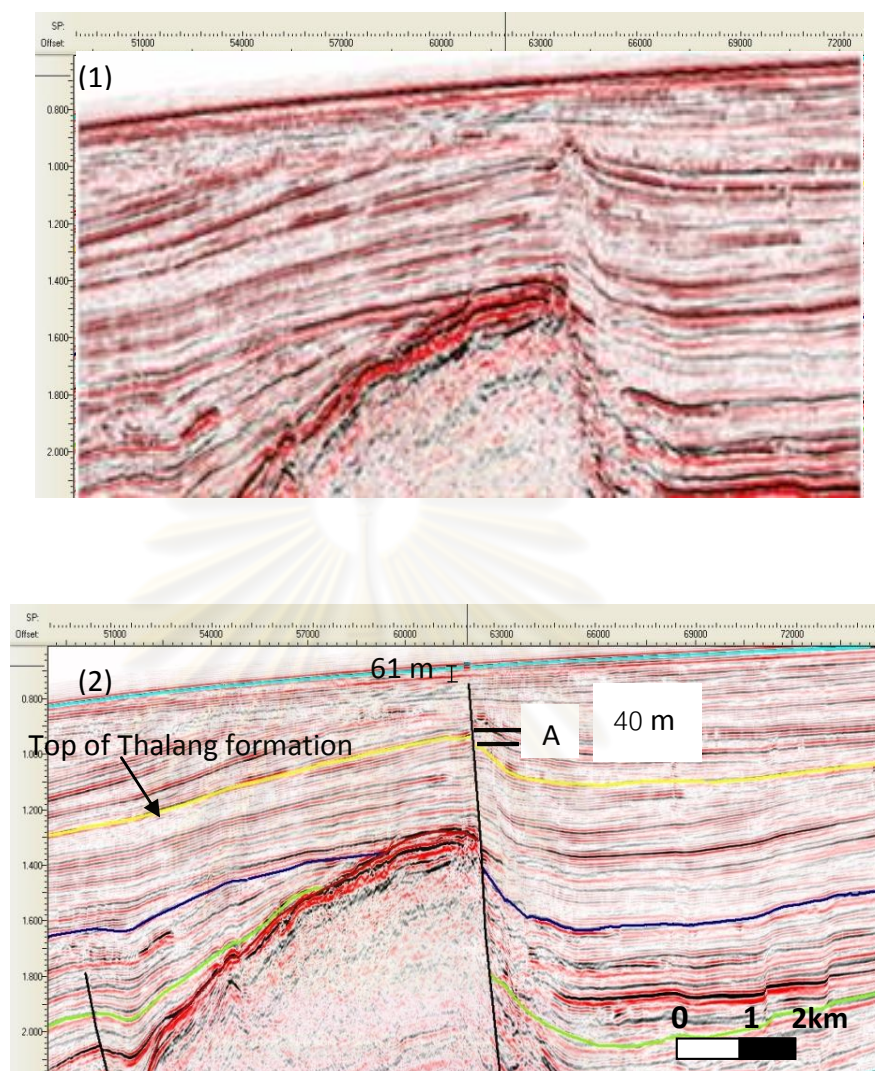


Figure 5.21 Seismic cross section of the enlarged line survey AN4 at Ranong ridge showing F1 almost reaching to the seafloor (point A).

ศูนย์วิจัยทรัพยากร
จุฬาลงกรณ์มหาวิทยาลัย

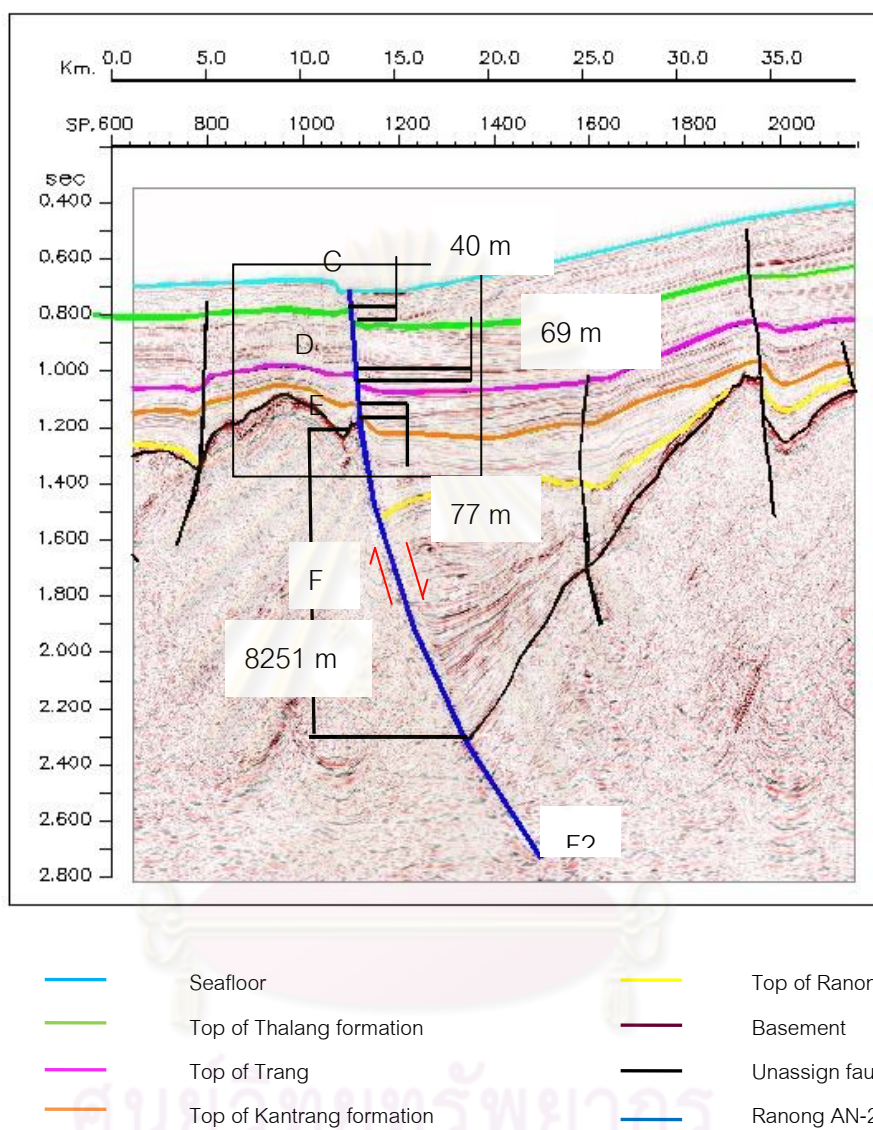


Figure 5.22 Seismic cross section of line survey AN4 near Ranong ridge showing normal movement at F2 cutting to the seafloor.

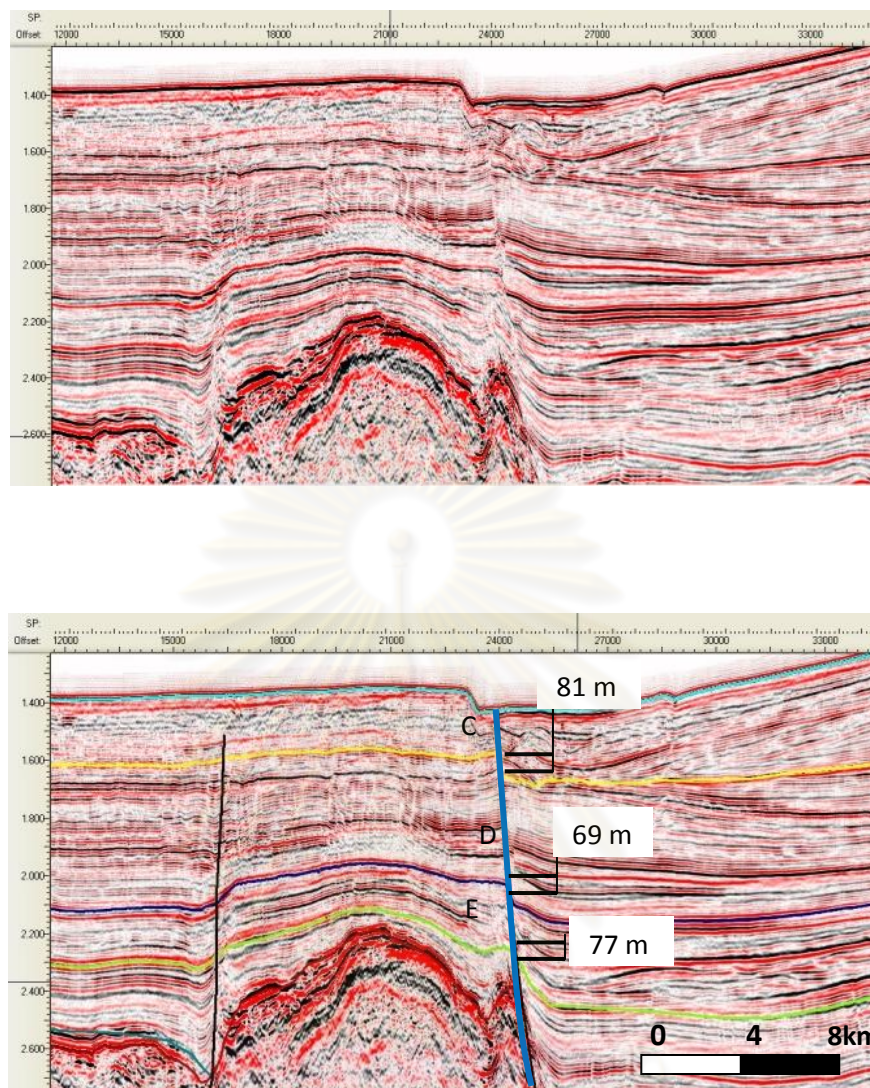


Figure 5.23 Seismic cross section of the enlarged line survey AN4 near Ranong ridge showing F2 reaching to the seafloor (point A).

ศูนย์วิทยทรัพยากร
จุฬาลงกรณ์มหาวิทยาลัย

Table 5.4 Displacement of faults in seismic line survey AN4.

Point	Vertical displacement		Vertical slip rate mm./yr	Dip angle (degree)	Age of top layer Ma.
	Sec.	m.			
A	0.047	40	0.0076	53	5.3
B	2.615	7039	0.2478	47	28.4
C	0.086	81	0.0153	60	5.3
D	0.057	69	0.0060	60	11.6
E	0.059	77	0.0048	60	16
F	2.254	8251	0.2905	56	28.4

5.1.2 Summary of seismic interpretation in Andaman sea

From the result of this section in Andaman Sea, it is observed that the Ranong fault zone is divided into many fault segments. The two most obvious fault segments (Figure.5.24) are the Ranong F1 shown as the red line and second and the Ranong F2 as to the blue line. When the collected data is compared with structure in Andaman Sea (Modified from DMR, STS. and BEICIP-FRANLAB, 1996) (Figure.5.25), it can be concluded that the two fault lines are fault segments of the Ranong fault zone that are still active fault because of the fault has cut through the basement to the seafloor. They are related to the earthquake coordinates that are found in that fault area with the size of 3.0-5.0 ML and there are many epicenters of earthquake with the magnitude of <3 ML in the northeastward of the area near Phanga province line in northeasth -southwest direction, they are probable occurred from RNF (Ranong F3) (Figure 5.25). These fault segments are also a strike slip fault. We can see that the movement of Ranong fault Zone in the Andaman Sea leads to the narrow push uplift (Ranong ridge) and the fault segments in the form of Horsetail spray (Cunningham and Mann, 2007 (Figure 5.26). From physiographic map of the Mergui Basin, Andaman Sea (Mahatanachai,1996) show Ranong fault through mergui shelf which left lateral movement (Figure 5.27).

From the interpreted data above, the special features of the three fault line can be identified

Table 5.5 Displacement of Ranong fault which cutting to the seafloor.

Line name	Dip angle		Vertical displacement				Vertical slip rate (mm./yr)	
			(m).		Sec			
	F1	F2	F1	F2	F1	F2	F1	F2
AN1	75		47		0.039		0.0029	
AN1	70		74		0.058		0.0036	
AN1	74		76		0.029		0.0031	
AN2	55		36		0.040		0.0068	
AN3	55		30		0.036		0.0057	
AN4	53	60	40	81	0.047	0.086	0.0076	0.0153

Table 5.6 Displacement of Ranong fault cutting the top of basement.

Line name	Dip angle		Vertical displacement				Vertical slip rate (mm./yr)	
			(m).		Sec			
	F1	F2	F1	F2	F1	F2	F1	F2
AN1	65	-	3640	-	-	-	0.1282	-
AN2	47	48	4328	2736	2.407	1.169	0.1524	0.0963
AN3	47	47	4419	3342	2.487	1.204	0.1556	0.1177
AN4	47	56	7039	8251	2.615	2.254	0.2478	0.2905

1. Ranong F1 (red line) identified by seismic interpretation, strikes in the northeast-southwest direction (NE-SW) N10E and dips about 47-60 degree to the southeast. Its length is approximately 100 kilometers. F1 cuts basement to the seafloor, the fault offsets seafloor and Thalang formation with the dip angle of 53-75 degree to east and with the vertical slip of 30-76 m (0.029-0.058 sec). This can give rise to the slip rate of about 0.0029-0.0076 mm/yr. The Ranong F1 offsets top of basement with the dip angle of 47-65 degree to east and the vertical slip of 3600-8500 meters (1.60-2.60 sec). The slip rate of about 0.1282-0.2478 mm./yr. is determined as shown in table 5.5.

2. Ranong F2 segment (blue line) identified by seismic interpretation and epicentral of earthquake, has strikes in the northeast-southwest direction (NE-SW) N24E and dips about 47-60 degree to the southeast with the approximate length of 45 kilometers. Ranong F2 cuts basement to the seafloor, the fault offsets seafloor with the dip angle of 60 degree to east with the vertical slip of 81 m (0.086sec) and slip rate of about 0.0153 mm/yr. Ranong F2 offsets top of basement with the dip angle of 47-56 degree to east with the vertical of 2,736-8,251 meters (1.169-2.254 sec) and slip rate of about 0.0963-0.2905 mm./yr. as shown in table 5.5. (Figures 5.28-5.29)

3. Ranong F3 (green line) identified by epicentral of earthquake, strikes in the northeast-southwest direction (NE-SW) N25E. The approximate length of 55 kilometers. Moreover, Ranong f3 is tentative fault segment of RNF and recommended for future active fault study.

Note that the slip rates determined from this study are regional (or long - term) sliprate which calculated from 2D seismic survey.

5.2 Seismic interpretation in Gulf of Thailand

In this part Kingdom 8.4 program was used to interpret 3 seismic lines located near the epicenters of earthquake event on 27th-28th September 2006 and 8th October 2006. These 2D seismic lines are G1, G2 and G3 as shown in the figure 5.30 . interpretation in this area does not have the borehole drilling hole log data to separate the sediment formation. It can only separates the layer into basement, sediment horizon seafloor and fault line.

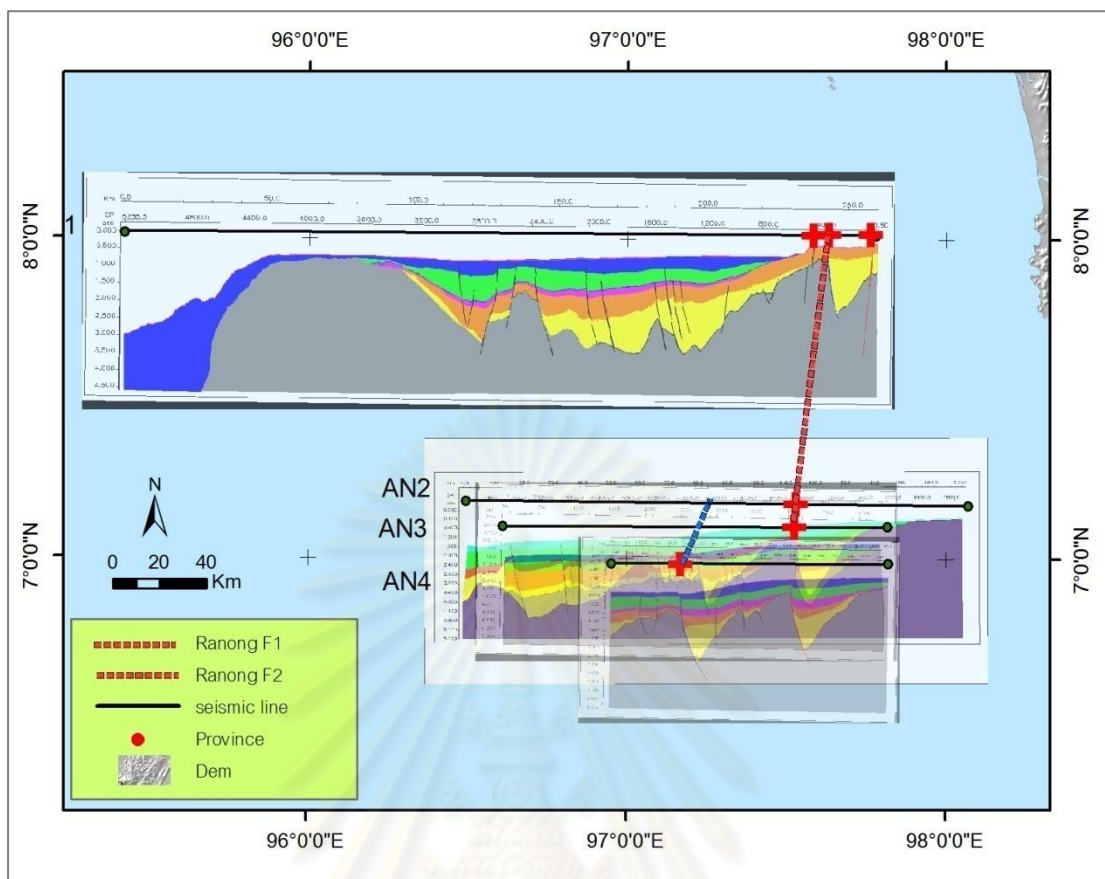


Figure 5.24 Map showing the direction of Ranong F1 and Ranong F2 from seismic interpretation in Andaman area. (The legend and explanation are as the same as these of Figure 5.14)

ศูนย์วิทยทรัพยากร
จุฬาลงกรณ์มหาวิทยาลัย

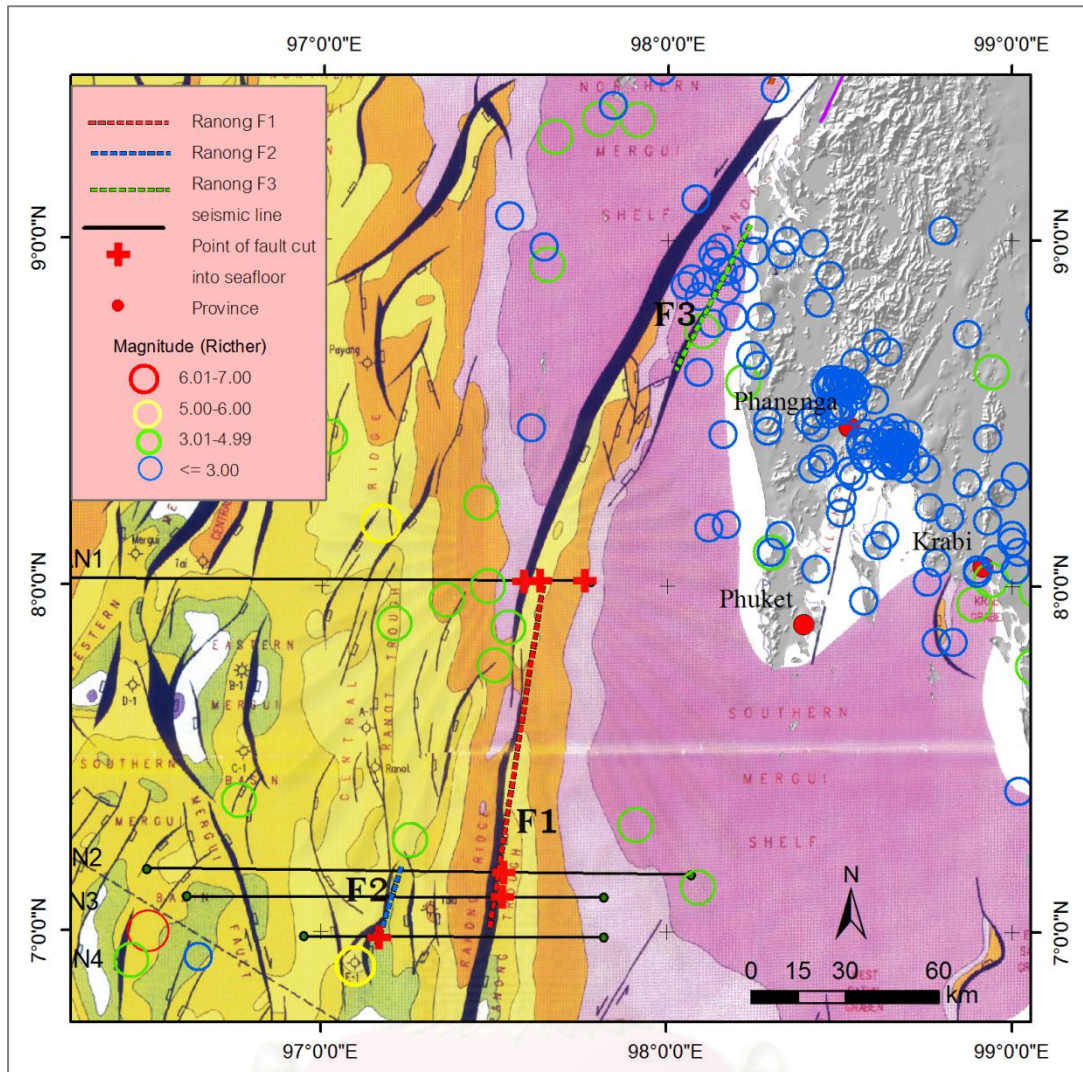


Figure 5.25 Map showing Ranong F1 Ranong F2 and Ranong F3 which are related to epicenters of earthquake with magnitudes about <3-5 ML and correspond with the structure map of Andaman (DMR,1996).

ศูนย์วิทยทรัพยากร
จุฬาลงกรณ์มหาวิทยาลัย

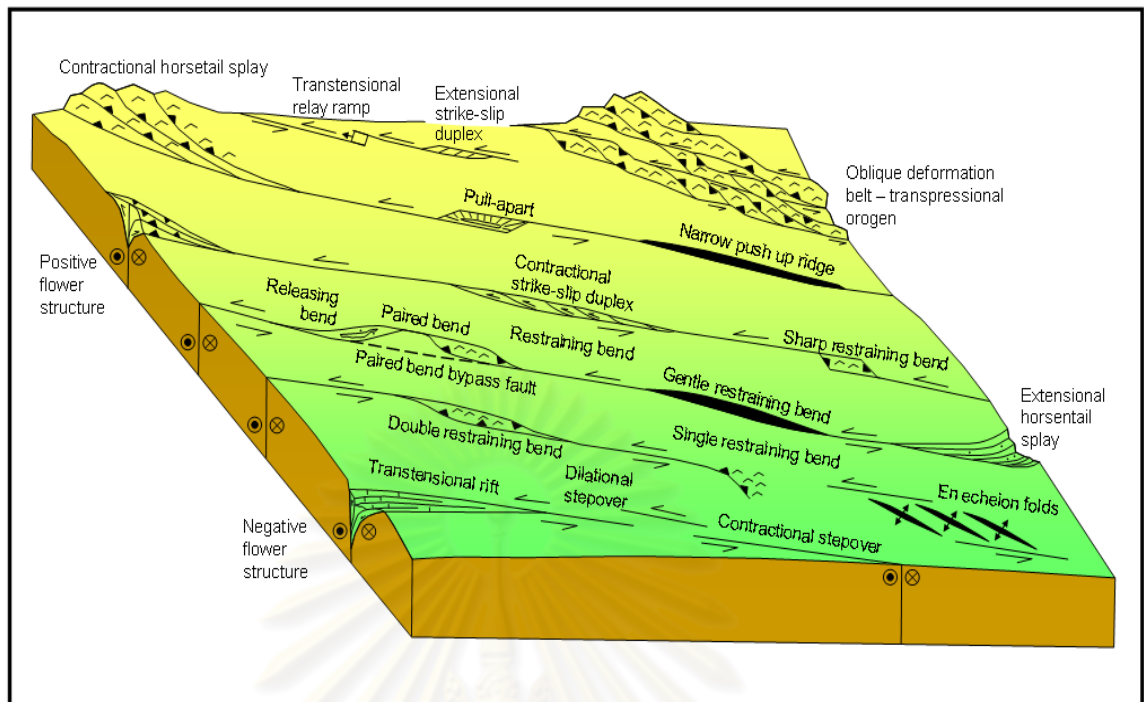


Figure 5.26 structural model from strike slip fault (Cunningham and Mann, 2007).

ศูนย์วิทยทรัพยากร
จุฬาลงกรณ์มหาวิทยาลัย

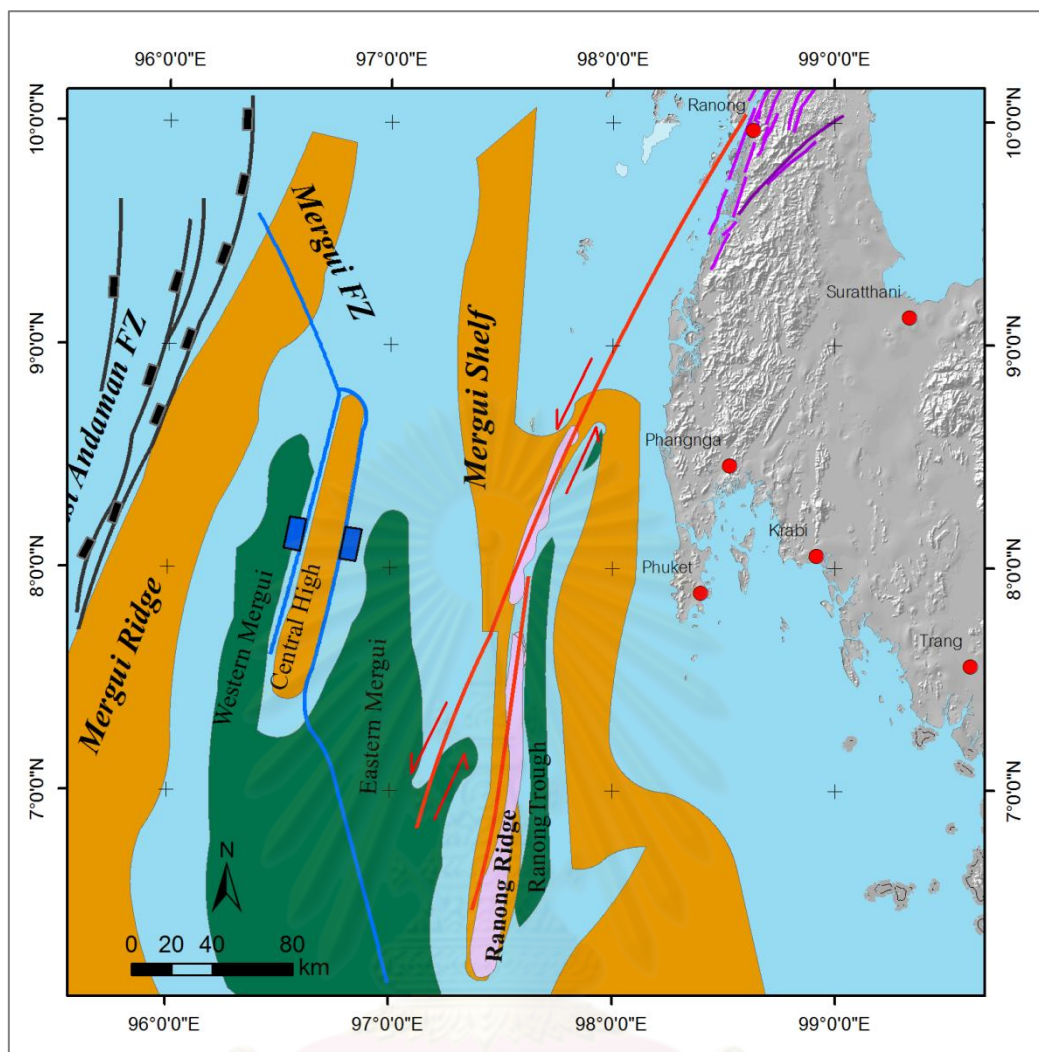


Figure 5.27 Map showing direction of movement of the RNF in the Andaman Sea and the main physiographic features of the Mergui Basin, Andaman Sea (Mahatanachai, 1996). Note that the RNF fault from structure map of Andaman by DMR (1996).

ศูนย์วิทยทรัพยากร
จุฬาลงกรณ์มหาวิทยาลัย

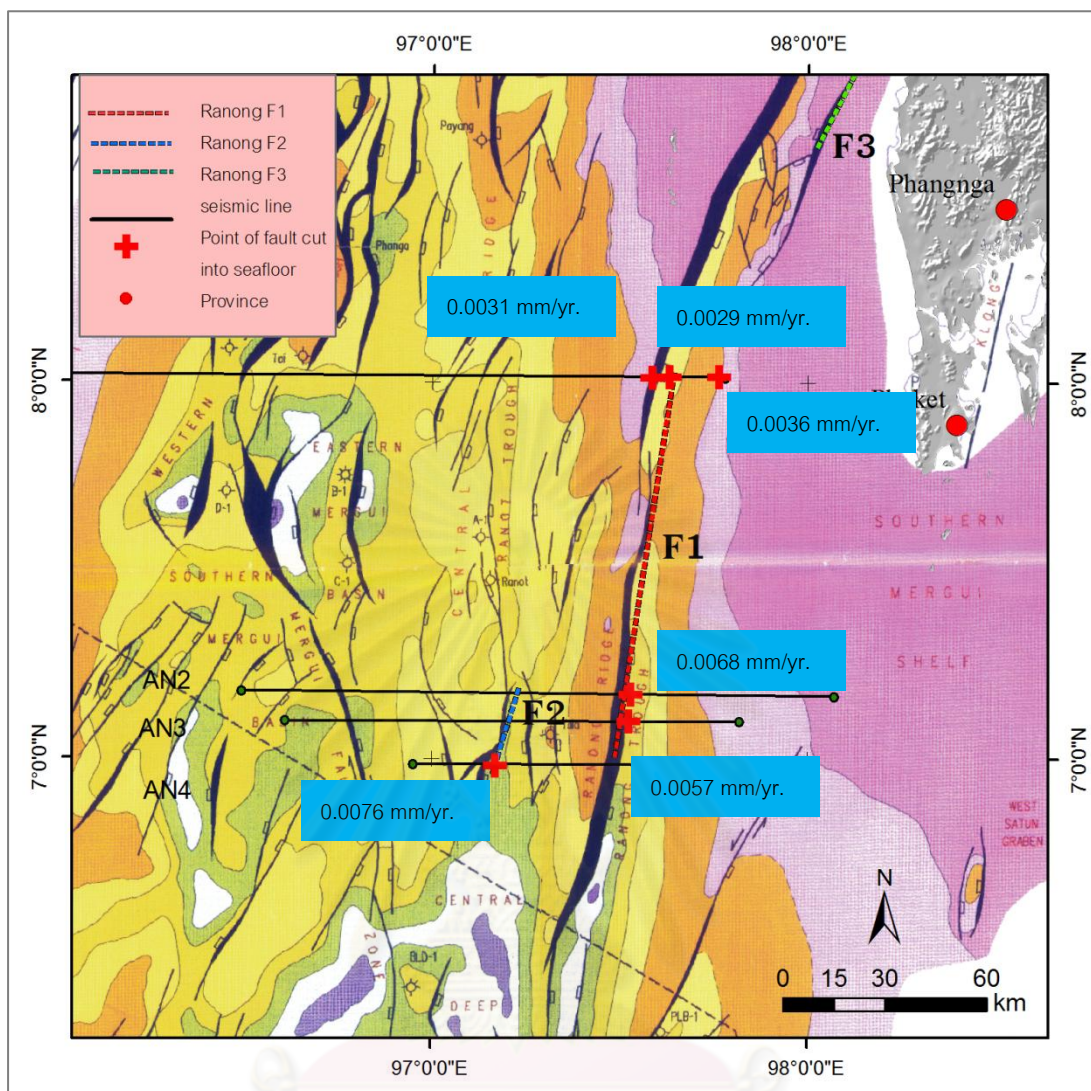


Figure 5.28 Map showing the computed average regional slip rates at the points which the Andaman seafloor was cut by Ranong F1 and Ranong F2. Note that the Ranong F1 from AN1 and AN2 is extrapolated based on the interpretation made by staff of DMF.

จุฬาลงกรณ์มหาวิทยาลัย

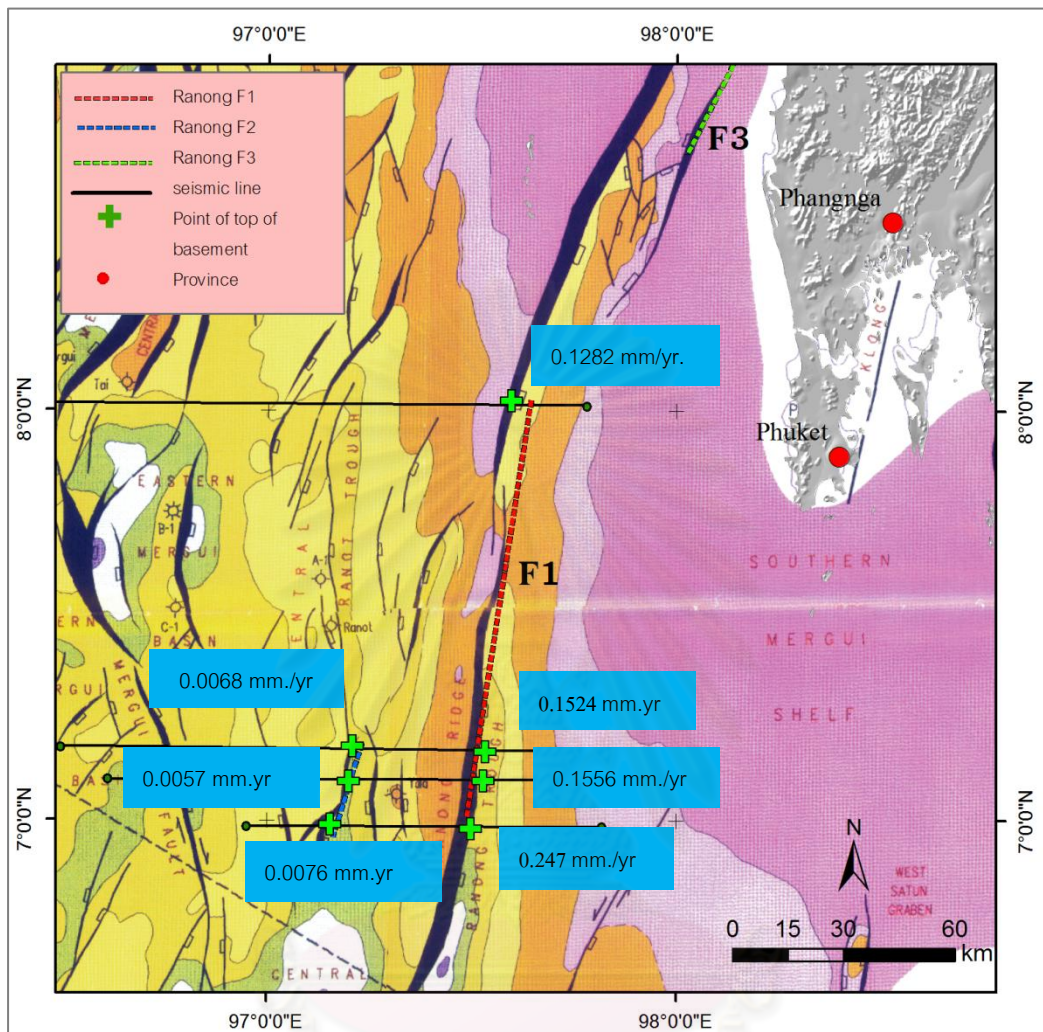


Figure 5.29 Map showing the computed average regional slip rate at the points which top of basement was cut by Ranong F1 and Ranong F2 .

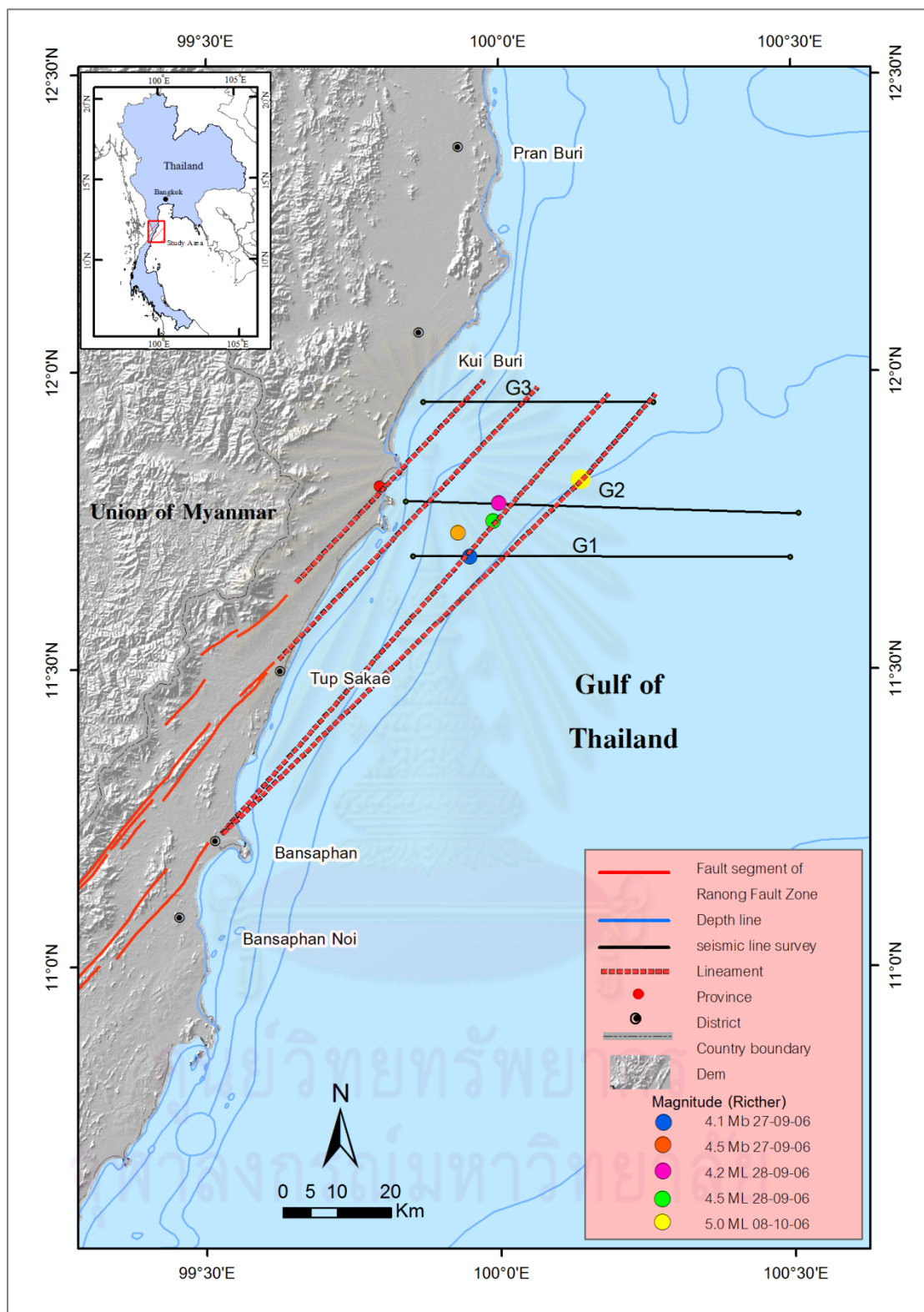


Figure 5.30 Map showing seismic line survey of this study (black line) and the extrapolated RNF in Gulf of Thailand.

In this study, the focus is on the Ranong fault zone that is suspected to pass into the gulf of Thailand and it could be the cause of the mentioned earthquake event. In this part use same formular as seismic interpretation in Andaman

From report of Basin Modelling of Hua Hin South Basin Block B3/32, Gulf of Thailand, Chaisilboon (1997) found sediment layer of Hua Hin basin at depth about 290-400m is the sediment in Pliocene -recent age (0-5.3 ma) and sediment layer in depth about 400-700 m is the sediment in Late Miocene (5.3-10 ma). Thus in this study used the age of sediment from above data to calculate slip rate.

5.2.1 Preliminary Result

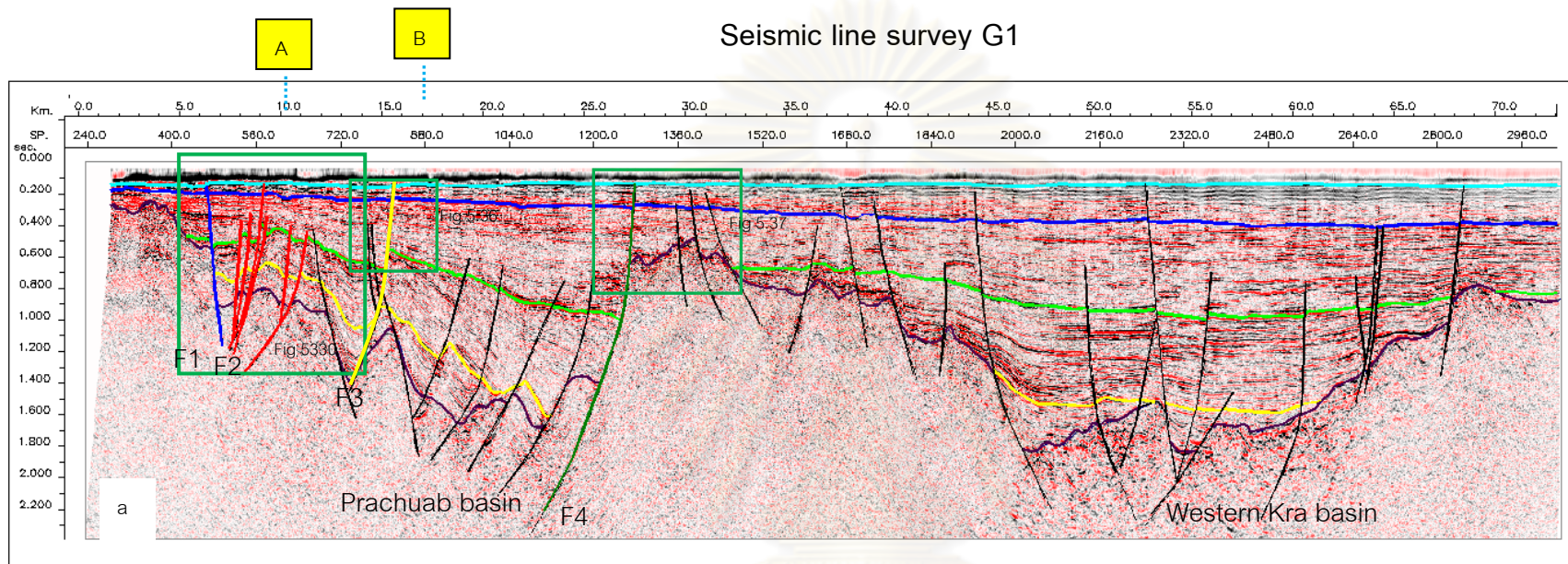
5.2.1.1 Seismic survey line G1

The basement, horizon layers and other fault lines can be separated as shown Figure 5.31 and 5.32.

F1 locates on the west side border of Prachuab basin (blue line) and cut the sediment into the seafloor. The faults offsets top of horizon A with the dip angle of 47degree to east with the vertical slip of 18m (0.015 sec), and slip rate of about 0.0034 mm/yr. F4 on the east side edge of Prachuab basin (green line) cut sediment to the seafloor which dip angle is 47 degree to west. F4 offsets top of horizon A with the vertical slip of 27m (0.021 sec) and slip rate of about 0.0051 mm/yr. Both faults show normal movement (Figure 5.33- 5.37).

When the Ranong fault segment is extrapolated to the sea, it reaches the seismic line G1 which is 10 km away (Figure 5.38) from the west seismic line. The line is within the point near the epicenter of earthquake event on 27 September 2006 when seismic interpretation indicates the fault associated with the negative flower structure (F2). The fault in the above structure cut through the sediment layer until it reaches the seafloor at Point A in the normal fault movement (Figure 5.35). F2 offsets horizon A with the vertical slip of 13m (0.014 sec) and slip rate of about 0.0025 mm/yr.,

Moreover, F3 (yellow line) which is 15 km west from the seismic line is found at point B. A fault dip 44 degree west cuts through the sediment layer until it reaches the seafloor as well and it a normal fault. F3 offsets top of horizon A with the dip angle of 44



- | | | | |
|--|-----------|--|----------------|
| | Seafloor | | Unassign fault |
| | Horizon A | | Fault F1 |
| | Horizon B | | Fault F2 |
| | Horizon C | | Fault F3 |
| | Basement | | Fault F4 |

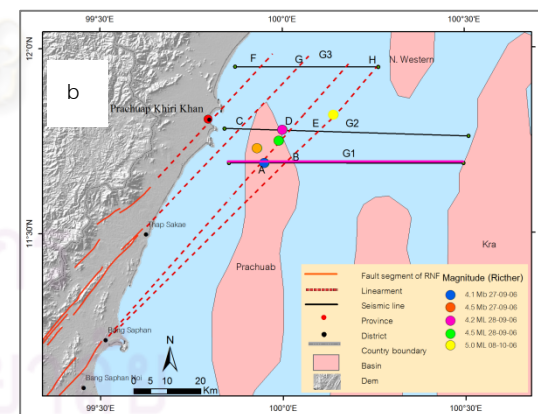
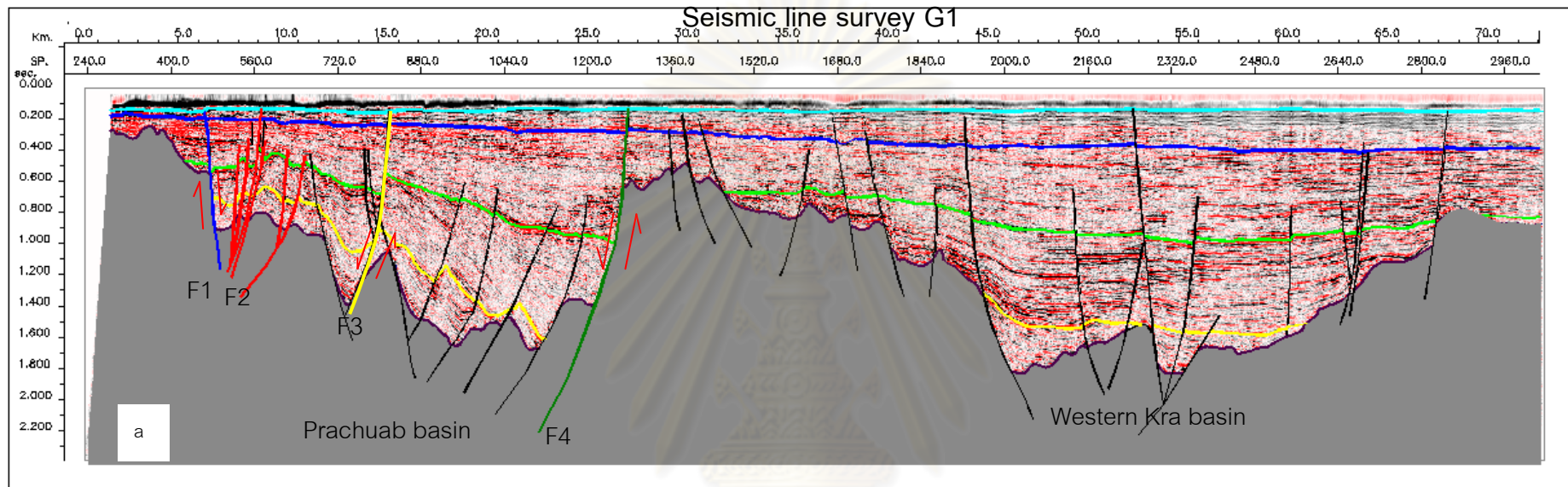
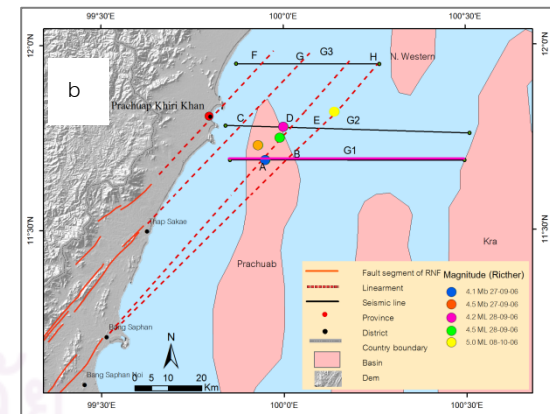


Figure 5.31 (a) seismic cross-section of seismic line survey G1. (b) Map showing seismic line survey G1, distribution of epicentral in Gulf of Thailand, lineament of Ranong fault zone and basin in Gulf of Thailand.



- | | | | |
|--|-----------|--|-----------------------|
| | Seafloor | | Unassign fault |
| | Horizon A | | Fault F1 |
| | Horizon B | | Fault F2 |
| | Horizon C | | Fault F3 |
| | Basement | | Fault F4 |
| | | | Direction of movement |



(DMF,TMD and USGS, 2009)

Figure 5.32 (a) Model of seismic line survey G1 showing direction of movement.

(b) Map showing seismic line survey G1, distribution of epicentral in Gulf of Thailand, lineament of Ranong fault zone and basin in gulf of Thailand.

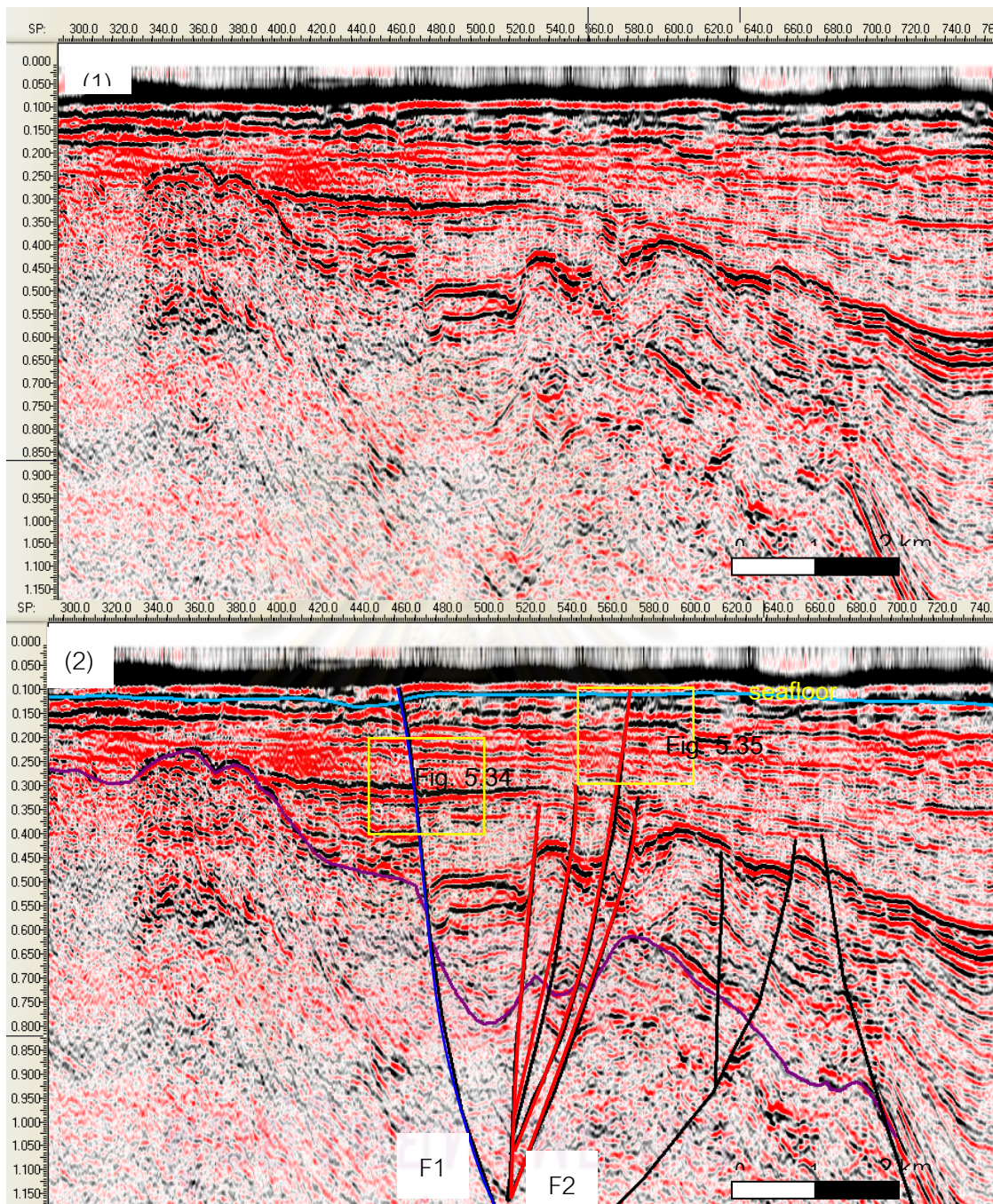


Figure 5.33 Seismic cross section of the enlarged seismic line G1 at Point A (Fig 5.31a) showing negative flower structure (F2, red line), suggesting the normal movement and F1 is the normal fault controlling the edge of Prachuab basin and cutting through into seafloor, layer.

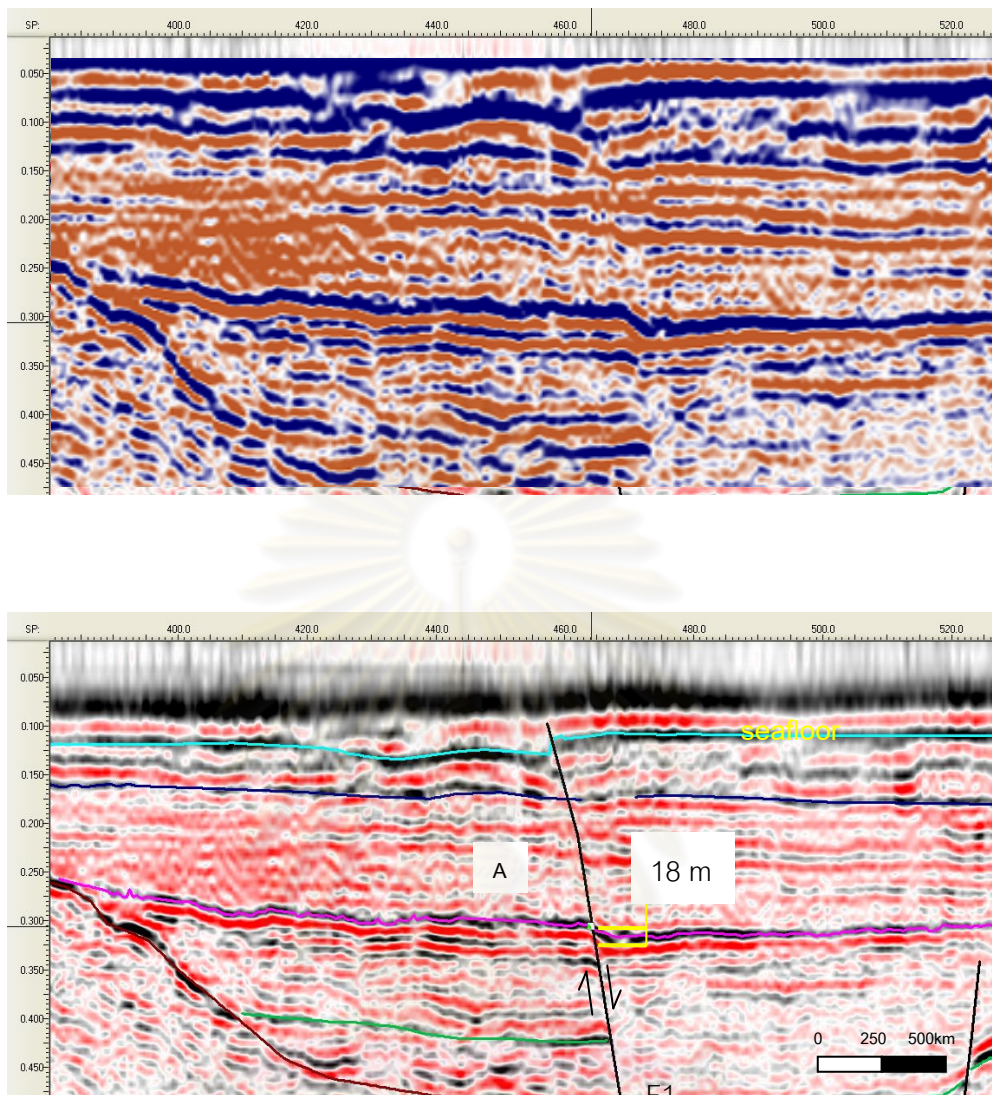


Figure 5.34 Seismic cross section of the enlarged seismic line survey G1 at the edge of prachuab basin in the west side showing normal movement of F1 reach to the seafloor .

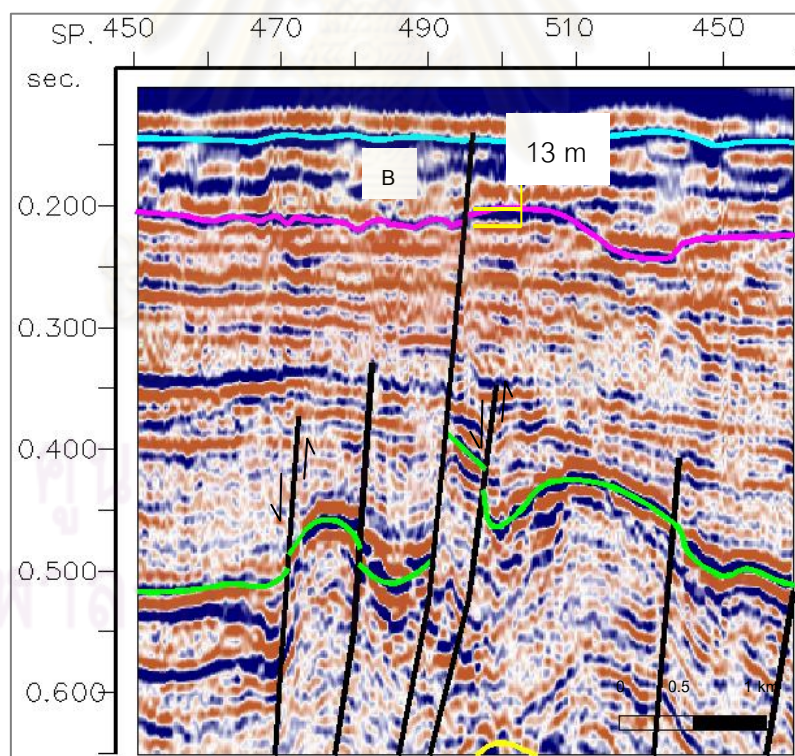
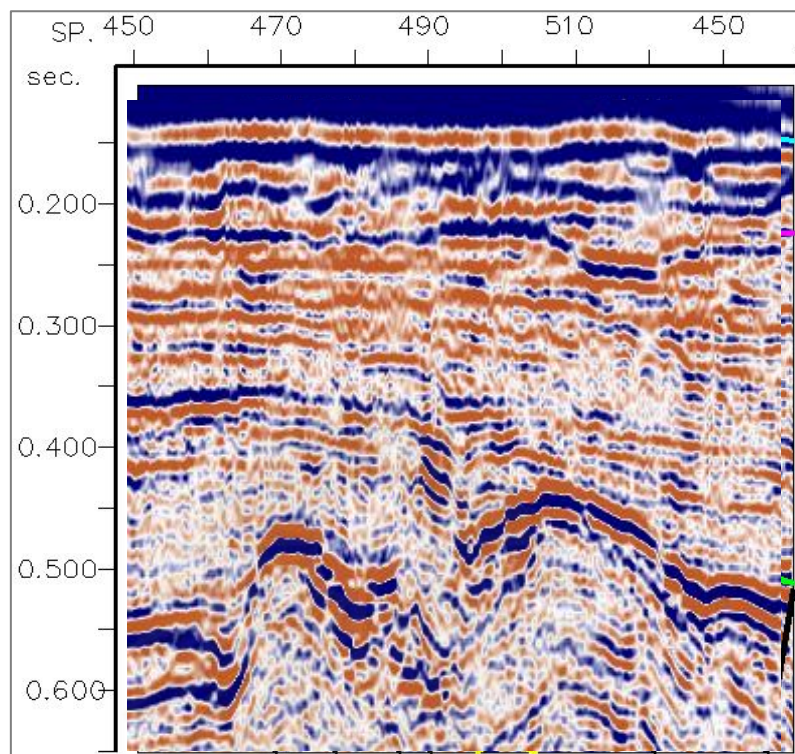


Figure 5.35 Seismic cross section of the enlarged seismic line survey G1 at Point A (Figure 5.31a) showing and reverse senses of normal movement in the flower structure reach to the seafloor.

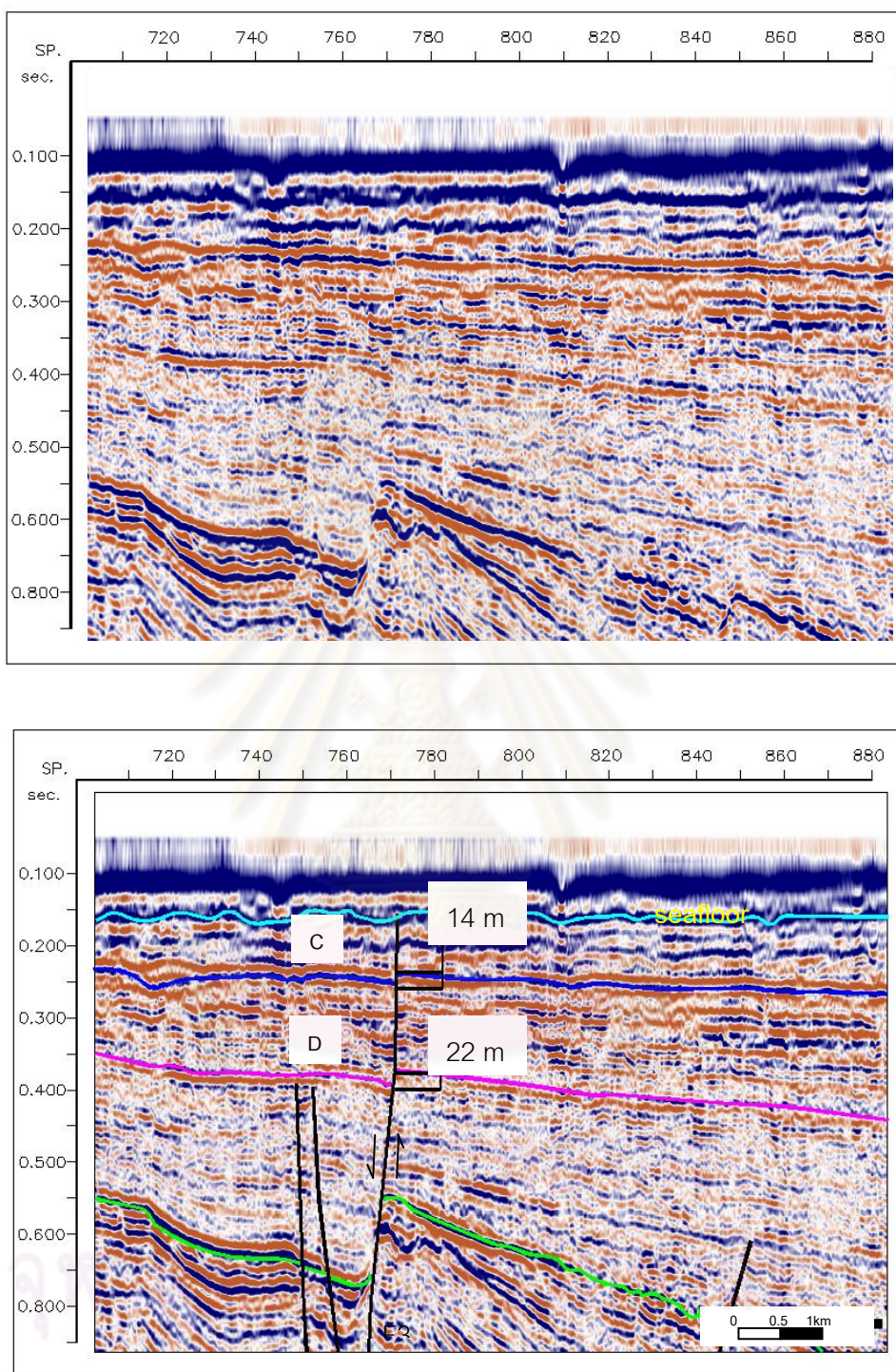


Figure 5.36 Seismic cross section of the enlarged seismic line survey G1 at Point B (Figure 5.31a) showing the normal movement of F3 that reaches to the seafloor.

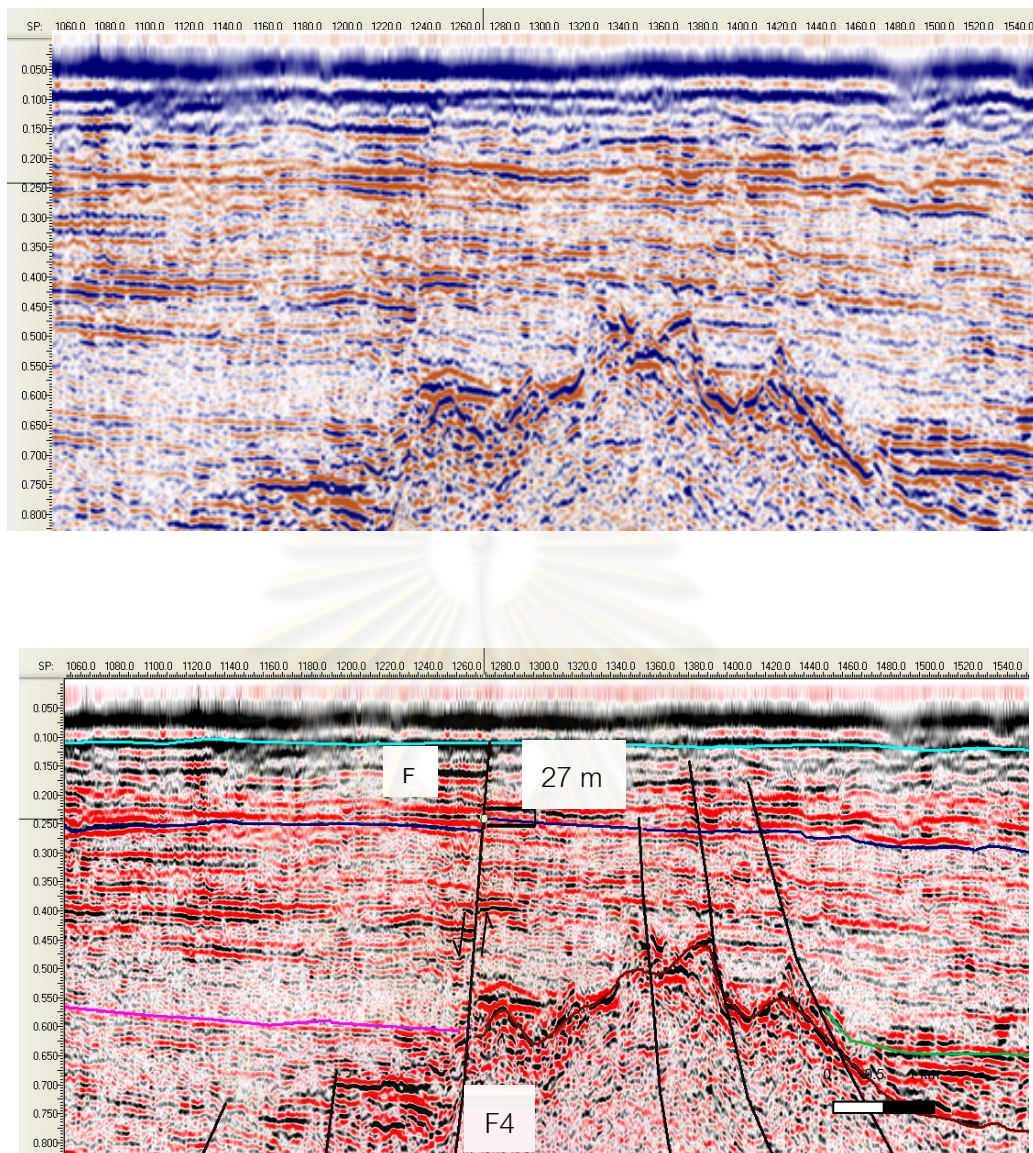


Figure 5.37 Seismic cross section of the enlarged seismic line survey G1 Point C (Figure 5.31a) showing the normal movement of F4 reach to the seafloor.

จุฬาลงกรณ์มหาวิทยาลัย

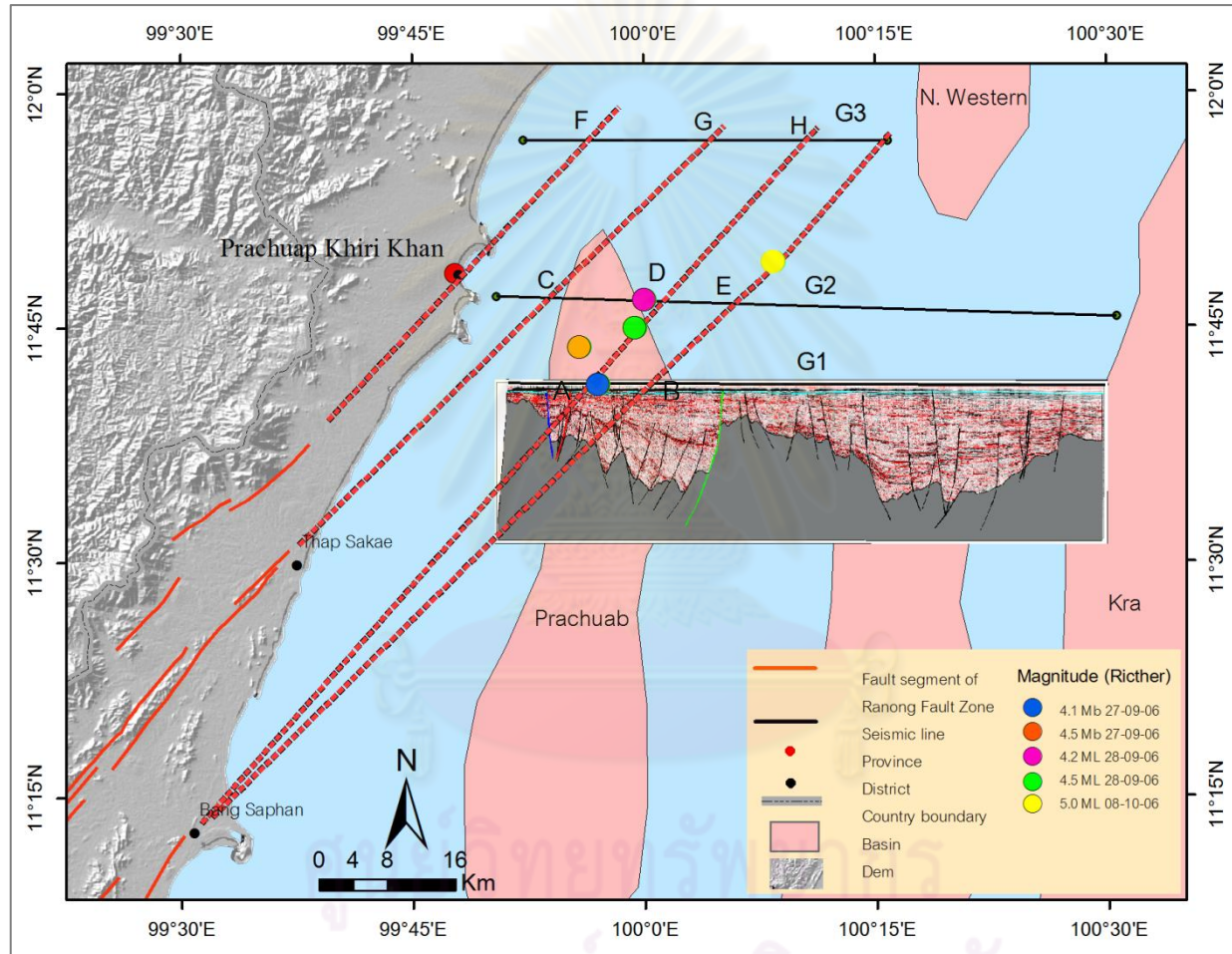


Figure 5.38 Map showing faults in seismic survey G1 and extended of lineament of RNF. Point A founded negative flower structure and it is location of epicenter of earthquake on 27 September 2006.

degree to west with vertical slip of 14-22 m (0.0014-0.016 sec) and slip rate of about 0.0022-0.0026 mm/yr. (Figure 5.36) as shown in table 5.7

Table 5.7 Displacement of faults in seismic line survey G1

Point	Vertical displacement		Vertical slip rate mm./yr	Dip angle (degree)	Age of top layer Ma
	Sec	m			
A	0.015	18	0.0034	47	5.3
B	0.014	13	0.0025	40	5.3
C	0.014	14	0.0026	44	5.3
D	0.016	22	0.0022	44	10
F	0.021	27	0.0051	47	5.3

5.2.1.2 Seismic survey line G2

The basement and other fault lines can be separated as shown in figures 5.39 and 5.41. Displacement of fault in seismic survey line G2 is shown in table 5.7. By extending Ranong fault segment until it reaches the seismic line, the fault is suspected to be found at point C, D and E which are 5,17 and 30 km away in the western direction respectively. The point C is the nearest to the epicenter of the earthquake event on 28 September 2006 with the size of 4.2 Richter. (Figure 5.44)

From the seismic interpretation, point C has the fault structure in the negative flower structure and the F2 (red line) in the above structure cut through the sediment layer until it reaches the seafloor near Point C in the normal fault movement. (Figure 5.41) F2 offsets horizon A with the vertical slip of 21m (0.017 sec) and slip rate of about 0.0040 mm/yr. (Figure 5.42),

At point D which locates near the epicenter of the earthquake, F3 (green line) dipping 40 degree west is found. It cuts through the sediment layer until it reaches the seafloor in the normal fault movement. The fault is also the eastern edge of the Prachuab basin (Figure. 5 45) and offset horizon A with the vertical slip of 25 m (0.024 sec) and slip rate of about 0.0047 mm/yr. (Figure 5.42),

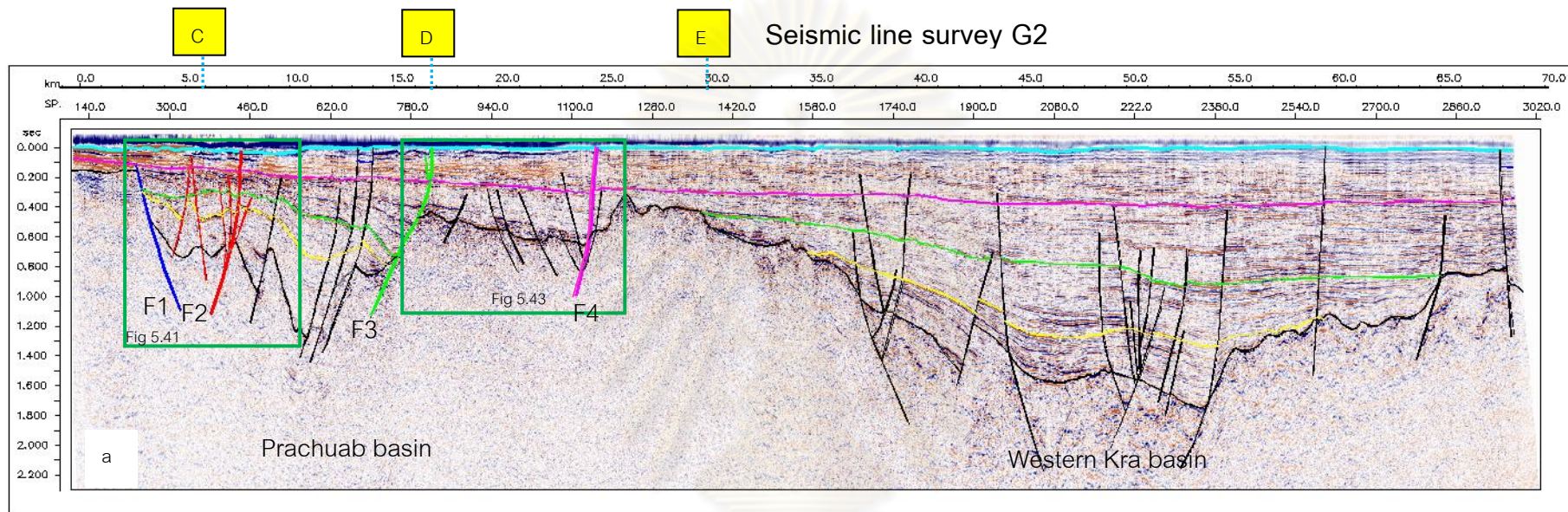
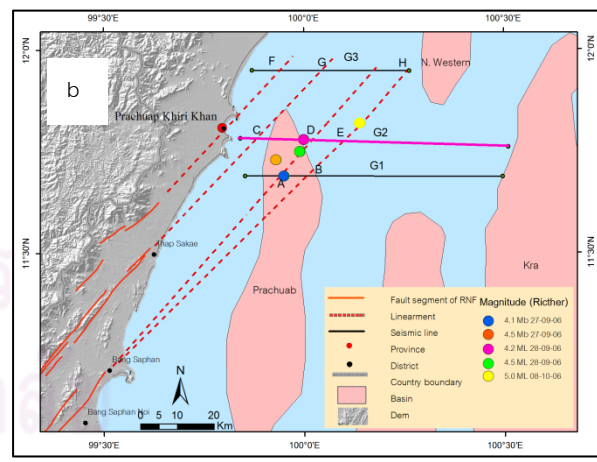
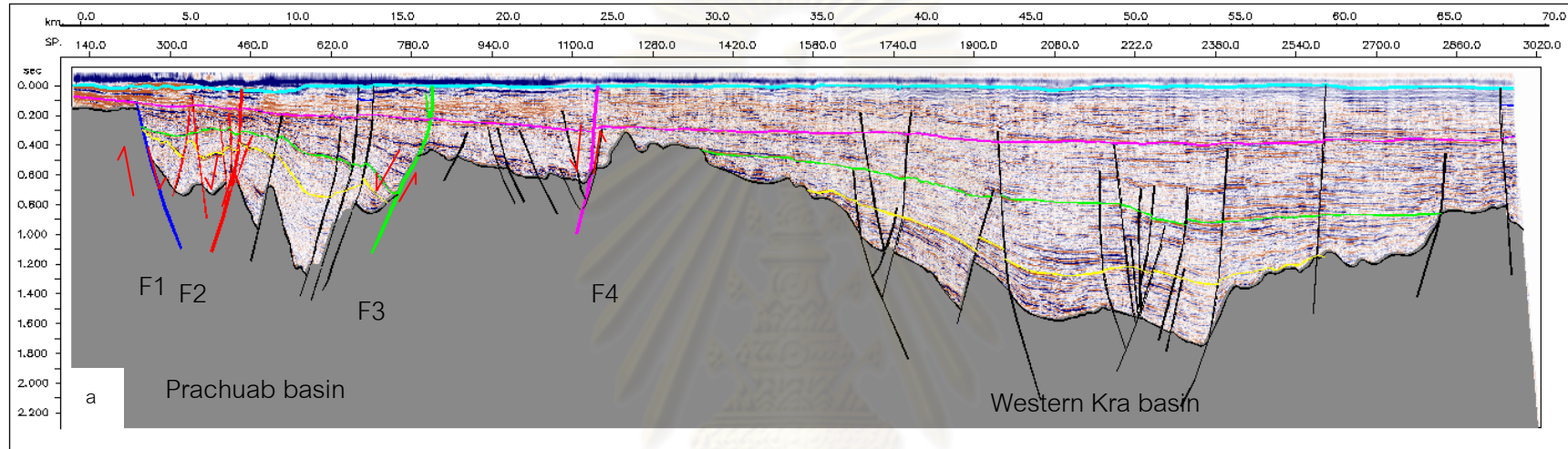


Figure 5.39 (a) seismic cross-section of seismic line survey G2. (b) Map showing seismic line survey G2, distribution of epicentral in Gulf of Thailand, lineament of Ranong fault zone and basin in gulf of Thailand.

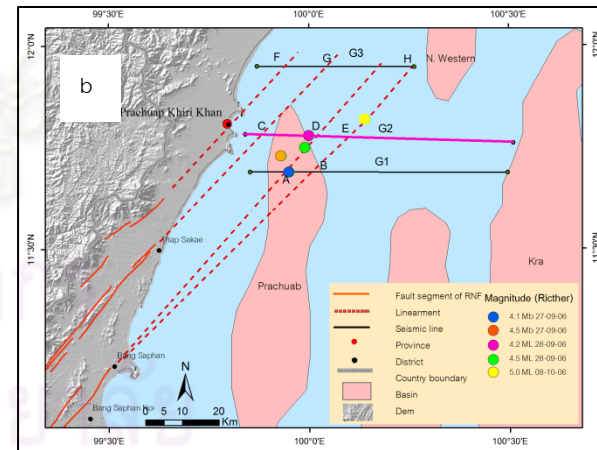


(DMF,TMD and USGS, 2009)

Seismic line survey G2



- | | | | |
|--|-----------|--|-----------------------|
| | Seafloor | | Unassign fault |
| | Horizon A | | Fault F1 |
| | Horizon B | | Fault F2 |
| | Horizon C | | Fault F3 |
| | Basement | | Fault F4 |
| | | | Direction of movement |



(DMF, TMD and USGS, 2009)

Figure 5.40 (a) Model of seismic line survey G2 showing direction of movement.

(b) Map showing seismic line survey G2, distribution of epicentral in Gulf of Thailand, lineament of Ranong fault zone and basin in gulf of Thailand.

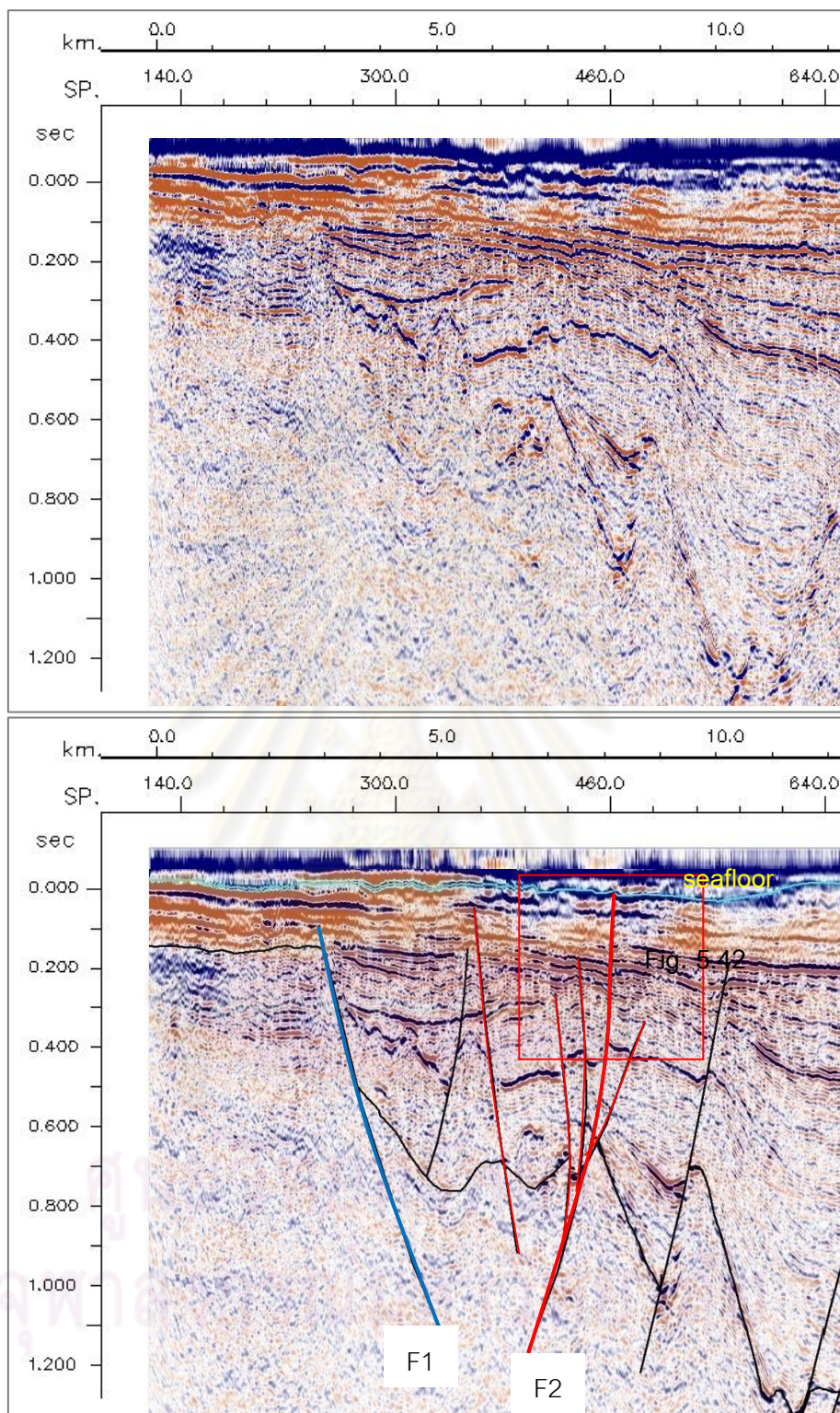


Figure 5.41 Seismic section of the enlarged line G2 at Point C (Fig 5.39a) showing the negative flower structure (F2, red line), suggesting the normal fault cutting through sediments into seafloor.

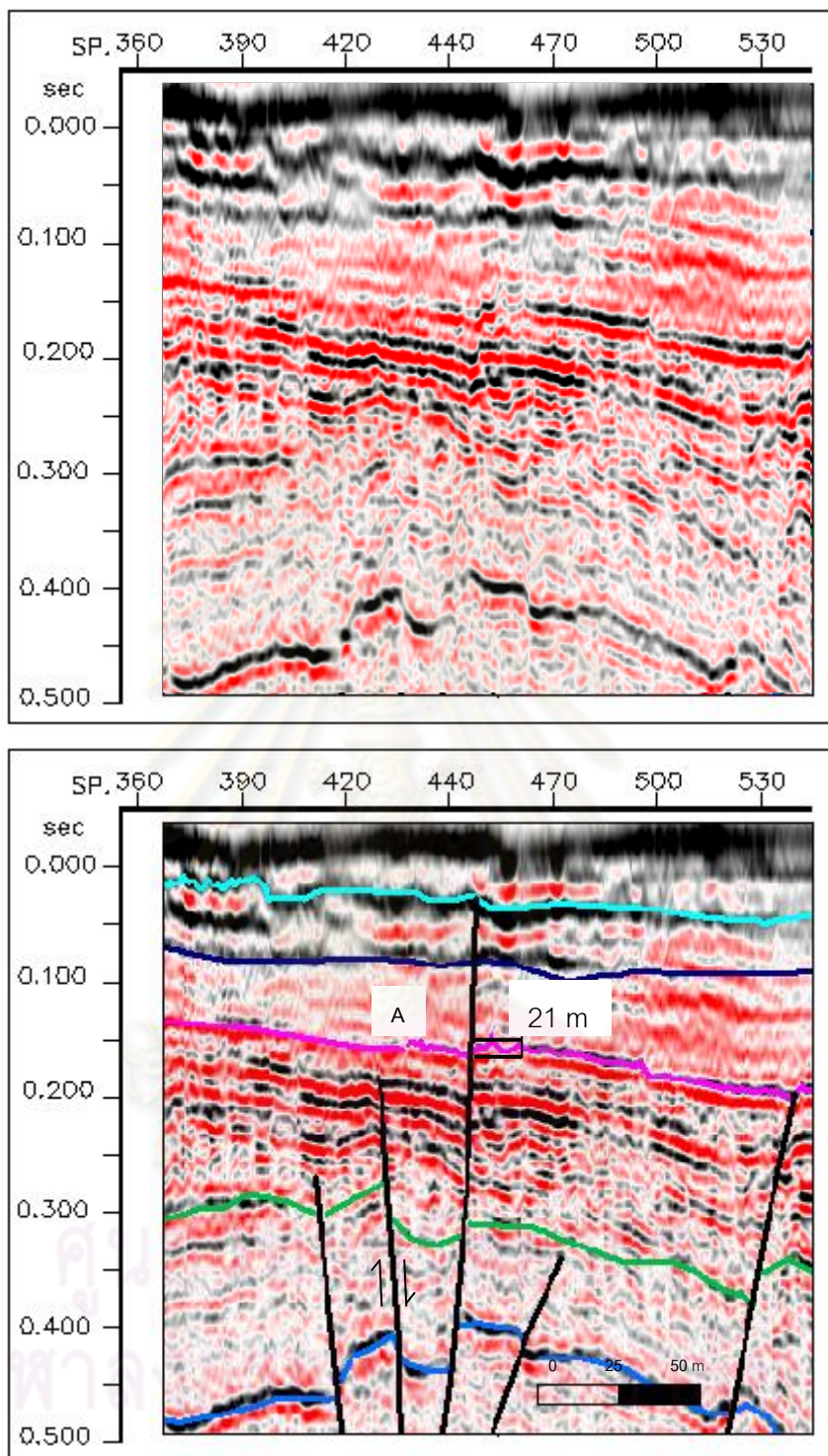


Figure 5.42 Seismic section of the enlarged line survey G2 at Point C (Figure 5.39a) showing normal movement in the negative flower structure with one fault reaching to the seafloor.

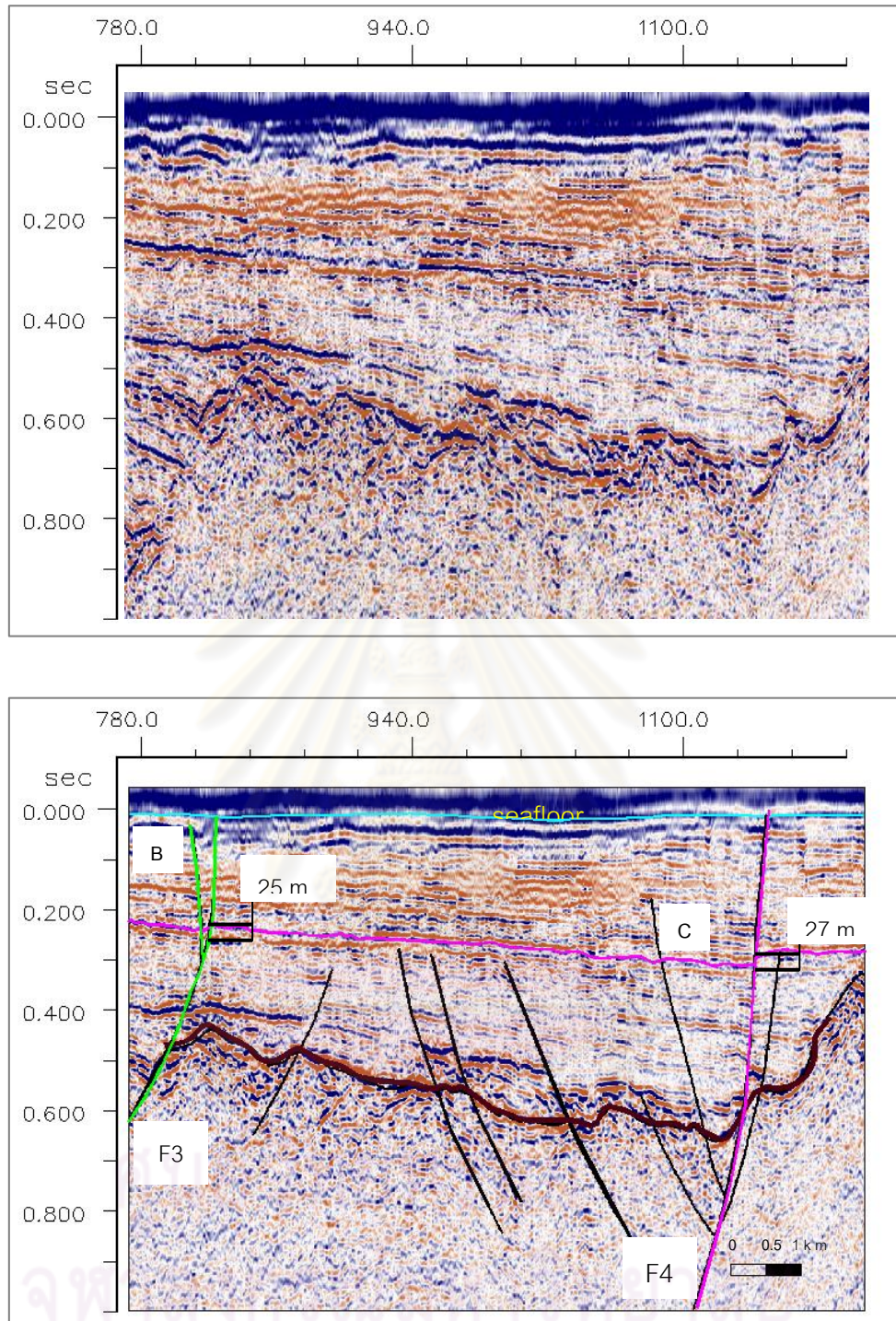


Figure 5.43 Seismic section of the enlarged line survey G2 at Point D and E (Figure 5.39a) showing normal movement of F3 and F4 (green line and pink line) reach to the seafloor .

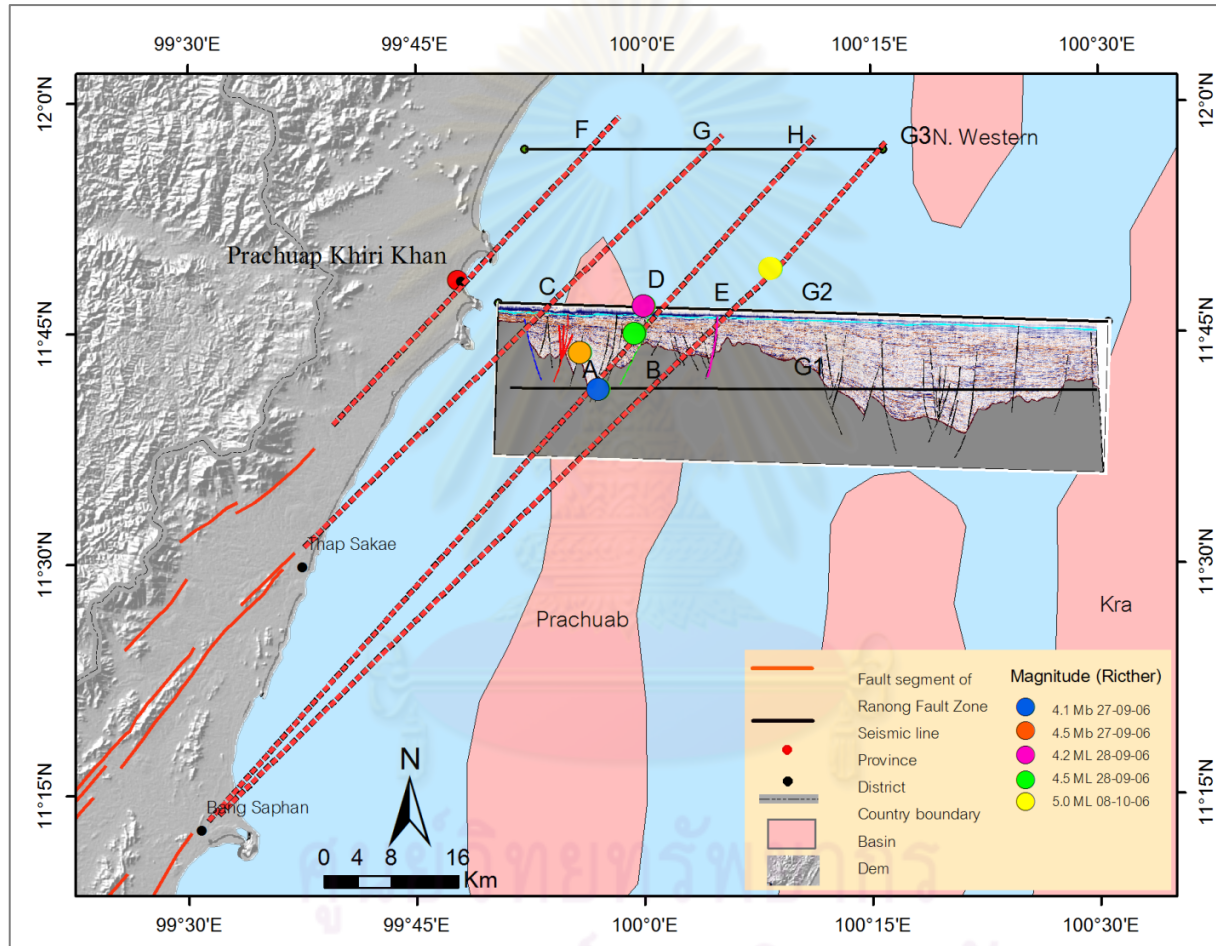


Figure 5.44 Map showing faults in seismic survey G2 and extended of lineament of RNF. Point C founded negative flower structure and Point D is location of epicenter of earthquake on 27 September 2006.

F4 cut the seafloor at point E in the movement of normal fault with dip angle of 60 degree to west and offset horizon A with thickness of 27 m (0.023 sec), slip rate about 0.0051 mm/yr.(Figure 5.42),

Table 5.8 Displacement of faults in seismic line survey G2

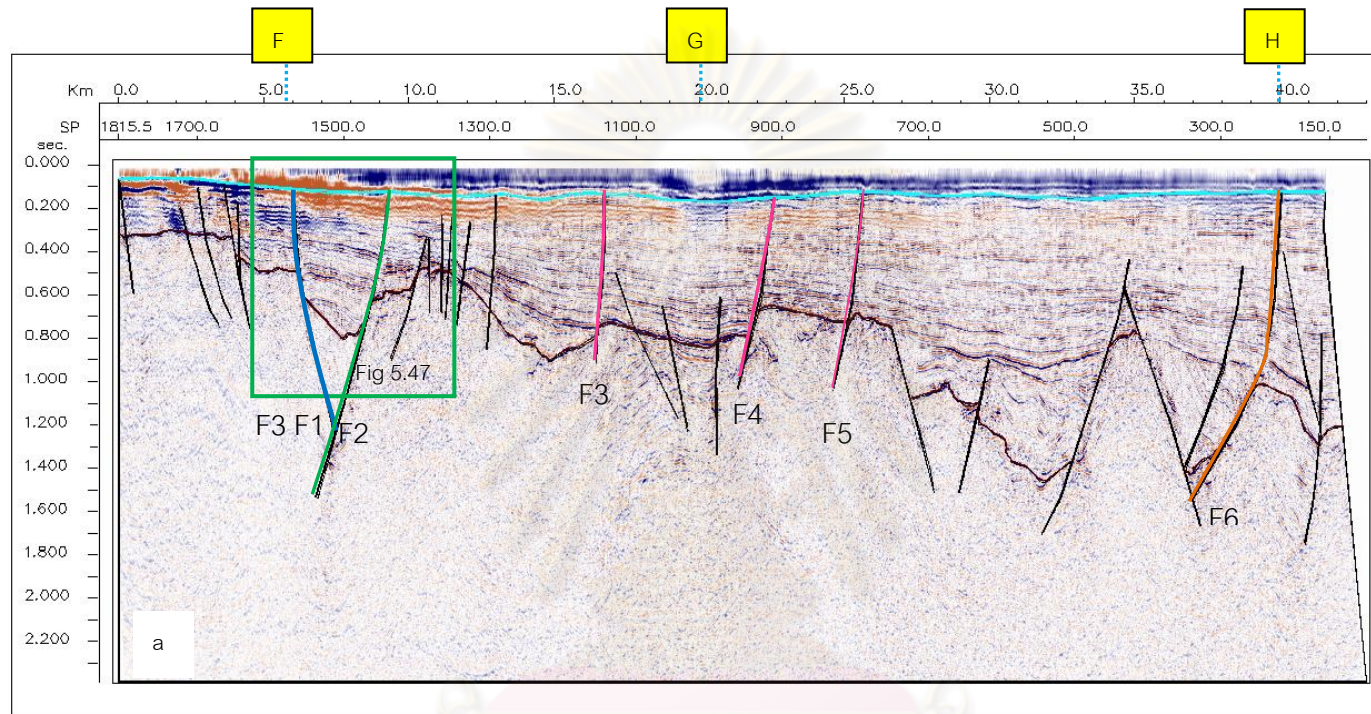
Point	Vertical displacement		Vertical slip rate mm./yr	Dip angle (degree)	Age of top layer Ma
	Sec	m			
A	0.017	21	0.0040	40	5.3
B	0.024	25	0.0047	40	5.3
C	0.023	27	0.0051	60	5.3

5.2.1.3 Seismic survey line G3

Basement and other fault lines can be separated as shown in figures 5.45 and 5.46. By extending Ranong fault segment until it reaches the seismic line G3, the fault is suspected to pass through at point F, G and H which are 5, 20 and 40 km away in the western direction respectively.

At point F, F1 with dip angle of 40 degree to east cuts the edge of the Prachuab basin until it reaches the seafloor in the normal fault movement. At point G, there is no fault that has the movement cutting through the sediment layer in the shallow level. However, in the area around 5-10 km, both east and west side(Figure 5.45),there are faults (F3, F4, and F5) with dip angle of 54 degree to west, they cuts through until it reaches the seafloor in the normal movement.

At point G, F6 cuts to the seafloor in the normal fault movement with dip angle of 60 degree to west.



- | | | | |
|--|----------|--|-----------------|
| | Seafloor | | Fault F4 |
| | Basement | | Fault F5 |
| | Fault F1 | | Fault F6 |
| | Fault F2 | | Unassign fault) |
| | Fault F3 | | |

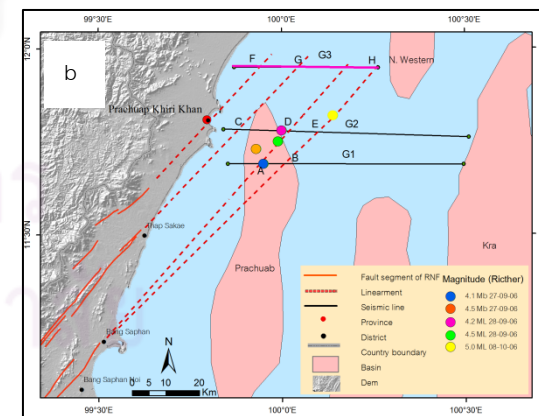
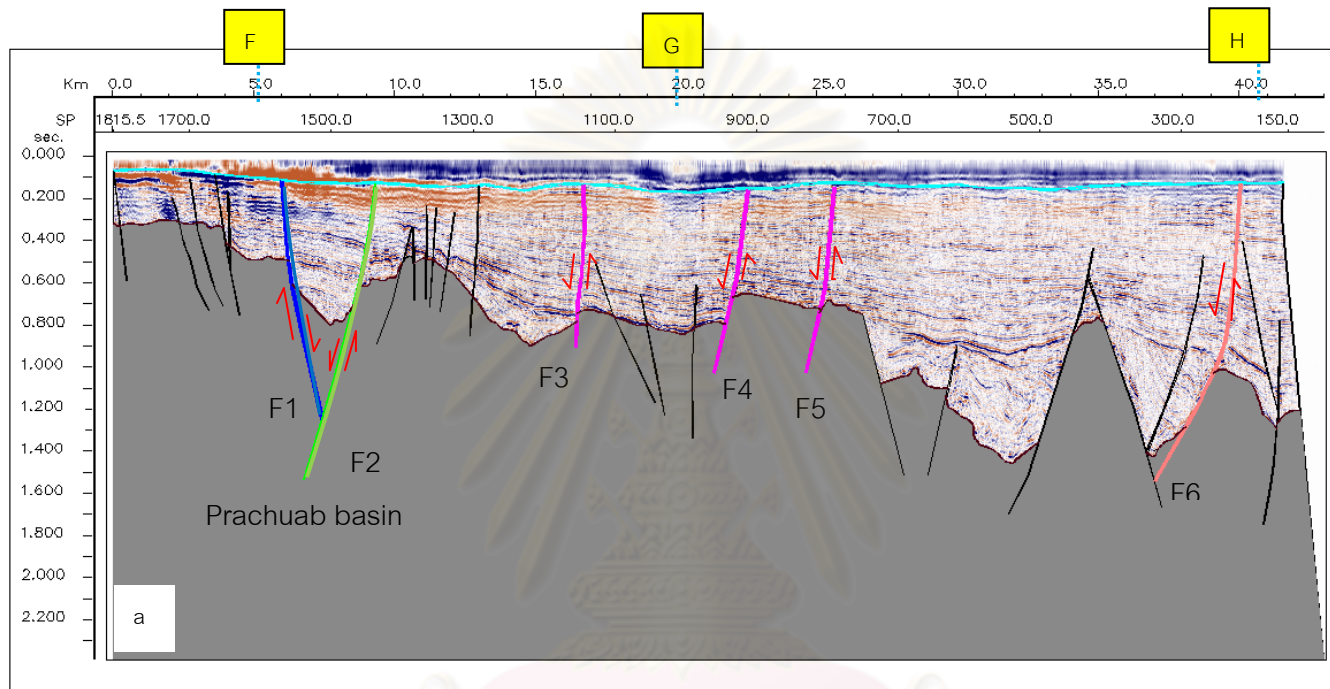


Figure 5.45 (a) seismic cross-section of seismic line survey G3. (b) Map showing seismic line survey G3, distribution of epicentral in Gulf of Thailand, lineament of Ranong fault zone and basin in gulf of Thailand.



- | | | | |
|--|----------|--|-----------------------|
| | Seafloor | | Fault F4 |
| | Basement | | Fault F5 |
| | Fault F1 | | Fault F6 |
| | Fault F2 | | Unassing fault |
| | Fault F3 | | Direction of movement |

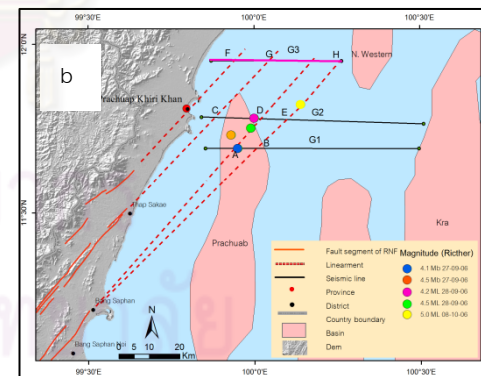


Figure 5.46 (a) Model of seismic line survey G3 showing direction of movement.
 (b) Map showing seismic line survey G3, distribution of epicentral in Gulf of Thailand, lineament of Ranong fault zone and basin in gulf of Thailand.

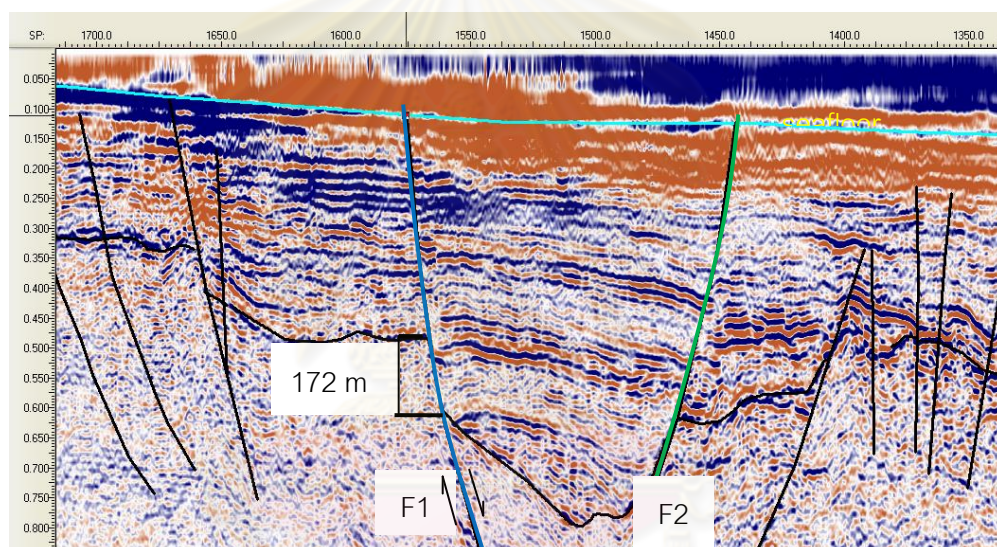
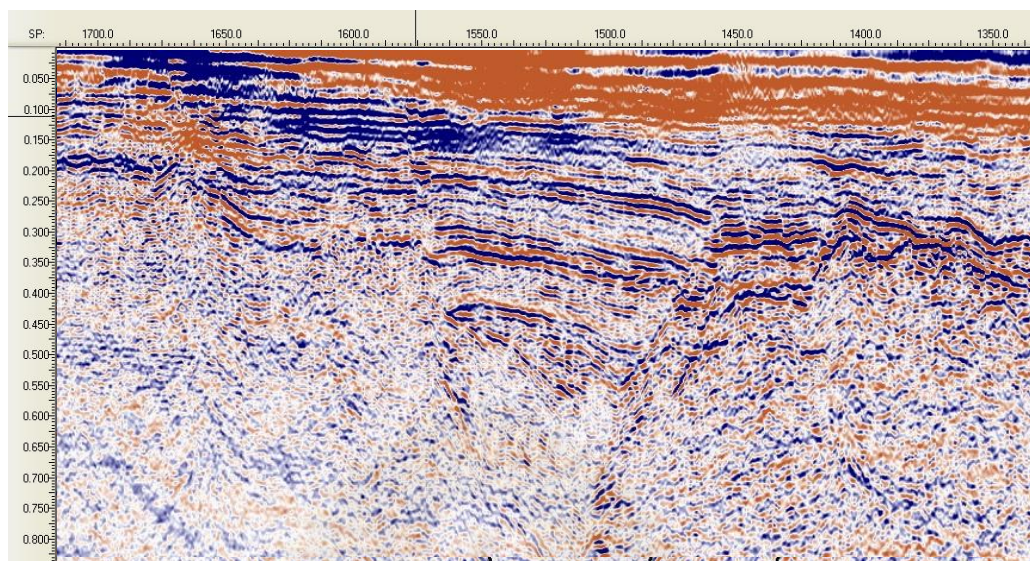


Figure 5.47 Seismic section of the enlarged line G3 at Point F (Figure 3.45a) showing normal movement along the F1 and F2 (blue line and green line) which cut through sediment into seafloor.

จุฬาลงกรณ์มหาวิทยาลัย

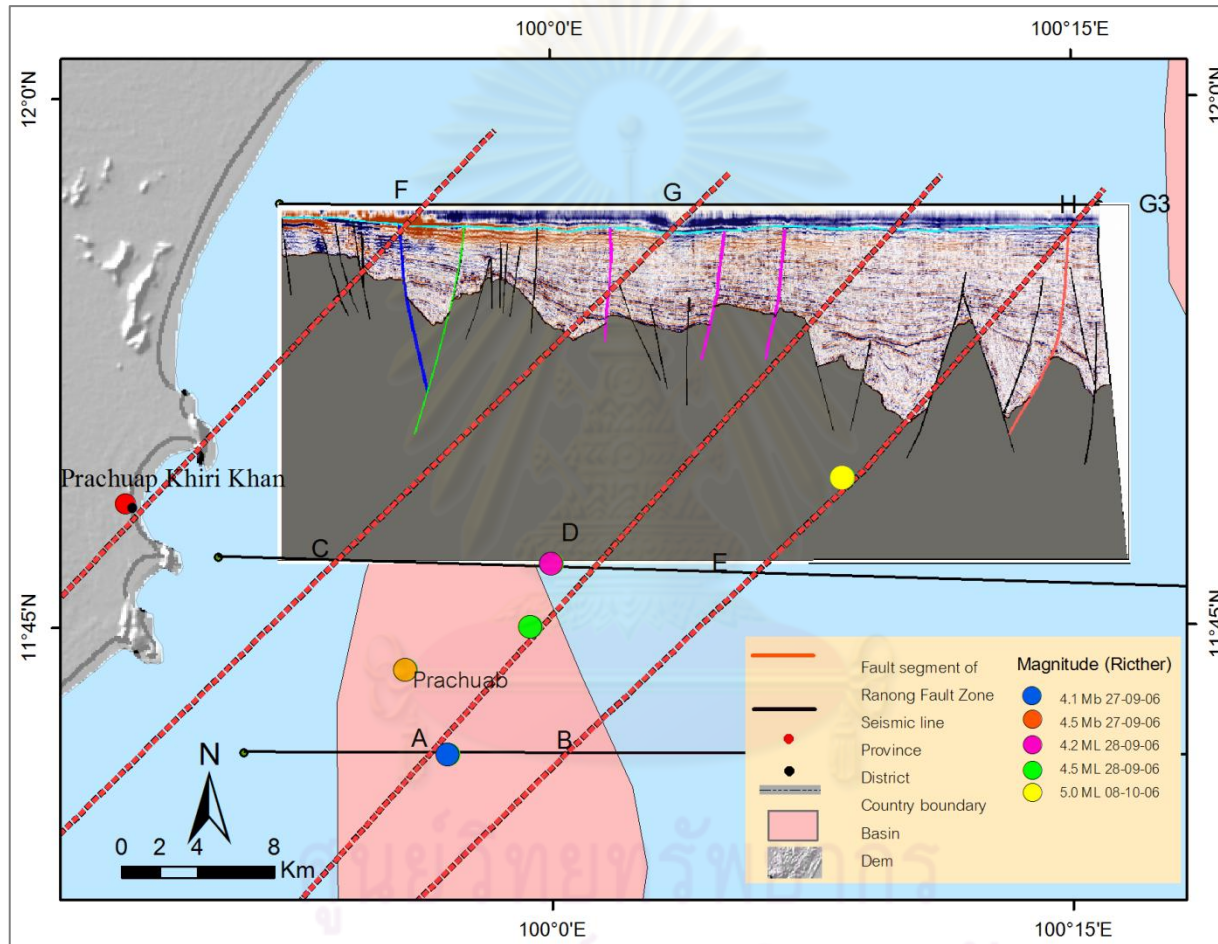


Figure 5.48 Map showing model of seismic line G3, epicenter of earthquake and extending lineament of Ranong Fault zone.

5.2.2 Summary of seismic interpretation in Gulf of Thailand

From the result we found

1. Faults at the edge of Prachuab basin, both western and eastern, has the movement that cut the seafloor showing that it still has continuous movement and they are active fault. The western side has the dip angle of 40-60 degree to east and the eastern side has the dip angle of 40-47 degree to west.

2. When the fault segment of Ranong fault zone is extended until it reaches all three seismic lines, there is some speculation that Bangsapan Noi segment might pass the point A and D, Bangsaphan and Nong Ya Plong fault segment might pass point C and G and the Thap sakae fault segment might pass point F. From the interpretation of all three seismic lines, the flower structure which creates the movement of strike slip fault is found at point A and D. It can be said that Bangsaphan, Nong Ya Plong fault segment and Bangsapan Noi segment moved into the gulf of Thailand and move until they reach the edge of the Prachuab basin cutting through the sediment layer until they reach the seafloor. This shows that they are all active fault. (Figure 5.50)

3. From the epicenter of the earthquake event on 27-28 September 2006 and 8 October 2006 locating in the area of Thai gulf, there are two seismic lines that pass this area.

The G1 seismic line passed the epicenter on 27 September 2006 with the size 4.1 mb at point A. The flower structure found at point A shows that it was the strike slip fault movement. There is a fault in the particular group of fault cut through until it reached the seafloor. Therefore, it is very likely that the earthquake incident on 27 September 2006 was caused by the oblique fault movement with the movement of normal with strike slip fault. This is because the fault in the flower structure group cut the sediment layer in the normal movement.

The G2 seismic line passed the epicenter on 28 September 2006 with the size 4.2 mb at point A. At point C, a fault dipping 40 degree cut the sediment until it reaches the seafloor in the normal fault movement. It also formed the east edge of the Prachuab basin. This makes me believe that the earthquake incident on the 28 September was caused by the normal fault movement.

For the earthquake incident on 8 October 2006, there is no seismic line passing through the area. The nearest to the epicenter of the earthquake is G2. When the perpendicular line from the epicenter is projected to the line of G2, there is still no fault cutting through the seafloor. However, when the Bangsaphan Noi is extended until it reaches the seismic line G2, a fault dipping 60 degree west cut through until it reached the seafloor in the normal fault movement is found. For that, the earthquake event on 8 October is related to a fault that moves in the oblique fault movement in normal with strike slip fault way. (Figure 3.50)

4. In this part we founded faults in 2D seismic survey cut in to the sea floor and can calculated regional slip rate of them as shown in figure 3.51.

5. With the small number of seismic lines used to carry out interpretation, the position of the fault plane might be inaccurate. Thus, more seismic lines are required to obtain the accurate value of the fault plane.



ศูนย์วิทยทรัพยากร
จุฬาลงกรณ์มหาวิทยาลัย

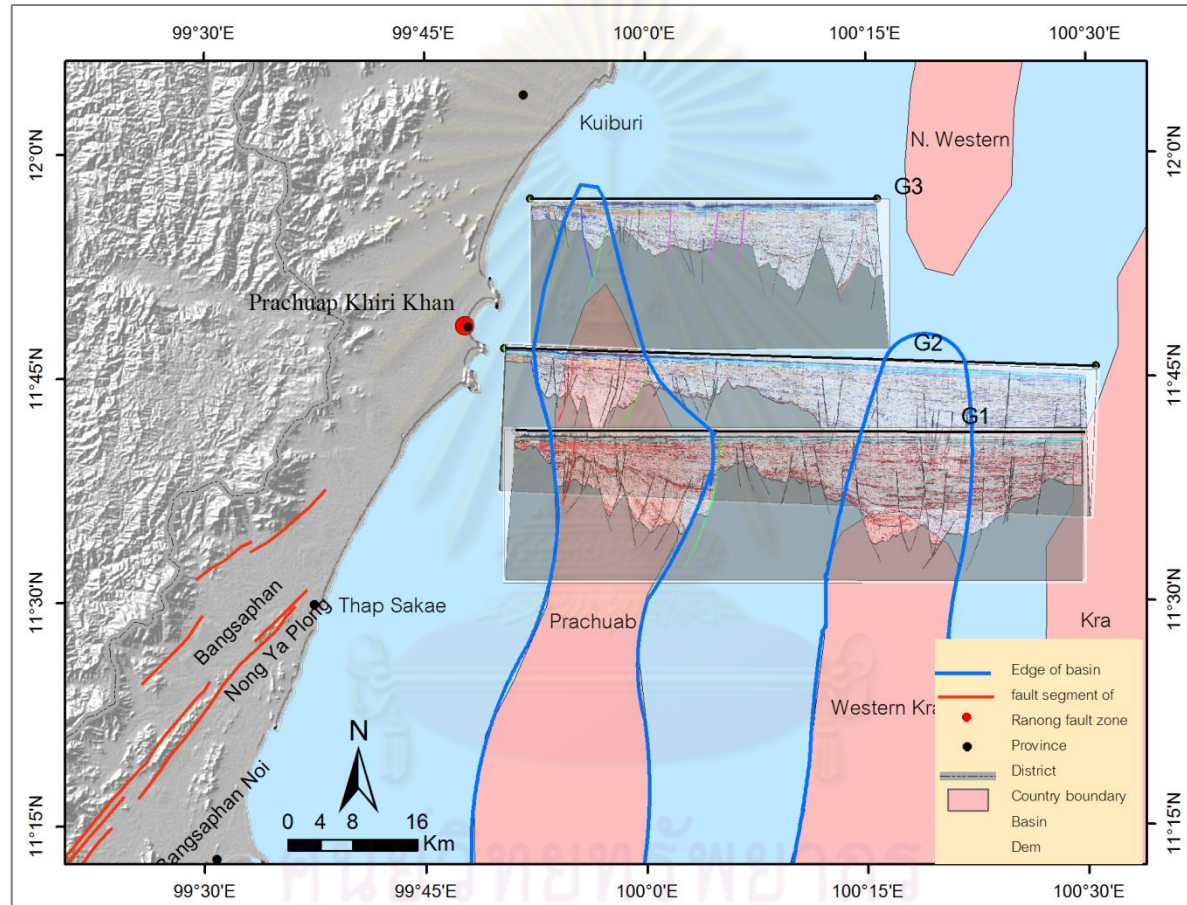


Figure 5.49 Map showing the newly proposed edge of basin (blue line) based on seismic interpretation in this study.

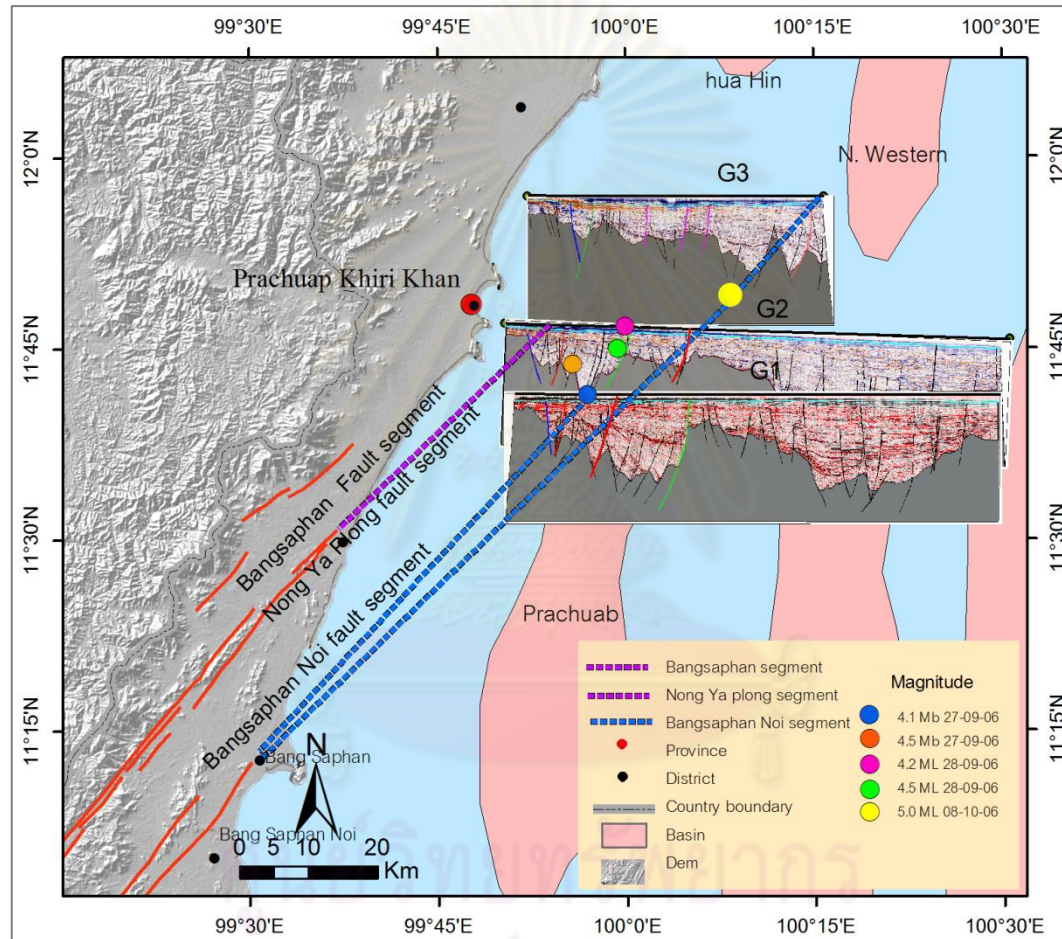


Figure 5.50 Map showing fault segments of the RNF (Nong Ya Plong segment, Bangsaphan segment and Bangsaphan Noi segment) that are extrapolated to the Gulf of Thailand.

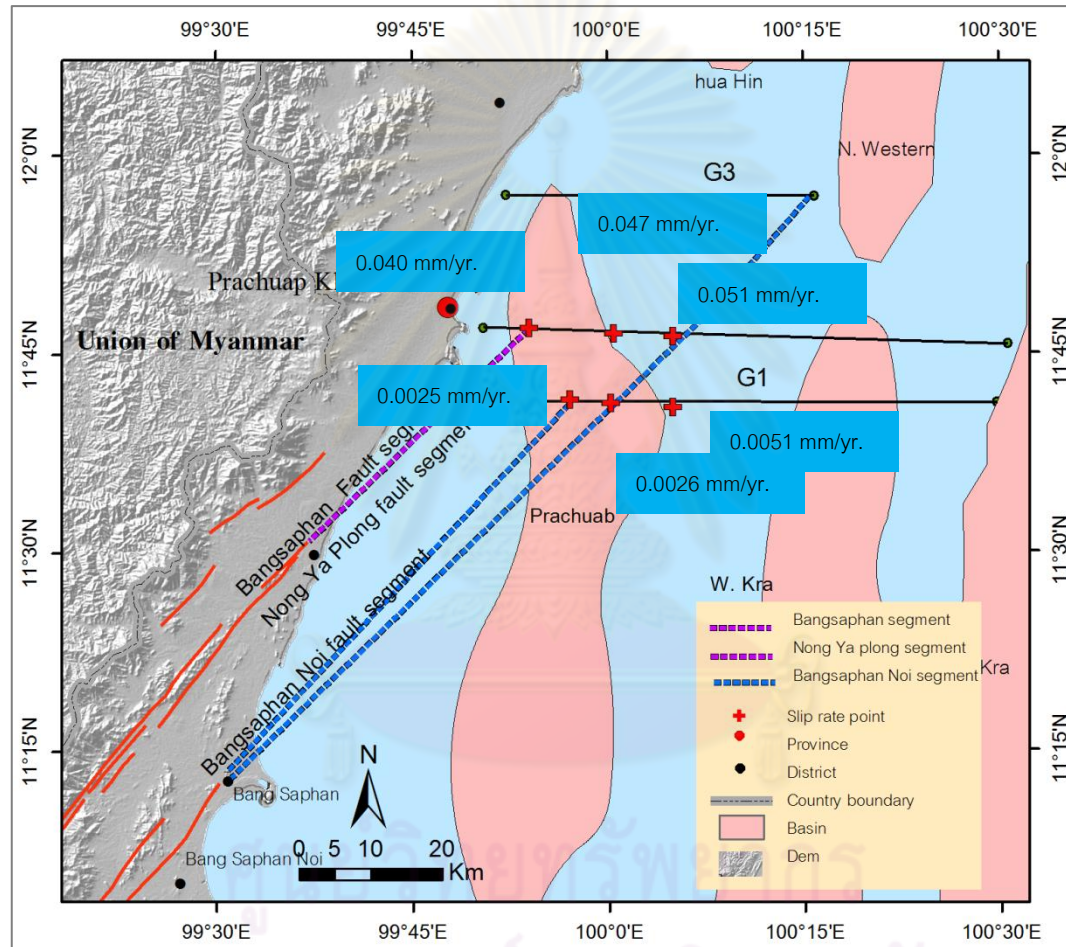


Figure 3.51 Map showing regional (or long-term) slip rate of the extrapolated lines of the RNF in Gulf of Thailand in this study.

Chapter VI

Field Investigations

This chapter covers description mainly from the results related to field investigations. Firstly, it involves the reviews of previous investigations of landform evidence perhaps related to active tectonics, such as hot spring locations in this study and nearby areas. Besides, radon survey were also used for locating fault segments. Secondary, emphasizes were placed on field evidences as expressed by morphotectonic features of landforms observed in the field along such relevant fault segments. In fact, tectonic evidence were very rarely discovered in field because dense vegetation and strong weathering process, so the 3D color orthographic were also helpful in this case. Lastly, the detailed field survey in the particular areas, including the detailed field observation by paleoseismic trenching traversed across the specific fault segments along main NE-SW trending accessibility road, are were performed.

6.1 Previous Investigations

There are some field surveys along the study area based on the results of morphotectonic evidence. Followings are the few descriptions of field surveys.

6.1.1 Natural Hot Spring

The history of the hot springs distribution in Thailand was first recorded by Brown and Buravas (1978). However, not many studies have been performed so far on the physio-chemical nature of hot springs in Thailand. Mostly they are only preliminary work or unpublished reports by Department of Mineral Resources and Electricity Generating Authority of Thailand.

Generally three important factors control the generation of hot springs, including heat sources, ground water and reservoir rocks. The main heat source is from active magmatic activity within the crust that emplace to shallower levels from unstable areas, such as active volcanic belts, fault zones, and subduction zones, or from areas dominated by high contents of radioactive elements, such as uranium (U), thorium (Th),

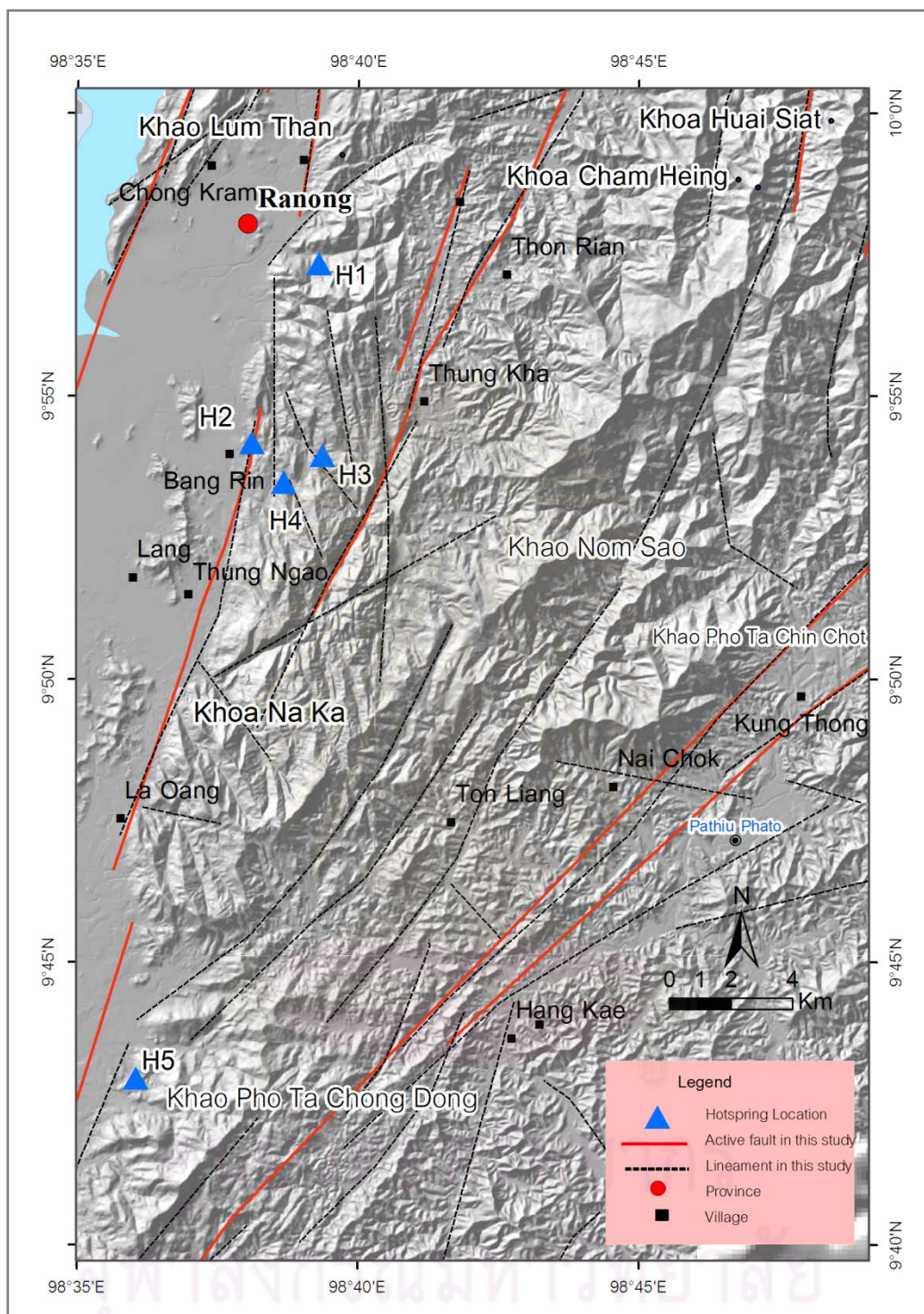


Figure 6.1 Map showing relationship between hotspring locations in Ranong province and active fault traces (data from Department of Mineral Resources, 2004).

and potassium (K). Groundwater is the main source of water supply. The water is principally derived from rain and cool water on the surface that percolates to the subsurface along bedding planes voids, fractures, joints, or faults of rocks. Some portions may be derived from steam of magmas in a cooling stage (magmatic or juvenile water) and water-bearing pore spaces of sediments (connate water). Good properties of reservoir rocks are high porosity and good permeability produced from both primary and secondary fractured or faulted rocks. When cool water from the surface percolates to reservoir rocks and receives heat transfer from the heat sources, the water will be heated and flow up along fractures or faults of rocks to the surface and become a hot spring. There are two well-known hot spring sites are in Ranong, in southern Thailand (Figure 6.1). However, a few hot spring location in adjustment area along the Ranong fault were found. As shown in Figure 6.1 hot springs are recognized in the study area, and several of them are located very close to fault termination. The H1 hot spring (Raksawarin hot spring), H4 (Rachakrut hot spring) and H5 (Nok Ngang hot spring) are discovered at middle of the Ranong fault segment, suggesting that there are subsegments nearby. The H2 (Bang Rin Hot spring) and H3 (Phon Lung hot spring) hot springs are located nearby Ranong fault segment and Laun fault segment. So it is quite clear that hot springs can, to some extent, help to locate the fault activity.

6.1.2 Radon gas survey

Radon gas was applied to surveying in the area of geothermal power resource, monitoring the explosion of a volcano, predicting earthquake events, seeking for sinkholes, and identifying active fault traces survey. Data of radon gas survey can indicate uncontinuity of tectonic or stability of geological structures because the area, dominated by active faults can show high concentrations of radon gas than the areas without active faults (Artyotha, 2007). In the case of active fault survey, sometimes the anomalous values are higher than the background values for more than 20.

The radon investigation at Si Yeak Ban Krut area (Bangsaphan Distrit, Prachuab Khiri Khan) was done by Artyotha (2009) in the northwest – southeast direction (Figure 6.3). Values of radon gas becomes higher than background value at approximately

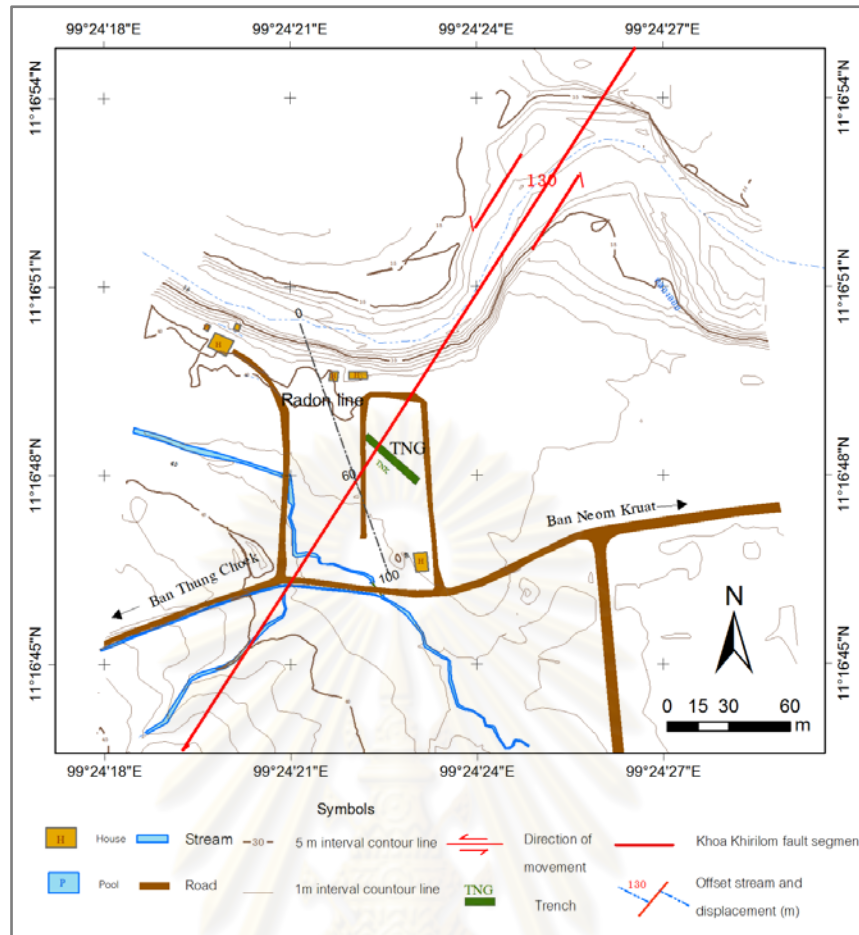


Figure 6.2 Detailed topographic map of Ban Neon Kruat , Bangsaphan district of Prachuab Khirikhan area, showing movement along the RNF segment with its left lateral sense of movement.

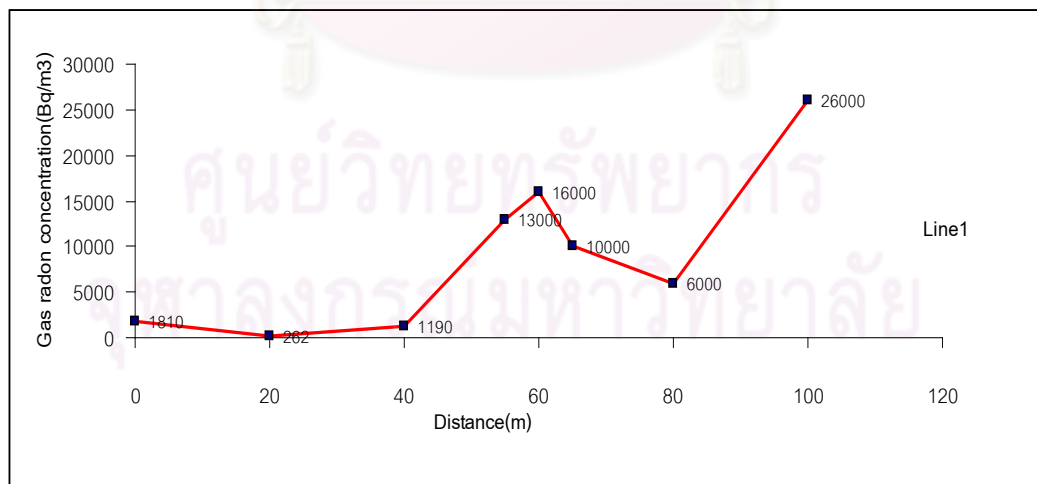


Figure 6.3 Plots of gas radon concentrations and distance in radon survey lines at Ban Neon Kruat area (Artyotha, 2007), showing the peak of random content immediately at the fault line (in Fig. 6.2)

distance of 60 and 100 meters (Figure 6.3). The result shows that the Ban Neon Kruat area of the Khoa Khirilom subsegment is also active based on the high radon contents.

6.2 Tectonic Geomorphology

In order to clarify and visualize the evidence of morphotectonic features as deduced from the results of remote-sensing interpretation, morphotectonic investigations were conducted. The followings are the descriptions of these evidences. Results of the remote-sensing interpretation and geomorphic indices can show the interesting areas in some area of field investigation nearby trenching location.

6.2.1 General Geology

The Ranong fault was the long active fault (300 km) and run through 3 provinces, i.e., Prachub Khiri Khan, Chumphon and Ranong. Generally, almost mountain range lie in the northeast-southwest direction. In this study, only 2 areas were chosen for representing active tectonical geomorphology. The first; Si Yeak Ban Krut area, which appears in 1:50,000 scale of topography map series L 7018 sheet 49314 (Amphoe Thap Sakae), can be accessed by asphalt road number 4 (Prachuab Khiri khan - Chumphon) in the western side of NE-SW trending hill namely Khao Nakkharat. This mountain range is characterized by narrow shape between basins. The channels are separated by this mountain such as Huai Kai To channel and flows northwestward but the some branches flow in the northeast direction. The plains at both sides of the mountain were supported by foothill sediments, the majority is the pebble gravel size until sand size, angular sharpen and poor sorted. The rocks in mountain zones are composed largely of sandstone, siltstone, claystone and quartzite (Figure 6.4).

The second is Ban Neon Kruat area, southward of Khoa Nakkharat and located in the eastern of Khoa Samianma, which appears in 1:50,000 scale of topography map series L 7018 sheet 48311 (Khao Neon Ya Nang) which the area can be accessed by asphalt road number 4 (Prachuab Khirikhan - Chumphon). In the western side is mountain range, which is characterized by sharpen line of northeast-southwest front mountain. The Khlong Thong and The Khlong Loi channels are the main channels, and

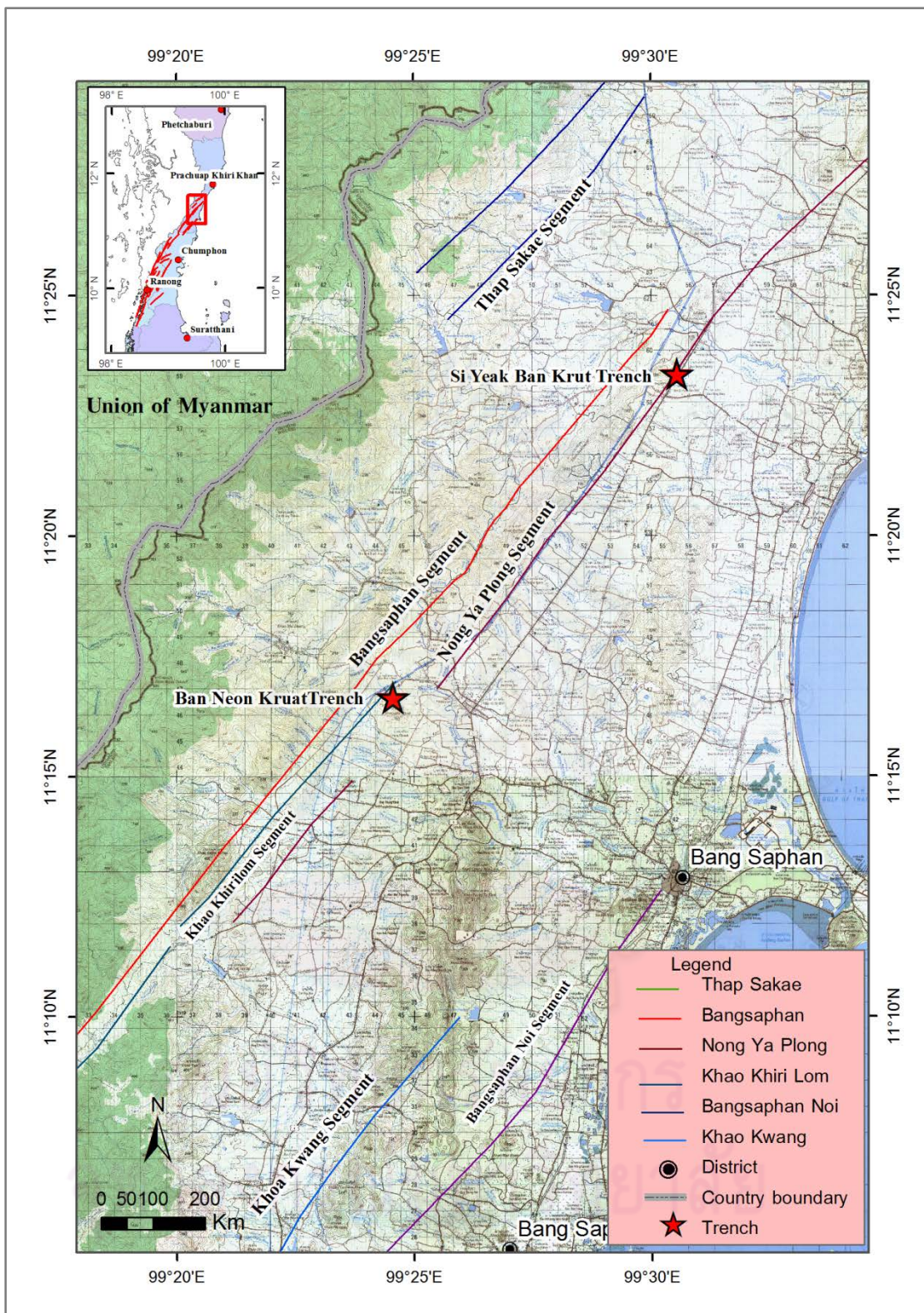


Figure 6.4 Locations of paleoseismic trenches (★) along the Nong Ya Plong and the Khao Khirilom segments of the RNF.

flow east – west direction(Figure 6.4). The basins were eastward of this area and supported by mountain sediment, whereas the rock in the mountain zone are composed largely of sandstone, siltstone, claystone and limestone.

6.2.2 Field investigations

In the field at center point of the junction of Si Yeak Ban Krut, mountain range, namely Khao Nakkharat, shows the west dipping triangular facets immediately at the foothill. The facet set was developed in the northeast trend along the Khao Nakkharat with the westward facing suggesting a fault running parallel to the mountain front (Figure 6.5). The appearance of triangular facets along the Nong Ya Plong segment is well developed as series of facet spurs. Perhaps this indicates that the fault shows several times of movements. Additionally, Khao Nakkharat is located within 2 fault segments (Bangsaphan segment and Nong Ya Plong segment)(Figure 6.5). There are significant lines of morphotectonic evidence including offset streams, a linear ridge and a fault scarp are found along fault traces. Similarly the Ban Neon Kruat area, shows a set of triangular facets northward and offset stream (Figure 6.7-6.12).

According to the result of the field investigation along the NE-SW trending traces, several lines of morphotectonic evidence indicate that the NE-SW traces have a potential to be the active faults and their movement are in normal sense together with the subordinate left-lateral movement.

6.3 Paleoseismic Trench

In as much as the reliable research is the supporting field evidences relevant to the fault segments concerned, it is necessity to study all the fault segment traces. Site selection of specific areas for detailed field investigation and paleoseismic trenching require some constraints to access the specified criteria. Therefore, selection of a specific area for this paleoseismic trenching covering three areas as mentioned before was conducted by compiling relevant supporting information of remotesensing and field morphology and showing the location of paleosiesmic trenching on topographic map

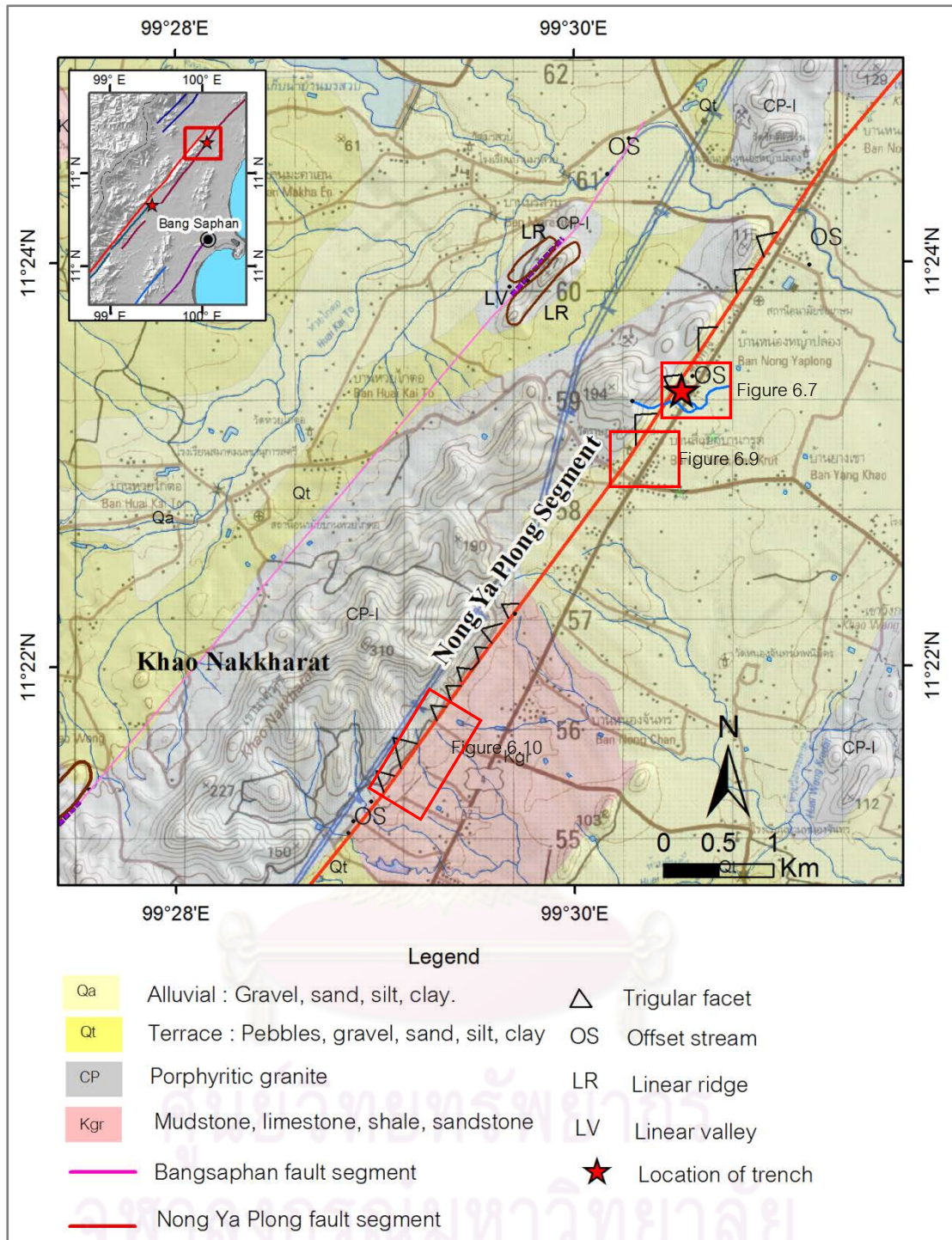


Figure 6.5 Topographic map of Si Yeak Ban Krut area showing the location of Nong Ya Plong segment and morphotectonic features offset streams, series of trigular facets, linear ridge and linear valley. Note that the red box represent the areas of photographs taken from field investigation.

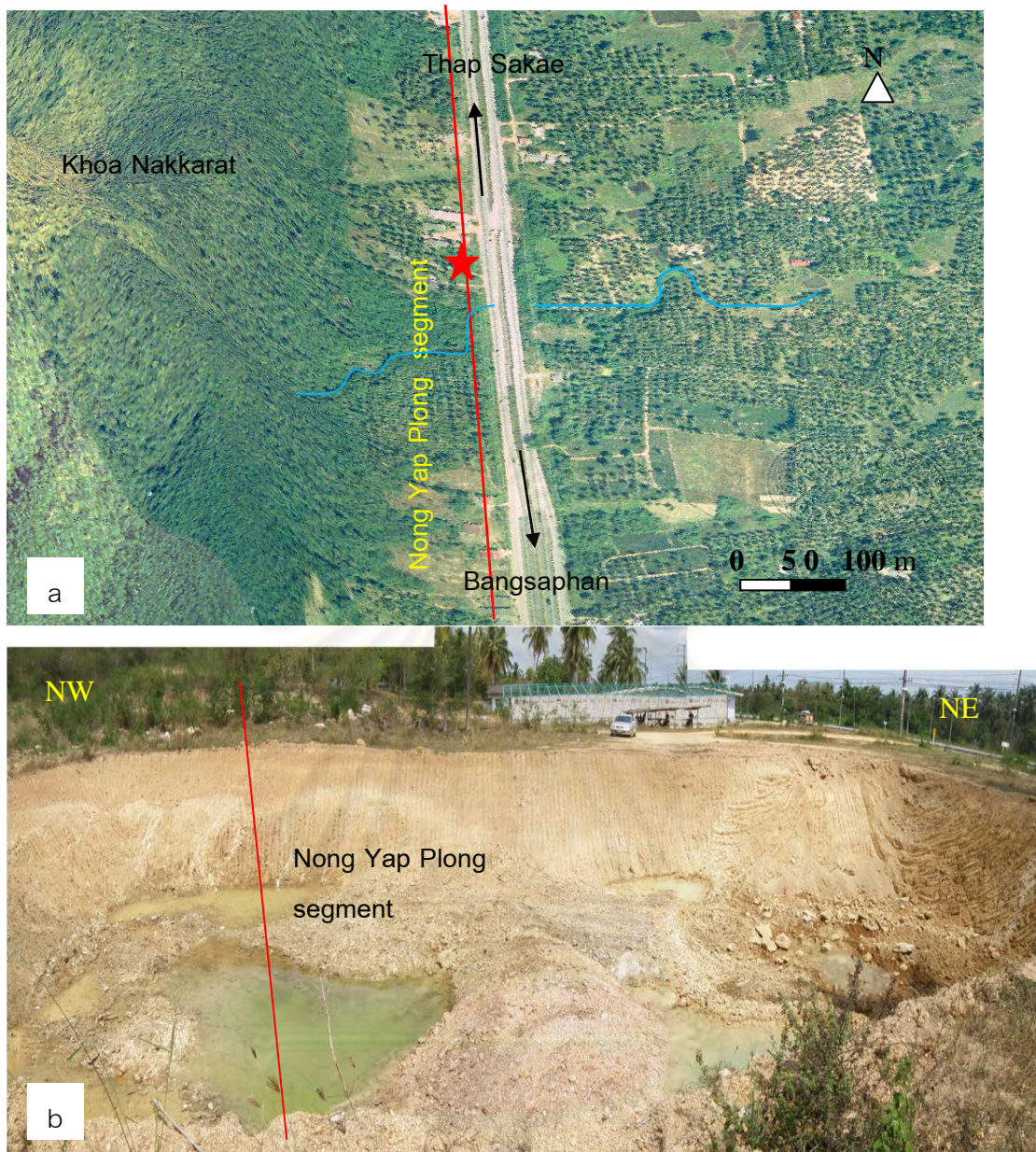


Figure 6.6 (a) color ortho- image showing location of Siyeak Ban Krut trench. (b) The artificial pool (Si Yeak Ban Krut Trench) at Ban Si Yeak Ban Krut , Thap Sakae district, Prachuab Khirikhan province. Note that the offer stream in (a) shows the left lateral sense of movement along the Nong Ya Plong segment of the RNF.

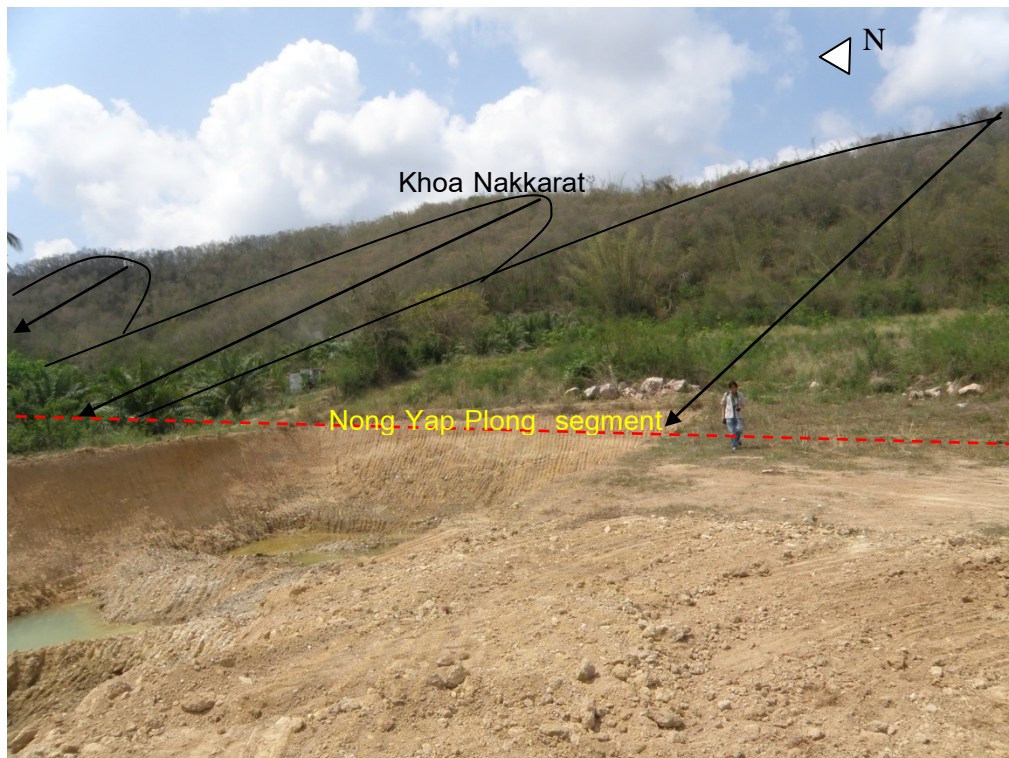


Figure 6.7 The artificial pool near Nakkarat mountain which cross cut by Nong Ya Plong segment and showing subdued trigular facets.



Figure 6.8 Quarry of weathered granite at Ban Nong Chun, Thap Sakae district, Prachuab Khirikhan showing the orientation of quartz vein in $20^{\circ}/68^{\circ}$, almost following the regional trend of the fault.

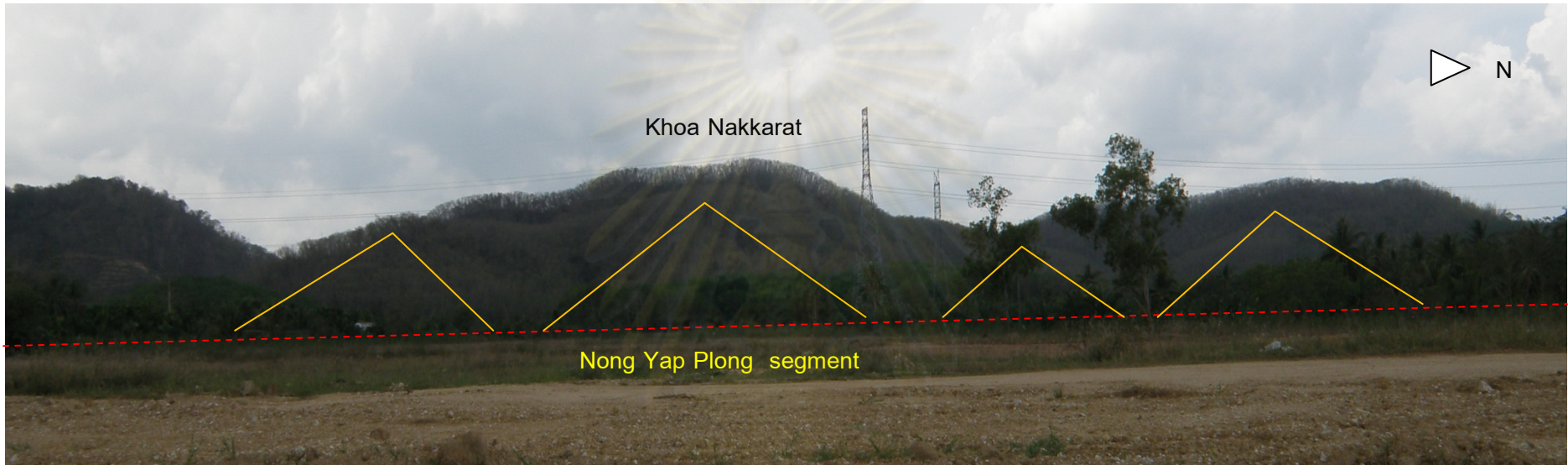


Figure 6.9 A panoramic view showing a series of trigular farcets along the Nong Yaplong segment of the RNF Ban Hin Thung, Thap Sakae district, Prachuab Khirikhan province. (Looking west). Note that the electric power line is behind this mountain.

ศูนย์วิทยทรัพยากร
จุฬาลงกรณ์มหาวิทยาลัย

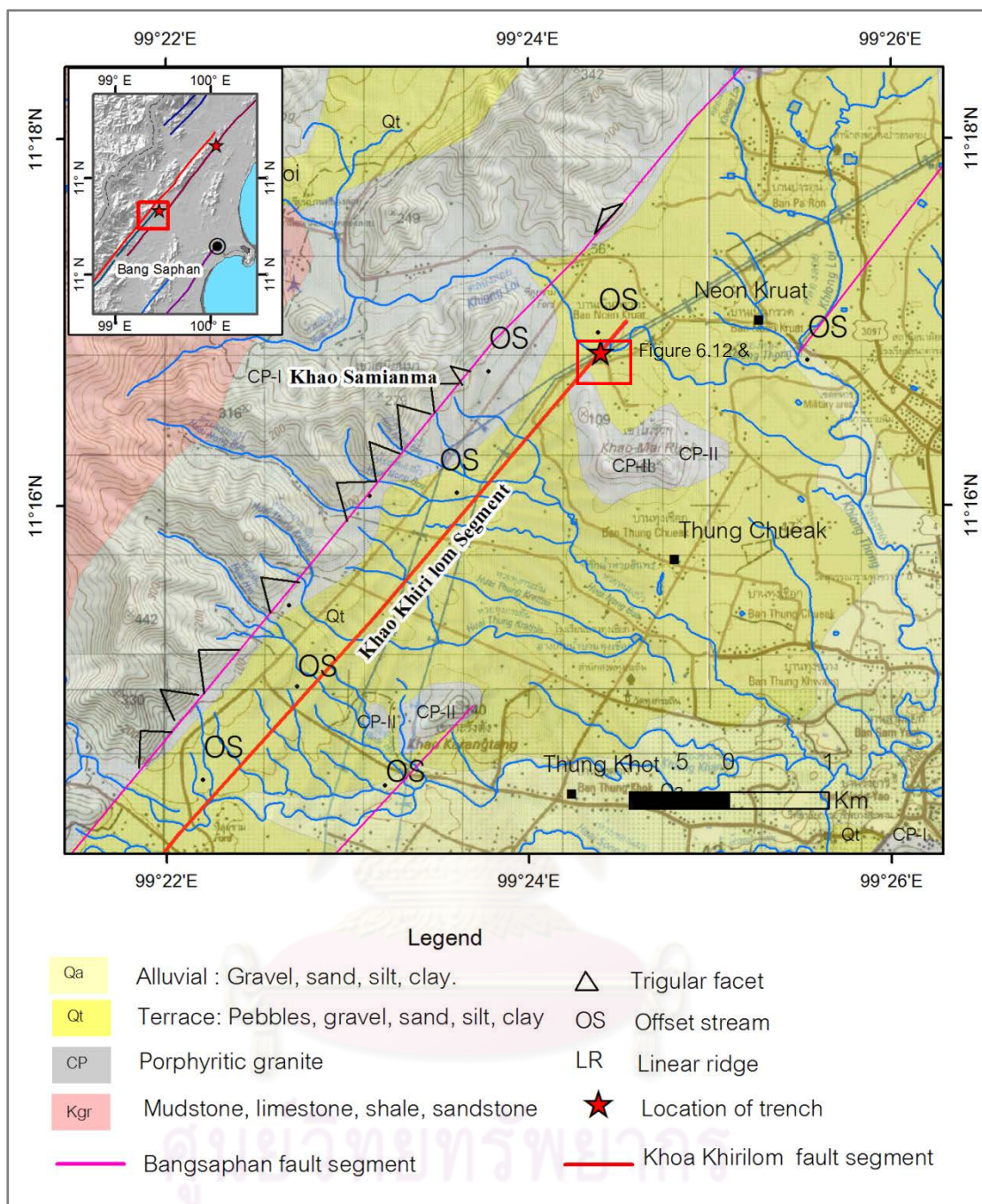


Figure 6.10 Topographic map of Ban Neon Kruat area showing the location of Khoa Khirilom segment, offset stream and trigonal facet. Note that the red box represent the areas of photographs taken from field investigation.

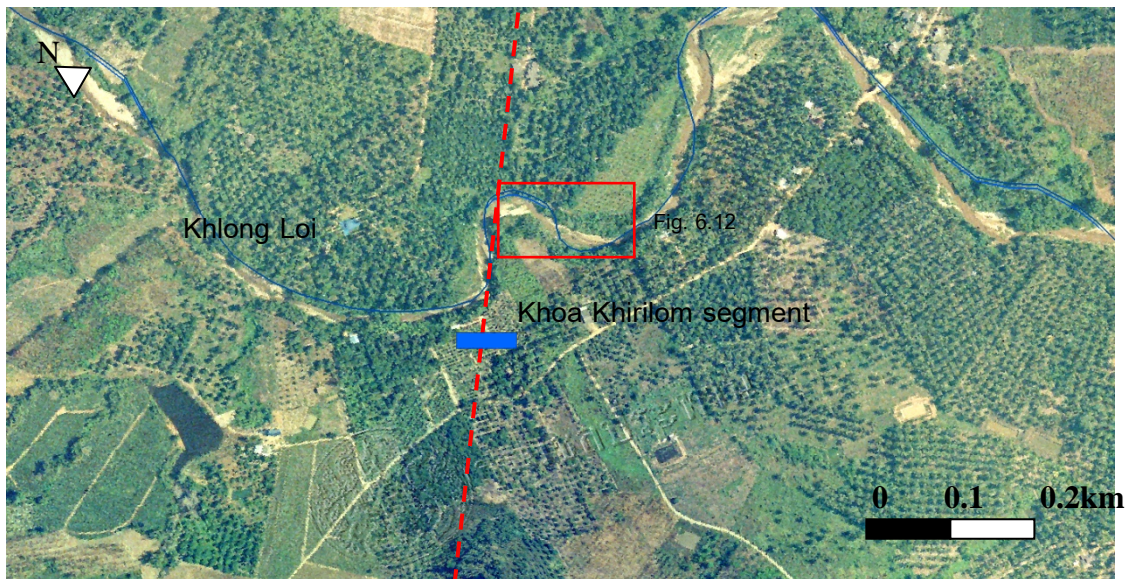


Figure 6.11 Color -orthographic image showing the offset stream of Khlong Loi stream channel and location of Neon Kruat trench.



Figure 6.12 A close-up view (Fig. 6.12) part of Khlong Loi river showing part of offset stream at Ban Neon Kruat area. (Looking west)

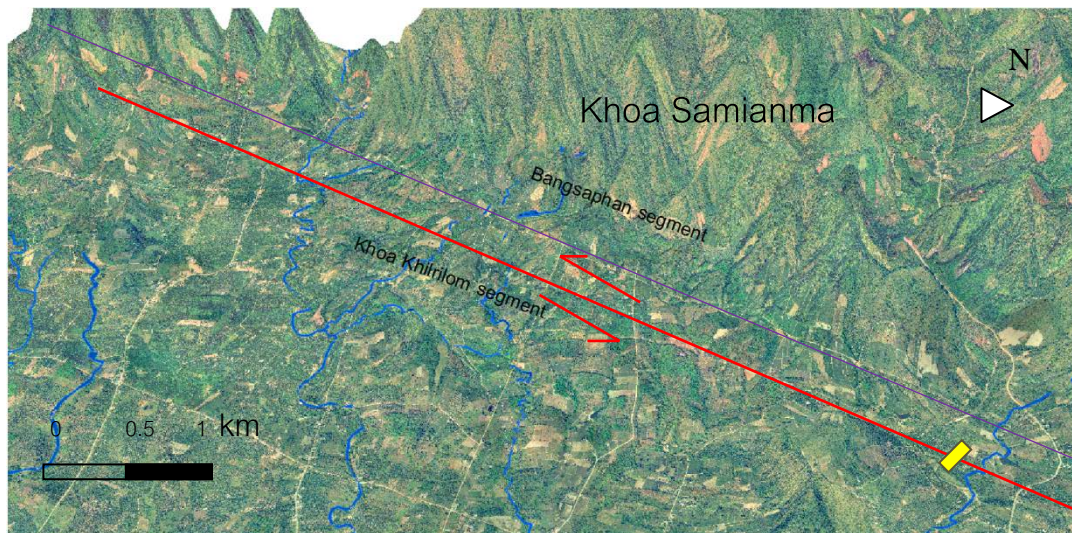


Figure 6.13 Color -Orthographic image showing offset stream evidence of Khoa Khirilom area and location of Neon Kruat trench (yellow colour).



Figure 6.14 Topography view of Neon kruat area around Neon Kruat trenching.

Note that the electric power line are located following the Kho Khirilom

(Figure 6.4). The most effective and suitable area was chosen for further detailed study and trench excavation. Nontechnically, the criteria are the accessibility.

Since backhole must be used for digging trench, and the ownership and authorization of the proposed area must be the second criteria. Three trench sites were selected in this study.

6.3.1 Trench 1: Si Yeak Ban Krut

Ban Nong Ya Plong trench is located north of Thap Sakae District along the main road no. 4. Remote-sensing interpretation shows a sharp lineament, and tectonic geomorphology indicates offset streams, shutter ridges, linear valleys, offset ridges, and triangular facets (see Figs. 6.6 to 6.10) on topographic map scale 1:50,000, sheet 49314 (Amphoe Thap Sakae). The trench site was an agricultural pool for rainfall support at grid reference 544673E/1246677N. As shown in figure 6.5 it is situated in the steeper slope at the left hand side of the main road near the offset stream and triangular facets. This artificial pool excavated into the young sediments deposits, traverse perpendicularly across the Nong Ya Plong fault segment. The pool's geometry is 30 m in width, 50 m in length, and 7 m in depth.

6.3.1.1 Stratigraphic Description

As shown in Figures 6.15 and 6.16, it is quite clear that the Si Yeak Ban Neon Kruat trench has relatively much more deformed stratigraphy. Trench-log stratigraphy is characterized by 4 unconsolidated sediment units and a one of granite rock basement. Detail of individual units is described below.

Unit A is the weathered granite, which is brown to yellowish brown and consists of pegmatite vein with orthoclase, mica and quartz are dominant. This unit appear at the bottom, which underlain by unit B and found at approximately 5-7 meters depth from surface.

Unit B is a completely weathered granite which is brown to dark yellow. This layer contains fracture zone with set of quartz veins. The weathering granite has the

characterize by shape brittle fracture, mix by iron oxide and very coarse sand to gravel but not show stratum. The thickness of this unit varies significantly from 1 - 3 meters.

Unit C is well-defined, grey to pale brown silty clay of alluvial deposit consisting of clay (70%) with silt to fine sand (25%) and iron oxide (5%). The deposit is well-sorted, and mainly matrix support. It is found as a small layer at the top of unit B in the middle of pool wall with thickness ranging from 30 to 50 cm.

Unit D is characterized by small zone of reddish brown, silty to sandy gravel layer. The gravels are mainly quartz rich sandstone with sub-angular shape. The unit is well-sorted and thickness is about 0.40 meter in the middle of pool wall and tendency more thickness in the right end of pool wall.

Unit E is light brown to reddish brown colluvial deposit clayey gravel. This layer consisting of gravel (70%), clay (25%) and rock fragment (5%). The thickness of this unit is about 0.80 -1.40 meter

6.3.1.2 Structural and Evidence of faulting

In the excavated trench, there are several pieces of evidence regarding faulting based on trench-log stratigraphy. One fault system was recognized (F1) which cut through the sedimentary units A, B, D and E. The important fault evidence includes the discontinuity of unit B and unit D, quartz veins in very weathered granite of unit B were broken off and throughout gravel of unit D as shown in figures 6.15 and 6.18. The F1 and offset (15-25 cm) of quartz veins referred type of normal fault. The other evidence is some gravels of unit E near the fault F1 change their orientation following the west-dipping fault plane at the shape contact between unit D and unit E.

According to the fault evidence mentioned above together with the current morphotectonic investigations, the sense of fault movement in the area is mainly normal with minor left-lateral slip movement. At the northeast wall, the fault F1 cuts through layers with strike N60E and dip angle 45 degree to east like to mountain front nearby trench location. Tri-angular facet were dipping to the east, too. The true displacement of F1 be not sure to observe because the hanging wall of units B, D and E are different thickness but at least, we can estimate the fault offset by assuming the top

Si Yeak Ban Krut Trench Logging
Northeast Wall



Figure 6.15 View of paleoseismic trench section on the north-east wall, Si Teak Ban Krut, Thap Sakae. Prachuab Khirikhan .

Si Yeak Ban Krut Trench Logging

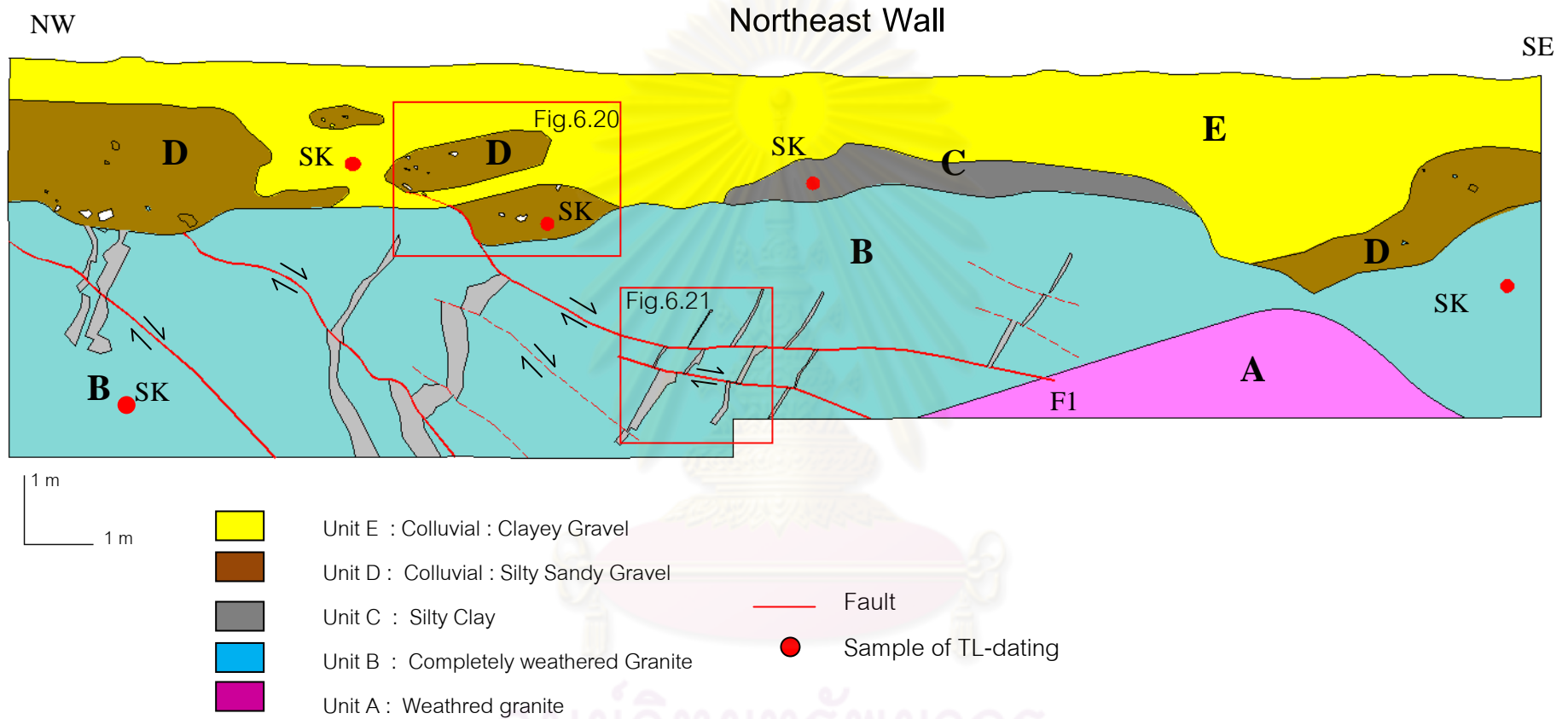


Figure 6.16 Trench log section of the north-west wall, Si Yeak Ban Krut, Thap Sakae, Prachuab Khirikhan showing 5 major stratigraphic units, major faults orientation and sample location for dating.

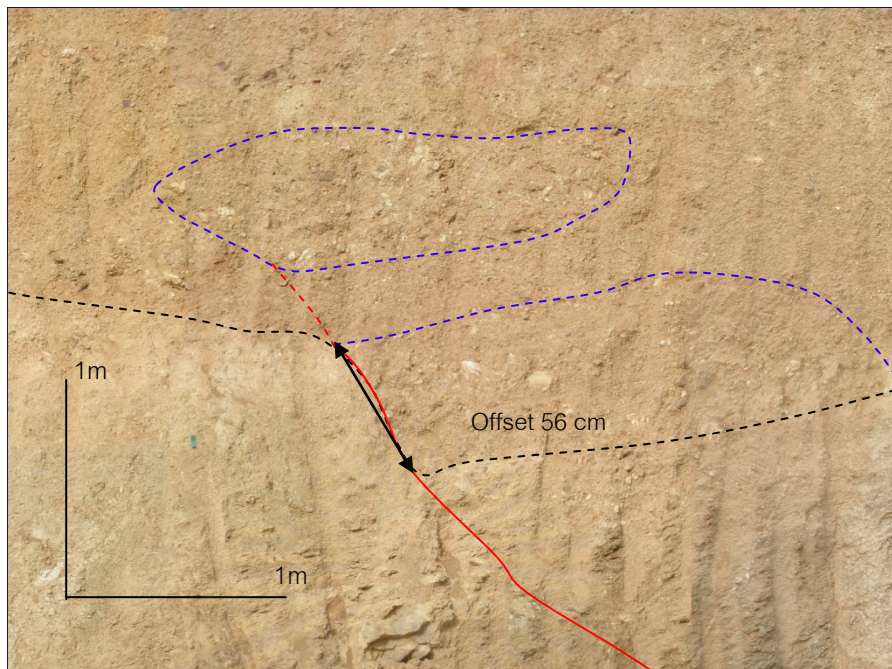


Figure 6.17 Trench log section at the northeast wall of Si Yeak Ban Krut showing
 Along the normal fault and the clear offset of Unit B which displacement
 approximately 56 cm.

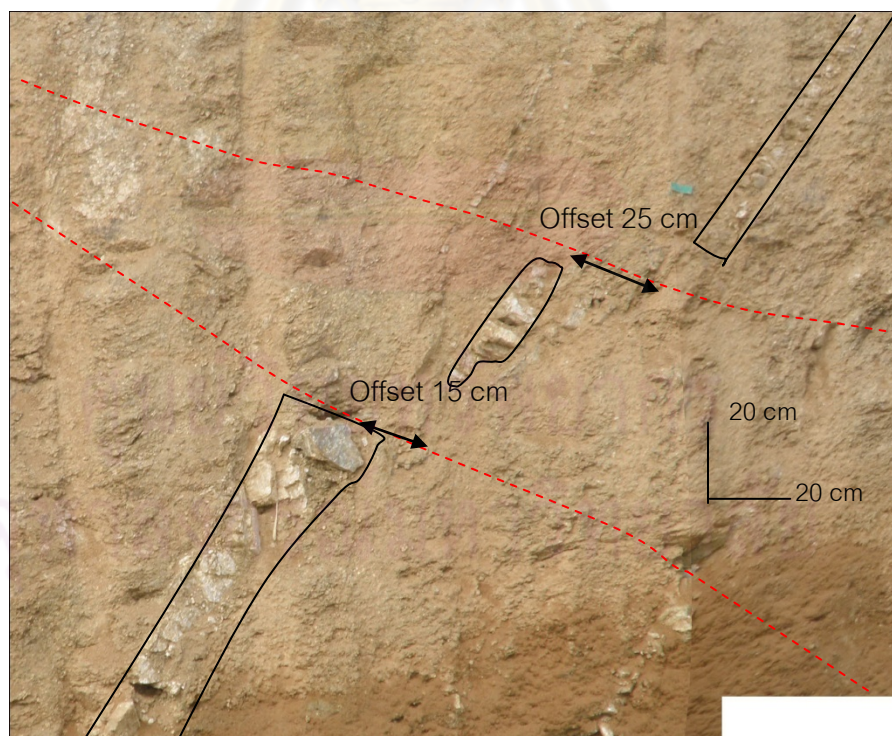


Figure 6.18 Trench log section at the northeast wall of Si Yeak Ban Krut showing
 the orientation of normal fault and the clear offset of quartz veins with
 separation of approximately 15-25 cm.

of layer B, which overlain by shape contact of unit D E. So its offset is approximately at least 0.56 m.

6.3.2 Trench 2: Ban Neon Kraut

This trench is the co-operating work between Chulalongkorn University and Department of Mineral Resources for preliminary earthquake investigation. Ban Neon Kraut trench is located at Ban Noen Kraut, Tambon Ron Thong, Bang Saphan, Distric, Prachuab Khirikhan, far from Bang Saphan distric about of 8 km. in northwestward, at grid reference 544378E / 1247328N. The result of investigation at Ban Noen Kraut suggests that the Khoa Khirilom segment in this study, orients in the northeast-southwest direction with the significance morphotectonic features include triangular facets, scarps and offset stream. This trench is excavated into young sediment deposits, orientation in the 135 degree in azimuth system and its shape is 3.7 m in width, 32 m in length, and 3.5 m in depth.

6.3.2.1 Stratigraphic Description

Results on exploratory paleoseismic trenching reveals 4 stratigraphic units from bottom to top as described below (Figure 6.19 and 6.20).

Unit A is characterized by reddish brown alluvial deposit gravel layer consisting of gravel 85 percent, sand 10 percent and clay 5 percent. Generally, gravel is quartz and shale, well sorted with 2-3 cm maximum gravel size, sub-angular to sub rounded and high sphericity. The thickness of this unit is more than 0.3 m.

Unit B is alluvial deposit containing light brown clayey sand, which composed of clay (20 percent), very fine sand to fine sand (65 percent), iron oxide and gravel (15 percent), well-sorted. Thickness of the unit is about 0.8-0.9 meter.

Unit C is alluvial deposit characterized by the brown sandy clay layer, which is 1.2-1.5 thick and overlying unit B in the left hand side of trench and fade out in the right hand side.

Unit D is alluvial deposit the gray clayey sand layer consists of very fine sand 80 percent, clay 20 percent. Unit D has the the thickness of 1.9-1.5 m.

6.3.2.2 Structural and Evidence of faulting

Main geological structures found in the trench include the F1 and F2 cutting through Unit B and Unit C. There two faults have the attitude of 60 degree strike with dipping angle 45 degree to southeast with reverse movement, F1 offset Unit C with the slip length of 62 cm. F2 cutting through Unit B and Unit C and has the attitude of 60 degree strike with dipping angle 45 degree to southeast with reverse movement (Figures 6.21 and 6.22). The slip along the F2 plane can not be estimated. This area is within the of Khao Khiri Lom segment with the offset stream northeastward of trench. The fault in this area is the reverse fault with left-lateral movement.

6.4 Conclusion

Base on both remote-sensing data and field investigation, it is evidenced that the RNF is active. This current line of evidence are similar to those report earlier by DMR (2007) and RID (2008). However, some detailed lineaments are quite contrast to these of earlier works.



ศูนย์วิทยธรณีวิทยา
จุฬาลงกรณ์มหาวิทยาลัย

Ban Neon Kruat Trench Logging
Northeast Wall



Figure 6.19 View of paleoseismic trench section (A-A'-A''-A''') on the north-east wall, Neon Kruat, Bangsaphan. Prachuab Khirikhan showing Cenozoic sediment

Ban Neon Kruat Trench Logging Northeast Wall

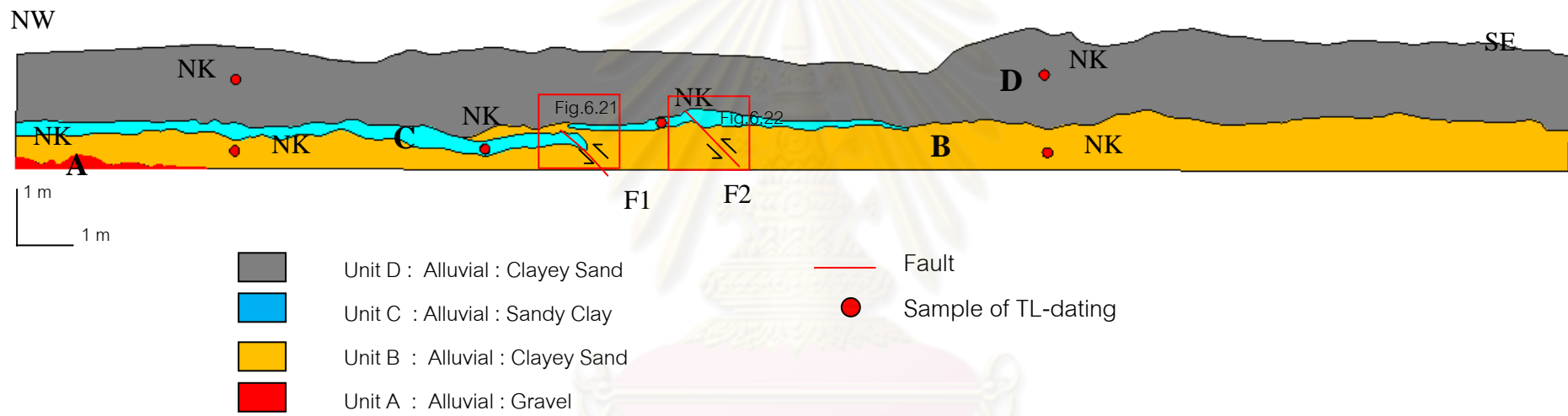


Figure 6.20 Trench log section of the north-west wall, Ban Neon Kruat, Bangsaphan Prachuab Khirikhan showing preliminary sediment stratigraphy, major faults orientation and sample location for dating.

ศูนย์วิทยทรัพยากร
 จุฬาลงกรณ์มหาวิทยาลัย

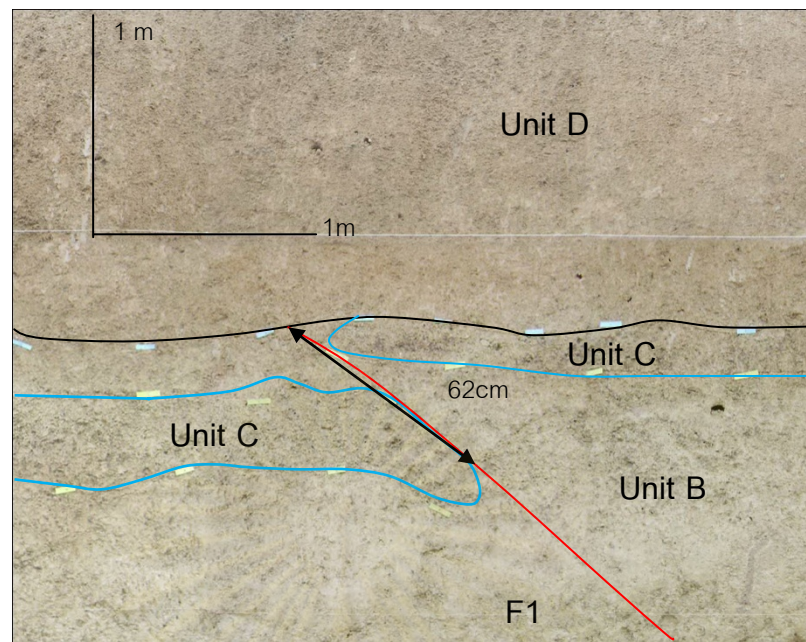


Figure 6.21 Trench log section at the northeast wall of Neon Kruat showing structure of reverse fault and clearly offset of Unit C which displacement approximately 62 cm.

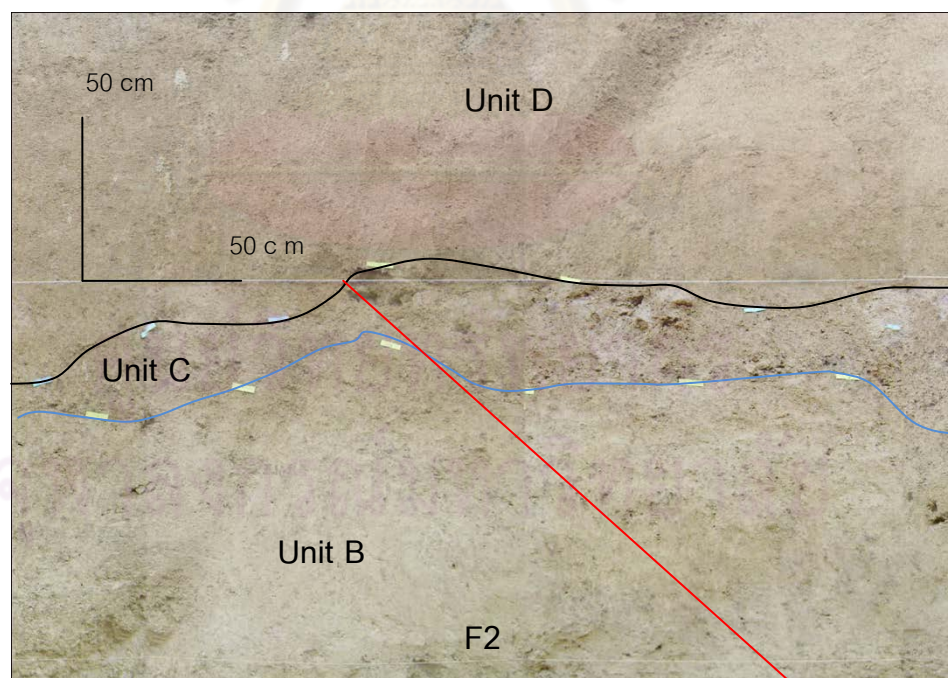


Figure 6.22 Trench log section at the northeast wall of Neon Kruat showing structure of reverse fault and clearly offset of Unit C .

Chapter VII

Luminescence Dating

There are many Quaternary Dating methods such as ESR, OSL and TL etc. The sample for dating in this study are from the paleoseismic trenches, and contain no organic materials for all the studied trench walls. Therefore only the TL methods were applied. Additionally, C-14 dating data from the earlier trench sites were also applied to constrain the most reliable earthquake events.

In this section, we reported the thermoluminescence (TL) dating procedures and results. The procedures are proposed by Takashima and Honda (1989). The methodology of analysis is composed of 2 main procedures, including equivalent dose evaluation and annual dose evaluation

7.1 Basic Concept

Thermoluminescence (TL) is the Quaternary dating techniques which measure when objects were last heated. Followings are the basic concept which is mainly from Aiken (1985).

TL is known as 'electron trap' techniques. Some natural materials such as various stones and soils (and also things made from them, such as pottery and stone tools) absorb or 'trap' naturally occurring electrons from their surroundings. This happens at a known and regular rate until the material becomes saturated with electrons after about 50,000 years. Since the world is much older than this, most objects are already saturated. However, if these substances are heated (such as when pottery is fired in a kiln or stones are dropped in a fire) this releases these trapped electrons and resets the 'clock' to zero. The object will then begin to trap electrons again. These electrons can be released and counted in a laboratory to give a date since the object was fired (TL). Some soils can have their electron 'clocks' reset simply by being exposed to sunlight. If they are then buried beneath later deposits, they begin to trap electrons again. This produces a date for the burial of the deposit.

The object to be dated is heated in a laboratory until it glows. Part of this is the ordinary glow of burning, the remainder is due to escape of these trapped electrons and

this is measured. These techniques can date objects up to 50,000 years old, although both are more accurate within the past 10,000 years. Even so, for the past 5000 years they are less accurate than other dating methods like radiocarbon. They can be useful for dating early sites and those that don't contain material suitable for radiocarbon or other dating methods (Figure 7.1).

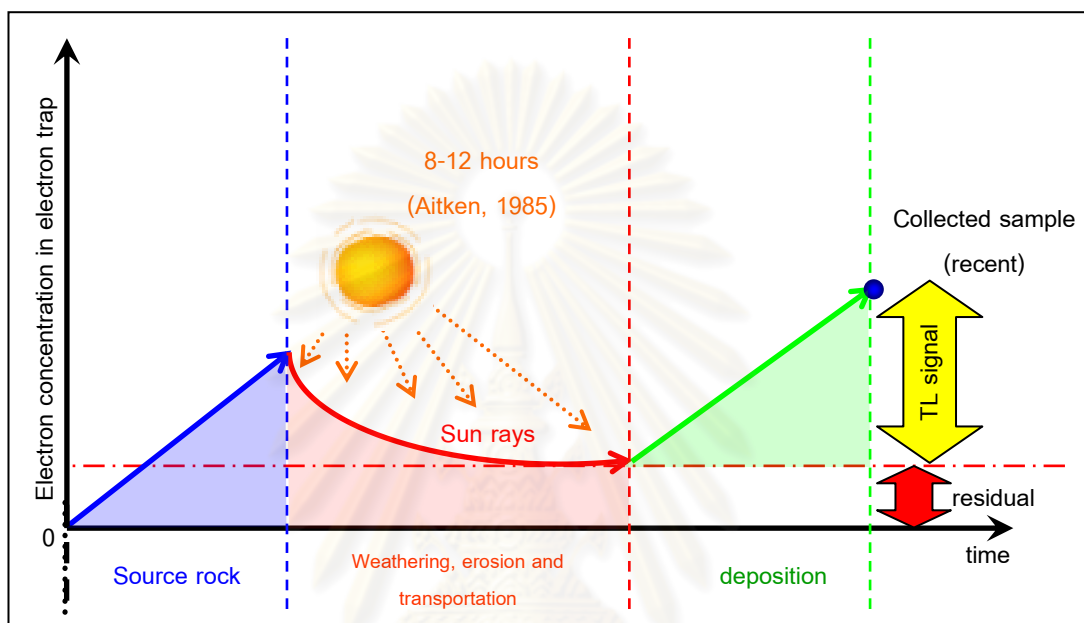


Figure 7.1 Applied thermoluminescence method for dating by showing relationship between amount electron in electron trap and time, (modified after Won-in, 2002).

Generally, insulators such as covalence solids and glasses can generate thermoluminescence (TL-dating) signal, but metals cannot. As a result, TL-dating method can be only applied with an insulator crystal. A simple model to review on general background of TL-dating method is based on ionic crystal model, which is simplified as shown in Figure 7.2

Ionic crystals, for example calcium carbonate and sodium chloride, are composed of lattice of positive and negative ions. In this lattice, it can be defected due to at least three reasons; an impurity atom, a rapid cooling from the molten stage, and damage by nuclear radiation. The defected lattice is presented by lacking of electron from its proper place or electron vacancy, called "electron trap", leads ionized electrons

from vicinity to fill up in this trap hole. In addition, ionized electron is the result of nuclear radiation from earth materials or solar radiation. However, both nuclear radiation and solar radiation have caused much less damages to the lattice structure.

Electrons have been trapped in trap holes lasted until shaken out due to the vibration of crystal lattice. A rapid increase of temperature to high in narrow range leads this vibration to be stronger. In addition, high temperature usually upward of 400°C can evict electrons from deep electron traps to be diffused around the crystal. Note that, because of different crystals, there are different types of traps, and then optimum temperatures to evict electrons in different crystal traps are unique. However, diffused electrons can be directed into two different ways; firstly to be retrapped at different types of defect which is deeper trap, and secondly to be recombined with an ion in lattice which electrons once have previously been evicted.

There are electron traps (T) and center of luminescence (L) located as intermediate between the valence band and the conduction band. The energy (E) is required in an optimum level to shaken out electrons from its deepest hole. In general, when electrons have already shaken out by heating, and recombination is done at the centers of luminescence, light is emitted. However, in some case which recombination has done at non-luminescence center or killer center, there is no emission of light and the energy is represented in the form of heat.

In summary, the luminescence process can be concluded in four steps (Figure 7.3). Firstly, ionization of electrons is caused by nuclear radiation. Secondly, some of these electrons are trapped in continuous and constant rates lasted until temperature has increased. Thirdly, some of electrons are heated at the optimized temperature level to evict electrons from deep trap hole. Fourthly, some of these electrons are then reach luminescence centers and in case of recombination process has done, light emission from luminescence centers is generated. The amount of emitted light or the number of photon in this stage is depended on the number of trapped electrons, which in turn is the amount of nuclear radiative proportion or paleodose. In addition, dose rate of nuclear radiative applied to environment is called annual dose.

Ultimately, based on TL process mentioned above, age of quartz-bearing sediments (such as those of this study) can be determined by simple equation 7.1

below;

$$\text{Age} = \frac{\text{Paleodose}}{\text{Annual dose}} \dots\dots\dots (7.1)$$

7.2 Laboratory Processes

The laboratory procedure in this study is mainly followed that of Takashima and Honda (1989). The methodology of analysis is composed of 2 main procedures, including paleodose or equivalent dose evaluation and annual dose evaluation (Figure 7.4).

7.2.1 Crushing and Sieving

Upon arrival in the laboratory, TL samples normally were dried by 40-50°C baked in the dark room. Water content is also measured for all samples being dated because it is the one significant parameter for annual dose determination. The formula of water content calculation is shown in equation 7.2.

$$\text{Water content} = \frac{(\text{weight of a wet sample} - \text{weight of a dried sample}) \times 100}{\text{weight of a dried sample}} \dots\dots\dots (7.2)$$

After getting dried sample, each sediment sample was shattered by using a rubber-hammer and the material passed through sieves to isolate the grain size fraction in 2 parts. Sediments which grain size pass through 20 mesh (<841 μm) were collected about 300 g and was separated to keep in plastic containers for annual dose determination. Remnant part from annual dose collection is carefully re-sieved and the material passed through sieves to isolate the grain size fraction between 60-200 mesh. Both of these portions were kept in beakers for purifying quartz grain and equivalent dose determination, respectively. In the annual dose, a sample portion is ready and skips to the measurement step but in both of two portions for equivalent dose determination is necessary to participate in chemical treatment.

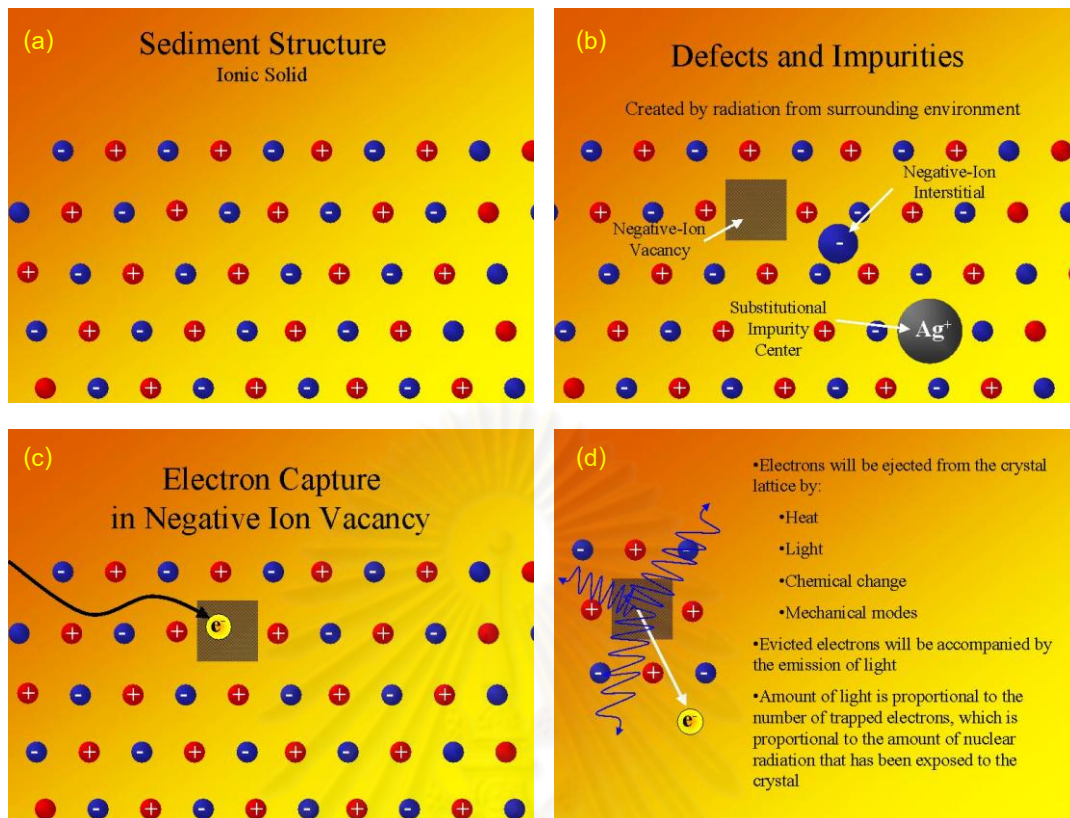


Figure 7.2 Simplified diagram of lattice structure and ionic crystal showing (a) ideal model of completely lattice (b) negative-ion vacancy occurred in ionic crystal cause negative-ion interstitial and substitution impurity center (c) electron capture by electron trap in negative ion vacancy and (d) electron escape from electron trap by heat or Light, (<http://www.rses.anu.edu.au>).

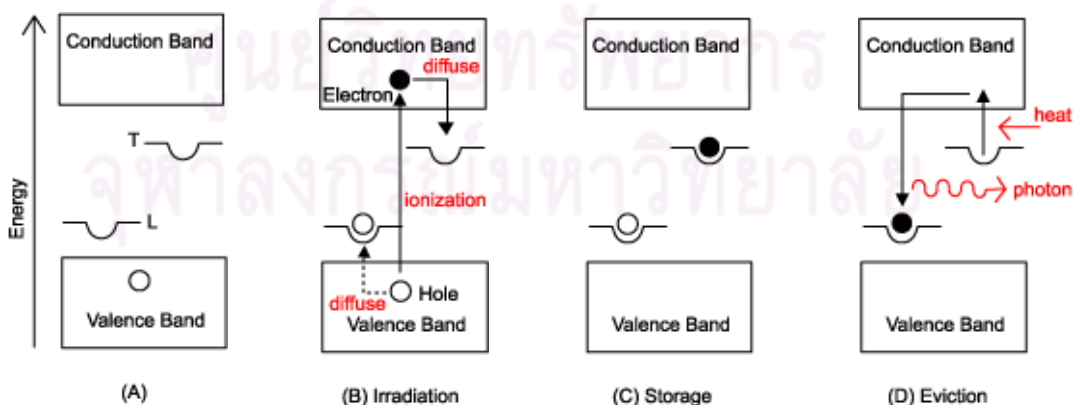


Figure 7.3 Simplified model showing energy states in Thermoluminescence processes, (Aitken, 1985).

7.2.2 Annual Dose Evaluation

Generally, sediments are exposed continuously to ionizing radiation, which originates from their radioactive contents, plus a small fraction from cosmic rays (Aitken, 1985). There are essentially 3 radioactive elements which contribute to the natural dose rate (annual dose) i.e. uranium (U), thorium (Th) and potassium (K). The decay of uranium and thorium results in α , β and γ radiation whereas potassium emits β and γ normally, the natural dose rates in most sediment are of the order of mGy/year.

For age determination it is necessary to evaluate the natural dose rate accurately. Several components are needed for an accurate annual dose is:

- Measurement of U, Th and K contents;
- Calculation of environmental water content in field at time of sample and
- Cosmic ray component evaluation

The annual dose to the sample is computed from the concentrations of K, U and Th by the method described by Bell (1979) and Aitken (1985), as shown in equation 7.3.

$$\text{Annual dose} = (AD) = D\alpha + D\beta + D\gamma + Dc \dots\dots\dots (7.3)$$

Where α = Alpha irradiation content,

β = Beta irradiation content,

γ = Gamma irradiation content, and

C = Cosmic ray irradiation content.

A) Measurement of Uranium, Thorium, and Potassium Contents

shows the schematic preparation and procedure for measurement of U, Th, and K contents by neutron activation analysis (NAA). The estimated standard errors were less than 10% for U and Th, and less than 3% for K using the fixed count error calculation method (Takashima and Watanabe, 1994).

B) Annual Dose Calculation

Annual dose is calculated from chemical data of U, Th, and K contents with the equations proposed by Bell (1979) and Aitken (1985), as shown

$$\begin{aligned}
 AD = & [0.15(2.783U + 0.783Th)/(1+1.50(W/100))] \\
 & + [(0.1148BU + 0.0514BTh + 0.2492BK)/(1+1.14(W/100))] \\
 & + [(0.1462U + 0.0286Th + 0.8303K)K/(1+1.25(W/100))] \\
 & + 0.15 \dots\dots\dots(7.4)
 \end{aligned}$$

Where ; AD = Annual dose (mGy/year),
 U = Concentration of uranium in ppm,
 Th = Concentration of thorium in ppm,
 K = Concentration of potassium oxide (%),
 B = Beta coefficient in quartz grains, and
 W = Water content (%).

7.2.3 Paleodose or Equivalent Dose Evaluation

7.2.3.1 Chemical Treatment

The main objective of chemical treatment is purification of quartz mineral in TL samples from the method in order to keep off destroying the signal of sample. The detail of chemical treatment is shown below:

- a) Washing the sample by distilled water 10 times for removing some organic materials and clay particles;
- b) Chemically cleansed the sample in dilute 35% HCl at 50°-60°C in a period of 15-30 minutes and re-washed several times with distilled water for eliminating carbonates and deep-rooted organic material;
- c) Etching the sample in 24% HF at 50°-60°C for 15-30 minutes and re-washed it several times with distilled water. HF was used to dissolve the plagioclase and outer layer of quartz grains to a depth sufficient for the core remaining to have a negligible component of alpha particle dosage; and
- d) After washing with water and drying in the dark room, the dried sample was then separated to remove out the dark minerals (e.g. zircon, garnet, and metallic minerals) by using an isodynamic separator (Frantz isodynamic magnetometer)

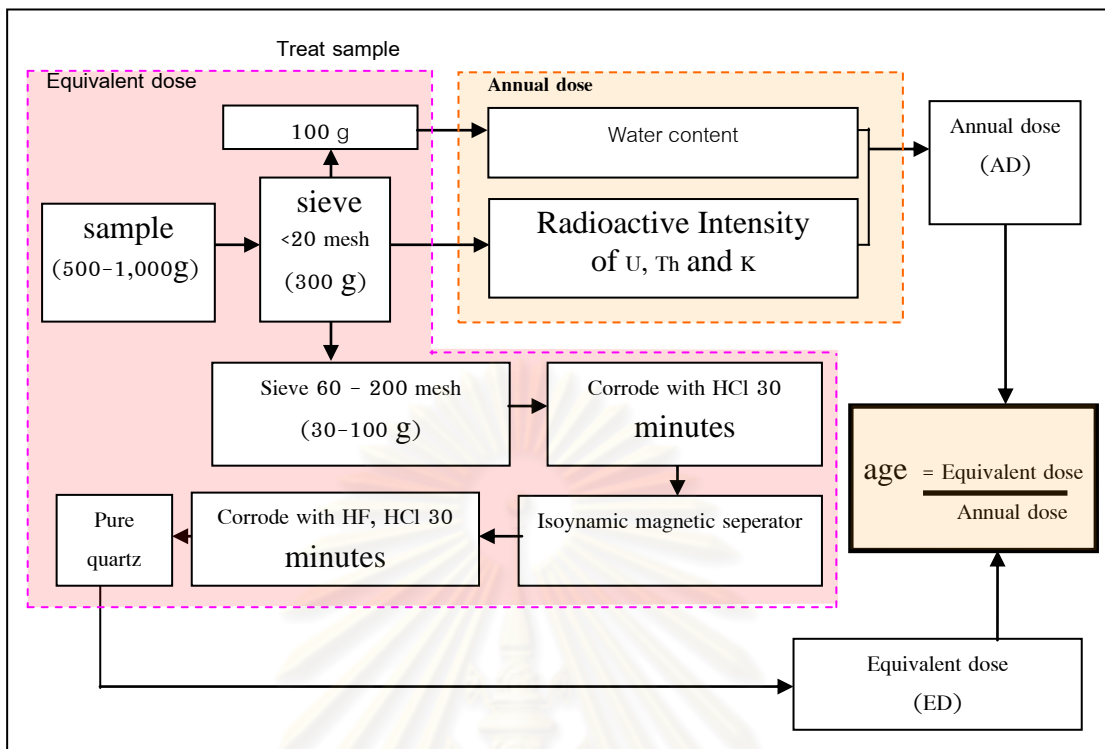


Fig 7.4 Chart of calculate annual dose and equivalent dose for TL and OSL dating, (modified after Takashima and Honda, 1989).

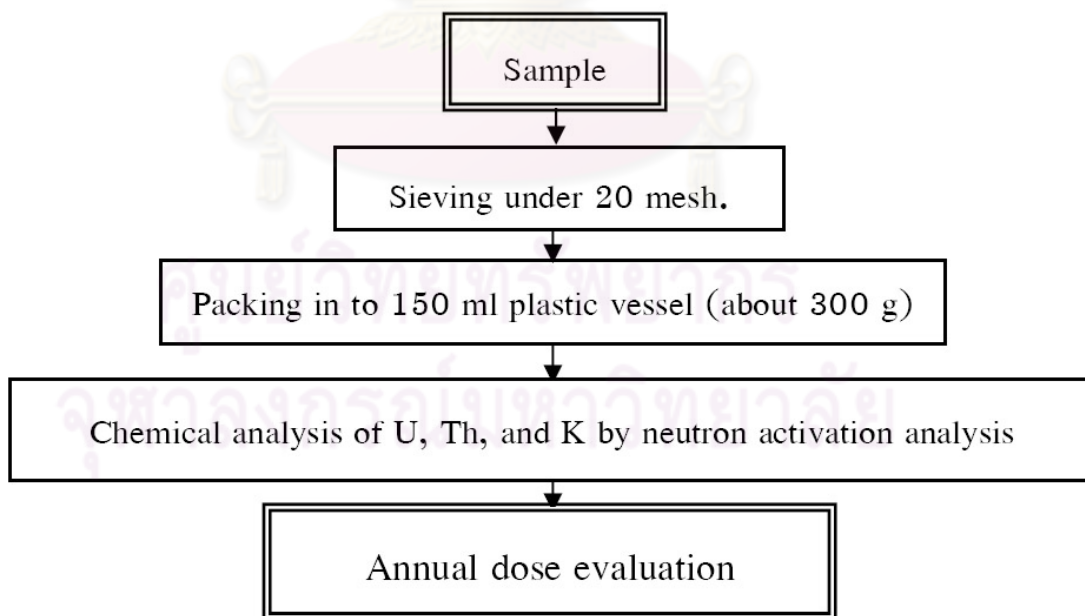


Figure 7.5 Summary of neutron activation analysis (NAA) procedures with sample preparation and annual dose determination.

After finishing sample treatment, it is necessary to check purity of quartz sample by XRD analysis. If the quartz-rich samples contain less than 10% of the other minerals, the samples were supposed to contain pure quartz concentrates. Then the sample was ready for determine equivalent dose in the next step.

7.2.3.2 Sample Preparation for Equivalent Dose Measurement

The pure quartz sample after chemical treatment is subdivided into 3 parts:

Part 1: Natural quartz sample was used for evaluated natural sensitivities of previously acquired TL signal;

Part 2: Sample was exposed directly with natural sunlight for 12 hours (Aitken, 1985) to effectively remove all of the previously acquired TL leaving only what is termed as the unbleachable TL signal. This part used for determining residual levels; and

Part 3: Sample used to find out the characteristic of quartz effective with artificial irradiation that amount of radioactive irradiation (in unit Grey) is known. The gamma ray source for artificial irradiation is a Co 60 from Office of Atomic Energy for Peace (OAEP), Bangkok.

7.2.3.3 Equivalent Dose Measurement

In this study used the Thermoluminescence Detector (TLD) at geology department, faculty of science, chulalongkorn university (Figure 7.6) was used for evaluation of equivalent dose commences with measurement of TL intensities on 3 sample portions: 1) natural sample portion, 2) artificial irradiation sample portion and, 3) residual sample portion (in sediment sample). About 20 mg of sample was filled in aluminum planchettes and placed on a molybdenum heater. The graph shows a relationship between TL intensity and temperature which is called "glow curve" (Aitken, 1985). The term glow curve is given to plot intensities of emitted light versus temperature (Figure 7.3a). Calculation of equivalent dose can be done by extrapolating natural signal intensity and residual signal intensity with a growth curve from artificial irradiated signal intensity. The result is assumed to be proportional to the equivalent dose of equation 7.1.

Although the glow curve shown in Figure 6.4b is smooth continuum, it is really composed of stable and unstable signals. This procedure makes by comparing the

shape of the natural glow-curve (i.e. the glow-curve observed from a sample which has not received any artificial irradiation in the laboratory) with the artificial glow-curve observed as a result of artificial irradiation. Thus a constant ratio between natural and artificial glow curves gives an indication that, throughout this plateau region, there has been negligible leakage of electrons over the centuries that have elapsed since all traps were emptied in the course of the stimulation by ancient environment.

The next step is for the construction of growth curve. This can be done by the increases of TL output with known amounts of additional radiation that 160 induced the sample. The graph showing this relationship is called “growth curve”.

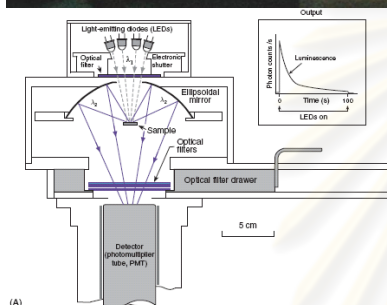
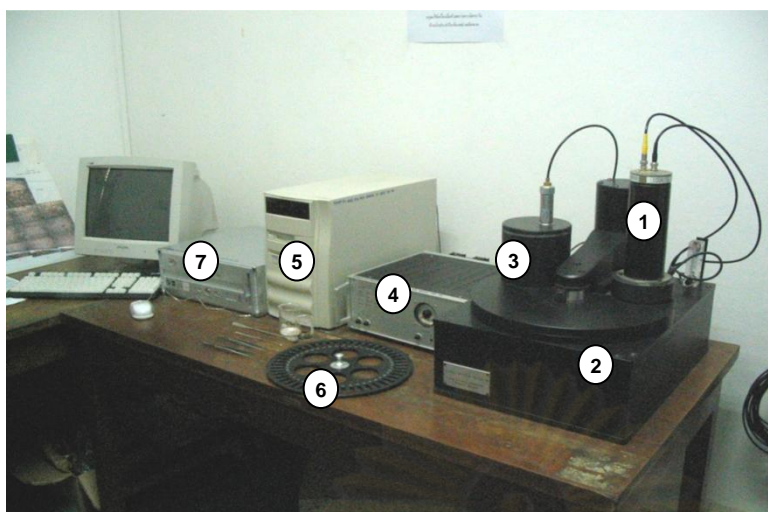
7.2.3.4 Regeneration Technique

In this technique, the simplest approach to the evaluation of equivalent dose is by the straight-forward procedure of measuring the natural TL intensity from a natural sample (N) and comparing it with the artificial TL intensity from the same sample that know certain dosage (artificial irradiate sample). In this study, after heating the quartz-extracted at 320°C for 5 hrs, individual samples were liquated for 5 sub-samples (Takashima et al., 1989). For each sub-sample, artificial irradiation was added with the doses of 44, 103, 303, 723, and 1,440 Gy. The values of TL intensity ($N/H+\gamma$) (as shown in Figure 7.6) versus temperature ranges were plotted for each sample and they are shown in Appendix.

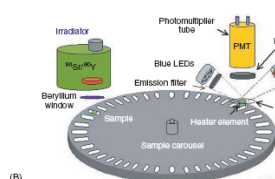
The growth curve plot is a graph of TL ratio or TL intensity (as shown in Appendix). It should be noted herein that most graphs of the natural intensity values close to the artificially irradiated liquated (i.e., H+1,440 Gy). Therefore their paleodose can be read after curve fitting for each aliquot. (Figure 7.8).

7.2.3.5 Residual Test

In case of sediment sample, evaluation of equivalent dose is complicated by the need to allow for the fact that the equivalent dose is composed of two components: the natural TL signal acquired since deposition and the residual signal that the sample had when it was deposited in the last time. Many scientists (e.g. Wintle and Huntley, 1980; Tanaka et. al., 1997) proposed several methods to simulate the light source exposures. Samples were exposed to some kinds of light sources. Natural sunlight, UV-ray lamp



(A)



(B)

- ① Photo detector and Photo multipliers
- ② Heater system
- ③ Radioactive Irradiation system
- ④ Hardware control system
- ⑤ Software control system
- ⑥ Sample dish
- ⑦ Output storage system

Figure 7.6 TL equipment component. (a) Thermoluminescence Detector (TLD) at geology department, faculty of science, Chulalongkorn University (b) Main equipment that comprises the “reader”, which is necessary for measuring the paleodose, irradiating the sample, heating the sample, and deriving a “growth” curve, (Lian, 2007).

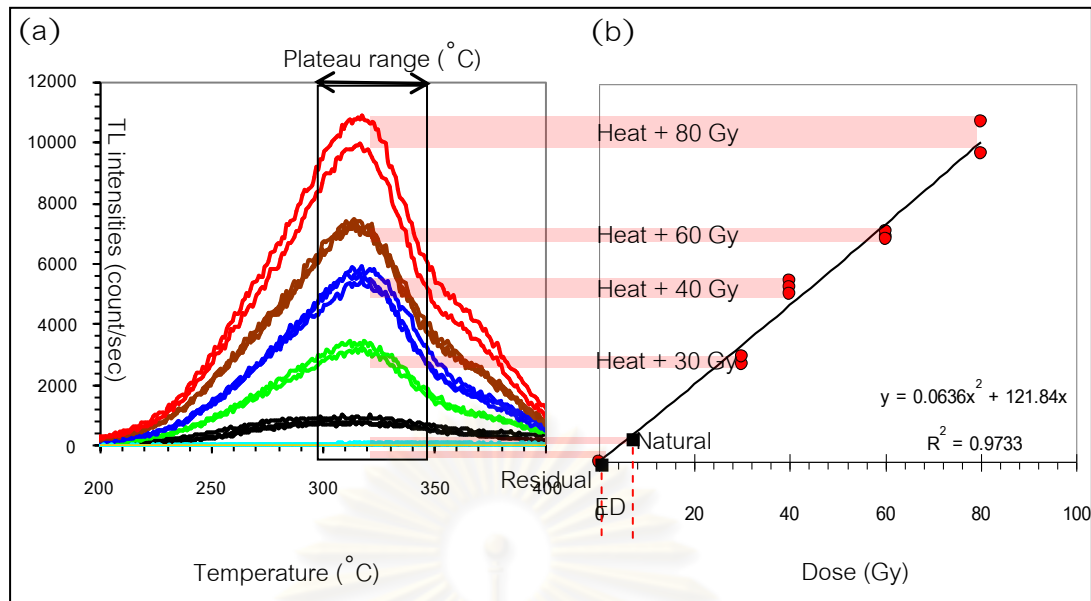


Figure 7.7 Result of example giagram after run with Thermoluminescence Detector for calculated equivalent dose (a) growth curve (b) grow curve.

(365 nm) and xenon lamp were the important illumination sources for bleaching experiments (Won-in, 2003).

In this research study, the naturally bleaching experiment by sunlight requires and depends significantly upon a long sunny day. For the artificial bleaching experiment, it is important to check the minimum of time that can completely bleach samples to the residual level and how much residual level in each sediment sample. The methodology of residual testing starts with bleaching sample and check TL intensity of sample in every 1 hour. Plotting graph showing a relationship between TL intensity and time used for bleaching reveal the minimum time that residual signal begin stable (unbleachable).

7.2.3.6 Plateau Test

According to glow-curve, there are overlapping peaks that may be raised to make misinterpretation of the peak, which is the result of electron emission from deep traps not other shallow traps. Glow-curve peak, which has located in the stable region, is that of interest. The stable region is usually at 300°C or higher where electrons from deep traps are evicted near zero. The method to recognize the stable region is a

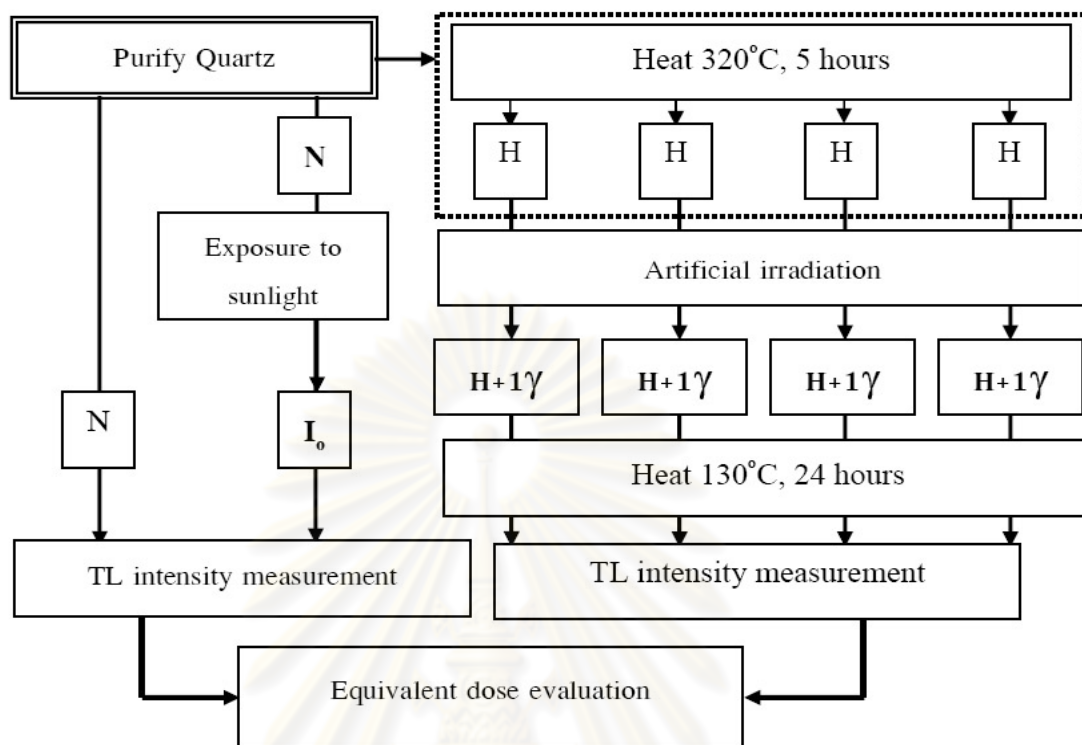


Figure 7.8 (a) Schematic charts of regeneration technique (Takashima et. al., 1989).

Note that several portions are used for measurement of the TL intensity; N is natural sample; I₀ is residual intensity from sample; H is 350°C heated sample; and γ is known dosage that irradiated sample.

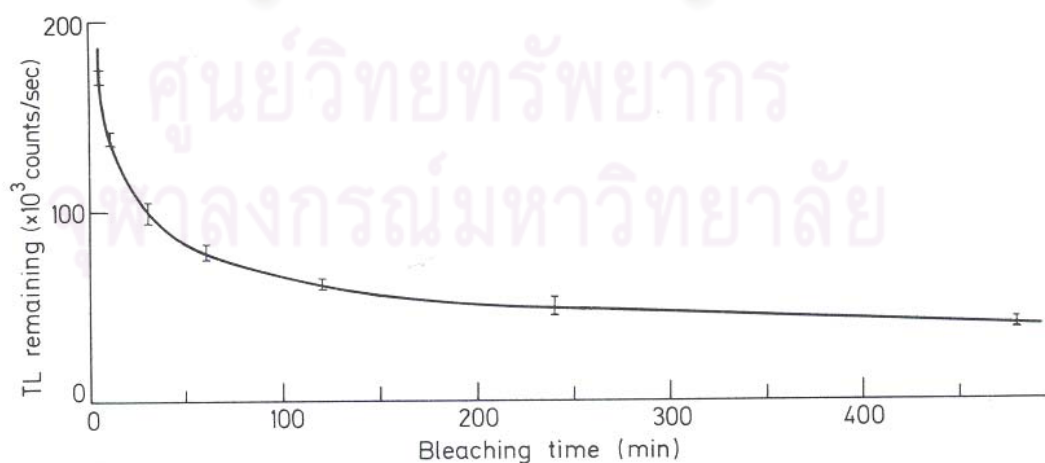


Figure 7.8 (b) Thermoluminescence remaining after bleaching by exposes to sunlight For various time (Aitken, 1985)

plateau test. There are two glow-curves of natural sample (N) and natural + artificial sample (N+ γ) that had been plotted as solid lines in the same graph. Ratio between N and N+ γ is shown as dots. The plateau of dots is the stable region red-colour zone or band. In addition, peaks of both samples have been generated at the same temperature, and N+ γ peak is higher than N peak, it means that deep traps are deep enough to contain other electrons.

7.2.4 Error Determination

Error in TL-dating result derives mainly from sample preparation and TL measuring apparatus (av. 10%), as well as standard deviation (SD) from measured values of ratio H+ γ / N on growth curve. So equation for dating errors is described as

$$\text{Error} = \text{Absolute} [(SD_{ED}^2) + (SD_{AD}^2)] \times \text{age} \dots\dots\dots (7.5)$$

Where $SD_{ED} = \text{Absolute} [(x-x)^2/N]$

$$SD_{AD} = 10 \%$$

7.3 Dating result from this study

A total of Quaternary sediment samples were selected from paleoseismic trench at Si Yeak Ban Krut and Ban Neon Kruat (as shown in Figure 7.9 - 7.11). Seven samples were collected from the northeast wall of Ban Neon Kruat trench (NK1-NK7) and there are five samples were collected from Siyeak Ban Krut Trench (SK1-SK5). The total of 12 samples were selected for TL dating and their results are shown in Table 7.1 respectively. For annual dose analysis, the dated samples contain U contents varying from 2.71 to 5.98 ppm, Th contents from 12.07 to 33.68 ppm, and K contents from 1.43 to 4.96 %. In general, water contents of the dated samples are between 1.66% and 34.13%. The annual dose of the dated samples vary from 3.68 to 7.81 mGy/Y, and the paleodose (or equivalent) dose range from 40.54 to 365.94 Gy. As shown in Table 7.1 ratios of paleodose to annual dose of individual dated samples give rise to the TL dates between 4,800 to 51,000 years. It is inferred from this study that the dating and geological results show more than one paleoseismic event. The oldest age of the fault movement is about 29,000 \pm 1,000 years are the latest movement took place at about 4,800 \pm 1000 years ago.

The detail of the results at Si Yeak Ban Krut trench are described below.

Sample no. SK1 from unit E shows good glow curves for both natural and artificially irradiated sample (appendix). The plateau test as shown in appendix is the rather stability line at 290° C onward. The growth curve for sample no. SK1 displays the stability TL intensity of a natural sample at 92,114 which is equivalent to the paleodose of 227.38 Gy. The sample has the annual dose about 7.81 m Gy/yr with the water content of 2.90%. These TL parameters reveal the date of sample no. SK1 as 29,100 yr.

Sample no. SK2 from unit D shows good glow curves for both natural and artificially irradiated sample (appendix). The plateau test as shown in appendix is the rather stability line at 320° C onward. The growth curve for sample no. SK2 displays the stability TL intensity of a natural sample at 100,795 which is equivalent to the paleodose of 243.04 Gy. The sample has the annual dose about 7.75 m Gy/yr with the water content of 4.13%. These TL parameters reveal the date of sample no. SK2 as 31,000 yr. Because this sample collected from the "in-situ" granite, then the data obtained from this sample is geologically meaningless.

Sample no. SK3 from unit B shows good glow curves for both natural and artificially irradiated sample (appendix). The plateau test as shown in appendix is the rather stability line at 280° C onward. The growth curve for sample no. SK3 displays the stability TL intensity of a natural sample at 82,291 which is equivalent to the paleodose of 369 Gy. The sample has the annual dose about 7.00 m Gy/yr with the water content of 6.97%. These TL parameters reveal the date of sample no. SK3 as 51,000 yr. Because the sample is not the transported material, so the data obtained yield geologically meaningless.

Sample no. SK4 from unit C shows good glow curves for both natural and artificially irradiated sample (appendix). The plateau test as shown in appendix is the rather stability line at 280° C onward. The growth curve for sample no. SK4 displays the stability TL intensity of a natural sample at 89,336 which is equivalent to the paleodose of 282 Gy. The sample has the annual dose about 7.14 m Gy/yr with the water content of 3.94%. These TL parameters reveal the date of sample no. SK4 as 39,500 yr.

Sample no. SK5 from unit C shows good glow curves for both natural and artificially irradiated sample (appendix). The plateau test as shown in appendix is the

rather stability line at 255° C onward. The growth curve for sample no. SK5 displays the stability TL intensity of a natural sample at 72,772 which is equivalent to the paleodose of 375.04 Gy. The sample has the annual dose about 7.38 m Gy/yr with the water content of 4.23%. These TL parameters reveal the date of sample no. SK5 as 51,000 yr. Similarly, this sample yields the unreliable data due to the sample is "in-situ".

The detail of the results at Ban Neon Kruat trench are described below.

Sample no. NK1 from unit D shows good glow curves for both natural and artificially irradiated sample (appendix). The plateau test as shown in appendix A is the stability line at 290° C onward. The growth curve for sample no. NK1 displays the stability TL intensity of a natural sample at 71,674 which is equivalent to the paleodose of 30.19 Gy. The sample has the annual dose about 6.24 m Gy/yr with the water content of 2.73%. These TL parameters reveal the date of sample no. NK1 as 4,800 yr.

Sample no. NK2 from unit B shows good glow curves for both natural and artificially irradiated sample (appendix A). The plateau tests are shown in appendix is the stability line at 280° C onward. The growth curve for sample no. NK2 displays the stability TL intensity of a natural sample at 112,727 which is equivalent to the paleodose of 40.79 Gy. The sample has the annual dose about 3.68 m Gy/yr with the water content of 2.10%. These TL parameters reveal the date of sample no. NK2 as 11,000 yr.

Sample no. NK3 from unit C shows good glow curves for both natural and artificially irradiated sample (appendix). The plateau test as shown in appendix is the stability line at 280° C onward. The growth curve for sample no. NK3 displays the stability TL intensity of a natural sample at 108,260 which is equivalent to the paleodose of 50.49 Gy. The sample has the annual dose about 5.50 m Gy/yr with the water content of 1.66%. These TL parameters reveal the date of sample no. NK3 as 9,100 yr.

Sample no. NK4 from unit C shows good glow curves for both natural and artificially irradiated sample (appendix). The plateau test as shown in appendix is the stability line at 280° C onward. The growth curve for sample no. NK4 displays the stability TL intensity of a natural sample at 108,260 which is equivalent to the paleodose

of 30.19 Gy. The sample has the annual dose about 4.11 m Gy/yr with the water content of 4.76%. These TL parameters reveal the date of sample no. NK4 as 7,300 yr.

Sample no. NK5 from unit A shows good glow curves for both natural and artificially irradiated sample (appendix). The plateau test as shown in appendix is the rather stability line at 290⁰ C on ward. The growth curve for sample no. NK5 displays the stability TL intensity of a natural sample at 119,256 which is equivalent to the paleodose of 109.76 Gy. The sample has the annual dose about 6.98 m Gy/yr with the water content of 2.43%. These TL parameters reveal the date of sample no. NK5 as 15,700 yr.

Sample no. NK6 from unit D shows good glow curves for both natural and artificially irradiated sample (appendix). The plateau test as shown in appendix is the rather stability line at 300⁰ C on ward. The growth curve for sample no. NK6 displays the stability TL intensity of a natural sample at 49,453 which is equivalent to the paleodose of 29.96 Gy. The sample has the annual dose about 5.88 m Gy/yr with the water content of 1.94%. These TL parameters reveal the date of sample no. NK6 as 5,000 yr.

Sample no. NK7 from unit B shows good glow curves for both natural and artificially irradiated sample (appendix). The plateau test as shown in appendix is the rather stability line at 285⁰ C on ward. The growth curve for sample no. NK7 displays the stability TL intensity of a natural sample at 61,014 which is equivalent to the paleodose of 50.33 Gy. The sample has the annual dose about 5.79 m Gy/yr with the water content of 3.18%. These TL parameters reveal the date of sample no. NK7 as 8,700 yr.

Table 7.1 TL dating results of quartz concentrates sediments for sample collected from the study area, Prachuap Kiri Khan and Ranong, Southern Thailand.

No.	Sample	U (ppm)	Th (ppm)	K (%)	Water Content (%)	Annualdose (mGy/yr.)	Paleo Dose(Gy)	Age (yrs)
1	SK1	4.77	25.87	4.45	2.90	7.81	227.38	29,100±5,000
2	SK2	5.98	25.47	4.18	4.13	7.75	243.04	31,000±4,700
3	SK3	5.46	26.71	3.56	6.97	7.00	369.08	51,000±9,600
4	SK4	5.08	23.67	3.92	3.94	7.14	282.55	39,500±5,400
5	SK5	4.76	23.52	4.24	4.23	7.38	375.04	51,000±6,000
6	NK1	5.19	15.45	3.57	2.73	6.24	30.19	4,800±1,000
7	NK2	3.43	16.21	1.43	2.10	3.68	40.79	11,000±3,000
8	NK3	4.26	17.56	2.89	1.66	5.50	50.49	9,100±2,000
9	NK4	3.06	22.50	1.53	4.76	4.11	30.19	7,300±2,200
10	NK5	5.18	21.10	3.88	2.43	6.98	109.76	15,700±4,300
11	NK6	4.19	18.77	3.20	1.94	5.88	29.96	5,000±1,000

NK = Noen Kruat and SK = Si Yeak Ban Kruat

ศูนย์วิทยทรัพยากร
จุฬาลงกรณ์มหาวิทยาลัย

Si Yeak Ban Krut Trench Logging

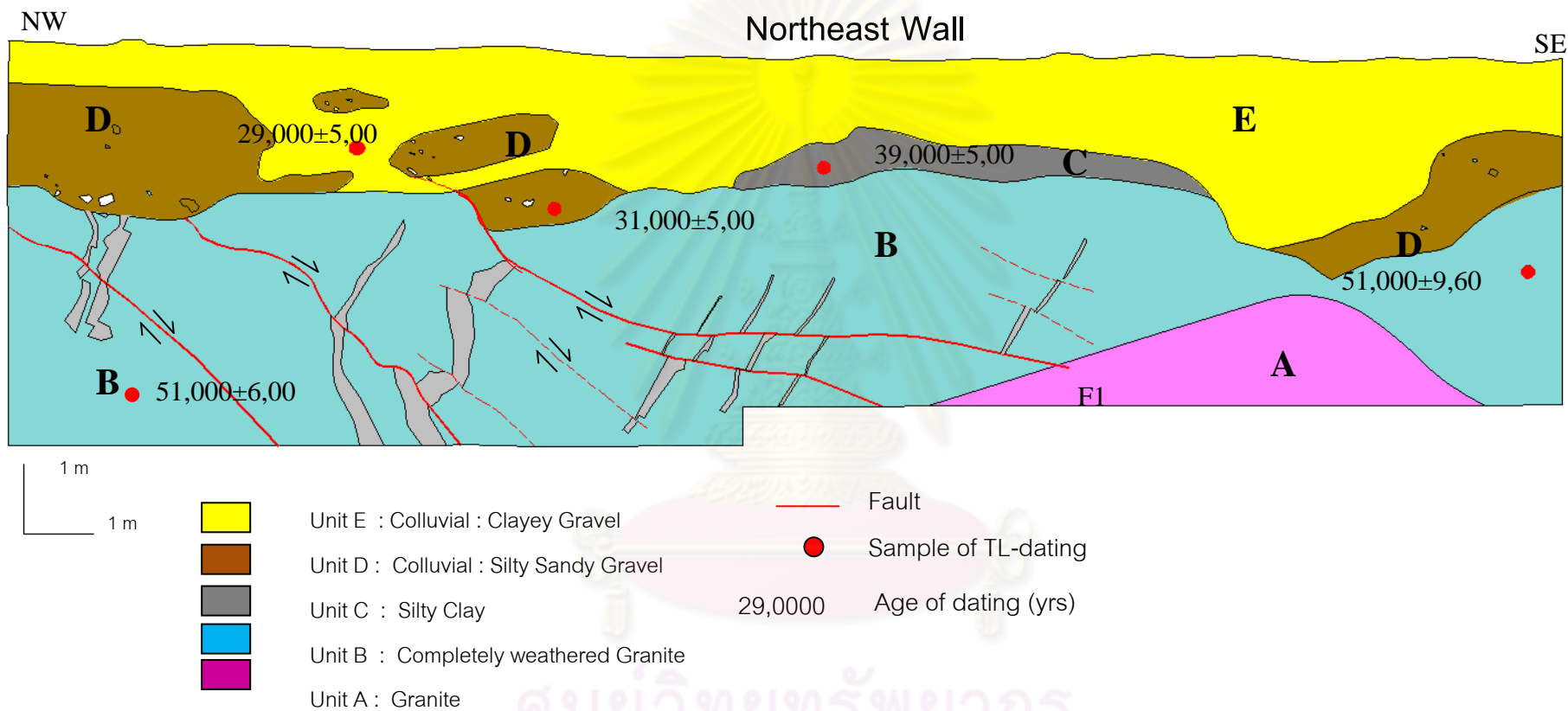


Figure 7.9 Trench log stratigraphy showing faults oriental and TL ages of sedimentary layers on northeast wall, Si Yeak Ban Krut trench.

Ban Neon Kruat Trench Logging

Northeast Wall

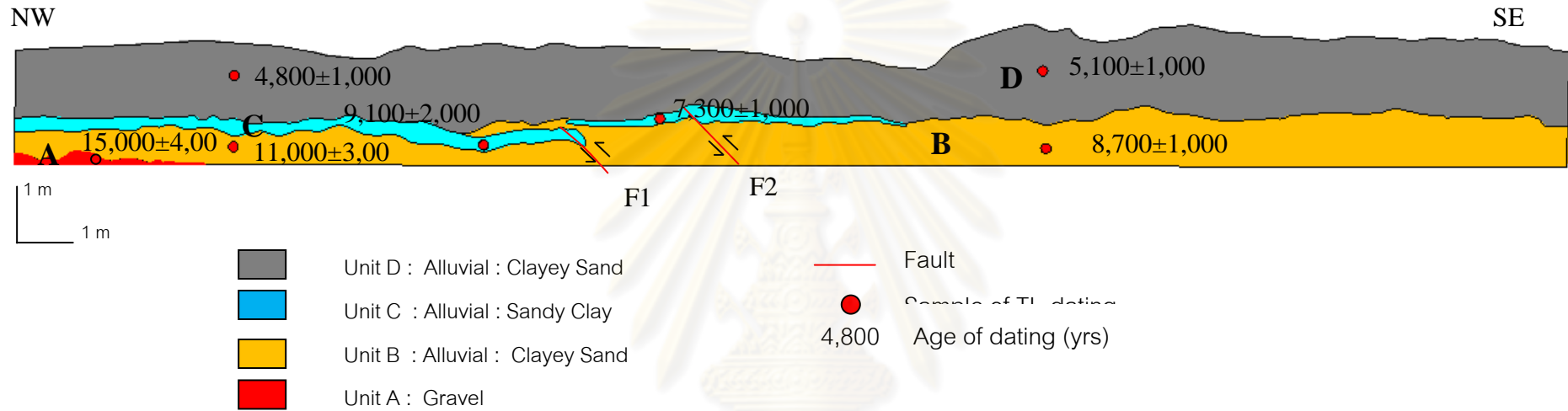


Figure 7.10 Trench log stratigraphy showing faults oriental and TL ages of sedimentary layers on northeast wall, Ban Neon Kruat trench.

ศูนย์วิทยทรัพยากร
จุฬาลงกรณ์มหาวิทยาลัย

Chapter VIII

DISCUSSION

In this chapter, a main point is described for the discussion related to the the results from current paleoseismic investigations along with the existing previous works. The discussion comprises of characteristics of the Ranong Fault zone, geomorphic features, maximum paleoearthquake magnitudes, their ages and slip rate, recurrence interval and evolution of active fault.

8.1 Characteristics of the RF

8.1.1 Sense of movement

Ranong fault zone (RNF) and Khlong Marui fault zone (KMF) are the major northeast -trending transform faults with the total length of 250 km and both are related to the development of the Andaman/Nicobar and Sumatra/Java island arc. The mega movement along these fault zones took place in late Jurassic to early Cretaceous times (Garson et al., 1975), the fault zone cut across Thai Peninsula with the left lateral sense of movement, However, Watkinson et al., (2003) found that this perhaps was the result of misinterpretation. These two faults are located to the south of the other two major faults which are the Three Pagoda (TPF) and Mae Ping Faults in western Thailand. Both RNF and KMF faults orientate about 100° to the TPF and MPF and act as the conjugate fault set (Lacassin et al., 1997; Tapponnier et al., 1986).

Garson et al. (1970) found that the western tin belt-granite displaced sinistrally at about 250 km to the south- west along the khlong marui fault, and 50-80km sinistral shift to south-west along the RNF and probable that Eastern belt of tin-bearing granite offset about 150 km along the RNF (Figure 8.1). Age determinations on muscovite and lepidolite from pegmatites intrude into fracture lines parallel to the main tectonic feature in the Khlong Marui transcurrent fault is about 52-57 Ma (Charusiri et al., 1993). Based on the above data it is quite possible that the KMF and RNF are sinistral movement after 52 Ma (Early Oligocene). This work by Garson et al. (1975) correspond well with that of Watkinson (2008). Based on Watkinson et al. (2008) the RNF is dextral movement before 52 Ma, after 52 Ma. RNF became sinistral sense and from 20 Ma (Miocene) began to

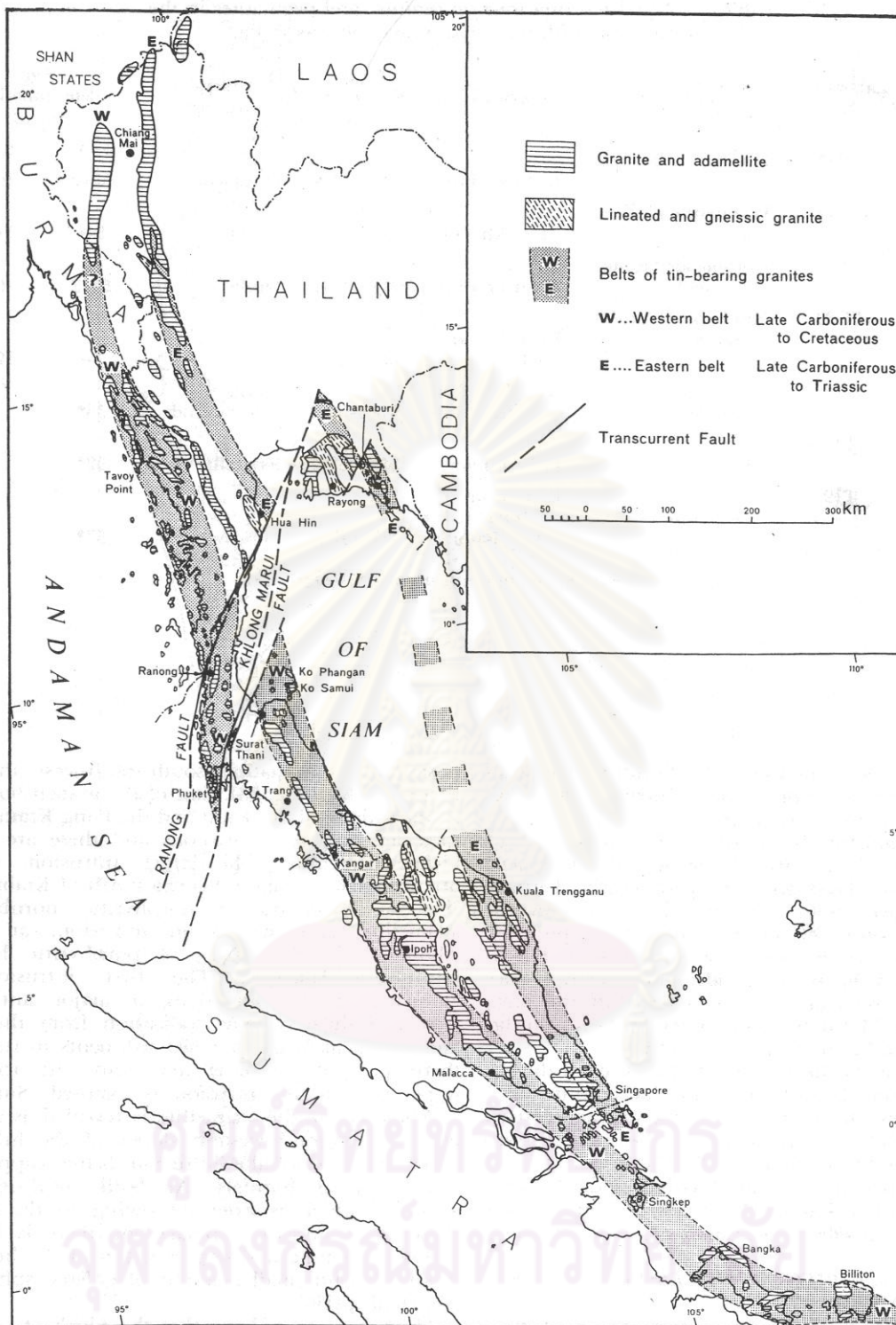


Figure 8.1 Regional distribution of tin -bearing granite belts in South-East asia (Garson et al., 1975).

dextral. However, from this study, morphotectonic feature in the present study show that the RNF shows the sinistral sense of movement. Due to the remote-sensing, ground geophysical data and paleoseismic trenching informations from this study, it reveals that the RNF is the strike-slip fault with the high dip angle ($>45^{\circ}$), corresponding to those reported by Watkinson et al. (2008) based on their field evidence.

Based upon this study the on- land RNF is the 300 km long fault extending from Prachuab Khirikhan to Ranong province. The left lateral movement is well observed along the NE-SW- trending fault trace such as at Khao Nakkharat, Prachuab Khiri Khan close to Nong Ya Plong segment and Mountain range in Ranong, which La-un segment is located. The results from paleoseismic trenching indicate that the RNF also shows its movement in both normal (Si Yeak Ban Krut trench) and reverse senses (Ban Neon Kruat trench). It is likely that in the trenches, the reverse fault are much more common. Such type of the RNF movement are also observed in the off-shore areas.

Based on their and the current studies, it is curtained that here is a change in tectonic-setting style through time, particularly between our result also confernces the movement along the on-land active RNF is largely lateral whereas the movement between Cretaceous and the present time.

8.1.2 Fault Extension

From the results of paleoearthquake investigations along the RNF in this study the RNF extends northward and southward to the Gulf of Thailand and Andaman sea, respectively and its characteristics are shown below (Figure 8.2).

Although Chantong (2010) first reported that the RNF was observed by 2D seismic survey to cut the sea floor of the Andaman Sea. No detailed study have been reported after that. It has been found from this study (chapter 5) that the RNF is the left-lateral strike-slip fault with the high dip angle (45° - 60°), The RNF extends from Ranong province into Mergui basin (from structure map of Andaman sea, DMR, 1996). The RNF runs into the Mergui basin as the low-magnitude epicenters can be extended and linked with the RNF in Andaman sea. Also, the Ranong fault has the strike slip fault movement that creates narrow push uplift (Ranong Ridge). It passes the Mergui Shelf with left lateral movement (Figure 5.27) resulting in the creation of the fault segment with horse

spray pattern (Cunningham and Mann, 2007). Based on the result of the seismic survey interpretation, the structure map in Andaman sea, the active fault map in Thailand and epicentral distribution in Andaman area, three fault segments are discovered. Ranong F1, Ranong F2, and Ranong F3. Ranong F1 move along the Ranong ridge with strike (northeast -southwest) N10E with dip angle 47-60 degree to east. Ranong F2 strike in N24E dip 47-60 degree to east and relation with earthquake 4.0-4.60 ML. Ranong F3 is tentatively active fault because this fault segment created from group of earthquake which size <3 ML near Pganga province, it will be more active fault study in the future and it has fault plane in the northeast-southwest direction (NE-SW) N25E. From the interpretation of data, Ranong F1 and F2 segments cut pass the sediment layer until the seafloor layer in the normal fault movement. This shows that the RNF which runs into the Mergui basin is the oblique fault with the major normal slip as the minor component of movement.

In the Thai gulf, it is possible that Bangsapan segment, Nong Yaplom segment and Bangsaphan Noi segment move into the gulf of Thailand. When the lines of all three faults are extrapolated to the Gulf of Thailand, the flower structure is found in the area of Prachuab basin where the RNF may cut pass. This structure is an evidence of the strike slip fault movement and these faults cut into the seafloor in normal movement and related to the epicenter of the earthquake event on 27 September 2006 (Figures 3.8 and 5.44) that show they are active fault and RNF movement in oblique fault (normal with strike slip movement). However, when RNF is extended into the Prachuab basin, no structure created by the strike slip fault movement is discovered. The faults mostly move with normal movement. Since the data used to interpret is little, it can be said that Bangsapan segment, Nong Ya Plong segment and Bangsaphan Noi fault segment runs into the gulf of Thailand. Nong Ya Plong segment and Bangsaphan segment that are extended into the sea which strikes at N40E direction. Bangsaphan Noi extended into the sea which strikes at N50E.

From the study of focal mechanism event on 8 October 2006 (chapter IV) and the preliminary result of the seismic interpretation (Chapter V), the analysis using beach ball reveals that the movement along the RNF is oblique (normal with minor strike slip component) with the dip of 30-60 degree. It is likely that the fault plane is in northeast-

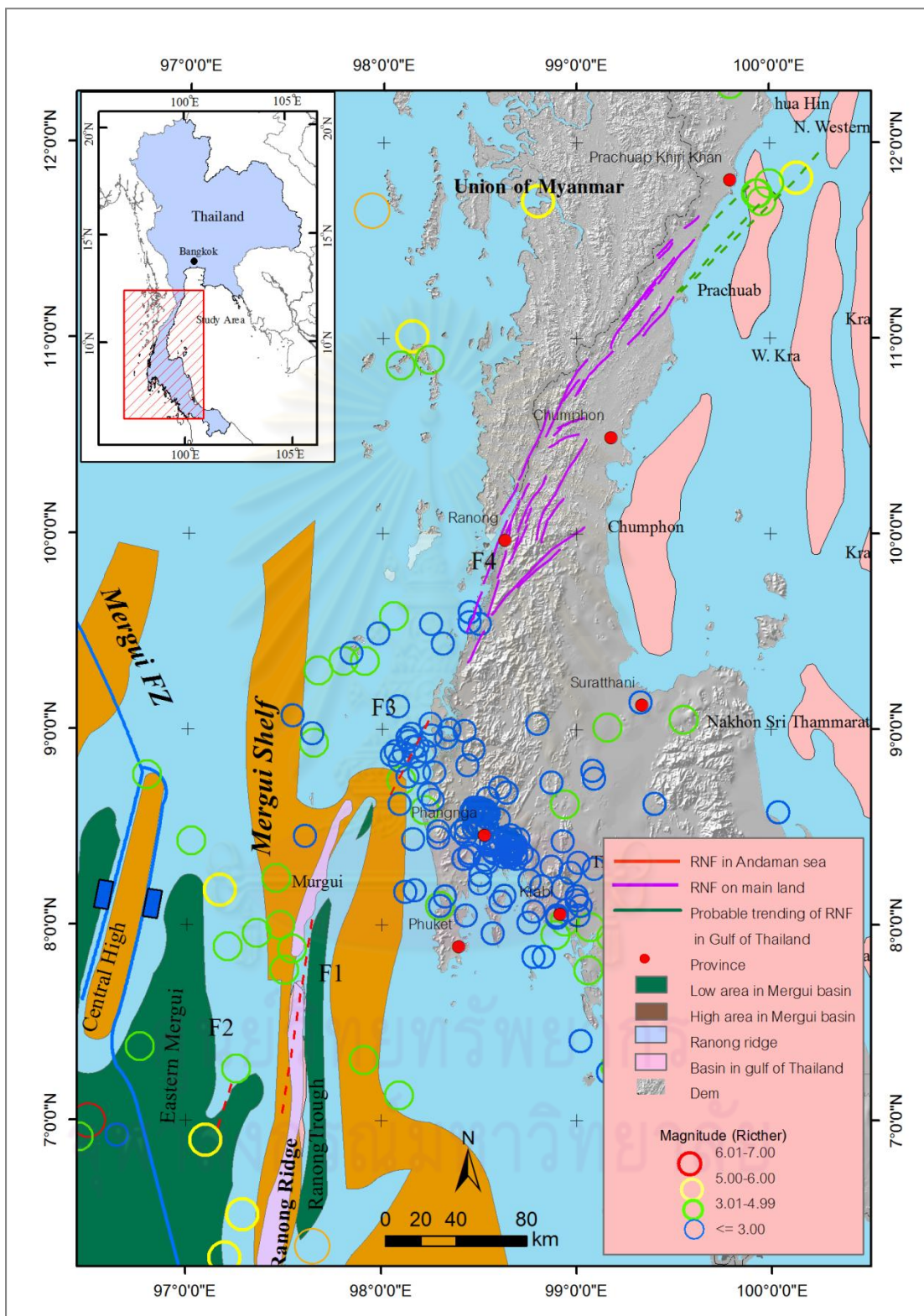


Figure 8.2 Map showing active fault segments of the RNF on main land and faults segments in the sea.

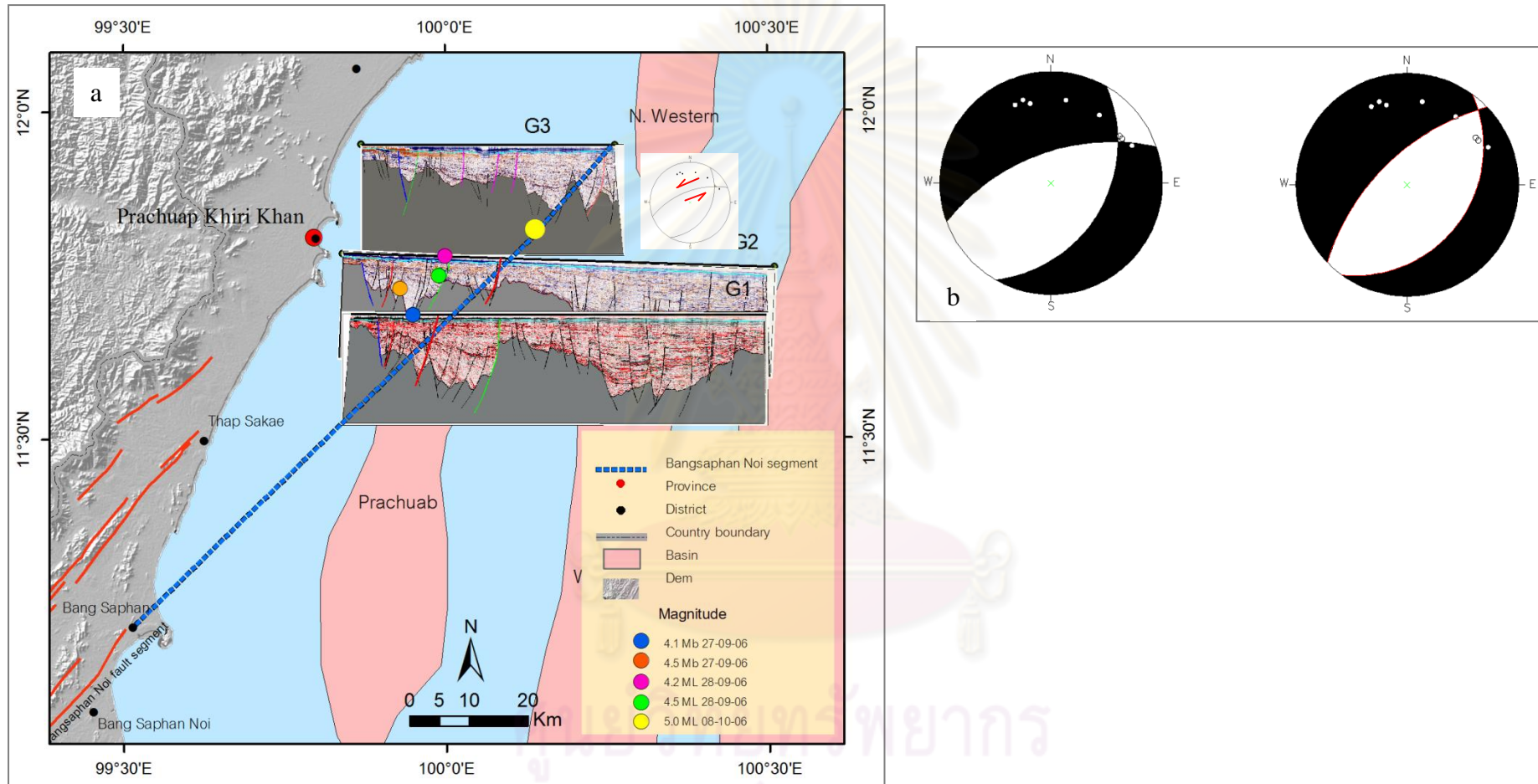


Figure 8.3 (a) Map showing the S46° W-trending Bangsaphan Noi extending to site of epicentral event on 8 October. (b) Beach balls of the same earthquake event on 8 October 2006.

southwest direction. From the seismic interpretation, there is no seismic line passing the point of earthquake and there is no fault line related to the earthquake when the point is projected. When the Bangsaphan Noi segment is extended towards the epicenter, the fault in all 3 seismic lines is found. At the area where Bangsaphan Noi segment cuts pass, there is a fault cutting through the sediment layer upon the seafloor with normal movement. The stated fault dips at 44-60 degree to the west which is related to the beach ball that strikes at S36W-S46W dip angle of 60 degree to west and the fault line of the Bangsaphan Noi segment. Therefore, it is possible that the earthquake incident is related to the Bangsaphan Noi segment that runs passing the gulf of Thailand and it is categorized as Oblique fault (normal with minor strike slip component) (Figure 8.3).

8.2 Geomorphic Features and Paleoearthquake Magnitudes

Department of Mineral Resources (2007) used the tectonic geomorphology in the RF and KMF and stated that both 2 faults are active. They found that the trend of all fault segments were in the northeast direction. However no northwest or the direction has been reported for the fault trend.

From the result of the remote-sensing interpretation, the fault segment can be divided into 19 sections on mainland. This is different from the result of DMR that divided the fault segment of RNF into 16 segments. In Prachuab Khirikhan DMR (2008), there are 8 fault segments and other 8 segments in Pananon(2009). In this study, it can be divided into 9 segments. In the area of Chumphon and Ranong DMR, there are 8 segments but the fault segments can be divided into 10 segments in this study. The faults that are added are Khoa khirilom segment (Bangsaphan segment, DMR (2007) and KhoaKhirilom (Pannanon, 2009) , Khoa Kwang segment , Khlong Nam Khoa segment (Na Khoa segment, DMR (2007)), Pato and Pathui fault segment supported by the detail of geomorphic evidence mentioning in Chapter III.

From the remote sensing interpretation with 2m contour line in the area of Khao Samianma, it is found that there is more than one fault segment (Figure 8.4), viz. Bangsaphan fault segment and Khoakhirilom segment and lines of evidence are shown in figures 3.18 and 3.20. In the area of Na Khoa segment (DMR, 2007) reported that geomorphic evidence such as trigular facets and offset stream in northern and southern

of this area. They are geomorphic evidence of Khlong Nam khoa segment (Figure 8.5) Therefore, the remote sensing interpretation by using the 2M contour interval DEM to divide the fault segment, the result of orientation and direction of the fault is more detailed and clearer as compared from the result of SRTM Dem as shown in figure 8.6.

From the above result, the fault segments on mainland orient mainly in the northeast-southwest direction. However, from the result of the remote sensing, there are lineaments in the north-south, northwest - south east and east-west direction. As the morphotectonic evidence is unclear and locates on the mountainous region, most of the fault segments are in the northeast-southwest direction. Most fault segments are in the value of N20E-N45E. Moreover, the Tha Mai Lai segment and Pak Jun segment are found to be in N70E-N75E near the East-west direction. From the data of the Park Jun seismic station in Chumphon province (Tha sea network, RID), the small magnitude of the earthquake can be measured at 2-3 ML. It was the only seismic station in Chumphon but the other network in Ranong province that could not detect the seismic wave of earthquake due to its small size. Thus, there might be a movement of fault in the vicinity. It is possible that Pak Jun segment had moved. According to Well and Coppersmith (1994) reported the relationship between surface rupture length (SRL) along the active faults and the paleoearthquake magnitudes. It is founded that fault segment on-land credible paleoearthquake as shown in table 8.1. Also, the maximum magnitude of the fault segment on mainland ranging from 6.4-7.0 Mw (Figures 8.7-8.8). Ranong fault segment has the longest surface rupture length and might be the cause of the earthquake with the magnitude of 7.4 Mw. In addition, the morphotectonic evidence proves that the major earthquake might be occurred on the mentioned fault segment.

From the result present above, there are small earthquakes along RNF in Andaman Sea and Gulf of Thailand (>100 events) that have been detected with the maximum magnitude of about 4 Mw. As shown in the earlier section, apart from the background earthquakes, many earthquakes are related to the movement along the RNF. As shown by USGS and TMD, there are moderate earthquakes in the Andaman and Gulf of Thailand, particularly in 2005 and 2006, respectively. Therefore, it is very likely that there could be more earthquake incidents occur on -land in the future since not many small earthquake events have been detected on land so far.

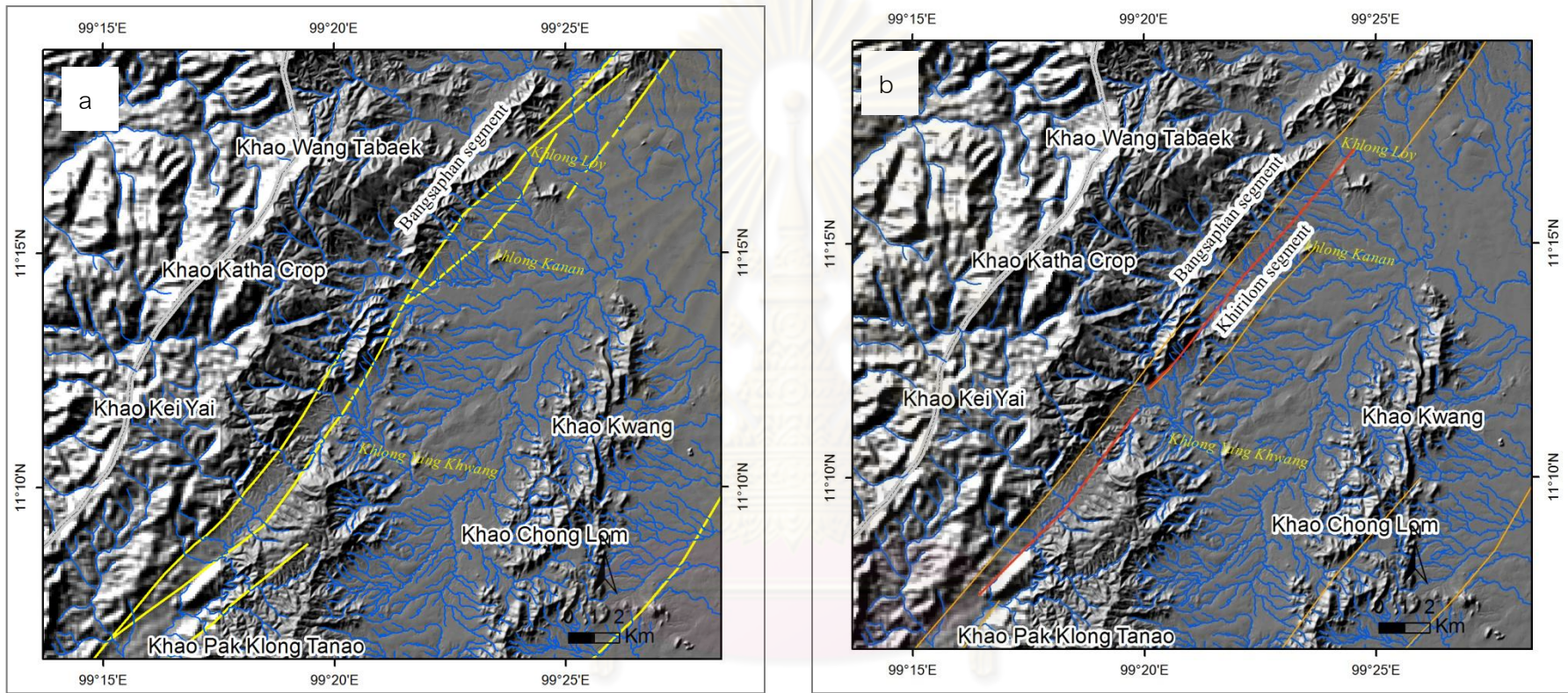


Figure 8.4 2m contour interval DEM showing (a) Bangsaphan segment from DMR (2007) and (b) Khoa Khirilom segment and Bangsaphan segment, Khoa Samianma, Bangsaphan district, Prachub Khilikhan province.

จุฬาลงกรณ์มหาวิทยาลัย

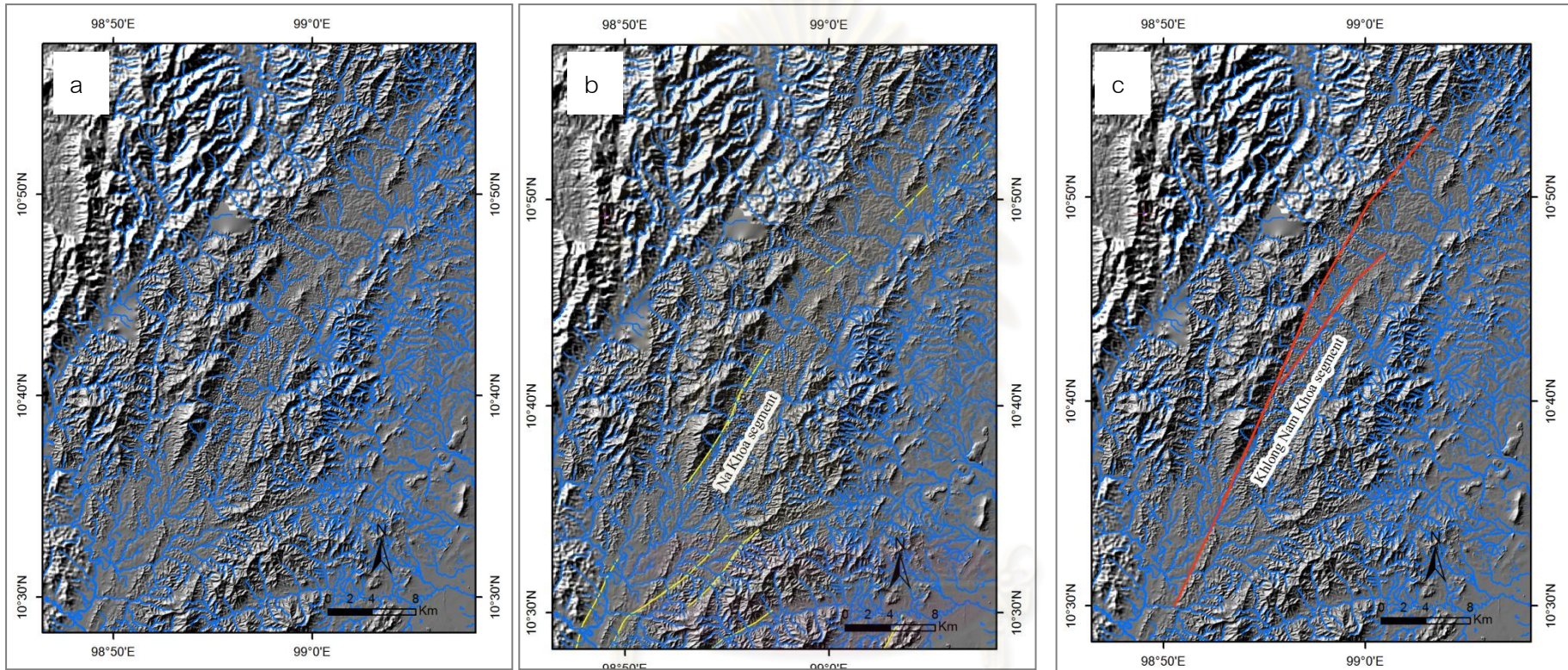


Figure 8.5 (a) 2m contour interval DEM showing (b) Na Khoa segment from DMR (2007) and (c) Khlong Nam Khoa segment from this study, Ranong -Kraburi district, Ranong province.

ศูนย์วิทยทรัพยากร
จุฬาลงกรณ์มหาวิทยาลัย

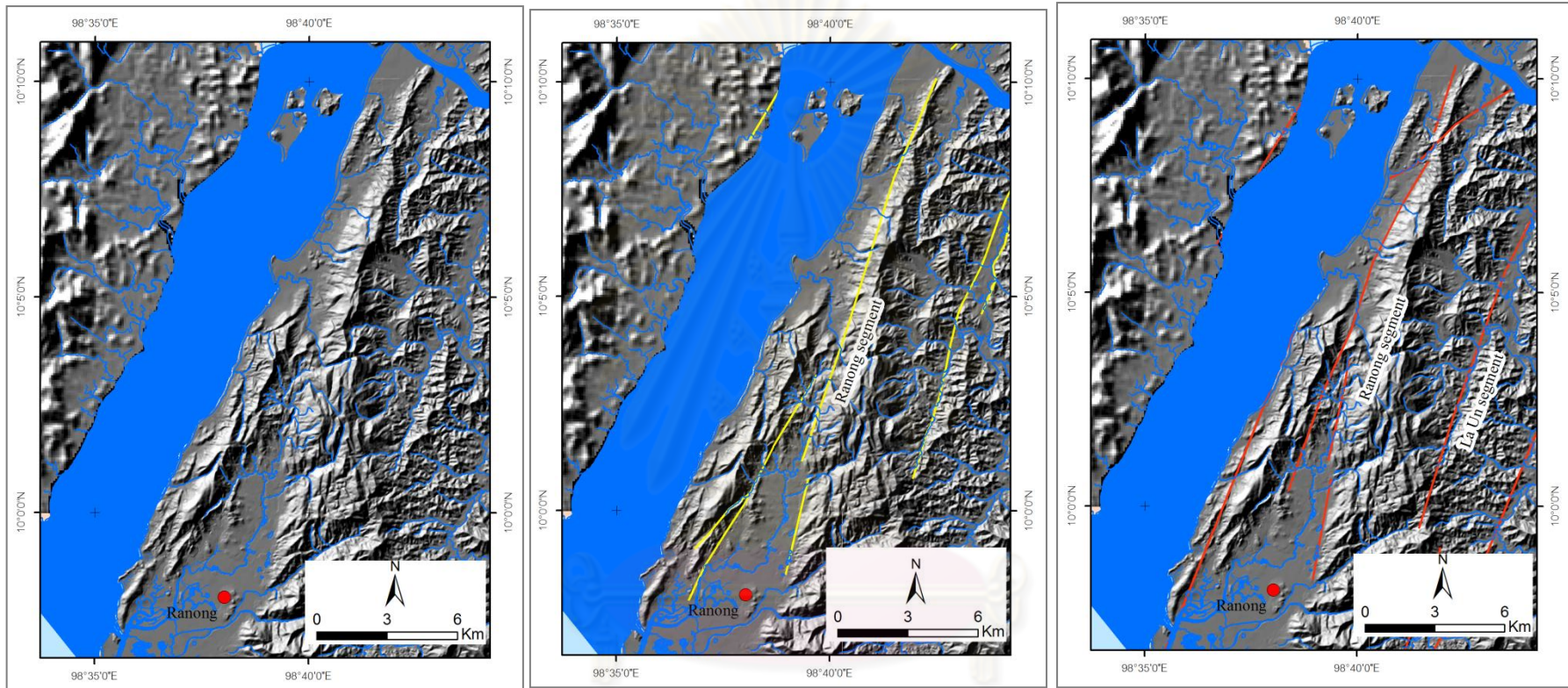


Figure 8.6 (a) 2m contour interval DEM showing (b) Ranong segment from DMR (2007) and (c) Ranong segment from this study, Ranong province

ศูนย์วิจัยทรัพยากร
 จุฬาลงกรณ์มหาวิทยาลัย

Table 8.1 Paleoearthquake magnitudes of the RNF in southern Thailand, estimation from Well & Coppersmith (1994).

No.	Fault segment	Surface Rupture Length (km)	Moment Magnitude (Mw)	Remark
1	Thap Sakae	11	6.3	
2	Khoa Mun	7	6.1	
3	Bangsaphan	45	7.0	
4	Nong Ya Plong	44	7.0	
5	Khoa Khirilom	22	6.6	
6	Khoa Daeng Noi	22	6.6	
7	Bangsaphan Noi	28	6.7	
8	Khoa Kwang	28	6.7	
9	Tha Sae	34	6.8	Peninsular
10	Khlong Nam Khoa	50	7.0	6.1-7.4 Mw
11	Pak Jun	20	6.6	
12	Tha Mai Lai	20	6.6	
13	Sawi	65	7.2	
14	Nong Ki	28	6.7	
15	Laun	54	7.1	
16	Ranong	98	7.4	
17	Kraburi	65	7.2	
18	Pato	70	7.2	
19	Pathui	32	6.8	

Mw can be calculated from the equation proposed by Well and Coppersmith (1994) as

$$M_w = 5.08 + 1.16 \log (\text{SRL})$$

Whereas:

Mw = moment magnitude;

SRL = surface rupture length;

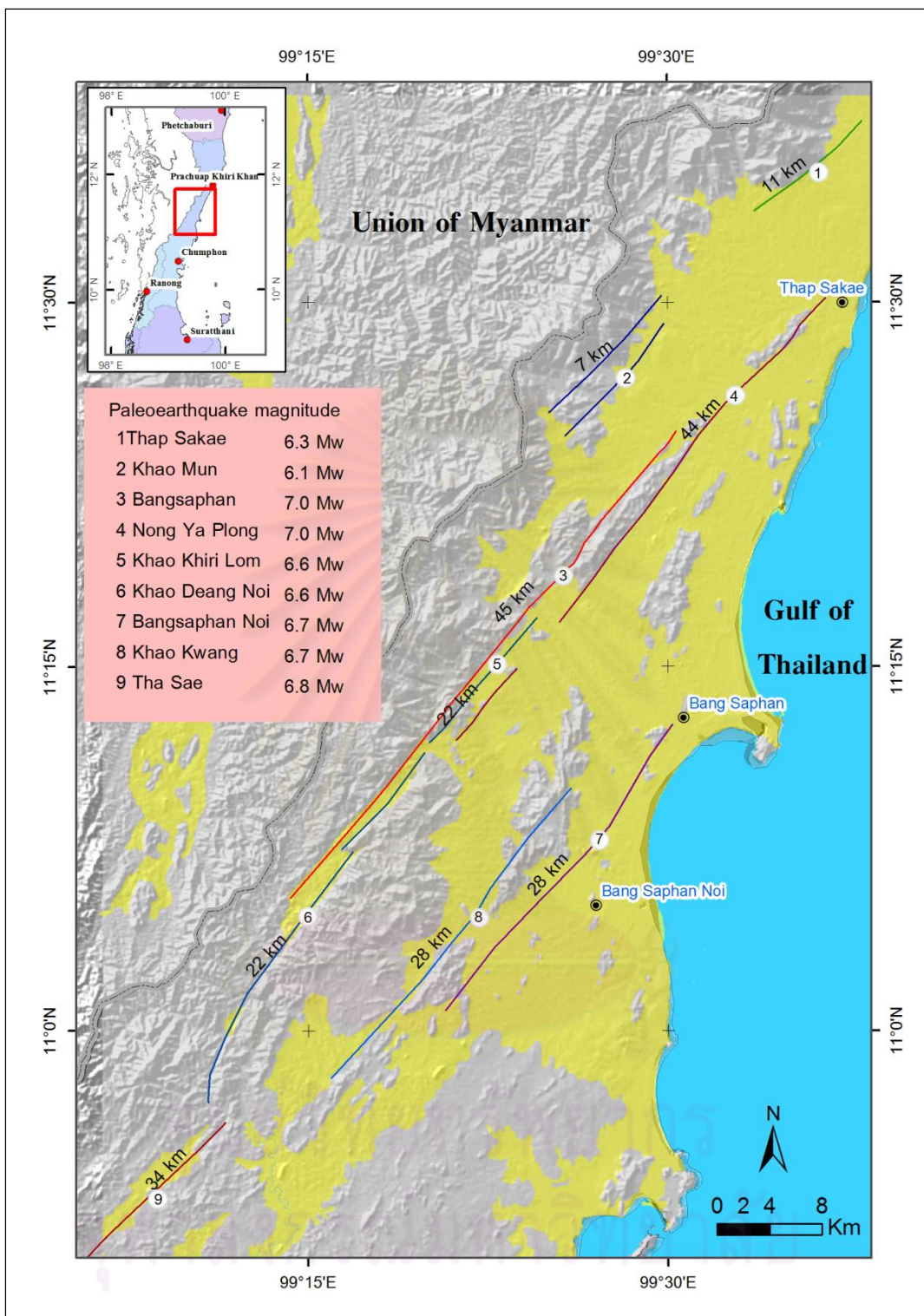


Figure 8.7 Map showing active fault segments, their length and estimated maximum credible earthquakes of paleomagnitudes of The Ranong Fault Zone in Prachuab Khirikhan province.

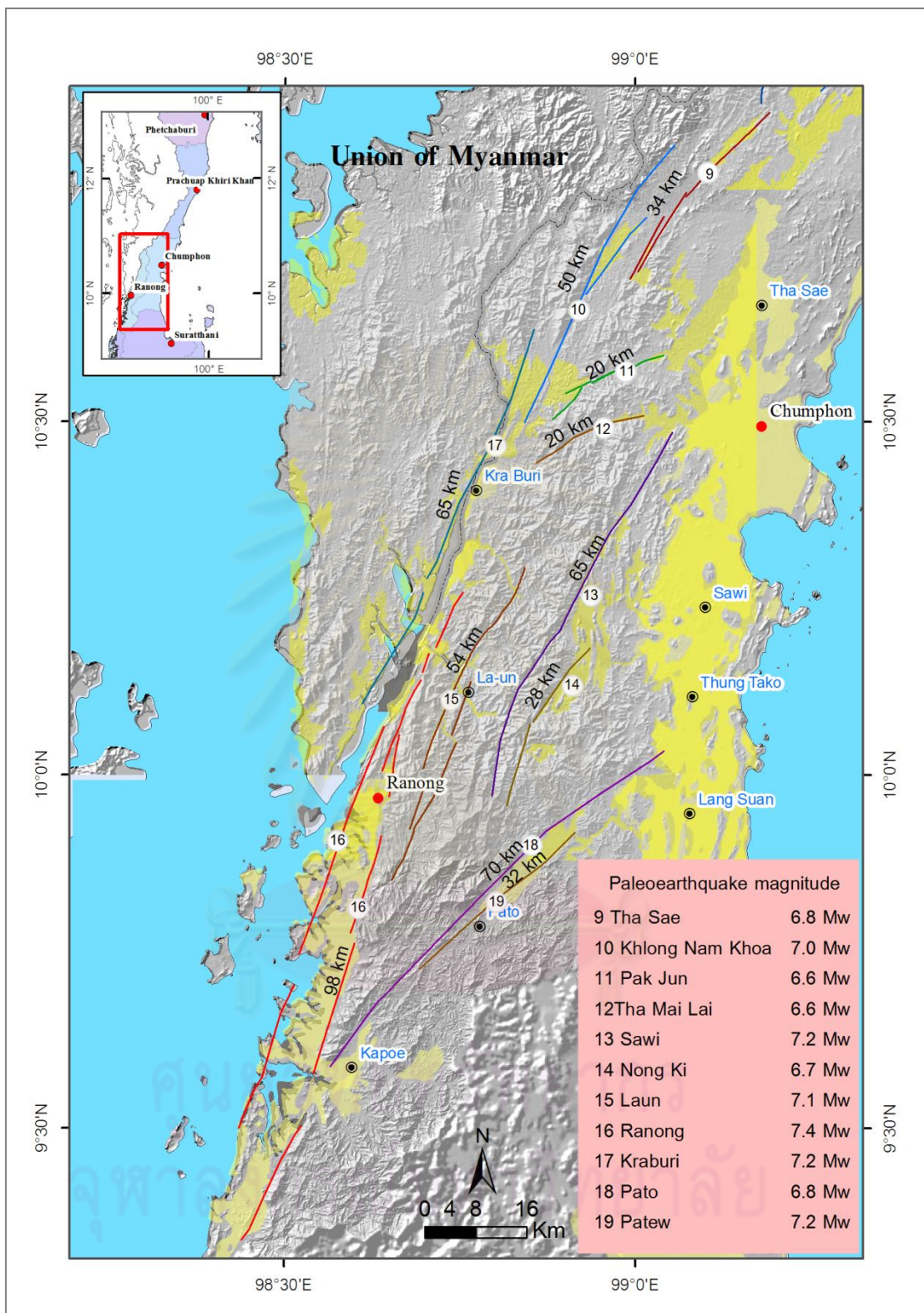


Figure 8.8 Map showing active fault segments, their length and estimated maximum credible earthquakes of paleomagnitudes of Ranong Fault Zone in Chumphon and Ranong province. (Cenozoic deposits data from DMR,2007)

8.3 Age, Slip Rates and Recurrence Interval

8.3.1 Earthquake faulting and recurrence interval

From the research of DMR, there are 5 earthquake events in the RNF and KMF. The earthquake events along RNF can only be detected for 3 times which are 40,000 years along the Nong Ki segment, 9,000 years along the Ranong segment and 2,000 yrs along Khoa Khirilom segment (Bangsaphan segment, DMR (2007). From the research study of Pananon(2009), the very rough earthquake faulting is reported to have occurred at about 4,500 yrs ago along Khoa Khirilom segment. However when all the mentioned data is added to the paleotrenching in this study, RNF on land has earthquake faulting for 6 events.

Detailed discussion of individual faulting events is discussed below.

The earliest faulting of the Ranong Fault Zones may have taken place at about 40,000 years age. The slip rate of 0.7 mm/yr is based on the offset sedimentary layers and the TL-dating methods from Ban Prachaseri area, (DMR, 2007) which took place at Nong Ki segment of the RNF.

The second faulting occurred at about 30,000 yrs based on the result of open wall at Si Yeak Ban Krut area which took place on Nong Ya Plong fault segment . The Faults F1 cut through and disturbed the layer bottom of unit E (Figures 6.16 and 6.17). However, the fault did not cut the upper part of unit E and bottom of unit D was dated by TL method to be about 29,000 yrs. So this represents the approximately fault ages, with the slip rate of fault at about 0.021mm/yr.

The third faulting event of the Ranong Fault Zones took place at about 7,300 yrs. The age of 7,300 yrs. Based on the result from Ban Neon Kruat area which occurred on Khoa Khirilom segment. The Faults F2 at Ban Neon Kruat trench cut through and disturbed the layer bottom of unit C (Figures 6.20, 6.22 and 8.9). However, the fault did not cut the upper of D. Unit C was dated by TL method to be about 7,300 yrs.

The fourth faulting event of the RNF at about 9,000 yrs with the slip rate of 0.18 mm/yr based on the trench log and the TL dating methods from Ban Bang Non Nai area, (DMR, 2007) which occurred on Ranong segment.

Ban Neon Kruat Trench Logging Northeast Wall

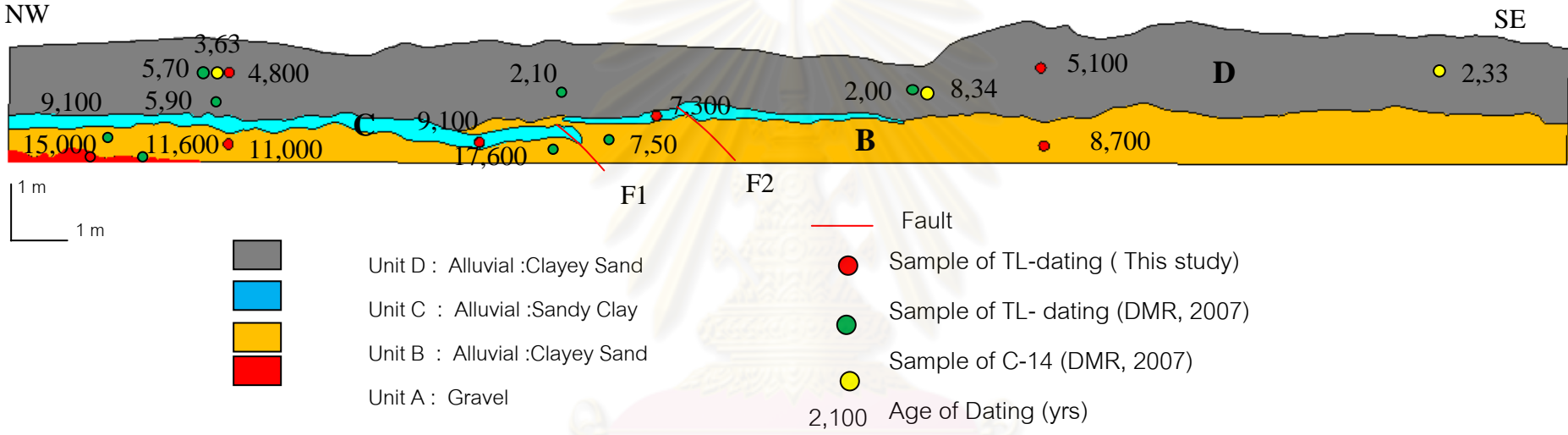


Figure 8.9 Trench log section at the northeast wall of Ban Neon Kruat, Prachuab Khirikhan showing principle stratigraphy and TL of this study, TL ages of Department of Mineral Resource (2007) and Carbon-14 dating of Department of Mineral Resource (2007).

ศูนย์วิทยทรัพยากร
จุฬาลงกรณ์มหาวิทยาลัย

The fifth faulting event of the RNF occurred at about 4,500 yrs. The slip rate 0.088 mm/yr is based on the results of exploratory trench at Ban Nong Chan area by TL dating (Pananon, 2009) which took place at Khoa Khirilom segment.

The last faulting of the RNF may have taken place at about 2,000 years ago with the slip rate 0.27 mm/yr based on the offset sedimentary layers and the C-14 AMS methods from Ban Neon Kruat area (Figure 8.9), (Department of Mineral Resources, 2009) which placed on Khoa Khirilom segment (Bangsaphan segment, DMR (2007)) of RNF.

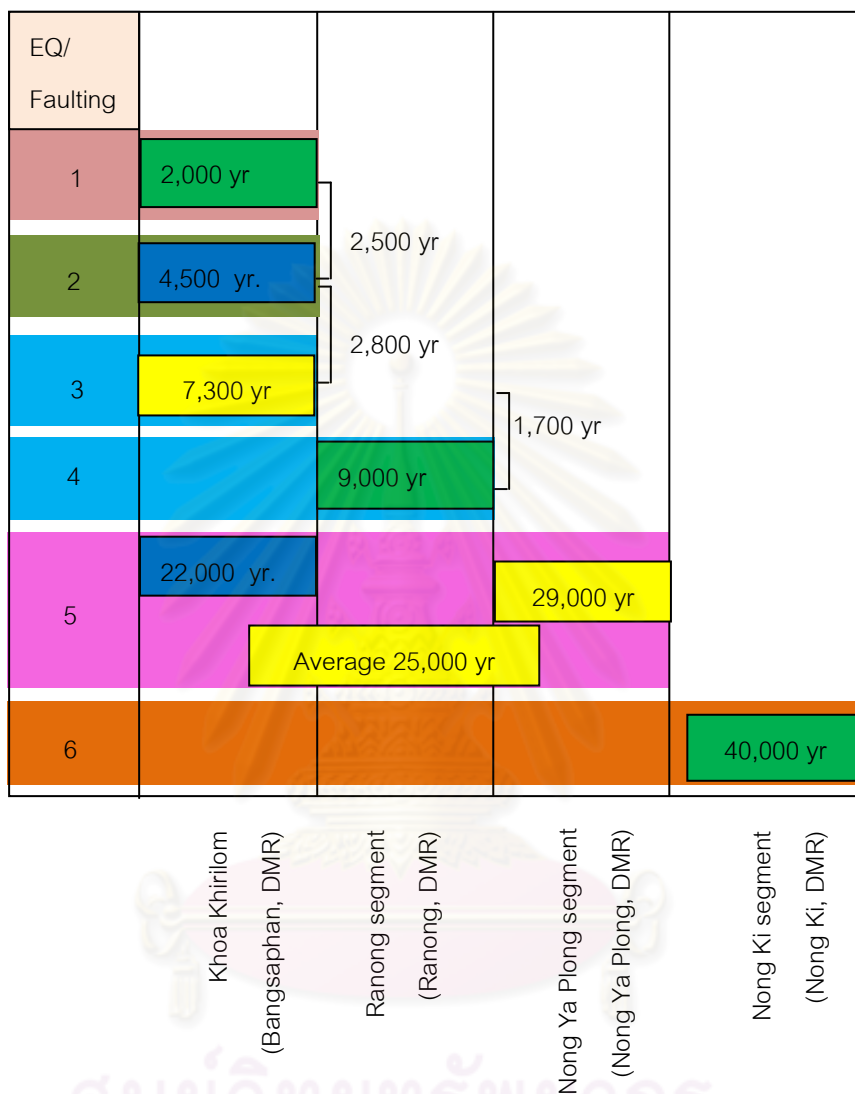
It is noted from the data of paleo-trenching in Ban Neon Kruat Area (Fig.8.9), that sediment of Unit D has the age of 4,800-5,100 years. Also, from the research result of DMR that had been tested by C 14 AMS, the age of sediment Unit D is about 2,330-3,630 yrs and ages by TL dating range from 2,000 to 5,900 years. From the result of the test and that of DMR, the value from the TL-dating that has the depth close to the area where the fault cut (F1) is used. Therefore, its age is 2000 yrs.

From the above discussion, a summary of earthquake events is shown in Table 8.2. Based upon the above result of discussion with earlier dating data and this study, it can be preliminarily deduced that the recurrence interval for 6.4 Mw of the Khirilom Fault segment is 2,000 yrs.

8.3.2 Slip rate

From this study we found the vertical slip rate along the RNF on main land range from 0.018-0.70 mm/yr from Quaternary sediment offsetted in paleoseismic trenching. The regional slip rate in long term of RNF in Andaman area about 0.0029-0.0076 mm/yr, or approximately about 0.01 mm/yr and the regional slip rate in long term of RNF Gulf of Thailand area about 0.0025-0.0051 mm/yr, or approximately about 0.01 mm/yr (Figure 8.10) which found from the 2D seismic interpretation. When we compare long term slip rate of active faults in northern -western Thailand (Fenton et. al, 2003) with long term slip rate in this study found that the long term slip rate of RNF in Andaman area and Gulf of Thailand less than the long term slip rate of active fault on land in the northern - western Thailand as shown in the table 8.3

Table8.2 Numbers of Earthquake faultings and recurrence interval of the fault segments belonging to RNF



- This study (TL dating)
- Pananon, 2009 (TL-dating)
- DMR, 2007 (TL & C-14 Dating)

Table 8.3 Slip rate and regional slip rate in long term of active fault

Fault	Age of most recent movement	Long term slip rate (mm/yr)	Slip rate (mm/yr)
Long	Late Pleistocene	0.04	
Nam Pat	Late Pleistocene	0.04	
Phayao	Late Pleistocene	0.05	
Phrae	Late Pleistocene	0.07	
Pua	Late Pleistocene	0.06	
Theon	Late Pleistocene	0.02	
RNF in Andaman sea	Early Pliocene	0.01	
RNF in Gulf of Thailand	Early Pliocene	0.01	
RNF on mainland			
- Khoa Khirilom segment	2,000		0.27
- Nong Ya Plong	29,000		0.021
- Nong Ki	40,000		0.70
- Ranong	9,000		0.18

*Data from Fenton et. al, (2003)

From the result above, the area with high slip rate is more likely to have higher seismic hazard, (P_{ga} value) than that of the area with low slip rate. Thus, it is more likely that the region on-land has more risk to suffer from the earthquake hazard more than that of the sea. It is shown from the calculation the slip rates in Andaman Sea and the Gulf of Thailand are not high those of Fenton et. al, (2003).

8.4 Neotectonic Evolution of The RF

Our integrated result reveals that the northeast-southwest-trending RNF shows its major sense of movement along its strikes with the sinistral movement on the land, and oblique fault movement (normal with minor strike slip component) in Gulf of Thailand and in Andaman area.

Based on the work of Watkinson et al. (2008) in the KMF and Ranong Fault using structural field and petrographic relations and geochronological synthesis, it is quite likely that during the Tertiary Period and shortly after the Indian-Asian collision at 52 Ma,

The RNF and Khlong Marui fault served as the major and deep fault (see Figures 8.11 and 8.12). They showed a sense of movement with the right lateral 250 km long, ductile displacement during 87 - 56 Ma. They also showed such the movement in the NNE to NE trends, which may have occurred at least 4 times. Sense of movement became reversed in Quaternary to late Tertiary Period after 52 Ma. Their field and petrographic lines of evidence strongly indicate that the brittle deformation may have occurred during 23 Ma.

Our TL age-dating data also indicate that the RNF has the strike slip movement with the sinistral offset and may have occurred before 290,000 yrs. (Prachaseri trench, Sawi segment, DMR (2007)) and latest movement about 2,000 yrs (Ban Neon Kruat trench, Khoa Khirilom segment, DMR (2007)). Such lateral movement occurred simultaneously with a vertical movement as shown by a slip in the paleoseismic trench at Ban Neon Kruat and Si Yeak Ban Krut trench. Our age dating data from the trenches were also confirmed by the work of Department of Mineral Resources (2007) and Pananon (2009).

Our results also illustrate that there are many times of displacement during Quaternary as shown in Table 8.2. Locations of hot springs provide the good supporting evidence for such neotectonic processes. Such the neotectonic activity and the epicentral distribution, all point to the fact that the RNF is still active till present with the major component of motion in the sinistral sense. However as quoted by Watkinson et al. (2008), the sense of movement may have been largely higher in the Tertiary Period than the present day.

ศูนย์วิทยทรัพยากร
จุฬาลงกรณ์มหาวิทยาลัย

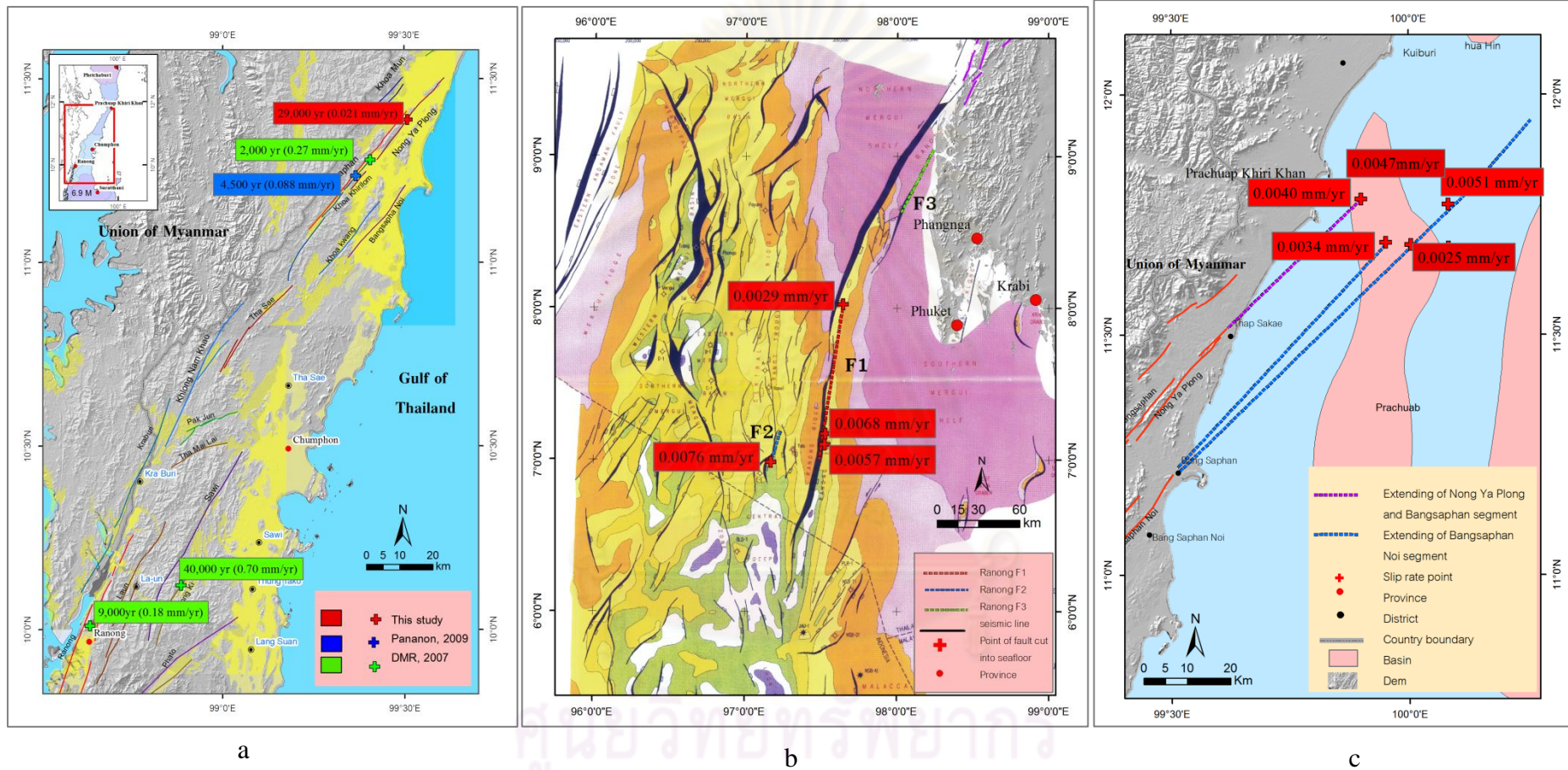


Figure 8.10 (a) Map showing slip rate on main land. (b) map showing regional slip rate -long term in Andaman Area. (c) Map showing regional slip rate - long term in gulf of Thailand.

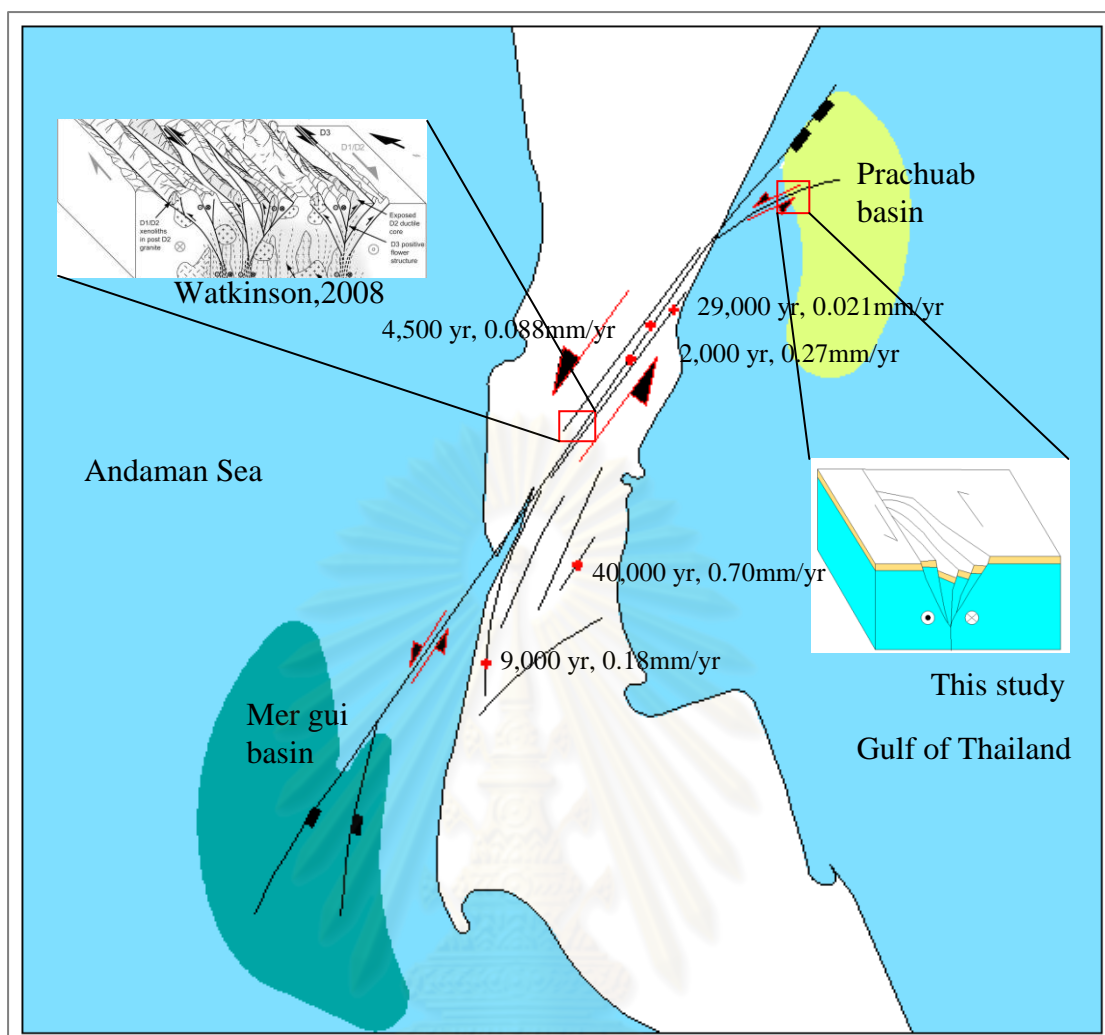


Figure 8.11 Simplified model of the RNF based on this study.

ศูนย์วิทยทรัพยากร
จุฬาลงกรณ์มหาวิทยาลัย

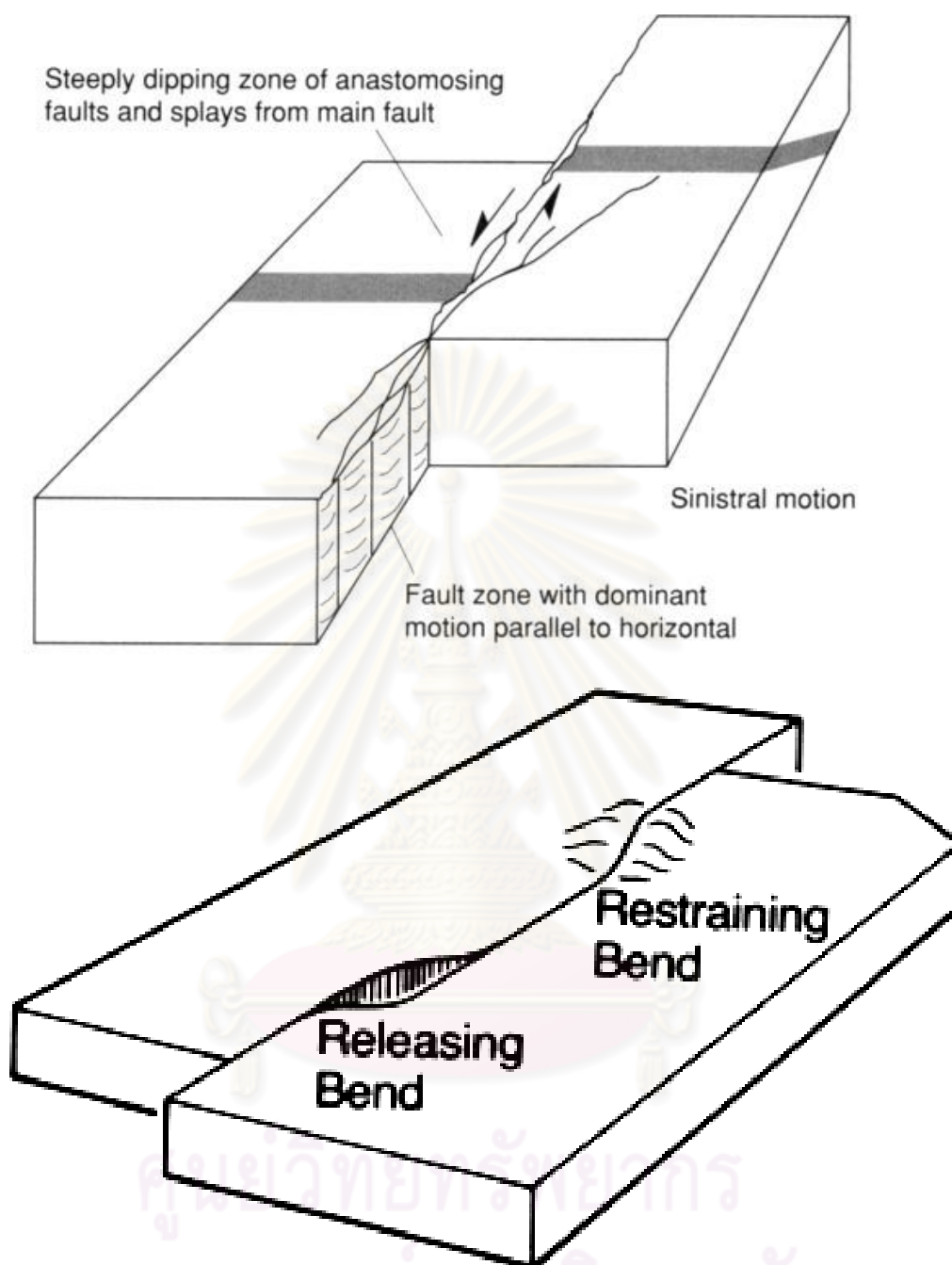


Figure 8.12 Geometry and anatomy of strike-slip fault showing releasing bend and restraining bend, which help in explaining evolution of Sinistral movement of the Ranong Fault Zone (Crowell, 1974).

CHAPTER IX

CONCLUSIONS

Based on the results of enhanced remote-sensing and aerial photographic interpretation integrated with ground-truth investigation, detailed topographic survey as well as those of TL-dating of fault related sediments, seismic interpretation in Gulf of Thailand and Andaman area and evolution of RNF, the conclusions can be drawn as the followings;

1) The Ranong Fault (RNF) is the northeast to north-northeast trending, 300 km-long fault extending from Prachuab to Ranong province. The RNF extends from Ranong into Mergui basin, Andaman sea and extends from Prachuab province to Prachuab basin, Gulf of Thailand.

2) Lineaments belong to the RNF orientated in the northeast – southwest, east-west and northwest – southeast directions. The major trends of lineaments are the northeast – southwest directions and are regarded as a major fault zone.

3) The Ranong Fault Zone can be divided into fault segments on main land based on discontinuity criteria into nineteen fault segments, viz, (1) Thap Sakae (11 km), (2) Khoa Mun (7 km), (3) Bangsaphan 45 km), (4) Nong Yaplong (44 km), (5) Khoa Khirilom (22 km), (6) Khoa Deang Noi (22 km), (7) Bangsaphan Noi (28 km), (8) Khoa Kwang (28 km), (9) Tha Sae (34 km), (10) Khlong Nam Khoa (50 km), (11) Pak Jun (20 km), (12) Tha Mai Lai (20km), (13) Sawi (65 km), (14) Nong ki (28 km), (15) Laun (54 km), (16) Ranong (98 km), (17) Kraburi (65 km), (18) Pato (70 km), (19) Pathui (32 km).

4) Significant and well-defined types of morphotectonic evidence can be seen both on the land and in the sea. On land they are triangular facets, fault scarp, offset streams, parallel ridge, linear ridge, pressure ridge and linear valley. They are well recognized along the RNF, particularly where bed rock connects with the Cenozoic basins boundary. In the sea seismic interpretation reveal that the RNF cut through Tertiary strata to seafloor, and many of them have the closed association with the epicenters.

5) Based on preliminary result of seismic interpretation section in the gulf of Thailand earthquake event on 27 September 2006 and 8 October 2006 occurred at the

point which Bangsaphan segment, Nong Ya Plong segment and bangsaphan Noi segment of RNF extended to Prachuab basin. Additionally, some part of fault segment of RNF seem to be located at the Prachuab basin boundary (or edge) and not related to earthquake event. In Andaman sea the earthquake swarms correspond with Ranong F1 and F2 which cut Tertiary layers up to the seafloor.

6) The result of focal mechanism based on beach ball analysis indict the RNF extends to the Gulf of Thailand with the normal sense of movement on the major component and in the left lateral sense of movement in the minor component.

7) The RNF used to trigger the largest earthquake with the magnitude of 7.4 Mw as evidenced by the Ranong segment and the fault has the maximum slip rate 0.7 mm/yr from the Nong Ki segment (DMR. 2007) based on the surface rupture length. The fault shows the left – lateral sense of movement at the present. However, the sense of movement became opposite in the Tertiary time.

8) There are six major earthquakes with the paleoearthquake of about 6.7-7.0 M along the RNF. They occurred about more than 40,000, 28,000, 9,000, 7,300, 4,500 and 2,000 years ago. Its recurrence interval is around 2,000 years for the Ranong Fault zone .

9) Based on classification of active fault as proposed by Charusiri et al. (2001), the Ranong fault zone is classified as active following the definition. Additional data of historical and instrumentally earthquake records in southern Thailand and adjacent area also indicated that this area is tectonically active.

10) The previous work and result of this study reveal that sense of movement of RNF have change in many times. First, ductile dextral strike-slip shear have develop during Late Cretaceous - Early Eocene (87– 56 Ma) next, RNF became sinistral reverse oblique strike-slip shear after 52 Ma. In the contrast, Watkinson founded brittle dextral strike-slip shear at Early Miocene (23 Ma.). Then it is left lateral after 0.29 Ma. till present.

11) However, at present-day sinistral movement along the studied RNF fault is responsible for the development of the opening of Andaman sea, and also seismic beach ball of the Ranong Fault Zone.

12) The present- day RNF shows that most earthquakes occur in the sea while, on land many action fault segments are recognized and they may experience major earthquake in the future.

REFERENCES

- Aitken, A. J. 1985. Thermoluminescence Dating. New York: Academic Press.
- Aki, K. 1984. Asperities of Barrier on an Earthquake Fault and Strong Motion Prediction. Jour. Geophys. Res., 98: 681-698.
- Albee, A. L., and Smith, J. L. 1966. Earthquake Characteristics and Fault Activity in Southern California. Engineering Geology in Southern California. Association of Engineering Geologists. Glendale, California. Los. Angeles Section Special Publication: 9-34.
- Allen, C. R. 1986. Seismological and Paleoseismological Techniques of Research in Active Tectonics. In: Wallace, R. E. ed. In: Active Tectonics: Studies in Geophysics. Natl. Washington: DC Acad. Press.
- Allen, C. R. Armand, F. Richter, C. F., and Nordquist, J. M. 1965. Relationship between Seismicity and Geologic Structure in the Southern California Region. Bulletin of the Seismological Society of America; 55, 4: 753-797.
- Artyotha, W. 2007. Radon Gas Investigation along the Ranong and Khlong Mauri Faults, southern Thailand. Master's thesis, Department of nucleartecnoogy Faculty of Engineer Chulalongkorn University.
- Barr, S. M., and Macdonal, A. S., 1979, Paleomagnetism age and geochemistry of the Denchai basalts, Northern Thailand, Earth Planet Science Letters, 46: 113-124.
- Biddle, K. T., and Christie-Blick, N. 1985. Glossary-Strike-Slip Deformation, Basin Formation, and Sedimentation. In Biddle, K. T., and Christie-Blick, N. eds., Strike-Slip Deformation, Basin Formation and Sedimentation, pp.375-385. Tulsa :Spec. Pub. Soc. Econ. Paleont. Miner.
- Bolt, B. A. 2006. Earthquake. 5th ed. New York: W.H. Freeman and Company.
- Bott, J. Wong, I. Prachuab, S. Wechbunthung, B. Hinthong, C., and S. Sarapirome. 1997. Contemporary seismicity in Northern Thailand and its tectonic implications, in Proceedings of the International Conference on Stratigraphy and Tectonic Evolution of Southeast Asia and the South Pacific, 453-464. Bangkok, Thailand.
- Botter-Jenson, L., McKeever, S.W.S., and Wintle, A.G. 2003. Optically Stimulated Luminescence Dosimetry. 1st ed. Netherland : ELSEVIER SCIENCE B.V.

- Bull, W.B., and L.D. McFadden, 1977, Tectonic geomorphology north and south of the Garlock fault, California, in *Geomorphology in arid regions*, D.O. Doehring, editor, Proceeding 8th Annual Geomorphology Symposium, pp.115-137. Binghamton: State University New York.
- Bunopas, S., 1981, Paleogeographic history of Western Thailand and adjacent parts of Southeast Asia - A plate tectonics interpretation, Doctoral dissertation, Victoria University of Wellington, New Zealand.
- Capetta, H., Buffetaut, E., and Suteethorn, V., 1990, A new hypodont shark from the Lower Cretaceous of Thailand, Neues Jahrbuch for Geologie und Paleontologie, Monatshefte, 11: 659-666.
- Carver, G. A., and McCalpin, J. P. 1996. Paleoseismology of Compression Tectonic Environment. In McCalpin, J. P. (ed.), Paleoseismology, New York: Academic Press.
- Chansawad, P., 2007. ESR-dating Investigations of Sediments by Using Soil Along the Southern Part of Khlong Marui fault, Phang Nga Province, Southern Thailand, Department of Geology Faculty of Science Chulalongkorn University.
- Chantong, W., et al. 2010. 2D Aeiamic Evidence for Recent Fault Activities in the Andaman Sea, Thailand. On the 5th International Conferences on Applied Geophysics; November 11-13, 2010, Phuket, Thailand. 50.
- Charusiri, P., Daorerk, V., and Supajanya, T. 1996. Applications of Remote-Sensing Techniques to Geological Structures Related to Earthquakes and Earthquake-Prone Areas in Thailand and Neighbouring Areas. A Preliminary Study. Journal of Scientific Research. Chulalongkorn University, 21, 1: 14-38.
- Charusiri, P., Daorerk, V., Kosuwan, K., and Choowong, M. 2004. Active Fault and Determination of Seismic Parameters Hutgyi Hydropower Project. Department of Geology, Faculty of Science, Chulalongkorn University submitted to Electricity Generating Authority of Thailand.
- Charusiri, P. Kosuwan, S. Fenton, C. H. Tahashima, T. Won-in, K., and Udchachon, M. 2001. Thailand Active Fault Zones and Earthquake Analysis: A Preliminary Synthesis. Jour. Asia Earth Sci. (submitted for publication).

- Charusiri, P., Kosuwan, K., Daorerk, V., Vajbunthoeng, B., and Khutaranon, S. 2000. Final Report on Earthquake in Thailand and Southeast Asia. Final Report Submitted to The Thailand Research Fund (TRF) (in Thai).
- Charusiri, P., Kosuwan, S., and Imsamut, S. 1997. Tectonic Evolution of Thailand: From Bunopas (1981)'s to a new scenario. The International Conference on Stratigraphy and Tectonic Evolution of Southeast Asia and the South Pacific, pp. 436-452. 19-24 August, Bangkok: Department of Mineral Resources.
- Charusiri, P. et al. 2006. The Study of Mae Yom Active Fault, Keang Sua Ten, Amphoe Song, Changwat Phare. Department of Geology, Faculty of Science, Chulalongkorn University submitted to Department of Royal Irrigation. Ministry of Natural Resources and Environment. Bangkok.
- Charusiri, P., Daorerk, V., and Supajanya, T. Applications of Remote-Sensing Techniques to Geological Structures Related to Earthquakes and Earthquake-Prone Areas in Thailand and Neighbouring Areas: A Preliminary Study. Journal of Scientific Research, 21, 1(1996) : 23-43.
- Charusiri, P., Kosuwan, S., Lumjuan, A., and Wechbunthung, B. 1998. Review of active faults and seismicity in Thailand. Proceedings of the Ninth Congress on Geology, Mineral, and Energy Resources of Southeast Asia-GEOSEA'98 and I GCP 383, Malaysia:symposium, pp.653-665. 17-19 August 1998, Kuala Lumpur : Geological Society of Malaysia.
- Christie-Blick, N., and Biddle, K. T. 1985. Deformation and Basin Deformation along Strike-Slip Fault. In: Biddle, K. T., and Christie-Blick, N. eds. Strike-Slip Deformation, Basin Formation, and Sedimentation, Society of Economic Paleontologists and Mineralogists, Spec. Pub. 37: 1-34.
- Chuaviroj, S. 1991. Geotectonic of Thailand. Bangkok: Geological Survey Division, Department of Mineral Resources.
- Cluff, L. S., and Bolt, B. A. 1969. Risk from Earthquake in the Modern Urban Environment with Special Emphasis on the San Francisco Bay Area, Urban Environmental Geology in the San Francisco Bay Region. In Association Engineering Geologist Sacramento, California: San Francisco Section Special Public: 25-64

- Daly, M. C. Cooper, M. A. Wilson, I. Smith, D. G., and Hooper, B. G. D. 1991. Cenozoic Plate Tectonics and Basin Evolution in Indonesia. Marine and Petroleum Geology. 8: 2-21.
- Department of Mineral Resources. 1999. Geologic Map of Thailand 1: 1,000,000. Department of Mineral Resources. Bangkok (with English explanation).
- Fenton, C. H., Charusiri, P., and Wood, S. H. 2003. Recent Paleoseismic Investigations in Northern and Western Thailand, Annals of Geophysics 2003: 957-981.
- Fenton, C. H., Charusiri, P., Hinthong, C., Lumjuan, A., and Mangkonkarn, B. 1997. Late Quaternary faulting in northern Thailand. Proceedings of the International Conference on Stratigraphy and Tectonic Evolution of Southeast Asia and the South Pacific, pp.436-452. August 1997, Department of Mineral Resources, Bangkok, Thailand.
- Garson, M.S., and Mitchell, A.H.G. 1970. Transform faulting in the Thai Peninsula. Nature 22, 45-47.
- Garson, M.S., Young, B., Mitchell, A.H.G., and Tait, B.A.R. 1975. The geology of the tin belt in peninsular Thailand around Phuket, Phangnga and Takua Pa. London: Overseas Mem. Inst. Geol. Sci.
- Gutenberg, B., and Richter, C. F. 1954, Seismic of the Earth and Associated Phenimena. New Jersey: Priceton University Press.
- Hall, R. 1996. Reconstructing Cenozoic SE Asia. In: Hall, R. and Blundell, D. eds., Tectonic Evolution of Southeast Asia. Geological Society of London Special Publication 106: 153-184.
- Hamblin, W.K. 1976. Patterns of displacement along the Wasatch Fault, Geology, 4: 619-622.
- Hinthong, C. 1991. Role of tectonic setting in earthquake event in Thailand. In ASEAM-EC Workshop on Geology and Geophysics, pp.1-37. Jakarta, Indonesia.
- Hinthong, C. 1995. The Study of Active Faults in Thailand. Proceedings of the Technical Conference on the Progression and Vision of Mineral Resources Development, pp.129-140. Department of Mineral Resources, Bangkok, Thailand.

- Hinthong, C. 1997. The Study of Active Faults in Thailand. Report of EANHMP. An Approach to Natural Hazards in the Eastern Asia: 17-22.
- Hobbs, W. H. 1972. Earth Features and Their Meaning. New York: Macmillan.
- Hoke, L., and Campbell, H. J. 1995. Active mantle melting beneath Thailand?. Proceedings of the International Conference on Geology, Geotechnology, and Mineral Resources of Indochina, pp.13-22. Department of Geotechnology, Khon Kaen University, Khon Kaen, Thailand.
- Huchon, P. LePichon, X., and Rangin, C. 1994. Indochina Peninsula and the collision of India and Eurasia. Geology, 22: 27-30.
- International Atomic Energy Agency. 1988. Code on the Safety of Nuclear Power Plants: Siting, Code 50-C-S. IAEA. Vienna.
- International Atomic Energy Agency. 1992. Code on the Safety of Nuclear Research Reactors: Design, Safety Series 35-S1. IAEA. Vienna.
- Keawmaungmoon, S., Thipyopass, S., and Charusiri, P. 2009. Preliminary Geomorphic Indices Associated to Active Faults in Khao Phanom area, Surat Thani Province. Journal of Remote Sensing and GIS Association of Thailand, Vol.10 No.2 May-August 2009: 54 -62.
- Keller, E. A., and Pinter, N. 1996. Active tectonics: Earthquake, uplift, and landscape, New Jersey: Prentice-Hall.
- Knuepfer, P. L. K. 1989. Implications of the Characteristics of End-Points of Historical Surface Fault Ruptures for the Nature of Fault Segmentation. In Schwartz, D. P. and Sibson, R. H. (ed.), Fault Segmentation and Controls of Rupture Initiation and Termination, pp.89-315, 193-228. U.S.: Geological Surv.
- Kosuwan, S. Saithong, P. Lumjuan. A. Takashima, I. and Charusiri, P. 1999. Preliminary Results of Studies on the Mae Ai Segment of the Mae Chan Fault Zone, Chiang Mai Northern Thailand. The CCOP Meeting on Exodynamic Geohazards in East and Southeast Asia, pp.1-8. July 14-16, Pattaya, Thailand.
- Lacassin, R. et al. 1997. Tertiary Diachronic Extrusion and Deformation of western Indochina: Structural and $^{40}\text{Ar}/^{39}\text{Ar}$ evidence from NW Thailand. Journal of Geophysical Research, 102: 10013 -10037.

- Landsat Thematic Mapper (TM) - USGS (U.S. Geological Survey), [online]. Available from: <http://eros.usgs.gov/products/satellite/tm.php>. [2009, August 5].
- Lee, T. Y., and Lawver, L. A. 1995. Cenozoic plate reconstructions of Southeast Asia. *Tectonophysics*, 251: 85–138.
- Loboonlert, P. 2007. Crustal Displacement after Earthquake in September 12th 2007, from August 1st to October 31th 2007, Using GPS Data at Phuket, Thailand. Department of Geology Chulalongkorn University.
- Lorenzetti, E.A. Brennan, P.A., and Hook, S.C. 1994. Structural styles in rift basins: interpretation methodology and examples from Southeast Asia, *Bull. Am. Assoc. Pet. Geol.*, 78, 1,152.
- MaCalpin, J. P. 1996. *Paleoseismology*. California: Academic press.
- Macdonald, A.S., Barr, S.M. Dunning, G.R., and Yaowanoyothin, W. 1993. The Doi Inthanon metamorphic core complex in NW Thailand: age and tectonic significance, *J. Southeast Asian Earth Sci.*, 8 (1-4), 117-125.
- Mahattanachai, T. 1996. *Seismic stratigraphy and Seismic Facies Analysis of the Mergui Basin, Thai Andaman Sea*. Master's Thesis. Department of Geology. Faculty of Science . Chiangmai University.
- Matthews, S. J. Fraser, A. J. Lowe, S. Todd, S. P., and Peel, F. J. 1997. Structure, Stratigraphy and Petroleum Geology of the SE Nam Con Son Basin, Offshore Vietnam. In: Fraser, A. Matthews, S. Murphy, R. eds., *Petroleum Geology of Southeast Asia*. *Geol. Soc. London, Spec. Publ.*, 126: 89–106.
- Mccabe, R. et al. 1988. Extension tectonics: the Neogene opening of the north-south trending basins of Central Thailand, *J. Geophys. Res.*, 93, 11,899-11,910.
- Mccabe, R. Harder, S. Cole, J.T., and Lumadyo, E. 1993. The use of paleomagnetic studies in understanding the complex Tertiary tectonic history of east and southeast Asia, *J. Southeast Asian Earth Sci.*, 8 (1-4), 257-268.
- Meesook, A. 2000. Cretaceous environments of Northeastern Thailand, in H. Okada and N.J. Mateer, eds. *Cretaceous environment of Asia*, *Elsevier Science B.V.*: 207-223.

- Ministry of Natural Resources and Environment, Department of Mineral Resources. 2007. Investigation on Recurrence Interval in Areas Showing Trace of Movement along the Faults in Prachuap Khiri Khan, Chumporn, Ranong, Surat Thani, Krabi, Phang Nga and Phuket Provinces (Ranong and Khlong Marui Faults). Bangkok: Environmental Geology Division.
- Molnar, P., and Deng, Q. 1984. Faulting Associated with Large Earthquake and the Average Rate of Deformation in Central and Eastern Asia. Journal of Geophysical Research, 89: 6,203-6,227.
- Molnar, P., and Tapponnier, P. 1975. Cenozoic tectonics of Asia: effects of a continental collision. Science, 280: 419-426.
- Ni, J., and York, J. E. 1978. Late Cenozoic Tectonics of the Tibetan Plateau. J. Geophys. Res., 83: 5,377-5,384.
- Nutalaya, P. Sodsri, S., and Arnold, E. P. 1985. Series on Seismology-Volume II-Thailand. In Arnold, E. P (ed.), Southeast Asia Association of Seismology and Earthquake Engineering.
- O' Leary, D. W., and Simson, S. L. 1977. Remote Sensing Application to Tectonism and Seismicity in the Northern Part of the Mississippi Embayment. J. Geophysics, 42, 3: 542-548.
- O' Leary, D. W., Fridman, J. D., and Pohn, H. A. 1976. Lineament, Linear, Lineation: Some Proposed New Standards for Old Terms. Bull. Geol.soc.Am, 87: 1463-1469.
- O'LEARY, J., and HILL, G. S. 1989. Tertiary basin development in the Southern Central Plains, Thailand. Proceedings of the International Symposium on Intermontaine Basins: Geology and Resources, pp. 254-264. Chiang Mai University, Chiang Mai, Thailand.
- Packham, G. 1996. Cenozoic SE Asia: reconstructing its aggregation and reorganization. In: Hall R., and Blundell, D. J. eds., Tectonic Evolution of Southeast Asia, pp. 123-152. London: Geol. Soc.
- Park, R. G., and Jaroszewski, W. 1994. Craton Tectonics, Stress and Seismicity. In: Hancock, P. L. ed., Continental Deformation, pp. 200-222. Oxford: Pergomon Press.

- Peltzer, G., and Tapponnier, P. 1988. Formation and evolution of strike-slip faults, rifts, and basins during the India-Asia collision: an experimental approach, J. Geophys. Res., 93: 15,085-15,117.
- Phillip, H. et al. 1992. The Armenian Earthquake of 1988 December 7; Faulting and Folding, Neotectonics and Paleoseismicity. Geophys. Jour. Int., 110: 141-158.
- Polachan, S. 1988. The Geological Evolution of the Mergui Basin, SE Andaman Sea, Thailand. Doctoral dissertation. Royal Holloway and Bedford New College, University of London.
- Polachan, S., and Satayarak, N. 1989. Strike-Slip Tectonics and the Development of Tertiary Basins in Thailand. Proceedings of the International Symposium on Intermountain Basin, Geology and Resources, pp.243-253. 30 Jan-2 Feb 1989, Chiang Mai, Thailand.
- Polachan, S. et al. 1991. Development of Cenozoic basins in Thailand, Mar. Pet. Geol., 8: 84-97.
- Rangin, C., Jolivet, L., and Pubellier, M. 1990. A Simple Model for the Tectonic Evolution of Southeast Asia and Indonesia Region for the past 43 m.y. Bulletin de la Société géologique de France, 8 VI: 889-905.
- Remus, D., Webster, M., and Keawkan, K. 1993. Rift architecture and sedimentology of the Phetchabun intermontaine basin, Central Thailand, J. Southeast Asian Earth Sci., 8 (1-4): 421-432.
- Rhodes, B. P., Perez, R., Lamjuan, A., and Kosuwan, S. 2002. Kinematics of the Mae Kuang Fault, Northern Thailand Basin and Range Province. The Symposium on Geology of Thailand, pp. 298-308. August 2002, Bangkok, Thailand.
- Saithong, P. 2006. Characteristics of the Moei-Mae Ping Fault Zone, Changwat Tak, Northwestern, Thailand. Master's Thesis. Department of Geology Faculty of Science Chulalongkorn University.
- Schwartz, D. P. 1998. Geological Characterization of Seismic Sources: Moving into the 1990's. In J.L. von Thun (ed.), Earthquake Engineering & Soil Dynamics II Proceedings; 2, Recent Advances in Group Motion Evaluation, pp.1-42. Spec. Publ. Am. Soc. Civil Engineers Geotech 20.

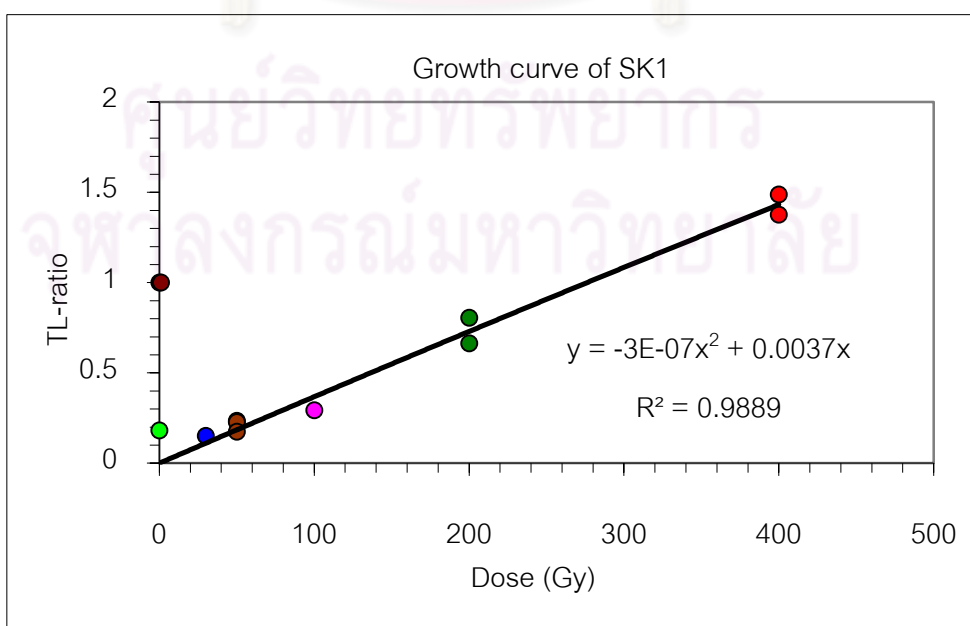
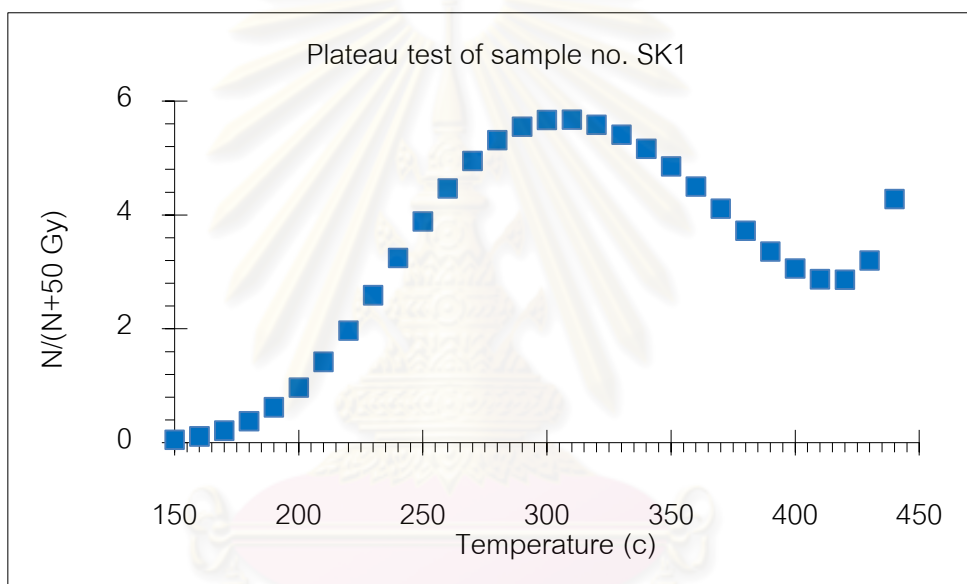
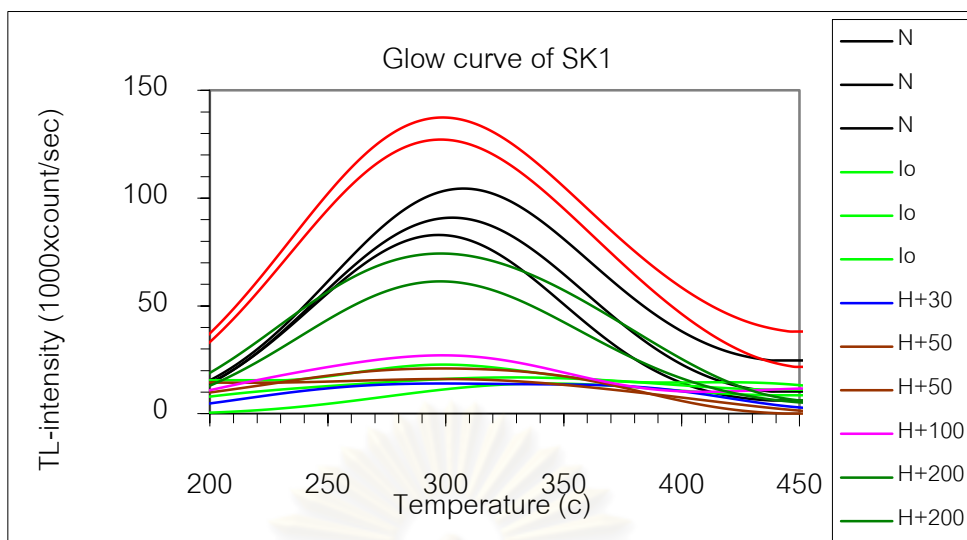
- Segall, D., and Pollard, D. D. 1980. Mechanics of Discontinuous Faults. J. Geophys. Res., 85: 4,337-4,350.
- Siribhakdi, K. 1986. Seismicity of Thailand and Periphery. Geological Survey Division, Department of Mineral Resources Bangkok. In: Panitan Lukleunaprasit et al. Proceedings of the 1 st Workshop on Earthquake Engineering and Hazard Mitigation, pp.151-158. November 1986, Bangkok, Chulaongkorn University.
- Smith, R.B., and Aabasz, W.J. 1991. Seismicity of the Intermountain Seismic Belt, in Neotectonics of North America, Geological Society of America Decade Map, vol. 1: 185-228.
- Strandberg, C. H. 1967. Aerial Discovery Manual. New York: John Wiley & Son.
- Stand Deyo earthquake's Warning. 2005. Subduction zone in the ring of fire. [Online]. Available from: <http://standeyo.com/Reports/041222.EQ.warning/050827.Deyo.EQs.html>. [2011, January 10].
- Sylvester, A. G. 1988. Strike-Slip Faults. Geol. Soc. Am. Bull., 100: 1666-1703.
- Takashima, I., and Walanabe, K. 1994. Thermoluminescence Age Determination of Lava Flows/Domes and Collapsed Materials at Unzen Volcano, SW Japan. Bulletin of the Volcanological Society of Japan, 39: 1-12.
- Tanaka, K. et al. 1997. Dating of Marine Terrace Sediments by ESR, TL and OSL Methods and their Applicabilities. Quaternary Science Reviews, 16: 257-264.
- Tapponnier, P., Peltzer, G., and Armijo, R. 1986. On the Mechanics of Collision between India and Asia. In: Coward, M. P., and Ries, A. C. eds., Collision Tectonics. Journal of the Geological Society of London. Special Publication, 19: 115-157.
- Tapponnier, P., Peltzer, G., Armijo, R., Le Dain, A., and Coobbold, P. 1982. Propagating Extrusion Tectonics in Asia: New insights from simple experiments with plasticine. Geology, 10: 611-616.
- Thailand Meteorological Department. 2008. Earthquake Information Catalogue. Report of Thailand Meteorological Department. Bangkok (digital files and unpublished Maunscript).

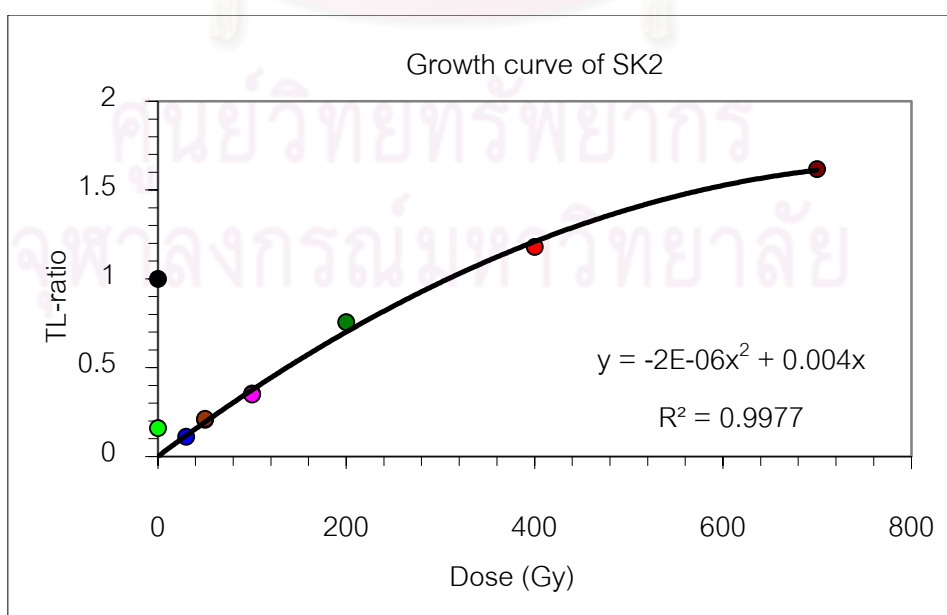
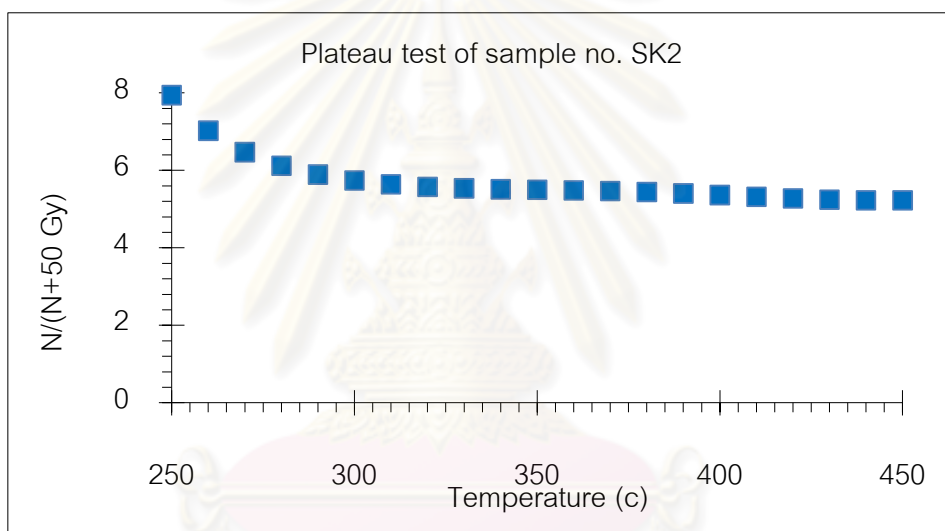
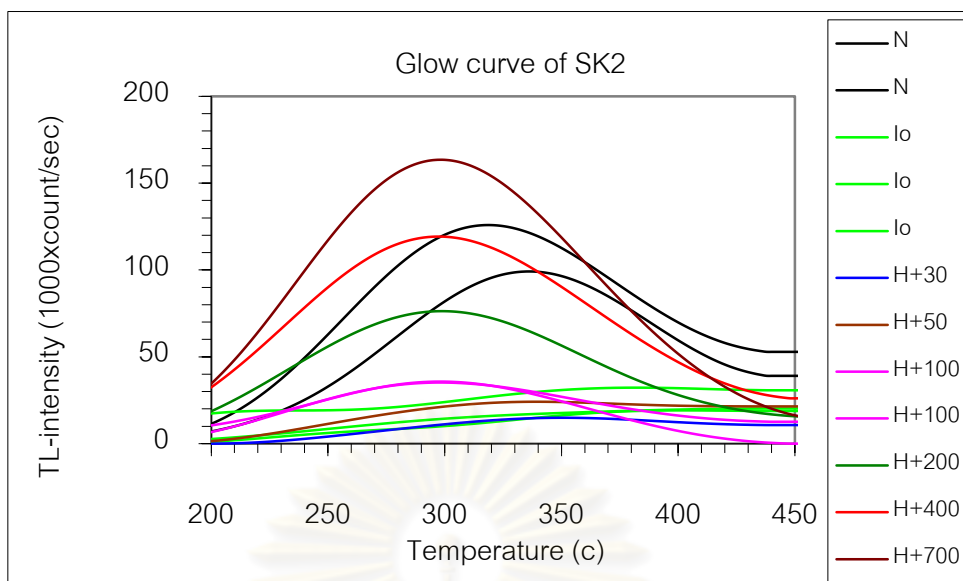
- Thipyopass, S. et al. 2008. Analysis of Macroseismic Intensities on the 2006 Earthquake Event in Prachuab Khirikhan Area, Central Thailand. On the Proceedings of the International Symposia on Geoscience Resources and Environments of Asian Terranes (GREAT 2008), 4th IGCP, and 5th APSEG; November 24-26, 2008 Bangkok, Thailand. 138-143.
- Thipyopass, S., and Charusiri, P. 2009. Preliminary Macroseismic Investigation of Earthquake Event on September – October 2006, 2009. Geographical Journal. Geographical Association of Thailand, Vol.33 No.1 April 2009, 64-65.
- University of Malaya. 2009. Seismicity of southeast asia. [online]. Available from: http://umfacts.um.edu.my/gallery/index.php?menu=research_details&cid=110. [2011, January 10].
- U.S. Nuclear Regulatory Commission. 1982. Appendix A: Seismic and geologic siting criteria for nuclear power plants. Code of Fed. Regul. 10. Chap. 1, Part 100. 1 September, 1982: 549-559.
- Weldon, R. J., McCalpin, J. P., and Rockwell, T. K. 1996. Paleoseismology of Strike-Slip Tectonic Environments. In: McCalpin, J. P. ed. Paleoseismology, pp.271-329. New York: Acad. Press.
- Wells, D. L., and Coppersmith, K. J. 1994. New Empirical Relationships among Magnitude, Rupture Width, Rupture Area, and Surface Displacement. Bulletin of the Seismological Society of America, 84: 974-1002.
- Wheeler, R. L. 1989. Persistent Segment Boundaries on Basin-Range Normal Faults. In: Stewart D. P. and Sibson, R. H. eds., Fault Segmentation and Controls of Rupture Initiation and Termination, U.S. Geol. Survey. 432-444.
- Won-in, K. 1999. Neotectonic evidences along the Three Pagoda Fault Zone, Changwat Kanchanaburi. Master's Thesis. Department of Geology Faculty of Science Chulalongkorn University.
- Wood, H. O. 1915. California Earthquake, A Synthetic Study of Recorded Shocks. Bulletin of the Seismological Society of America, 6: 54-196.

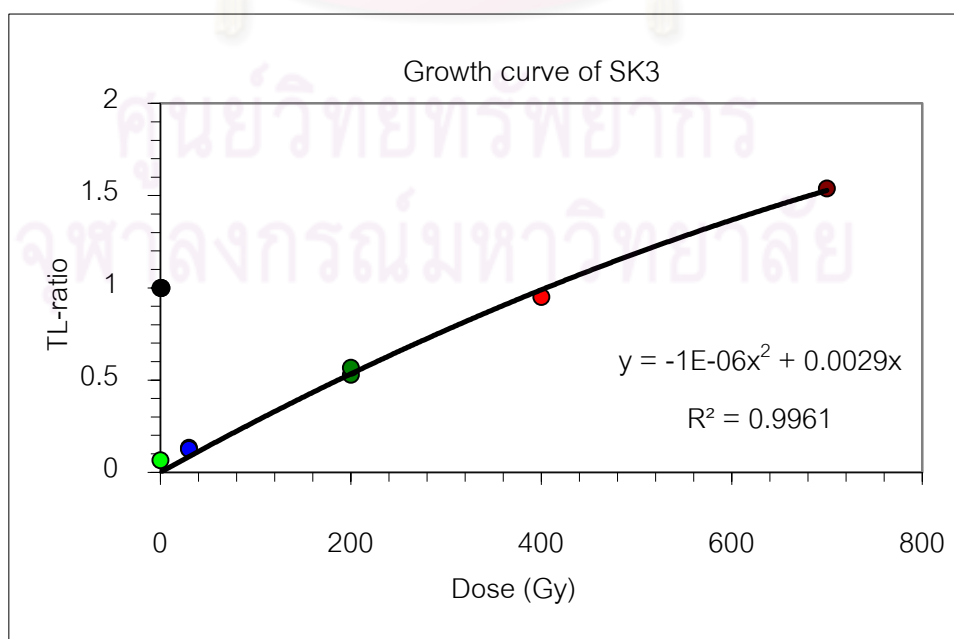
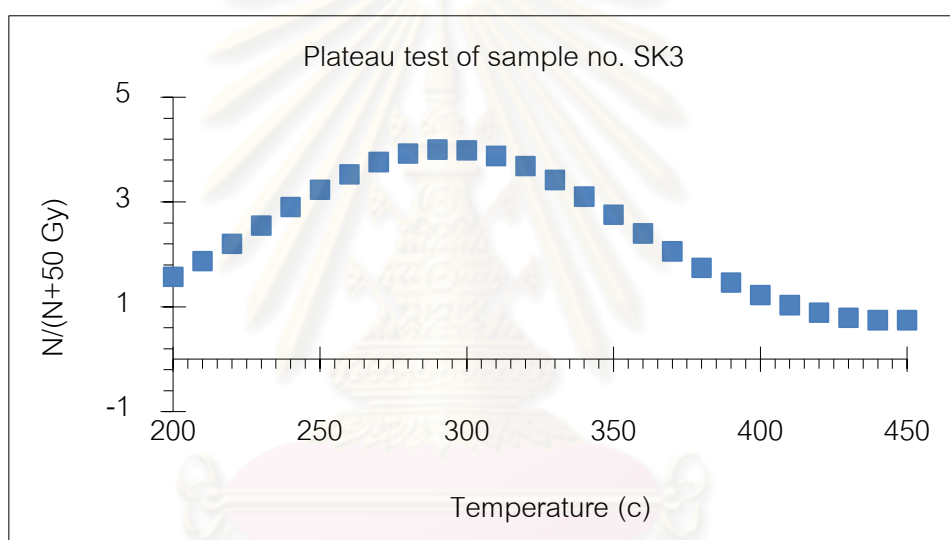
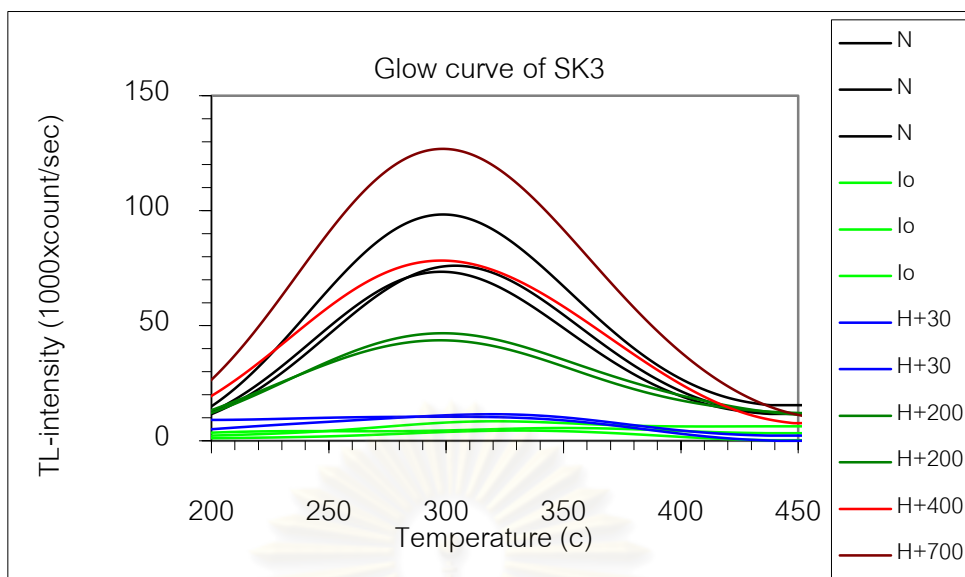


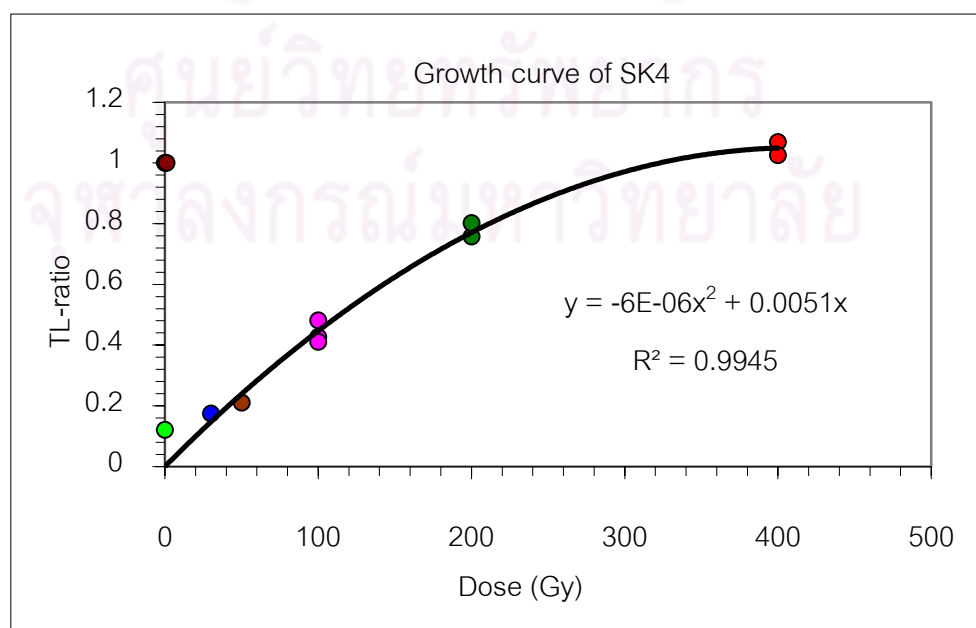
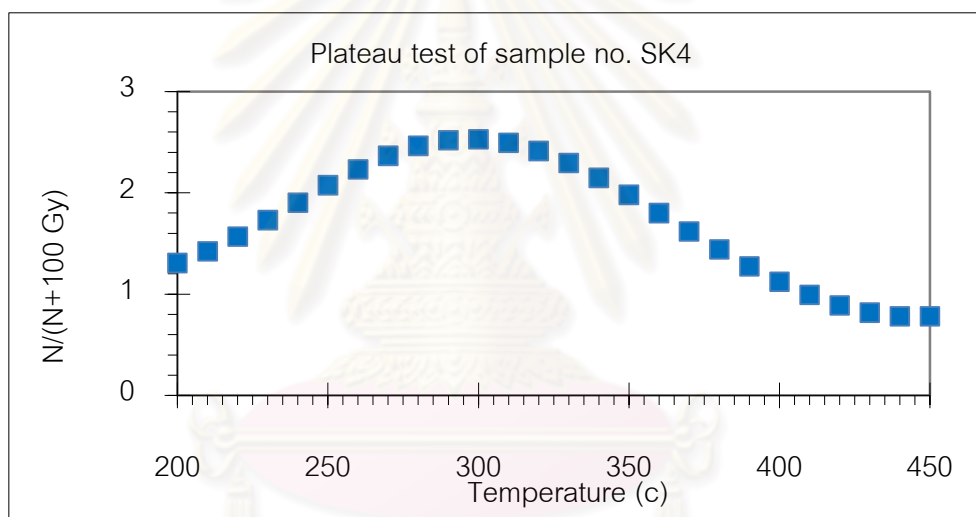
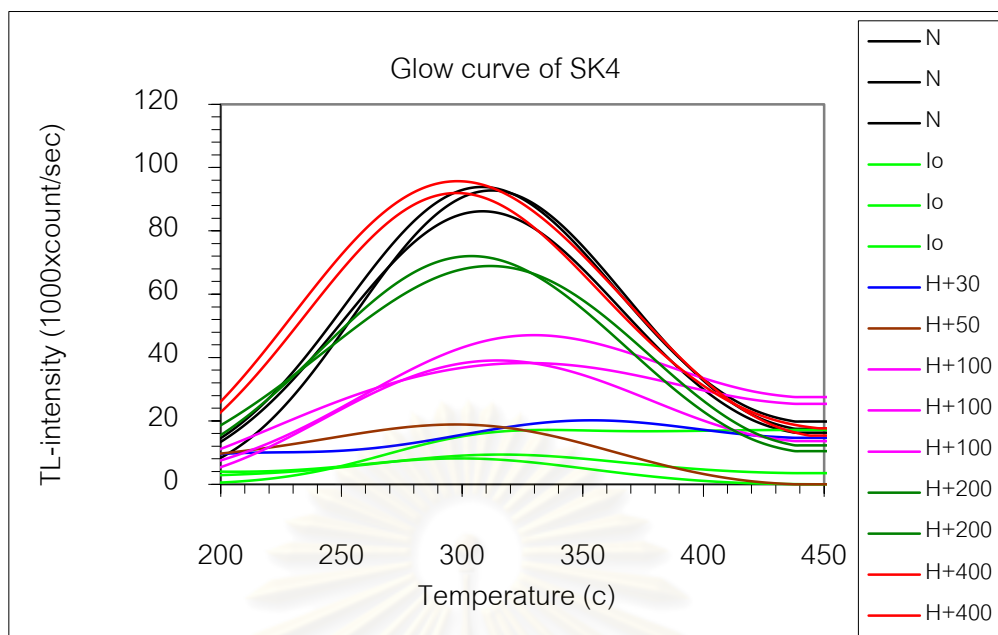
APPENDIX

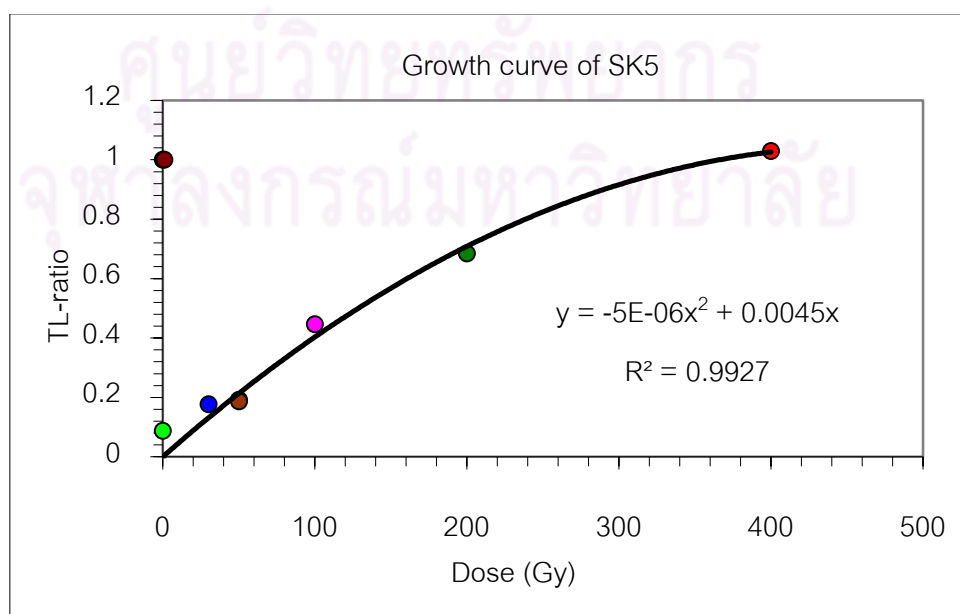
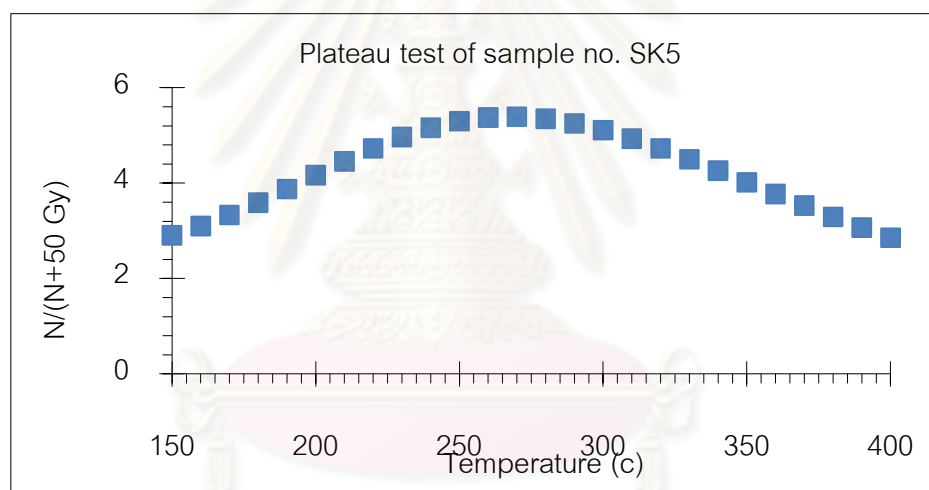
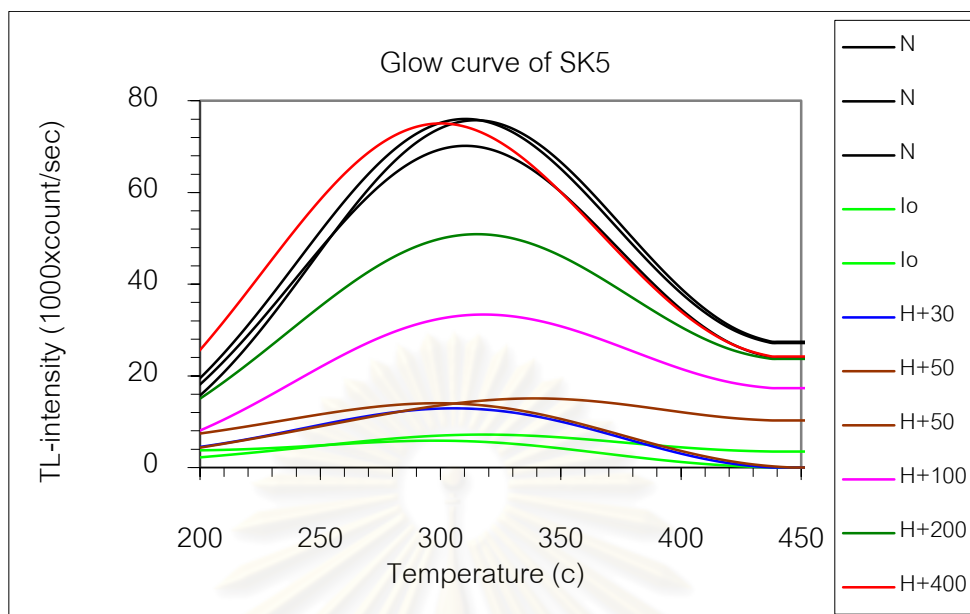
ศูนย์วิทยทรัพยากร
จุฬาลงกรณ์มหาวิทยาลัย

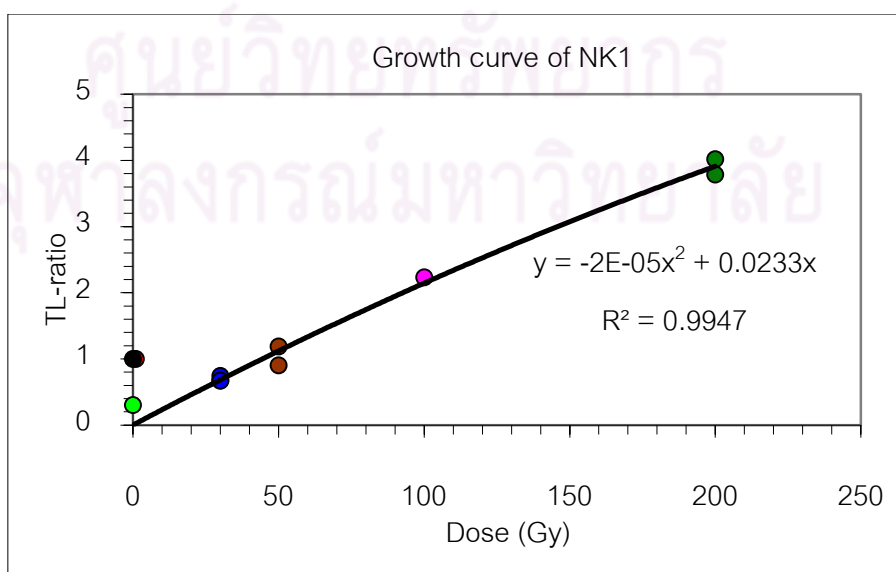
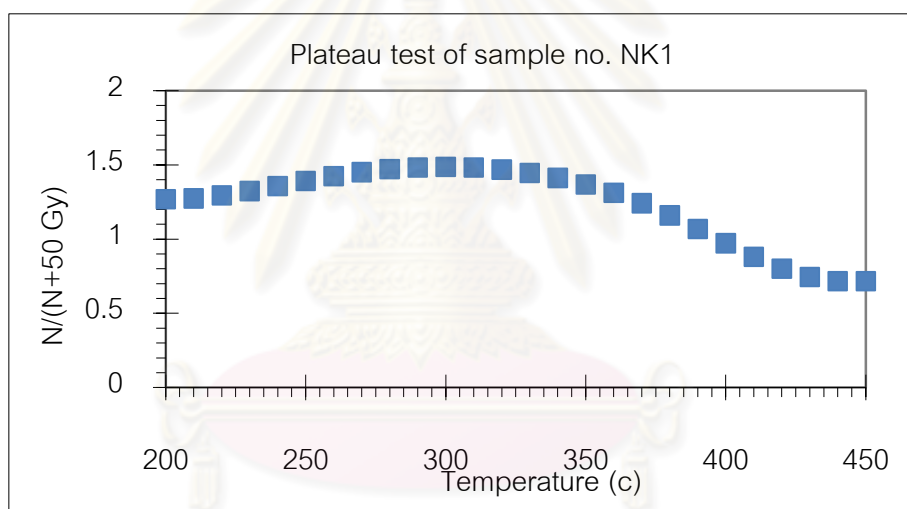
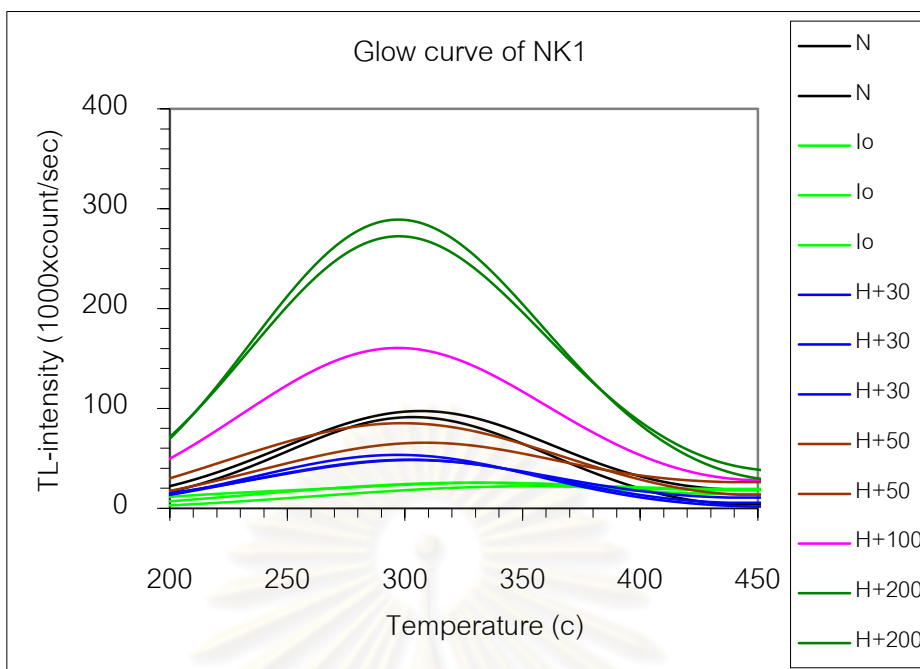


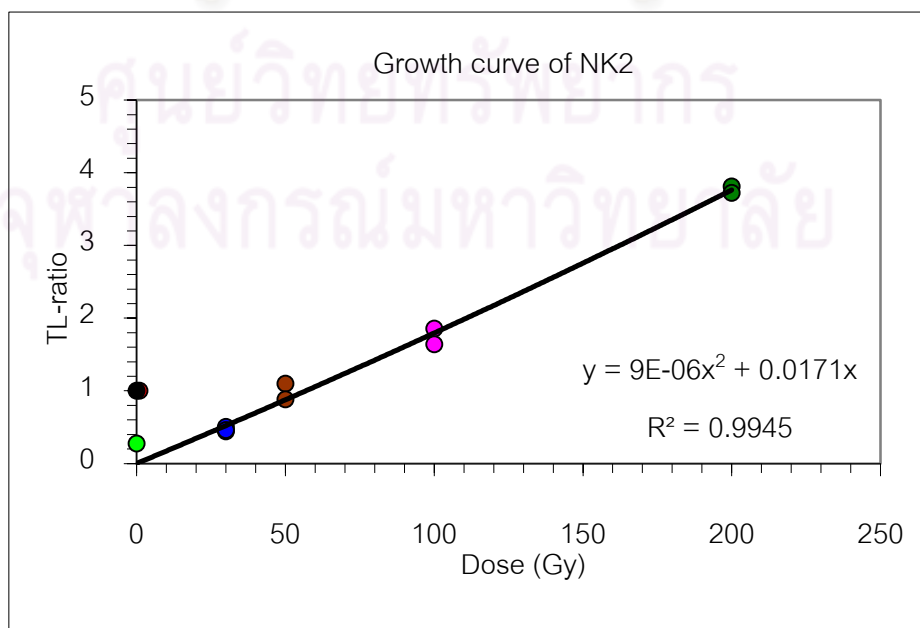
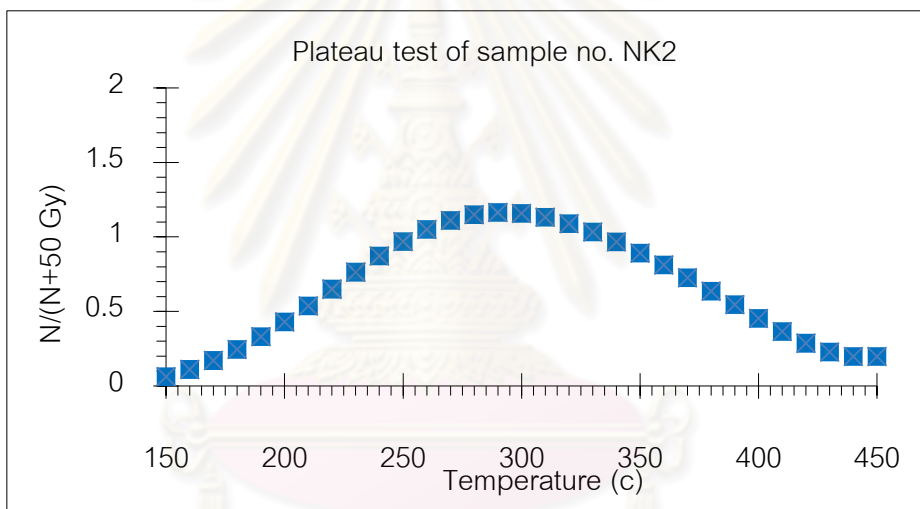
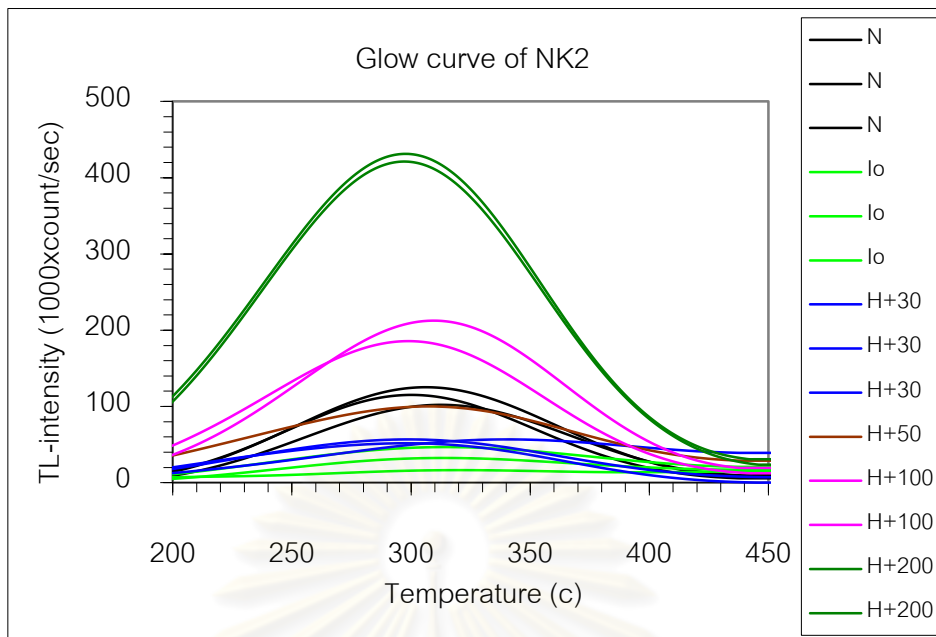


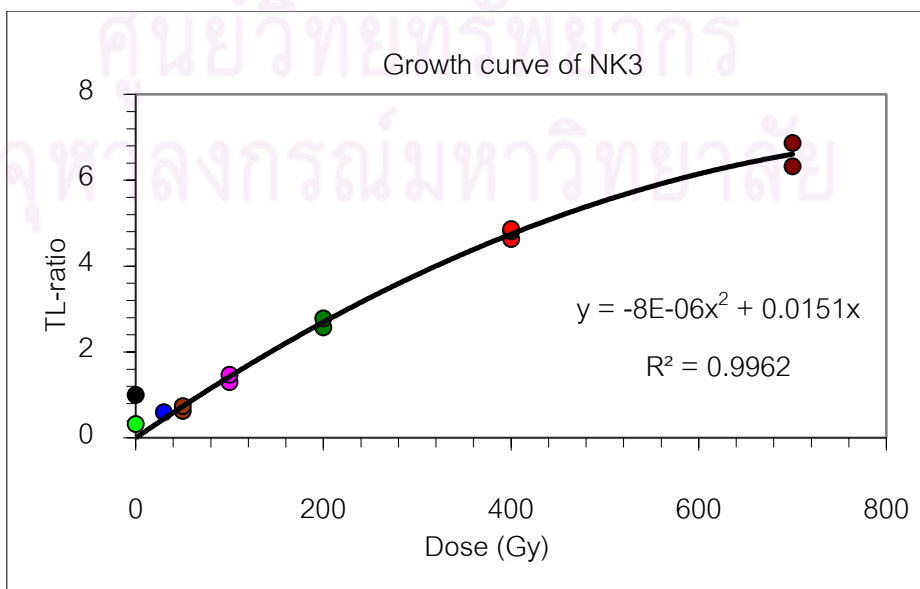
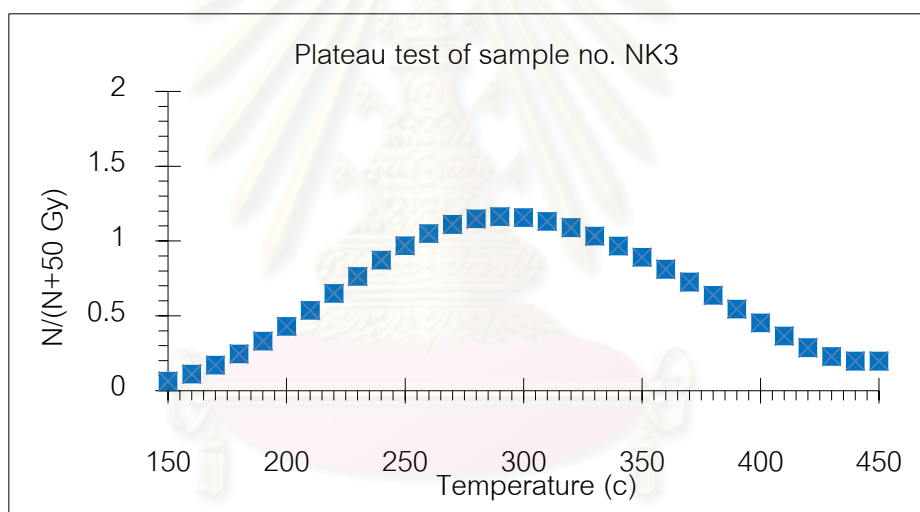
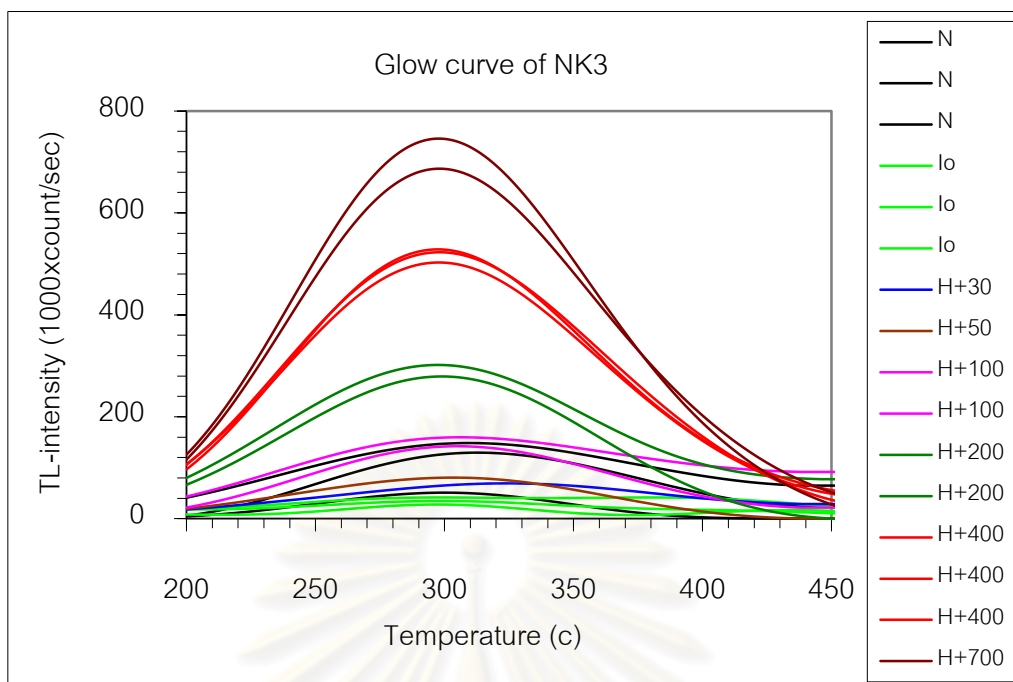


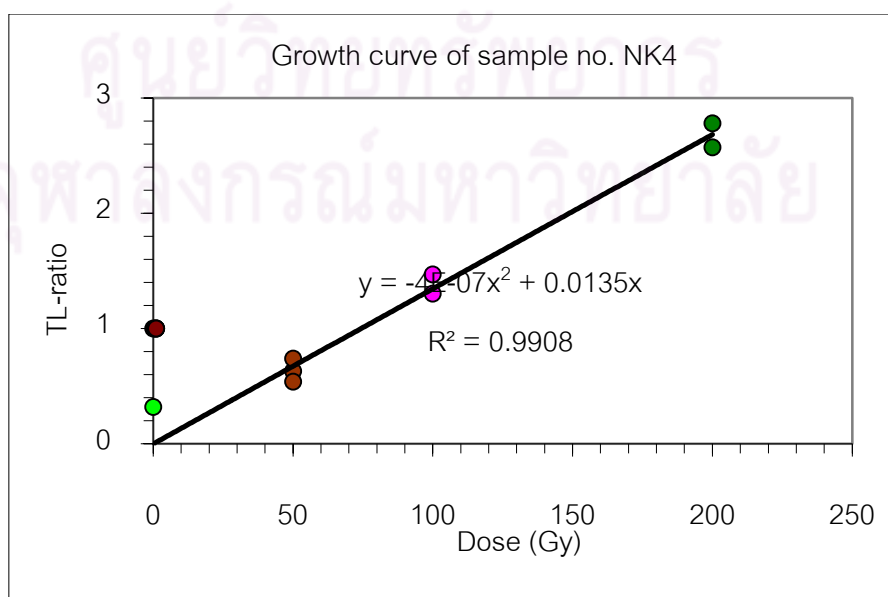
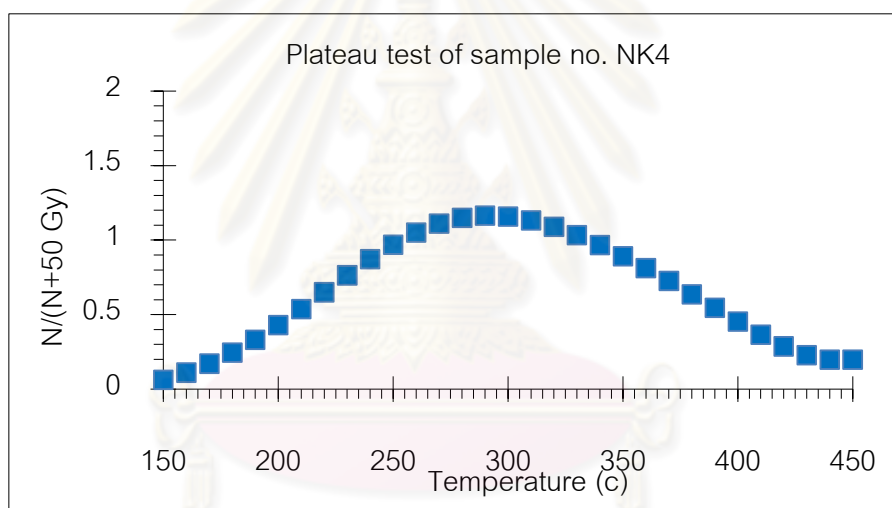
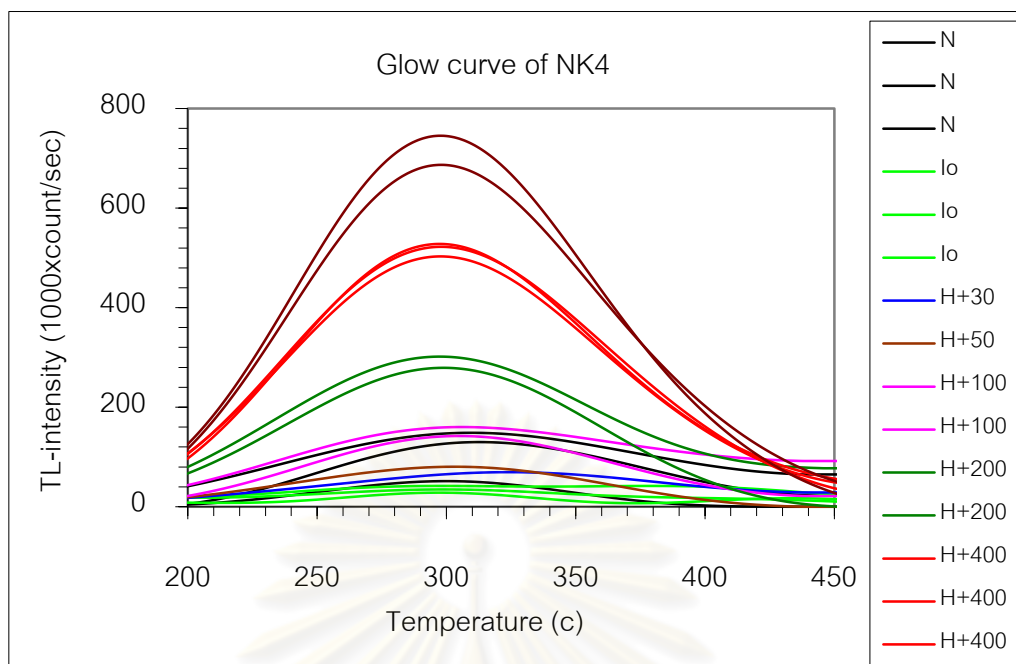


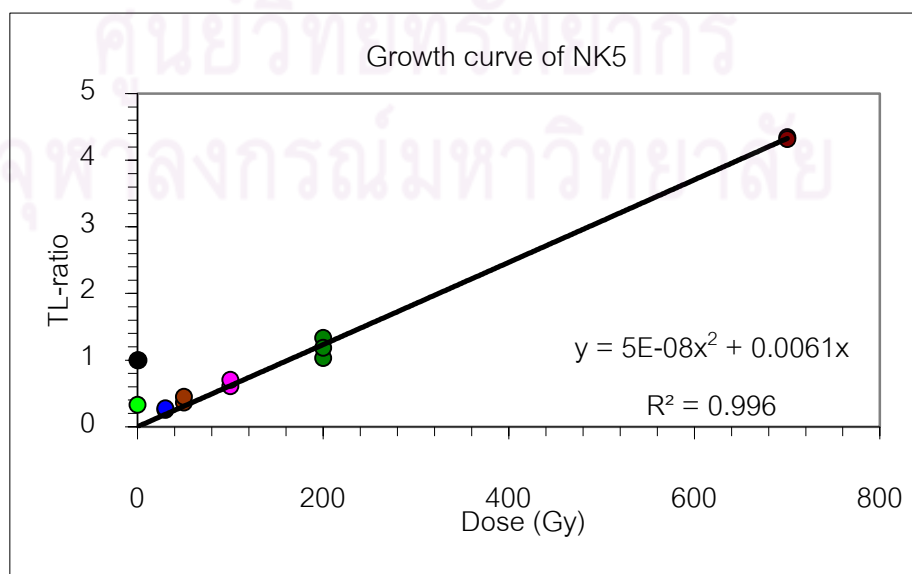
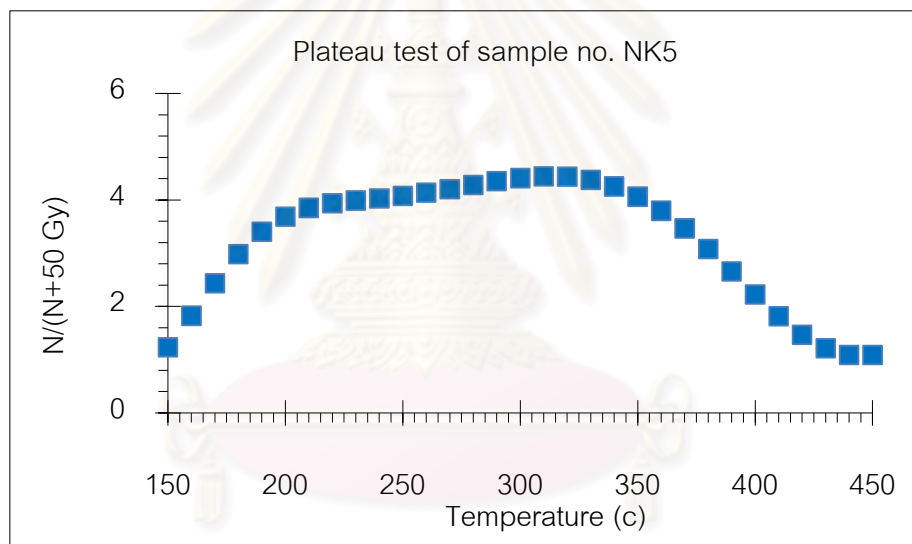
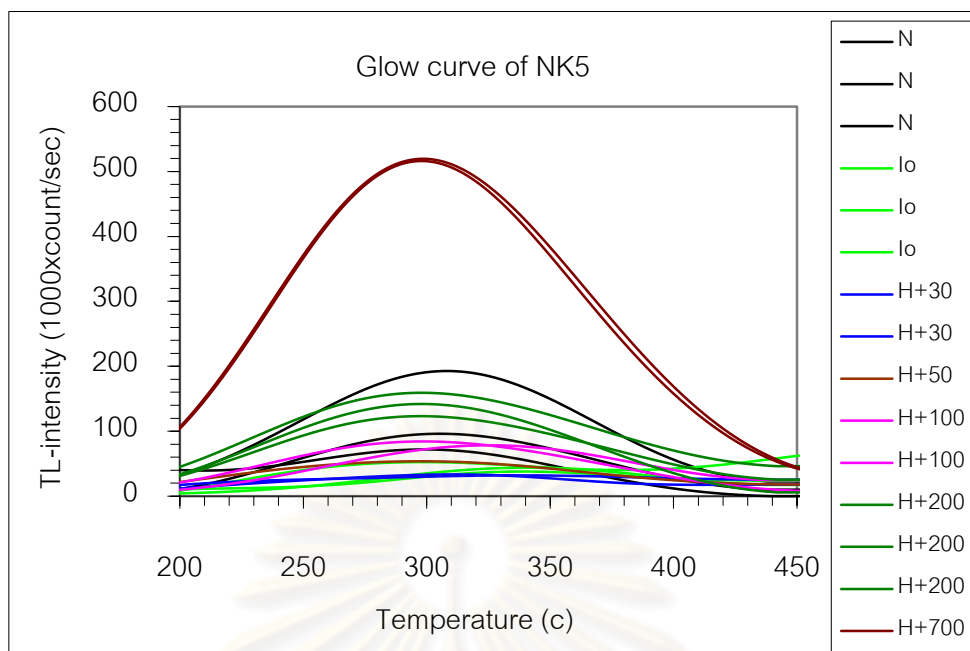


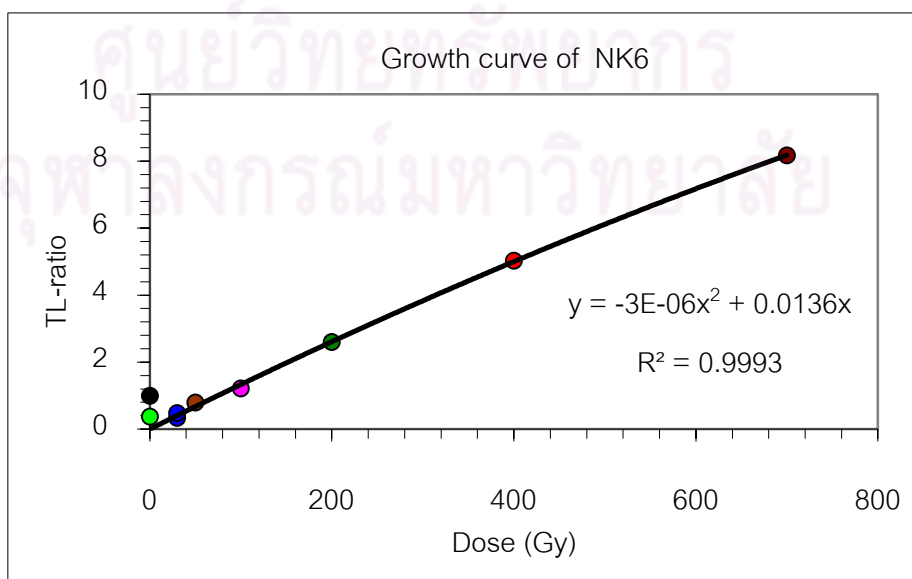
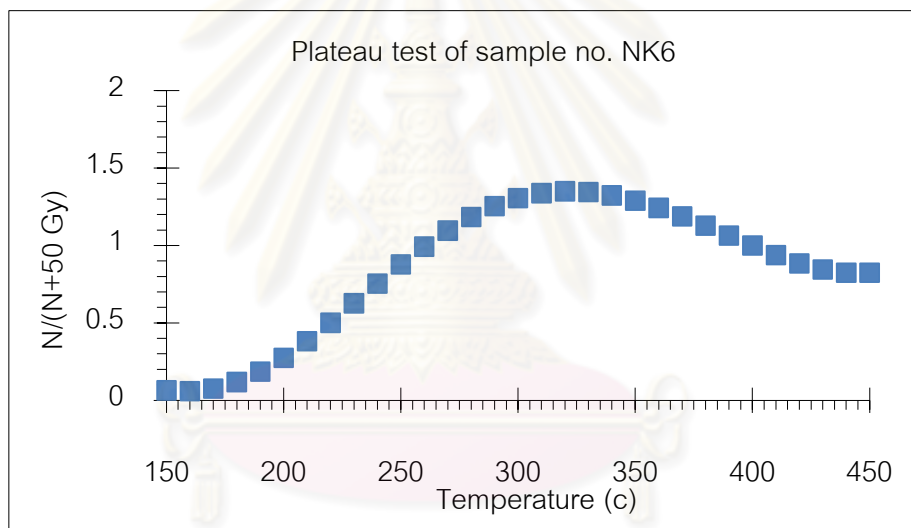
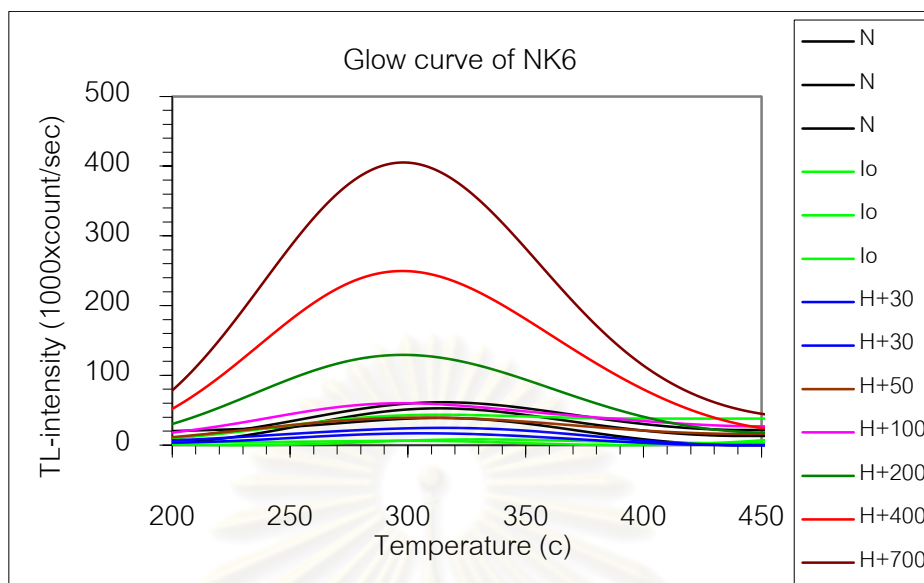


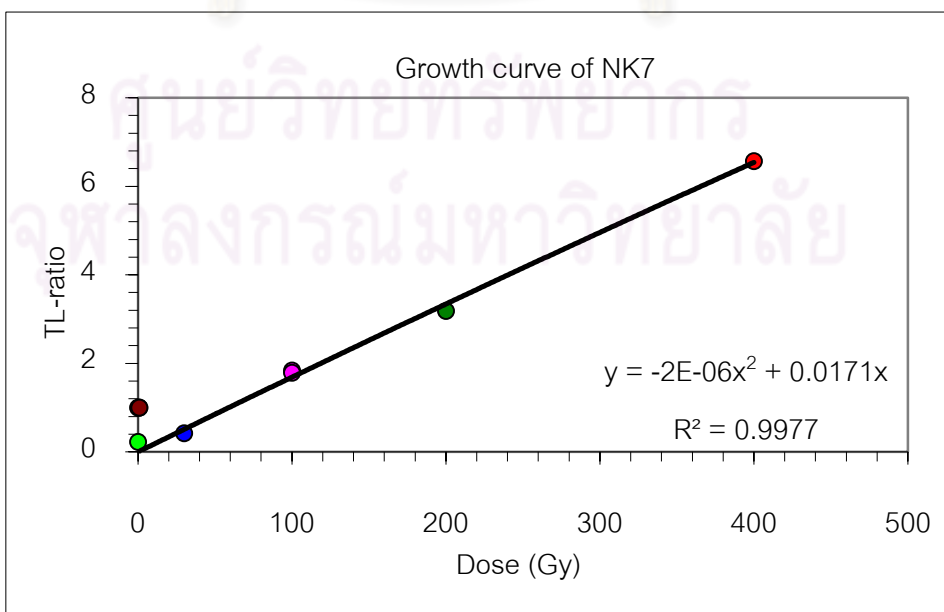
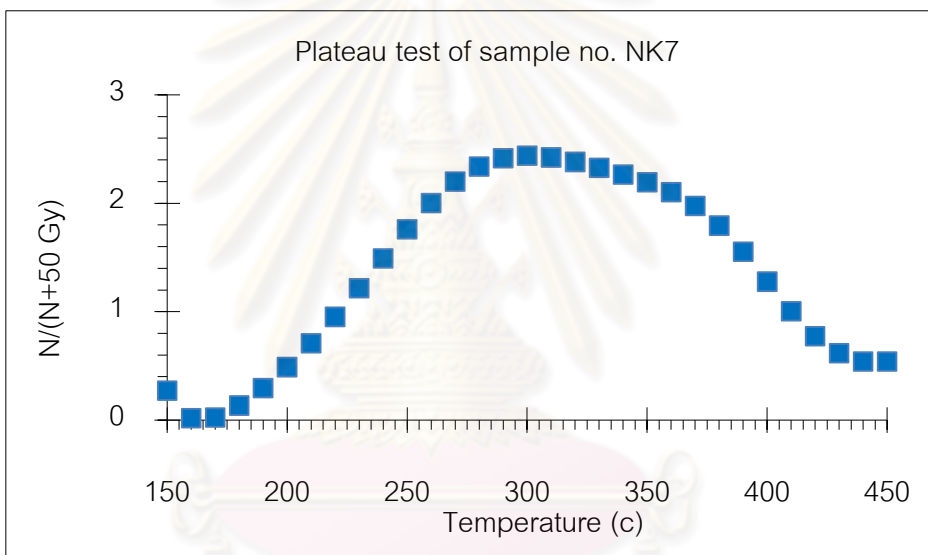
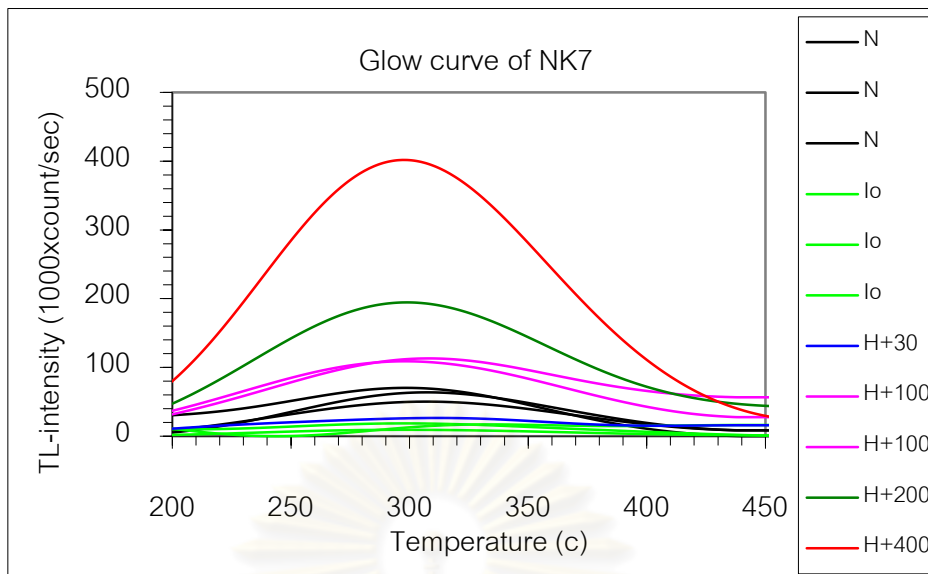












BIOGRAPHY

Miss Sumalee Thipyopass was born on February 15, 1976 in Khon Kaen, northeastern Thailand. She graduated at high school level from Ban Pai School, Khon Kaen, in 1993. In 1997, she received a B.Sc. degree in geotechnology from the Department of Geotechnology, Faculty of Technology, Khon Kaen University, Thailand. After she graduation, she started her work in 1997 as a both of geologist and head of laboratory researcher at the PVC Engineering Co. Ltd., Bangkok and six month later she move to work at department of Geotechnology, Faculty of Technology, Khon Kaen University as scientist , head of laboratory section . In 1998 she fill the post as a government official geologist of the Royal Irrigation Department (RID) at central office, Bangkok and few years later she moved to work at office section 13, Prachub Khiri khan until present time. In 2008 she enrolled as a graduate student for the M.Sc. program of Geology program at Graduate School, Chulalongkorn University, Bangkok, Thailand.

During her research study, in 2008, she published a geoscientific paper on “Analysis of Macroseismic Intenities on the 2006 Earthquake Event in Prachub Khirikhan Area, Central Thailand” which appeared on Proceedings of International Syposia on Geoscience Resources and Environments of Asian Terranes, GREAT 2008/4th IGCP 516/ 5th APSEG, Bangkok, Thailand. In the late 2009, she published the other paper on “Preliminary Macrosiesmic Investigation of Earthquake Event on September – October 2006 in Prachub Khirikhan ” in the Journal of Geography, ISSN 0857-6025 Vol. 33 No.2 August, Geographical Association of Thailand.

ศูนย์วิทยทรัพยากร
จุฬาลงกรณ์มหาวิทยาลัย